

Green Energy and Technology

Sudipta Chakraborty  
Marcelo G. Simões  
William E. Kramer *Editors*

# Power Electronics for Renewable and Distributed Energy Systems

A Sourcebook of Topologies,  
Control and Integration

 Springer

# Green Energy and Technology

For further volumes:  
<http://www.springer.com/series/8059>

Sudipta Chakraborty · Marcelo G. Simões  
William E. Kramer  
Editors

# Power Electronics for Renewable and Distributed Energy Systems

A Sourcebook of Topologies, Control  
and Integration

 Springer

*Editors*

Sudipta Chakraborty  
William E. Kramer  
National Renewable Energy Laboratory  
Golden, CO  
USA

Marcelo G. Simões  
Electrical Engineering and Computer  
Science  
Colorado School of Mines  
Golden, CO  
USA

ISSN 1865-3529

ISSN 1865-3537 (electronic)

ISBN 978-1-4471-5103-6

ISBN 978-1-4471-5104-3 (eBook)

DOI 10.1007/978-1-4471-5104-3

Springer London Heidelberg New York Dordrecht

Library of Congress Control Number: 2013938758

© Springer-Verlag London 2013

This work is subject to copyright. All rights are reserved by the Publisher, whether the whole or part of the material is concerned, specifically the rights of translation, reprinting, reuse of illustrations, recitation, broadcasting, reproduction on microfilms or in any other physical way, and transmission or information storage and retrieval, electronic adaptation, computer software, or by similar or dissimilar methodology now known or hereafter developed. Exempted from this legal reservation are brief excerpts in connection with reviews or scholarly analysis or material supplied specifically for the purpose of being entered and executed on a computer system, for exclusive use by the purchaser of the work. Duplication of this publication or parts thereof is permitted only under the provisions of the Copyright Law of the Publisher's location, in its current version, and permission for use must always be obtained from Springer. Permissions for use may be obtained through RightsLink at the Copyright Clearance Center. Violations are liable to prosecution under the respective Copyright Law. The use of general descriptive names, registered names, trademarks, service marks, etc. in this publication does not imply, even in the absence of a specific statement, that such names are exempt from the relevant protective laws and regulations and therefore free for general use.

While the advice and information in this book are believed to be true and accurate at the date of publication, neither the authors nor the editors nor the publisher can accept any legal responsibility for any errors or omissions that may be made. The publisher makes no warranty, express or implied, with respect to the material contained herein.

Printed on acid-free paper

Springer is part of Springer Science+Business Media ([www.springer.com](http://www.springer.com))

# Foreword

Energy is one of the major challenges for the human being; maybe ranked as number three of all critical factors in order to survive. First priority is water; many areas are globally lacking on this and humans cannot live without it for many days. The second is food and the third in my opinion is energy. In a modern society, energy is necessary for almost all functions in life in order to create a sustainable society. For the moment, we are consuming fossil fuel very fast to generate energy for living. Even with the continuous increase on consumption, the fossil fuel resources are available for our life-time; but for future generations such energy resource will be a limiting factor for our society and global instability can appear very fast—maybe much faster than we can foresee today.

As engineers, we have to come up fast with solutions to solve that challenge in order to make the global energy system sustainable. It is a significant challenge, which needs to be solved by new technological innovations combined with a careful awareness about the energy we are using and what we are using it for. I think more and more people are aware of their water consumption and such awareness should also be developed for the energy consumption. In order to create energy sustainability, four important issues need to be addressed: first is to make the power production sustainable by renewable energy generation; second is to increase the electrification of the transportation sector; third is to make the energy consumption much more efficient; and fourth is to develop the necessary infrastructure to take care of the large-scale energy transport for large distances.

This book discusses many of the required energy technologies that would create a sustainable world. For renewable and distributed energy in general, power electronics is an important enabling technology which allow us to convert electrical power from one form to another very efficiently and very fast. The technology is under steady development with continuously decreasing costs and increasing reliability. It is used in electrical power production, electric transmission, distribution, and efficient consumption. In the past decade, the technology is also dramatically more utilized in the automotive sector toward electrification of vehicles.

This book is an excellent contribution to the power electronics technology as it explains different ways to generate sustainable electricity, also how to obtain efficient electrical power consumption and how to do system engineering and

control of the future grid configures into a microgrid structure. It also covers the emerging areas such as smart grid and electric vehicles.

Good luck with the reading of this comprehensive book and hope this book will lead to the innovations to create a sustainable world.

Frede Blaabjerg  
IEEE Fellow  
Aalborg University  
Denmark

# Preface

Although the cost of electricity has significantly decreased since the 1930s, it is still not readily available to the disadvantaged in countries and regions of poverty. One of the single most ways to reduce poverty is to find ways to reduce the cost of energy. Renewable resources can play a significant role to reduce these costs. Electricity across our world is primarily produced from fossil fueled resources. There is significant debate about the energy sources on today's fossil-fueled power plants and the affects they may be having on climate. A primary product of combustion of fossil generation is carbon dioxide, CO<sub>2</sub>. Many of today's computer simulations suggest that as the atmospheric concentration of CO<sub>2</sub> increase, the earth's average temperature will continue to increase. The earth is made up of countless ecosystems. Laboratory and field studies show that most ecosystems will collapse when subjected to fast temperature changes.

In order to reduce the production of CO<sub>2</sub> globally, we must focus on getting the amount of CO<sub>2</sub> produced per unit of energy as close to zero as possible. As researchers, scientists, and engineers, we must focus on using our energy more efficiently and finding alternative energy sources that are competitive with fossil fuel energy sources. In the near term, we must find ways to mitigate CO<sub>2</sub> production from our existing fossil fuel plants using technologies such as carbon capture and carbon storage. Wind, solar photovoltaic (PV), and solar thermal are becoming cost competitive but can be intermittent in nature and must be coupled through the use of power electronics to existing energy systems. As the penetration of renewable resources increase, we must effectively use renewable energy when it is produced through advanced load control strategies. Low cost, energy storage technologies will continue to develop and can be used to abate renewable energy variability. Power electronics and their respective control systems is the enabling technology that will define our future energy.

This book is an excellent reference that provides insights into the world of power electronics for renewable resources. I recommend that this book be used as a resource text together with instructor-developed exercises and laboratories at both the undergraduate and graduate level. The book provides background

material for students and seasoned engineers to gain broader understanding of the application of power electronics and control systems for renewable energy applications.

William E. Kramer



# Contents

<b>1</b>	<b>Introduction</b> . . . . .	<b>1</b>
	Marcelo G. Simões and Sudipta Chakraborty	
<b>2</b>	<b>Fundamentals of Power Electronics</b> . . . . .	<b>7</b>
	Edison R. C. da Silva and Malik E. Elbuluk	
<b>3</b>	<b>Photovoltaic Power Electronics</b> . . . . .	<b>61</b>
	Felix A. Farret	
<b>4</b>	<b>Wind Power Generation</b> . . . . .	<b>111</b>
	Mohit Singh, Eduard Muljadi, Vahan Gevorgian and Surya Santoso	
<b>5</b>	<b>Small Hydroelectric Systems</b> . . . . .	<b>151</b>
	Felix A. Farret, Marcelo G. Simões and Ademar Michels	
<b>6</b>	<b>Fuel Cell System</b> . . . . .	<b>185</b>
	Fei Gao, Mohammad Kabalo, Marek S. Rylko, Benjamin Blunier and Abdellatif Miraoui	
<b>7</b>	<b>Variable-Speed Power Generation</b> . . . . .	<b>235</b>
	Wlodzimierz Koczara and Grzegorz Iwanski	
<b>8</b>	<b>Microturbines</b> . . . . .	<b>295</b>
	Stephen Gillette and Mark Gilbreth	
<b>9</b>	<b>Battery Energy Storage System</b> . . . . .	<b>333</b>
	Stan Atcitty, Jason Neely, David Ingersoll, Abbas Akhil and Karen Waldrip	
<b>10</b>	<b>Fast Response Energy Storage Systems</b> . . . . .	<b>367</b>
	Juan M. Carrasco, Eduardo Galván, Sergio Vázquez, Luis García-Tabarés and Marcos Lafoz	

<b>11</b>	<b>Modular Power Electronics</b> . . . . .	429
	Sudipta Chakraborty	
<b>12</b>	<b>Resource Aggregation Using Microgrids</b> . . . . .	469
	Giri Venkataramanan and Sandeep Bala	
<b>13</b>	<b>Power Electronics for Smart Distribution Grids</b> . . . . .	493
	Danilo I. Brandão, Renata Carnieletto, Phuong H. Nguyen, Paulo F. Ribeiro, Marcelo G. Simões and Siddharth Suryanarayanan	
<b>14</b>	<b>Advanced Electric Vehicles</b> . . . . .	525
	Giampaolo Carli, Arash Shafiei and Sheldon S. Williamson	
<b>15</b>	<b>Multi-Agent Technology for Power System Control</b> . . . . .	567
	Robin Roche, Fabrice Lauri, Benjamin Blunier, Abdellatif Miraoui and Abderrafîa Koukam	

# Chapter 1

## Introduction

Marcelo G. Simões and Sudipta Chakraborty

**Abstract** In this chapter, a brief discussion on renewable energy and distributed power generation is presented followed by a discussion on characteristics of power electronics and requirement of power electronics for these energy sources. Brief summary for each of the following chapters are provided to introduce the readers to rest of this book.

### 1.1 Introduction

Modern societies require significant energy resources that define the way we live. The food we eat, clothes we wear, buildings we live, appliances we use, and cars we drive require different forms of energy in their production or operation. A common metric that describes economic production performance is the ratio of energy consumption per capita income divided by the energy consumed. Today, there is a 200-fold disparity in income per capita between Great Britain and Ethiopia but the ratio of income to energy consumption between these countries is only 0.30–0.32. The fact that the two ratios are nearly identical, suggests that

---

Views expressed in this chapter are personal with no implied endorsement of the same by NREL/DOE.

---

M. G. Simões (✉)  
Colorado School of Mines, 1610 Illinois Street, Golden, CO 80401, USA  
e-mail: msimoes@mines.edu

S. Chakraborty  
National Renewable Energy Laboratory, 15013 Denver West Pkwy,  
Golden, CO 80401, USA  
e-mail: sudipta.chakraborty@nrel.gov

increased standards of living will require increased energy in order to maintain such a ratio. Over the past 200 years, developed countries consumed more energy per capita than all the other previous societies throughout the history. Since fossil-fuel resources are limited, a drive toward more energy sustainability leads to renewable energy-based power generation. The costs of renewable resources such as solar, and wind have decreased in recent years due to technology and material production advances. Different forms of renewable energy are available in every country across the globe. For the developed world, a new paradigm of distributed power generation that is less dependent on fossil-fuel resources must be developed, in order to maintain the standard of living and sustainable growth. Developing countries growth and prosperity should increase as they begin to access to electric power through locally occurring natural energy sources providing them a new way of life through energy solutions that are sustainable.

The technology of power electronics is fundamental for renewable energy systems. Many renewable resources are intermittent and, without power electronics, we could not regulate voltage, frequency, and power output characteristics. Depending on the available renewable sources, DC–AC inverters, AC–DC rectifiers, and DC–DC converters are required. A rectifier might be a frontend for an electric grid connected to a load or an inverter can be the interface with local generation. There are other converters for intermediate stages, necessary for adapting the energy produced by the source in such a way that both the energy source and the power conversion operate at their highest efficiencies. Rotating machines are typically used to produce power from sources such as hydro and wind; and storage systems can be used to compensate for intermittency. Resources such as sunlight, hydrogen, and sometimes natural gas require DC–DC conversion, followed by the DC–AC inverter to integrate to the AC grid. In the past 20 years, new energy storage technologies such as ultracapacitors and electrochemical storage have been developed. The output of these devices tends to be DC. A Power electronic converter is needed to convert the power from DC to AC during discharge and AC back to DC during energy storage charging. Energy storage systems can be used to help regulate intermittent renewable energy systems by providing power when the output power is low or by absorbing power when excess power is available.

Power converters for renewable energy integration present a higher complexity when compared with those used in industrial or stand-alone systems because they have to efficiently manage power flow and stay synchronized with the grid. Power electronics for renewable and alternative energy systems require the following attributes:

- High efficiency: A negligible part of the power should be lost during conversion. This requirement is affected by input and output energy fluctuations and by conversion efficiency, changing with the quantity of energy at input/output terminals. The converter has to operate in continuous tracking of the input/output quantities and a subsequent real-time adjustment of the converter operation ensuring the highest energy transfer. This requires two or more power conversion stages (typically AC–DC and/or DC–DC and/or DC–AC).

- **Optimal energy transfer:** All renewable sources are energy constrained and as such, they need control algorithms to achieve a maximum power point operation. For example, PV arrays must be interconnected with maximum power point tracking (MPPT) in order to optimize their energy transfer.
- **Bidirectional power flow:** In some cases, the power converter has to be able to supply either the local load and/or the grid.
- **High reliability:** The continuity of service is a major issue when delivering energy.
- **Synchronization capabilities:** All power sources connected with the grid have to be fully synchronized and operate in a safe manner thus ensuring high efficiency and reliability, plus conforming to electrical requirements such as the IEEE 1547 interconnection standard for utility grid applications.
- **Electromagnetic interference (EMI) filtering:** The quality of the energy injected on the grid must respect electromagnetic compatibility (EMC) standards.
- **Smart metering:** The converter between the local source/load and the grid must be capable of tracking the energy consumed by load or injected on the grid. Real-time information can be passed to an automatic billing system capable of taking into account parameters as the buy/sell energy in real time at the best economic conditions and informing the owner of the installation of all required pricing parameter decisions.
- **Communication:** Intelligent functioning of power electronics depends on their capability to support communications at the same time that power flows in the systems. Such functions are fundamental for overall system optimization and for implementing sophisticated dispatching strategies.
- **Fault tolerance:** A key issue for a modern grid is the built-in ability of avoiding propagation of failures among the nodes and to recover from local failures. This capability should be managed by the power converter, which should incorporate monitoring, communication systems, and reconfiguration systems.
- **Additional functions capable of making the interface user-friendly and accessible anywhere through Internet-based communications.**

Different aspects of these attributes are covered in the 14 chapters written by well-known educators, engineers, and scientists who have developed products and prototypes in their respective areas of expertise and with a focus on renewable and distributed energy applications. The book provides background knowledge for the reader to understand how to enable efficient interconnection and economical operation of dispersed installations to the utility grid. Achieving one of the tenets of the smart grid initiative—enabling active participation of consumers in the demand response using timely information and control options.

**Chapter 2** gives a description and overview of power electronic technologies including a description of the fundamental systems that are the building blocks of power electronic systems. Technologies that are described include: power semiconductor switching devices, converter circuits that process energy from one DC level to another DC level, converters that produce variable frequency from DC sources, principles of rectifying AC input voltage in uncontrolled DC output

voltage and their extension to controlled rectifiers, converters that convert to AC from DC (inverters) or from AC with fixed, or variable output frequency (AC controllers, DC–DC–AC converters, matrix converters, or cycloconverters). The chapter also covers pulse width modulation control techniques in detail.

**Chapter 3** discusses photovoltaic systems and describes how semiconductor devices can directly convert solar energy into direct current. PV cell technology is explained and a description of how, incident light spectrum, panel tilt, cell temperature, panel design, surface deposits, shadows, and materials on the solar cell can influence performance. In order to have modules or arrays for higher voltage or current, the cells must be associated, and control algorithms must be implemented in order to make the system operate with high efficiency. Descriptions of power electronics, digital controls, sun tracking, and remote monitoring are provided as the basis for the modern PV energy systems.

**Chapter 4** presents wind energy systems, with coverage on the basic energy conversion from wind, wind turbines, and their aerodynamic and control issues. The chapter continues with a discussion on how wind energy systems can be isolated or grid-connected and the difference between onshore and offshore applications. Specific power electronics for wind turbine applications include: partially rated power electronics, full scale power electronics, FACTS, and advanced topologies. The chapter concludes in how wind turbines can be controlled and integrated.

**Chapter 5** gives examples and applications of small hydropower systems. A small hydropower can be used as stand-alone cost-effective solution to provide remote power or enhance grid connected power systems. This chapter provides a discussion of basic principles of hydropower resources, how to find the best places to site hydropower in rivers. Power turbine system technologies that can be used for small-hydro applications are also discussed. Systems such as fixed-speed with induction generator, variable-speed with a cage-bar induction generator or synchronous generator, variable-speed with a multiple-pole synchronous generator or multiple-pole permanent magnet synchronous generator; and variable-speed with a doubly-fed induction generator are described.

**Chapter 6** introduces fuel cell systems and their associated power electronic converter topologies. The introduction includes a description of different fuel cell technologies and the physics behind the characteristic polarization curve and dynamic behavior. Two models for control applications are discussed, one for a proton exchange membrane fuel cell (PEMFC) and another for the solid oxide fuel cell (SOFC) with detailed equations. The chapter presents specific power converter topologies used for fuel cell systems highlighting their advantages and drawbacks.

**Chapter 7** explains how variable (adjustable) speed generation systems provide reduction of fuel consumption and improve electrical power generation systems. Two basic topologies are presented; one is based on the application of permanent magnet generator and another one on slip-ring induction machines. A description of how power is controlled from engine driven generators is described. A variable-speed power generation with the slip-ring induction machine system is introduced that utilizes a control method based on space vector theory. In the chapter,

discussions were provided showing how the reference stator voltage vector, rotor current amplitude, frequency, and phase are controlled to provide a stable sinusoidal three-phase stator voltage.

**Chapter 8** provides the basics of micro turbines operation and integration techniques. Microturbines are a relatively new technology for generation of electric power, and are commercially available in ratings from 30 kW up to 1 MW or more. This chapter describes how microturbines perform, and how they differ from other more traditional forms of electric power generation. Emphasis is placed on the power electronics and control features of typical microturbines.

**Chapter 9** provides a discussion on the various technical components that are used for battery energy storage systems for utility-scale energy storage and how these technical components are interrelated. A basic description of how battery energy storage systems work is provided with several examples to illustrate how battery energy storage can be used in large-scale applications. An overview of how the storage system's power electronics work is given in the chapter followed by a more detailed description of possible power electronic topologies and power electronic controls that are used to ensure that the system can be properly integrated with the generation source and, if necessary, the load. Battery management and monitoring through the power electronic controls are discussed and a detailed example of battery energy storage system integration is provided.

**Chapter 10** introduces the concept of fast response energy storage systems that have the ability to provide or to absorb a high amount of electrical energy in a short period of time without diminishing the lifetime of the storage device. Major technologies discussed in this chapter are: electric double layer capacitors (EDLC) that store energy in the electrical field of a capacitor; Flywheels that utilize kinetic energy, and superconducting magnets (SME) where energy is kept in the magnetic field of a lossless inductor. Fast storage technologies show promise to allow increasing penetration of renewable energy sources and support Smart Grid. In this chapter, the power converters that are used to manage power delivered and stored for these fast response energy storage systems are provided along with descriptions of how to integrate these technologies for renewable energy system applications.

**Chapter 11** covers application of modular power electronics for renewable and distributed energy applications. The chapter starts with basics of modular power electronics such as power electronics building block (PEBB) and integrated power electronics module (IPEM). A description of common power electronics topologies for different renewable and distributed energy applications are given showing that generalized power electronic topologies can be formalized to design building block modular power electronics interfaces. The chapter concludes by giving examples suggesting that such modular power electronics can eventually improve the overall life-cycle cost and reliability for renewable and distributed energy systems.

**Chapter 12** provides a fundamental description of microgrids. The current and future capability of microgrids for aggregating multiple resources is described. Concepts such as plug-and-play technologies need to be developed to accommodate the addition or removal of different sources and loads without a need to

develop complex interconnection, load flow, and dispatch studies. Dynamic microgrid interactions between different aggregated resources and their power electronic controllers are discussed.

**Chapter 13** focuses on the role that power electronics will have in future smart-grids. The operation of future electricity grids will be multi-disciplinary in nature with merging of energy and communication infrastructures, and interaction of state-of-the-art technologies such as power electronics, computational intelligence, signal processing, or smart metering. The chapter provides good background information of emerging distribution systems, evolutionary changes, and enabling the technologies that will be needed. Power electronic-based interface systems with smart topologies and controls are explained. Three examples of smart interface control systems are described including smart inverters, smart power router, and the concept of the virtual synchronous generator.

**Chapter 14** explains practical issues for commercialization of current and future plug-in hybrid electric vehicles and focuses primarily on power electronics-based solutions for both current as well as future electric vehicle technologies. New plug-in hybrid vehicle power system architectures are discussed in detail together with key battery technologies that are used for transportation applications. Advanced power electronics battery management techniques and charging infrastructures for electric vehicles and plug-in hybrid electric vehicles are also described in this chapter.

**Chapter 15** introduces a new distributed control paradigm for power system control, called multi-agent systems (MAS). The development of advanced communication infrastructures can provide power electronics interfaces with the ability to control complex power systems in efficient and scalable ways and in real-time. Multi-agent systems (MAS) are based on distributing information and computing algorithms for complex networks, and are an excellent technological solution for power electronics applications. This chapter focuses on applications of MAS in power systems and provides applications how MAS can be used with other artificial intelligence techniques in order to make the grid smarter and more flexible.



# Chapter 2

## Fundamentals of Power Electronics

Edison R. C. da Silva and Malik E. Elbuluk

**Abstract** This chapter gives a description and overview of power electronic technologies including a description of the fundamental systems that are the building blocks of power electronic systems. Technologies that are described include: power semiconductor switching devices, converter circuits that process energy from one DC level to another DC level, converters that produce variable frequency from DC sources, principles of rectifying AC input voltage in uncontrolled DC output voltage and their extension to controlled rectifiers, converters that convert to AC from DC (inverters) or from AC with fixed or variable output frequency (AC controllers, DC–DC–AC converters, matrix converters, or cyclo-converters). The chapter also covers control of power converters with focus on pulse width modulation (PWM) control techniques.

### 2.1 Definition, History, Applications and Trends of Power Electronics

Power electronics (PE) experienced tremendous growth after the introduction of the first solid-state power switch, the silicon controlled rectifier (SCR) in 1957. Today, almost all of the technologies that require control of power control utilize PE technology. This chapter will give the reader an overview on the field of PE including:

---

E. R. C. da Silva (✉)  
Departamento de Engenharia Eletrica, Universidade Federal de Campina Grande,  
Campina Grande, Brazil  
Rua Rodrigues Alves, 1090—Bela vista, Campina Grande, PB CEP 58428-795, Brazil  
e-mail: ercdasilva@gmail.com

M. E. Elbuluk  
The University of Akron, Akron, OH 44325, USA  
e-mail: melbuluk@uakron.edu

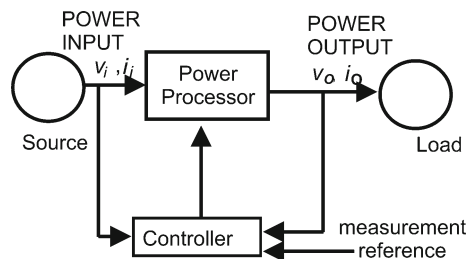
- A description of the fundamentals of the power semiconductor switching devices.
- Converter circuits that process energy from one DC level to another DC level.
- Converters that produce variable frequency from DC sources.
- Principles of rectifying AC input voltage in uncontrolled DC output voltage and their extension to controlled rectifiers.
- Converters that convert to AC from DC (inverters) or from AC with fixed or variable output frequency.
- AC controllers.
- DC–DC–AC converters.
- Matrix converters or cycloconverters.
- Detailed description of pulse width modulations control techniques.

Power electronic circuits are used to control the power conversion from one or more AC or DC sources to one or more AC or DC loads, and sometimes with bidirectional capabilities. In most power electronics systems, this conversion is accomplished with two functional modules called the control stage and the power stage. Figure 2.1 shows the topology for a single source and single load converter application that includes a power processor (the power stage) and a controller (the control stage). The converter, handles the power transfer from the input to output, or vice versa, and is constituted of power semiconductor devices acting as switches, plus passive devices (inductor and capacitor). The controller is responsible for operating the switches according to specific algorithms monitoring physical quantities (usually voltages and currents) measured at the system input and/or output.

The modern PE era began in 1957. It was during that year the first commercial thyristor, or Silicon Controlled Rectifier (SCR), was introduced by General Electric Company. The SCR, started replacing the mercury arc rectifiers, invented in 1902, and the later developed thyatron (invented in 1923) and ignitron (invented in 1931), allowed the commercialization of several industrial circuits conceived during the 1920s and 1940s (like the cycloconverter, the chopper, and the parallel inverter) as well as the Graetz bridge conceived in 1897.

The SCR was the only available power device for more than 25 years after its invention (and still is very useful for extremely high power applications). Since it is very difficult to impose turn-off conditions for SCR's, faster devices, with higher voltage and current capabilities, with better controllability were developed,

**Fig. 2.1** A general power electronic system

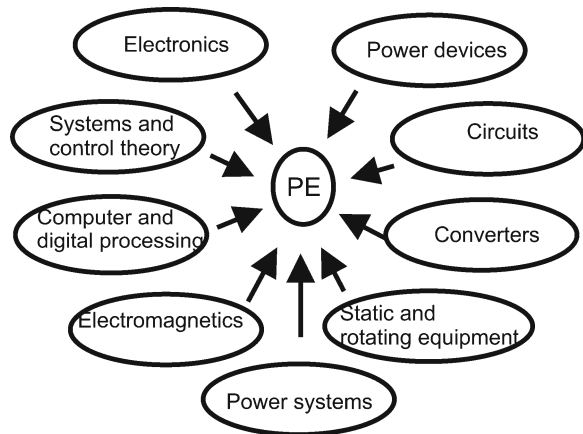


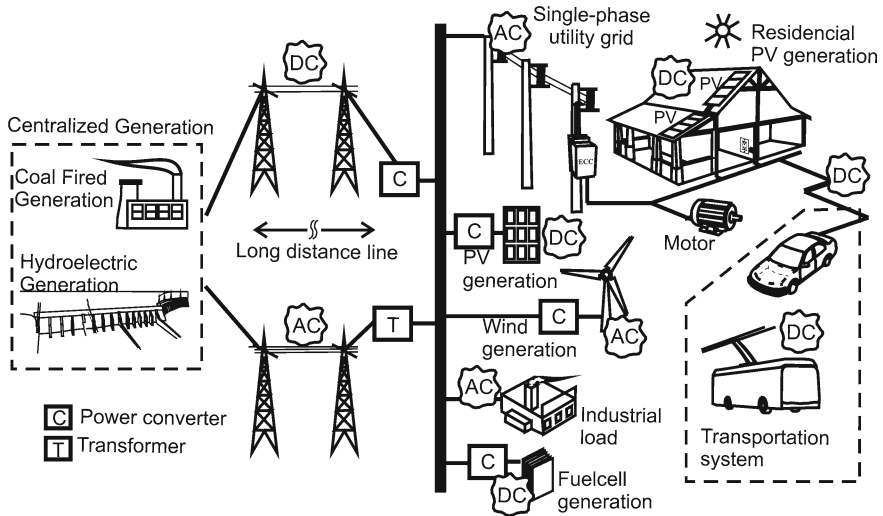
including the bipolar junction transistor (BJT) invented in 1970. The BJT was used in applications from low to medium power and frequency and now is considered obsolete. The metal oxide semiconductor field effect transistor (MOSFET) was invented in 1978 and is used for power electronic switching applications of low power and high frequencies. The gate turn-off thyristor (GTO), is used in applications from medium to high power and from low to medium frequencies. The insulated gate bipolar transistor (IGBT) developed in 1983 is used in applications from low to medium power and frequency. The integrated gate commutated thyristor (IGCT) invented in 1997 is used in applications from medium to high power and from low to medium frequencies.

Through the use of this switching technology power electronics systems can operate in the range from few watts up to GW, with frequency range from some 100 Hz up to some 100 kHz, depending on the power handled [1]. The advent of microelectronics and computer control made it possible to apply modern control theory to PE and at same the time made possible very complex circuit functions. Therefore, the area of PE, became interdisciplinary, as indicated in Fig. 2.2. At the high power level, PE deals with static and rotating equipment for generation, transmission, and distribution handling large amount of power. For consumer electronic applications power converters and circuits are important for information processing, employing analog and digital circuits, or microprocessors including microcontrollers, digital signal processors (DSP), and field programmable gate arrays (FPGA). In the area of control, PE deals with stability and response characteristics in systems with feedback loops, based on classical or modern control. With the development of very large system integration (VLSI), ultra large system integration (ULSI), and other sophisticated computer-assisted designs; advanced control systems could be used to develop new power electronic topologies.

The development of devices and equipment able to individually or in combination convert efficiently electric energy from AC to DC, DC to DC, DC to AC, and AC to AC together with the changes that occurred in electrical power engineering has resulted in wide spread of PE in a large spectrum of applications.

Fig. 2.2 Power electronics and related topics





**Fig. 2.3** Power electronics and electrical energy generation transmission, storage, and distribution

Figure 2.3 shows how electrical energy generation is distributed for the end-user, showing transmission, distribution, storage, renewable energy sources and users. In fact, nowadays PE is a key technology for all those sub-systems, and has spread in many applications, examples including:

- Residential: heaters, home appliances, electronic lighting, equipment sources;
- Commercial: heaters, fans, elevators Uninterruptible Power Supply (UPS), AC and DC breakers, battery chargers;
- Industrial: pumps, blowers, robots, inductive heaters, welding, machine drive, portable sources;
- Transportation: electrical and hybrid vehicles, battery chargers, railroad electric system;
- Utility systems: high voltage direct current, generators, reactive compensators, interface for photovoltaic, wind, fuel cells systems, Flexible AC Transmission System (FACTS) equipment;
- Aerospace: sources for spacecrafts, satellites, planes;
- Communication: sources, RF amplifiers, audio-amplifiers.

Power electronics will continue to be an enabling technology to address our future electricity needs. It is expected that new power devices for higher power, higher frequency, and lower losses will continue to be invented. Global energy concerns will provoke a large interest in the increase of the conversion efficiency and more application of PE in power quality, distributed generation, energy conservation, and smart grids. The integration of power and control circuitry into functional modules will result in systems solutions that are highly integrated into packaged products that will be both more reliable and affordable.

## 2.2 Power Semiconductor Devices

Electronic switches capable of handling high voltage and current operations at high frequency (HF) are the most important devices needed in the design of energy conversion systems that use PE. For the purposes of this discussion we will define the concept of an ideal switch. An ideal power electronic switch can be represented as a three terminals device as shown in Fig. 2.4. The input, the output, and a control terminal that imposes ON/OFF conditions on the switch. A switch is considered “ideal” when it is open, it has zero-current through it and can handle infinite voltage. When the switch is closed it has zero-voltage across it and can carry infinite current. Also, an ideal switch changes condition instantly, which means that it takes zero-time to switch from ON-to-OFF or OFF-to-ON. Additional characteristics of an ideal switch include that it exhibits zero-power dissipation, carries bidirectional current, and can support bidirectional voltage. If we plot the switch current ( $i$ ) with respect to its voltage ( $v$ ) we define four quadrants that are often referred to as the  $v$ - $i$  plane and are shown in Fig. 2.5. By definition, an ideal switch can operate in all four quadrants.

Practical or real switches do have their limitations in all of the characteristics explained in an ideal switch. For example, when a switch is on, it has some voltage across it, known as the on-voltage and it carries a finite current. During the off stage, it may carry a small current known as the leakage current while supporting a finite voltage. The switching from ON-to-OFF and vice versa does not happen instantaneously. Of course, all actual switching devices take times to switch and we define these characteristics as the delay, rise, storage, and fall times. As a consequence of the above two non-ideal cases, there is voltage and current across the switch at all times, which will result in two types of losses. The first loss occurs during the on and off-states and is defined as the “conduction loss”. The second loss is defined as the “switching loss” which occurs just as the switch changes state as either opening or closing. The switch losses result in raising the overall

Fig. 2.4 Ideal switch

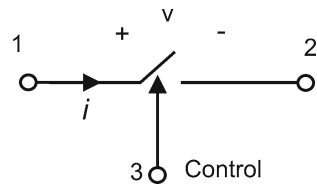
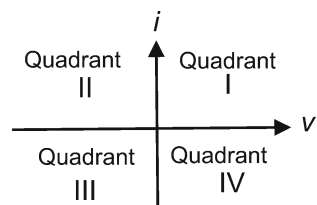


Fig. 2.5 4-quadrant switch  $v$ - $i$  characteristics



switch temperature. Further, the ON/OFF-state of the power switch must be controlled through an external signal.

### 2.2.1 Classifications of Power Switches

The concept of the ideal switch is important when evaluating circuit topologies. Assumptions of zero-voltage drop, zero-leakage current, and instantaneous transitions make it easier to simulate and model the behavior of various electrical designs. Using the characteristics of an ideal switch, there are three classes of power switches:

1. *Uncontrolled switch*: The switch has no control terminal. The state of the switch is determined by the external voltage or current conditions of the circuit in which the switch is connected. A diode is an example of such switch.
2. *Semi-controlled switch*: In this case the circuit designer has limited control over the switch. For example, the switch can be turned-on from the control terminal. However, once ON, it cannot be turned-off from the control signal. The switch can be switched off by the operation of the circuit or by an auxiliary circuit that is added to force the switch to turn-off. A thyristor or a SCR is an example of this switch type.
3. *Fully controlled switch*: The switch can be turned-on and off via the control terminal. Examples of this switch are the BJT, the MOSFET, the IGBT, the GTO thyristor, and the MOS-controlled thyristor (MCT).

#### 2.2.1.1 Uncontrolled Switches

A diode, also known as rectifier, is an *uncontrolled switch*. It is a two terminal device with a symbol depicted in Fig. 2.6a. The terminals are known as Anode ( $A$ ) and cathode ( $K$ ). In the ideal case, the diode current ( $i_d$ ) is unidirectional and current can only flow from the anode to the cathode. The diode voltage ( $v_d$ ) is measured as being positive from the anode to the cathode.

The  $v$ - $i$  characteristics for a real (non-ideal) diode are shown in Fig. 2.6b. In quadrant I, the diode is in the ON-state, and is known as the forward-biased region. When it is ON the diode carries a positive current while supporting a small voltage. The diode current varies exponentially with the diode voltage. The diode is reversed-biased in quadrant III, which is the OFF-state. When it is OFF, the diode supports a negative voltage and carries a negligible current (leakage current). When the negative voltage exceeds a certain limit, known as the breakdown voltage, the leakage current increases rapidly while the voltage remains at the breaking value, which potentially damages the device. Therefore, operation that exceeds the breakdown voltage must be avoided.

The ideal diode characteristics are shown in Fig. 2.6c. During the ON-state, the diode has zero-voltage across it and carries a positive current. During the OFF-state, the diode carries zero-current and supports a negative voltage.

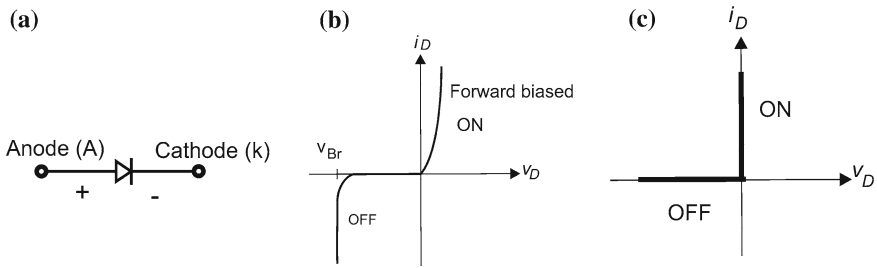


Fig. 2.6 Diode: a symbol, b  $i$ - $v$  characteristics, and c idealized characteristics

2.2.1.2 Semi-controlled Switches

The thyristor or SCR is a power semiconductor switch whose turn-on can be activated from the control terminal Gate but once it turns ON, the control terminal becomes ineffective and the thyristor behaves similar to a diode. Therefore, the thyristor is considered a *semi-controlled switch*. The name, controlled rectifier, is an indication that a thyristor is a device that can be considered as a diode whose turn-on can be commanded externally. Figure 2.7a shows the circuit symbol for a thyristor. Although there are similarities between the diode and the thyristor circuit symbols, their operation is very different. The thyristor current,  $I_A$ , flows from the anode (A) to the cathode (K) and the voltage  $V_{AK}$ , across the thyristor is positive when the anode is at higher voltage than the cathode. Figure 2.7b shows the  $v$ - $i$  characteristics of a real or non-ideal thyristor. In quadrant I, in the absence of a gate current, the device is OFF in the forward blocking region and supports a positive voltage. If a gate current is applied, the device switches to the on-state region and the device has a  $v$ - $i$  characteristic similar to that of a diode. In quadrant III, the device is OFF and the region is known as the reverse blocking region. Again the characteristics are similar to those of a diode. Comparing the switching characteristics of a diode and a thyristor, it appears that when the thyristor is OFF, it can block large positive or negative voltage, which is a fundamental feature that is important in circuit applications, such as AC/AC converters. This can be clearly seen in the ideal characteristics of the thyristor as shown in Fig. 2.7c. In the ON-state, the thyristor has zero-voltage across it and carries a positive current. In the

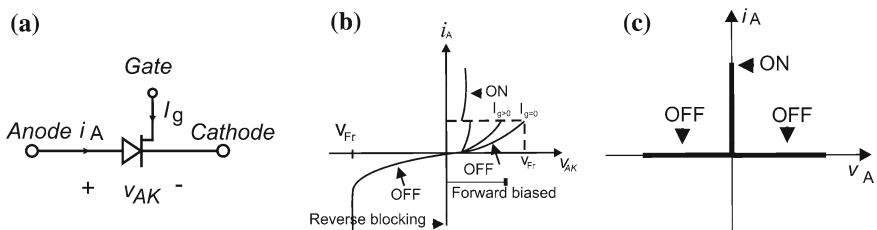
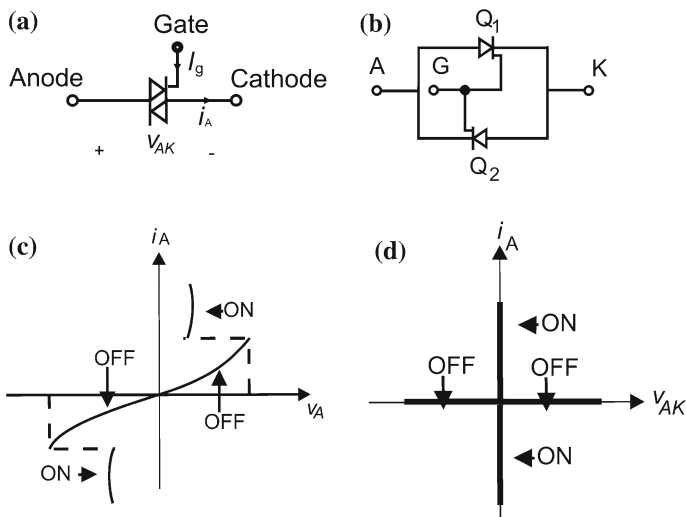


Fig. 2.7 Thyristor: a symbol, b  $i$ - $v$  characteristics, and c idealized characteristics



**Fig. 2.8** The triac: **a** symbol, **b** two-thyristor-representation, **c**  $i$ - $v$  characteristics, and **d** idealized characteristics

OFF-state, the thyristor can support a positive voltage in the forward blocking region or a negative voltage, similar to a diode, in the reverse blocking region. Therefore, the thyristor can be considered to carry an unidirectional current and supports a bidirectional voltage.

The triac, shown in Fig. 2.8a, is also a semi-controlled switch. A triac can be modeled as two thyristors connected back-to-back as shown in Fig. 2.8b. Triacs are considered as bidirectional voltage and bidirectional current devices, as shown by the  $v$ - $i$  characteristics in Fig. 2.8c. The ideal characteristics are in Fig. 2.8d. As a low-cost bidirectional switch, the triac is the primary switch that is used for low power electronic commercial circuits such as light dimmers and control circuits for single-phase motors used in home appliances.

### 2.2.1.3 Fully Controlled Switches

In a *fully controlled switch* the ON- and OFF-states can be activated externally through a control terminal. A number of power switches fall into the category of controlled switches; some of them are transistor-based devices and others are thyristor-based devices. A brief description of each device is given in the following sections:

#### A. The Bipolar Junction Transistor

Figure 2.9a shows the circuit symbol for an npn-type BJT. The base ( $B$ ) is the control terminal, where the power terminals are the collector ( $C$ ) and the emitter ( $E$ ). The  $v$ - $i$  characteristics of the device are shown in Fig. 2.9b. The device



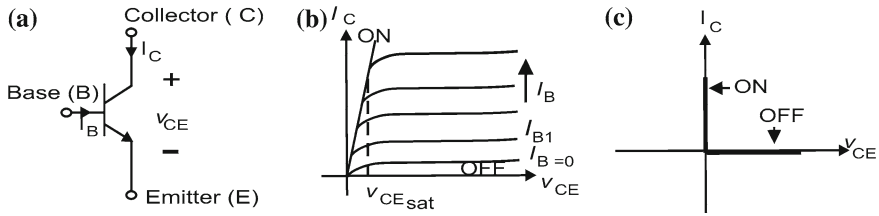


Fig. 2.9 The BJT: **a** symbol, **b**  $i$ - $v$  characteristics, and **c** idealized characteristics

operates in quadrant I and is characterized by the plot of the collector current ( $I_C$ ) versus the collector to emitter voltage ( $v_{CE}$ ). The device has three regions two of them where the device operates as a switch and the third is where the device operates as a linear amplifier. The device is OFF in the region below  $i_B = 0$  and is ON in the region where  $v_{CE}$  is less than  $v_{CE(sat)}$ . Neglecting the middle region, the idealized device characteristics as a switch are shown in Fig. 2.9c. During the ON-state the device carries a collector current  $I_C > 0$  with  $v_{CE} = 0$ . In the OFF-state, the device supports positive  $v_{CE} > 0$  with  $I_C = 0$ . Therefore, the BJT is unidirectional current and voltage device. The BJT has historical importance, but today most of its function are covered by devices like the IGBT.

**B. The Metal Oxide Semiconductor Field Effect Transistor**

Figure 2.10a shows the circuit symbol for an n-channel, enhancement mode MOSFET. Similar to the BJT, it has a control terminal known as the gate ( $G$ ) and the power terminals are the drain ( $D$ ) and source ( $S$ ). The device is controlled by supplying a voltage ( $v_{GS}$ ) between the gate and the source. This makes it a voltage-controlled device compared to the BJT, which is a current-controlled device. The real  $v$ - $i$  characteristics of device are shown in Fig. 2.10b. Similar to the BJT, the MOSFET operates within three operating regions. Two of the regions are used when the device is operated as a switch, and the third is when the device is used as an amplifier. To maintain the MOSFET in the off-state,  $v_{GS}$  must be less than a threshold voltage known as  $v_T$ , which is the region below the line marked OFF. And when the device is ON it act as resistance determined by the slope of the line marked ON. The idealized characteristics of a MOSFET switch are shown in Fig. 2.10c. When the device is ON, it has zero  $v_{DS}$  and carries a current  $I_D > 0$  and when the device is OFF it supports a positive  $v_{DS}$  and has zero drain current ( $I_D = 0$ ).

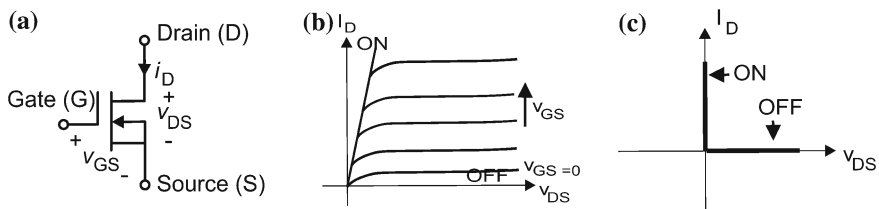
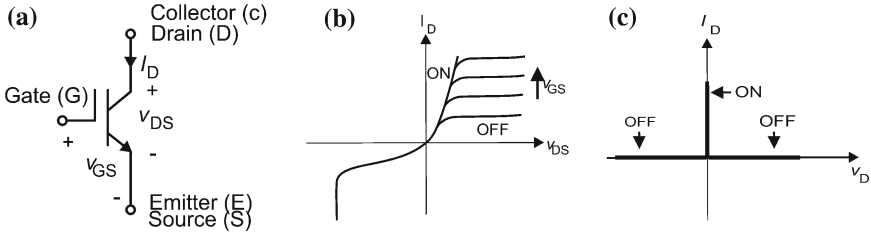


Fig. 2.10 The MOSFET: **a** symbol, **b**  $i$ - $v$  characteristics, and **c** idealized characteristics



**Fig. 2.11** The IGBT: **a** symbol, **b**  $i$ - $v$  characteristics, and **c** idealized characteristics

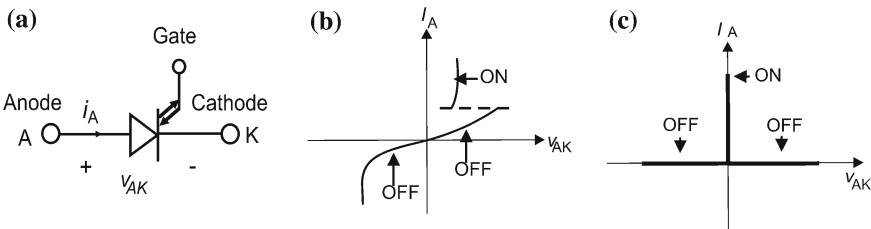
Three other MOSFET configurations include: n-channel depletion mode and p-channel enhancement and depletion modes.

*C. The Insulated Gate Bipolar Transistor (IGBT)*

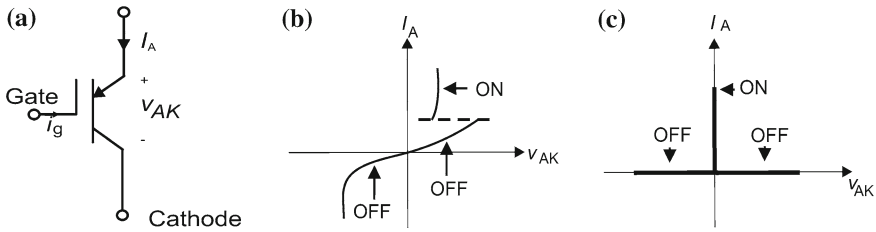
The IGBT is a hybrid or also known as double mechanism device. Its control port resembles a MOSFET and its output or power port resembles a BJT. Therefore, an IGBT combines the fast switching of a MOSFET and the low power conduction loss of a BJT. Figure 2.11a shows a circuit symbol that is used for an IGBT, which is slightly different from the MOSFET with similar terminal labels. The control terminal is labeled as gate (G) and the power terminals are labeled as collector (C) and emitter (E). The  $i$ - $v$  characteristics of a real IGBT are shown in Fig. 2.11b, which shows that the device operates in quadrants I and III. The ideal characteristics of the device are shown in Fig. 2.11c. The device can block bidirectional voltage and conduct unidirectional current. An IGBT can change to the ON-state very fast but is slower than a MOSFET device. Discharging the gate capacitance completes control of the IGBT to the OFF-state. IGBT's are typically used for high power switching applications such as motor controls and for medium power PV and wind PE.

*D. The Gate Turn-Off Thyristor*

The GTO thyristor is a device that operates similar to a normal thyristor except the device physics, design and manufacturing features allow it to be turned-off by a negative gate current which is accomplished through the use of a bipolar transistor. The circuit symbol for a GTO is shown in Fig. 2.12a. The  $v$ - $i$  characteristics and the ideal switch characteristics are shown in Fig. 2.12 b, c. Although the device has been in existence since the late 1960s, and it has been successfully used in high power drives, IGBTs have reached price and rating parity and are expected to replace GTO's in new power electronic designs.



**Fig. 2.12** The GTO: **a** symbol, **b**  $i$ - $v$  characteristics, and **c** idealized characteristics



**Fig. 2.13** The MCT: **a** symbol, **b**  $i-v$  characteristics, and **c** idealized characteristics

### E. The MOS-Controlled Thyristor

Similar to the IGBT, the MCT is a hybrid or double mechanism device that was designed to have a control port of a MOSFET and a power port of a thyristor. The circuit symbol for the device is shown in Fig. 2.13a. The real device characteristics and the idealized characteristics are shown in Fig. 2.13b, c. The characteristics are similar to the GTO, except that the gate drive circuitry for the MCT is less complicated than the design for a GTO as the control circuit of the MCT uses a MOSFET instead of a transistor. As a result, the MCT was supposed to have higher switching frequency. Although the MCT was invented at the same time period of the IGBT it never became fully commercially available and at the time of writing this book it is unknown the future market plans.

## 2.3 Power Electronic Converter Topologies

Power electronic converters are switch-mode circuits that process power between two electrical systems using power semiconductor switches. The electrical systems can be either DC or AC. Therefore, there are four possible types of converters; namely DC/DC, DC/AC, AC/DC, and AC/AC. The four converter types are described below:

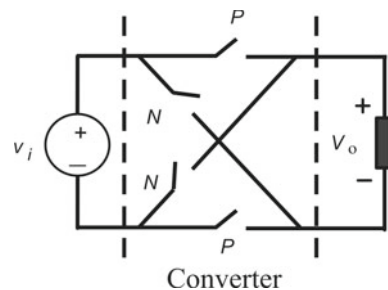
1. *DC/DC Converter*: is also known as “Switching Regulator”. The circuit will change the level voltage available from a DC source such as a battery, solar cell, or a fuel cell to another DC level, either to supply a DC load or to be used as an intermediate voltage for an adjacent power electronic conversion such as a DC/AC converter. DC/DC converters coupled together with AC/DC converters enable the use of high voltage DC (HVDC) transmission which has been adopted in transmission lines throughout the world.
2. *DC/AC Converter*: Also described as “Inverter” is a circuit that converts a DC source into a sinusoidal AC voltage to supply AC loads, control AC motors, or even connect DC devices that are connected to the grid. Similar to a DC/DC converter, the input to an inverter can be a stiff source such as battery, solar cell, or fuel cell or can be from an intermediate DC link that can be supplied from an AC source.

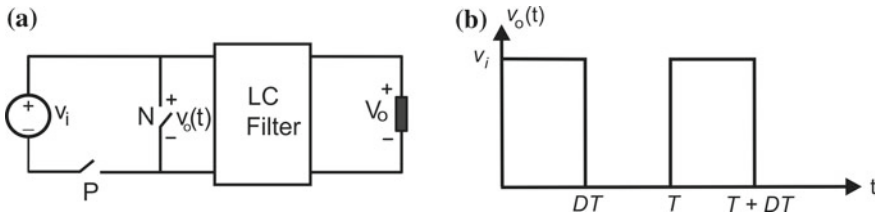
3. *AC/DC Converter*: This type of converter is also known as “Rectifier”. Usually the AC input to the circuit is a sinusoidal voltage source that operates at 120 V, 60 Hz or a 230 V, 50 Hz, which are used for power distribution applications. The AC voltage is rectified into a unidirectional DC voltage, which can be used directly to supply power to a DC resistive load or control a DC motor. In some applications the DC voltage is subjected to further conversion using a DC/DC or DC/AC converter. A rectifier is typically used as a front-end circuit in many power system applications. If not applied correctly, rectifiers can cause harmonics and low power factor when they are connected to the power grid.
4. *AC/AC Converter*: This circuit is more complicated than the previous converters because AC conversion requires change of voltage, frequency, and bipolar voltage blocking capabilities, which usually requires complex device topologies. Converters that have the same fundamental input and output frequencies are called “AC controllers”. The conversion is from a fixed voltage fixed frequency (FVFF) to a variable voltage fixed frequency (VVFF). Applications include: light dimmers and control of single-phase AC motors that are typically used in home appliances. When both voltage and frequency are changed, the circuits are called “Cycloconverters”, which convert a FVFF to variable voltage variable frequency (VVVF) and when fully controlled switches are used, this class of circuit is called “Matrix Converter”. Another way of achieving AC/AC conversion is by using AC/DC and DC/AC through an intermediate DC link. This type of combined converter approach can be complex as the correct control approach must be implemented including simultaneous regulation of the DC link, injection of power with a prescribed power factor and bidirectional control of energy flow.

### 2.3.1 DC/DC Converters

A generalized circuit for a DC/DC converter is depicted in Fig. 2.14 where all possible switches connecting the input to the output are represented. If one P-switch and one N-switch are used, the resulting circuit is shown in Fig. 2.15a. The switches are controlled ON and OFF within a specified period  $T$ . The output

**Fig. 2.14** Generalized circuit for DC/DC converter circuits





**Fig. 2.15** Non-isolated down (buck) DC/DC converter: **a** circuit and **b** waveforms

voltage is equal to the input voltage when the P-switch is ON, and is equal to zero when the N-switch is ON. The ratio of the ON-time of switch P switch to the period  $T$  is defined as the duty ratio or duty-cycle ( $D$ ). The waveform of the output voltage  $v_o(t)$  is shown in Fig. 2.15b. Since  $v_o(t)$  is a pulsating waveform, an LC circuit is used to filter the voltage to a DC. In this case the average  $V_o$  or DC component of the output voltage is given by Eq. (2.1),

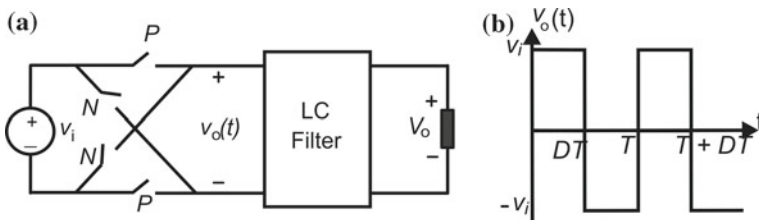
$$V_{avg} = \frac{1}{T} \int_0^{DT} V_i dt = DV_i \tag{2.1}$$

Since  $D < 1$ , the DC output voltage of this converter is always less than the input voltage.

When all the generalized converter switches are used, the resulting circuit is shown in Fig. 2.16. When the P-switches are ON, the output voltage is equal to the input voltage and when the N-switches are ON, the output voltage is equal to the negative of the input voltage. The resulting waveform is shown in Fig. 2.16b. The DC component or the average of the output voltage is given by:

$$V_{avg} = \frac{1}{T} \left[ \int_0^{DT} V_i dt + \int_{DT}^T -V_i dt \right] = (2D - 1)V_i \tag{2.2}$$

Equation (2.2) indicates that the output voltage is less than the input voltage with a changed polarity. For duty-cycle  $D > 0.5$  the output has a positive value and for



**Fig. 2.16** Full-bridge non-isolated down (buck) DC/DC converter: **a** circuit, and **b** waveforms

duty-cycle  $D < 0.5$  the output has a negative value. The LC circuit in the design is used to filter the harmonic components of the output voltage so that the load receives a DC voltage with negligible ripple. Both voltages given by Eqs. (2.1) and (2.2) indicate that output has a lower DC value than the input voltage. Therefore, the converters are referred to as step-down or buck converters.

Two other basic DC/DC converters include the boost and buck/boost converters. A boost converter can be defined as when the DC output voltage is higher than the input voltage. This design is also referred to as a step-up converter and a typical design is shown in Fig. 2.17. In this circuit, the switches are inserted between the inductor and the capacitor. If the converter is lossless, the ratio of the output DC voltage to the input DC voltage is given by Eq. (2.3). Since  $D$  is less than one, the output voltage is always higher than the input voltage.

$$V_{\text{avg}} = \frac{V_i}{D} \tag{2.3}$$

A buck/boost or step-up/down converter is shown in Fig. 2.18. This converter is capable of providing a DC output voltage that can be lower or higher than the input DC voltage. The input/output conversion ratio is given by Eq. (2.4).

$$\frac{V_o}{V_i} = \frac{D}{1 - D} \tag{2.4}$$

When the  $D$ , is less than 0.5 the converter operates as a buck or step-down converter and when  $D > 0.5$  the converter operates as step-up or boost converter.

For all basic DC/DC converters discussed so far the switch is implemented by a controlled switch (transistor) and an uncontrolled switch (diode). When the transistor and the diode are alternately switched, the mode of operation is referred to as

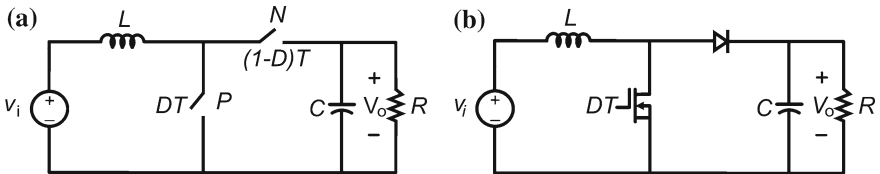


Fig. 2.17 Non-isolated boost (up) DC/DC converter: **a** circuit, and **b** switch implementation

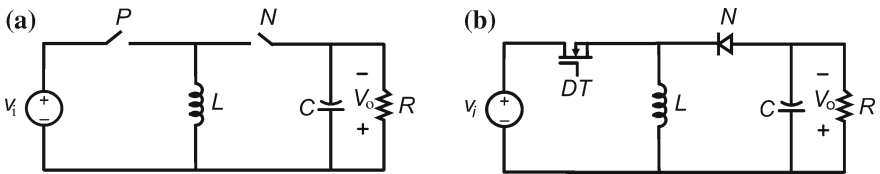


Fig. 2.18 The buck-boost (up/down) non-isolated DC/DC converter: **a** circuit, and **b** switch implementation

continuous conduction mode (CCM). In this mode, the inductor current never reaches zero and the output voltage-to-input voltage conversion ratio becomes only a function of the duty ratio. If the inductor current is zero for a portion of the cycle, the mode of operation is known as the discontinuous conduction mode (DCM). The converter will operate at DCM when circuit parameters such as inductance is decreased or when the switching frequency is decreased or when the load resistance is increased. Therefore, the output-input conversion ratio is a function of the duty ratio and several of those parameters.

The three basic DC/DC converters discussed so far are referred to as non-isolated converter topologies. Another class of converter is called isolated converters whose utilize a transformer that is placed directly between the input and output and usually have more switches and more filter components than non-isolated converters. Isolated DC/DC converters can be designed to provide multiple output DC voltages. There are some non-isolated converters that use higher order filter such as the ‘Cuk converter, the SEPIC converter and the ZETA converter. For complete types and analysis of non-isolated and isolated converters, please refer to Chaps. 6 and 7 in [1], Chaps. 7 and 10 in [2], Chaps. 4 and 5 in [3] and Chaps. 6 and 7 in [4].

### 2.3.2 DC/AC Converters (Inverters)

Inverters are power electronic circuits that transform DC voltage from sources such as batteries, solar cells or fuel cells (or the output of a rectifier) into AC, for powering motor drives, providing stand-alone AC output, or interconnecting to the AC grid. Inverters can be usually classified according to their AC output as single-phase or three-phase and also as half- and full-bridge converters.

#### 2.3.2.1 Single-Phase Inverters

Figure 2.19a represents a generalized DC/AC single-phase inverter. Figure 2.19b shows the resulting AC waveform when the P- and N-switches operate at a  $D = 0.5$ . The graph shows that the AC waveform is a square wave  $D = 0.5$ . Further, the voltage has no DC component which can also be shown by substituting  $D = 0.5$  in Eq. (2.2). A half-bridge converter can be obtained using two DC sources of equal voltages, one P-Switch and one N-switch as shown in Fig. 2.20. The output is a square wave with a period  $T$ , which corresponds to an AC fundamental frequency as:

$$f = \frac{1}{T} \text{ Hz} \quad \text{or} \quad \omega = 2\pi f = \frac{2\pi}{T} \text{ rad/s} \quad (2.5)$$

The amplitude of the  $n^{\text{th}}$  sinusoidal voltage can be evaluated by Fourier series of the square wave  $v_o(t)$  as

$$v_{on} = \frac{2}{T} \int_0^T v_o(t) \sin n\omega_a t dt = \frac{4V_i}{n\pi} \rightarrow n = 1, 3, 5, \dots \text{odd} \quad (2.6)$$

A filter such as a resonant LC-type circuit can be designed to filter most of the harmonics present in the square wave and prevent them from appearing across load.

The fundamental voltage available from the square voltage has a fixed amplitude (as obtained by substituting  $n = 1$  in Eq. (2.6)). Half-bridge converters have

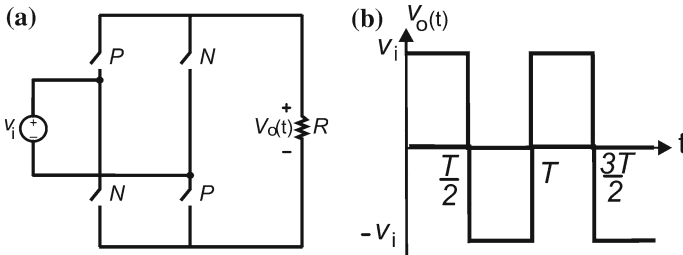


Fig. 2.19 Full bridge (FB) DC/AC converter: **a** circuit, and **b** waveforms

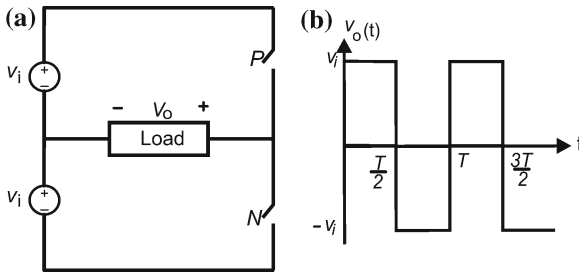


Fig. 2.20 Half-bridge (HB) DC/AC converter (inverter): **a** circuit, and **b** waveforms

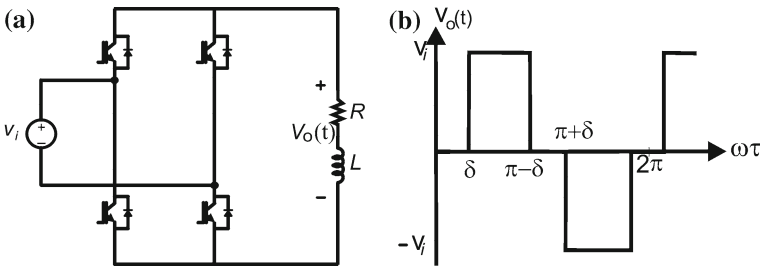


Fig. 2.21 Full-bridge (FB) DC/AC converter with variable AC voltage: **a** circuit, and **b** waveforms



fixed amplitude, but the full-bridge ones (as shown in Fig. 2.21) do not have this limitation.

Rather than having the voltage  $v_o$  to have only two levels  $V_{dc}$  or  $-V_{dc}$ , a third level can be used where the voltage  $v_o$  is zero and is called a three-level inverter. The resultant voltage waveform is shown in Fig. 2.21b. The angle  $\delta$  is a phase-shift between the two transistor legs and is used to control the amplitude of the sinusoidal  $n^{\text{th}}$  voltage, as demonstrated by Fourier series of  $v_o$ .

$$v_{on} = \frac{4}{T} \int_0^T v_o(t) \sin n\omega_a t \, d(\omega t) = \frac{4V_i}{n\pi} \cos n\delta \quad \rightarrow n = 1, 3, 5, \dots \text{odd} \quad (2.7)$$

It can be seen that by varying  $\delta$  from zero to  $\pi$ , the output voltage can be varied from a fixed voltage at  $\delta = 0$  to zero-voltage at  $\delta = \pi$ . This  $\delta$ -control introduces a variable AC voltage and also can eliminate one harmonic voltage as long as Eq. (2.8) is observed.

$$\cos n\delta = 0, \text{ which means } n\delta = \frac{\pi}{2} \quad (2.8)$$

For example, if the third harmonic voltage is chosen to be eliminated then  $\delta = \pi/6$ . This method of harmonic elimination is known as active filtering contrasted to passive filtering that requires actual filter components. Another method of active filtering is known as harmonic cancellation where harmonics are eliminated by processing waveforms. Figure 2.22a shows two converters where both converters are switched at a steady square wave voltage. The output waveforms  $v_{o1}(t)$  and  $v_{o2}(t)$  of the two converters are shown in Fig. 2.22b. It can be seen that each of the two converters produces a fixed two-level square wave voltage. By shifting the control of one converter by angle  $\delta$ , and adding the two voltage the resulting output voltage  $v_o(t)$  is a variable three-level inverter, similar to the one shown in Fig. 2.21. Each of the inverters output contains a third harmonic. However, by adding the two inverters output, the resulting voltage will not have third harmonic voltage if  $\delta$  is chosen to be  $30^\circ$ . Numerous control methods for

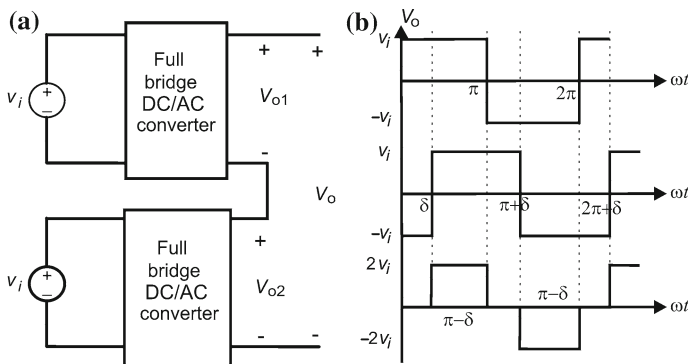
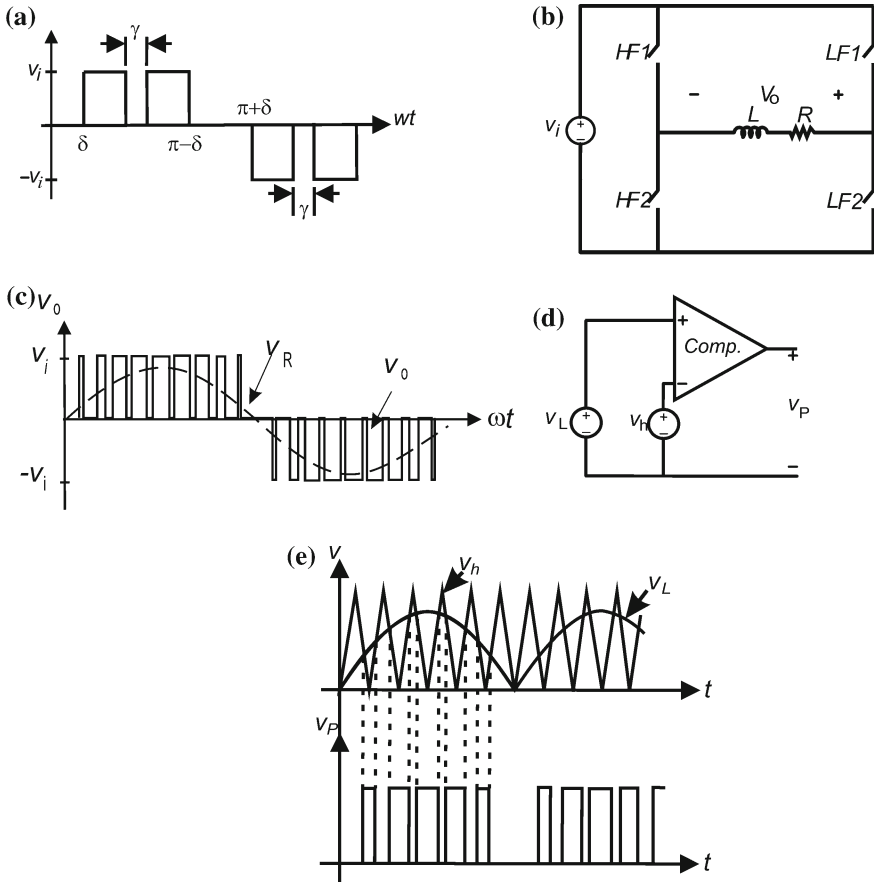


Fig. 2.22 Active filtering using harmonic elimination: **a** circuit, and **b** waveforms



**Fig. 2.23** Pulse-width modulation (PWM) switching technique: **a** multiple harmonic elimination, **b** PWM circuit, **c** PWM AC output, **d** PWM generation, and **e** PWM signal

harmonic elimination and harmonic cancellation have been proposed in the literature. These methods have resulted in two major breakthroughs in active-wave shaping or active filters; namely the method of pulse-width modulation (PWM) and the method of multilevel inverters, which will briefly be discussed later.

The  $\delta$ -control method imposes a zero-voltage on the output voltage and if more of the zero-voltage segments are introduced, the harmonic content of the AC voltage can be reduced. For example, if two segments are introduced as shown in Fig. 2.23a, with  $\delta = 30^\circ$  and  $\gamma = 12^\circ$ , then it can be shown that both the third and fifth harmonic voltages can be eliminated [1]. Also, if these zero-voltage regions can be introduced at high frequency (HF) with a variable width that is sinusoidally distributed at the fundamental frequency of the AC voltage, the resulting AC

voltage will contain only the fundamental AC component and components at the HF of the  $\delta$ -control.

Figure 2.23b shows a converter similar to the full-bridge topology where the switches are controlled at either HF or a low frequency (LF). The HF switches operate at a frequency known as the carrier frequency, which is much higher than the fundamental AC frequency. The LF switches are operated at the fundamental frequency, referred to as the modulating frequency. During the positive half cycle of the LF switches, the HF switches are alternating at the constant carrier frequency with different on-times, i.e., a variable duty ratio. The duty ratio can be obtained by comparing a triangular wave signal at the carrier frequency with a sine wave signal at the modulating frequency, as shown in Fig. 2.23c. The resulting output waveform has a constant frequency with a modulated pulse width so this technique is called PWM. Although no specific harmonic elimination (or cancellation) is introduced, the unwanted frequencies are pushed to higher frequency decades above the fundamental AC frequency and, as a result, the amount of passive filtering that is required can be minimized.

### 2.3.2.2 Three-Phase Inverters

Three-phase DC/AC converters can be constructed using single-phase DC/AC converters (one leg branch). Three single-phase inverters can be connected to a common DC source, as shown in Fig. 2.24a. Their switch controls are shifted by  $120^\circ$ , with resulting output voltages shown in Fig. 2.24b. The three outputs can be connected in  $Y$  or  $\Delta$  as shown in Fig. 2.24c. It can be shown that the number of switches for the three independent single-phase bridge converters can be reduced to six switches rather than twelve and this design is shown in Fig. 2.25a and b. This converter design is the standard circuit topology that is used for conversion of DC to three-phase AC. The AC output depends on the control of the six switches. For example, if the switches are controlled with a phase-shift command of  $60^\circ$ , the resulting waveforms are shown in Fig. 2.25c.

When a DC voltage is the input to a converter, the design is defined as voltage-fed inverter (VFI) or voltage source inverter (VSI). When a DC current is the input to a converter it is defined as either a current-fed inverter (CFI) or current source inverter (CSI) as depicted in Fig. 2.26. The CSI operation constraints are: (1) there must always exist a current path for the current source; (2) the output phases cannot be short-circuited. The DC current is unidirectional, and only two switches conduct at same time providing the path for current circulation. The switch types for this design must be fully controlled in current and bidirectional in voltage. Switches that meet this requirement include: SCR, GTO, and the recently introduced IGBT.

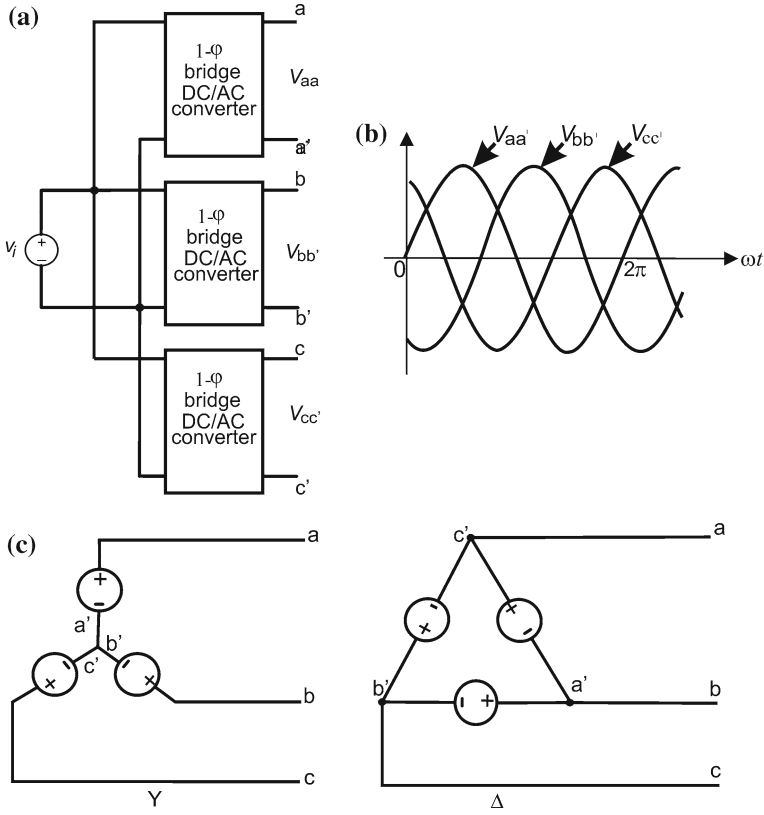


Fig. 2.24 Three-phase AC/DC converter: a circuit, b waveforms, and c connections

### 2.3.3 AC/DC Converters (Rectifiers)

AC/DC converters are called rectifiers circuits, which can be broadly classified based on the type of AC source and the type of semiconductor switch is used as shown in Fig. 2.27. Rectifiers are usually used in either single-phase or three-phase applications, but multi-phase topologies are possible for high power applications. Switches that are used in rectifier's designs can be either uncontrolled (diode) or controlled devices (thyristor). Single-phase rectifiers can be classified as either half-wave or full-wave circuits. Three-phase rectifiers are classified based on the number of pulses of the rectified output voltage, i.e., 3-pulse rectifiers, 6-pulse, 12-pulse, or more generally  $3 \times 2^n$ -pulse (where  $n = 0, 1, 2, 3, \dots$ ). The number of pulses is the ratio of the fundamental frequency of the rectifier output to the frequency of the AC input.

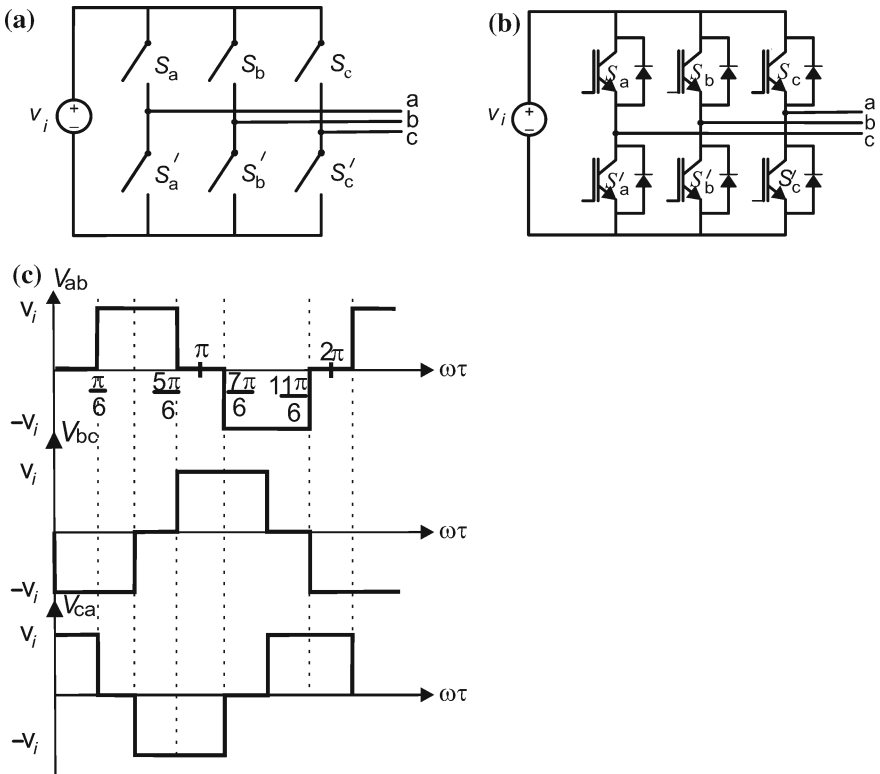
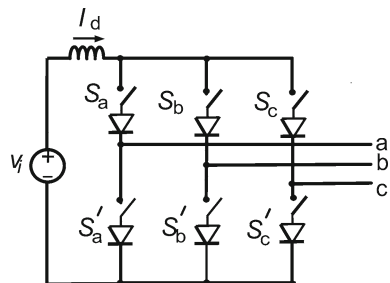


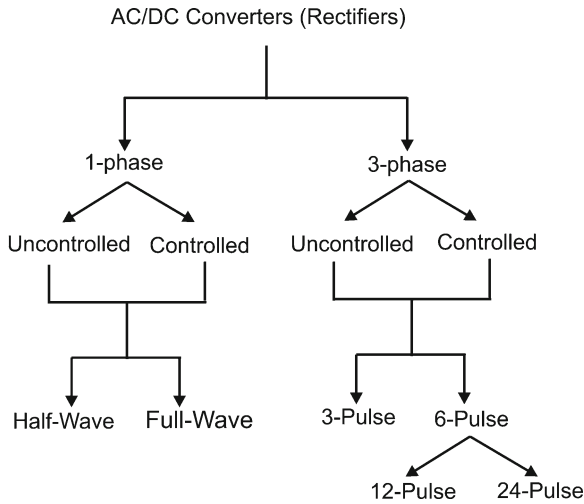
Fig. 2.25 Six-step inverter and waveforms: **a** circuit, **b** switch implementation, and **c** waveforms

Fig. 2.26 Current source inverter (CSI)

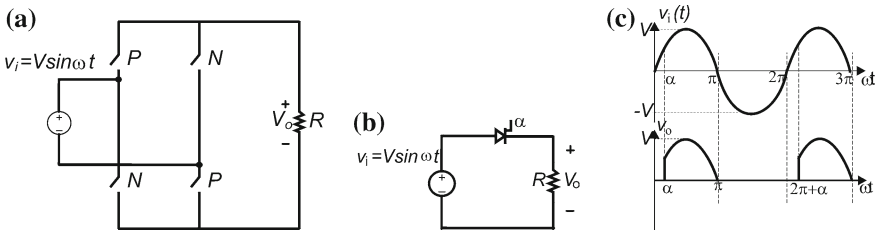


### 2.3.3.1 Single-Phase Rectifiers

A general circuit for a single-phase rectifier is illustrated in Fig. 2.28. Note that this design is the same as the generalized DC/DC converter shown in Fig. 2.14 except that a sinusoidal voltage replaces the input DC source. The basic single-phase rectifier circuits are completed by setting the P- and N-switches to be either permanently closed or open. For example, if all the N-switches are permanently



**Fig. 2.27** Classifications of rectifier circuits

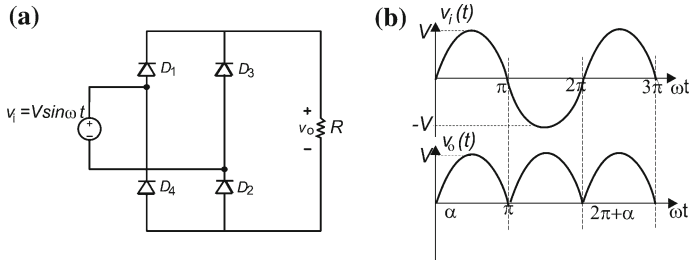


**Fig. 2.28** **a** General 1-phase rectifier circuit, **b** 1-phase controlled rectifier, and **c** Input and output voltage waveforms

open and the bottom P-switch is permanently closed, the resulting circuit is a half-wave rectifier circuit. If the remaining P-switch is a thyristor, then the resulting circuit is a controlled half-wave rectifier. A depiction of this topology is shown in Fig. 2.28b and resulting waveforms are shown in Fig. 2.28c. In such case, the angle  $\alpha$  is the thyristor turn-on delay angle, which is measured starting at the zero-crossings of the input voltage source. The output waveform has an average value (the required DC component), which can be calculated using Eq. (2.9) as,

$$V_{avg} = \frac{1}{T} \int_0^T v(t) dt = \frac{1}{2\pi} \int_{\alpha}^{\pi} V \sin \omega t d(\omega t) = \frac{V}{2\pi}(1 + \cos \alpha) \quad (2.9)$$

Equation (2.9) shows that the value of the DC voltage can be varied as  $\alpha$  is changed. A half-wave uncontrolled rectifier is possible when the remaining P-switch is implemented through the use of a diode; this circuit is the same as in



**Fig. 2.29** Examples of uncontrolled rectifiers: **a** full-bridge (FB), and **b** waveforms

Fig. 2.28b except the thyristor is replaced by a diode. Since the diode is an uncontrolled switch,  $\alpha$  is set to zero and the diode will turn-on at the zero-crossings of the supply voltage. When  $\alpha = 0$  is substituted into Eq. (2.9) then average voltage is given as:

$$V_{avg} = \frac{1}{2\pi} \int_0^{\pi} V \sin \omega t \, d(\omega t) = \frac{V}{\pi} \tag{2.10}$$

Equation (2.10) shows that the DC voltage is fixed and cannot be changed and as a result this type of rectifier is defined as uncontrolled.

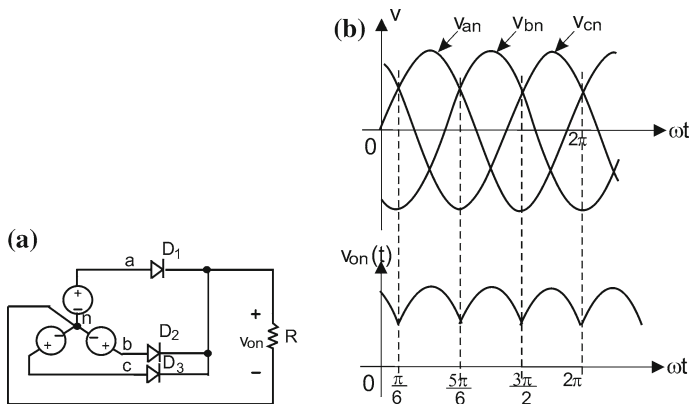
If all the switches of Fig. 2.28a are used then the resulting circuit is a full-wave rectifier as shown in Fig. 2.29a. When all the switches are diodes, the resulting waveform is illustrated in Fig. 2.29b. The DC voltage in a full-wave rectifier design will be double the one from the half-wave rectifier.

There are circuit topologies, such as one-quadrant, two-quadrant, and four-quadrant, for half- or full-wave types. Some of them are uncontrolled, and others are fully controlled depending on the combination of diodes and thyristors, which are usually classified as semi-controlled or hybrid rectifiers. Some rectifiers use transformers for isolation for further rectification capability [1, 2].

### 2.3.3.2 Three-Phase (3-Φ) Rectifiers

As mentioned in the classification of three-phase rectifiers, the output is defined in terms of the number of pulses per one cycle of the input voltage. The 3-pulse rectifier is a basic three-phase rectifier circuit (connected to a three-phase system), and can be used as building block for most of other three-phase rectifiers. Each of the three-phase input voltages can be determined using Eq. (2.11). The operation of a three-phase 3-pulse rectifier is shown in Fig. 2.30a, b.

$$\begin{aligned} v_a &= V \sin \omega t \text{ V} \\ v_b &= V \sin(\omega t - 120^\circ) \text{ V} \\ v_c &= V \sin(\omega t + 120^\circ) \text{ V} \end{aligned} \tag{2.11}$$

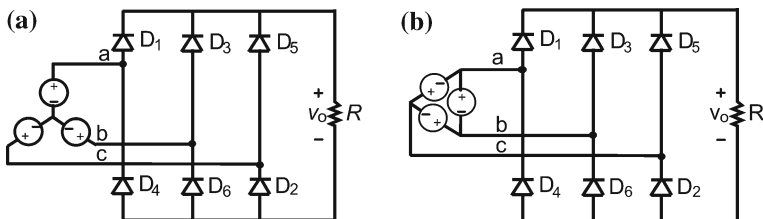


**Fig. 2.30** three-phase, 3-pulse rectifier circuit: **a** circuit and **b** waveforms

In this case the switches are implemented with diodes (uncontrolled rectifier). A diode will turn-on when its voltage is higher than the other two diodes, i.e., the diode connected to the highest of the three voltages will conduct. The resulting output is shown in Fig. 2.30b; notice that the diode conduction starts and ends when two of the three voltages are equal. Also, each diode conducts for an angle of  $120^\circ$ , and the output voltage has 3 pulses, during one cycle of the input. Therefore, the fundamental frequency of the output voltage is three times the frequency of the input voltage. The DC component of the output of each of them can be calculated by the average over its period as:

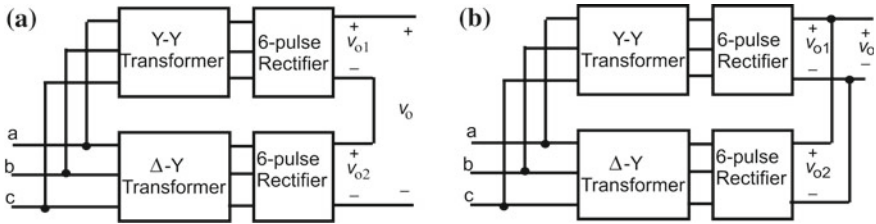
$$V_{avg} = \frac{1}{(2\pi/3)} \int_{\frac{\pi}{6}}^{\frac{5\pi}{6}} V \sin \omega t d(\omega t) = \frac{3\sqrt{3}V}{2\pi} \tag{2.12}$$

The DC voltage, given by Eq. (2.12), is higher than the output voltage of a single-phase full-wave rectifier. Of course, the drawback is the need of a three-phase source, which is most common for industrial applications.



**Fig. 2.31** 6-pulse rectifier circuits: **a** Y-connected source, and **b** Δ-connected source





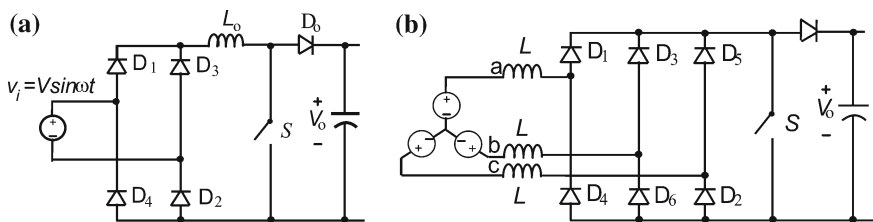
**Fig. 2.32** 12-pulse rectifier circuits: **a** high voltage 12-pulse rectifier, and **b** high current 12-pulse rectifier

If two 3-pulse rectifiers are connected the resulting topology is shown in Fig. 2.31. This circuit is known as a 6-pulse rectifier, and it is the building block for all high power multiple-pulse rectifier circuits.

Two 6-pulse rectifier circuits can be connected through the use of Y–Y and Δ – Y transformers for building 12-pulse rectifiers. If the two rectifiers are connected in series, the resulting circuit is shown in Fig. 2.32a and is suitable for high voltage, whereas the converter is connected in parallel as shown in Fig. 2.32b, the circuit is suitable for high current.

### 2.3.3.3 Controlled Rectifiers

When diodes are replaced by thyristors, the three-phase rectifier circuit becomes a controlled one, and the delay angle  $\alpha$  (measured relative to the time where the diodes start to conduct) will control the output voltage. Similar to single-phase rectifiers, there are combinations of switches and transformers that result in higher pulse three-phase rectifiers. For complete understanding on the types and analyses of single-phase and three-phase rectifiers, the reader is referred to Chaps. 4 and 5 of reference [1], Chap. 7 of reference [2], Chaps. 5 and 6 of reference [3], and Chaps. 4 and 5 of reference [4].



**Fig. 2.33** PWM rectifier: **a** single-phase, and **b** three-phase

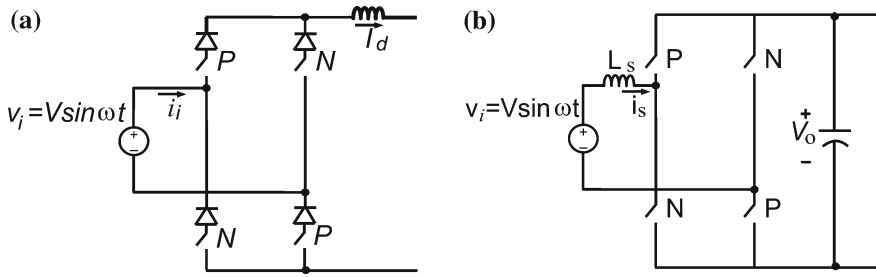


Fig. 2.34 Single-phase PWM rectifiers

### 2.3.3.4 PWM Rectifiers

PWM rectifiers can be implemented as unidirectional or bidirectional as regarding their power flow capabilities. A basic unidirectional boost version consists of an uncontrolled diode bridge followed by a boost converter as shown in Fig. 2.33a. When the switch is ON the inductor current increases proportionally to the input voltage (which is sinusoidal). When the switch is OFF, the inductor current decreases, and its energy is transferred to the capacitor, repeating such cycle with variable input voltage. The boost converter regulates the capacitor voltage, and also impresses a sinusoidal input current profile, which improves the input power factor. Since this converter can operate in either Continuous Conduction Mode (CCM) or in Discontinuous Conduction Mode (DCM), its control should be designed to be stable and work in both conditions. A three-phase version of the unidirectional boost rectifier is shown in Fig. 2.33b, but the inductors are connected at the AC side.

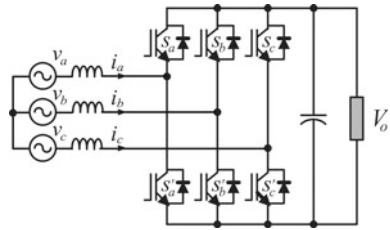
In order to implement a bidirectional converter fully controlled switches replace the diodes, as shown in Fig. 2.34a. This topology is called a current source rectifier (CSR). In this design, the output voltage,  $V_0$ , is smaller than the amplitude of the input voltage,  $V$ , as indicated in Eq. (2.13). Therefore, the CSR is also defined as a Buck Rectifier, where the objective is to provide a constant current  $I_d$  at the output.

$$V_0 < \frac{\sqrt{3}}{2} V \quad (2.13)$$

The boost function is possible by connecting the boost converter inductor on the AC side, as shown in Fig. 2.34b. When the AC voltage is positive and the switch  $T_2$  is ON, the inductor current increases proportionally to the AC voltage and when  $T_2$  turns-off the inductor energy is pumped to the capacitor via diodes  $D1$  and  $D4$ . Similarly, when the AC voltage is negative  $T4$  is turned-on. When it turns-off the energy flows via diodes  $D2$  and  $D3$ . This topology is known as the voltage source rectifier (VSR). In VSR the output voltage,  $V_0$  is greater than the amplitude of the input voltage,  $V$ , as indicated in Eq. (2.14).

$$V_0 > V \quad (2.14)$$

**Fig. 2.35** Implementation of the three-phase VSR



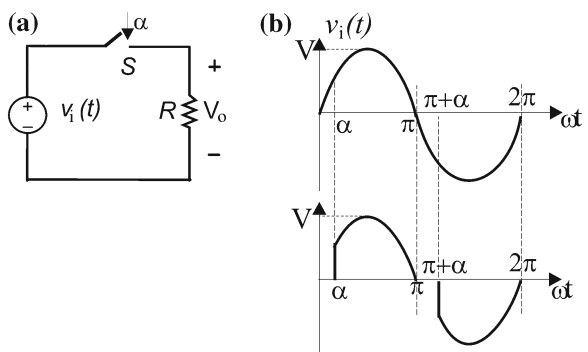
The VSR is also known as Boost Rectifier with objective to provide a constant voltage  $V_0$  at the output. The CSR and the VSR are dual from each other. Figure 2.35 shows the implementation of a three-phase version of the PWM VSR (with IGBTs). The VSR requires a large capacitor across the output, it is inherently bidirectional and can be applied in several applications where the line side converter must be able to deliver energy back to the source, such as in locomotives, cranes, and renewable energy sources connected to the DC link side.

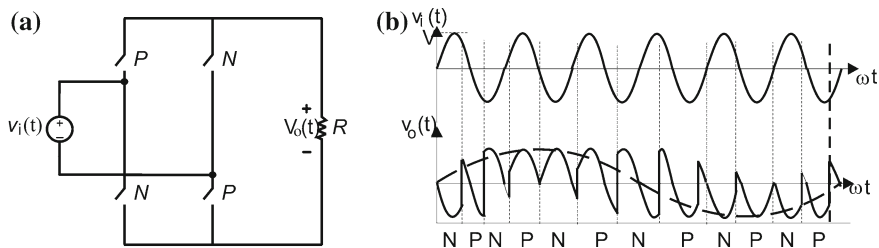
### 2.3.4 AC/AC Converters

AC/AC converters are used to interconnect AC sources, for example from single-phase or a three-phase source to single-phase or a three-phase source. In applications that require variable AC such as light dimmers and AC motor drives, energy is converted from a FVFF to a single-phase or three-phase VVFF or VVVF.

A very simple AC/AC converter circuit, to regulate the AC power for a resistive load is shown in Fig. 2.36a and the waveform shown in Fig. 2.36b. This circuit is known as AC controller, which converts from single-phase AC FVFF to VVFF single-phase AC. The fundamental frequency of the input and output is the same. By varying the switch turn-on delay angle  $\alpha$ , the amplitude of the fundamental voltage is varied. Typical applications of this circuit are light dimmers and single-phase motor drives used in home appliances. The switch implementation is usually a

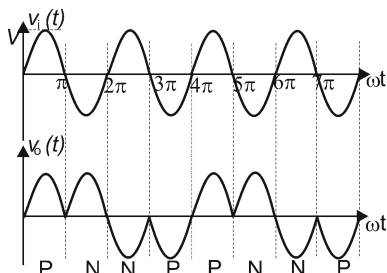
**Fig. 2.36** Variable voltage fixed frequency (VVFF) AC/AC converter



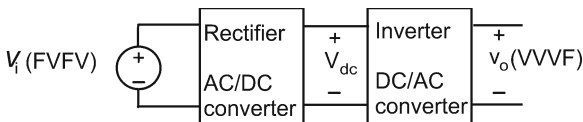


**Fig. 2.37** Cycloconverter as VVVF AC/AC converters

**Fig. 2.38** Integral-cycle control for (VVVF) AC/AC converter



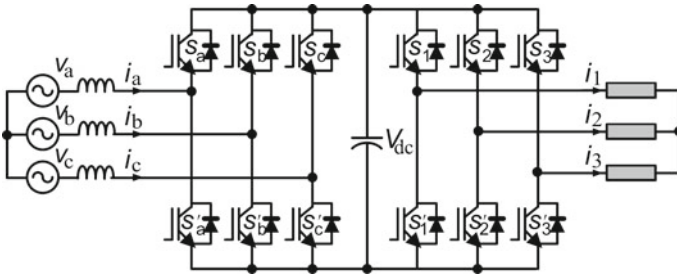
**Fig. 2.39** FVFF to VVVF AC/AC converter through a DC link



triac (combination of two SCR's in anti-parallel) controlling the positive half cycle of the AC source with one thyristor and the negative half cycle with the other one.

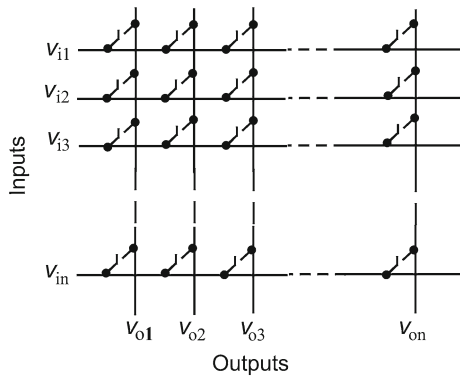
The circuit shown in Fig. 2.37a is a general AC/AC converter, referred to as a cycloconverter. The switches can be controlled to produce an output voltage with variable amplitude and variable frequency. This is referred to as VVVF output as shown in Fig. 2.37b [1]. The P- and the N-switch are controlled to achieve an output voltage at a frequency lower than the input frequency. Another possible approach for controlling AC/AC converter is known as integral-cycle control, as shown by the waveforms in Fig. 2.38, exemplifying a case where the fundamental frequency of the output is twice the input [2].

AC/AC conversion can also be obtained by cascading an AC/DC converter with a DC/AC converter, as shown in Fig. 2.39; the approach is known as “DC link conversion” approach. The implementation of this converter with IGBTs is shown in Fig. 2.40. This design allows two-way energy flow and four-quadrant operation and is usually applied to motor drives, electric power generation using asynchronous machines, energy storage systems (such as batteries, UPS, and flywheel energy systems), and the connection of two independent grids. Because a CSR can



**Fig. 2.40** Implementation of a FVFF to VVVF AC/AC converter through a DC link

**Fig. 2.41** Generalized matrix converters



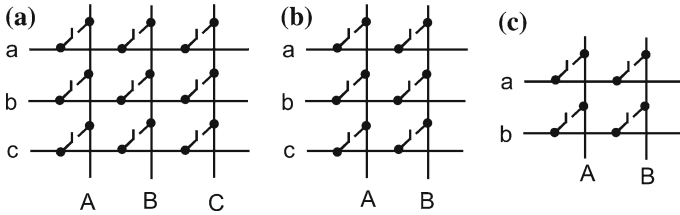
be modeled as a controllable DC current source, the natural load is a CSI that supports a FVFF to VVVF AC/AC converter through an inductive DC link.

### 2.3.5 Advanced Converter Topologies

Several advanced circuits have been developed and the field of PE is still an emerging and rapidly growing field with new converters. Some of those topologies are application-specific and will be discussed in the next sections.

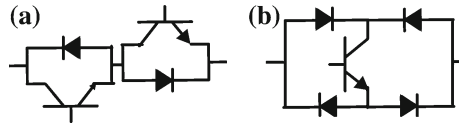
#### 2.3.5.1 The Matrix Converter

A matrix converter consists of a multi-input multi-output switching matrix that can represent all the switching converters. It can be considered as a fully controlled four-quadrant bidirectional switch, which allows HF operation. Figure 2.41 has an example of a matrix converter with  $n$ -inputs and  $m$ -outputs. Figure 2.42a shows a specific case where  $n = m = 3$ , i.e., a three-phase to three-phase AC/AC



**Fig. 2.42** Examples of converters derived from the matrix converter: **a** AC/AC, **b** AC/DC, and **c** AC/DC and DC/DC

**Fig. 2.43** Implementation of a fully bidirectional switch

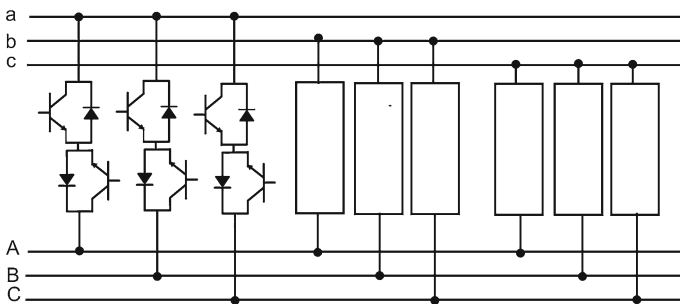


converter, while Fig. 2.42b shows the case for  $n = 3$  and  $m = 1$ , which can be either a three-phase AC/DC converter or a DC to three-phase AC converter. Figure 2.42c shows the converter for  $n = m = 1$  (i.e., any DC/DC converter, single-phase AC/DC converter, or DC to single-phase AC converter).

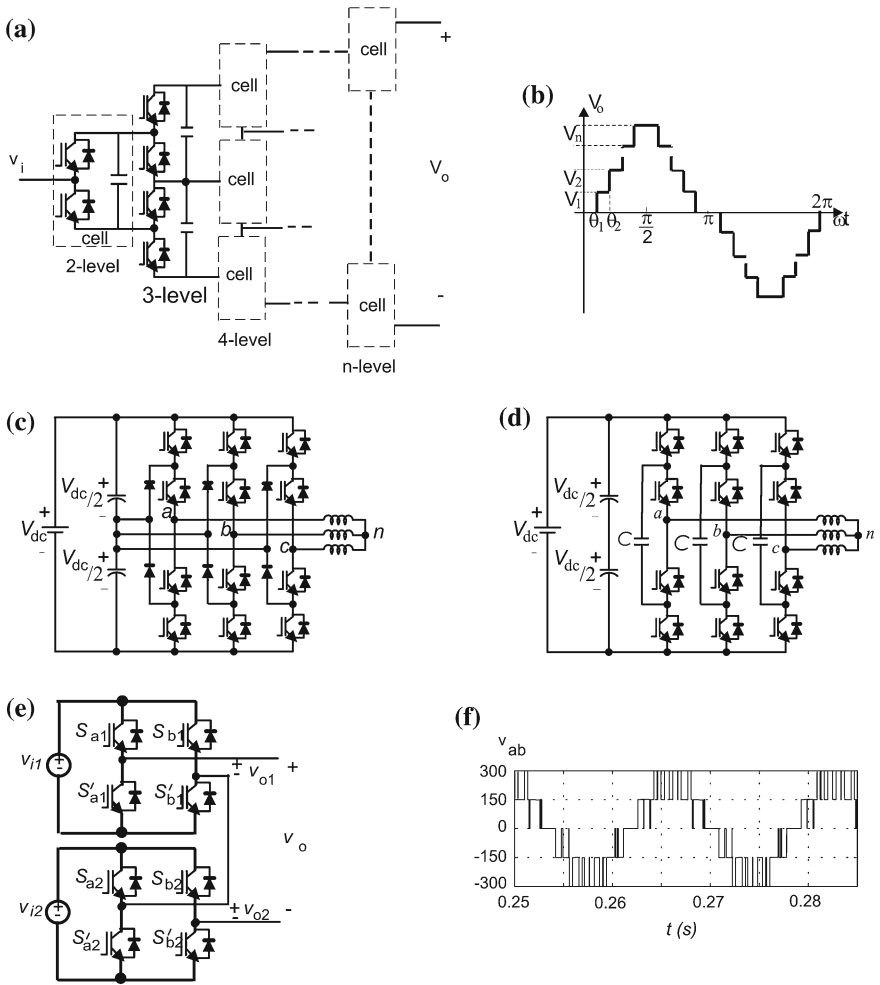
The bidirectional voltage and current switch can be made of diodes and controlled switches as indicated in Figs. 2.43a, b. A three-phase AC to AC converter is shown in Fig. 2.44. Although the matrix converter topology has been around for quite some time, it has gained attention in many applications because of the recent availability of switching power electronic devices and controllers.

**2.3.5.2 Multilevel Inverters**

Multilevel inverters are AC/DC converters where a series connection of power electronic devices and split capacitors allow high voltage applications. These inverters are modulated in a way such that the output voltage resembles a staircase



**Fig. 2.44** Implementation of a three-phase AC/AC converter



**Fig. 2.45** Multilevel inverter: **a** generalized multi-level converter, **b** generalized waveforms, **c** NPC inverter, **d** flying capacitor inverter, **e** H-bridge cascaded inverter, and **f** NPC line voltage waveform

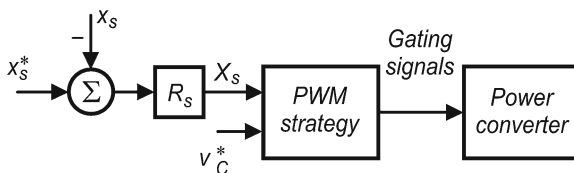
as shown by the generalized multilevel inverter in Fig. 2.45a. A three-level converter consists of series capacitor with a center tap as the neutral where each phase leg of the converter has two pairs of switching devices in series. As the number of levels increase, the synthesized output waveform adds more steps, producing a more refined staircase wave with minimum harmonic distortion, as shown in Fig. 2.45b. Of course, a zero-harmonic distortion of the output wave can be obtained by an infinite number of levels. More levels also mean that series device can provide higher output voltages without any device voltage-sharing problems. Such multiple switches and circuits usually make multilevel inverters more expensive than two-level inverters and are cost-effective only for very specific

utility and transmission or distribution power system applications. Different multilevel inverter topologies can be developed from the basic circuit of Fig. 2.45, for example the Diode Clamped (or Neutral-Point Clamped, NPC), and of the Capacitor Clamped or flying capacitor (FC) inverters, as shown in Fig. 2.45c, d, respectively, for three-level inverters. Another popular configuration is the Cascaded H-Bridge, with separate DC sources that is evolved from the two-level inverter, shown in Fig. 2.45e for five-level inverter. All these inverters can also be controlled by PWM techniques [5, 6], of which one example is shown in Fig. 2.45f for the three-level NPC inverter.

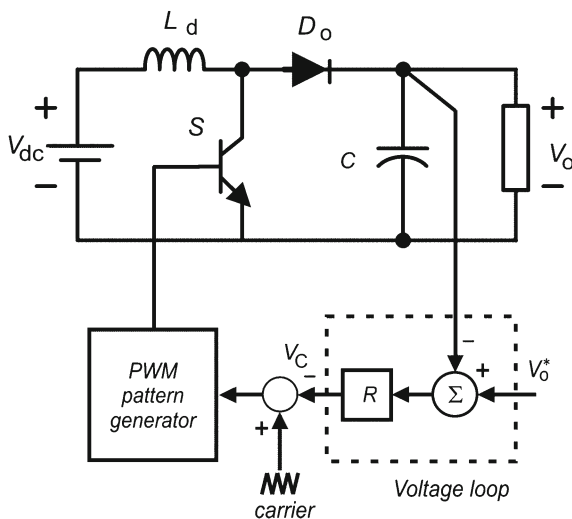
### 2.4 Control of Power Converters

There are several objectives in the applications of the power converters, such as control of grid voltage, control of current, control of DC link voltage or current, as load or DC connection, control of AC load voltage or current, control of harmonics, control of speed, and so on. The control strategy applied to these cases often deal with the regulation of two variables with different dynamics, one is probably slow and another fast. Examples are: (1) for a rectifier: capacitor voltage (slow) and grid current (fast), (2) for a motor drive: motor speed (slow) and motor current (fast), (3) grid connected inverter: output current (slow) and input voltage (fast).

**Fig. 2.46** Slow variable controller



**Fig. 2.47** Voltage control of a boost converter





This section will only consider the control of voltages and currents. Figure 2.46 shows a typical PWM control for a slow variable, defined as  $X_s$  is compared with its reference  $X_s^*$ .

The resulting error is regulated by the slow variable regulator,  $R_s$ . This regulator has a dynamic performance such as  $D$  is directly adjusted so that the slow variable remains regulated. This scheme can be directly applied to DC/DC converters. An example is for a boost DC/DC converter shown in Fig. 2.47, where the objective is to regulate the output voltage,  $V_O$ . For this, the error between the reference and the actual output voltage typically feeds a proportional-integrative (PI) regulator,  $R$ . The output of the regulator, the voltage control  $X_s = v_c$  is compared to the carrier signal to produce a direct duty ratio PWM control. This type of control can also be employed when only one variable is controlled, such as the voltage in the PWM VSI, and the current in the PWM CSI.

The control scheme can be generalized by using a cascaded strategy, in which any external (slow variable) control defines the reference for an internal (fast variable) control. This kind of control is most often stable since both loops have different dynamics. In order to ensure a desired fast variable profile, the output of regulator  $R_s$  is synchronized with a template signal to define the internal control reference,  $x_f^*$ . As an example, for obtaining near unity power factor operation, the PWM input line current pattern is synchronized with the grid voltage. This can be achieved in two ways: (1) the grid voltage, after filtering, can be used directly as a template for current, or (2) the zero crossing of the grid or the capacitor voltage can be used as a synchronization signal.

Two schemes for internal control will be now considered: the first one is shown in Fig. 2.48, where  $x_f$  is compared with the internal loop reference,  $x_f^*$ , in order to generate the gating pulses. Considering only CCM operation, this comparator can: (1) employ hysteresis (bang–bang) techniques, in which the regulated variable is maintained inside a tolerance band; (2) compare directly  $x_f^*$  and  $x_f$ , and (3) compare the integral of  $x_s$  with  $x_f^*$ . These three principles are indicated in Fig. 2.49 when the controlled variable is the current and the template is a sinusoidal waveform. In the hysteresis technique shown in Fig. 2.49a the measured current is compared with a tolerance band around the reference. The corresponding switch is turned-on when the current reaches the lower limit of the band,  $I_{min}^*$ , and is turned-off when the actual current reaches the upper limit of the band,  $I_{max}^*$ . The switching frequency varies along the current waveform. Different from the previous technique, case (2),

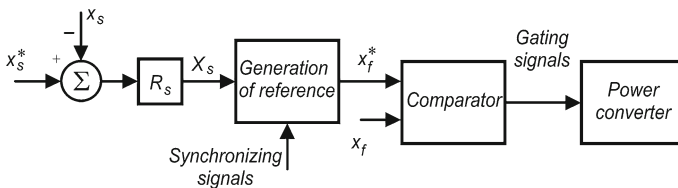


Fig. 2.48 Block scheme for both slow and fast variable control

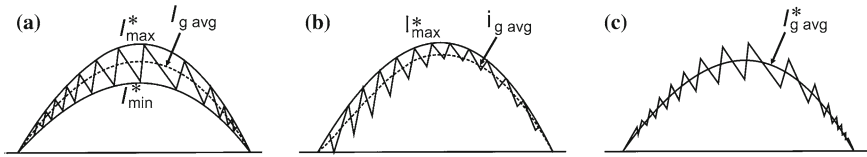


Fig. 2.49 CCM: **a** hysteresis control, **b** current peak control, and **c** average current control

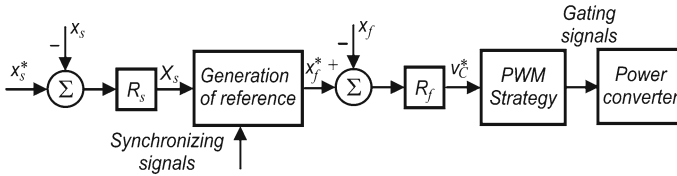


Fig. 2.50 Generalized control strategy applied to power converters

Fig. 2.49b, operates with constant switching frequency: the corresponding switch is turned-on by a clock at the beginning of each switching interval and is turned-off when the actual current tries to go beyond the reference. This technique is known as current peak control. In Fig. 2.49c the measured current is integrated so that its average value can be compared with the current reference. For this reason this approach is known as average current control. For more information on these and other current control schemes the reader is referred to [7– 9].

A possible scheme is given in Fig. 2.50 where the control error is regulated by the regulator  $R_f$ , whose output furnishes the modulating signal to be applied to the chosen PWM strategy.

Consider, as an example, the control of the PWM VSR circuit, as shown in Fig. 2.51. In this case, the output voltage and the grid current are the main objectives of the converter control. In the scheme of Fig. 2.51,  $x_s$  is the capacitor voltage and  $x_f$  is the grid current.

The scheme in Fig. 2.51 includes a fast current controller, a slow DC voltage controller, such as PI, P, Fuzzy or other, and a PWM generator. Since, for power factor control, the input current reference,  $i^*$ , must be sinusoidal, and the voltage controller output is multiplied by a sinusoidal signal (template signal) with the same frequency and the same phase-shift angle of the mains supply. This template is used to produce the PWM pattern that forces the input currents to follow the desired current template  $I^*$ . This voltage source current controlled PWM rectifier is simpler and more stable than the voltage source voltage controlled PWM rectifier method. Its stability can be ensured by adequate choice of the controller gains [9].

Other control strategies such as the space vector scheme are also used (Fig. 2.52). In this case the voltage controller provides the value of the reference of the  $d$  component current,  $X_d^*$ , while the reference of the  $q$  component current,  $X_q^*$ , is fixed to zero in order to obtain unitary power factor. These references are compared with the input currents that are represented in  $d$ - $q$  coordinates.

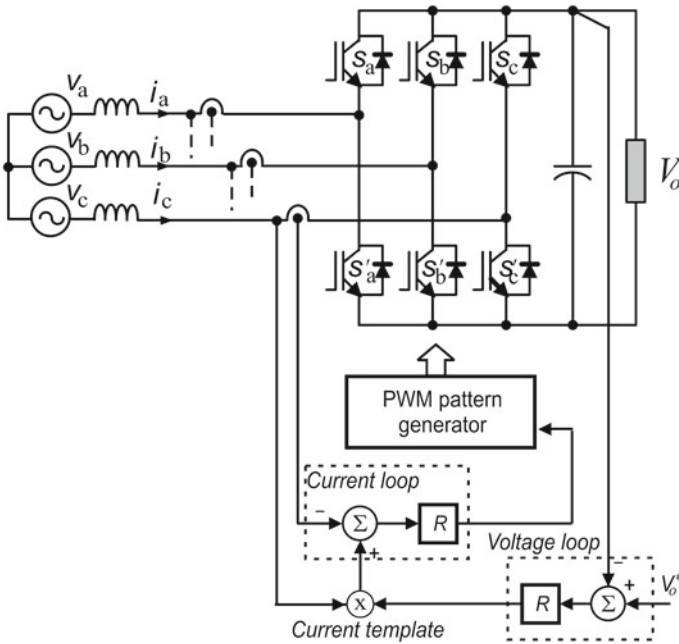
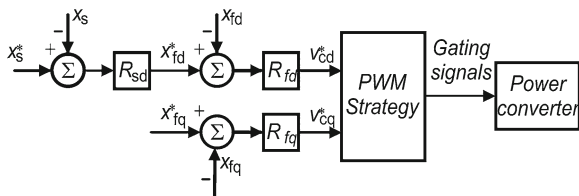


Fig. 2.51 Voltage current controlled PWM rectifier

Fig. 2.52 Space-vector control scheme

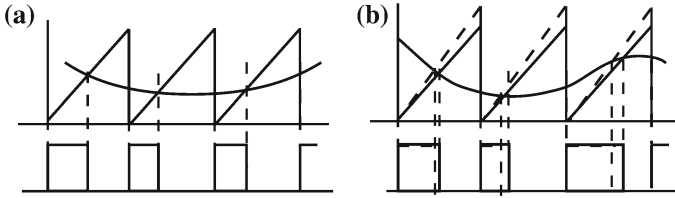


Two controllers, typically PI, give the control values  $v_{cd}^*$  and  $v_{cq}^*$  that generate the PWM pattern which controls the VSR. The inverse transformation  $dq/abc$  allows for obtaining the gate drive pulses for the switches.

An important point is that the current controller can be modified by other signals like the signal of balancing capacitor voltages in NPC multilevel converter.

### 2.5 Pulse Width Modulation

A PWM pattern is essential in the schemes shown in Figs. 2.46, 2.48, and 2.52. The following sections will present more advanced PWM strategies that are used in control of DC/DC and DC/AC converts. The PWM strategies will be applied to a three-phase PWM VSI and then used for a PWM CSR. It will also be indicated how these strategies can also be applied to three-phase PWM CSIs and PWM VSRs.



**Fig. 2.53** Two principles of PWM modulators: **a** variation of the control voltage and saw-tooth carrier with constant slope, and **b** variation of the carrier amplitude

### 2.5.1 PWM Techniques for DC/DC Converters

The most popular DC PWM is the voltage-mode control. It is obtained by comparing a saw-tooth (carrier) with a control voltage (modulating signal). The adjustment of the control voltage allows adjustment of the output pulse width and is shown in Fig. 2.53a. As the control voltage is increased or decreased, the  $D$  is increased or decreased, causing an increase or decrease in the converter output voltage. For this reason the voltage-mode control is also called duty-cycle control, which is largely employed to control DC/DC power converters. The pulse-width control can also be obtained by varying the carrier amplitude as shown in Fig. 2.53b. For digital implementation, a digital comparator and the modulating signal are replaced by a sampled signal [8].

### 2.5.2 PWM Techniques for Two-Level Voltage Source Converters

PWM has been the subject of intensive research and is widely employed to control the output voltage of static power converters. A large variety of feed forward and feedback control schemes has been described in the literature [5, 10], such as the Selective Harmonic Elimination PWM, but the most widely used methods of PWM are the sinusoidal pulse-width modulation (SPWM), the non-sinusoidal carrier PWM techniques, the space vector modulation (SVPWM), and the hybrid PWM (HPWM) [11].

Although most of comments in the following will be addressed to the VSIs, PWM rectifiers are very important because of several advantages such as: regulation of input power factor to unity, minimum harmonic distortion of input line currents, near sinusoidal current waveforms, precise regulation of output DC voltage, and bi-directional power flow.

The PWM techniques discussed for the VSI can be directly applied to the VSR or Boost Rectifier. Although the basic operation principle of VSR consists in keeping the load DC link voltage at a desired reference value, the PWM scheme for the VSR must provide an adjustable modulation index for the DC voltage

control in addition to the reduction in the total harmonic distortion at the input current, mainly by controlling the input power factor.

**2.5.2.1 Selective Harmonic Elimination PWM**

Selective harmonic elimination (SHE) PWM can be explained from the output voltage waveform in Fig. 2.54, obtained by operating the circuit in Figs. 2.3 and 2.19, with  $2V_i = V_{dc}$  and four extra commutations per cycle in relation to the square wave. The choice of the values of the angles  $\alpha_1$  and  $\alpha_2$  allows to eliminate or reduce two selected harmonics in the square-wave form. The Fourier analysis of the waveform given in Fig. 2.19 allows for determining the amplitude of the fundamental and harmonic voltage content of the pole voltage waveform, that is,

$$V_{ao(n,m)} = \frac{4 V_{dc}}{\pi} \frac{2}{2} \left( \frac{1 - 2 \cos n\alpha_1 + 2 \cos n\alpha_2}{n} \right) \tag{2.15}$$

Specific harmonics will be eliminated when the numerator of Eq. (2.15) is set equal to zero for a given value of  $n$ . For example, the third and fifth harmonics are the largest present in the square-wave voltage, and because they are relatively close to the fundamental frequency they are also the most difficult to filter. Their elimination is obtained by solving two trigonometric equations issued from (2.15), assuming that  $0^\circ < \alpha_1 < 90^\circ$ ,  $0^\circ < \alpha_2 < 90^\circ$  and  $\alpha_1 < \alpha_2$ , which results in

$$\alpha_1 = 23.62^\circ \tag{2.16}$$

$$\alpha_2 = 33.30^\circ \tag{2.17}$$

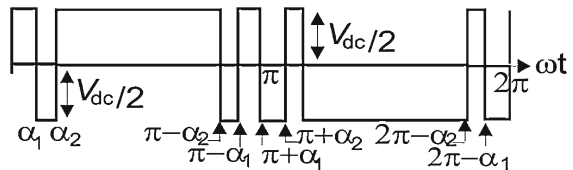
However, in most multiple phase circuits the third harmonics and multiples are eliminated by connections that include the addition of the two “notches” in the voltage waveform can eliminate the fifth and seventh harmonics, allowing for no harmonics below the eleventh on the inverter output voltage waveform. The angles  $\alpha_1$  and  $\alpha_2$  for this case are

$$\alpha_1 = 16.25^\circ \tag{2.18}$$

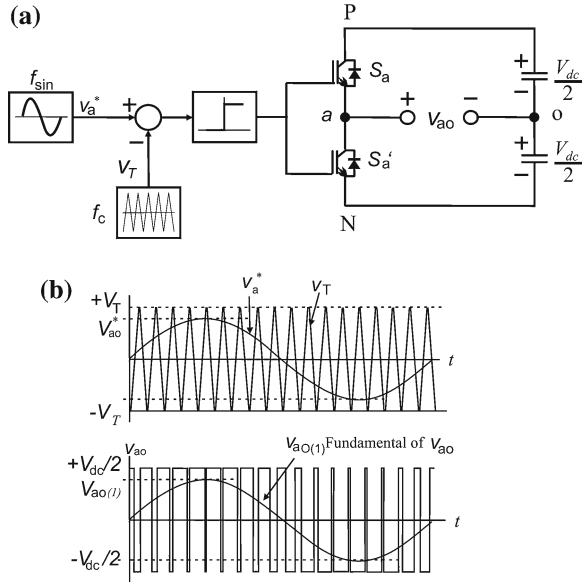
$$\alpha_2 = 22.07^\circ \tag{2.19}$$

More harmonics can be eliminated by the introduction of additional notches.

**Fig. 2.54** Selective harmonic elimination PWM



**Fig. 2.55** Sinusoidal PWM  
**a** bipolar voltage switching for half-bridge inverter,  
**b** control signals (*upper*) and pole voltage (*lower*)



### 2.5.2.2 Carrier Modulation

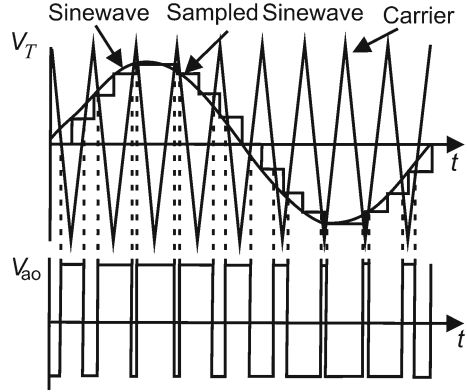
In Sect. 2.3, a modulated pulse width is obtained by comparing a triangular wave at the carrier frequency with a sine wave signal at the modulating frequency. This technique is known as Sinusoidal PWM [1, 3, 5, 12]. Its principle is shown in Fig. 2.55a, b, for a half-bridge inverter. When the modulating signal,  $v_a^*$ , is higher than the carrier signal,  $v_T$ , the upper switch is turned-on and the inverter leg assumes a switching state “P”. The pole voltage is then equal to  $V_{dc}/2$ . When the modulating signal is lower than the carrier signal, the lower switch is turned-ON and the inverter leg assumes a switching state “N”. The pole voltage is then equal to  $-V_{dc}/2$ .

The ratio between the amplitudes of the sine wave and the carrier signals is defined as amplitude modulation ratio  $m_a$ , and that between the carrier frequency and the modulating frequency is defined as the frequency modulation ratio,  $m_f$ . In order to avoid the effects of sub-harmonics  $m_f$  should be an odd integer.

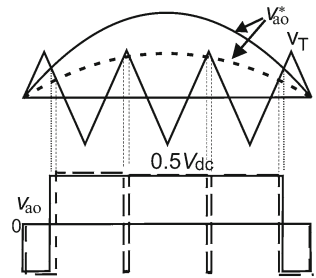
When  $m_f$  is high enough, the amplitude of the fundamental frequency component of the pole voltage,  $V_{ao}$ , in Fig. 2.55a is linear with the variation of  $m_a$ , that is,

$$V_{Ao1m} = m_a \frac{V_{dc}}{2} \quad (2.20)$$

**Fig. 2.56** Regular-sampled PWM



**Fig. 2.57** Operation in over modulation region



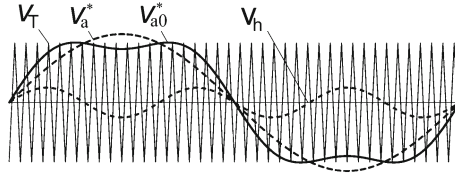
Also, the harmonics of the output voltage waveform appear centered around harmonics  $m_f$ ,  $2m_f$ , and so on, as sidebands.

The pulses are almost centered inside the switching interval; the use of high switching frequencies to improve this location can be avoided by sampling the signals as done for the regular sampled modulation (RSPWM) [13] shown in Fig. 2.56. Nevertheless, sinusoids will continue to be used in the examples that follow.

A value of  $m_a > 1$  causes over modulation with a reduction in the number of pulses in the pole voltage  $v_{ao1}$  waveform, as shown in Fig. 2.57, and loss of linearity. However, the addition of an adequate zero-sequence component, either continuous or discontinuous, to each of the pole voltage reference waveforms makes possible to increase in 15.5 % the fundamental of the output voltages [14]. Figure 2.58 shows an example of the third harmonic injection PWM (THIPWM), which is somewhat flattened on the top [15]. Injection of other zero-sequence components makes possible to generate different PWM strategies such as Symmetrical PWM and Discontinuous PWM [5, 14–20].

The above concept can be expressed in terms of the sinusoidal reference plus a zero-sequence signal  $v_h$ , that is,

$$v_a^{*'} = v_a^* + v_h \tag{2.21}$$



**Fig. 2.58** Operation in over modulation region—non-sinusoidal PWM: sinusoidal reference,  $v_a^*$ , modulating signal generated,  $v_{a0}^*$ , and zero-sequence signal  $v_h$  (middle) for the THIPWM strategy

From (2.21), the SPWM corresponds to  $v_h = 0$ .

For the three-phase inverter shown in Fig. 2.59a there are three modulating signals, one for each of the phases, and one carrier signal, as shown in Fig. 2.59b. This figure shows the pole voltage and the line–line voltage of the inverter.

In the following section, it will be shown how to build different PWM techniques for the three-phase VSI, using the concepts mentioned above. The extension of Eq. (2.21) to the three-phase case results in

$$v_j^* = v_j^* + v_h \quad (j = a, b, c) \quad (2.22)$$

An important feature is that the injected zero-sequence signal  $v_h$  will not increase the LF harmonic distortion in the inverter output voltage.

The most used  $v_h$  signal can be easily determined for any of the Sectors from I to VI, which divide the fundamental period, as shown in Fig. 2.60, from [21].

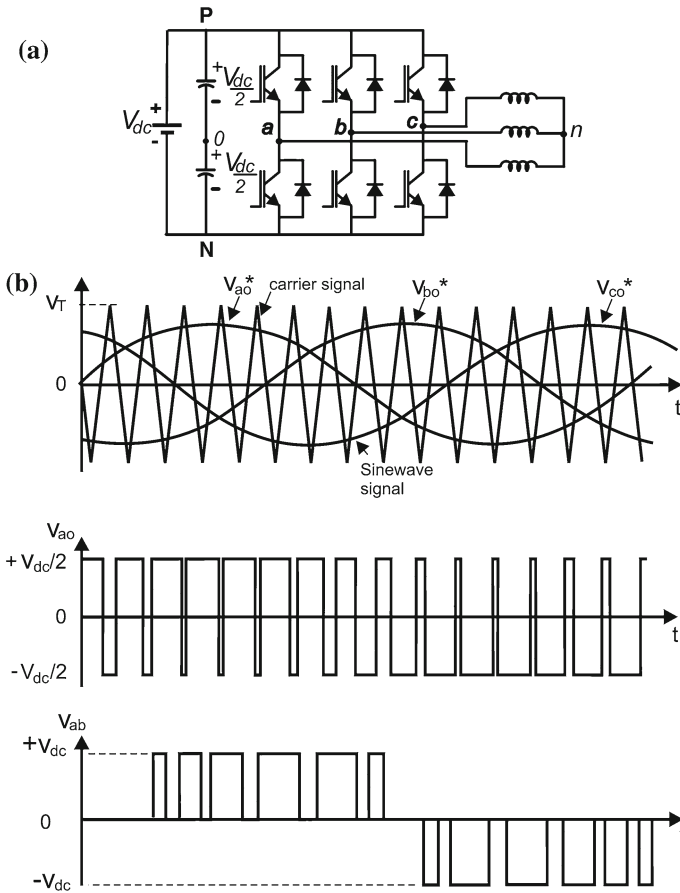
$$v_h = \frac{v_M + v_m}{2} \quad (2.23)$$

That is, from the average value of  $v_M + v_m$ , where  $v_M$  and  $v_m$  are the maximum and the minimum values among the three sinusoidal reference voltages,  $v_a$ ,  $v_b$  and  $v_c$ , respectively. In the switching interval considered,  $v_a$  and  $v_c$  have the maximum and minimum values, respectively, while  $v_b$  is at an intermediate value. Therefore, in the case,  $v_h$  corresponds to the intermediate values,  $v_{mid}$ , along the three references along the fundamental period (see the dashed line in Fig. 2.60), since  $v_a$ ,  $v_b$  and  $v_c$  change position in the different sectors. The continuous line in Fig. 2.61 represents the new modulating signal for one phase.

As mentioned, many other continuous and discontinuous zero-sequence components can be employed in Eq. (2.22), resulting in different non-sinusoidal carrier-based PWM techniques, but their discussion is out of the scope of this chapter.

The combination of the conduction of the switches “P” (upper switches) and the switches “N” (lower switches) in legs  $a$ ,  $b$ , and  $c$  of the inverter in Fig. 2.59a, allows for eight possible switch combinations, denoted by  $SC_i$  ( $i = 0, 1, \dots, 7$ ). Six of these switch combinations,  $SC_1 = PNN$ ,  $SC_2 = PPN$ ,  $SC_3 = NPN$ ,  $SC_4 = NPP$ ,  $SC_5 = NNP$ , and  $SC_6 = PNP$ , apply voltage to the output (active switch combinations) while switch combinations  $SC_0 = NNN$  and  $SC_7 = PPP$  correspond to the short circuiting of the lower switches and of the upper switches, respectively.





**Fig. 2.59** Three-phase sinusoidal PWM: **a** inverter circuit, **b** principle, pole voltage, and inverter output voltage

**Fig. 2.60** Sectors inside one period

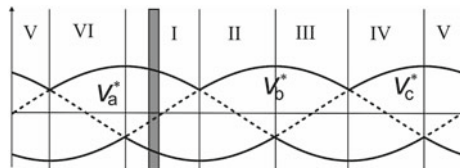
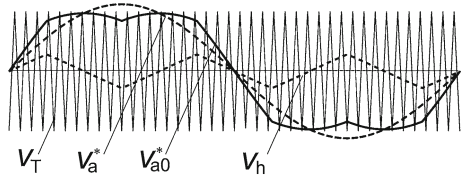
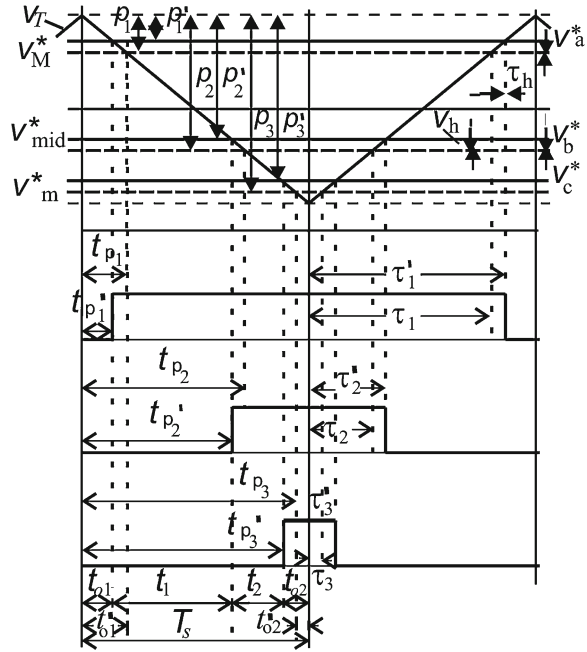


Figure 2.62 shows the representation of the modulated pulse waveforms inside a switching interval of Sector I. The intersection of modulating voltages (references)  $v_M(v_a^*)$ ,  $v_m(v_b^*)$ , and  $v_{mid}(v_c^*)$  with the triangle defines: (1) the pulse widths for each of the phase voltages,  $\tau_1$ ,  $\tau_2$ , and  $\tau_3$ , (2) the distances between the switching instants for phases  $a$ ,  $b$ ,  $c$ , the delay of the first switching procedure  $t_{01}$ , the distances of the switching instants,  $t_1$  and  $t_2$ , and the remaining time of the

**Fig. 2.61** Operation in over modulation region—non-sinusoidal PWM:  $v_a^*$ , modulating signal generated,  $v_{a0}^*$ , and zero-voltage signal  $v_h$  (middle) generated for Symmetric PWM



**Fig. 2.62** Pole voltage pulse width inside a switching interval



sampling period  $t_{02}$ , and (3) the time intervals  $t_{p1}$ ,  $t_{p2}$ , and  $t_{p3}$  (switching delays) before each leg changes in a given switching interval. When the zero-sequence component is added to the sinusoidal reference, the intervals  $t_1$  and  $t_2$  between the phase pulses remain the same. Instead, the pulse widths for each of the phase voltages,  $\tau_1$ ,  $\tau_2$ , and  $\tau_3$ , do change, and become  $\tau_1'$ ,  $\tau_2'$ , and  $\tau_3'$ . Note that, inside the switching interval, the intervals  $t_{01}$ ,  $t_1$ ,  $t_2$ , and  $t_{02}$  indicate the duration of the switch combinations NNN, ONN, PPN, and PPP, which occur in all switching periods inside Sector I. Note, also, that

$$t_z = t_{01} + t_{02} = T_s - (t_1 + t_2) \tag{2.24}$$

In Eq. (2.24),  $t_z = t_{01} + t_{02}$  constitutes the total freewheeling interval. Note, finally, that  $t_{01}$  and  $t_{02}$  are equally distributed at the beginning and at the end of the switching interval. In reality, these zero interval constituents can assume different values provided that the condition in (2.24) is observed.

It is possible to have a digital implementation where the calculation of the pulse widths  $\tau'_1$ ,  $\tau'_2$ , and  $\tau'_3$  in Fig. 2.62 after the addition of the zero-sequence signal  $v_h$ . These are obtained from the triangle equivalences found in that figure [18, 22–25], that is,

$$\tau'_i = \left( \frac{v_j^* + v_h}{E} + \frac{1}{2} \right) T_s \quad (i = 1, 2, 3; j = a, b, c; i \neq j) \quad (2.25)$$

$$t_{01} = T_s - \tau'_M \quad (2.26)$$

$$t_{02} = \tau'_m \quad (2.27)$$

The comparison of  $\tau'_i$  allows to determine  $\tau'_M$ ,  $\tau'_m$ , and  $\tau'_{\text{mid}}$ . This method corresponds to the digital Scalar PWM and DSPWM strategy with direct measurement of the average values of the three modified reference phase voltages at a given switching interval [24].

### 2.5.2.3 Space Vector Modulation

The space vector pulse-width modulation (SVPWM) technique [4, 5] does not consider each of the three-phases as a separate entity. The three-phase voltages are simultaneously performed within a two-dimensional reference frame (plane), the complex reference voltage vector being processed as a whole. Because of its flexibility of manipulation, the SVPWM technique became popular [5, 10, 26, 27].

In a balanced system, the three-phase voltage can be represented by a vector  $v(t)$

$$\vec{v}(t) = \frac{2}{3} \left[ \vec{1}v_{a0}(t) + \vec{a}v_{b0}(t) + \vec{a}^2v_{c0}(t) \right] = Ve^{j\omega_s t} \quad (2.28)$$

where:  $\vec{a} = e^{j\frac{2\pi}{3}} = -\frac{1}{2} + j\frac{\sqrt{3}}{2}$ ,  $\vec{a}^2 = e^{j\frac{4\pi}{3}} = -\frac{1}{2} - j\frac{\sqrt{3}}{2}$ . Variables  $v_{a0}(t)$ ,  $v_{b0}(t)$ , and  $v_{c0}(t)$  are the instantaneous values of the three-phase system defined by the unity vectors  $\vec{1}$ ,  $\vec{a}$ , and  $\vec{a}^2$ .

Consider the eight possible switching configurations  $SC_1 = \text{PNN}$ ,  $SC_2 = \text{PPN}$ ,  $SC_3 = \text{NPN}$ ,  $SC_4 = \text{NPP}$ ,  $SC_5 = \text{NNP}$ ,  $SC_6 = \text{PNP}$ ,  $SC_0 = \text{NNN}$ , and  $SC_7 = \text{PPP}$ . It can be seen that for  $SC_1$   $v_{a0} = V_{dc}/2$ ,  $v_{b0} = -V_{dc}/2$ , and  $v_{c0} = -V_{dc}/2$ . For  $SC_2$ , the values of the variables are  $v_{a0} = V_{dc}/2$ ,  $v_{b0} = V_{dc}/2$ , and  $v_{c0} = -V_{dc}/2$ , and so on. The application of values  $v_{a0}(t)$ ,  $v_{b0}(t)$ , and  $v_{c0}(t)$ , obtained for each of the active switching configurations, into (2.28) results in six active six space vectors,  $\vec{V}_i$  ( $i = 1, \dots, 6$ ), of amplitude  $2V_{dc}/3$  and phase shifted of  $60^\circ$  from each other. For the freewheeling configurations  $SC_0$  and  $SC_7$ , the amplitude of the resultant vectors,  $\vec{V}_0$  and  $\vec{V}_7$  is zero, originating the zero space vectors. Therefore, for each  $SC_i$  ( $i = 1 \dots 6$ ) there is a corresponding vector  $\vec{V}_i$  ( $i = 1 \dots 6$ ), as shown in Fig. 2.63.

Space vector modulation consists in synthesizing a reference vector with the help of two adjacent state vectors, which define the sectors of the three-phase reference voltages, as shown in Fig. 2.64. As shown in Fig. 2.64b for Sector I, the reference vector  $\vec{v}_{dq}^*$  can be synthesized by applying vectors  $\vec{V}_0$ ,  $\vec{V}_1$ ,  $\vec{V}_2$ , and  $\vec{V}_7$  (adjacent vectors) during the intervals of time  $t_0$ ,  $t_1$ ,  $t_2$  and  $t_7$  as defined in the switching pattern in Fig. 2.64c, which obey the volt-second balancing equation

$$V_{dq}^* T_s = V_0 t_0 + V_1 t_1 + V_2 t_2 + V_7 t_7 \quad (2.29)$$

Knowing that:

$$t_z + t_1 + t_2 \leq T_s \quad (2.30)$$

In which:  $t_z = t_0 + t_7$  is the total zero-voltage interval distributed at the beginning,  $t_0$ , and at the end,  $t_7$ , of the switching interval  $T_s$ . In space vector PWM this means that the upper and bottom freewheeling interval are distributed inside the switching interval.

In space Vector PWM where:  $t_0 = t_7$ , and intervals  $t_1$  and  $t_2$  are the same as in Fig. 2.62, but they are calculated from the knowledge of the vector position determined by the angle  $\theta$ , that is,

$$t_1 = \sqrt{3} \frac{V_s}{V_{dc}} T_s \sin\left(\frac{\pi}{3} - \theta\right) \quad (2.31)$$

$$t_2 = \sqrt{3} \frac{V_s}{V_{dc}} T_s \sin(\theta) \quad (2.32)$$

where  $V_s$  is the amplitude of the reference vector,  $\vec{V}_s$ .

Note that the values of the intervals  $t_1$  and  $t_2$ , calculated from (2.31) and (2.32), can also be calculated from the triangle equivalences in Fig. 2.62, that is,

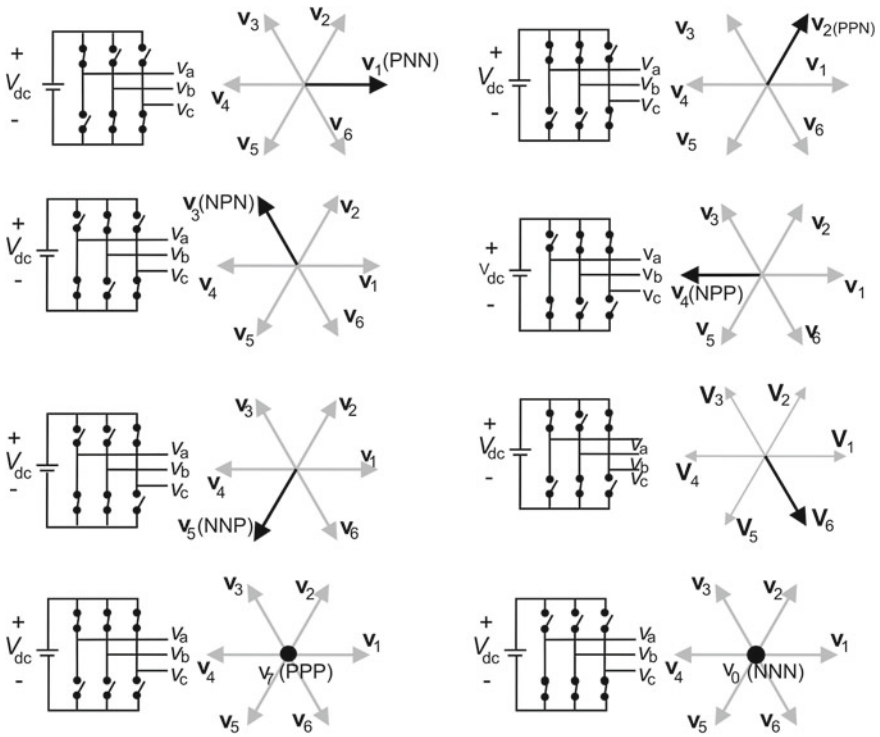
$$t_1 = \frac{T_s}{E} (v_M^* - v_{mid}^*) \quad (2.33)$$

$$t_2 = \frac{T_s}{E} (v_{mid}^* - v_m^*). \quad (2.34)$$

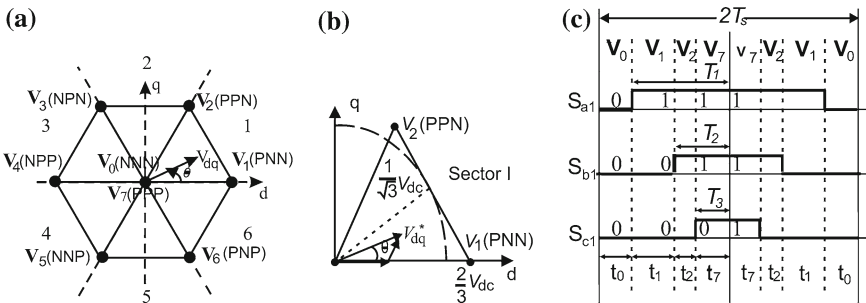
and  $t_{01} + t_{02} = T_s - (t_1 + t_2)$  as in Fig. (2.24).

Note that  $v_M$ ,  $v_m$ , and  $v_{mid}$  can be used to calculate the values of  $t_1$  and  $t_2$  since these durations do not change with  $v_h$ . This technique is known as Hybrid PWM, HPWM [17, 18, 20, 28].

Figure 2.65 shows the block diagram for calculating the gating pulses, that is, the determination of  $v_M$  and  $v_m$  among the three reference voltages, defines  $v_h$  from (2.23), which in turn determines the new modulating voltages with the help of (2.22). The width of the gating pulses can be calculated from either the trigonometric Eqs. (2.31) and (2.32) or the algebraic Eqs. (2.33) to (2.34).



**Fig. 2.63** Relation of the inverter switching configurations and the state vectors

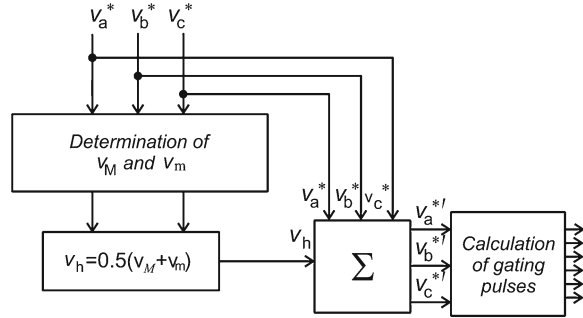


**Fig. 2.64** **a** Space vector diagram and sector definition, **b** synthesis of the reference state vector in Sector I using switching vectors  $\vec{V}_0$ ,  $\vec{V}_1$ ,  $\vec{V}_2$ , and  $\vec{V}_7$ , and **c** switching pattern

### 2.5.3 PWM Techniques for Other Two-Level Converters

In the following section on the PWM techniques for the CSI and the CSR and AC/AC converters will be introduced.

**Fig. 2.65** Block diagram for calculation of the pulse width



### A. Current Source Converters

The three-phase CSI is the dual of the voltage source three-phase inverter [29, 30]. Because of this the line-to-line output voltage waveform of a VSI is the line output current waveform of a CSI. Using this knowledge, the CSI can be controlled by the same PWM techniques used to control the VSI. However, there are two differences [29]:

1. In CSI the current signals are used as references, instead of voltages as in VSI.
2. For VSI, the PWM pattern can be used to directly control the switching devices and in the CSI the phase switching states cannot be used directly to control the switching devices, since these are controlled by line switching states [5]. References [29–31] have established a PWM equivalence between these circuits so that any PWM techniques developed for VSI can also be applied to current-type inverters, such as SHE PWM [32], SVPWM, HPWM, and other techniques, including those of third harmonic injection and discontinuous PWM to reduce losses [11].

High power and its high quality as current source PWM has applications in AC drives, VAR generator, active filters, and superconductive magnetic energy storage (SMES) [33]. But it is much less used than the VSR. The PWM techniques used for the CSI can be directly applied to the CSR. However, the PWM scheme for the CSR must provide an adjustable modulation index for the DC current control in addition to the reduction in the total harmonic distortion. CSR or Buck Rectifier

### B. AC/AC Converters

PWM techniques for indirect and direct (matrix) AC/AC converters will be examined next. Due to the fact that the VSR can be modeled as a controllable DC voltage source, its natural load is a VSI. The connection of these two voltage source converters sharing a common capacitor DC link (as in Fig. 2.40) allows two-way energy flow and four-quadrant operation. This four-quadrant converter is presently applied to asynchronous drives, electric power generation using asynchronous, energy storage systems, like UPS and flywheel energy storage systems, and transmission and distribution systems multilevel converter-based (Universal Power Flow Controller, UPFC, High Voltage DC-Light, HVDC-Light, Dynamic Voltage Regulation, DVR) [34, 35].

The major objective in matrix converters is to simultaneously control their input currents, managing inclusively the reactive power flowing between the grid and the load. This is also the major difficulty found in PWM schemes to control these converters. Many schemes have been proposed to solve this problem [36]. This problem does not exist in indirect converters because of the independent control of the input currents (at the rectifier stage) an output voltages is independent from the control (in the inverter stage) due to the capacitor in DC link. The two-stage direct power converter (DPC) topology has a structure similar to the AC/DC/AC converter, but without the DC link capacitor [37, 38]. Based on this, *dissociation* between input currents and output voltages controls in the matrix converter was proposed in [37]. The space vector modulator implemented includes the adaptation of the DPC duty-cycles to the matrix converter topology.

The technique was also implemented using a generalized PWM strategy similar to those studied for two-level converter to control both input currents and output voltages. This technique is well detailed in [39].

#### ***2.5.4 PWM Techniques for Multilevel Converters***

Multilevel inverters have emerged as the solution for working with higher voltage levels. They have been considered for an increasing number of applications due to not only their high power capability, but also lower output harmonics and lower commutation losses.

The three-level NPC inverter topology shown in Fig. 2.66a will be used as an example. This topology has 12 active switches (note that the number of switches increases with the number of level  $K$ ). In each leg of the inverter, the switches can be positive ( $S_1$  and  $S_2$ ) or negative ( $S_3$  and  $S_4$ ), which in turn can be external ( $S_1$  and  $S_4$ ) or internal ( $S_2$  and  $S_3$ ), in phase  $a$  of inverter. Also, each inverter leg can assume three switching states, “P”, “O”, and “N”, as shown from the equivalent circuit in Fig. 2.66b. Taking into account the three-phases, the inverter has a total of 27 possible combinations of switching states as indicated in the three-level space vector diagram in Fig. 2.67, obtained through the same procedure used for the two-level inverter. Such representation allows not only to establish the correlation between the state vectors and the switching configurations but, also, to visualize the division of the voltage vectors into four groups as a function of the vector amplitude: Large Vectors, when the three pole voltages assume only the states  $P$  and  $N$ ; Medium Vectors, when the three pole voltages assume the states  $P$ ,  $O$ , and  $N$ ; Small Vectors, when the three pole voltages assume only the states  $P$  and  $O$  or  $O$  and  $N$ ; Null Vectors: NNN, PPP, OOO. In SVPWM, in order to optimize the modulation, each sector is typically divided into four triangles (regions 1 to 4). The knowledge of the position of the reference vector inside a region of a certain sector allows for calculating the pulse widths of the gating pulses. One possibility is to consider the space vector diagram as formed of six small two-level hexagons, each of them centered in one vector of the small vectors

$\vec{V}_1, \vec{V}_2, \dots, \vec{V}_6$ , as shown in Fig. 2.67. Using the adjacent state vectors of the small hexagon reproduces a partial reference vector. The reference voltage vector  $V^*$  is then obtained by subtracting the center vector of the corresponding small hexagon from the original reference vector (see vectors in triangle  $D$  of Sector I). This means that in that region the pole voltage modulates, for instance, between  $P$  and  $O$  levels. For a  $K$ -level inverter, its state phase-diagram is simplified to that of a  $K-1$  level inverter and so on, till that of the two-level inverter.

Alternatives are the use of SHE modulation or the use a carrier-based PWM, such as the in-phase disposition (IPD) modulation [6] illustrated in Fig. 2.68a for the three-level inverter ( $K = 3$ ). The number of carrier signals is  $K-1 = 2$ . For this reason, the modulating signal intersects two triangular waves, generating the pulse widths of each pole voltage.

Similar to two-level inverters, the correlation between space vector PWM and hybrid PWM has been established for multilevel inverters [40]. The steps for implementing the symmetrical hybrid PWM will be given next, using the case of a three-level NPC inverter [25] as an example.

Step 1. Determine the values of the three-levels—If these values are nominated as Axis, then the three axes for the case are  $\text{Axis}(1) = +V_{dc}/2$ ,  $\text{Axis}(2) = 0$ , and  $\text{Axis}(3) = -V_{dc}/2$ . A general expression that permits to calculate these values for  $K$  levels is

$$\text{Axis}(k) = \left( \frac{1}{2} - \frac{(k-1)}{(K-1)} \right) v_{dc} \quad (k = 1, 2, \dots, K) \tag{2.35}$$

Step 2. Determine the values of variables  $p_i$  ( $i = 1, 2, 3$ ), as defined in Fig. 2.68b. In this step consider  $v_1^*, v_2^*$  and  $v_3^*$  as the maximum,

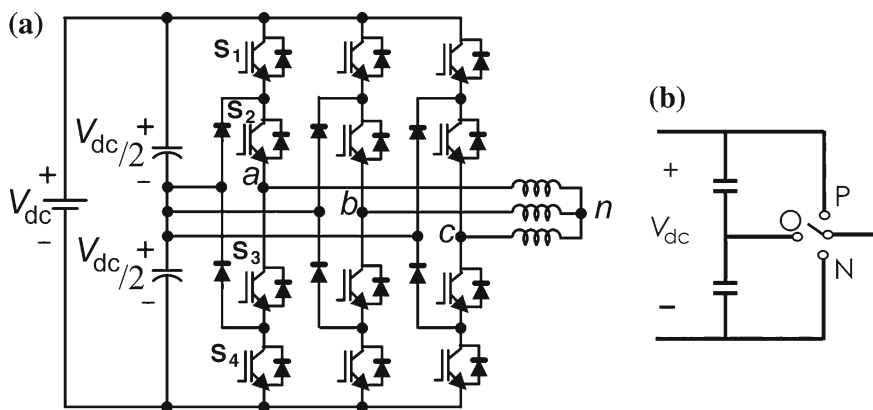
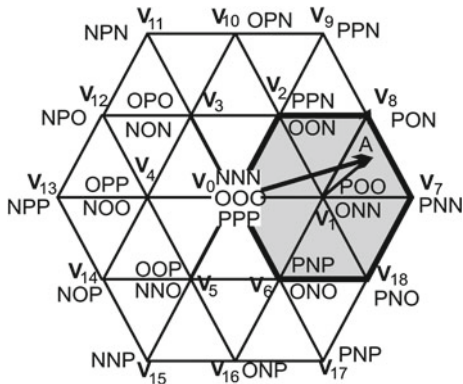


Fig. 2.66 a Three-level NPC inverter topology and b equivalent circuit



**Fig. 2.67** Space vector diagram of a three-level converter



intermediate, and minimum values among the reference signals  $v_a^*$ ,  $v_b^*$  and  $v_c^*$ , respectively, within the switching interval. Remembering that references  $v_a^*$ ,  $v_b^*$  and  $v_c^*$  change for each sector, the values of  $p_i$  can be calculated from

$$\text{If}(\text{Axis}(k) > v_i^* > \text{Axis}(k + 1))$$

then:

$$p_i = \text{Axis}(k) - v_i^* \quad (i = 1, 2, 3) \tag{2.36}$$

where, for the case,  $v_1^* = v_a^*$ ,  $v_2^* = v_b^*$ , and  $v_3^* = v_c^*$ . Then:

$$\begin{aligned} p_1 &= p_{\min} = \frac{V_{dc}}{2} - v_1^* = \frac{V_{dc}}{2} - v_a^* \\ p_2 &= p_{\text{mid}} = 0 - v_2^* = 0 - v_b^* \\ p_3 &= p_{\max} = 0 - v_3^* = 0 - v_c^* \end{aligned} \tag{2.37}$$

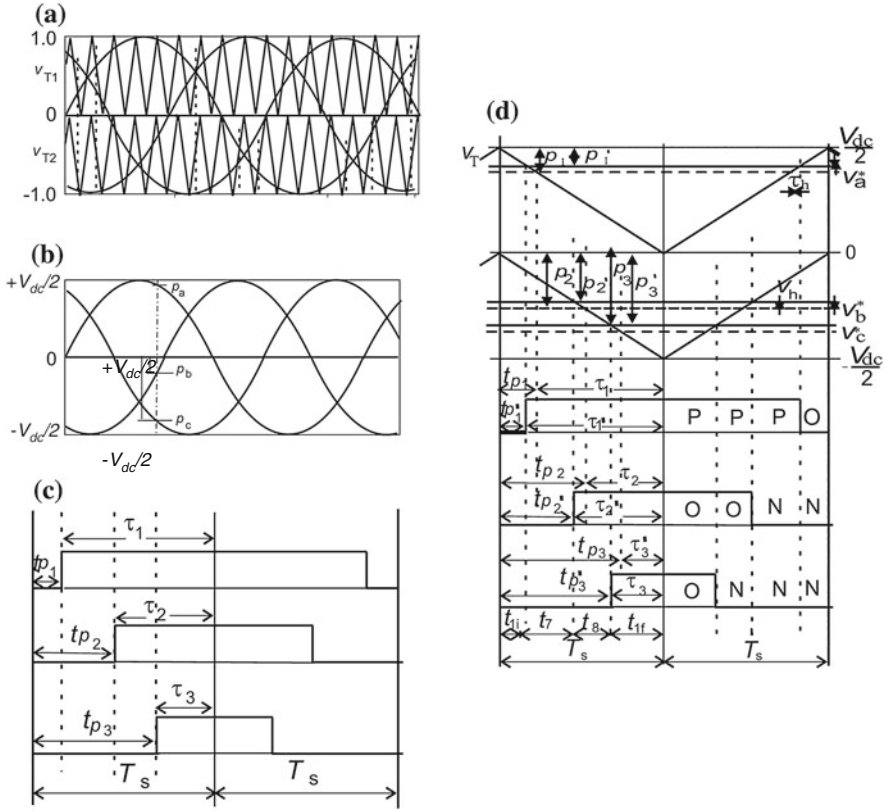
Each of these values is proportional to a corresponding delay time  $t_{pi}$  of the switching pulses for each of the inverter phases, as shown in Fig. 2.68c.

Step 3. Calculate

$$v_h = 0.5 \left( p_{\min} + p_{\max} - \frac{V_{dc}}{2} \right) \tag{2.38}$$

and then find the new references  $v_j^{*h}$  by using (2.22). For the general case,

$$v_h = 0.5 \left( p_{\min} + p_{\max} - \frac{V_{dc}}{K - 1} \right) \tag{2.39}$$



**Fig. 2.68** Three-level inverter: **a** modulation principle (IPD), **b** definition of  $p_i$  ( $i = 1, 2, 3$ ), **c** the relation of  $p_i$  with the pulse delays in the switching interval  $t_{p_i}$ , and **d** the switching interval considering the addition of the zero-sequence signal,  $v_h$

Step 4. Calculate the new  $p_i^{*}$ —When  $v_h$  is added to each reference signal to generate the new references  $v_i^{*}$ , new values  $p_i^{*}$  are generated, as shown in Fig. 2.68d and which are given by:

$$\text{If } (\text{Axis}(k) > v_i^{*} > \text{Axis}(k + 1)), \text{ then } p_i = \text{Axis}(k) - v_i^{*} \quad (i = 1, 2, 3) \tag{2.40}$$

and determine  $t'_{p_i}$  from

$$t'_{p_i} = \frac{2p_i^{*}T_s}{V_{dc}}, \quad (i = 1, 2, 3) \tag{2.41}$$

The corresponding generalized expression for (2.41) is

$$t'_{pi} = \frac{p'_i T_s}{\left(\frac{V_{dc}}{K-1}\right)} \quad (2.42)$$

From Fig. 2.68d, the width signals to command the inverter switches ( $\tau'_1$ ,  $\tau'_2$  and  $\tau'_3$ ) can be found from

$$t'_i = T_s - t'_{pj}, \quad (i = 1, 2, 3). \quad (2.43)$$

If necessary, the line pulse widths can be easily calculated.

Step 5. The determination of the pole voltages ( $v_{ao}$ ,  $v_{bo}$ , and  $v_{co}$ ) for  $k = 1, 2, \dots, (K - 1)$  is given by:

$$\text{If } (t < t'_{pi}) \text{ or } (t > t'_{pi} + 2\tau'_{pi}), v_{jo} = \text{value of axis } (k + 1) \quad (2.44)$$

$$\text{If } (t'_{pi} < t < t'_{pi} + 2\tau'_{pi}), v_{jo} = \text{value of axis } (k) \quad (2.45)$$

For  $K = 3$ ,

$$\begin{aligned} &\text{If } (t < t'_{pi}) \text{ or } (t > t'_{pi} + 2\tau'_{pi}), v_{jo} = 0 \text{ and} \\ &\text{If } (t < t'_{pi}) \text{ or } (t > t'_{pi} + 2\tau'_{pi}), v_{jo} = +V_{dc}/2 \end{aligned} \quad (2.46)$$

## 2.6 Conclusions

This chapter gives an overview of PE. The authors expect to help readers to understand the main principles and obtain base for further studies. Besides the examination of basic devices and converter topologies, the digital PWM control was largely focused for control scheme since this is an important topic. However, further reading is highly recommended and future expectation in PE can be found in [41–44]. Also, there is an extensive technical literature on topics not covered in this chapter including: isolated DC-to-DC converters [45], soft switching [1, 45, 46], phase-controlled converters [47], and control design [45, 48].

## References

1. Kassakian J, Schlecht M, Verghese G (1991) Principles of power electronics. Addison-Wesley, Reading
2. Batarseh I (2004) Power electronic circuits. Wiley, New York
3. Mohan N, Undeland T, Robbins W (2003) Power electronics: converters, applications, and design. Wiley, New York
4. Hart D (2011) Power electronics, 2nd edn. McGraw Hill, New York
5. Holmes D, Lipo T (2003) Pulse width modulation for power converters. IEEE/Wiley-Interscience, New York
6. Wu B (2006) High-power converters and AC drives. Wiley, New York
7. Rossetto L, Spiazzi G, Tenti P (1994) Control techniques for power factor correction converters. In: Proceedings of PEMC, pp 3310–1318
8. Buso S, Matavelli P (2006) Digital control in power electronics. Morgan & Claypool, San Rafael
9. Rodriguez J, Dixon J, Espinoza J et al (2005) PWM regenerative rectifiers: state of the art. IEEE Trans Ind Electron 52:5–55
10. Holtz J (1994) Pulse width modulation for electronic power conversion. Proc IEEE 82:1194–1214
11. da Silva E, dos Santos E, Jacobina C (2011) Pulsewidth modulation strategies. IEEE Ind Electron Mag 5:37–45
12. Schönung A, Stemmler H (1964) Static frequency changers with sub-harmonic control in conjunction with reversible variable speed AC drives. Brown Boveri Rev 51:555–577
13. Bowes S, Mount M (1981) Microprocessor control of PWM inverters. IEEE Proc B:293–305
14. Depenbrock M (1977) Pulse width control of a 3-phase inverter with non-sinusoidal phase voltages. In: Proceedings of the IEEE international semiconductor power converter conference, ISPC'77, pp 399–403
15. Houldsworth J, Grant D (1984) The use of harmonic distortion to increase the output voltage of a three-phase PWM inverter. IEEE Trans Ind Appl IA-20:1224–1228
16. Kolar JW, Ertl H, Zach FC (1990) Influence of the modulation method on the conduction and switching losses of a PWM converter system. In: Proceedings of the IEEE-IAS'90, pp 502–512
17. Sun J, Grotstollen H (1996) Optimized space vector modulation and regular-sampled PWM: a reexamination. In: Proceedings of the IEEE-IAS'96, pp 956–963
18. Blasko V (1996) A hybrid PWM strategy combining modified space vector and triangle comparison methods. In: Proceedings of the IEEE PESC, pp 1872–1878
19. Hava A, Kerkman R, Lipo T (1998) A high-performance generalized discontinuous PWM algorithm. IEEE Trans Ind Appl 34:1059–1071
20. Alves A, da Silva E, Lima A, Jacobina C (1998) Pulse width modulator for voltage-type inverters with either constant or pulsed DC link. In: Proceedings of IEEE IAS'98, pp 229–1236
21. Seixas P (1988) Commande numérique d'une machine synchrone autopilotée. D.Sc. Thesis, L'Institut Nationale Polytechnique de Toulouse, INPT, Toulouse
22. Holmes D (1996) The significance of zero space vector placement for carrier-based PWM schemes. IEEE Trans Ind App 32:1122–1129
23. Grotstollen H (1993) Line voltage modulation: a new possibility of PWM for three phase inverters. In: Proceedings of the IEEE IAS'93, pp 567–574
24. Jacobina C, Lima A, da Silva E, Alves R, Seixas P (2001) Digital scalar pulse-width modulation: a simple approach to introduce non-sinusoidal modulating waveforms. IEEE Trans Power Electron 16:351–359
25. Oliveira A, da Silva E, Jacobina C (2004) A hybrid PWM strategy for multilevel voltage source inverters. In: Proceedings of the IEEE PESC'2004, pp 4220–4225

26. Van der Broeck H, Skudelny H, Stanke G (1988) Analysis and realization of a pulse width modulator based on voltage space vector. *IEEE Trans Ind Appl* 24:142–150
27. Jacobina C, Lima A, da Silva E (1977) PWM space vector based on digital scalar modulation. In: *Proceedings of the IEEE PESC*, pp 100–105
28. Zhou K, Wang D (2002) Relationship between space-vector modulation and three-phase carrier-based PWM: a comprehensive analysis. *IEEE Trans Ind Appl* 49:186–196
29. Ledwich G (2001) Current source inverter modulation. *IEEE Trans Power Electron* 6:618–623
30. Dahono P, Kataoka T, Sato Y (1997) Dual Relationships between voltage-source and current-source three-phase inverters and its applications. In: *Proceedings of the PEDS*, pp 559–565
31. Zmood D, Holmes DG (2001) Improved voltage regulation for current-source inverters. *IEEE Trans Ind Appl* 37:1028–1036
32. Espinoza J, Joós G, Guzmán J et al (2001) Selective harmonic elimination and current/voltage control in current/voltage source topologies: a unified approach. *IEEE Trans Ind Electron* 48:71–81
33. Zargari N, Geza J (1993), A current-controlled current source type unity power factor PWM rectifier. In: *Proceedings of the IEEE IAS'93*, pp 793–799
34. Acha E, Agelidis V, Anaya-Lara O et al (2002) *Power electronic control in electrical systems*. Newnes, Oxford
35. Simões G, Farret F (2008) *Alternative energy system*. CRC Press, Boca Raton
36. Casadei D, Serra G, Tani A et al (2002) Matrix converter modulation strategies: a new general approach based on space-vector representation of the switch state. *IEEE Trans Ind Electron* 49:370–381
37. Huber L, Borojevic D (1995) Space vector modulated three-phase to three-phase matrix with input power factor correction. *IEEE Trans Ind Appl* 31:1234–1246
38. Klumpner C, Blaabjerg F (2005) Modulation method for a multiple drive system based on a two-stage direct power conversion topology with reduced input current ripple. *IEEE Trans Power Electron* 20:922–929
39. Accioly AGH, Bradaschia F, Cavalcanti M et al (2007) Generalized modulation strategy for matrix converters, part I. In: *Proceedings of the IEEE PESC'07*, pp 646–652
40. Wu H, He M (2001) Inherent correlation between multilevel carrier-based PWM and space vector PWM: principle and application. In: *Proceedings of the IEEE PEDS'01*, pp 276–281
41. Strzelecki R, Zinoviev GS (2008) Overview of power electronics converters and controls. In: Strzelecki R, Benysek G (eds) *Power electronics in smart electrical energy networks*. Springer, London
42. Lorenz, L (2009) Power semiconductor devices and smart power IC's: the enabling technology for future high efficient power conversion systems. In: *Proceedings of the IPEMC*, pp 193–201
43. Shigekane H, Fujihira T, Sasagawa K et al (2009) Macro-trend and a future expectation of innovations in power electronics and power devices. *Proceedings of the IPEMC*, pp 35–39
44. Bose B (2006) *Power electronics and AC drives*. Elsevier, Amsterdam
45. Kazimierczuk M (2008) *Pulse-width modulated DC–DC power converters*. Wiley, New York
46. Krein P (1998) *Elements of power electronics*. New York, Oxford
47. Shepherd W, Zhang L (2004) *Power converter circuits*. CRC, New York
48. Erickson R, Maksimovic D (2001) *Fundamentals of power electronics*. Springer, New York

# Chapter 3

## Photovoltaic Power Electronics

Felix A. Farret

**Abstract** Photovoltaic electricity (PV) is produced by semiconductor devices capable of directly converting the incident solar energy into DC current with a theoretical efficiency varying from 3 to 31 %. Such efficiencies will depend on the manufacturing technology, incident light spectrum, panel tilt, cell temperature, panel design, surface deposits, shadows, and materials on the solar cell. The photovoltaic electric system is usually constituted by many photovoltaic solar cells arranged in modules or arrays of modules. Many algorithms of control and power electronics arrangements have been proposed in the literature to operate such systems going from interconnections of individual cells to the connection of a single module or groups of them to the grid. Electronically, interconnected panels can be adapted to best suit a given situation like operation under intermittent shadows, network surges, load insertion, and other peculiarities. This chapter includes power electronics, digital controls, sun tracking, and remote monitoring as the basis for the modern PV production of electricity from solar radiation.

### 3.1 Introduction

Solar energy is vital for our planet. As a whole, it is the most perennial, silent, and nonpolluting source of energy. It has been responsible for all life forms on the planet for millions of years. It is the largest renewable energy source and the origin of many others on Earth such as: wind, hydro, photosynthesis, superficial geothermic, sea thermal, and sea tides.

---

F. A. Farret (✉)  
Federal University of Santa Maria, Campus-Camobi, Santa Maria, RS, Brazil  
e-mail: fafarret@gmail.com

The sunlight energy produces an average of  $1,372 \text{ W/m}^2$  on the earth’s outer atmosphere, which is filtered through the whole atmosphere and received at the surface at about  $1,000 \text{ W/m}^2$  or less, an average of  $345 \text{ W/m}^2$ . Most of the energy has wavelengths in the range of  $300 \text{ nm} \leq \lambda \leq 3,000 \text{ nm}$  (average  $\lambda = 556 \text{ nm}$ ).

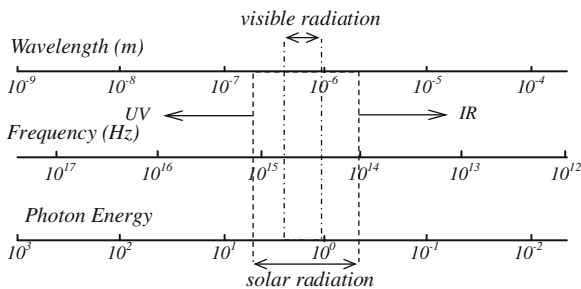
Solar energy can be captured as heat (thermal energy) and by photovoltaic conversion yielding directly electrical energy. Variations in surface energy affect the potential capture. On their way to the Earth surface the sunrays go through air layers, clouds, and haze, reducing the received surface energy. Any flat-plate absorber directed normally to the sun will receive energy that can vary according to the amount of atmosphere path through (overhead air mass  $\equiv 1$ ). Because of this, the total specific radiant power, or radiant flux, per area reaching the Earth is defined as Spectrum AM (air mass) 0 (extraterrestrial). If the Sunray is perpendicular to the Earth’s surface, sunlight only has to pass once through the air mass of the atmosphere. Therefore, this state is called AM 1. In all other cases, the route of the solar radiation through the atmosphere is longer. Therefore, it depends on the Sun’s height. As a worldwide terrestrial average, the Spectrum AM 1.5 is used, but the Solar “constant” varies with sun radiation and measurement accuracy.

The received energy around the world varies due to local cloud attenuation reflecting about 18 % of the sunlight back into space, 9 % is scattered backwards by air molecules and 9 % is actually directly reflected off the surface back to space. Therefore, the travel through the atmosphere decreases the radiation at the Earth’s surface to less than 40 % than the level in the stratosphere. As a result, the received energy by direct normal radiation, for example in Arizona, is 5.0–5.5 kWh/(m<sup>2</sup>-day). In the USA, daily solar energy varies from less than 3.0–7.0 kWh/(m<sup>2</sup>-day).

Solar irradiance decreases with the square of the distance to the Sun. Since the distance of the Earth to Sun changes during the year, solar irradiance outside the Earth’s atmosphere also varies between 1,325 and 1,420 W/m<sup>2</sup>. In March, the solar irradiance is below 600 W/m<sup>2</sup>—a factor to be considered when designing PV-powered satellites.

The irradiance is measured in W/m<sup>2</sup> (power) and has the symbol  $E$  and depends on the amount of energy contained in the light photons and on the wavelength (see Fig. 3.1). When integrating the irradiance over a certain period of time it becomes

**Fig. 3.1** Solar radiation and the visible spectrum



the solar irradiation (energy). Irradiation is measured in either  $J/m^2$  or  $Wh/m^2$  (energy), and represented by the symbol  $H$ . For daylight purposes, only the visible part of the sunlight is considered.

To have a rough evaluation of how much solar energy strikes earth some figures can be discussed as follows. The Sun gives off  $3.9 \times 10^{26}$  W and the Earth intercepts this energy equal to a disk as big as its diameter. The Earth's radius is 3,393 km, so the Earth's solar interception area is  $\pi \times 3,393 \times 10^6$ , or  $3.62 \times 10^{13}$  m<sup>2</sup>. The amount of power crossing Earth's orbit is 1,388 W/m<sup>2</sup> therefore the Earth intercepts  $5.02 \times 10^{16}$  W or 50 quadrillion W/day. The direct and global radiation at a 37° tilt defined by the American Society for Testing and Materials (ASTM) norm G173-03 is depicted in Fig. 3.2 [1].

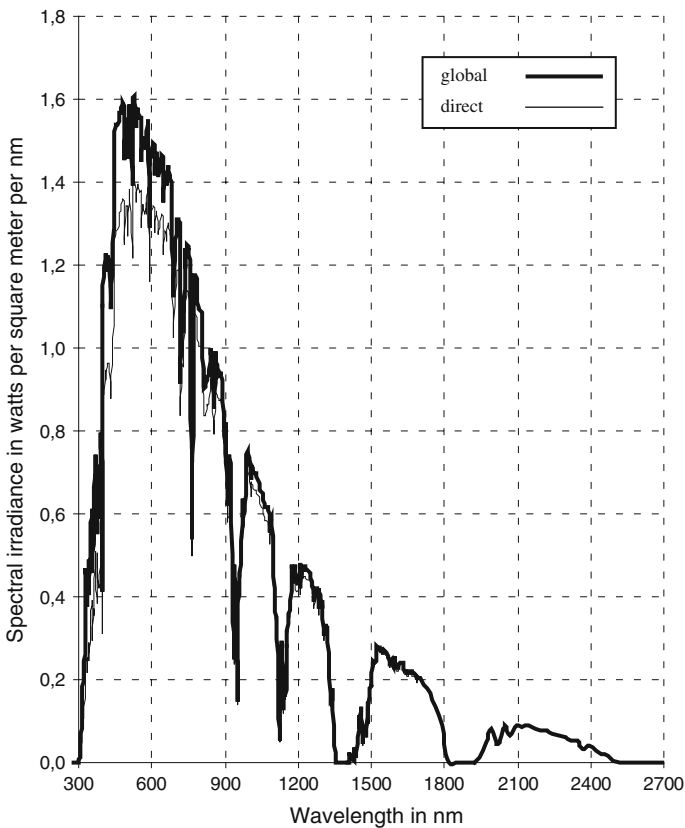


Fig. 3.2 Direct and global irradiance 37 deg tilt (ASTM G173-03)



## 3.2 PV Energy Basics

Solar energy can be directly or indirectly converted into electricity:

1. Indirectly by transforming solar radiation into heat, vapor, and then electricity such as the large-scale applications using: parabolic plate, parabolic trough, or tower of energy to concentrate heat on a boiler with efficiency between 50 and 74 %.
2. Directly by transforming solar light into electricity such as photovoltaic whose current commercial converting efficiency is between 3 and 25 %.

### 3.2.1 PV Energy Generation

The generation of photovoltaic electrical power with modules is constituted of many photovoltaic solar cells arranged in modules and arrays of modules. Every module must face South in the northern hemisphere and North in the southern hemisphere, depending on the local use interests. The recommended panel tilt angle can be calculated by using the site latitude plus 15–20°. Many algorithms of control have been proposed in the literature for interconnections of the individual cells to the connection of a full module or group of them to the grid. For best results, it is necessary to alter the interconnection schemes of each panel in a power system to find the best configuration to a given situation such as operations under intermittent shadows, network surges, load insertion, and other peculiarities. Power electronics, digital controls, and remote monitoring are the basis for production of electricity from solar radiation.

Photovoltaic electrical power generation is a very attractive means to produce energy for several reasons:

- It is quick to install.
- It is modular.
- The solar energy that is produced can match well with daylight loads.
- The systems do not produce noise.
- The power density (power/kg) is high.
- It does not produce pollution.
- It has no moving parts.
- Low maintenance.
- It is highly portable.
- Highly reliable and can produce power for a long period of time.

The manufacturing of solar cells is usually in the form of fine films or wafers. These semiconductor devices are able to directly convert the solar radiant energy light into electricity with modules constituted of many photovoltaic solar cells. The radiant energy is not continuous but according to Max Planck can exist only in

quanta or photons. The number of photons is associated with light of frequency  $f$  (in hertz), each of which has an energy  $hf$  (in Joules) where  $h$  is the Planck's constant. So the more intense the sunlight, the larger number of photons will be present.

There is a certain amount of energy being carried with each photon. This energy will vary depending on the light color that depends on the light frequency. Semiconductor materials can be technologically arranged to let photon energy be transferred into their atoms. The electron in the valence band will leave that energy level of the atom's core, which is filled with protons and neutrons. The electron in the conduction band is the result of the energy received from outside the atom and is called free electron. These bands are illustrated in Fig. 3.3.

Photons from the sun's energy can reach the atom through solar radiation. The amount of photons with  $300 \text{ nm} \leq \lambda \leq 3,000 \text{ nm}$  reaching the Earth is:

$$\text{photon flux/m}^2\text{s} \approx 3.44 \times 10^{21} \text{ photons/m}^2\text{s} \tag{3.1}$$

For a  $\lambda = 500 \times 10^{-9}$ , every photon stores:

$$E = \frac{hc}{\lambda} = \frac{(6.63 \times 10^{-34} \text{ J/s}) \times (3.0 \times 10^8 \text{ m/s})}{500 \times 10^{-9} \text{ m}} = 3.978 \times 10^{-19} \text{ J/photon} \tag{3.2}$$

where

$h$  is the Max Planck constant,

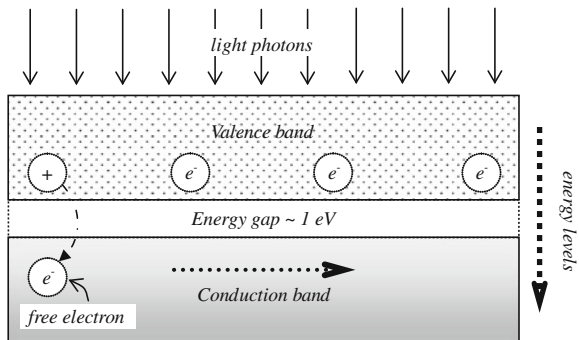
$c$  Is the light speed.

Multiplying Eq. (3.1) by Eq. (3.2) gives the power flux expressed as:

$$G_{sc} \approx (3.44 \times 10^{21} \text{ photons/m}^2\text{s}) \times (3.978 \times 10^{-19} \text{ J/photon}) = 1,367 \text{ kW/m}^2$$

This is the power peak reaching the outer atmosphere of the Earth fetching in it heat and light. Solar light can be directly converted into electricity with modules constituted of many photovoltaic solar cells.

**Fig. 3.3** Energy levels in semiconductor atoms



When dealing with light radiation measurements there are always terms that may look complex at first sight. They depend on the study field in consideration. Table 3.1 lists some of these units. One of these terms is the radiant flux, which gives the number of joules per second (power in watts). Irradiance is used when the electromagnetic radiation from the sun is incident on a surface and it is measured in  $\text{W}/\text{m}^2$ . Irradiance due to solar radiation is also called insolation. By its turn, irradiation is defined as the total radiant power density incident upon a receiving surface along a period of time in  $\text{Wh}/\text{m}^2$  or  $\text{J}/\text{m}^2$ .

Illumination is the ability of the human eye to see different wavelengths of radiation which is the radiant power density weighted in proportion to the standard luminosity intensity. The luminous flux is measured in lumen, so that  $1 \text{ lm} = 0.0016 \text{ W}$  for yellow–green light. One candlepower corresponds to a total light flux of 12.5664 lm. The standard illumination wavelength curves go from about 0.2 to 0.8  $\mu$ , covering the ultraviolet (UV) radiation to the infrared (IR) energy. In particular, pyranometers are frequently used to measure broadband solar irradiance (UV + IR + light) or the solar radiation flux density (in watts per square meter) on planar surfaces like in meteorology, climatology, solar energy studies, and building physics.

### 3.2.2 Electrical Efficiency

The electrical power supplied to the load has to pass through several pieces of equipment and steps: the PV module itself, DC–DC converter, DC–AC inverter, sun tracker, maximum power point tracker, electronic controllers, battery bank, and battery charge/discharge regulator. All these energy processors have their own characteristic efficiency and if they are not properly dimensioned, the overall efficiency will degrade itself causing heavy waste of energy. To evaluate that, there are two measurable types of efficiency in PV systems: the panel efficiency across its terminals and the PV generating system efficiency. The panel efficiency is obtained from the photo conversion efficiency of a PV cell defined as:

$$\eta_{\text{pv}} = \frac{P_{\text{dc}}}{P_{\text{irr}}} \quad (3.3)$$

where

$P_{\text{dc}}$  is the module DC output power,

$P_{\text{irr}}$  is the irradiance level on the panel surface.

The efficiency levels of the panel vary during the day according to the irradiance levels, temperature, and other constructional factors. When all parts of the whole PV system are taken into consideration but the load, the PV system efficiency will be given as:

**Table 3.1** SI radiometry units

Quantity	Symbol	Unit	Notes
Radiant energy	$Q_e$	J	Energy
Radiant flux	$\Phi_e$	W	Radiant energy per unit time, also called <i>radiant power</i>
Spectral power	$\Phi_e$	W/m	Radiant power per wavelength
Radiant intensity	$I_e$	W-s/r	Power per unit solid angle
Spectral intensity	$I_e$	W-s/r-m	Radiant intensity per wavelength
Radiance	$L_e$	W-s/r-m <sup>2</sup>	Power per unit solid angle per unit <i>projected</i> source area and confusingly called “intensity” in some other fields of study.
Spectral radiance	$L_{e,\lambda}$ or $L_{e,\nu}$	W-s/r-m <sup>3</sup> or W-s/r-m <sup>2</sup> -nm	Commonly measured in W-s/r-m <sup>2</sup> -nm with surface area and either wavelength or frequency
Irradiance	$E_e$	W/m <sup>2</sup>	Power incident on a surface, also called <i>radiant flux density</i> and sometimes confusingly called “intensity” as well
Spectral irradiance	$E_{e,\lambda}$ or $E_{e,\nu}$	W/m <sup>3</sup> or W/m <sup>2</sup> -z	Commonly measured in W/m <sup>2</sup> -nm or 10 <sup>-22</sup> W/m <sup>2</sup> -Hz, known as solar flux unit

Source [http://en.wikipedia.org/wiki/Template:SI\\_radiometry\\_units](http://en.wikipedia.org/wiki/Template:SI_radiometry_units)

$$\eta_s = \frac{P_o}{P_{\text{irr}}} \quad (3.4)$$

where

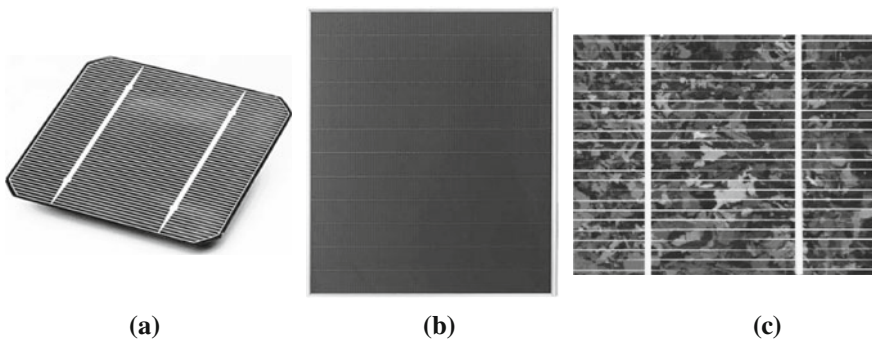
$P_o$  is the output power.

### 3.2.3 Construction of PV Cells and Panel Modules

Photovoltaic electricity is produced by semiconductor devices capable of directly converting the incident solar energy into DC current with a theoretical efficiency varying from 3 to 31 %, depending on the manufacturing technology, incident light spectrum, panel tilt, cell temperature, panel design, deposits, shadows, and materials on the solar cell. Individual wafers are sliced from ingots using wire saws and then subjected to a surface etching process. In this process, the cell adopts an individual shape so as to fit it with others installed on the same panel.

Solar cells created from monocrystalline technology are cut into wafers from a silicon ingot grown from a single crystal; in other words, a crystal that has grown in only one plane (or one direction) (see Fig. 3.4). Single crystalline wafers are more expensive to manufacture and typically they have a slightly higher efficiency than conventional polycrystalline cells resulting in smaller sized individual cells, and thus typically in a slightly smaller module.

Solar cells created from polycrystalline technology are cut from a silicon ingot that is grown from multifaceted crystalline material, or a crystal that grows in multiple directions. Polycrystalline solar cells typically have a slightly lower efficiency resulting in larger sized individual cells, and thus typically a slightly larger module.



**Fig. 3.4** Appearance of the three most common types of solar cells. **a** Monocrystalline. **b** Amorphous thin-film (Sharp's). **c** Polycrystalline

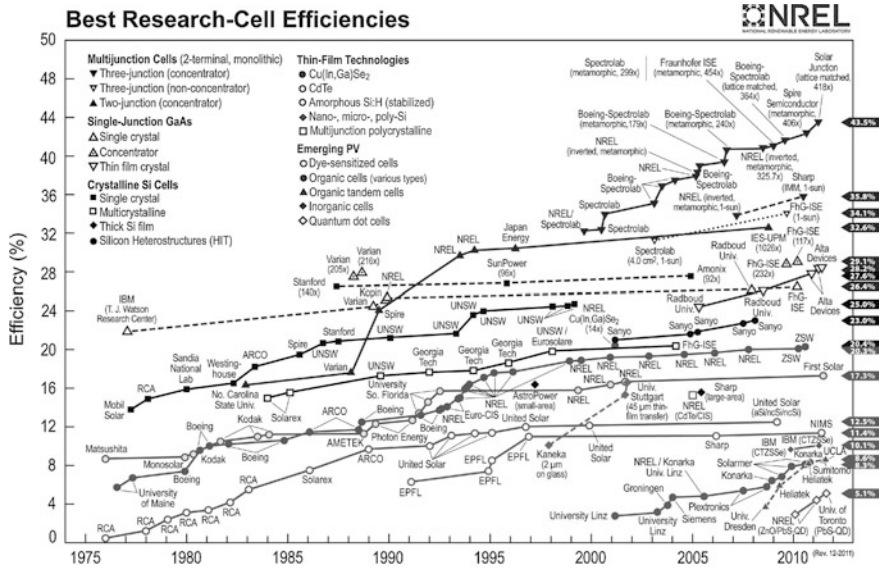


Fig. 3.5 Research-cell efficiencies of PV modules

Amorphous silicon wafers have no crystal structure and are gradually degraded by exposure to light. The mechanism of degradation is called the Staebler–Wronski effect. Better stability requires the use of thinner layers in order to increase the electric field strength across the material. However, this reduces light absorption and hence the cell efficiency. It is important to bear in mind that a 100 W module is a 100 W module whether it was made from polycrystalline cells, monocrystalline, or amorphous cells; the panel area is certainly different. Figure 3.5 illustrates the studies on some of these PV materials in terms of efficiency.

### 3.2.4 PV Modules and Strings

The voltage across a single wafer is typically 0.5 V at a current of 5 A. These wafers are grouped in a series–parallel connection to form a module or solar panel. One or more of the solar modules constitute a solar array to form a power system. The whole solar power system is usually constituted of additional items including: structures or support of light metal such as aluminum, sun trackers, power converters, bank or set of batteries, indicator of battery charge level, and points of load consumption. Furthermore, the photovoltaic plant needs a place where the solar panels will be positioned, which should be an open area without constant shadows and close to the points of load consumption or to the grid to avoid mismatch losses and unexpected operations.

### 3.2.5 Mismatch Losses

Mismatch losses are related to the adverse operation of a PV panel by defective or shaded cells such as the presence of dirt, changes in temperature, damaged cells, and nonuniform irradiation or partial shadows. The defective or shaded cells will let currents from other cells go through its stray parallel resistance producing a reverse voltage. After having a cell fail in the panel array, the rest of the array can force the current through itself, producing a significant temperature rise in the other cells and leading to further damage. These effects can be minimized by anti-parallel power diodes in the module wiring [2, 3]. The operating module or array on which reverse voltage appeared across a defective or shaded cell can be automatically bypassed by this diode providing an alternative path for current from other cells. These reverse current blocking diodes may be used in series with the solar arrays in case the solar panel supplies battery charging or is connected in parallel with other arrays.

According to the manufacturers, the use of blocking diodes is recommended in most applications of 24 V or higher using multiple parallel circuits. It is recommended to use Schottky diodes in these cases placed in the positive pole of the wiring box. The main purpose of the reverse biased diode is to prevent the current from flowing backwards through the cells in dark conditions or into a faulty parallel string. Such conditions affect the efficiency and operation of the panels and may cause heavy losses and damages [2–5].

Mismatching may occur due to internal or external cell events and it is still an open technical issue. The internal mismatch is linked to variations in the PV cell parameters with the temperature and the fabrication process. The external mismatch is linked to any possible external phenomenon disturbing the photo current intensity on the cells. The external events are mostly related to transient shadows, permanent shadows, shadow intensity, and dust on the panel cover. Most of these loss effects are caused randomly and they have to be dealt with as such. All of these events affect the cell parameters and are related to the maximum power point (MPP) of the PV plant. These influences come with the number of modules per string, the number of strings, the shading factor, bypassing diodes, and the topology.

Only the selection of panel topology may not be effective against internal mismatching. A better way to fight internal mismatching is mitigating it through the connection of a set of modules with very low variation in their parameters. Some topologies are very efficient in mitigating these effects in some cases, but each shadow may have a different influence and may need a specific topology that best mitigates these types of losses.

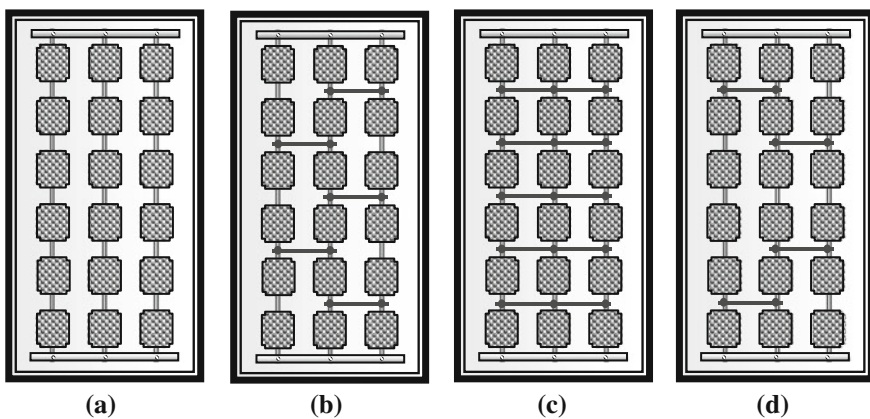
The best mitigation of the external mismatching is through different arrangements of the cell strings in the modules by the use of electronic switching such as: (a) in series–parallel strings [5, 6]; (b) in series with interconnection between them following a bridge-like shape known as bridge-like; (c) all modules connected in series with interconnections in parallel, called total cross tied; and (d) the modules

connected in series and with two connections and two holes known as a honey comb [7–11]. Figure 3.6 displays the four most common internal topologies of PV cell arrangements of photovoltaic panels.

Each shadow needs a different and specific topology to best mitigate the mismatching losses giving always at least two pathways for the output current. Figure 3.7 shows an example of a PV plant topology and its connection to the grid. The interconnection between solar cells is a subject related to power electronic switching and control. Artificial intelligence could be of good help in many cases. The best connection between these pairs has to take into account several factors such as: type of module interconnection, shade scenario, DC bus voltage, power electronic devices, overall costs, and environment [11, 12].

Short and wide shadows do not seem to be mitigated by any of the currently studied topologies. A short and narrow shadow can be expressed by a single-shaded module. The evolution of the power loss with the shading factor indicates that the shadow distribution is strongly affected by the shading factor and the bypass diodes. Hence, the total cross-tied topology is best adapted for low shading factors, before the activation of the bypass diodes. After these became biased, the performance of the series–parallel topology improves, while performance of the total cross-tied topology deteriorates.

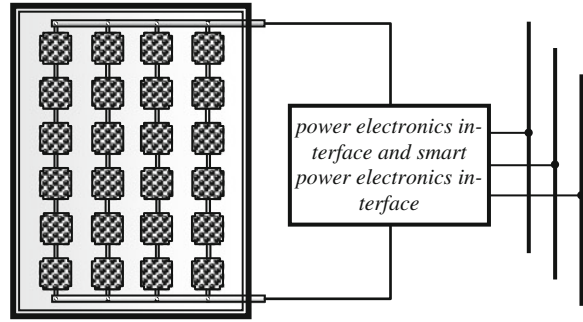
Some experimental works on alternative array configurations show that modifying the module configuration scheme inside a PV plant can raise the maximum temperature by up to 4 %, especially in partially shaded conditions with respect to traditional series–parallel connection [8–12]. Automated DC electronic switches should be used to modify the configurations on-line according to some control strategies for degraded mode operations. Electronic switching may be a very costly solution and it has to be carefully compared with other ways of increasing efficiency gains.



**Fig. 3.6** The four commonest internal topologies of cell arrangements series parallel (a), bridge-like (b), total cross-tied (c), and honey comb (d)



**Fig. 3.7** A model of PV panel integration



### 3.3 Determination of PV Panel Parameters

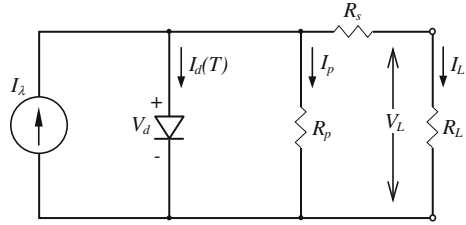
Under the point of view of maximum power transfer from a source to its load, it is theoretically known from the basic circuit theory that the impedance of the power generator must match the load impedance, as discussed in Sect. 3.4. If it has produced more energy than the load is able to absorb the excess will have to be stored. However, energy storage demands for inherent additional losses. This excess of energy can be dissipated in heaters, coolers, and electrolysis to produce hydrogen, and/or battery charging. This will be reflected in economical and energy losses and in a lowered utilization factor.

#### 3.3.1 Models of PV Cells

When considering solar panels, as any other alternative source of energy, the maximum power transfer to the load is more important than the maximum efficiency, since if the sunlight is not used at the moment it is available in nature it will be useless later on. Of course, efficiency is important, however, the efficiency of commercial silicon-based photovoltaic modules is still much lower than 30 % as discussed in Sect. 3.2.2. Furthermore, the output power of a solar panel has strong dependence on the climate conditions, forcing extraction of all possible energy whenever it happens. Thus, the correct modeling of a solar cell becomes necessary, either for a good panel-array design or to enjoy the correct knowledge of the PV behavior when connected to the load.

A reasonable representation of a PV cell has to take into account its current versus voltage output characteristic. This is a very nonlinear relationship and has moderate complexity, consisting of several parameters that need to be adjusted from experimental data using actual devices [13–15]. Such characteristics can be mathematically modeled by an electric equivalent circuit that is usually composed of a DC current source, a diode and two resistances, as shown in Fig. 3.8. Sometimes this model includes a stray capacitance across the parallel resistor  $R_p$  in such a way that a

**Fig. 3.8** One diode equivalent circuit of a photovoltaic cell



high frequency switching distortion may be included. It is clear from this model that PV solar panels are closer to a current source than any other alternative sources such as fuel cells and rotating generators, which are essentially voltage sources.

The output current of a PV panel can be derived from the Kirchoff's law, as depicted in Fig. 3.8, to give  $I_L = I_\lambda - I_d - I_p$  where  $I_L$  is the load current,  $I_\lambda$  is the photocurrent,  $I_d$  is the internal diode current and  $I_p$  is the shunt current across the p-n junction.

The internal diode current is given by the Shockley's Equation (3.5) as:

$$I_d = I_s(e^{qV_d/\eta kT} - 1) \tag{3.5}$$

then

$$I_L = I_\lambda - I_s(e^{qV_d/\eta kT} - 1) - V_d/R_p \tag{3.6}$$

where

$I_s$  is the reverse saturated current of the diode, typically 100 pA for small silicon cells,

$k = 1.38047 \times 10^{-23}$  J/K is the Boltzman constant,

$q = 1.60210 \times 10^{-19}$  C is the electron charge,

$V_d$  is the diode voltage expressed in volts,

$\eta$  is an ideality constant depending on the material used in the cell manufacturing,

$T = 273.2 + t_C$  is the absolute temperature given as a function of temperature Celsius or Centigrade,  $t_C$ , generally taken as  $T = 298.2$  K (that is, 25 °C),

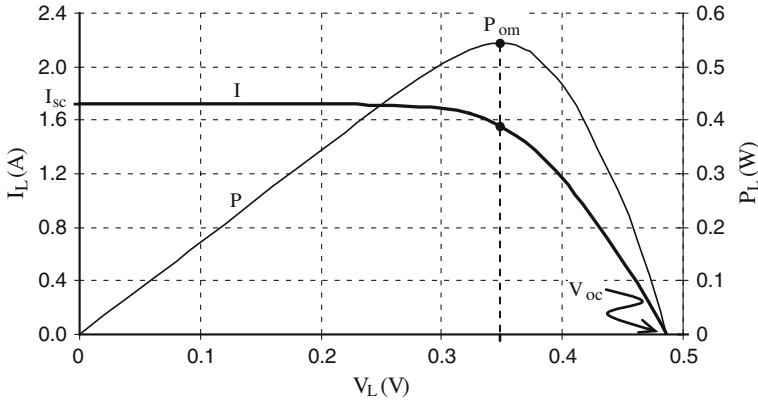
$V_T = kT/q = T/11, 600$  J/C where:  $t_C = 25$  °C

$R_p$  is the equivalent shunt resistance.

In a more general way, for any temperature:  $q/k = 11, 605.4677$  C, known as the equivalent voltage of the temperature  $T$ ; particularly for  $t_C = 25$  °C,  $V_T = 26$  mV.

### 3.3.2 Output Characteristics of a PV Cell

Once again using the model given in Fig. 3.8, it is possible to construct the output characteristics of a PV cell based on its parameters. Equation 3.4 and the equations below also derived from Fig. 3.8 may be used to plot the characteristics given in Fig. 3.9.



**Fig. 3.9**  $V \times I$  and  $P \times I$  output characteristics of a PV cell

$$V_L = V_d - I_L R_s$$

$$P_L = V_L I_L$$

Notice that the photocurrent  $I_\lambda(T)$ , the saturation current of the diode  $I_s(T)$  and its exponential term are dependent on the absolute temperature, as discussed in Sect. 3.5. Parameters  $V_{oc}$  and  $I_{sc}$  are the voltage and current limiting values when designing PV converters. They also help when selecting the proper PV panel for a certain application and are the basis for accessing the quality factor of a PV panel, as discussed in Sect. 3.9.

With the open circuit voltage  $V_{oc}$  conditions, Eq. (3.6) becomes:

$$0 = I_\lambda - I_s(e^{qV_{oc}/\eta kT} - 1) - V_{oc}/R_p \quad (3.7)$$

Eq. (3.7) can be solved for  $V_{oc}$  by a numerical method or by an approximate solution. As for the usual values of photo cells  $R_p$  is something in between 200 and 400  $\Omega$  and  $V_{oc}$  is around 0.5 V,  $V_{oc}/R_p$  is negligible. With these assumptions Eq. (3.7) becomes  $e^{qV_{oc}/\eta kT} \sim (I_\lambda + I_s)/I_s$  or giving it in terms of  $V_{oc}$  comes:

$$V_{oc} \cong (\eta kT/q) \ln(I_\lambda + I_s)/I_s \quad (3.8)$$

The short-circuit current ( $V_d \approx 0$ ) may be obtained from Eq. 3.4 and approximated by:

$$I_{sc} \approx I_\lambda \quad (3.9)$$

### 3.3.3 Approximate Determination of the PV Panel Parameters

Finding a reasonable direct equation for each parameter of Fig. 3.8 is not a trivial task, since the circuit can be considered a “black-box” system with transcendental relationships. A PV cell can also be simulated by through the use of spreadsheet such as Microsoft Excel or dynamically using simulation programs such as Matlab-Simulink using experimental data that defines the I-V curve characteristics [11, 14, 15]. Most of the mathematical models to represent PV panels do not consider either one of the key parameters, or that their values change along the I-V curve or with temperature, as discussed in Sect. 3.5.

The equations and methods to determine all key parameters in this section consider: the ideality diode factor,  $\eta$ , diode reverse saturation current,  $I_s$ , shunt resistance,  $R_p$  and series resistance,  $R_s$ . All these relationships are based on an experimental data acquisition from I-V characteristics, diode biasing, and other curves as presented below. In this context, Table 3.2 presents an approximate methodology to determine the parameters of photovoltaic panels based on the lab conditions of the operation.

Table 3.3 is a summary of the test conditions in order to have an approximate determination of PV panel parameters.

## 3.4 Determination of the PV Panel Maximum Power

It is noticeable in Fig. 3.9 that the maximum output power does not correspond to either the maximum voltage or the maximum current. However, using the parameters determined in Sect. 3.3, it is possible to obtain the maximum power point of a PV panel as follows.

To obtain the maximum power of a PV cell, as represented in Fig. 3.8, depending only on the cell parameters we use the product  $P_d = V_d I_d$ . Then, with the help of Eq. (3.6), the PV power across the internal diode terminals is defined as:

**Table 3.2** Definitions of test conditions for voltage across and current through a PV cell

Condition	Load	Load voltage	Load current	PV diode voltage	PV diode current
Short-circuit	$R_L = 0$	$V_L = 0$	$I_L = I_{sc}$	$V_{d(sc)} = I_{sc} R_s$	$I_{d(sc)} = I_s (e^{I_{sc} R_s / \eta V_T} - 1)$
Rated	$R_L$	$V_L = R_L I_L$	$I_L$	$V_d = I_L (R_s + R_L)$	$I_d = I_s (e^{V_d / \eta V_T} - 1)$
Open circuit	$R_L = \infty$	$V_L = V_{oc}$	$I_L = 0$	$V_{d(oc)} = V_{oc}$	$I_{d(oc)} = I_s (e^{V_{oc} / \eta V_T} - 1)$

where  $I_L, V_L, R_L$  are rated current, voltage and load,  $I_{L(sc)}, V_{L(sc)}, R_{L(sc)}$  are the short-circuit current, voltage, and load,  $I_{L(oc)}, V_{L(oc)}, R_{L(oc)}$  are the open circuit current, voltage, and load

**Table 3.3** Test conditions to obtain PV cell parameters

Parameter	Test conditions	Experimental formula
$R_p$	$I_s \approx 0$ and $R_p \gg R_s$	$R_p \cong \frac{V_{\text{ext}}}{I_L}$
$I_\lambda$	$I_{\lambda 0} \propto G_0$ and $I_\lambda \cong I_{\text{sc}}$	$I_\lambda = I_{\lambda 0} \frac{G}{G_0}$
$I_d$	$I_\lambda \cong I_{\text{sc}}$	$I_d \approx I_{\text{sc}} - I_L - \frac{V_d}{R_p}$
$\eta$	Measure $I_{d1}$ , $I_{d2}$ , $V_{L1}$ and $V_{L2}$ for $V_d > 0.3$ V	$\eta = \frac{q(V_{L1} - V_{L2})}{kT \ln(I_{d1}/I_{d2})}$
$I_s$	Use $R_p$ , $\eta$ and $V_{L(\text{oc})}$	$I_s \cong \left[ \frac{I_\lambda - \frac{V_{L(\text{oc})}}{R_p}}{e^{aV_{L(\text{oc})}/\eta kT} - 1} \right]$
$R_s$	Measure $V_{\text{ext}(1)}$ and $V_{\text{ext}(2)}$ for $I_{\text{ext}(1)}$ and $I_{\text{ext}(2)}$ , respectively	$R_s \cong \frac{\Delta V_{\text{ext}}}{\Delta I_{\text{ext}}}$

$$P_d = V_d \left[ I_\lambda - I_s (e^{aV_d} - 1) - \frac{V_d}{R_p} \right] \quad (3.10)$$

To obtain the maximum power point from this function the derivative of  $P_d$  is taken with respect to  $V_d$  and equating it to zero. For simplicity  $a = q/\eta kT = 11,600/\eta T$  and  $V_{\text{dm}}$  is the voltage across the internal diode terminals at the maximum power point. After some mathematical developments is obtained:

$$P_{\text{dm}} = V_{\text{dm}}^2 \left[ \frac{a(I_\lambda + I_s) + \frac{1 - aV_{\text{dm}}}{R_p}}{1 + aV_{\text{dm}}} \right] = \frac{V_{\text{dm}}^2}{(R_s + R_{\text{Lm}})} \quad (3.11)$$

where

$P_{\text{dm}}$  is the maximum power under the point of view of the internal diode terminals,

$V_{\text{dm}}$  is the internal diode voltage,

$R_{\text{Lm}}$  is load resistance at the maximum power point.

To transfer the point of view from the internal diode terminals power to the PV cell output terminals, we use the following equation based on Eq. 3.10:

$$P_{\text{Lm}} = I_{\text{Lm}}^2 R_{\text{Lm}} = \left( \frac{V_{\text{dm}}}{R_s + R_{\text{Lm}}} \right)^2 R_{\text{Lm}} \quad (3.12)$$

where

$P_{\text{Lm}}$  is the maximum output power of the PV cell.

### 3.5 Temperature Effects

The P-N junction temperature affects the rate of the PV output current with respect to the radiation current. Several environmental factors contribute for the current–voltage performance such as irradiance ( $G$ ), wind speed and module temperature ( $T$ ). The characteristics of the relating voltage and currents are usually based on the short-circuit current ( $I_{sc}$ ) and open circuit voltage ( $V_{oc}$ ) at the given environmental conditions ( $G, T$ ) from a reference I-V curve taken as ( $G_{ref}, T_{ref}$ ). The current output of the modules is usually specified for standard test conditions (STC) or for a more common condition, the nominal operating condition (NOC). The STC stands for 1,000 W/m<sup>2</sup> irradiance and 25 °C cell temperature and the NOC for 800 W/m<sup>2</sup> irradiance and 42 °C cell temperature as summarized in Table 3.4. To pass from one intermediary condition to another, several converting equations have been proposed in the literature [16–20].

$$I(G_2, T_2) = I(G_1, T_1) \frac{G_2}{G_1} [1 + \alpha(T_2 - T_1)] \quad (3.13)$$

$$V(G_2, T_2) = V(G_1, T_1) [1 + \beta(T_2 - T_1)] \left[ 1 + \delta \ln \left( \frac{G_2}{G_1} \right) \right] \quad (3.14)$$

where  $\alpha$ ,  $\beta$  and  $\delta$  are adjusted from a previous determined condition.

**Table 3.4** The standard (STC) and nominal (NOC) operating conditions

Parameter	Standard conditions	Nominal conditions	Equation
Solar irradiance, $G$	1,000 W/m <sup>2</sup>	800 W/m <sup>2</sup>	–
Cell temperature, $T_r$	25 °C	42 °C	–
$I_s(T) = [I_{sc} + K_I(T - T_r)] \frac{G}{1,000}$			(3.15)
$I_s(T) = KT^m e^{-V_{GO}/\eta V_T^a}$	–	–	(3.16)
$\frac{dI_s/I_s}{dT} = \frac{m}{T} + \frac{V_{GO}}{\eta T V_T}$	About 7 %/°C for Si	–	(3.17)
$I_s(T) \cong I_{s0} \times 2^{(T-T_0)/10}$	–	–	(3.18)
$I_{sc} = I_{sc0}(1 + \alpha\Delta T)$	$\alpha \approx 500 \mu$ units/K	PTC	(3.19)
$\frac{dV_d}{dT} = \frac{V_d - (V_{GO} + m\eta V_T)}{T}$	$dV_d/dT \cong -2.5$ mV/°C	–	(3.20)
$V_{oc} = V_{oc0}(1 - \beta\Delta T)$	$\beta = -5 \mu$ units/K	NTC	(3.21)

<sup>a</sup> Terms in this table are defined as

$K$  is a constant independent of temperature

$m = 1$  for silicon

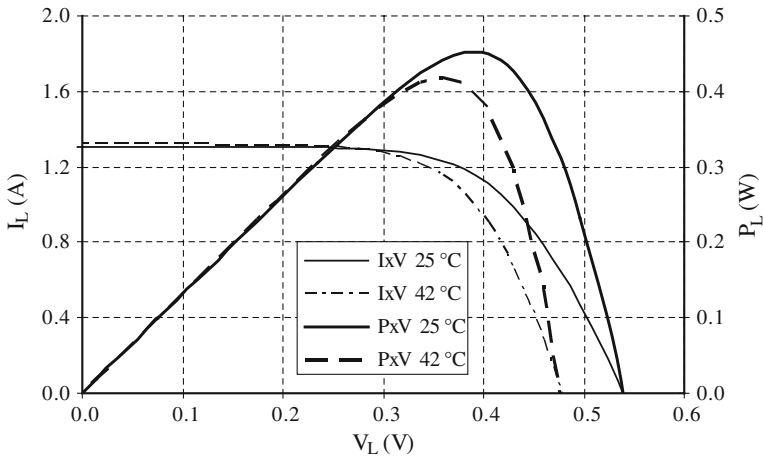
$\eta = 1.2 \sim 1.8$  for silicon (it depends on the position in the diode curve  $I_d \times V_d$ )

$V_{GO} = 1.210$  V for silicon and it is known as the equivalent voltage to the prohibited band in electron volts

$V_T = kT/q = T/11,605.4677$  is an equivalent voltage to the junction temperature

PTC is the  $\alpha$  positive temperature coefficient

NTC is the  $\beta$  negative temperature coefficient



**Fig. 3.10** Effects of the temperature on the PV cell characteristics

As the decrease in voltage predominates over the increase in current, the overall effect of an increased temperature is a reduced output power across the PV panel terminals, as illustrated in Fig. 3.10.

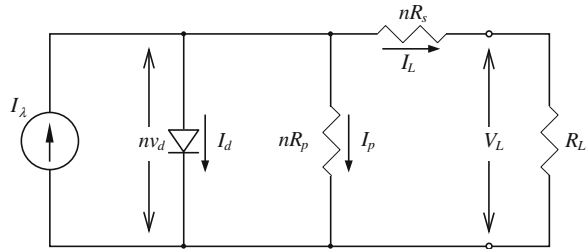
### 3.6 Parameters of PV Cell Associations

Manufacturers do their best to have identical cells in the construction of their PV panels. Nevertheless, in practice, small differences do occur in their individual manufacturing parameters (internal mismatches) and these differences have to be evaluated and considered theoretically. An approximate performance of PV cell series association can be obtained for practical panels by considering them as panel chains of identical series-connected cells, as the circuit depicted in Fig. 3.11 [2]. With the above differences, in a series connection, the yielding current will be equal to the minimum current provided by the one supplying the smallest power. The voltages of individual modules are then added together. An exact evaluation is very difficult because of the enormous amount of different possibilities among individual cell performances.

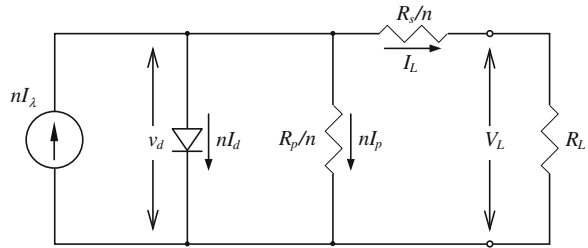
Similarly, when dealing with panel chains of identical parallel-connected cells, the circuit is as depicted in Fig. 3.12. In a parallel connection, the voltage is the same and equal to the average output of parallel modules and the current is the summation of output currents from each module.

The configurations shown in Figs. 3.11 and 3.12 can be used during practical tests to obtain the PV panel parameters in such a way that the average cell parameters are obtained by dividing them or multiplying them by  $n$  according to each case indicated in these two figures.

**Fig. 3.11** Equivalent circuit of a PV panel with identical series-connected cells



**Fig. 3.12** Equivalent circuit of a PV panel with identical parallel-connected cells



### 3.7 PV System Configurations

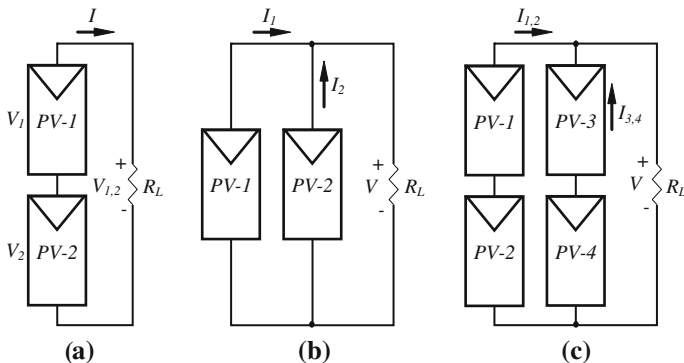
This section discusses the various combinations of photocells used to form strings, the combinations of strings used to form panels or modules, and combinations of panels used to form arrays and systems. A photovoltaic solar array is constituted of one or more solar modules connected in a series and/or parallel. The PV modules are mounted on structures or supports of aluminum. Good control practices of power converters are used to guarantee that the load is supplied with a good quality voltage, and that the solar panel is not going to either affect or be affected by the load behavior in cases of short circuits, shadowing, failures, over voltages, over current, atmospheric surges, and other unpredicted phenomena. All these combinations can operate either in a stand-alone basis or connected to the grid.

Stand alone or autonomous photovoltaic systems are those PV arrays feeding a load directly independently of the main supply. For this reason they have to use battery banks for those periods without sufficient irradiance since they will depend only on the energy produced by the PV panels. In any case, as discussed in Sect. 3.2, it is always possible to have a series and/or parallel combination of photovoltaic modules, strings, and arrays to reinforce the output voltage and/or current.

As a result of a series connection there is only one path for the current to follow as illustrated in Fig. 3.13a. With a parallel connection there is only one common voltage to all modules as illustrated in Fig. 3.13b. By combining the features of both series and parallel strings any voltage or current can be arranged to match a certain load, as illustrated in Fig. 3.13c.

In order to interconnect PV modules to the load or to the grid, there are several types of DC–AC power inverters discussed in the technical literature.

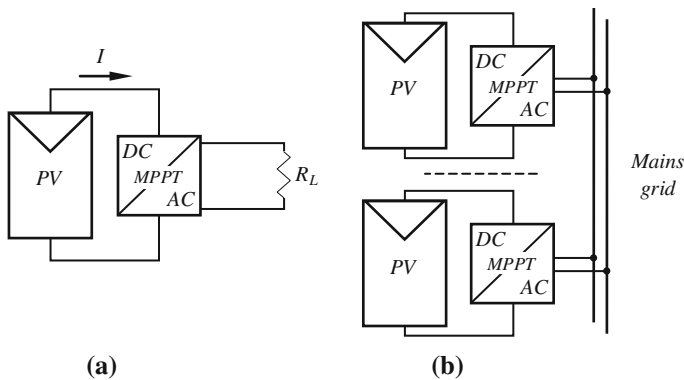




**Fig. 3.13** Solar module strings. **a** PV series connection. **b** PV parallel connection. **c** PV series-parallel connection

### 3.7.1 Module Inverter

In this configuration, every solar panel or small set of them is connected to an inverter forming an independent module, usually up to 48 V and 500 W, and ready to be connected to the load or single-phase main grid, as illustrated in Fig. 3.14. Many modules can be added together to work on a standalone basis or connected to the grid. There is no need for any DC cabling from the array and the solar panel can also be connected to the grid at its own location. Some of these inverters do not use any isolating transformer but most of them do use an isolating low-frequency (LF) conventional transformer or a high-frequency (HF) transformer to ground these panels and to minimize presence of DC currents through the grid. HF transformers are small, highly efficient, easily manufactured in series, and light-weight but need more complex circuitry, they are more expensive in \$/W and have



**Fig. 3.14** Module PV inverter. **a** Module inverter connected to an AC load. **b** Module inverter connected to the grid

shorter useful life. Module inverters are more suitable to detect the maximum power point (MPP) of individual panels since each of them could be exposed to environmentally distinct locations [4, 5, 21–24].

### 3.7.2 String Inverter

An extension of the module inverter is the string inverter where a single inverter is suitable for a string or parallel strings of panels connected in series, as depicted in Fig. 3.15. The input voltage may be high enough to avoid voltage amplification. The string inverters are used for smaller PV systems up to 10 kW and are usually connected to the main grid. Since PV panels are essentially a current source, the connection of parallel strings in a single string inverter without current circulation inter panels is possible, but each string will have its own or a common maximum power point tracking (MPPT), as illustrated in Fig. 3.15b [5, 25, 26]. All current sources represented by the panels will contribute to the load current node and from that, to the load or output. The main problem in this case is in the event of failures or shadowing effects on individual panels, as discussed in Sect. 3.2. Use of multiple MPPT inputs in the inverter allows a remarkable increase in the total output power for when all modules in the same string are facing the same direction (see Sect. 3.10) [4, 25, 27].

Another aspect of the maximum power generation is when individual strings are connected to a dedicated MPPT such that the total output power would be greater than if the strings were connected to an inverter with only one overall MPPT. This arrangement is cheaper than using a number of individual inverters. This means that every string will have its own DC–DC converter all connected to a common DC–AC inverter [28].

The multi-string inverter is a further development of the string inverter, where several strings are interfaced with their own DC–DC converter and then connected

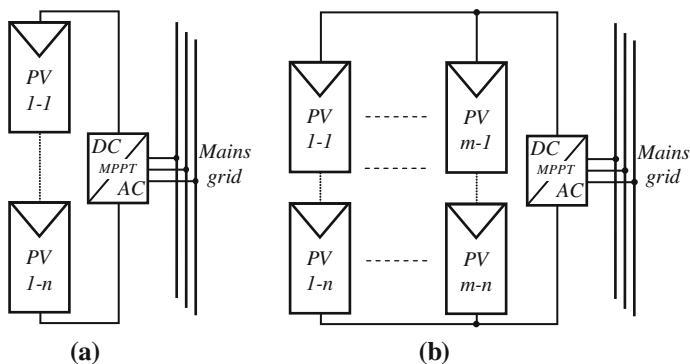
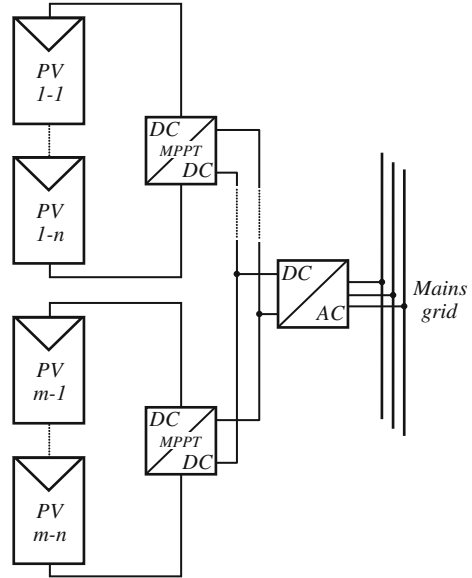


Fig. 3.15 String PV inverter. a String inverter. b String inverter with parallel PV strings

**Fig. 3.16** String module DC–DC converters with a common DC–AC inverter



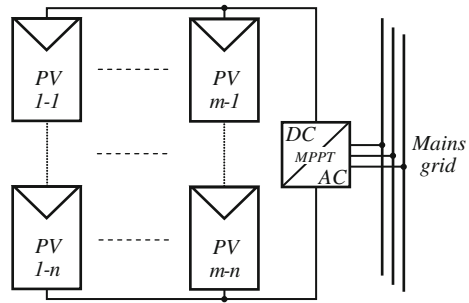
to a common DC–AC inverter (see Fig. 3.16). Thus, the PV power plant may start with few modules and later increase according to the evolution of the load. In this case, the strings can operate at their individual MPPT, therefore a better overall efficiency is expected [4, 22–25].

### 3.7.3 Central Inverter

One variation of the string panel is the central panel for higher PV power levels to be injected into the mains grid. This configuration resembles the string inverter with parallel strings except that the central panel array can be divided into a number of sub-arrays comprising a number of ten's of PV modules connected in series and/or parallel strings. The expression “central inverter” is generally used to refer to large systems in the order of ten's of kW, so as to distinguish it from string inverters (see Fig. 3.17). The power losses are normally higher in this configuration, than for the string inverter or module inverter, mainly due to mismatches between the modules and the necessity of string diodes. Also, when using a single inverter for the whole array, the system may suffer from power shortages if the only inverter fails or even during maintenance services in the whole set.

As system connections of the central inverter configuration may be complex, some manufacturers have developed the master-slave arrangement, such that in low irradiance, the whole PV array will be only connected to a master inverter. As the irradiance increases, other slave inverters will be gradually introduced similarly to what is explained in Sect. 3.7.4. The manufacturers claim that such

**Fig. 3.17** Central inverter

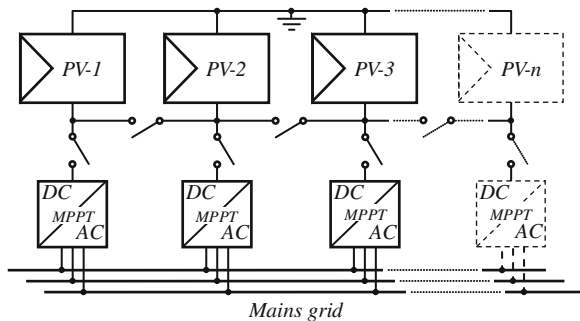


procedures will increase the system efficiency at lower irradiance levels, because the losses in the inverters are minimized at lower current levels [4, 29–32].

### 3.7.4 Team Concept Inverters

Power inverters are designed to have a maximum efficiency at their own rated values. To enjoy this feature under low irradiance levels, in the team concept all panels are connected to a single inverter or a group of inverters such that they will operate close to their rated values, increasing their individual efficiency, as illustrated in Fig. 3.18. Under lower irradiance levels the PV array will be distributed to fewer strings, until all inverters can be fully operative again according to local irradiance. The set of inverters use the same concept of the module inverter, except for the possibility of changing the way the panels are interconnected between them to allow highly efficient operations. Such arrangements were developed to use the rated power of the inverters reducing losses with respect to their off nominal operation. This procedure enjoys all advantages of the module inverter, but needs a more complex power and control circuitry. Furthermore, this arrangement keeps the advantage of each array having its own MPPT control.

**Fig. 3.18** Team concept PV inverter for low irradiance



### 3.7.5 *Energy Storage for PV*

It is possible to store energy in large scale using water dams or fuel reservoirs. Ideally, when using electricity it has to be produced as it is being consumed. Unfortunately, the photovoltaic energy has to be stored since during the night or periods of cloudy days there is not enough production of electricity. Energy storage then becomes an essential item to assure a continuous power supply.

The most widely used means of storage for PV systems is the battery bank, because it is inexpensive and simple to manufacture, it has a mature, reliable, and well-understood technology and when used correctly, is durable and provides a dependable service. Its self-discharge is relatively low and demands for low maintenance requirements with high charge/discharge rates.

There are several types of batteries on the market such as: nickel cadmium, lithium ion, lithium polymer, nickelmetal hydride, lead acid and, more recently zinc air. They serve a variety of modern purposes for many things including spacecrafts, electrical vehicles, motorbikes, domestic utilities, and also to level off renewable sources of energy. Each one of them is more or less convenient for a specific application and they are normally judged by criteria such as their specific energy, energy density, pollution residues, specific power, nominal cell voltage, memory effect, energy efficiency, charge/discharge rate, self-discharge, dependence on temperature, and market availability and lifetime. As a rule, batteries are very much dependent on their range of operation. The integration details of battery storage technologies can be found in a later chapter of this book.

The variables usually monitored and controlled in battery banks with power electronics and instrumentation are related to voltage and current magnitudes, cell temperature, ranges of Ah, charge/discharge cycles, rate of charge and discharge, dept of discharge, gassing index, overcharging, electrolyte levels, and many more [21]. It is particularly critical when a photovoltaic module does not use a charge regulator to avoid overcharging events. Shortened lifetime and danger of explosions are points strongly considered by designers of photovoltaic system.

Other energy storage technologies exist and are classified according to the energy as well as the time and transient response required by their operation [2, 26]. It is convenient to define storage capacity in terms of the time that the nominal energy capacity can cover the load at the rated power. Storage capacity can then be categorized in terms of energy density requirements (for medium- and long-term needs) or in terms of power density requirements (for short- and very short-term needs). The details of various storage technologies can be found in later chapters of this book.

### 3.8 Power Electronic Topologies in PV Systems

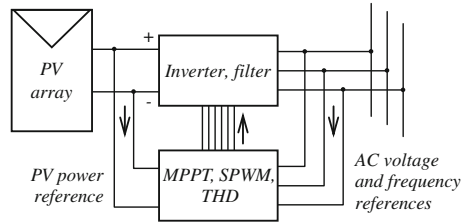
The electronic connection between PV systems and their load or the grid may have several purposes: (1) convert PV–DC voltage into an AC voltage; (2) adjust the PV panel load to obtain the maximum output power; (3) perform harmonic compensation; (4) match the voltage level differences between the PV generator and load; (5) perform legal and quality standards such as IEEE19 and EN61000-3-2 regulations; (6) shut the system off in case of any failures or islanding; and others. This multi-functional ability of the power electronics is mostly related to new devices and circuits, new topologies, digital electronic controls, and telemetering. Topologies of power electronics is the subject of this section.

PV modules supply only DC voltages and currents from their terminals, so any energy processing in a stand-alone system will have to use some sort of self commutated device. The most suitable switches for self-commutated inverters use mostly semiconductor switches as IGBT or MOSFET which are used to control the voltage pulse width to synthesize the converter output, for example a voltage sine wave to feed an isolating transformer.

The PV–DC output current can be converted into AC current using line commutated or self commutated power inverters. Most of the PV panels are electrically isolated from the grid by transformers. The connection to the grid may be through a single inverting stage for when the PV and the load voltage are comparable or a double stage for when the difference between the load or grid voltage level is considerable. The usual HF isolation for the inverter is to reduce the size of the bulky LF transformer placed across its terminal and to produce a voltage level enough to reduce switching losses in the inverter. The number of stages will increase with this difference of voltage. The single stage inverter uses the conventional converter topologies such as series resonant, push–pull DC–DC, H-bridge DC–DC and flyback current-fed [22, 33–38]. The double stage is made of a DC–DC switched converter connected to a DC–AC inverter and then to the load or grid. The usual switching frequencies may be a low frequency for 60 Hz (LF) or high frequency (HF) for up to 50 kHz with the present commercial technology. The HF converters have higher efficiency and use small transformers. In compensation, they use a more complex circuitry and are subject to shorter useful life, noise and magnetic conducted, and irradiated interferences [36–38].

Power electronics circuitry may be linked to PV generation when interconnecting PV cells to allow intelligent controls, when interconnecting strings to form intelligent panels or modules, when interconnecting PV panels to form arrays and when interconnecting arrays to inject power into the grid of power systems. Power electronics contribute for higher efficiency levels of PV generation incorporating environmental conditions (temperature, clouding, shadowing, earth positioning, and seasons). MPPT is embedded in the DC–DC converter for the dual stage PV converters (typically small residential ones). These interconnections may be controlled by artificial intelligence, conventional digital circuitry, or manually.

**Fig. 3.19** PV generation controls



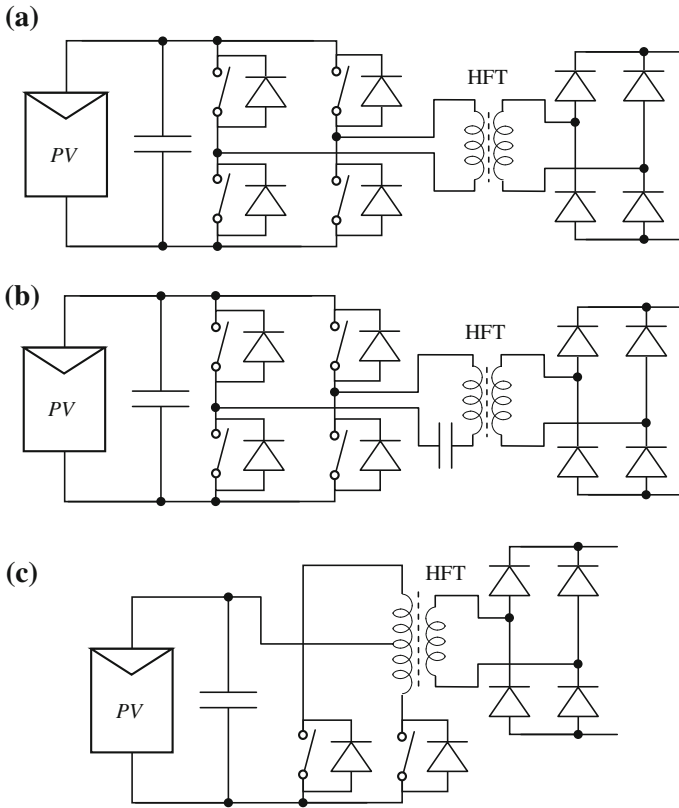
As it was already stated in Sect. 3.5, the output voltage of a solar module, and therefore an array output current will be dependent on the irradiance and the temperature. So good designing practices would recommend that the inverter operates within the solar array operating range for all the expected day time temperatures at the actual location where the solar array is installed. Of course, the inverter must be suitable for the power rating of the total power rating of the array.

Generally speaking, modern PV systems are very flexible in altering the arrangements to best match a power system through electronic switching devices and digital controllers. Among these devices are the thyristors (SCR/GTO/IGCT), IGBT and MOSFET. Thyristors are the most powerful, durable, and robust devices and they are well suited for high voltages and high currents but can be used also for low cost applications though they are not very flexible to control [34–39]. IGBT suits for medium voltages and high current and they are fully controllable and fast switching devices. MOSFET suits for low voltages and high currents and they are also fully controllable as well as being the fastest switching device among the most usual devices used in PV inverter technology. Therefore, power electronics may help the PV generation controls both in stand-alone PV schemes and in grid connected systems, as illustrated in Fig. 3.19 where maximum power point tracker, the sinusoidal PWM driver and control of the total harmonic distortion, harmonic filter, and output voltage are all included [40–44]. Some commercial trademarks are Enphase, Solectria, Siemens, XantrexGT, Toshiba, and SMA.

### 3.8.1 Transformer Isolated Converters

Considering that PV panels are mostly current sources, a decoupling capacitor must be placed across the panel terminals to avoid photo current interruption by the converter switching. Nonisolated DC–DC converters are recommended when there is no need for galvanic isolation and to increase the resulting low voltage ratio between the load and the PV panel output. The rectifier is usually placed across the transformer output and may not be a full diode bridge, since it can be replaced by a half-bridge rectifier either with a single or double secondary transformer configuration.

The ordinary types of transformer isolated converters are shown in Fig. 3.20. The forward H-bridge is a straight version of the theory of power converters, since



**Fig. 3.20** Transformer isolated DC–DC converters forward H-bridge (a), series resonant H-bridge (b), and push–pull DC/DC (c)

it converts the DC power from the PV panels and injects it in the elevating transformer to rectify it in a higher voltage level. Switching losses are considerable because of the low voltage commutation in the converter. Such losses can be reduced by using an H-bridge series resonant converter as shown in Fig. 3.20b which adds the advantages of its natural short-circuit protection and no saturation problems guaranteed by the presence of the resonant capacitor in the transformer input. The disadvantage of this configuration is the necessity of a precise hard switching on the forward converter otherwise it can produce core saturation and so extra losses. Under special conditions of high DC voltage and high DC current it may be more indicated the used of the push–pull configuration shown in Fig. 3.20c.



### 3.8.2 *Stand-Alone PV Systems*

As a general rule, selection of the right converter or inverter for a specific application will depend on the difference between the PV source and the load voltages. Among the DC–DC converters are the following well-known configurations: buck, boost, buck boost, Cúk, Sepic, Zeta, and others dealt in full details in good power electronics text books [32, 33, 45]. Some examples of their applications are discussed as follows.

The buck converter is the most usual form of DC–DC conversion, sometimes called a chopper (see Fig. 3.21a). A buck converter can create an average DC output less than or equal to its DC voltage source. The switch used in a buck converter must be fully controllable, i.e., a MOSFET or an IGBT, so that the switch can forcibly turn off its current. The PWM modulates its output by turning the switches on and off, so that a variable average voltage can be synthesised at the output.

In the boost converter, the load voltage is always higher or equal to the source voltage (see Fig. 3.21b). In the buck–boost converter the load voltage can be higher, lower or equal to the source voltage (see Fig. 3.21c). The Cúk converter has the interesting feature of adapting its input impedance to the output impedance of the PV panel through the switching frequency increasing so its output power (see Fig. 3.21d). A detailed analysis of this converter has been adequately reported in the technical literature and will not be undertaken here [26, 33, 45, 46].

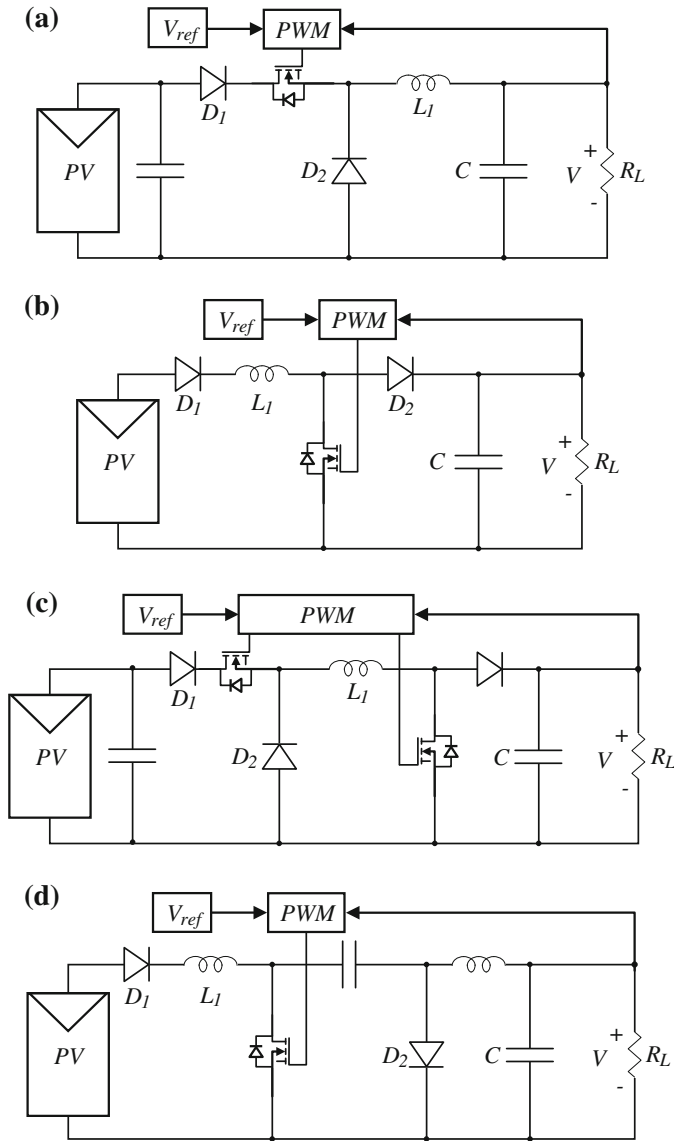
A very simple power electronic solution for remote places is used when the generation of solar electricity may become temporarily too high with respect to the load demands. The load voltage will surpass the limit voltage  $V_{\text{lim}}$  of the load and it will have to be somehow curbed. The easiest way to do that is by using a shunt power switch across the module output dispensing any battery or grid connection. Figure 3.22 depicts this situation where the PV panel will work as a heat sink with zero power to the load.

In a stand-alone configuration, the PV generator can be connected to the load through a series or a parallel connection as discussed below.

### 3.8.3 *Series Connected Inverters*

A series connection is when the converter is connected in between the source and the load. The literature is rich in connection types for solar panels to obtain electrically regulated load voltages and maximized output power. Figure 3.23 presents the most common types of autonomous series inverters for voltage regulation and battery charging. The voltage panel has a different voltage level with respect to the battery bank and load.

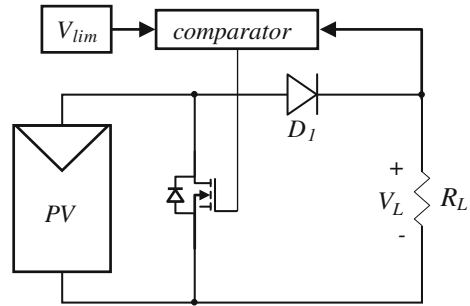
The buck converter is used when the PV voltage is higher than the battery voltage, the boost converter is used when the PV voltage is lower than the battery



**Fig. 3.21** Basic types of self-commutated converters buck (a), boost (b), buck boost (c), and Cúk (d)

voltage and the buck–boost converter is for when the PV voltage and battery voltage have about the same voltage level. In these configurations, the battery charger adjusts the charge/discharge cycles of the battery bank and searches for the maximum power point of the primary source. They have the same voltage level

**Fig. 3.22** Shunt transistor to limit the load voltage



across the batteries and across the DC bus bar to avoid a voltage elevating stage or any transformers.

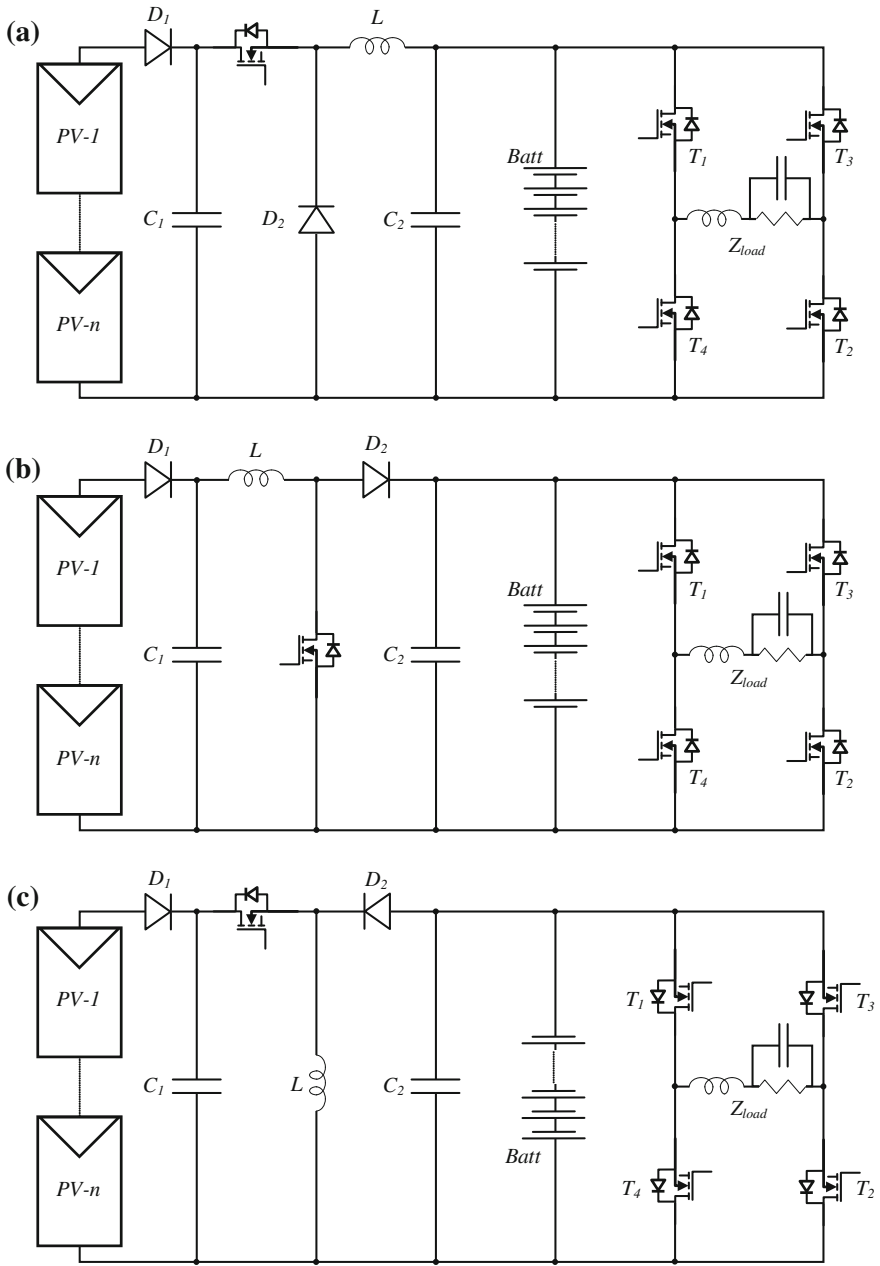
Other configurations may be used as series connected inverters, but they usually present higher levels of losses, are more expensive, and have more volume and weight. In the series configuration, the number of stages and the converter topology to convert PV energy into useful electrical energy may vary according to the voltage levels across the load and the battery bank [47, 48]. One example of application of this series connected inverter is a typical boost inverter for load integration of stand-alone PV arrays to feed an H-bridge, and then the load, is illustrated in Fig. 3.23. This is the one usually preferred for solar panels because of its flexibility and the low voltage generated in the panels. A battery bank should guarantee the load supply for a predicted period of low irradiance or none at all. Diode  $D_1$  assures that the battery bank is not going to be discharged over the PV module terminals or other surges able to damage the PV cells.

The problems of the series buck, boost, and buck–boost configurations as presented in Fig. 3.23 are that the load current passes through the battery bank and that there are different voltage levels across the PV panels and the battery bank plus DC bus demanding for further voltage adjustments in the power converters. These difficulties increase the complexity and cost of the PV installations.

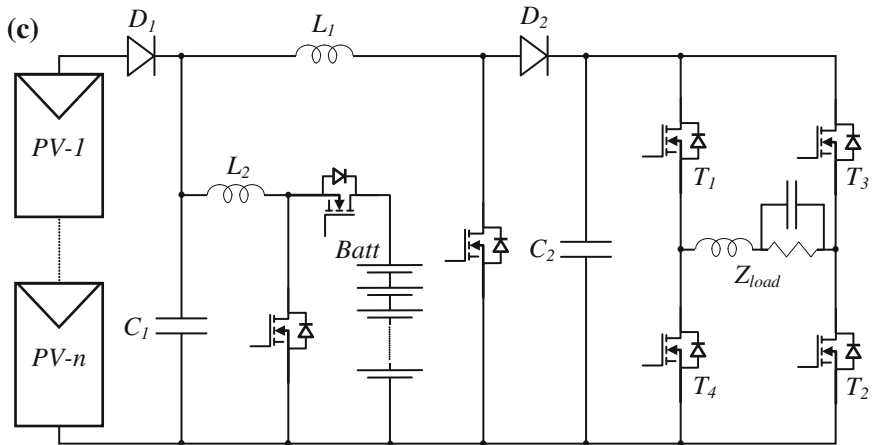
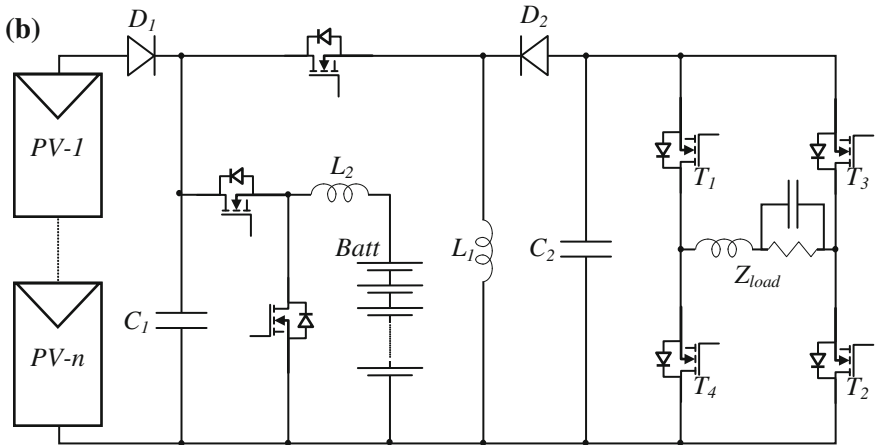
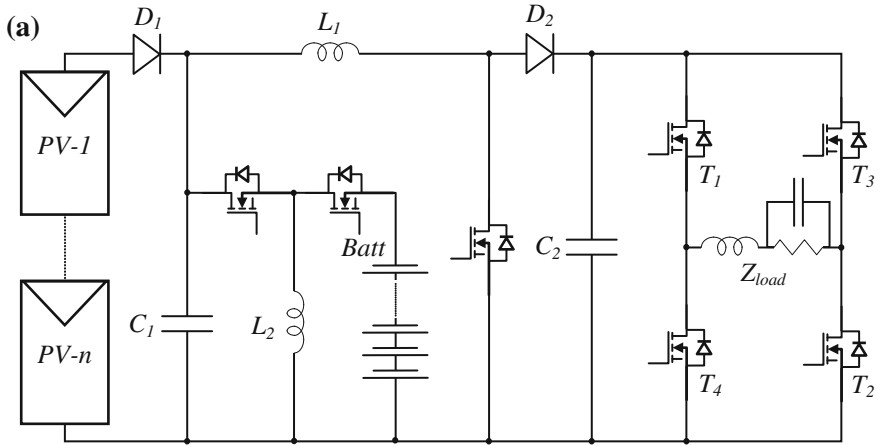
### 3.8.4 Parallel-Connected Converters

A parallel-connected converter is when there are two independent converters, one connecting the PV panel to the battery bank and another one connecting it to the DC bus. Figure 3.24 presents the most common types of autonomous parallel inverters for voltage regulation and battery charging.

Similarly with the series autonomous inverters, the buck converter is used when the PV voltage is higher than the battery voltage and DC bus bar. The boost converter is used when the PV voltage is lower than the battery voltage and the DC bus bar and buck–boost converter is for when the PV voltage and bus bar have the same level.



**Fig. 3.23** Autonomous series converters for voltage regulation and battery charging buck converter for voltage regulation and battery charging (a), boost converter for voltage regulation and battery charging (b), and buck-boost converter for when the PV voltage and battery voltage have about the same voltage level (c)



- ◀ **Fig. 3.24** Autonomous parallel converters for voltage regulation and battery charging bidirectional buck–boost inverter for battery regulation and boost inverter for DC bus voltage regulation (a), buck–boost inverters for both battery regulation and DC bus voltage regulation (b), and bidirectional boost inverter for battery regulation and boost inverter for DC bus voltage regulation (c)

The parallel configuration has some advantages with respect to the series configuration: (a) the load current does not go through the battery bank except when it is necessary to enter into operation decreasing in this way the battery's number of charge/discharge cycles; (b) it charge/discharges the batteries independently of the load therefore allowing a better mastering of the battery cycles; (c) the components are dimensioned only for the specific use below the rated values, for controlling the battery cycles and for regulating the load voltage so they last longer; and (d) voltage elevation and battery cycles are controlled by a single bidirectional converter [49].

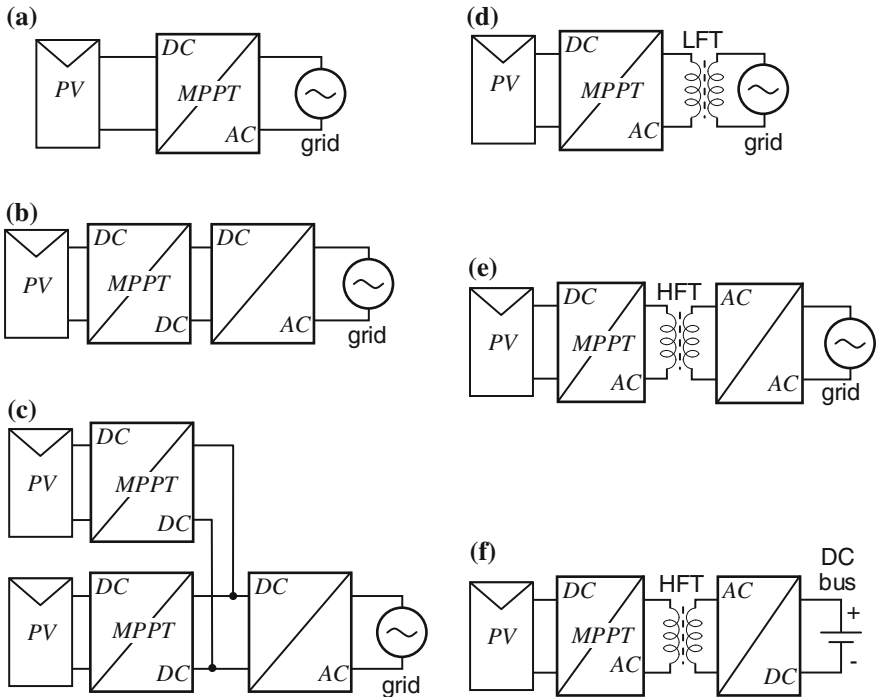
### 3.8.5 Grid-Connected PV Systems

As PV panels generate only DC current, to integrate a solar panel to an AC distribution system or to supply common consumer AC loads, it is necessary to invert its current and adjust it in voltage and frequency to feed it correctly into the main grid. The vast majority of the small grid-connected systems are single phase and arrays of three of them may form a three-phase system. Integration of PV modules producing a direct current in a typical AC electrical distribution system is not a difficult task for power electronic converters and inverters.

The power electronic devices operate as an interface between the DC generation and the AC load, represented by the main grid or any other passive or active load. The function of these power converters is to convert DC power into AC power. For the large single stage ones, the maximum power point tracking is done in the DC–AC inverter. Active and passive protection on the grid side can be treated as well to ensure the inverter will be isolated from the grid when either of them fail or are operating out of their tolerance range.

For grid connected inverters, typically the small residential ones are single phase, whereas the large ones (>30 kW) are three-phase inverters. Stand-alone inverters (i.e., not connected to grid) can be of single- or three-phase based on the load they are supplying. There is no need to install a battery bank in a grid-integrated configuration since the grid will assure continuity of the supply like an “AC battery”.

Several arrangements can be made to connect a PV panel string to the electrical load aiming at different applications. A single-stage inverter can be used to cope with grid current control, voltage amplification, and MPPT, as depicted in Fig. 3.25a. In the dual stage processing there is one converter doing the MPPT and/or voltage amplification and an inverter doing the grid current control and/or



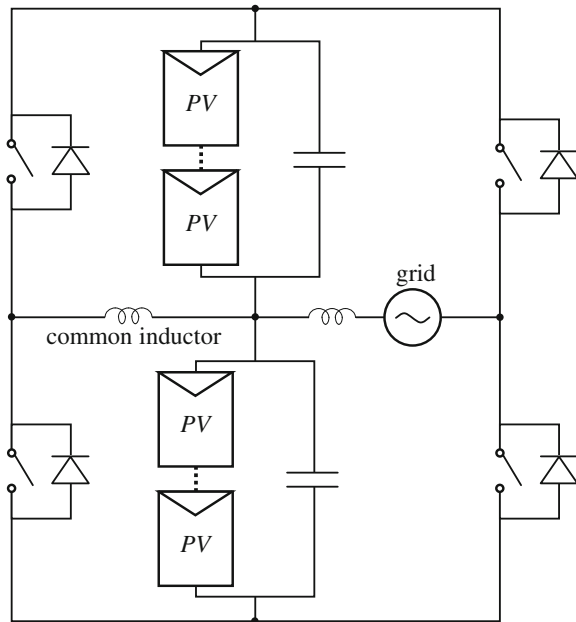
**Fig. 3.25** Common arrangements for connecting PV strings or panels to the load or the grid single-stage inverter (a), double-stage inverter (b), dual-stage processing for parallel connections (c), connection through low frequency transformer (d), connection through high-frequency transformer (e), and connection to a DC bus through high-frequency transformer (f)

voltage amplification, as illustrated in Fig. 3.25b. In the dual-stage converter, a single DC–AC inverter processes the power produced in two or more PV panels with individual DC–DC converters (see Fig. 3.25c). DC current can be avoided in the grid through the use of a line transformer (LFT), as shown in Fig. 3.25d. To reduce transformer size, weight, price, and power losses it is better to use a high frequency transformer (>20 kHz) for connection of solar panels to the grid as in Fig. 3.25e. In some cases, a direct connection to the DC bus is useful, such as for battery chargers or remote loads, as illustrated in Fig. 3.25f.

The connection of PV panels to the grid may involve a number of power processing stages, grounding strategies, form of decoupling between the PV module and the grid, presence of LF or HF transformers and circuit configuration of grid interfaces.

Two buck–boost converters using a common inductor may individually control the load voltage of each string forming a generation control circuit (GCC) as shown in Fig. 3.26. Each buck–boost inverter is formed by the two switches in one leg of the bridge with their free-wheeling diodes, one capacitor and the common input inductor. The current injected into the grid is controlled by the right leg of

**Fig. 3.26** Generation control circuit (GCC) for photovoltaic inverter



the inverter through the output inductor. This is a straightforward way of a MPPT controlling each string voltage. More chopper stages can be added to this configuration forming an efficient multi-mode system [44, 50].

Another buck–boost flyback-converter sharing a transformer and a cyclo converter in the output stage is presented in Fig. 3.27. At the present stage of development stage of this circuit, the minimum number of components is its strong point [22, 27, 50].

Figure 3.28 shows an example of a DC–DC converter operated at high frequencies ( $>50$  kHz) with a selectable voltage transfer ratio allowing virtually any desired voltage level across its output. The PV panels feed the primary voltage of such a transformer through a full-bridge or a half-bridge inverter topology. This figure presents a series resonant DC–DC converter feeding a resonant tank creating zero-voltage switching opportunities from a full bridge grid-connected inverter. Reduced switching losses are assured by the resonant converter associated with a MPPT algorithm realized by the grid inverter [51].

Multi-level topologies are required for high-voltage, high-power PV systems. Figure 3.29 shows an example of a high-voltage, high-power topology of a Cascaded H Bridge (CHB) multilevel converter to set a symmetrical nine-level inverter with four cascaded cells. This type of converter is a cascaded connection of a number of conventional two-level bridges, whose AC terminals are connected in series to synthesize sinusoidal output waveforms or any other more convenient shape for some particular application.

The number of output phase voltage levels is defined by  $n = 2N + 1$ , where  $N$  is the number of independent PV panels. Each converter level can generate three



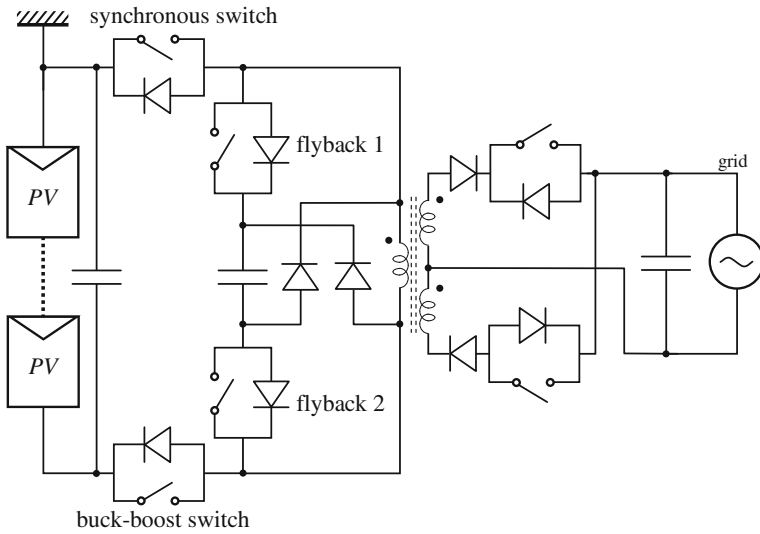


Fig. 3.27 Transformer isolated inverter

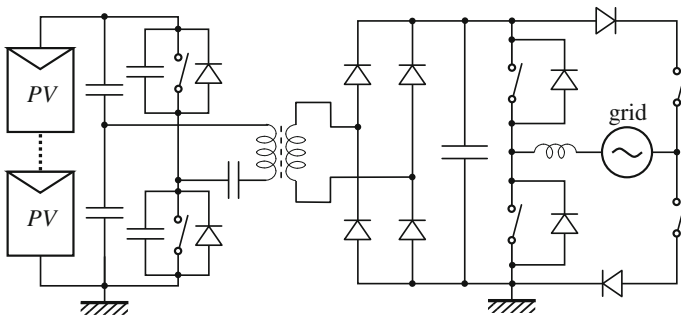
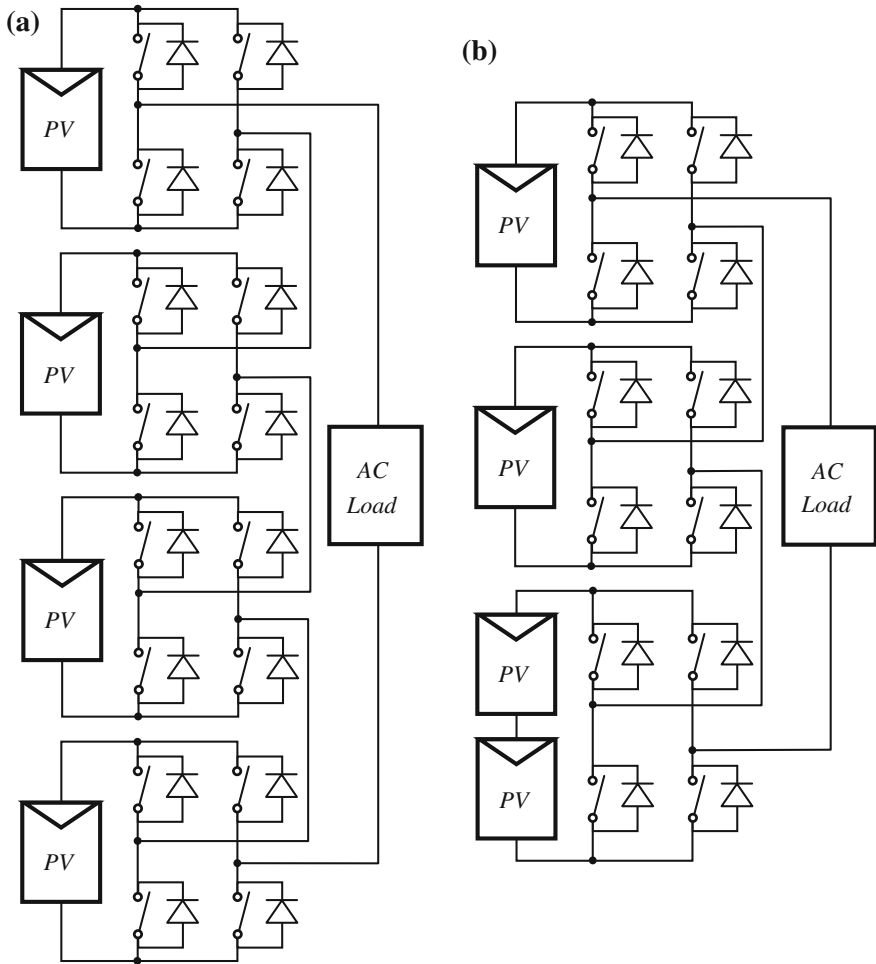


Fig. 3.28 A series-resonant transformer isolated DC/DC inverter feeding a grid connected inverter

different voltage outputs,  $V_{cell}$ , 0 and  $-V_{cell}$  to compose the AC output as the summation of the individual converter outputs. This is known as symmetric CHB inverter where the separate DC sources have same magnitude. If at least one of them is different from the others, the converter is known as an asymmetrical multi-level converter. This topology is more flexible since it allows a higher number of synthesised voltage levels, high-conversion efficiency, smaller number of power components, reduced THD, reduced voltage stress, and can also be easily interfaced with PV panels [52].

Figure 3.30 shows an inverter PowerLynx for 4.5 kW satisfying the NEC690 standard since there is galvanic isolation in between the solar panels and the grid and all equipment is grounded to the same level. A boost converter matches the



**Fig. 3.29** Cascaded H bridge (CHB) inverter for practical PV cells. **a** Symmetrical. **b** Asymmetric

voltages between the PV panels and the full-bridge inverters to feed the high-frequency transformers (HFT). The DC–DC converters are based on current full-bridge inverters with an embedded HF transformer and rectifier. Current commutated inverters assure certain characteristics such as low reverse charge recovery of the diodes, no need for filter capacitor and low-voltage stress [39, 40, 53]. The presence of the HFTs may avoid resonance in between the PV modules and any inductances in the current path helped by the grounding connections on both output and input terminals.

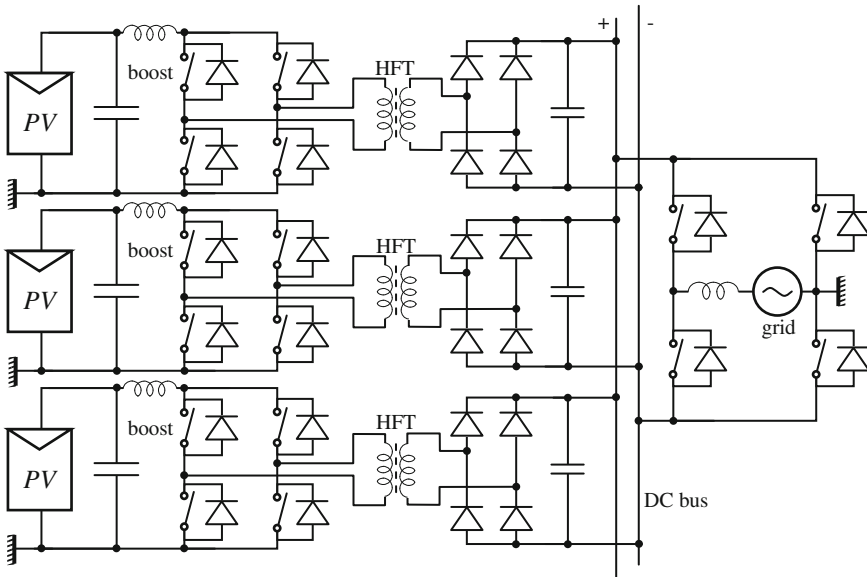


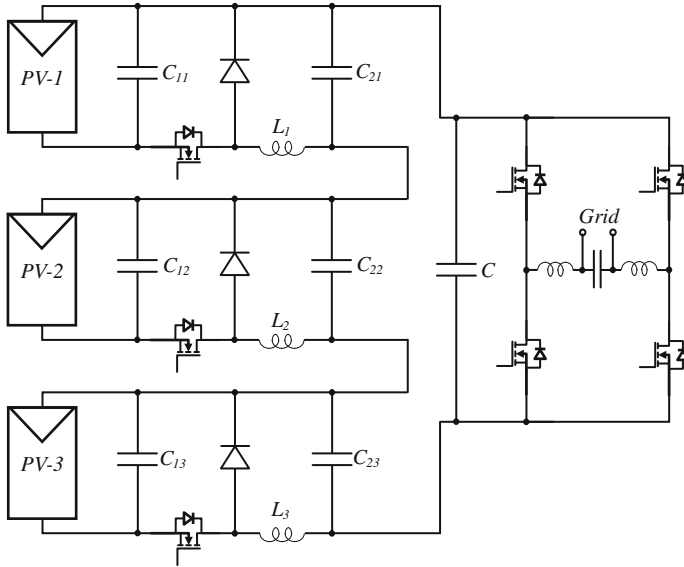
Fig. 3.30 An example of an isolated multi-string inverter

### 3.8.6 Distributed Photovoltaic Systems

The distributed photovoltaic systems are characterized by the connection of a smaller number of series and/or parallel modules. Such PV systems are connected in several points of the distribution network or the transmission system. They differ from the sparse connection in the sense that the latter are not connected to the grid but in several stand-alone sparse locations with the capability of being connected or not connected to the grid. As shown in Fig. 3.31, in distributed photovoltaic systems the panel arrays are arranged in subsets of panels and each one with its own DC-DC converter, all connected in a series to form a DC bus of its own [54, 55].

## 3.9 Maximum Power Point Tracking

When dealing with alternative sources of energy, the search for the point of maximum power becomes more important than the maximum efficiency. This is because when the energy from the primary sources such as sunrays, wind, river currents, sea waves, and sea tides are not used at the moment they are present in nature, they are lost for good. This is not different for solar panels, and with a good sun tracker it is possible to increase the electricity production from about 15 to 30 % [56–59].



**Fig. 3.31** Distributed PV arrays for grid connected systems [49, 54]

Without other losses, there is a theoretical maximum power point expected from PV solar panels and that value would occur at the open circuit voltage  $V_{oc}$  and short-circuit current  $I_{sc}$ . Such maximum value cannot be achieved in practical cases, so a numerical factor is created to estimate how close the production capability of a panel can go. This is called the fill factor defined as:

$$FF = \frac{I_{Lm} V_{Lm}}{I_{sc} V_{oc}} \tag{3.22}$$

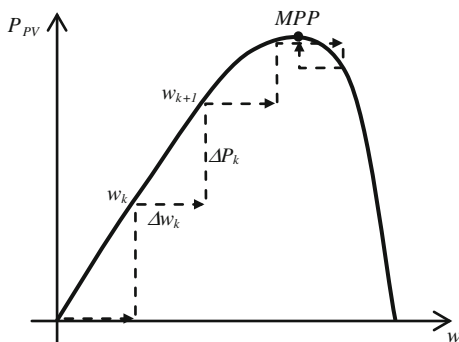
where  $I_{Lm}$  and  $V_{Lm}$  are the current through and voltage across the load at the maximum power point.

The most well-known methods for maximum power tracking are Hill Climbing Control, Constant Voltage, Perturb and Observe, and Incremental Conductance.

### 3.9.1 Hill Climbing Control

Several algorithms using the hill climbing control (HCC) are discussed in Farret and Godoy Simões [2], Hohm and Ropp [60]. This technique is based on the successive increments of a selected pulse width  $w$  in a PWM control incremental step of voltage across terminals or in a current through the PV inverter, then increasing its output power  $P_{PV}$  up to the maximum point. This process continues until the output power passes the maximum power point for the first time ever, as illustrated in Fig. 3.32. After that, it goes backwards to the MPP and so forth.

**Fig. 3.32** Hill climbing control



HCC may be a very precise approach to reach the MPP under the ever changing meteorological or shadowing condition the solar panel may go through [15, 37]. The HCC can be used either to adjust the best direction of the solar panel with respect to the solar rays or to let it draw the right voltage or current step at the maximum power point.

### 3.9.2 Constant Voltage

This oversimplified technique is based on the assumption that the maximum power point for any PV panel happens at about 76 % of its open circuit voltage  $V_{oc}$  and should be used only with a very poor budget [61]. According to the meteorological variations and shadows in the location of the PV array and in order to always have refreshed open circuit voltages, the panels are periodically disconnected from the load to allow sampling of a new  $V_{oc}$ . This value is used to establish the new maximum power point voltage with a constant steady-state error. Additional electronic switches have to be used to implement this periodical operation. Interruptions of energy and relatively extended periods off the maximum power point are the main drawbacks of this technique.

### 3.9.3 Perturb and Observe

The Perturb and Observe method is very similar to the HCC. A small output power increase or decrease is introduced through the voltage or current reference level. Based on the resulting output power before and after this alteration is established the direction of the next maximum power point. As the array comes closer to its maximum power point, the steps of reference signal are gradually decreased or increased according the variations of power until the steady-state condition is reached. This introduces a steady-state error. With very low levels of irradiance,

the performance of this technique is aggravated even more. Also, regular disturbances in resonant systems may cause undesired problems. Furthermore, the dynamical control response of this algorithm is slow and may stay off the maximum power point for some time, since it is commonly expected to change in solar irradiance or temperature [62, 63].

### 3.9.4 Incremental Conductance

This method depends on the on-line derivative solution of the output power given by  $P = V_L I_L$  with respect to the load voltage at the maximum power point, that is:

$$\left. \frac{dP}{dV_L} \right|_{P_m} = I_{Lm} + V_{Lm} \left. \frac{dI_{Lm}}{dV_{Lm}} \right|_{P_m} = 0$$

which gives

$$\frac{dI_{Lm}}{dV_{Lm}} = -\frac{I_{Lm}}{V_{Lm}} \approx -\frac{\Delta I_{Lm}}{\Delta V_{Lm}} \quad (3.23)$$

Another way of looking at this question is to obtain the power derivative with respect to the load current, that is:

$$\left. \frac{dP}{dI_L} \right|_{P_m} = V_{Lm} + I_{Lm} \left. \frac{dV_{Lm}}{dI_{Lm}} \right|_{P_m} = 0$$

which gives

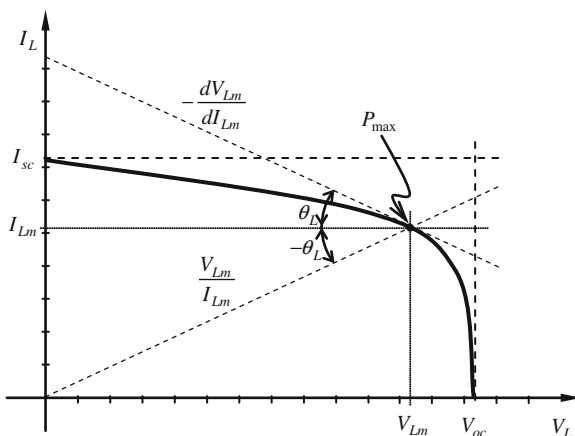
$$\frac{dV_{Lm}}{dI_{Lm}} = -\frac{V_{Lm}}{I_{Lm}} \approx -\frac{\Delta V_{Lm}}{\Delta I_{Lm}} \quad (3.24)$$

The incremental derivative is continuously measured to solve:

$$\frac{V_{L(\text{old})} - V_{L(\text{new})}}{I_{L(\text{old})} - I_{L(\text{new})}} \quad (3.25)$$

Based on this information, the reference voltage to the PWM algorithm is adjusted to move the panel current to the maximum power point. The steady-state error is small. A graphical interpretation of these relationships is given in Fig. 3.33. As it can be noticed in this Fig. 3.33, the point of maximum power is determined by the intersection point between two lines determined from Eq. (3.24). The terms on both sides of this equation are obtained from Eq. 3.6 [21, 64–68].

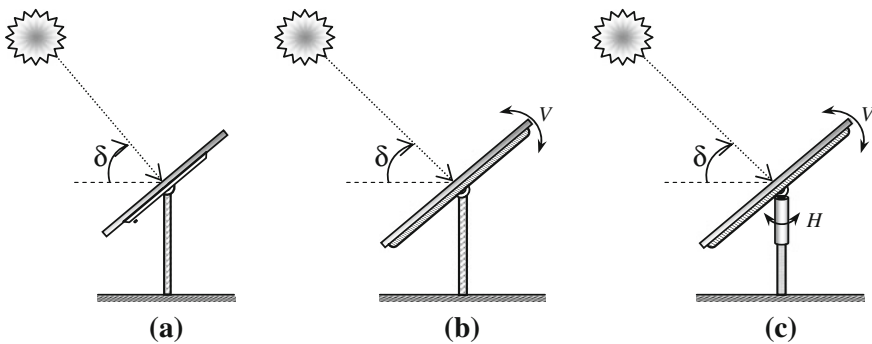
**Fig. 3.33** A graphical interpretation of the maximum power point



### 3.10 Sun Trackers

To maximize the solar energy, differences between angles of incidence in winter and summer days have to be considered and these differences will be added to the overall efficiency of the PV system. Efficiency of a PV solar panel is a crucial point to make any solar plant viable. The best Azimuth angle of the PV array to generate more energy is when it faces South in the Northern hemisphere and vice versa in the Southern hemisphere. To select the installation site the surroundings must also be evaluated to decide on the best orientation. A North–South cross-section cut may help in evaluating the incidence angle and any possible obstruction to the sunlight. An East–West cross-section is a wide open view on how the sun will travel from sunrise to sunset and possible shading along that path. For best results, differences between incidence angles of winter and summer days have to be considered. The angle at which sunlight hits the solar array changes every day. March 20 and September 22 are the dates of the vernal and autumnal equinoxes of the Northern hemisphere, where the array angle should be equal to the latitude. The ground mounted array has to be adjusted to  $+15^\circ$  for winter or  $-15^\circ$  for summer correction. This situation is illustrated in Fig. 3.34. In spring and fall, it is typical to set the module angle at the local latitude.

The structure of PV modules can be fixed or adjusted according to the position of the sun with respect to the ground or with the season of the year. The azimuth angle determines the direction the array faces with respect to South. For the southern hemisphere the array will have to face north. The array tilt will determine how much energy the PV array will generate as well. The array face will generate the most energy annually when it faces South (or North in the Southern hemisphere) and has an array tilt that has to be continuously corrected from summer to winter. This correct positioning can be obtained through intelligent cell arrangements, sun trackers, optimum control strategies, and well-designed arrays. A good cleaning of the solar panels surface may also increase the energy production by 8–12 %.



**Fig. 3.34** Spring and fall with the array angle equal to the latitude fixed structure (a), single axis (b), and double axis (c)

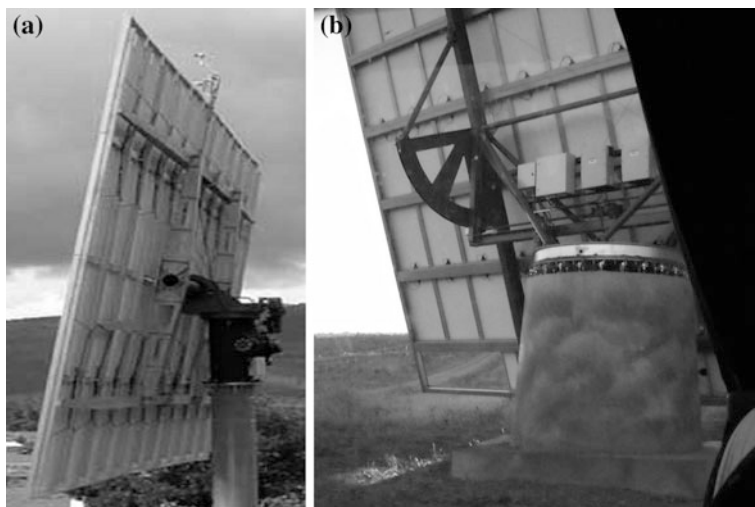
Also, concentration of the solar rays can produce electricity by using mirrors or lenses. The four best-known technologies are parabolic troughs, dish-Stirling engine systems, central receivers, and concentrating photovoltaic systems. The efficiency of a PV panel when collecting energy from the sun between sunrise and sunset can be increased by about 40 %, more or less depending on location, if the solar panel is kept directly following the sun track. This is done automatically by sun trackers.

There are two types of electromechanical sun trackers: the one-axis tracker, which keeps the PV module pointing horizontally to the North during the day in the Northern Hemisphere (or South in the Southern Hemisphere) and the two-axis tracker which has exactly the same role as the one-axis except that it also follows the sun's vertical movement during the seasons of the year as in Fig. 3.35a, b. Figure 3.36 illustrates two cases where two linear actuator motors are independently used to position the horizontal and vertical movements. At the end of the day, these motors are used to reposition the panels to begin all over again next morning.

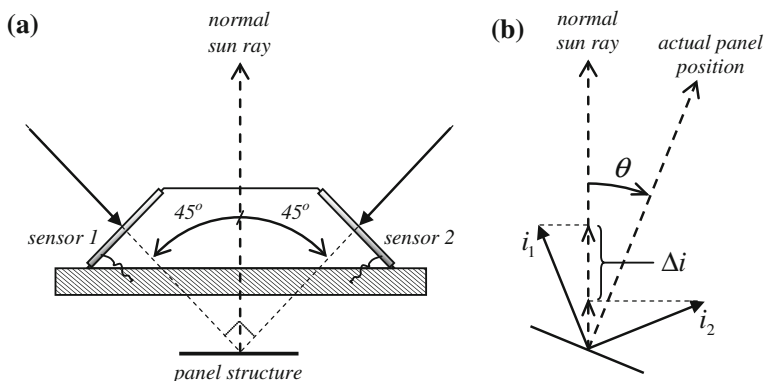
Two sensors are mounted on the panel structure positioned at  $45^\circ$  with respect to the normal sun rays as shown in Fig. 3.36. When the sun rays are exactly at the normal direction to the ground, the irradiation on both panels will be the same, so the current resulting from a differential combination of both panels will be null and the motor will be idle. The further the sun rays travel from the normal direction, the more the current will be available to drive the linear motor making it go at a higher velocity. Each sensor current follows approximately a cosine law as  $i = I_n \cos \theta$ . There is no need for keeping the motor activated at all times but only periodically.

There are two methods for controlling the linear motor. The first method is to use the current operating range of the linear motor by applying the resulting current from the differential sensors. The second way is by receiving the solar sensor data of the maximum unbalance range that is acceptable to let the solar module off the ideal direction to drive the linear motor at its rated current. The first method is more precise since it obeys every new sun position. The second method is simpler but it does not maximize the use of solar irradiance.





**Fig. 3.35** Example of solar trackers for PV panels. **a** Lugo, Galicia-Spain. **b** Extremadura-Spain (personal files)



**Fig. 3.36** Electromechanical sun trackers. **a** Location of a pair of PV sensors on the panel structure. **b** Phasor diagram of the current signal mismatch

Another type of sun tracker is the one based on satellite information. With the present knowledge of the astronomical position of the Earth with respect to the Sun's position, it is possible to estimate very accurately the best direction of the solar panel with respect to the position of the sun. This type of sun tracker has been tested in Extremadura and Andalusia PV Power Plants in Spain.

A third type of sun tracker still being researched uses a pair of sensors not mechanically connected to the structure of the solar panels. This sun tracker is based on the hill climbing strategy to determine the best position for the solar irradiance.

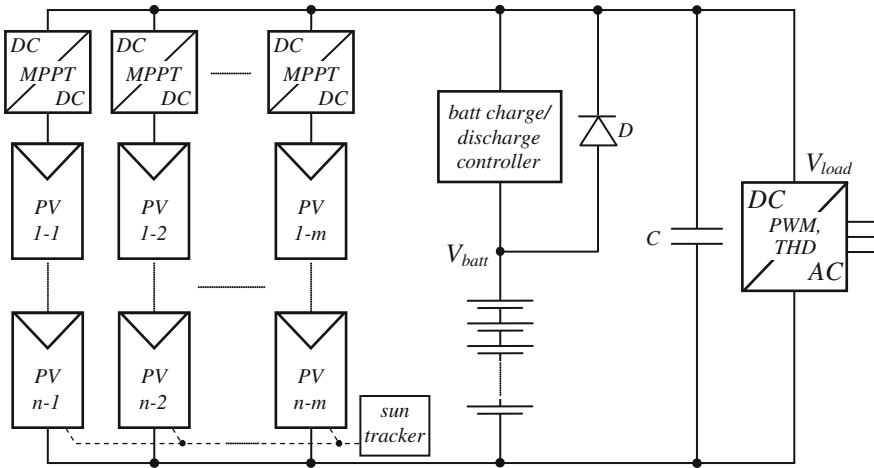


Fig. 3.37 Generic example of double stage PV integration with battery storage

This information is then passed to a computer which determines the correct position of the solar panels for both the vertical and horizontal positions.

### 3.11 Generic Example of PV Integration

A typical PV system including most of the parts discussed in this chapter is presented in Fig. 3.37 shows that the PV cells are organized into modular panels as usual to produce electricity with voltage standards of 12, 24, and 48 V well adapted to the lead–acid battery levels.

The standard 12 V strings can be associated with others of the same level in series and/or parallel to produce the commercial PV power plants. It is always possible to group panels or modules in arrays like the one shown in Fig. 3.37 to produce the levels of power required by the consumer or the grid. Their output is generally converted into AC through DC–AC converters as discussed in this chapter to feed most of the modern loads or to be connected to the grid. However, there are several types of DC loads supplied directly from solar panels as well and manufacturers are opening a slice of their market for these products, for example DC bulbs, television sets, computers, water pumps, washing machines, and many others.

## References

1. <http://rredc.nrel.gov/solar/spectra/am1.5/ASTMG173/ASTMG173.html>
2. Farret FA, Godoy Simões M (2006) *Integration of alternative sources of energy*. Wiley, Boca Raton
3. Villa LFL (2010) Maximizing the power output of a partially shaded PV plant by optimizing the interconnections among its modules. M.Sc. research 2 in electrical engineering, EEATS Grenoble INP/UJF Grenoble, France
4. Stapleton G, Garrett S, Thorne B (2007) *Grid connected PV systems, design and installation*, 1st edn. Global Sustainable Energy Solutions Pty Ltd, Ulladulla
5. Wang YJ, Hsu PC (2009) Analysis of partially shaded PV modules using piecewise linear parallel branches model. *World Acad Sci Eng Technol*, vol 60
6. Chamberlin CE, Lehman P, Zoellick J, Pauletto G (1995) Effects of mismatch losses in photovoltaic arrays. *Sol Energy* 54(3):165–171
7. Picault D, Raison B, Bacha S, de la Casa J, Aguilera J (2010) Forecasting photovoltaic array power production subject to mismatch losses, science direct. *Sol Energy* 84(2010): 1301–1309
8. Bratcu AI, Munteanu I, Bacha S, Picault D, Raison B (2011) Cascaded DC-DC converter photovoltaic systems: power optimization issues. *IEEE Trans Ind Electron* 58(2):403–411
9. Kaushika N, Rai AK (2007) An investigation of mismatch losses in solar photovoltaic cell networks. *Energy* 32(5):755–759
10. Alonso-García M, Ruiz J, Chenlo F (2006) Experimental study of mismatch and shading effects in the i-v characteristic of a photovoltaic module. *Sol Energy Mater Sol Cells* 90(3):329–340
11. Patel H, Agarwal V (2008) MATLAB-based modeling to study the effects of partial shading on PV array characteristics. *IEEE Trans Energy Convers* 23(1):302–310
12. Wang X, Yang L, Yan P (2010) Parameter optimization of MPPT and simulation of PV grid-connected system. In: 2nd international conference on information science and engineering (ICISE), pp 6752–6755. doi:[10.1109/ICISE.2010.5691939](https://doi.org/10.1109/ICISE.2010.5691939)
13. Villalva MG, Gazoli JR, Filho ER (2009) Analysis and simulation of the P&O MPPT algorithm using a linearized PV array model. In: *Brazilian power electronics conference (COBEP 09)*, pp 189–195. doi:[10.1109/COBEP.2009.5347755](https://doi.org/10.1109/COBEP.2009.5347755)
14. Villalva MG, de Siqueira TG, Ruppert E (2010) Voltage regulation of photovoltaic arrays: small-signal analysis and control design. *Power Electron IET* 3(6):869–880. doi:[10.1049/iet-pel.2008.0344](https://doi.org/10.1049/iet-pel.2008.0344)
15. Kajihara A, Harakawa AT (2005) Model of photovoltaic cell circuits under partial shading. In: *IEEE international conference on industrial technology (ICIT 2005)*, pp 866–870. doi:[10.1109/ICIT.2005.1600757](https://doi.org/10.1109/ICIT.2005.1600757)
16. Farret FA, Lenz JM, Trapp JG (2011) New methodology to determinate the parameters of photovoltaic solar panels. In: *Brazilian conference on power electronics (XI COBEP 2011)*, Natal-RN, Brazil
17. Jagannathan B, Anderson WA (1996) Properties of sputtered amorphous silicon/crystalline silicon solar cells. In: *Conference record of the 25th IEEE photovoltaic specialists conference*, pp 533–536. doi:[10.1109/PVSC.1996.564061](https://doi.org/10.1109/PVSC.1996.564061)
18. Marion B (2008) Comparison of predictive models for photovoltaic module performance (PVSC08). In: *33rd IEEE photovoltaic specialists conference*, pp 1–6. doi:[10.1109/PVSC.2008.4922586](https://doi.org/10.1109/PVSC.2008.4922586)
19. Tsuno Y, Hishikawa Y, Kurokawa K (2006) Curves of various PV cells and modules. In: *Conference record of the 2006 IEEE 4th world conference on photovoltaic energy conversion*, vol 2, pp 2246–2249. doi:[10.1109/WCPEC.2006.279619](https://doi.org/10.1109/WCPEC.2006.279619)
20. Millmann J, Halkias CC (1967) *Electronic devices and circuits*. McGraw-Hill Book Co, New York
21. Patel MR (1999) *Wind and solar power systems*. CRC Press, Boca Raton

22. Blaabjerg F, Chen Z, Kjaer SB (2004) Power electronics as efficient interface in dispersed power generation systems. *IEEE Trans Power Electron*, vol 19(5)
23. Rahim NA, Selvaraj J (2010) Multi string five-level inverter with novel PWM control scheme for PV application. *IEEE Trans Ind Electron* 57(6):2111–2123
24. Meinhardt M, Cramer G (2000) Past, present and future of grid connected photovoltaic- and hybrid-power-systems. In: *Proceedings of the IEEE power engineering society summer meeting*, vol 2, pp 1283–1288
25. Meinhardt M, Wimmer D (2001) Multistring-converter: the next step in evolution of string-converter technology. In: *Proceedings of the EPE01 conference*
26. Brunet Y (ed) (2011) *Energy storage*. ISTE Ltd, London. ISBN 978184821834
27. Kjaer SB, Pedersen JK, Blaabjerg F (2005) A review of single-phase grid-connected inverters for photovoltaic modules. *IEEE Trans Ind Appl* 41(5):1292–1306
28. KanEnergi AS (1998) *New renewable energy: Norwegian developments*. In: *The research council of Norway in cooperation with the Norwegian water resources and energy directorate (NVE)*. Hanshaugen, Oslo, Norway
29. [http://www.leonics.com/product/renewable/inverter/inverter\\_fronius-ig-central\\_en.php/](http://www.leonics.com/product/renewable/inverter/inverter_fronius-ig-central_en.php/)
30. <http://www.sunways.eu/en/products/solar-inverter/pt-series/>
31. <http://www.aegps.com/solarinverters/products/central-inverters/>
32. Johns M, Hanh-Phuc Le, Seeman M (2009) EE-290 N-3: contemporary energy issues: grid-connected solar electronics, technical report. Department of Electrical Engineering and Computer Sciences, University of California at Berkeley, Berkeley
33. Rashid MH (2003) *Power electronics, circuits, devices and applications*. Prentice Hall International Editions, New Jersey. ISBN 13: 9780131011403
34. Oishi H, Okada H, Ishizaka K, Itoh R (2002) Single-phase soft-switched current-source inverter for utility interactive photovoltaic power generation system. In: *Proceedings of the power conversion conference. PCC Osaka 2002*, vol 2. Oita National College of Technology, Osaka, Japan. ISBN: 0-7803-7156-9, INSPEC accession number: 7261748, pp 632–637. doi:10.1109/PCC.2002.997591
35. Ertasgin G, Whaley DM, Ertugrul N, Soong WL (2008) Implementation and performance evaluation of a low-cost current-source grid-connected inverter for PV applications. In: *IEEE international conference on sustainable energy technologies (ICSET 2008)*, pp 939–944. doi:10.1109/ICSET.2008.4747142
36. Shanthy T, Gounden AN (2007) Power electronic interface for grid-connected PV array using boost converter and line-commutated inverter with MPPT. *Intelligent and advanced systems (ICIAS 2007)*. Sri Ramakrishna Institute of Technology, Coimbatore. International conference on November 2007, E-ISBN 978-1-4244-1356-0, print ISBN: 978-1-4244-1355-3, INSPEC accession number 10368603, pp 882–886. doi:10.1109/ICIAS.2007.4658513
37. Komoto K, Ito M, Vleuten PV, Faiman D, Korokawa K (2009) *Energy from the desert: very large scale photovoltaic systems: socio-economic, financial, technical and environmental aspects*. Earthscan, Photovoltaic Power Systems Executive Committee of the International Energy Agency, London, UK. ISBN 978-1-84407-794-6
38. Sarwar A, Asghar MSJ (2010) Multilevel converter topology for solar PV based grid-tie inverters. In: *IEEE international energy conference and exhibition (Energy Con)*, Electrical Engineering Department, Aligarh Muslim University, Aligarh, India. ISBN: 978-1-4244-9378-4, INSPEC accession number: 12007879, pp 501–506. doi:10.1109/ENERGYCON.2010.5771733
39. Dorofte C (2001) *Design of a dc/dc converter for photovoltaic grid interconnection*. Aalborg University, Denmark
40. Timbus AV, Teodorescu R, Blaabjerg F, Borup U (2004) Online grid measurement and ENS detection for PV inverter running on highly inductive grid. *IEEE Power Electron Lett* 2(3):77–82

41. Achille E, Martire T, Glaize C, Joubert C (2004) Optimized DC-AC boost converters for modular photovoltaic grid-connected generators. In: IEEE international symposium on industrial electronics, vol 2, pp 1005–1010. doi:[10.1109/ISIE.2004.1571951](https://doi.org/10.1109/ISIE.2004.1571951)
42. Johns M, Hanh-Phuc Le, Seeman M (2009) Grid-connected solar electronics, EE-290 N-3-contemporary energy issues-grid-connected solar electronics, technical report. Department of Electrical Engineering and Computer Sciences, University of California at Berkeley, Berkeley
43. Fang C, Zhou Y (2010) Study on soft-switching technology of photovoltaic grid-connected system. In: International conference on communications, circuits and systems (ICCCAS). School of Informatics and Electronics Engineering, Panzhuhua University, Panzhuhua, China. ISBN: 978-1-4244-8224-5, INSPEC accession number: 11555617, pp 612–615. doi:[10.1109/ICCCAS.2010.5581920](https://doi.org/10.1109/ICCCAS.2010.5581920)
44. Shimizu T, Hashimoto O, Kimura G (2003) A novel high-performance utility-interactive photovoltaic inverter system. IEEE Trans Power Electron 18:704–711
45. Mohan N, Undeland TM, Robbins WP (2003) Power electronics: converters, applications and design, 3rd edn. Wiley, Hoboken
46. Schuch L, Dalla Costa MA, Rech C, Michels L, Costa GH, Santos AS (2011) Autonomous system of high efficiency public illumination based on solar energy and LEDs. Power Electron Mag Campinas Brazil 16(1):17–27
47. Wu T, Chang C, Wu Y (1999) Single-stage converters for PV lighting systems with MPPT and energy backup. IEEE Trans Aerosp Electron Syst 35:1306–1317
48. Wu TF, Chang CH, Wu YJ (1999) Single-stage converters for PV lighting systems with MPPT and energy backup. In: IEEE transactions on aerospace and electronic systems, vol 35(4). National Chung Cheng University, Taiwan
49. Walker GR, Sernia PC (2005) Cascaded dc-dc converter connection of photovoltaic modules. IEEE Trans Ind Appl 41:1292–1305
50. Shimizu T, Wada K, Nakamura N (2002) A flyback-type single-phase utility interactive inverter with low-frequency ripple current reduction on the dc input for an ac photovoltaic module system. In: Proceedings of the PESC02 conference, vol 3, pp 1483–1488
51. Lohner A, Meyer T, Nagel A (1996) A new panel-integrated inverter concept for grid-connected photovoltaic systems. In: Proceedings of the ISIE96 conference, vol 2, pp 827–831
52. Chithra M, Dasan SGB (2011) Analysis of cascaded H bridge multilevel inverters with photovoltaic arrays. In: 2011 international conference on emerging trends in electrical and computer technology (ICETECT). Tamil Nadu, India. ISBN: 978-1-4244-7923-8, INSPEC accession number: 11973746, pp 442–447. doi:[10.1109/ICETECT.2011.5760157](https://doi.org/10.1109/ICETECT.2011.5760157)
53. Dorofte C (2001) Comparative analysis of four dc/dc converters for photovoltaic grid interconnection. Aalborg University, Denmark
54. Calais M, Myrzik J, Spooner T, Agelidis VG (2002) Inverters for single-phase grid connected photovoltaic systems: an overview. Power Electron Specialists Conf 4:1995–2000
55. Caricchi F, Crescimbeni F, Napoli AD, Honorati O, Santini E (1993) Testing of a new dc-dc converter topology for integrated wind-photovoltaic generation system. In: 5th European conference on power electronics and applications, pp 83–88
56. Enslin JHR, Wolf MS, Snyman DB, Swiegers W (1997) Integrated photovoltaic maximum power point tracking converter. IEEE Trans Ind Electron 44:769–773
57. Snyman DB, Enslin JHR (1993) Simplified maximum power point controller for PV installations. In: 2nd IEEE photovoltaic specialists conference, pp 1240–1245
58. Koutroulis E, Kalaitzakis K, Voulgaris N (2001) Development of a microcontroller-based photovoltaic maximum power point tracking control system. IEEE Trans Power Electron 16:46–54
59. Szabados B, Wu F (2008) A maximum power point tracker control of a photovoltaic system. In: IEEE international instrumentation and measurement technology conference Victoria, Vancouver Island, Canada

60. Hohm DP, Ropp ME (2000) Comparative study of maximum power point tracking algorithms using an experimental, programmable, maximum power point tracking test bed. In: 3rd IEEE photovoltaic specialists conference, pp 1699–1702
61. Hsiao YT, Chen CH (2002) Maximum power point tracking for photovoltaic power system. *Ind Appl Conf* 2:1035–1040
62. Santos JL, Antunes FLM (2003) Maximum power point tracker for PV systems. In: World climate and energy event, pp 75–80
63. Kuo YC, Liang TJ, Chen JF (2001) Novel maximum-power-point-tracking controller for photovoltaic energy conversion system. *IEEE Trans Ind Electron* 48(3):594–601
64. Hsieh GC, Chen HL, Chang CY (2009) Energy management for interleaved PV stand-alone system with incremental conductance MPPT (TENCON 2009). In: IEEE region 10 conference, pp 1–6. doi:[10.1109/TENCON.2009.5395896](https://doi.org/10.1109/TENCON.2009.5395896)
65. Valenciaga F, Puleston PF, Battaiotto PE (2001) Power control of a photovoltaic array in a hybrid electric generation system using sliding mode techniques. *IEE Proc Control Theor Appl* 148(6):448–455
66. Xiao W, Dunford WG (2004) A modified adaptive hill climbing MPPT method for photovoltaic power systems. In: 35th annual IEEE power electronics specialists conference (PESC 04), vol 3, pp 1957–1963. doi:[10.1109/PESC.2004.1355417](https://doi.org/10.1109/PESC.2004.1355417)
67. Chambouleyron I (1989) Solar electricity. *Sci Today* 9(54):32–39
68. Messenger R, Ventre J (2000) Photovoltaic systems engineering. CRC Press, Washington, DC

# Chapter 4

## Wind Power Generation

Mohit Singh, Eduard Muljadi, Vahan Gevorgian and Surya Santoso

**Abstract** Wind power is a fast growing source of renewable energy. In this chapter, the process of conversion of the kinetic energy inherent in the wind to electrical energy is described. Numerous technologies exist and compete in order to achieve this objective, but in general, wind turbines and wind power plants (WPPs) rely on electrical machinery and power converters working together to achieve this purpose in an optimal and stable fashion. In this chapter, prevailing generator and converter types are discussed, as are some designs which may be seen in future turbines. Turbine and plant level control is also discussed.

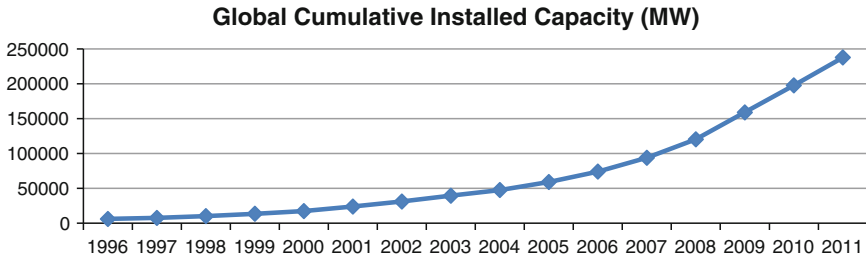
### 4.1 Introduction

The wind is a free, clean, and renewable energy source on our planet. It has served mankind for centuries to pump water, grind grain, and move ships. With the discovery of electricity and development of electric power, wind energy found new applications in human society in the form of providing clean and inexhaustible electric power in a wide range of scales and capacities. Nowadays, wind powered generation operates at variety of sizes between small residential and utility scales. Modern utility-scale wind power is the fastest growing energy sector in the world. It is becoming an important part in the national energy mix for many countries including the US. At the end of 2009, worldwide nameplate capacity of wind power generators was 159.2 GW producing about 2% of worldwide

---

M. Singh · E. Muljadi (✉) · V. Gevorgian  
National Renewable Energy Laboratory, MS ESIF200, 15013 Denver West Parkway,  
Golden, CA 80401, USA  
e-mail: eduard.muljadi@nrel.gov

S. Santoso  
Univeristy of Texas at Austin, Austin, TX 78712, USA  
e-mail: ssantoso@ece.utexas.edu



**Fig. 4.1** Wind energy global growth (*source* GWEC)

electricity usage [1]. The US continued to see growth and remains on top in total installed capacity followed by China and Germany. Wind power is capable of becoming a major contributor to America's electricity supply over the next three decades, according to a report by the U.S. Department of Energy [2]. US wind capacity has more than doubled in the past three years. Despite this growth, the technology used in wind turbines has not yet coalesced around one particular design. A wide variety of designs, especially for power conversion, are in use and on the drawing board. This makes wind turbines and WPPs an interesting study from the power conversion point of view. The upward trend in wind turbine installation worldwide is shown in Fig. 4.1.

## 4.2 Wind Energy Basics

The atmosphere surrounding our planet acts as a gigantic heat engine that extracts energy from the sun and reflects it back to a space. In the process, regions of lower and higher pressure are developed in the air. This pressure differences cause winds to blow. There are many factors affecting development of high and low pressure regions, and therefore the wind patterns. Such factors include solar radiation, surface cooling, humidity, complexity of terrain, rotation of the earth, etc. The greater is pressure difference between two neighboring regions the greater is the force on the air and the stronger is the wind speed. Accurate estimation of wind energy potential is the most important element in selecting a site for a future WPP. The stochastic nature of wind makes it hard to predict and is best described using statistical methods. Another complicating factor to note is that wind speed distributions are non-Gaussian. The two most common probability density functions used to describe the wind speed frequency are Weibull and Rayleigh functions. The Weibull function is considered more versatile since it uses a two-parameter distribution as opposed to the Rayleigh function which uses a single-parameter distribution. The Weibull density function for wind speed  $V$  can be described as



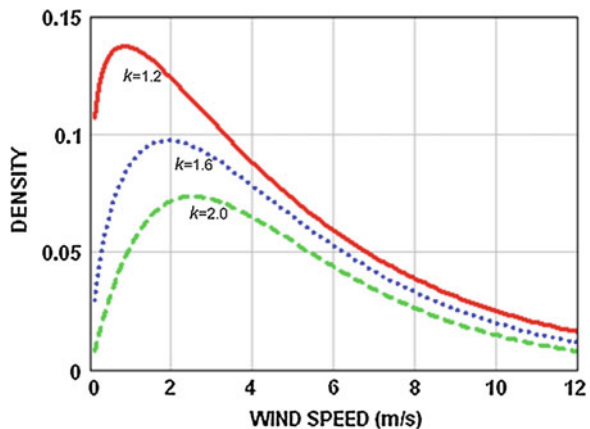
$$f(V) = \frac{k}{c} \left(\frac{V}{c}\right)^{k-1} e^{-\left(\frac{V}{c}\right)^k} \tag{4.1}$$

Here  $c$  and  $k$  are the scale and shape parameters respectively. Some example Weibull distribution curves are shown in Fig. 4.2, with each curve representing a different geographical region. For each of the three curves, the scale parameter is  $c = 5$  m/s. The top curve shows a distribution for a relatively low wind speed region. In this curve, the density of measured wind speeds peaks at around 0.75 m/s. The bottom curve shows a higher wind speed region, where the density of wind speed measurements peaks at around 2 m/s. Typically, long-term wind speed data collection (1 year or longer) is needed for statistically meaningful determination of Weibull  $c$  and  $k$  parameters. From this data, the WPP’s annual energy production can be estimated.

Another important aspect of wind speed nature is a variation with height. This is why it is important to collect wind speed data at different heights to understand the wind shear profile. Depending on the capacity of a prospective wind farm, more than one meteorological tower may be required for wind speed and direction measurements.

A high-quality wind speed measurement is essential in reducing the uncertainties in predicted energy production and economic feasibility assessments of a proposed project. Wind speeds can be measured in a wide variety of ways. A typical anemometry mast has number of anemometers, wind vanes, and ambient sensors (temperature, pressure, wetness, etc.). In many cases, the classic rotational cup anemometers still remain the primary means for wind speed measurements. Other technologies, such as ultrasonic anemometers have been used as well. In recent years, more advanced ground-based remote sensing devices such as sound detection and ranging (SODARs) and light detection and ranging (LIDARs) have been entering the market for wind site assessments. Such devices can measure wind speeds at a range of heights without the need for conventional mast.

**Fig. 4.2** Weibull density function curves ( $c = 5$  m/s)



## **4.2.1 Energy Generation**

### **4.2.1.1 History of Wind Power**

One of the earliest non-animal sources of power used by man was the wind turbine. Wind turbines have been in documented use for more than 1,000 years. The earliest wind turbine designs were extremely simple; turbines were allowed to rotate at a rate proportional to the velocity of the wind. They were used to pump water, grind grain, cut lumber, and perform a myriad of other tasks. For these purposes, varying speed seldom impacted the effectiveness of the windmill enough to justify the complications of closely controlling rotational speed. Allowing the machines to run at variable speed was in fact highly advantageous as it greatly increased the total energy that could be extracted from the wind.

The earliest horizontal-axis windmill to use the principles of aerodynamic lift instead of drag may have been introduced in the twelfth century. These horizontal-axis sail turbines were allowed to run at varying speeds, limited only by braking or furling to control their speed during storms. These designs operated throughout Europe and in the Americas into the present century. In the 700 or so years since the first sail-wing turbine, designers discovered many of the key principles of aerodynamics without understanding the physics behind them. It was not until the nineteenth century that these principles began to be clearly understood.

In the early nineteenth century the classic American water pumper was introduced. The need for this machine was driven by the phenomenal growth of agriculture in the American Midwest, beginning with the opening of the North-western prairie states in the early 1800s. More than a million of these machines dotted the Midwest and West starting in the early 1850s. Even now these multi-bladed farm windmills can be seen throughout the western United States and Canada, where the energy and storage requirements for providing drinking water for cattle are well matched to the wind water pumper's power, the storage capacity of the associated stock tank, and the wind statistics of the Great Plains. These machines use the most rudimentary airfoils (often flat plates or slats of wood) and are allowed to rotate proportionally to wind velocity. For the purposes of direct mechanical water pumping, this variable-speed operation works effectively. Although the American water pumping design gives up something by its dependence on a flat-plate airfoil, its simplicity, ease of construction, and reliability still make it ideal for its intended purpose.

The early twentieth century saw the start of the electric era. The rapid advances in motor, generator, lighting, and appliance designs by Edison, Steinmetz, Tesla, and others offered the promise of an electric-powered utopia. The homes and farms of America were not immune to this desire, and for remote locations wind turbines offered great promise. As early as 1888 the Brush wind turbine in Cleveland, Ohio, had produced 12 kW of direct current (DC) power for battery charging at variable speed. DC and variable-speed wind turbines seemed only natural. Many early electric motors required DC and the varying voltage due to turbulent winds was

held relatively constant by the associated battery bank. At remote farms, where power lines might never reach, a DC wind turbine could charge batteries, and operate equipment that could never cope with varying alternating current (AC) frequencies caused by constantly changing wind speeds.

In 1925 Marcelleus and Joseph Jacobs began work on the first truly high-speed, small-size, affordable battery charging turbine. Thousands of their 32 and 110 V DC machines were manufactured starting in the late 1920s and running into the 1950s. This machine was followed by others such as the Windcharger. They could be setup easily and required little if any maintenance. All of these machines were allowed to run at variable speed. Even after AC utility power had begun to spread through cities and towns, Sears Roebuck and others manufactured and distributed a wide range of products designed to run on DC to satisfy the needs of remote farms and ranches using batteries and variable-speed DC turbines.

In 1937 the creation of the Rural Electric Associations started the demise of these stand-alone variable-speed DC machines. As AC power lines spread throughout rural America, the need for such machines began to fade. America was becoming connected, and in the future would depend upon large central power plants to produce electricity for all. Long transmission lines required much higher voltage for efficient distribution. Electric transformers and their required AC were the obvious technology to employ. It was then necessary to standardize on a constant voltage levels and a constant frequency. In North America, this fixed frequency became 60 Hz (Hz or cycles per second). The simple variable-speed wind turbines had no economical way of either interconnecting to these grids or supplying power for the many new appliances that began to fill farm households. The prudent farmer or rancher might keep his old machines running for emergencies; however, his wife began depending on cheap, dependable AC to wash the clothes and run the phonograph. The return to power independence for the American farmer and rancher would have to wait for a new generation of technologies.

Despite the apparent difficulties of connecting a wind turbine to the AC electrical grid, as early as 1939 in the United States, such a step had been explored. Even earlier examples of large turbines used to produce electricity tied to an established AC electrical grid may be cited; however, for depth of engineering and breadth of vision, few early pioneers have surpassed Palmer Putnam's Grandpa's knob machine. This machine was incredibly advanced for its day, with full-span pitch control, active-yaw drive, two-bladed flapping rotor, and 1.25 MW (megawatt) rating. However, the Smith-Putnam turbine rotor avoided the problem of variable speed and ran at a fixed rpm locked to a synchronous generator directly tied to the electrical grid. However, by fixing the rotational rate of the turbine to that of the electric grid, the turbine lost a great deal of wind potential. Allowing the machine to rotate at a varying rate would optimize the aerodynamics of the rotor by allowing its speed to be proportional to wind speed. In this operating mode, as we will see later, the machine can capture the maximum fraction of available wind energy. Not only would it gain more aerodynamic efficiency in high winds, but it would also be able to run at lower speeds and gather more energy than a fixed-speed machine.

The dream of a variable-speed wind turbine tied to the AC electrical grid began to become a viable reality in the early to mid-1970s. Machines went on-line in the United States and Europe, using several different methods for transforming variable-voltage, variable-frequency outputs to reliable constant voltage, constant frequency outputs. In addition to large grid-connected machines, small stand-alone machines were developed that incorporated these new technologies and would allow the farmer or homeowner to produce his own power, and to someday allow him to sell his excess power back to the utility grid. For example, the 8 kW *Windworks* machine of the early 1970s used a diode bridge to rectify the variable-frequency output of the permanent magnet generator. Silicon controlled rectifiers (SCRs) were used in an inverter module to convert the resulting rectified DC output to produce AC synchronized to the grid. Technologies like these are still in use, as described below, and are being further developed. New technologies are under constant development.

Variable-speed wind turbines provide the ability to control the rotor speed. This allows the wind turbine system to operate constantly near to its optimum tip-speed ratio. Current variable-speed-based turbine technologies have enabled wind energy to become a viable power source in today's energy market. In spite of the progress, wind energy provides approximately 1% of total U.S. electricity generation. Advancements in turbine technology that have the potential to increase wind energy's presence are currently being explored. These areas of study include reducing capital costs, increasing capacity factors, and mitigating risk through enhanced system reliability. With sufficient research, development, and demonstration (RD&D), these new advances could potentially have a significant impact on commercial product lines in the next 10–20 years.

Commercial, utility-scale wind turbines have evolved significantly from their early days in the 1980 and 1990s. Today, typical commercial turbine installation is 2.5 MW although some 5.0–6.0 MW wind turbines are being installed in Europe. Most manufacturers have larger (up to 10 MW) machines in design stages targeting offshore markets. For example, Clipper Wind Power is fine-tuning plans for the 10 MW Britannia wind turbine which will be one of the world's largest wind machines.

### ***4.2.2 Wind Turbines***

Wind turbines produce electrical power by converting the kinetic energy of wind into mechanical power with subsequent conversion into electrical power by means of an electrical generator. Gearboxes are used to increase the speed of rotating shaft to a level appropriate for generator to operate. Power electronic converters are used in variable-speed wind turbines to convert generator varying voltage and frequency to the constant level required by the utilities. The power output then goes to a transformer, which converts voltage to a collection level (usually 35 kV).

### 4.2.2.1 Aerodynamic Power

The kinetic energy in a section of air of length  $l$  and mass  $m$  moving at speed  $V$  through cross-sectional area  $A$  is

$$E = \frac{1}{2}mV^2 = \frac{1}{2}\rho AV^2 l \quad (4.2)$$

The power in the wind is the first derivative of kinetic energy

$$P_{\text{air}} = \frac{1}{2}\rho AV^2 \frac{dl}{dt} = \frac{1}{2}\rho AV^3 \quad (4.3)$$

An ideal wind turbine cannot extract more 16/27 of  $P_{\text{air}}$  (or 0.593—so-called Betz limit). Even smaller amount of power can be extracted by a real rotor. The fraction of power extracted by a real wind rotor is determined by the power coefficient  $C_p$ :

$$P_m = C_p P_{\text{air}} = \frac{1}{2}C_p \rho AV^3 \quad (4.4)$$

The maximum value of  $C_p$  is determined by Betz limit. The practical maximum values of  $C_p$  are in the range of 25–46%. The power coefficient  $C_p$  depends on many design and operational factors. It is a conventional method to define the  $C_p$  as a function of a tip-speed ratio  $\lambda$  of wind turbine rotor. Here,  $\omega$  is rotor angular speed (rad/s), and  $R$  is rotor radius (m).

$$\lambda = \frac{\omega R}{V} \quad (4.5)$$

### 4.2.2.2 Control of Wind Turbines

In the past, wind harnessing devices such as sails or windmills employed manual controls to change the amount of energy extracted from the wind. In modern wind turbines, automated control systems employing electronic or hydraulic control schemes are employed. These controls are necessary for maximization of energy extraction from the wind and for protection of the mechanical and electrical machinery comprising the turbine from the stresses imposed by adverse wind conditions. Four control techniques are discussed here [3]:

- Turbine yawing.
- Pitch control.
- Stall control.
- Speed variation.

Turbine yawing refers to the rotation of the turbine about the vertical axis (perpendicular to the ground, along the wind turbine tower). Within the operating

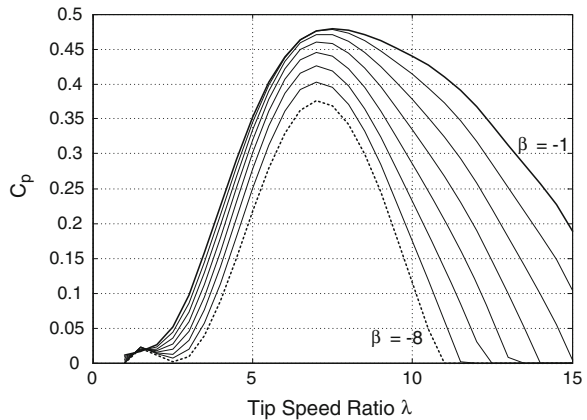
range of wind speeds, yawing is employed to allow the turbine to track the wind direction. The wind turbine's plane of rotation aligns itself perpendicular to the wind flow, resulting in optimal energy extraction. If wind speeds exceed the cut-out speed of the turbine, the yaw mechanism is employed to move the turbine's plane of rotation parallel to the wind flow direction to reduce the effective cross section of the rotor and protect the machine. Small machines (such as the ubiquitous 'Western wheel' turbines) use passive yaw systems, typically wind vanes. Downwind turbines are steered by wind pressure on the blades. However, the majority of modern wind turbines are upwind turbines. Modern turbines employ electric or hydraulic azimuth drives consisting of a motor and gearbox, a ring gear, and a yaw controller.

As mentioned earlier, the rotor power coefficient  $C_p$  depends on the blade pitch angle. Rotating the blades about their long axes changes the pitch angle, modifying  $C_p$ , and thus changing the power extracted from the wind. The relation between  $C_p$  and tip-speed ratio for different pitch angles is shown in Fig. 4.3 for an example turbine. Blade-pitching can be achieved precisely and quickly with the use of electric controls, allowing smooth control of output power. Most wind turbines rated above 0.5 MW employ this control method for power regulation.

There is a nonlinear relationship between blade pitch angle and rotor power coefficient, and any controller design must take this fact into account. Blade pitch angle controllers must also be able to contend with dynamic torques acting on the turbine blades during pitch angle changes. A simplified pitch angle control implementation has been discussed in Sect. 4.4.1.1.

For turbines of rating less than 0.5 MW, a technique known as stall regulation is employed to limit power extraction from the wind. No active controllers are used, and the turbine performance characteristics are influenced through blade design. This technique employs a blade design in which during normal operation, airflow at the blades is laminar, i.e., the flow can be considered to be smooth streamline flow with no turbulence. This condition persists for all wind speeds from cut-in wind speed to rated wind speed (wind speed at which rated power is

**Fig. 4.3** Change in  $C_p$  curves with change in pitch angle ( $\beta$ )

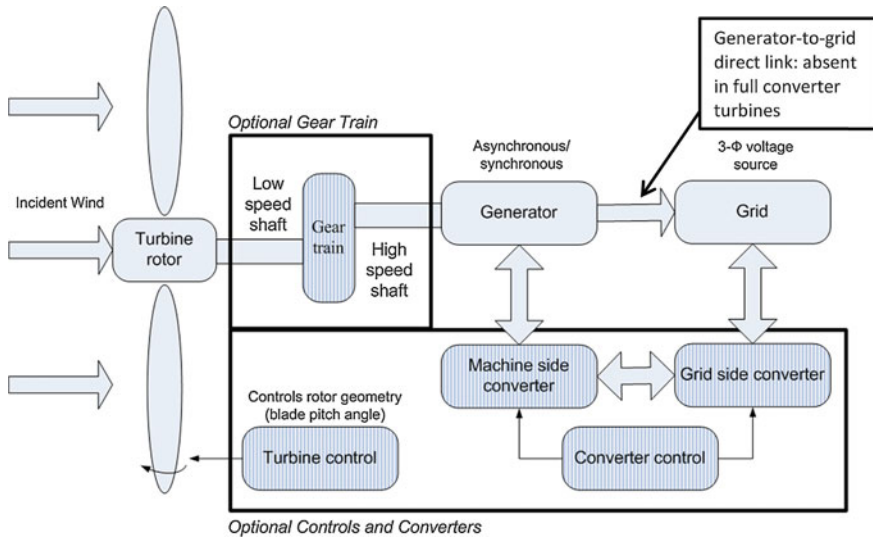


developed). At wind speeds higher than rated, the blade design results in non-laminar or turbulent airflow, thus reducing the lift force on the blades and increasing the drag force. The result of these changes is that the power output reduces, since power output is largely dependent on the lift force. Thus, even though there is more energy available for extraction is higher than rated wind speeds, the turbine output reduces in order to protect the turbine. While this technique is relatively simple to implement, power extraction is not maximized.

The first modern upwind turbines to be deployed in megawatt-scale wind farms employed induction machines operating at a fixed speed, and came to be known as fixed-speed wind turbines. The rotor speed variation for these turbines is kept to a minimum. The allowable variation is typically less than 1% of rated rotor speed. Maintaining this constant speed under diverse wind conditions causes huge stresses on wind turbine gearboxes, bearings and other components, leading to increased maintenance requirements. Variable-speed turbines (with rotor speed variation of up to 30% of rated rotor speed allowable) have since been introduced and have captured the majority of the market. These variable-speed turbines employ a number of different methods to achieve their goals (and these are discussed in [Sect. 4.2.3.1](#)). While both mechanical (changing of gear ratios) and electrical methods (frequency converters) are feasible for speed changing, in practice electrical methods are preferred since they offer faster and more reliable methods of speed control. Variable-speed turbines have reduced dynamic loading on the mechanical as well as electrical systems, and also increase the time spent operating at optimal performance levels.

### ***4.2.3 Wind Generators***

A wide variety of wind turbine technologies are in use today [4, 5]. Typical WPPs consist of hundreds of turbines, usually all employing the same technology. These technologies vary in cost, complexity, efficiency of wind power extraction and equipment used. A typical wind turbine employs a blade and hub rotor assembly to extract power from wind, a gear-train to step up the shaft speed at the slowly spinning rotor to the higher speeds needed to drive the generator, and an induction machine or synchronous machine as an electromechanical energy conversion device. Induction machines are popular as generating units due to their asynchronous nature. Maintaining a constant synchronous speed in order to use a synchronous generator is difficult due to variable nature of wind speed. However, full converter turbines are able to employ high pole count permanent magnet synchronous generators, since the generator is completely decoupled from the grid frequency. Power electronic converters may be used to regulate the real and reactive power output of the turbine. [Figure 4.4](#) shows a general framework for representation of most typical wind turbine technologies. The different types of wind turbines are discussed in more detail in this subsection.



**Fig. 4.4** Block diagram of typical wind turbine

#### 4.2.3.1 Different Types of Wind Turbines

The dominant technology for utility-scale applications is the horizontal axis wind turbine (HAWT). These turbines are called so because the axis of rotation of the turbine blades is parallel to the ground. Vertical axis wind turbines (VAWTs) have been developed but are not yet technologically mature enough for utility-scale applications. Typical power ratings for HAWTs range from 500 kW to 7 MW. It must be noted that the power output is inherently fluctuating and nondispatchable.

According to differences in generation technology, in [6, 7], wind turbines have been classified into four basic types:

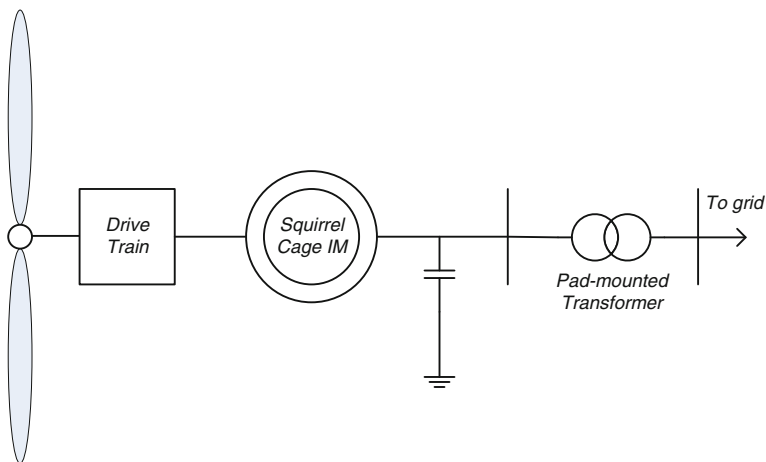
- Type 1: Fixed-speed wind turbines.
- Type 2: Variable-slip wind turbines.
- Type 3: Doubly-fed induction generator (DFIG) wind turbines.
- Type 4: Full converter wind turbines.

Fixed-speed wind turbines (popularly known as the “Danish concept”) are the most basic utility-scale wind turbines in operation. They operate with very little variation in turbine rotor speed, and employ squirrel-cage induction machines directly connected to the grid. External reactive power support is necessary to compensate for the reactive power consumed by the induction machine. Due to the limited speed range over which these turbines operate, they are prone to torque spikes which may be damaging to the mechanical subsystems within the turbine and may cause transients in the electrical circuitry. These turbines may employ passive stall regulation, active stall regulation, or blade pitch regulation in order to regulate power at high wind speeds. For turbines employing passive stall



regulation, the blades are designed to cause turbulent flow at high wind speeds, creating stall conditions, and thus reducing lift force and aerodynamic power. Turbines employing pitch regulation employ blades which can be rotated about their long axes by the use of actuators. The blades are rotated (pitched) to change their angle of attack, thus lowering lift forces and aerodynamic power at high wind speeds. Active stall turbines also employ pitchable blades, but they are rotated in the opposite direction with respect to blades for pitch controlled turbines. This rotation leads to turbulent air flow and stalling. Although relatively robust and reliable, there are significant disadvantages of this technology, namely that energy capture from the wind is sub-optimal and reactive power compensation is required. An example of a popular fixed-speed wind turbine is the NEG Micon NM64/1 500 turbine, rated at 1.5 MW. A schematic for fixed-speed wind turbine is shown in Fig. 4.5.

Variable-speed wind turbines (the broad category into which the other three dominant technologies fall) are designed to operate at a wide range of rotor speeds. These turbines usually employ blade-pitching for power regulation. Speed and power controls allow these turbines to extract more energy from a given wind regime than fixed-speed turbines can. Variable-slip turbines employ wound rotor induction machines, which allow access to both the stator and the rotor of the machine. The rotor circuit of the machine is connected to an AC–DC converter and a fixed resistance. The converter is switched in such a manner to control the effective resistance in the rotor circuit of the machine, in order to allow a wide range of operating slip (speed) variation (up to 10%). However, power is lost as heat in the external rotor circuit resistance. A controller may be employed to vary the effective external rotor resistance for optimal power extraction. Reactive power compensation is still required. Vestas OptiSlip turbines such as the Vestas V66

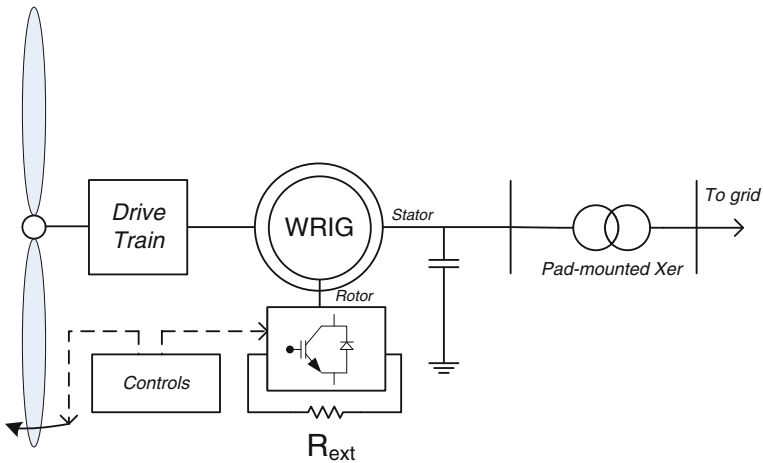


**Fig. 4.5** Fixed-speed wind turbine schematic

(1.65 MW) were the most successful turbines to employ this technology. A schematic for this technology is shown in Fig. 4.6.

DFIG turbines remedy the problem of power loss in the rotor circuit by employing a back-to-back AC/DC/AC converter in the rotor circuit to recover the slip power. Flux-vector control of rotor currents allows decoupled real and reactive power output, as well as maximized wind power extraction and lowering of mechanical stresses. These turbines also usually employ blade-pitching for power regulation. Since the converter is only handling the power in the rotor circuit, it does not need to be rated at the machine's full power output. The disadvantages of this technology, namely higher cost and complexity, are offset by the ability to extract more energy from a given wind regime as compared to the preceding technologies. The GE 1.5 MW turbine is an example of a successful DFIG design, with over 15,000 turbines installed. A schematic for this technology is shown in Fig. 4.7.

In full converter turbines, a back-to-back AC/DC/AC converter is the only power flow path from the wind turbine to the grid. The converter has to be rated to handle the entire power output of the turbine. There is no direct connection to the grid. These turbines usually employ high pole count permanent magnet synchronous generators, but use of induction generators is also possible. The reason for using high pole count machines is that they allow the elimination of the gearbox from the drive-train, thus increasing reliability. These turbines also offer independent real and reactive power control, and typically employ blade-pitching for power regulation. A schematic for this technology is shown in Fig. 4.8. While these turbines are relatively expensive, the increased reliability and simplicity of the control scheme vis-à-vis DFIG turbines are attractive features especially for offshore installations where maintenance is costly. Enercon manufactures turbines based on this technology, such as the popular E82, a 2 MW turbine.



**Fig. 4.6** Variable-slip wind turbine schematic

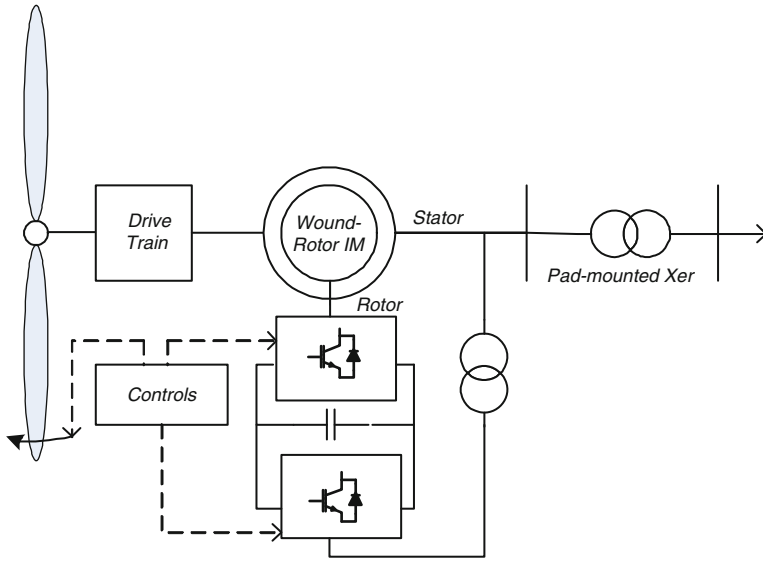


Fig. 4.7 Doubly-fed induction generator wind turbine schematic

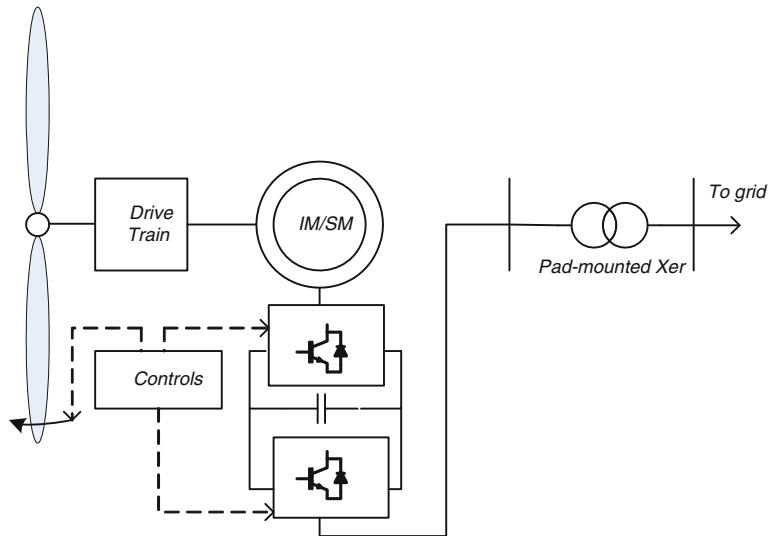


Fig. 4.8 Full converter wind turbine schematic

The four turbine technologies discussed here are found in the majority of wind turbines already installed and planned for installation. However, many other significantly different technologies exist, and minor variations based on these four dominant technologies are also being explored [8]. New and emerging technologies may also challenge the dominant technologies in the future. Trends indicate

that DFIG and full converter turbines will enjoy strong growth as they are the preferred options for new WPPs and as older turbine types are replaced with newer ones in existing WPPs.

#### 4.2.3.2 Different Levels of Connection

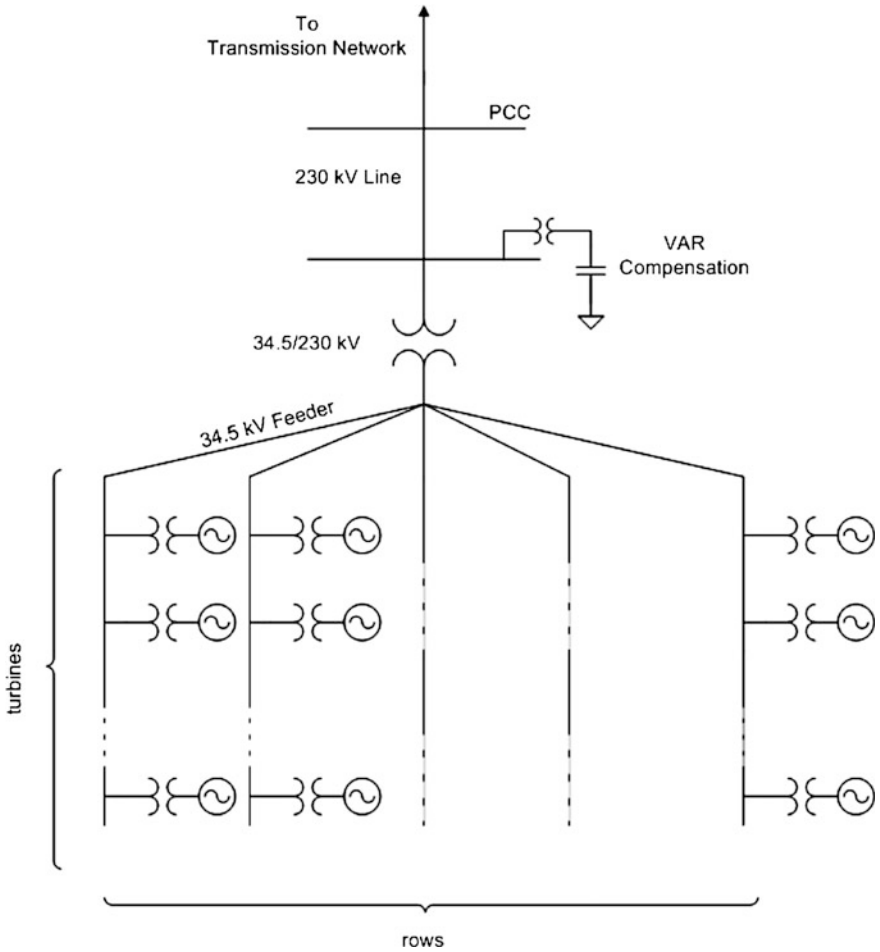
The majority of installed wind turbines are connected to the bulk power system. They are rarely installed singly, instead being installed in groups of tens or hundreds of similar turbines (wind farms) which pool the generated power and supply it to the power system through an interfacing network known as the collector system [9]. The collector system typically consists of the following passive elements:

- Individual generator transformers (usually pad-mounted units at the base of each turbine) that step-up voltage from the sub-1 kV level at the generator to medium-voltage levels (34.5 kV is typical).
- Medium-voltage underground cables connecting the turbine rows.
- Medium-voltage overhead lines from the turbine rows to the main substation.
- Step-up transformer(s) at the main substation that raise the voltage to transmission levels (Fig. 4.9).

A WPP consists of many individual wind turbine generators (WTGs) tied to a medium voltage collector system, and connected to the transmission system at the interconnection point. Modern utility-scale WTGs have nameplate ratings ranging from 1 to 4 MW. Terminal voltage typically ranges from 575 to 690 V. A step-up transformer, generally a pad-mounted unit, connects each WTG to a medium-voltage collector system operating at 12–34.5 kV. The collector system consists of one or several feeders connected together at a collector system station. One or more station transformers at the collector system station are used to achieve transmission system voltage. Unless the collector system station is adjacent to the interconnection point, an interconnection transmission line is needed.

Reactive compensation in the form of mechanically switched capacitors and continuously variable devices such as STATCOMs or static var systems (SVS) may be installed at the collector system station. Depending on the type of WTG, shunt reactive compensation at the WTG terminals may be installed for power factor correction. The amount and nature of reactive compensation is driven by interconnection requirements and collector system design considerations, including voltage regulation and losses.

The effects of wind turbines and wind farms on the bulk power system depend on the voltage level at which the collector system interconnects with the power system. The voltage level of interconnection depends on the size of the WPP and its location. Grid codes set the rules for acceptable behavior for wind farms interconnected to the power system [10–12]. The dominant concerns are voltage control and reactive power compensation. Voltage stability may be the limiting factor when it comes to deciding the maximum size of a wind plant allowable for

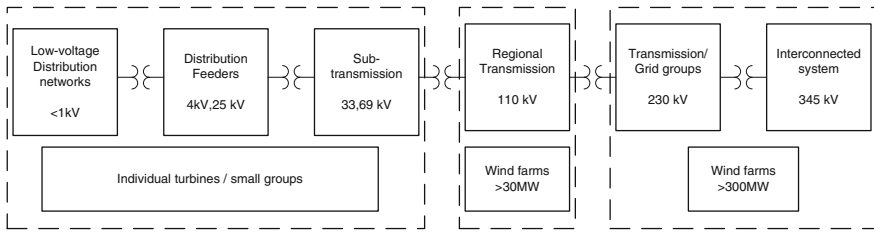


**Fig. 4.9** Collector system for wind farm

interconnection at a particular node. These concerns are particularly acute when wind farm sites are far away from load centers or connected to the power system through a weak network. Wind turbines may also be connected individually or in small groups to distribution networks, however, in these networks power quality rather than stability is the main concern (Fig. 4.10).

#### 4.2.3.3 Fault Ride Through

The main causes of voltage faults on wind turbine terminals are short circuits that can occur in various locations of the power system in a number of different ways including line-to-ground and line-to-line faults. Such faults can be symmetrical or



**Fig. 4.10** Connection at different voltage levels

nonsymmetrical depending on the fault scenario. The amplitude of a voltage dip on a single wind turbine or whole wind farm terminals depends on the type of the fault and electrical distance to the location of the fault. Traditionally, wind turbines were disconnected from the grid immediately after abnormal voltage conditions were detected by wind turbine control systems. This type of response to voltage faults cannot be used in power systems with higher levels of wind penetration. Disconnecting large number of wind turbines from the grid in response to voltage faults may cause instability problems for the whole power system. Modern wind turbines are now required to stay connected during voltage faults of certain durations and depths, and continue normal operation immediately after fault is cleared. This is called a fault ride through (FRT) capability, and applies to both low and high-voltage conditions. Such capability is nowadays an interconnection requirement for wind power in many grid codes. Wind turbine response to voltage faults largely depends on wind turbine electrical topology. Some topologies are prone to producing large currents in response to voltage drops on wind turbine terminals. This category includes wind turbines with generators directly coupled to the grid. In such cases, some power electronic devices can be applied on the wind farm level to improve FRT characteristics of the whole WPP. Other topologies use full capacity power converters isolating the generator from grid voltage. Such topologies allow control over the amount of current that the wind turbine contributes to the fault.

#### ***4.2.4 Onshore and Offshore Wind Power Plants***

In the early development of WPPs only onshore WPPs were considered, however, with the immense potential for offshore wind (50 GW in the US alone), offshore wind is now the focus of much research. The best locations for a WPP must have several attributes: high wind resource, close to the transmission line access, close to the load center, easy access to major highway for transportation, availability of inexpensive land, environmentally suitable for WPP.

**Table 4.1** Comparison of conventional power plant and wind power plant

Conventional power plant	Wind power plant
Single or several large (40–1,000 MW+) generators	Many (hundreds) of wind turbines (1–5 MW each), covers a very large area
Generator: synchronous generator	Generator: four different types (fixed speed, variable slip, variable speed, full converter)
Fixed speed—no slip: Flux is controlled via exciter winding. Flux and rotor rotate synchronously	Type 3 and 4: variable speed with flux oriented controller (FOC) via power converter. Rotor and flux do not rotate synchronously
Prime mover: steam, combustion engine—non-renewable fuel	Prime mover: wind turbine—wind
Located where convenient for fuel and transmission access	Located at wind resource, it may be far from the load center
Controllability: adjustable up to max limit and down to min limit	Controllability: curtailment, ramp rate limit, output limit
Real power is scheduled with power droop capability	Real power follows the wind speed variation
Reactive power is controllable up to its maximum limit for a PQ bus, or it is used to control the voltage for a PV bus	Reactive power is controllable by the wind turbine control and/or plant level compensation to control the reactive power Q, the power factor, or the voltage

**4.2.4.1 Differences Between Wind Plant and Conventional Power Plant**

Comparison between a conventional power plant and WPP is presented in Table 4.1. Modern WPPs employ turbines equipped with power converters (DFIG and full converter turbines). In a conventional (synchronous) generator, the rotor flux is attached to the rotor pole (no slip); any oscillation at the generator shaft appears as oscillations at the grid and the generator shaft. The oscillation of a large generator will appear as a large power oscillation on the grid and may affect other generators connected to the same line. In a WPP (type 3 and type 4), the rotor does not have to rotate synchronously with the flux. The flux can glide on the rotor surface at adjustable speed by controlling the power converter connected to the winding. If there is an oscillation at one of the turbines, the mechanical rotor oscillations do not have to be translated to the grid, because the rotor flux can be controlled independently from the rotational rotor speed by a flux orientation controller via the power converter. In addition, the diversity within the WPP allows each individual turbine to operate at its own operating point. Thus, the response of an individual turbine within the entire wind plant may appear as distributed responses from hundreds of turbines instead of a single large response as in a conventional power plant.

**4.2.4.2 Offshore Wind Power Plants**

Many of the prime locations on shore are reserved by early wind developers, the future WPPs may be easier to get in the offshore locations. Another consideration

of offshore WPPs is easy transportation by ship. As the size of wind turbines gets larger, the turbine components will inevitably be larger in size and heavier in weight. For example for 5 MW wind turbines the size of wind turbine blades becomes excessively long and transportation by road access can be a challenge. With offshore locations, there are certain additional costs that incurred due to the transportation, the foundation, the installation, the power transmission, and the operation and maintenance (O&M) costs of the WPPs. Deep water installation will be more expensive than shallow water installation. For a WPP located near the shore, AC transmission can be used. However, if the distance from the shore is far away (>35 miles) AC transmission might not be appropriate due to the excessive reactive power generated by the submarine cables, which may cause over voltage at several buses, thus, inductive compensation must be included. On the other hand, with DC transmission, additional cost may be incurred as we must install power converters to interface with the grid at the on-shore substation and at the WPP substation.

### **4.3 Power Electronics for Wind Power**

Solid-state power converters are based on the use of power electronic devices such as insulated gate bipolar transistors (IGBTs), grid-commutated thyristors, integrated gate commutated thyristors (IGCTs), gate turn-off thyristors (GTOs), and MOSFETs as switches [8]. They perform the task of interfacing WTGs to the grid. Interfacing the power output of WTGs to the grid is a challenging task due to the diversity of generator types and the constantly varying nature of the output. An additional challenge is that generating units are also expected to be able to perform voltage control and reactive power support functions. Power converters are employed to address these issues. The grid consists largely of synchronous machines rotating at the same constant electrical angular speed, and consequently operating at the same frequency. In wind turbines, maintaining the rotational speed constant is difficult due to variations in wind speed, and hence it may be preferred to decouple the wind turbine from the grid. This decoupling is also achieved through the use of converters. In addition, tracking the maximum power available in the wind can also be accomplished through control of these converters. Switching frequencies for the IGBT-based converters are high (kHz) and hence the bandwidth of controllers for the power electronic converters is much higher than bandwidth of the generator. Thus, these converters enable faster control actions. These converters can also improve the steady-state and dynamic performance of wind turbines. Most modern wind turbines employ converters in some capacity, and in this section the topologies of these converters employed are discussed and contrasted.



### **4.3.1 Partially-Rated Power Electronics**

Fixed-speed, variable-slip, and DFIG turbines employ partially-rated power electronics. The power electronic circuitry does not handle the entire output of the generator at any time. These turbines employ induction machines in various configurations, and the converters employed handle the power in the induction machine's rotor circuit alone. The advantages are lower costs in terms of initial cost and in terms of cooling technology required, and reduced conduction losses as compared to full converter solutions. The disadvantages are that control schemes may be more complex (such as in DFIG turbines), and the induction generator may not be fully decoupled from the grid by these schemes.

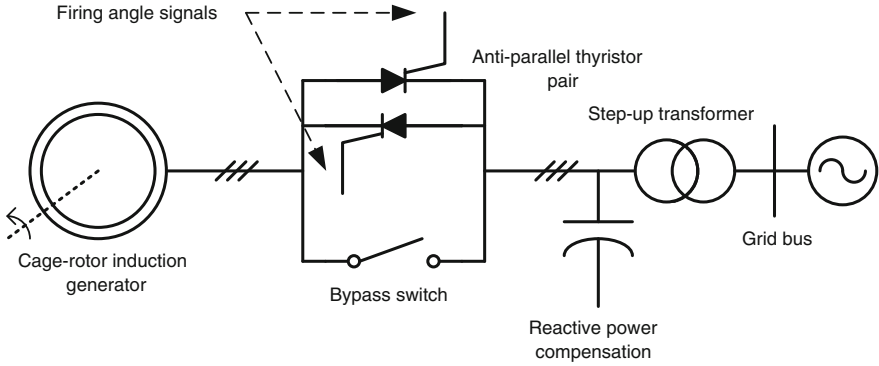
#### **4.3.1.1 Soft Starters for Fixed-Speed Turbines**

Fixed-speed wind turbines employ cage rotor induction machines as generating units. Induction machines can be connected to the grid only at rotor speeds close to or above synchronous speed, since they only act as generators at speeds higher than their synchronous speed. The purpose of the soft starter is to reduce the inrush current when this connection takes place [13]. In the absence of a soft starter, inrush current can be several times higher than the rated current, causing torque spikes and electrical transients. Voltage sags and gearbox damage may result from this sudden start. The soft starter raises the voltage at the machine terminals gradually rather than instantly, and thus allows the magnetic flux in the generator to grow slowly over a few cycles, eliminating transients.

A soft starter typically consists of two anti-parallel thyristors in each phase (see Fig. 4.11). The firing angle for these thyristors is varied from  $90^\circ$  (full off) to  $0^\circ$  (full on) for a resistive load, and from  $180^\circ$  (full off) to  $90^\circ$  (full on) for an inductive load, in order to raise voltage at machine terminals gradually. The wind turbine is predominantly an inductive load. The relationship between firing angle and voltage seen at machine terminals is nonlinear. Once the thyristors are fully on, they are bypassed using a switch. This is done to minimize heat losses once normal operation commences. Soft starters are inexpensive and readily available, since they are also used for induction motors in many other applications.

#### **4.3.1.2 Power Converter for External Resistance Control in Variable-Slip Turbines**

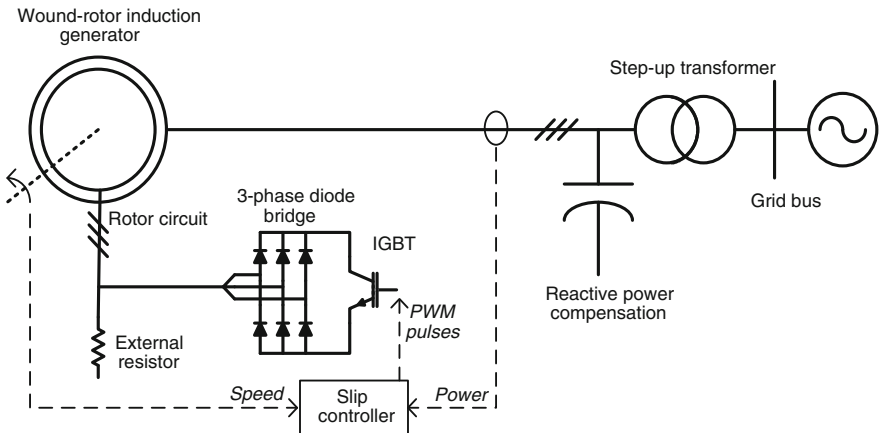
Variable-slip turbines employ wound rotor induction machines. Brushes and slip rings are used to access the rotor windings. In order to achieve the desired output power, the torque-slip (and consequently power-slip) curve of the machine is modified, by modifying the effective external rotor resistance [14]. The higher the external resistance value, the higher the value of slip is. Use of a mechanically-



**Fig. 4.11** Soft starter for fixed-speed wind turbines

variable resistor in each phase is impractical, slow and expensive, and therefore a power electronic AC/DC converter and a static resistor are employed to achieve the same effects. The converter typically consists of a three-phase diode bridge rectifier, and an IGBT chopper as shown in Fig. 4.12.

The diode bridge rectifier consists of six diodes (three legs with two diodes each) and converts the three-phase AC voltages at the rotor terminals to a DC voltage. The reason for employing the AC/DC conversion is that it reduces the number of IGBTs required from three (one per phase) to just one. The IGBT is employed on the DC side of the diode bridge rectifier and, when it is in the on state, it shorts the rotor circuit, reducing external rotor resistance to near zero. When the IGBT is in the off state, the external resistance is not bypassed, and forms a part of the rotor circuit. By varying the duty cycle of the IGBT switching, the effective rotor resistance as seen by the machine can be varied. The effective rotor resistance is a value between zero and the fixed value of the external resistor.



**Fig. 4.12** Power converter for external resistance control in variable-slip turbines

The higher the duty cycle is, the lower the effective external resistance. A detailed explanation of the effects of external resistance on the torque-slip characteristics of the wound rotor induction machine, and a controller to change external resistance, are described in Sect. 4.4.

The effective external resistance can be varied smoothly, and allows the machine to operate at different operating speeds for the same output power. This flexibility reduces the strain on the gearbox. However, some portion of the extracted energy is lost in the rotor resistances as heat. Slip power recovery schemes such as the static Kramer drive (unidirectional power flow) and static Scherbius drive (bidirectional power flow) may be employed to recover this energy. Also, reactive power compensation (as well as a soft starter) is still required in variable-slip turbines.

### 4.3.1.3 Back-to-Back PWM VSI for DFIG Turbines

DFIG turbines offer significant advantages over variable-slip turbines, as they extract more power from wind with an induction machine of the same size, and they can control real and reactive power output independently, eliminating the need for reactive power compensation [15, 16]. These turbines also do not require soft starters. They are easier to interface with the grid as compared to fixed-speed and variable-slip turbines, as the fast and independent control over real and reactive power allows them to quickly respond to grid conditions and wind speed changes.

DFIG turbines employ a modified static Scherbius drive configuration [17] to recover slip power. In this configuration, the induction machine stator is directly connected to the grid (see Fig. 4.13). The rotor circuit consists of a controlled AC/DC converter consisting of six IGBTs (three legs with two IGBTs each) to control AC currents in the rotor circuit, a DC link capacitor which acts as an energy storage and filter for the DC link voltage, and an identical DC/AC converter to

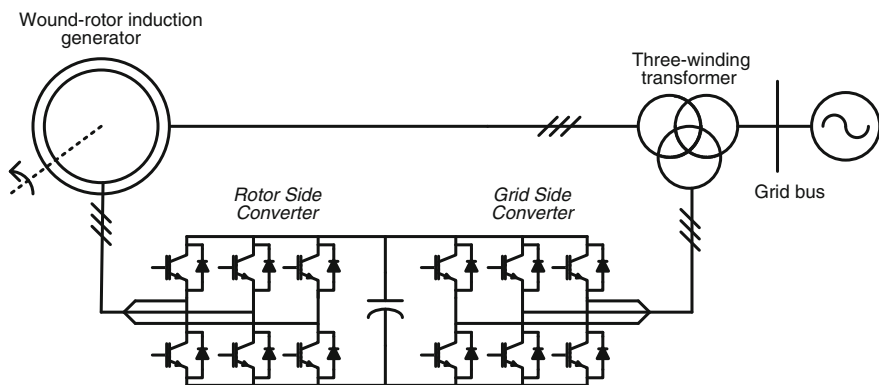


Fig. 4.13 Back-to-back PWM VSI for doubly-fed induction generator turbines

interface with the grid. Each of the converters is a voltage-source inverter (VSI) switched using PWM. This back-to-back PWM-VSI configuration is the most studied and most frequently used three-phase frequency converter configuration. It should be noted that for typical DFIG turbines, this configuration only needs to be rated at about 30% of the induction generator's total power rating, and will allow about a 30% speed variation above synchronous speed.

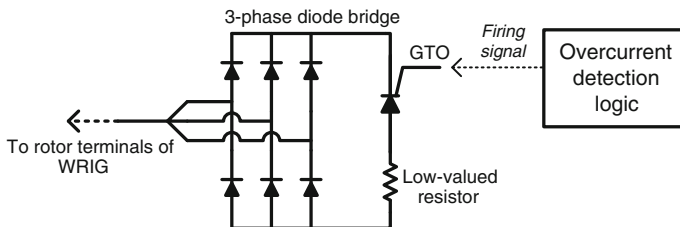
The grid side converter (GSC) is typically employed to keep the DC link voltage constant and provide limited reactive power support to the grid, while the rotor side converter (RSC) controls the active and reactive power output of the induction generator. A flux-vector control approach is employed for decoupled control of real and reactive power. This approach has been described in detail in Sect. 4.4.

### 4.3.2 Crowbar for Rotor Circuit of DFIG Turbines

When severe voltage sags occur on the grid side, the power generated by the DFIG turbine cannot be delivered to the grid, leading to large fault currents in the stator, which are transferred by transformer action to the rotor side. These rotor side over-currents can damage the RSC. In order to protect the RSC from these over-currents, a power electronic device known as a crowbar is used to short the rotor windings [18]. The crowbar is connected between the rotor windings and the RSC. The crowbar consists of a three-phase diode bridge for AC/DC conversion, and a switching device such as a GTO in series with a small resistance on the DC side, as shown in Fig. 4.14. When an over-current condition is detected, the GTO is switched from the off to the on state and shorts the rotor windings, bypassing the RSC.

### 4.3.3 Full-Scale Power Electronics

In full converter turbines, a converter is the only power flow path from the wind turbine to the grid. The converter has to be rated to handle the entire power output



**Fig. 4.14** Crowbar for protection of DFIG rotor circuit

of the turbine. These turbines usually employ high pole count permanent magnet synchronous generators, but use of induction generators is also possible.

### 4.3.3.1 Back-to-Back PWM VSI for Full Converter Turbines

Figure 4.15 shows a configuration for a full converter wind turbine. The configuration is similar to that of a DFIG, but with the important distinction the rotor is not accessed, and the stator is not connected directly to the grid. Instead, the stator interfaces with a PWM VSI converter (machine-side converter or MSC). This converter, as in the DFIG RSC, employs flux-vector control for maximum power point tracking and control the DC link voltage. As in DFIG turbines, a DC link capacitor is employed to smooth the DC link voltage. The GSC transfers power to the grid, and controls the amount of active and reactive power sent to the grid [8]. Though the back-to-back PWM VSI configuration here appears similar to that of the DFIG, the MSC and DFIG RSC actually perform different functions, as does the GSC in each case. This configuration is typically used for permanent magnet synchronous generator (PMSG) machines, but may also be used for other generator types. This converter is a four-quadrant converter and real and reactive power can be moved in both directions, i.e., to and from the turbine.

### 4.3.3.2 Converter Exclusively for Full Converter Turbines with Permanent Magnet Synchronous Generators

A synchronous generator or alternator (in this context the term alternator is preferred, since synchronous or fixed-speed operation is not possible) with permanent magnets on the rotor is typically employed for full converter solutions. By employing a large number of rotor poles (often over 100 poles) the machine can directly output three-phase currents and voltages with frequency around 15–20 Hz, without requiring a gearbox [5]. These voltages are rectified to DC using a diode bridge rectifier. A change in speed of the generator changes the DC link voltage. A boost or buck/boost DC/DC converter is used to interface the DC link voltage set by the rectifier and the voltage set by the grid side converter (see Fig. 4.16). The grid side converter is a PWM VSI. This converter tracks maximum power, and sends output real and reactive power to the grid. An inductive filter may be

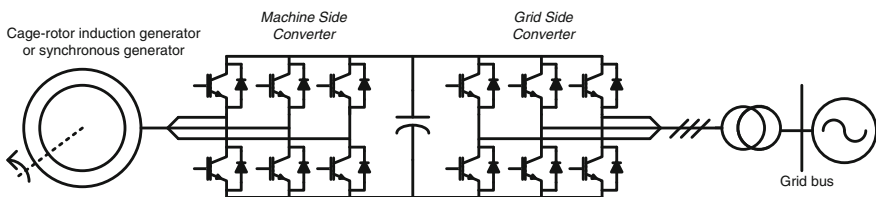
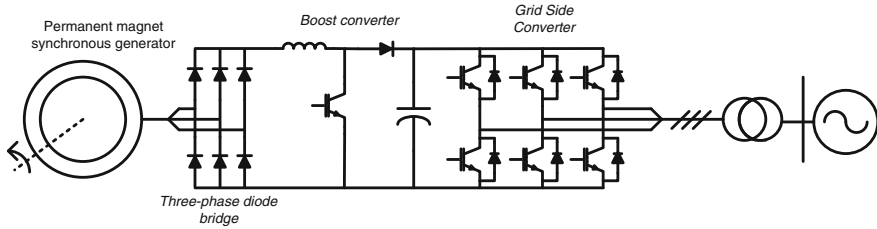


Fig. 4.15 Back-to-back PWM VSI for full converter turbines



**Fig. 4.16** Converters for PMSG full converter turbines

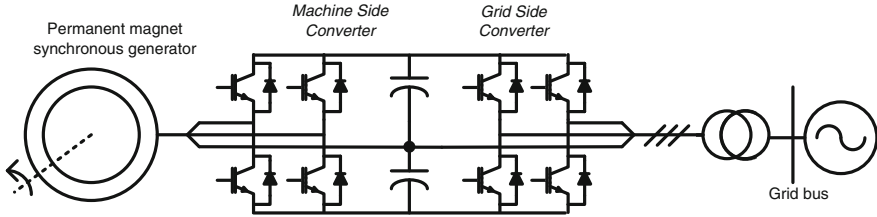
employed to improve quality of the power sent to the grid. The reason this topology may be preferred is that it is cheaper and more reliable since fewer IGBT switches are required compared to the back-to-back PWM VSI. Details about controllers for such systems are provided in Sect. 4.4. Note that this configuration does not allow power flow to the generator from the grid since it is a two-quadrant converter.

### 4.3.4 New and Advanced Topologies

A number of alternative technologies are competing to replace the standard back-to-back PWM VSI in wind turbines [5, 8]. Multilevel converters offer the prospect of eliminating the bulky transformer, matrix converters allow elimination of the DC link capacitor, and the tandem and resonant converters offer improved higher converter efficiency (lower switching losses). Each of these converters offers an improvement over the standard back-to-back PWM VSI but none can so far match it in cost and simplicity. A brief explanation of each of these converter types is provided.

#### 4.3.4.1 Reduced Switch Count PWM VSI Full Converter Configuration for PMSG Turbines

A new type of converter for use with PMSGs has been recently proposed (see Fig. 4.17) [5]. This type of converter employs four-switch PWM VSI converters, and two DC link capacitors. Maximum power point tracking is possible with this configuration, and both converters operate with unity power factor. The machine-side converter is responsible for the power tracking, and the grid side converter controls the DC link voltage. Flux-vector control is employed for both converters. This configuration is lower in cost than a conventional back-to-back PWM VSI and also has fewer losses. However, it does not allow as much flexibility in reactive power control.



**Fig. 4.17** Reduced switch count converter for PMSG turbines

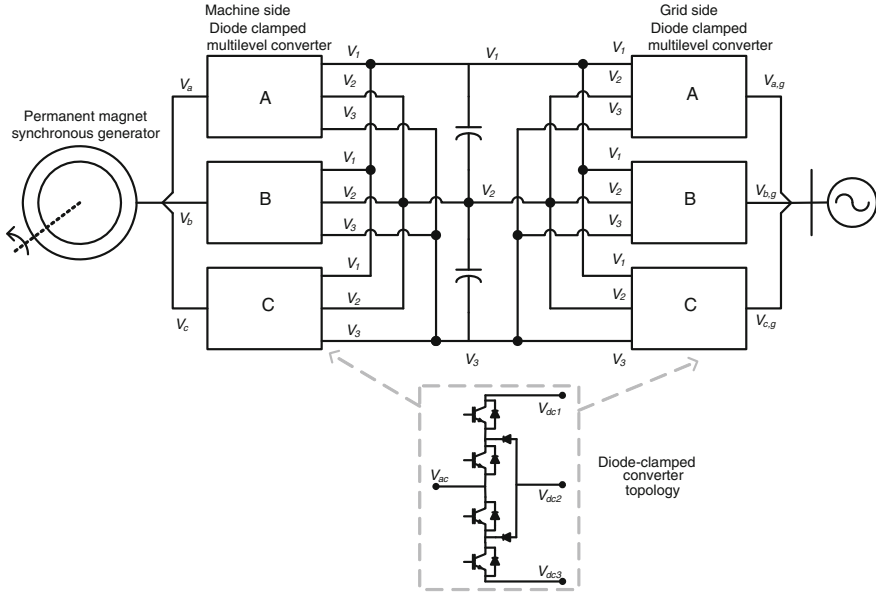
#### 4.3.4.2 Multilevel Converters

The multilevel converter concept is a technique for generating sinusoidal voltages from a number of DC voltage levels [8]. Multiple possible multilevel configurations exist:

- (1) Diode-clamped multilevel converter,
- (2) Bidirectional switch interconnection multilevel,
- (3) Multilevel configurations with flying capacitors,
- (4) Multilevel configurations with multiple three-phase inverters,
- (5) Multilevel configurations with cascaded single-phase H-bridge inverters.

In theory, the number of DC voltage levels that can be employed is not limited, but in real-world applications employing more than three DC voltage levels leads to a huge increase in number of switching devices and complexity (leading to a decrease in reliability). Some of the above configurations may not be easily controllable with more than three voltage levels. The main benefit of employing these converters rather than back-to-back PWM VSI is that they boost the voltage at the output, reducing current demands, thus allowing the use of lower rated switching devices. If the voltage level at the output can be raised high enough, the bulky transformer that is typically used to interface wind turbines to the grid can be eliminated. They also offer superior power quality with fewer harmonics seen in the input and output voltage, thus reducing the need for filtering. As power ratings of turbines increase, multilevel converters are expected to become increasingly viable. An application of a multilevel converter using the diode-clamped configuration is shown in Fig. 4.18 [8]. Multilevel converters are particularly suited to solutions incorporating high pole count PMSGs. In such cases, the multiple stator windings can be used to generate many different DC voltage levels. Power electronic building blocks (PEBBs) [19] may also be assembled into multilevel converters.

Multilevel converters, despite the advantage of higher voltage capability, do have some disadvantages. There are concerns about unequal stress on the switches, as well as voltage imbalances between the upper and lower DC link capacitors [8]. The increased number of devices may contribute to higher conduction losses, though this may be offset by lower switching losses since the switching frequency can be lower than the back-to-back PWM VSI configuration.



**Fig. 4.18** Three-level converter for PMSG turbine interfacing to grid without transformer (based on diode-clamped multilevel converter)

#### 4.3.4.3 Matrix Converters

Matrix converters do not employ an intermediate DC conversion between the variable-frequency and variable-voltage AC from the generator and the fixed-frequency and fixed-voltage AC at the grid side. They are capable of a single-stage AC/AC conversion. This allows the elimination of passive elements such as DC link capacitors and other filtering devices. However, this converter requires nine bidirectional switches. In practice, each of the bidirectional switches comprises two unidirectional switching devices such as IGBTs. This raises the number of required switching devices to eighteen. Since there is only one converter, the control algorithm is simpler, though implementing this algorithm is harder due to increased number of switches. Due to the high number of switches present it is preferred to use cheaper devices with lower ratings, hence application of matrix converters has typically been considered for rotor circuits of DFIG turbines (see Fig. 4.19), although they may also be used for full converter turbines [8]. A flux-vector control scheme is employed.

The idea behind the matrix converter is that a desired input current from the generator, a desired output voltage at the grid, and a desired output frequency at the grid can be generated by appropriately connecting the output terminals of the converter to the input [5]. In other words, the nine bidirectional switches arranged in such a manner that any input phase can be connected to any output phase at any time. Each of the bidirectional switches is capable of both rectification and



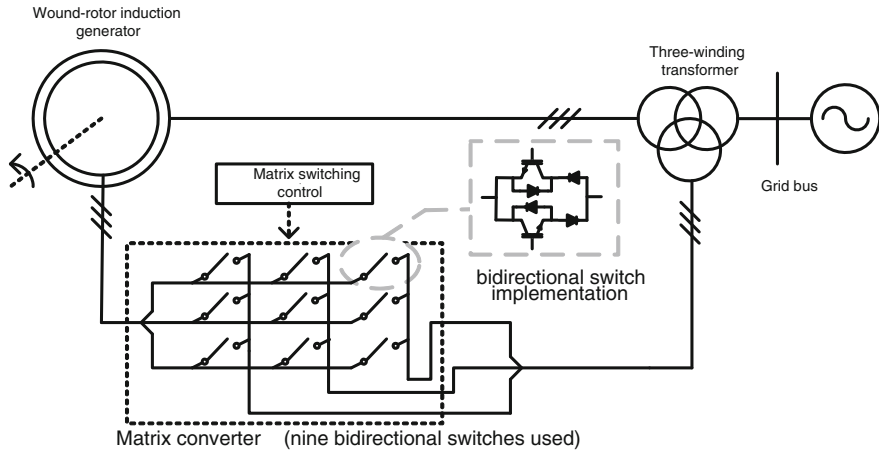


Fig. 4.19 Matrix converter for DFIG turbine

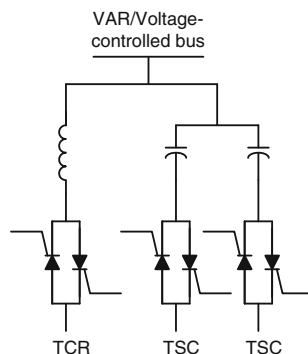
inversion. Two control rules must be followed for protection of the converter: first, only one switch in an output leg can be on at a time, and second, each of the three output phases must be connected to an input phase at any instant of time.

There are significant advantages associated with the use of matrix converters. Each of the switches is equally stressed, reducing the likelihood of thermal problems such as hotspots. The elimination of the DC link capacitor boosts reliability, and the harmonic content of the output is lower due to three effective DC voltage levels being employed rather than two. The switching losses may also be lower, despite the increase in switching devices. However, the output voltage is at most 0.866 times the input voltage, forcing the use of switches with higher current ratings for a converter with the same power rating as compared to a back-to-back PWM VSI. Also, a true bidirectional switch is hard to implement, and following the two aforementioned control rules is not strictly possible due to the fact that no real-world devices can switch instantaneously. The lack of the DC link also poses a problem; during a grid fault, unbalance, or voltage event, the converter has no protection.

### 4.3.5 FACTS Devices

WPPs may employ variety of flexible AC transmission systems (FACTS) devices to improve power quality and voltage stability, typically by providing reactive power compensation. These devices employ power electronics in conjunction with passive elements such as capacitors or reactors for power factor correction at the point of interconnection (also known as the point of common coupling or PCC) of the WPP and the grid. For WPPs consisting of fixed-speed and variable-slip turbines, these devices are necessary, since induction machines are consumers of

**Fig. 4.20** Static VAR compensator (SVC) with one TCR and two TSCs

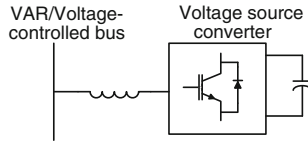


reactive power. WPPs consisting of DFIG and full converter turbines may also employ FACTS devices for additional reactive power support [19].

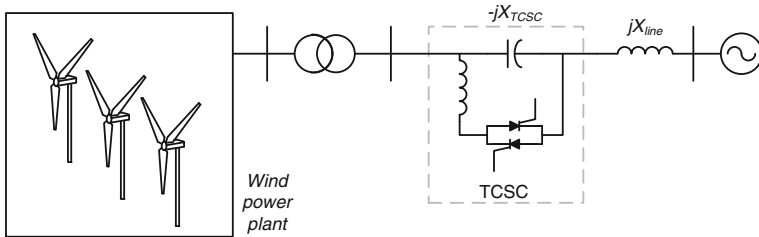
Different systems are employed for power factor correction within the WPP and outside the WPP. In the past mechanical switched capacitor banks were employed for reactive power compensation within WPPs, but these banks are unable to vary the capacitance smoothly, instead providing voltage step-up or step-down in fixed increments. These step-changes increase the stress on the capacitors, turbines, and other power system equipment and reduce reliability. There are two alternatives for the use of mechanical switched capacitors: static VAR compensators (SVCs) and static synchronous compensators (STATCOMs).

The SVC can adjust reactive power output smoothly and continuously, to compensate for reactive power demand and correct power factor. It is connected at the collector bus of the WPP. SVCs employ thyristor controlled components, specifically thyristor switched capacitors (TSCs) and thyristor controlled reactors (TCRs), shown in Fig. 4.20. Fixed capacitors or reactors may also be employed in addition to TSCs and TCRs. One leg (for one phase) of the TSC consists of a pair of anti-parallel thyristors in series with a capacitor. The TCR is similar but employs a reactor instead of a capacitor. Controlling the firing angle of the thyristors changes the effective voltage at the terminals of the capacitor or inductor, thus changing its reactive power output (or intake). Combinations of these components can provide good compensation in subtransmission and distribution applications. However, the TCR operation introduces current harmonics, and the TSC operation introduces voltage harmonics. If fixed capacitors or reactors are used, they may be tuned for filtering out these harmonics. SVCs are suited only for steady-state operation [19].

STATCOMs are based on PWM VSI technology. They typically consist of a PWM VSI with a capacitor across the DC terminals, connected through a reactor to the bus at which compensation is required (see Fig. 4.21). IGBTs are typically employed for STATCOMs. Using the PWM VSI to vary the DC voltage across the capacitor can change the reactive power output of the combination of elements. STATCOMs react faster than SVCs, and also provide better performance and lower voltage levels. They can cope with both steady-state and transient events.



**Fig. 4.21** Static synchronous compensator (STATCOM)



**Fig. 4.22** Thyristor controlled series capacitor (TCSC)

In addition, in an SVC, if grid voltage level at the collector bus drops, the reactive power output drops with the square of the voltage, hence reactive power output collapses quickly. In STATCOMs, the reactive power output drop is proportional to the bus voltage drop, hence reactive power output does not collapse quickly [19].

Typically, WPPs are located far from load centers and are situated at the end of a long transmission line. Some compensation may be installed outside the WPP to compensate for the line reactance. Typically a thyristor controlled series capacitor (TCSC) is employed (see Fig. 4.22). It consists of a combination of passive and active elements in series with the line. Specifically, it consists of two parallel legs, one of which consists of a fixed capacitor, and the other consists of a reactor in series with a pair of anti-parallel thyristors. Controlling the firing angle of the thyristors controls the effective series capacitance of the line. The TCSC can be used to improve voltage regulation of the line, improve power-carrying capability, and also improve dynamic stability [19].

**4.3.5.1 HVDC Systems for Wind Power Plants**

For long transmission distances or offshore applications, high-voltage DC (HVDC) transmission systems may be used to interface WPPs to the grid. HVDC transmission systems typically consist of two AC/DC converter stations connected by a DC line. For long distances, the high cost of the converter stations is balanced by the lower cost of the DC line vis-à-vis an AC line. For offshore WPPs, undersea cables are employed, which have a very high distributed capacitance. This limits the maximum feasible length of the AC cable and maximum power carrying capacity of the cable. HVDC can connect the offshore WPP to the grid without

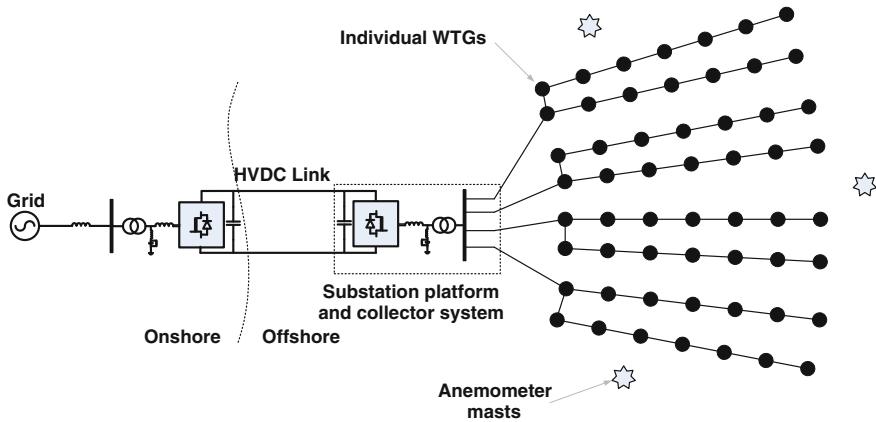


Fig. 4.23 Offshore wind power plant

encountering these limitations. HVDC transmission offers many advantages. Frequency synchronism with the grid is no longer required due to the converters' decoupling effects and the WPP is isolated from grid disturbances, power flow is fully controllable. For offshore applications, power losses are lowered as well, and power transmission capability is increased (Fig. 4.23) [19].

Classical HVDC systems employ current source converters consisting of thyristors. Thyristors are line-commutated devices (they switch off only when AC voltage across them falls to zero during an AC voltage cycle) and thus require active AC networks at both ends in order to transfer power. These systems are thus not very useful for offshore wind, since most WPPs need to be powered up by the grid before they can begin to generate power. Additionally, they cannot control real and reactive power throughput independently, and also generate a lot of harmonics, which necessitates the use of large filters. Due to these limitations, PWM VSI HVDC systems (such as ABB's HVDC Light and Siemens' HVDC Plus) are preferred for offshore WPPs. These systems employ IGBTs, which can be force-commutated by PWM pulses. Thus, they do not require AC networks to be connected at both ends to transmit power, and can even start up without an AC network at either end. They can also control real and reactive power independently.

#### 4.4 Controls for Power Electronics for Wind Power

There are many control methodologies and techniques in use in modern wind turbines and WPPs. The main objectives of these controls are [19]:

- To maximize power extracted from the wind (maximum power point tracking or MPPT).

**Table 4.2** Turbine types and the controls they employ

Turbine types	Pitch control	Real power control for MPPT	Independent reactive power control
Fixed speed (type 1)	Yes	No	No
Variable-slip (type 2)	Yes	No	No
Doubly-fed induction generator (type 3)	Yes	Yes	Yes
Full converter (type 4)	Yes	Yes	Yes

- To ensure that power extracted from wind does not exceed generator ratings by modifying blade characteristics at high wind speeds (pitch control).
- To regulate real and reactive power sent to or received from the grid.

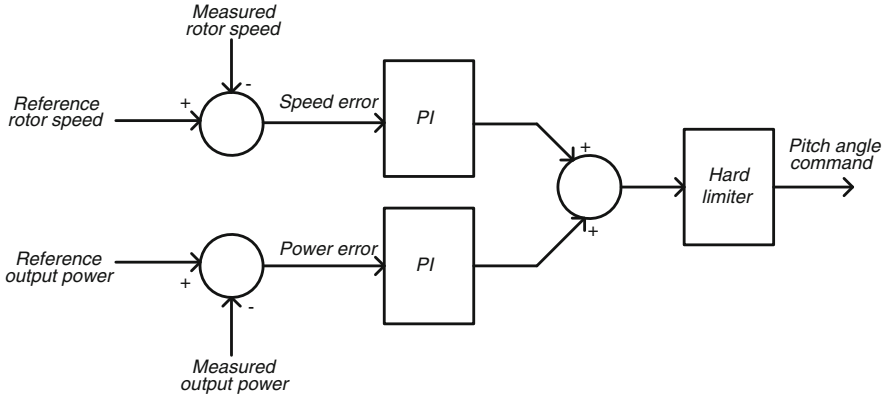
Controllers for each of these purposes must be capable of stable operation in unison with the other turbine controllers. Table 4.2 summarizes the controls employed based on turbine type. Numerous other control systems (such as yaw control and brakes) are utilized but since their functions lie outside the objectives mentioned above, they are omitted from this discussion. In addition to individual turbine controls, WPPs also require controls in order to meet system operator requirements. These controls are usually intended to meet requirements regarding power system control and stability. Some of the existing and proposed plant level controls are also discussed here.

### 4.4.1 Controlling Wind Turbines

Each of the types of turbine listed in Table 4.2 has a different control strategy. Fixed-speed turbines are the most simple type of turbine and usually the only active controller they employ is for pitch control (many such turbines employ stall control instead, a passive form of power regulation at high wind speeds). Variable-slip turbines add a simple real power controller for MPPT, while DFIG and full converter turbines employ flux-vector control, requiring more sensors, hardware, and software.

#### 4.4.1.1 Blade Pitch Control

The power available in the wind increases with the cube of wind speed. As wind speeds increase it becomes necessary to leave the MPPT path and limit power extracted from the wind to the generator's rated power output. The pitch controller (Fig. 4.24) changes blade pitch angle at higher than rated wind speeds, changing the angle of attack of the wind with respect to the blades to spill excess power [5]. Thus, power output is maintained at rated value even though wind speed exceeds rated wind speed. The reference speed and actual speed is compared and the error drives upper PI controller. Reference power and actual power is also compared and



**Fig. 4.24** Blade pitch angle controller

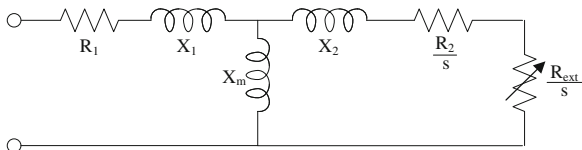
the error drives the lower PI controller. PI controller outputs are summed and hard limited to generate the pitch angle signal. The pitch angle signal is active only when wind speed is close to rated, and otherwise is fixed at zero.

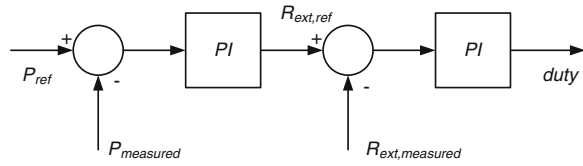
**4.4.1.2 Controls for Variable-Slip Turbines**

The per phase equivalent circuit of a wound rotor induction machine with external rotor resistance is shown in Fig. 4.25. This circuit approximates the machine’s behavior when all three-phase voltages are balanced. The effect of the rotor circuitry described in the previous section (see Fig. 4.12) is to approximate a variable resistance in the rotor circuit. The parameters  $R_1$  and  $X_1$  represent the stator resistance and reactance, while  $X_m$  represents the magnetizing reactance. The parameters  $R_2$  and  $X_2$  represent the rotor resistance (at standstill) and reactance referred to the stator side across the transformer turns ratio from stator to rotor.  $R_{ext}$  is the external resistance (at standstill) referred to the stator side. Note that the effective value of both the internal and external rotor resistance is dependent on the slip  $s$  which represents the per unit deviation of the machine’s rotor speed from the synchronous speed.

A variable resistor is present in each phase, since the equivalent circuit represents one phase of a balanced three-phase circuit. A desired value of torque can thus be achieved at many different speeds, by varying the external rotor resistance. The power and torque equations are modified as follows:

**Fig. 4.25** Per phase induction machine equivalent circuit with external resistor



**Fig. 4.26** External resistance controller

$$P_{\text{airgap}} = 3V_s^2 \frac{R_2 + R_{\text{ext}}}{s} \frac{1}{\left(R_1 + \frac{R_2 + R_{\text{ext}}}{s}\right)^2 + (X_1 + X_2)^2} \quad (4.6)$$

$$\Gamma = \frac{3}{\omega_s} V_s^2 \frac{R_2 + R_{\text{ext}}}{s} \frac{1}{\left(R_1 + \frac{R_2 + R_{\text{ext}}}{s}\right)^2 + (X_1 + X_2)^2} \quad (4.7)$$

In the above equations,  $V_s$  is the per phase Thevenin equivalent voltage at the machine terminals,  $\omega_s$  is the synchronous speed,  $P_{\text{airgap}}$  is the airgap power, and  $\Gamma$  is the machine electromagnetic torque. The most straightforward way of controlling the output power is to use the measured power value as the process variable for comparison. The rotor resistance controller implementation is shown in Fig. 4.26. A reference power signal  $P_{\text{ref}}$  is generated by measuring the machine slip, and using a nonlinear characteristic to find the desired value of power for that value of slip. This reference power value is compared with the measured power  $P_{\text{measured}}$  and the error signal is fed to the PI control. The output of the PI controller is the reference external rotor resistance  $R_{\text{ext,ref}}$  required to maintain the generator power output at its rated value [20]. This rotor resistance value is compared with the measured external rotor resistance  $R_{\text{ext,measured}}$ , and the error is fed to another PI control. The output of the PI control is duty cycle for the rotor resistance control IGBT shown in Fig. 4.12. This duty cycle is compared to a triangle wave to generate the firing pulses for the IGBT.

The controller allows speed variation of up to 10%, thus reducing the likelihood of torque spikes and other transients seen in fixed-speed turbines. It performs MPPT by calculating the maximum deliverable power based on the machine speed and sending the same amount to the grid. Reactive power control cannot be achieved using this technique, and some power is lost in the rotor resistance.

#### 4.4.1.3 Controls for DFIG Turbines

Space-vector theory allows the transformation of three-phase time varying currents and voltages to two constant orthogonal time-invariant vectors, in a rotating frame of reference, known as the  $dq0$  or  $qd0$  frame, depending on the convention chosen. This transformation is achieved using the Clarke and Park transforms [21]. Since the two current vectors in the  $dq0$  frame are orthogonal, they can be controlled independently (Fig. 4.27).

The RSC (see Fig. 4.28) of the DFIG is connected to the grid side converter through a DC link capacitor. Assuming that the grid side converter maintains a

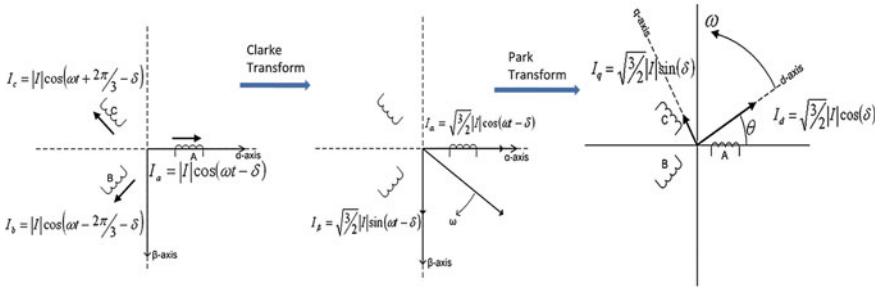


Fig. 4.27 Transformation from time-variant to time-invariant frame

constant DC link voltage, the role of the rotor side converter is to inject rotor frequency (variable) currents into the rotor circuit in such a manner as to achieve decoupled active and reactive power control. In our chosen convention, the converter operates in a stator-flux  $qd0$ - reference frame and the rotor current is decomposed into an active power ( $q$ -axis) and a reactive power ( $d$ -axis) component. With change in wind speed, slip changes the frequency of rotor currents. Actual active power ( $P_{actual}$ ) is compared with the set point value ( $P_{ref}$ ) which is determined by the wind speed. Similarly, actual reactive power ( $Q_{actual}$ ) is compared with the set point value ( $Q_{ref}$ ). The errors between reference and actual real and reactive power are fed into PI controllers to generate the required value of  $q$ -axis rotor current  $I_{qref}$  and  $d$ -axis rotor current  $I_{dref}$ . These values of  $I_{qref}$ , and  $I_{dref}$  are transformed back into the  $abc$  frame to obtain the required value of rotor currents  $I_{ar\_ref}$ ,  $I_{br\_ref}$ , and  $I_{cr\_ref}$ . These reference  $abc$  frame currents are compared to the actual  $abc$  frame currents  $I_{ar\_act}$ ,  $I_{br\_act}$  and  $I_{cr\_act}$ . The errors are fed to a hysteresis controller which generates the switching sequence for the IGBT switches in the rotor side converter. Required rotor currents obtained in  $abc$  frame are thus generated by using hysteresis control [22].

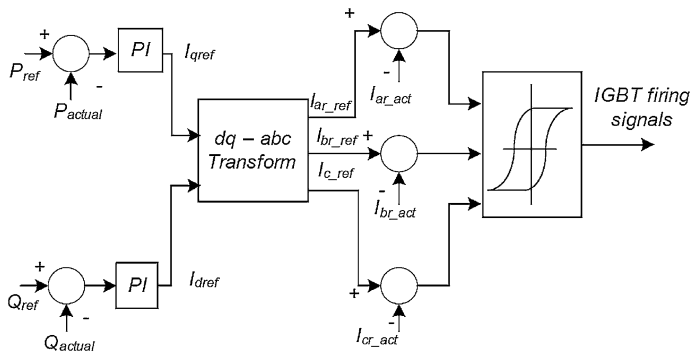
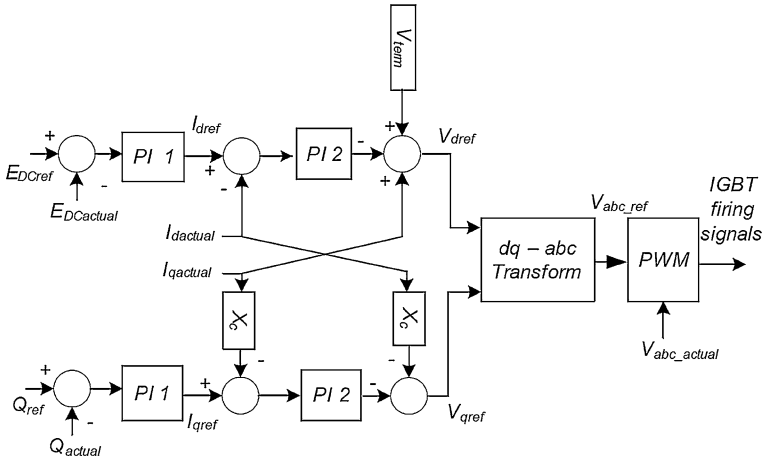


Fig. 4.28 Rotor side converter controller for DFIG turbines





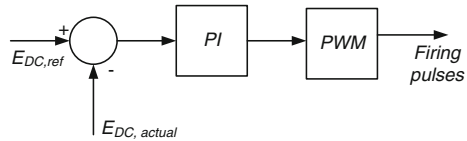
**Fig. 4.29** Grid side converter controller for DFIG turbines

The converter at the grid side is controlled in a manner so as to achieve constant link voltage across the DC link capacitor. A relation between the DC link voltage and the  $qd0$ -axis stator currents and stator voltages is used to model the control and firing circuit for the grid side converter. Vector control, using Clarke and Park transforms is used to obtain the actual  $qd0$ -axis stator currents and stator voltages. The desired  $qd0$  voltages to keep the DC link voltage constant are obtained by comparing the actual value of the DC link voltage. A PI controller is used to obtain the desired values of the stator voltages in  $qd0$  frame. These desired  $qd0$  voltages are then transformed to  $abc$  frame by applying the inverse Park and Clarke transforms to fire the IGBTs. Figure 4.29 shows the block diagram for the grid side converter control circuit [22]. The reference DC link voltage  $E_{DCref}$  is compared to the actual DC link voltage  $E_{DCactual}$ , and the error is fed to a PI control, the output of which is the  $d$ -axis reference current  $I_{dref}$ . This reference current is compared to the actual  $d$ -axis current  $I_{dactual}$  and the error is fed to another PI control. A reference  $d$ -axis voltage signal is generated using the output of the aforementioned PI control, summed with the terminal voltage  $V_{term}$  and a cross-coupling term from the  $q$ -axis current. Likewise, a  $q$ -axis reference voltage  $V_{qref}$  is generated based on the comparison between reference and actual reactive power and cross-coupled terms from the  $d$ -axis current. Reactance  $X_c$  is the output reactance of the converter. These  $q$ - and  $d$ -axis reference voltages are then converted into  $abc$  frame voltages and compared with the actual  $abc$  frame voltages, with the errors then being used to drive a PWM to generate the IGBT switching signals for the GSC.

#### 4.4.1.4 Controls for Full Converter Turbines

Full converter turbines often use a diode-bridge rectifier, a boost or buck/boost converter to increase the voltage level at the DC link, and a PWM VSI to interface

**Fig. 4.30** Boost converter controller for DC link of full converter turbine [22]



with the grid. A typical full converter design was described in the previous section (see Fig. 4.16). The rectifier and buck/boost converter are responsible for converting the AC output of the PMSG to a fixed DC voltage. The boost converter topology is shown in Fig. 4.16. A three-phase diode bridge converts PMSG output to a variable DC voltage. The boost converter maintains the DC link at an appropriate voltage level to interface with the grid side converter. The controller for the buck-boost converter is shown in Fig. 4.30. This controller is based on PI control; error between the desired DC link voltage set-point  $E_{DC,ref}$  and the actual DC link voltage  $E_{DC,actual}$  drives the PI controller and generates a duty signal output. The duty is compared to a triangle wave to generate firing signals for the IGBT in the boost converter.

The grid side inverter is a typical three-phase six-IGBT current controlled inverter. It is similar in design to the rotor side converter of the DFIG turbine (shown in Fig. 4.28) and works on the same principles to achieve decoupled real and reactive power control.

For full converter turbines employing back-to-back PWM VSI converters, the grid side inverter and the machine-side inverter are similar in operation to the grid side inverter and rotor side inverter for a DFIG. Like in the DFIG turbine, the GSC controls DC link voltage, while the machine-side converter is responsible for extracting the desired real and reactive power from the electric machine. However, the grid side converter may also be used to control the reactive power output of the turbine.

#### 4.4.2 Controlling Wind Power Plants

Large WPPs are being increasingly required to behave as controllable elements in the power system as they gain parity with conventional generation. They may have to regulate active and reactive power and perform frequency and voltage control on the grid in order to meet grid connection requirements, specifically those regarding FRT capabilities and power control. WPPs consisting of fixed-speed wind turbines do not operate with centralized control, and are incapable of meeting these grid requirements. However, more modern WPPs employ turbines capable of variable-speed operation and connected to the grid through power electronic converters. The presence of these converters offer better control capabilities, and offer opportunities to develop automated centralized controls [23].

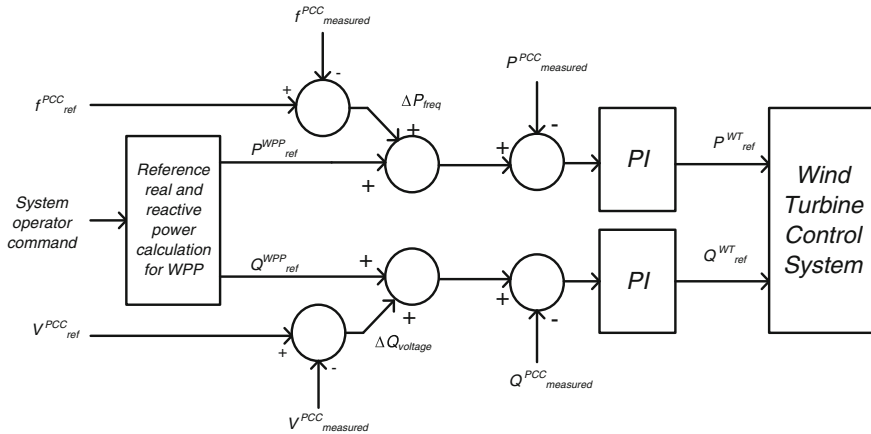


Fig. 4.31 Supervisory control for wind power plants

WPPs with DFIG or full converter wind turbines must be able to provide both real and reactive power control, as per the system operator’s demand. The real power controls desired by system operators are:

- Balance control: system operators may require the WPP to increase or decrease power production.
- Delta control: WPPs in the future may be required to hold part of their output power in reserve so it can be used for frequency control; however, the variability of WPP output poses problems.
- Power gradient limiter for ramp rate control.
- Automatic frequency control: the frequency at the PCC between the WPP and the grid must be held constant, by production of more or less real power in order to compensate for changes from rated value.

The reactive power controls desired by the system operators are:

- Reactive power control: the WPP should be able to produce or absorb a constant specific amount of reactive power.
- Automatic voltage control: the voltage at the PCC between the WPP and the grid must be held constant, by production of more or less reactive power in order to compensate for changes from rated value.

Based on these requirements, a plant level controller is shown in Fig. 4.31. The effect of these controllers is to add another supervisory control loop to the existing turbine level controls. The inputs to the plant level controllers may be reference (desired) values of frequency  $f_{ref}^{PCC}$  and  $V_{ref}^{PCC}$  at the PCC from which desired real and reactive power ( $P_{ref}^{WPP}$  and  $Q_{ref}^{WPP}$ ) can be calculated, or desired real and reactive power commands may be directly issued by the system operator. These real and reactive power reference values can be modified based on measured frequency and voltage at the PCC ( $f_{measured}^{PCC}$  and  $V_{measured}^{PCC}$ ). These real and

reactive power reference values are compared with measured real and reactive power at the PCC ( $P_{\text{measured}}^{\text{PCC}}$  and  $Q_{\text{measured}}^{\text{PCC}}$ ), and the error signals between the two are used to drive PI controllers. The outputs of the PI controllers are real and reactive power commands for individual wind turbines ( $P_{\text{ref}}^{\text{WT}}$  and  $Q_{\text{ref}}^{\text{WT}}$ ). The turbines use these values as reference values and attempt to match their output to these references [24].

## References

1. World Wind Energy Association (WWEA) Website (2010) <http://www.wwindea.org/home/index.php>
2. Lindenbergh S, Smith B, O'Dell K, DeMeo E (2008) 20 % wind energy by 2030: increasing wind energy's contribution to U.S. electricity supply. U.S. Department of Energy. <http://www.nrel.gov/docs/fy08osti/41869.pdf>
3. Heier S (1998) Grid integration of wind energy conversion systems. Wiley, New York
4. Hansen L, Madsen P, Blaabjerg F et al (2001) Generators and power electronics technology for wind turbines. The 27th annual conference of the IEEE industrial electronics society (IECON)
5. Baroudi J, Dinavahi V, Knight A (2005) A review of power converter topologies for wind generators. In: IEEE international conference on electric machines and drives
6. Muljadi E, Ellis A (2008) Validation of wind power plant models. In: IEEE power and energy society general meeting-conversion and delivery of electrical energy in the 21st century, pp 1–7
7. Behnke M, Ellis A, Kazachkov Y et al (2007) Development and validation of WECC variable speed wind turbine dynamic models for grid integration studies. AWEA WindPower conference
8. Hansen L, Helle L, Blaabjerg F et al (2001) Conceptual survey of generators and power electronics for wind turbines. Risø National Laboratory. [www.risoe.dk/rispubl/VEA/ris-r-1205.htm](http://www.risoe.dk/rispubl/VEA/ris-r-1205.htm)
9. Muljadi E, Butterfield CP, Ellis A et al (2006) Equivalencing the collector system of a large wind power plant. In: IEEE power engineering society general meeting
10. Ackermann T (2005) Wind power in power systems. Wiley, New York
11. Tsili M, Papathanassiou S (2009) A review of grid code technical requirements for wind farms. IET Renew Power Gener 3:308
12. Jauch C, Matevosyan J, Ackermann T et al (2005) International comparison of requirements for connection of wind turbines to power systems. Wind Energy 8:295
13. González-Rodríguez AG (2006) Improvement of a fixed-speed wind turbine soft-starter based on a sliding-mode controller (PhD Thesis). Department of Electrical Engineering, University of Seville
14. Novak P, Ekelund T, Jovilk I et al (1995) Modeling and control of variable speed wind turbine drive systems dynamics. IEEE Control Syst Mag 15(4):28–38
15. Slootweg JG, Polinder H, Kling WL (2001) Dynamic modeling of a wind turbine with doubly fed induction generator. In: Proc IEEE Power Eng Soc Summer Meeting
16. Muller S, Deicke M, de Doncker RW (2002) Doubly fed induction generator systems for wind turbines. Ind Appl Mag 8(3):26–33
17. Pena R, Clare JC, Asher GM (1996) Doubly fed induction generator using back-to-back PWM converters and its application to variable-speed wind-energy generation. Proc Inst Elect Eng (Electr Power Appl) 143(3):231–241

18. Morren J, De Hann S (2007) Short-circuit current of wind turbines with doubly fed induction generator. *IEEE Trans Energy Convers* 22:174–180
19. Carrasco J, Franquelo L, Bialasiewicz J et al (2006) Power-electronic systems for the grid integration of renewable energy sources: a survey. *IEEE Trans Ind Electron* 53:1002
20. Burnham D, Santoso S, Muljadi E (2009) Variable rotor-resistance control of wind turbine generators. In: *IEEE power and energy society general meeting*
21. Krause P, Wasynczuk O, Sudhoff S (2002) *Analysis of electric machinery and drive systems*. IEEE Press, NJ
22. Singh M, Vyas M, Santoso S (2010) Using generic wind turbine models to compare inertial response of wind turbine technologies. In: *IEEE power and energy society general meeting*
23. Hansen D, Sorensen P, Iov F et al (2006) Centralised power control of wind farm with doubly fed induction generators. *Renew Energy* 31:935
24. Rodriguez-Amenedo JL, Arnalte S, Burgos JC (2002) Automatic generation control of a wind farm with variable speed wind turbines. *IEEE Trans Energy Convers* 17(2):279–284

# Chapter 5

## Small Hydroelectric Systems

Felix A. Farret, Marcelo G. Simões and Ademar Michels

**Abstract** In present days, most government policies plan to increase their national electricity grid. The reality is that several villages, farmers, and settlers will not have access to electricity because of infrastructural and economic constraints. Although high technological solutions can be necessary to expand the main grid, small stand-alone projects may sometimes require very simple solutions. Even so, there is a lack of knowledge and understanding of how to implement them without major social or environmental impacts. This chapter shows the basic principles of hydropower resources, how to plan sites in rivers where the water flow and height differences are large enough so that new small hydropower plants can be built. Usually these plants will have a capacity of 10–20 kW, for runoff the river applications, or from 20 to 100 kW for water flows above  $0.3 \text{ m}^3/\text{s}$  during the dry season, and a height difference of at least a few meters. Even during the dry season, the electricity is often sufficient for powering light at night, computers or television sets and a refrigerator, which will already have major impacts on such places. In this chapter, the following hydro turbine systems are discussed: fixed-speed with an induction generator; variable-speed with a cage-bar induction generator; variable-speed with a multiple-pole synchronous generator or multiple-pole permanent magnet synchronous generator; and variable-speed with a doubly-fed induction generator.

---

F. A. Farret (✉)  
Federal University of Santa Maria, RS, Brazil  
e-mail: fafarret@gmail.com

M. G. Simões  
Colorado School of Mines, Golden, CO, USA  
e-mail: msimoes@mines.edu

A. Michels  
Faculty of Horizontina, RS, Brazil  
e-mail: ademarmichels@gmail.com

## 5.1 Determination of the Hydro Turbine Output Power

In the project and installation of hydroelectric power plants, it is essential to know the water flow rate and the fall height to access the potential energy. It is still important to know the maximum flow or maximum water discharge for construction of the engine room in a safe place outside of the flooding area. Knowing the water flow rate in various periods of the year can also set the pluviometric ranges (amounts of rain) in the area.

The output power of a water turbine is based on a Bernoulli's derived equation as follows:

$$P_t = \eta_t \rho g Q H_m$$

where

- $\eta_t$  is the turbine efficiency
- $\rho$  is the water density in  $\text{kg/m}^3$
- $g$  is the acceleration of the gravity in  $\text{m/s}^2$
- $Q$  is the water flow in  $\text{m}^3/\text{s}$
- $H_m$  is the water head in m.

### 5.1.1 Measuring Methods of the Water Flow $Q$

One of the first methods to measure the water flow rate ( $Q$ ) is based on the continuity equation of the Fluid Mechanics

$$Q = A \times v$$

where

- $A$  cross-sectional area, in  $\text{m}^2$ ;
- $v$  speed, in  $\text{m/s}$

To obtain the speed at various points along a single vertical line, a water flow detector can be used to measure the speed of the water in streams, creeks, and even in small rivers. A water flow detector is a device that produces a voltage signal proportional to the water flow. The advantage of the water flow detector in the measurement of speed is that corresponding sub-areas can be determined to calculate the water discharge. If an ordinary water flow detector is not available, expeditiously, the next simplest methods are those using ordinary floats.

To measure the water speed by float, initially is necessary to choose a length  $L$  along the edge of the watercourse, longer than 10 m if possible, whose bed is as uniform as possible with minimal turbulence. The method uses a float, consisting of a sealed flask containing water (ballast) to about 1/3 of its volume. The distance is measured by marking its starting and ending point, delimiting it with two strings

perpendicular to the waterway. The float is placed a few meters upstream from the first string. With a stopwatch, one verifies the time required for the float to cover the distance between the strings. This operation must be repeated several times taking care to discard the measures that deviate too much from the average. With the elapsed time so determined and knowing the distance  $L$ , the speed is calculated. The continuity equation must be multiplied by a correction coefficient for surface speed, considering the boundary layers of water. In practice, this correction coefficient is equal to 0.8 and the continuity equation becomes:

$$Q = 0.8L\bar{A}/t \tag{5.1}$$

At least two areas must be measured and then the arithmetic average of the areas is calculated as depicted in Fig. 5.1. The cross-section areas are limited by the upper water level and by the stream, creek, or small river bottom.

A second method to obtain the water flow rate in streams, creeks, and small rivers is to use a rectangular spillway. This method leads to more accurate results than that of ordinary floats, but it requires more work and it is limited to the cases

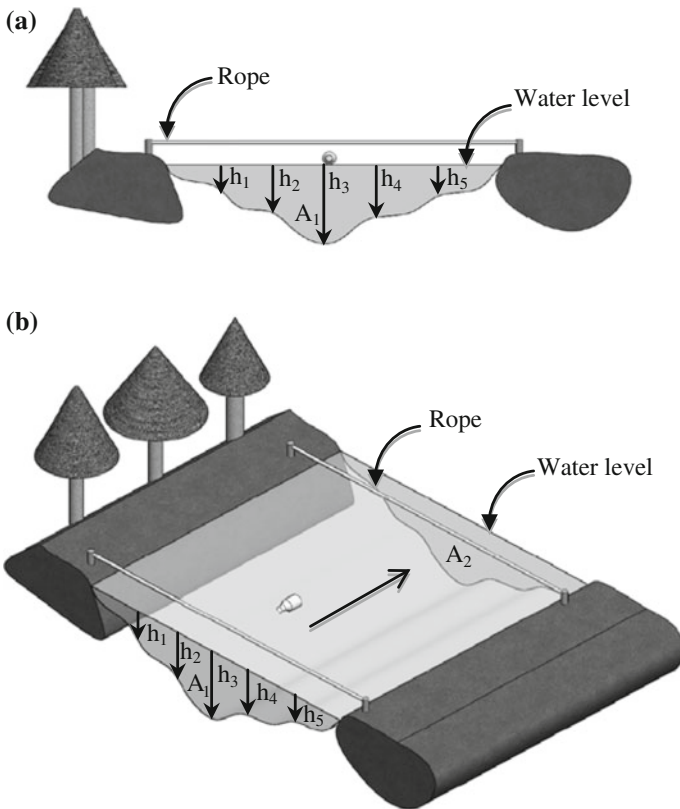
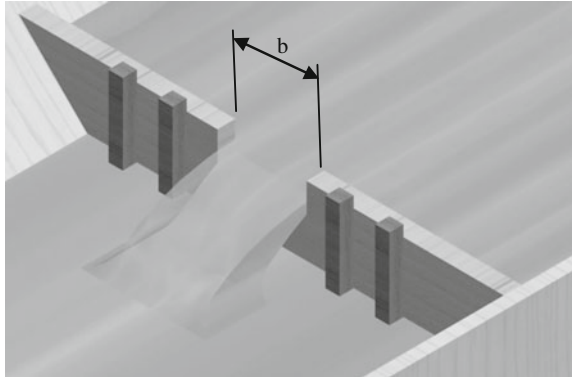
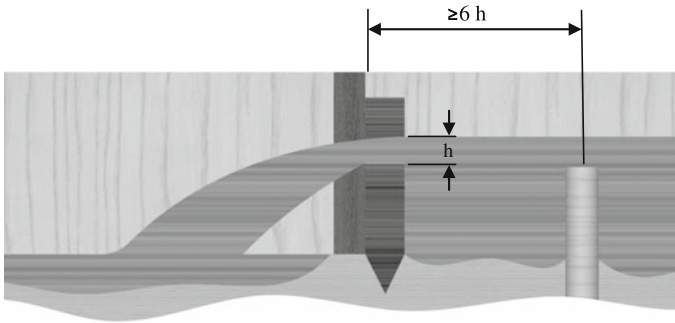


Fig. 5.1 Cross-sectional depths in a water stream





**Fig. 5.2** Rectangular spillway



**Fig. 5.3** Positioning a rectangular spillway

where the morphological conditions of the watercourse allow its use. In this case, the watercourse is dammed with a panel made of wood boards with a rectangular opening on its upper center by where all water to be measured must pass. The width of the opening must have at least half the width of the watercourse and a maximum of two-thirds of the width. Then a stake is driven into the bed upstream to the panel, at a minimum distance of six times the water surface height and leveled with the spillway crest. After reaching the steady-state flow the height  $h$  of the water level is measured on the top of the stake.

The water flow can be calculated using the Francis formula shown here:

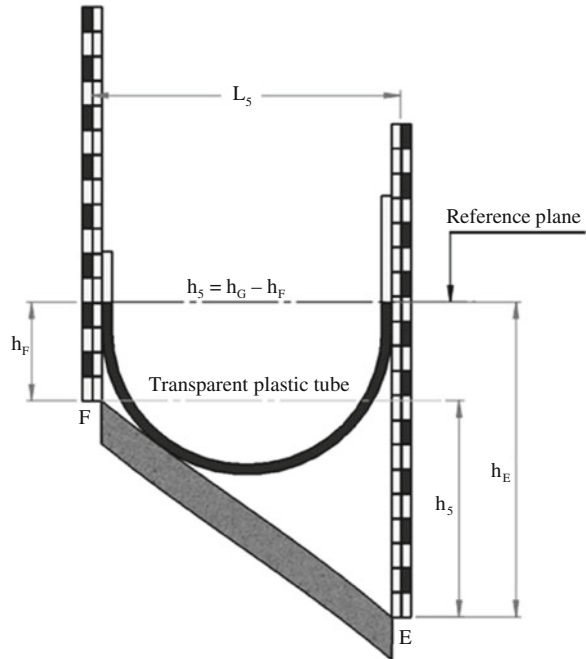
$$Q = 1.84 \times b \times h^{3/2} \quad (5.2)$$

where

$Q$  water flow rate, in  $\text{m}^3/\text{s}$

$b$  width of the opening of the spillway, in m

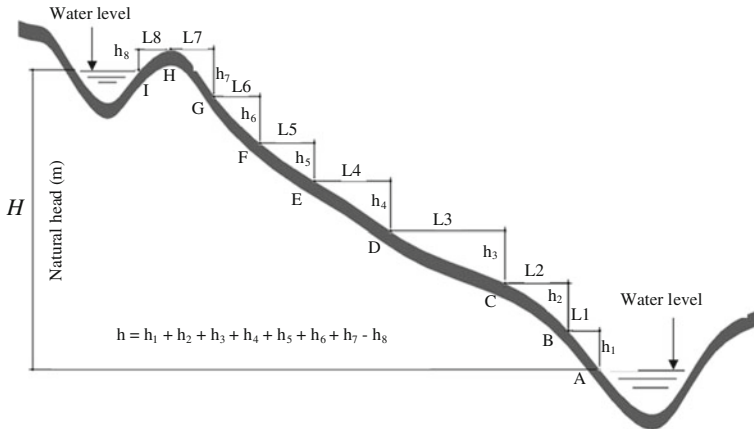
**Fig. 5.4** Method of the rulers and flexible transparent plastic tube



$h$  height of the water level over the spillway crest, in m, measured upstream, where the stake was driven as in Figs. 5.2 and 5.3.

### 5.1.2 Measuring Methods of the Water Head $H$

There are several methods to determine the water head in the local for a mini hydroelectric central. Among these methods, the most recommended is the GPS, which easily and quickly gives a notion of the water head. If there is not a GPS, the method of slopes and profiles can be recommended. To use this method graduated rulers of about 2 m long and a flexible and transparent plastic tube, about 6 m long are required. The two rulers are placed in an upright position, on any two points,  $E$  and  $F$ , for example, in the place to measure the level difference as shown in Fig. 5.4. With the help of the flexible and transparent plastic tube filled with water, the points are determined on each ruler at the same level, thus creating a horizontal plane of reference. Good care should be taken to eliminate any air bubbles that could have by any chance remained in the flexible tube. The difference between the heights of this plan on the two points  $E$  and  $F$  will give the level difference  $h_5$  between these two points. Adding these differences,  $h_1 + h_2 + h_3 + \dots + h_n$ , as illustrated in Fig. 5.5 one obtains the natural fall  $H$  of that site.



**Fig. 5.5** Referential *horizontal planes*

## 5.2 Specification of Small Hydro Turbines

The turbine is a machine that uses the kinetic and/or potential energy of the water to produce a rotational movement on the central rotor shaft, which is transferred to the generator shaft directly or through a belt, being able to produce electric energy.

Regarding the principle of operation, the hydraulic turbines are classified into two major groups:

- action turbines;
- reaction turbines.

The difference between the two types is that the action turbines use the speed of the water flow to turn the turbine, while reaction turbines use the speed and the pressure difference during the water passage through the turbine. Therefore, reaction turbines use the whole existing upstream to downstream height, while the action turbines use only the height between the upstream and the turbine shaft.

Francis, Kaplan, propeller, and Dériaz turbines are good examples of reaction turbines. The best known action turbine is the Pelton turbine, but there are many others, such as the double effect or cross-flow turbine, also known as Ossberger or Michell-Banki turbine. Figure 5.6 gives the application ranges of water flow and dam height recommended for various types of hydraulic turbines. This diagram is commonly used to establish the application ranges of water flow  $Q$  in cubic meters per second, and the height  $H$  in meters for each type of turbine discussed here.

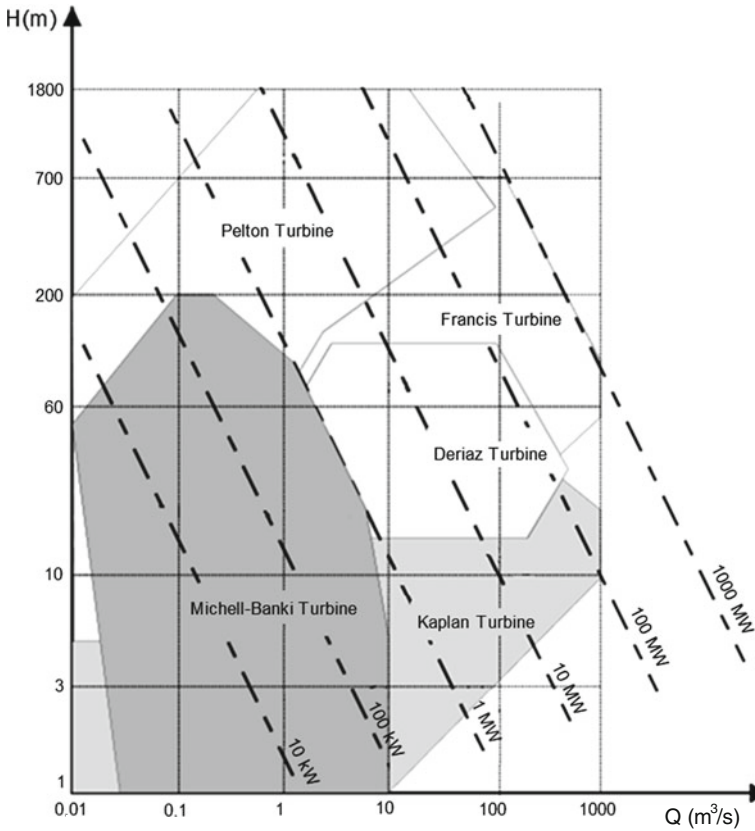


Fig. 5.6 Application field recommended for various types of hydraulic turbines

### 5.2.1 Pelton Turbine

The Pelton turbine is the most used action turbine. It consists of a circular disk, with a set of shells mounted on its periphery (blades). The directed water flow to these blades is regulated by an injector acting in such a way to cause a rotation movement in the turbine shaft. The output power is regulated by an injector which increases or decreases the water flow rate into the turbine. In an emergency a flow diverter is used, which directs the water stream to the tailrace, without reaching the turbine shovels, thus avoiding high rotor speeds. This way, one can perform a slow closure of the injector without causing pressure blows (water hammer) through the forced pipe. This type of turbine is indicated for high falls and low water flows. The energy production with these machines is over 90 % of the operating design conditions. It presents a fairly flat power curve, reaching from 80 % to approximately 20 % of the water flow design rates. Design details about this turbine and some others used in small power plants are presented in references [1, 2].

### **5.2.2 *Michell-Banki Turbine***

The Michell-Banki is an action, cross-flow, and double effect turbine. The rotor consists of two circular disk with fixed blades. The water is directed to the rotor through a guiding-blade that also serves to regulate the water flow rate.

The greatest advantage of this turbine is its robustness and ease of construction, considering the fact that it does not use castings. As this is an action machine, the change in speed direction is used to obtain mechanical work. The Michell-Banki turbine does not present cavitation problems.

The disadvantage of the Michell-Banki turbine is its low power production, especially the volumetric production. It presents a fairly flat production curve. This type of turbine is recommended to generate electricity in isolated houses where the electric power is more important than the efficiency. The Michell-Banki turbine is not recommended for energy injection into the grid, since high production, and sale cost of the electric energy are important matters.

## **5.3 Electrical Generators for Small-Scale Hydro Turbines**

Hydro and wind power generation are very much alike in the sense that their operation follows Bernoulli's Law for fluids in motion. The similarities come from the fact that both hydro and wind turbines can operate either at fixed or variable speeds. Fixed-speed turbines use an old and relatively simple technology with constant-speed mechanical input. They are often intended for a certain fluid speed at which the maximum efficiency can be achieved. They need a water or air flow regulator, which is not usually very cheap. However, they differ mostly in the means of storage, since the air in motion cannot be viably stored, but water dams can be used for massive storage hydro power. Another difference is in mass density given in  $\text{kg}/\text{m}^3$ , which is a lot higher for water. Variable-speed hydro turbine is a rich field for power electronics and digital control applications.

For the run-of-a-river hydro turbines, the rotational speed of the electrical generator can be changed in a stepwise manner by changing the pole number in accordance with the speed of the water. For example, for a 60 Hz network, the synchronous speed can be changed from 1,800 to 1,200 rpm by switching the pole number from four to six without the need of mechanical gear boxes. Because the fluctuations of the generated power, fixed-speed turbines have a less positive impact on power systems, as compared to the variable-speed turbines. Variable-speed hydro turbines can also be designed for broader hydro speed ranges. Turbines for this type of power generation have the possibility to control the amount and the frequency of the produced electricity, although it requires a more complicated electrical system.

For connection of a generator to the network, an electronic converter scaled either for the full output power in a stator connection or to the reduced output power in a wound rotor connection is required. In both cases, this introduces extra

costs and additional losses. However, the efficiency of such a system can be somewhat higher than the efficiency of the system containing an induction generator directly connected to the grid. On the other hand, a full-scaled converter offers an opportunity of a variable-speed control over a large speed range. This allows a better utilization of the available hydro power and therefore has a potentially higher energy yield.

For best results, in the connection of a small generator to the mains grid one will have to use power electronics and digital controls. In this section, such electronic connections can be separated for the following hydro turbine systems: (1) Fixed-speed with an induction generator; (2) Variable-speed with a cage-bar induction generator; (3) Variable-speed with a multiple-pole synchronous generator or multiple-pole permanent magnet synchronous generator; and (4) Variable-speed with a doubly-fed induction generator.

A direct-driven relatively low-speed generator with a large number of poles and with the outer diameter larger than conventional generator is required in small hydro systems. Electrically excited direct-driven synchronous and induction generators are utilized by a number of hydro turbine manufacturers. Wound rotor induction generators are also present in many larger power plants [3].

### ***5.3.1 Permanent Magnet Generator***

In the past few decades, reduced magnet prices made synchronous generator with permanent magnet excitation (PMSG), also known as brushless dc generator (BLDC), an attractive alternative for hydro power generation. In comparison to the conventional electrical excitation, the permanent magnet excitation favors a reduced active weight, decreased copper losses, and the output energy should be somewhat higher. This topology is being utilized with large commercially available direct-driven permanent magnet generators. A number of studies have been conducted investigating different topologies of PMSG suited for direct-driven low-speed hydro and wind generators [4, 5].

The PMSG is a permanent magnet generator so the brush and the commutator used for supplying the magnetic flux are not necessarily compared with the usual DC machine; therefore, the maintenance for those components is not required. As the field winding is replaced by a permanent magnet, the copper losses of the field winding are absent. The stator has laminated steel to reduce the eddy current loss and the structure is the same as the PMSG motor.

Because of the variable-speed, the permanent magnet generator uses alternating currents of variable frequency so this AC current has to be converted from a DC supply. Because its speed/torque characteristic is very similar to the ordinary dc motor with brushes, it is sometimes known as a brushless dc generator. With its variable frequency including the synchronous frequency, perhaps the best name for it would be the permanent magnet synchronous generator. The PMSG is mostly related to its minimal sizing, low maintenance, and lighter weight in the same rated

machines. They are especially suitable for many applications, such as small power plants, remote area off-grid power supply systems, and isolated loads.

There are features in the PMSG construction dependent on the manufacturer as the location within multiple turbine blades which supply mechanical drive to the shaft on which they are placed via motion of water thus rotating the shaft. The magnetic field move through aluminum bars of traditional commutation devices and thereby create electrical currents through those bars, most metallic components embedded in polymer or Teflon limiting oxidation, and fewer components and needing less maintenance.

The PMSG generator is specially suited for hydro turbines since the primary machines depend on the fluid moving through their blades. Hydro turbines have smaller and larger numbers of blades than wind turbines and being the permanent NdFeB magnets integrated into smaller hydraulic turbine blades, the turbine blades turn more efficiently and are less easily damaged than the ordinary types of generators. The PMSG can be used for the generation of electrical energy from rivers by using variable-speed hydro turbines or from sea waves by using tides and waves, as well as from other forms of water motion energy.

### 5.3.2 Principle of Operation of the PMSG

The concept of PMSG is based on the standard way of creating an electrical current that allows a wire wound rotor to spin in a circumferential magnetic field located in the stator with brushes. These brushes are fitted to contact the wires extruded into a commutator on the spindle of the rotor shaft. If this wire is moving through a magnetic field, a voltage is induced on it and vice versa. From basic physics, the e.m.f. is given by:

$$e = Blv \quad (5.3)$$

where

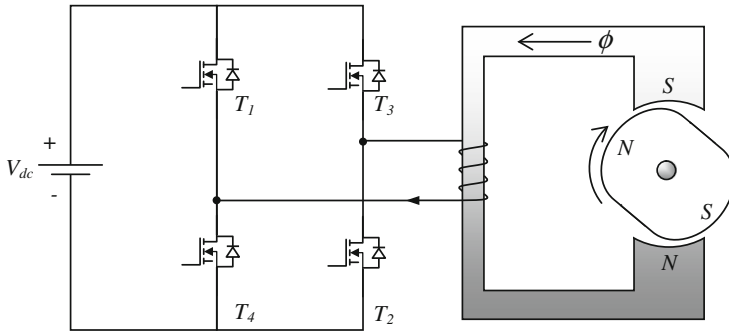
$e$  is the voltage induced in the wire

$B$  is the magnetic flux density

$\ell$  is the conductor length in the magnetic field

$v$  is the velocity of the wire passing through the magnetic field.

The basic electronic principle of the PMSG, as depicted in Fig. 5.7, is based on the fact that after production of the electric current a set of brushes contacts the commutator to allow the electric current to be connected to the exterior of the power generator. The basic difference between the conventional DC generator and PMSG is with respect to the commutator function placed on the outside of the magnetic field moving cyclically on the spindle, and thus eliminating so the brushes. In the PMSG, the permanent or electro magnets are put on the rotor. High power electronic switches change up from one electromagnet to the next as the shaft turns.



<i>switches</i>	<i>position</i>	<i>switches</i>	<i>position</i>	<i>motor torque</i>	<i>generator torque</i>
1-2	on	3-4	off	positive spin	negative spin
1-2	off	3-4	off	inertia	primary drive
1-2	off	3-4	on	positive spin	negative spin
1-2	off	3-4	off	inertia	primary drive

Fig. 5.7 Operating principle of the PMSG generator

The PMSG model with a single coil shown in Fig. 5.7 is not usual because its torque is very unsteady and a higher number of coils would be advisable. Once the rotor began its movement by one of the poles, the next one will be just near enough to receive the next magnetic push and so on. With such configuration, the rotor movement will be smoothed out as the number of poles increases. More typically, the number of poles could be three or a multiple of three as shown in Fig. 5.8. This generator can be modeled much like the ordinary salient pole synchronous generator with the stator connected in the star and the two rotor poles seen as an electromagnet. The stator windings are sinusoidally distributed and shifted from each other by 120° as the phases represented in Fig. 5.9 by resistors and inductances. In the rotor magnetically coupled to the stator there is an equivalent

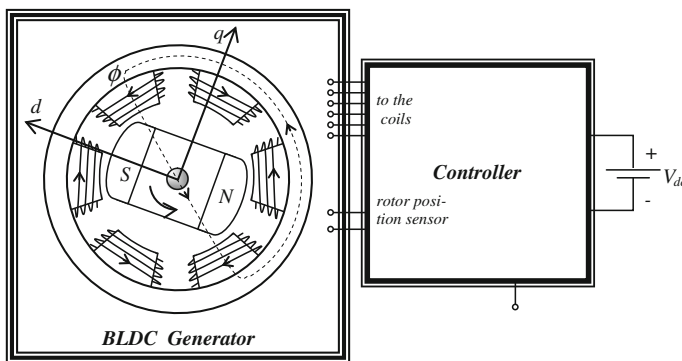
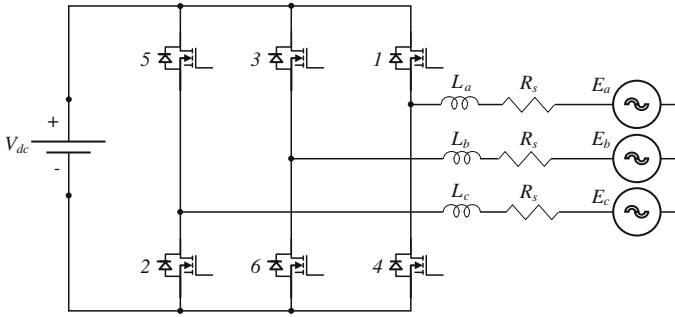


Fig. 5.8 Structure of a typical multi-pole permanent magnet generator





**Fig. 5.9** Equivalent driving circuit of the PMSG generator

winding to the magnet that is represented also by a resistance and an inductance. The current going through the stator coils is assumed as the positive sense to describe the generator excitation.

### 5.3.3 Simplified Model of the PMSG Generator

In a sinusoidal power supply system, a pulse-width modulated (PWM) rectifier is generally used for voltage control and power factor correction. In the given sinusoidal current reference waveform, six active switches are used, as shown in Fig. 5.9, to control the distribution of currents through the phases and to keep them in phase with the voltage of the generator. However, note that a PMSG generator is a non-sinusoidal power supply system. Therefore, the optimal current waveform for power density maximization is not sinusoidal. Hence, a sinusoidal PWM rectifier cannot maximize the output power. The most popular and practical method is to use a diode rectifier for a PMSG generator system. However, since the voltage and current are out-of-phase and the current waveform is uncontrolled, the maximum power and efficiency available cannot be achieved. To control the current waveform, it is necessary to use a PWM rectifier. However, a PMSG generator is a non-sinusoidal power supply with an induced e.m.f. waveform [6].

A mathematical representation of a multi-pole permanent magnet generator can be made by using phases a, b, and c of the stator while the rotor is represented by the direct  $d$  and quadrature  $q$  axis with the rotor magnetic axis coinciding with the quadrature axis  $q$ . Figure 5.9 shows also the equivalent driving circuit of the PMSG generator. The stator resistances are defined as to  $R_s$ , the self-inductances for phases  $a$ ,  $b$  and,  $c$  are defined, respectively, as  $L_a$ ,  $L_b$  and  $L_c$  and the mutual inductances are defined as  $M_{ij}$  where  $i, j$  refer to the phase combination as presented in the matrix equation. The analysis is based on the following assumptions for simplification: (1) The generator is operated within the rated condition, so the generator is not saturated; (2) All three phases have an identical and balanced induced e.m.f. shape; (3) Iron losses are negligible; and (4) Power semiconductor

devices in the converter are ideal. Using the notation of Fig. 5.9 we can write the matrix equation below:

$$\begin{bmatrix} v_a \\ v_b \\ v_c \end{bmatrix} = \begin{bmatrix} R_s & 0 & 0 \\ 0 & R_s & 0 \\ 0 & 0 & R_s \end{bmatrix} \begin{bmatrix} i_a \\ i_b \\ i_c \end{bmatrix} + \frac{d}{dt} \begin{bmatrix} \psi_a \\ \psi_b \\ \psi_c \end{bmatrix} \quad (5.4)$$

where

$$\begin{bmatrix} \psi_a \\ \psi_b \\ \psi_c \end{bmatrix} = \begin{bmatrix} L_a & M_{ab} & M_{ac} \\ M_{ab} & L_b & M_{bc} \\ M_{ca} & M_{bc} & L_c \end{bmatrix} \begin{bmatrix} i_a \\ i_b \\ i_c \end{bmatrix} + \frac{d}{dt} \begin{bmatrix} \psi_{pma} \\ \psi_{pmb} \\ \psi_{pmc} \end{bmatrix}$$

and  $\psi_{pma}$ ,  $\psi_{pmb}$  and  $\psi_{pmc}$  are, respectively, the coupled magnetic fluxes through phase poles  $a$ ,  $b$  and,  $c$ .

According to the position of the rotor with respect to the fixed frame  $a$ ,  $b$  and,  $c$  the rotor position is defined by an electrical angle  $\theta_e$  as follows [7, 8]:

$$\begin{aligned} L_a &= L_0 + L_m \cos(2\theta_e) \\ L_b &= L_0 + L_m \cos\left(2\theta_e - \frac{2\pi}{3}\right) \\ L_c &= L_0 + L_m \cos\left(2\theta_e + \frac{2\pi}{3}\right) \\ M_{ab} &= -\frac{1}{2}L_0 + L_m \cos\left(2\theta_e + \frac{2\pi}{3}\right) \\ M_{bc} &= -\frac{1}{2}L_0 + L_m \cos(2\theta_e) \\ M_{ca} &= -\frac{1}{2}L_0 + L_m \cos\left(2\theta_e - \frac{2\pi}{3}\right) \end{aligned} \quad (5.5)$$

In Eq. 5.5 the physical reactive parameters of the generator are represented by  $L_0$  and  $L_m$ . The varying magnetic sinusoidal coupling between stator and rotor are expressed as a function of the maximum magnetic phase flux  $\psi_{pm}$  for phases  $a$ ,  $b$  and  $c$  as follows:

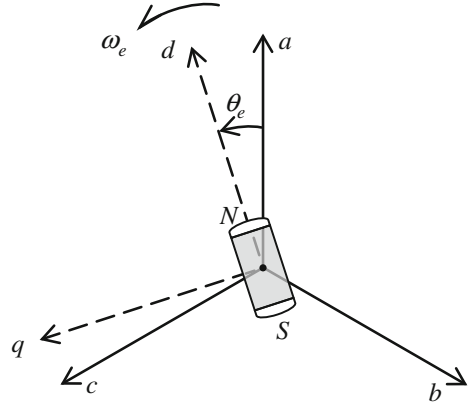
$$\begin{aligned} \psi_{pma} &= \psi_{pm} \cos(\theta_e) \\ \psi_{pmb} &= \psi_{pm} \cos\left(\theta_e - \frac{2\pi}{3}\right) \\ \psi_{pmc} &= \psi_{pm} \cos\left(\theta_e + \frac{2\pi}{3}\right) \end{aligned} \quad (5.6)$$

It is usual to transform the three-phase matrixes represented in Eqs. 5.5 and 5.6 in a two-phase system with invariant inductances with respect to  $\theta_e$  where the winding magnetic axis are denoted by  $a$ ,  $b$  and  $c$ ; the direct and quadrature axes are denoted  $d$  and  $q$ , as depicted in Fig. 5.10.

The abc to dq transformation matrix for the balanced system is:

$$T_{dq0} = \frac{2}{3} \begin{bmatrix} \cos(\theta_e) & \cos\left(\theta_e - \frac{2\pi}{3}\right) & \cos\left(\theta_e + \frac{2\pi}{3}\right) \\ -\sin(\theta_e) & -\sin\left(\theta_e - \frac{2\pi}{3}\right) & -\sin\left(\theta_e + \frac{2\pi}{3}\right) \\ \frac{1}{2} & \frac{1}{2} & \frac{1}{2} \end{bmatrix} \quad (5.7)$$

**Fig. 5.10** Coordinate transformation from abc to dq frame



The voltage equation for the synchronous coordinates is:

$$\begin{bmatrix} v_d \\ v_q \end{bmatrix} = \begin{bmatrix} R_s & 0 \\ 0 & R_s \end{bmatrix} \begin{bmatrix} i_d \\ i_q \end{bmatrix} + \omega_e \begin{bmatrix} 0 & 1 \\ -1 & 0 \end{bmatrix} \begin{bmatrix} \psi_d \\ \psi_q \end{bmatrix} + \frac{d}{dt} \begin{bmatrix} \psi_d \\ \psi_q \end{bmatrix} \quad (5.8)$$

where

$$\begin{bmatrix} \psi_d \\ \psi_q \end{bmatrix} = \begin{bmatrix} L_d & 0 \\ 0 & L_q \end{bmatrix} \begin{bmatrix} i_d \\ i_q \end{bmatrix} + \begin{bmatrix} \psi_{pm} \\ 0 \end{bmatrix}$$

$$L_d = \frac{3}{2}(L_0 - L_m)$$

$$L_q = \frac{3}{2}(L_0 + L_m)$$

The state equation is given by:

$$\frac{d}{dt} \begin{bmatrix} i_d \\ i_q \end{bmatrix} = \begin{bmatrix} -\frac{R_s}{L_d} & \frac{\omega_e L_q}{L_d} \\ -\frac{\omega_e L_d}{L_q} & -\frac{R_s}{L_q} \end{bmatrix} \begin{bmatrix} i_d \\ i_q \end{bmatrix} + \begin{bmatrix} \frac{1}{L_d} & 0 \\ 0 & \frac{1}{L_q} \end{bmatrix} \begin{bmatrix} v_d \\ v_q \end{bmatrix} + \omega_e \begin{bmatrix} 0 \\ -\frac{\psi_{pm}}{L_q} \end{bmatrix} \quad (5.9)$$

From Eqs. 5.8 and 5.9, it can be built the equivalent circuit in synchronous coordinates like the circuits shown in Fig. 5.11.

Digital technology, multi-phase converters, and position sensors are well suited for synchronizing the switching current with the rotor position. These sensors are often optical or Hall Effect devices using the rotor magnetism to sense its position. It is expected that the torque reduces as the speed increases since the rotor generates proportionally a counter e.m.f. (electromotive force) across the coil that is coming closer to the pole. There will be a current reduction and so, a reduction of the magneto-motive force (m.m.f.) and, as a consequence, the torque. The maximum speed will be reached when the counter electromotive force (c.e.m.f) is equal to the DC source voltage. This feature let the PMSG generator also be used for dynamic or regenerative braking.

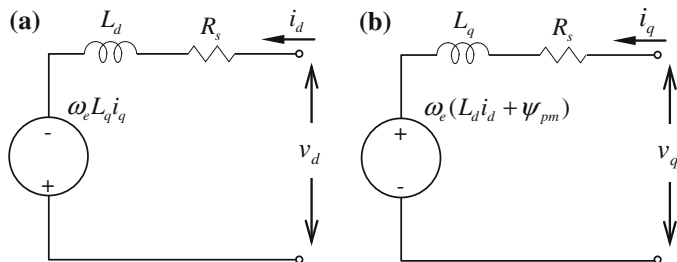


Fig. 5.11 Equivalent circuits of the  $d$ - $q$  axis: **a** direct axis; **b** quadrature axis

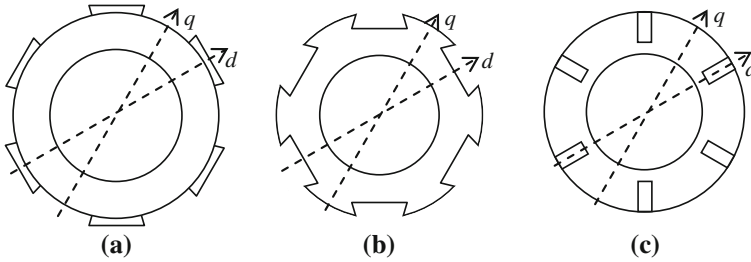
### 5.3.4 Types of Permanent Magnet PMSG

The permanent magnet PMSG generator can be categorized according to the way the permanent magnets are mounted on the rotor and the shape of the induced e.m.f. The permanent magnets can either be surface-mounted, interior-mounted, or buried in the rotor, and the induced e.m.f. shape in the stator can either be sinusoidal or trapezoidal [9].

Most electrical machines can be manufactured in two different ways: with inner rotor (external stator) or outer rotor (internal stator). For the given torque, the air gap area remains the same in either case. However, from the design point of view, an outer rotor is preferable, as the machine’s outer diameter becomes smaller. This results in a better utilization of the available volume. The windings are also easier to place in the slots of the internal stator. On the other hand, it requires a considerably more complex supporting structure like bearings and mounting in order to keep the air gap constant. The internal stator design might also have a poorer heat transfer capability as the main heat source—copper losses in the conductors—are located further away from the cooling surface in case of an air-cooled machine.

The heat transfer of the outer rotor can be improved by introducing an internal water cooling system. Depending on the type of excitation, a transverse flux machine can be either electrically or magnetically excited. An electrically excited machine normally has a more massive rotor and larger weight as compared to the magnetically excited one. The recently reduced magnet prices are making permanent magnet machines more feasible than ever.

Depending on the way the permanent magnets are placed in the rotor, the permanent magnet machine may have several design possibilities. As stated above, the most common designs used in the conventional radial-flux machine are the surface-mounted, interior-mounted, and buried designs. Selection of the proper design would affect the machine’s performance, as well as its weight and the overall production cost. The three rotor designs with the direct  $d$  and quadrature  $q$  axes are depicted in Fig. 5.10 and presented in Fig. 5.12.



**Fig. 5.12** Cross-sectional view of the permanent magnet types of rotor: **a** surface-mounted magnets; **b** interior-mounted magnets; **c** buried magnets

### 5.3.4.1 Surface-Mounted Permanent Magnet Type (SPM)

Figure 5.12a shows the rotor type of a surface-mounted permanent magnet. Each permanent magnet (PM) is mounted on the round surface of the rotor. It is easy to build up but there is a possibility for the attached PM to fly apart during a high-speed operation. Typically, for this type of generator, the inductance variation by rotor position is negligibly small.

In the configuration with the surface-mounted magnets (Fig. 5.12a), the magnets are polarized radially or sometimes circumferentially. The bandaging of such a machine is often necessary in order to protect magnets from the centrifugal forces. The reactances in the  $d$ - and  $q$ -axis are nearly the same. The construction of such rotor is relatively simpler, in comparison to the other rotor designs.

### 5.3.4.2 Interior-Mounted Permanent Magnet Type (IPM)

Figure 5.12b shows how each permanent magnet is mounted inside of the interior-mounted rotor of the PM type. The use of the interior-mounted PM is not as common as the surface-mounted type, but the interior-mounted PM is a good candidate for a high-speed operation of the hydro turbines because of its robustness and smaller diameter. It is noted that there is an inductance variation for this type of machine because the effective air gap varies by rotor position.

The interior-mounted rotor shown in Fig. 5.12b has radially polarized magnets embedded in slots on the rotor surface. The  $q$ -axis synchronous reactance is larger than in the  $d$ -axis. The rotor is likely to be lighter in this case since the e.m.f. induced by the magnets is generally lower than in surface-mounted design due to the larger flux leakage.

### 5.3.4.3 Buried-Mounted Permanent Magnet Type (BPM)

In the buried-magnet rotor depicted in Fig. 5.12c, the magnets are circumferentially magnetized. The synchronous reactance in the  $q$ -axis is larger than in the  $d$ -axis. The thickness of the bridge between the magnets should be carefully chosen.

In this configuration a non-magnetic shaft should preferably be used. The advantage of this rotor design is that the air-gap flux density can be greater than the remanent flux density of the permanent magnets [10–12].

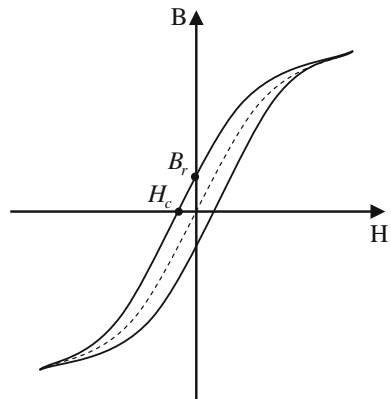
### 5.3.5 Permanent Magnets of the PMSG Generator

Permanent magnets are essential ingredients to the PMSG generator. In last two decades, permanent magnet technology has been substantially improved. When a permanent magnet has been magnetized by an external magnetic field, it will remain magnetized even if the magnetic field intensity is gone. The magnetic flux density at this point is called the remanence, denoted  $B_r$ . The remanence is the maximum flux density that the magnet can produce by itself. On the other hand, if magnetic field intensity has increased in the opposite polarity, the flux density will eventually become zero. The magnetic field intensity at this point is called the coercivity, denoted  $H_c$ .

The absolute value of the product of the magnetic flux density,  $B_r$  and the magnetic field intensity,  $H_c$  at each point along the magnetization curve in the second quadrant region is called the energy product, or the density of magnetic energy as it is illustrated in Fig. 5.13. The higher the density of magnetic energy is, the smaller the machine dimensions and core losses are. The operating point can be determined by the intersection between the permeance line and the hysteresis curve in the second quadrant region. The permeance line is determined by the characteristics of the machine structure: air gap length, magnetic path length, and number of coil turns. The large  $B_r$  produces a large flux in the machine, while the large  $H_c$  means that a very large current would be required for demagnetizing the poles [13].

Nowadays, many different types of permanent magnet materials are available. The types available include Alnico, Ferrite (ceramic), Rare-earth samarium-cobalt, and Neodymium-iron-boron (NdFeB). The NdFeB magnets, which have been

**Fig. 5.13** Typical magnetization curve of ferromagnetic materials



**Table 5.1** Characteristics of the permanent magnets

Type of PM	$B_r$	$H_c$	Performance	Cost
Alnico	High	Low	Excellent mechanical strength	Inexpensive
Ferrite	Low	Medium	Fragile	Moderately inexpensive
NdFeB	High	High	Excellent performance	Moderately expensive
Rare-Earth Samarium-Cobalt	High	High	Small temperature coefficient	Very expensive

developed recently, have the highest energy product. Ferrite magnets are the most commonly used due to their cost effectiveness and widespread usage. Each magnet type has different properties leading to different constraints and different levels of performance. The characteristics of the permanent magnet materials are compared in Table 5.1. NdFeB magnets have the highest remanence and coercivity but the initial price is very high. Ferrite magnets are widely used because the material and production costs are both low, even though they have low remanence, coercivity, and power product.

### 5.3.6 Advantages and Disadvantages of the PMSG Generator

The PMSG generator offers many advantages. The PMSG machine is the most efficient of all electric machines since it has a movable magnetic source inside itself. Use of permanent magnets for the excitation consumes no extra electrical power. Therefore, copper loss of the exciter does not exist and the absence of mechanical commutator and brushes or slip rings means low mechanical friction losses. Another advantage is its compactness.

The recent introduction of high-energy density magnets (rare-earth magnets) has allowed the achievement of extremely high flux densities in the PMSG generator, therefore rotor winding is not required. These in turn allow the generator to be of small, light, and rugged structure. As there is no current circulation in the rotor to create a magnetic field, the rotor of a PMSG generator does not heat up. The only heat production is on the stator, which is easier to cool down than the rotor because it is on the periphery of the generator and the static.

The absence of brushes, mechanical commutators, and slip rings suppresses the need for the associated regular maintenance and suppresses the risk of failure in these elements. They have very long lasting winding insulation, bearing, and magnet life length. Since no noise is associated with the mechanical contacts and the driving converter switching frequency could be above 20 kHz producing only ultrasound inaudible for human beings.

When the PMSG generator is compared with respect to the conventional ones for low-speed water flows, the list of advantages is increased: (1) No speed multiplier or gears since there may be multiple permanent or electromagnets in the rotor for more current production; (2) Few maintenance services because of its

simplified mechanical design; (3) Easy mechanical interface; (4) Cost optimization; (5) Highest power-to-weight ratio in a direct drive; (6) Location of a moving magnetic field being generated in the center of the field; (7) More precise operations since a microprocessor controls the generator/motor electrical output and current instead of mechanical brushes; (8) Higher efficiency for the brushless generation of electrical current and digitally controllable flexible adjustment of the generator speed with less friction, fewer moving components, less heat, and reduced electrical noise; (9) Since the permanent or electromagnets are located on the rotor, they are kept cooler and thus have a longer life.

The PMSG generator has some inherent disadvantages. Two of them are related to the high cost of the permanent magnets and the commercial availability. The cost of higher energy density magnets prohibits their use in applications where initial cost is a major concern. Another problem is the field-weakening operation for the PMSG machine is somewhat difficult due to the use of permanent magnets. An accidental speed increase might damage the power electronic components above the converter rating, especially for vehicle applications. In addition, the surface-mounted permanent magnet generators cannot reach high speeds because of the limited mechanical strength of the assembly between the rotor yoke and the permanent magnets. Finally, the demagnetization of the permanent magnet is possible by the large opposing magneto-motive-force (m.m.f.) and high temperatures. The critical demagnetization force is different for each magnet material (see Table 5.2) where  $B_r$  stands for relative flux density,  $\mu_r$  is the corresponding relative magnetic permeability and  $\rho$  is the volumetric density. Also, extreme care must be taken to cool the generator, especially if it is compact.

There are several types of PM generators: the conventional PM synchronous machine, the conventional PM synchronous machine with flux concentration, the slotted axial-flux PM machine, TORUS, the surface-mounted transverse-flux PM machine, and the flux-concentrating trans-verse-flux PM machine. In order to select the best type of PMSG generator, one has to consider four main characteristics among the various topological variants of the PM machines such as: (1) air gap orientation with respect to the rotational axis: radial or axial; (2) stator core orientation with respect to the direction of the movement: longitudinal or transverse; (3) PM orientation with respect to the air gap: surface-mounted or flux-concentrating; and (4) copper housing: slotted or slotless [11, 12].

**Table 5.2** Types of permanent magnets for PMSG generators

Magnet type	NdFeB (Vacodym 633 PT)	Ferrite (Oe MagnetY30 BH)
$B_r$ (Tesla)	1.32	0.3663
$\mu_r$	1.06	1.0600
$\rho$ (kg/m <sup>3</sup> )	7,700	4,700



## 5.4 The Induction Generator

The induction generator is an induction machine that is converted in some way into a generator as discussed in this section. The term “asynchronous generator” is avoided in this text since it has been inconveniently used many times for induction machines not considering that every alternative source of energy operates at some asynchronous mode, not only the induction generator. This can be misleading since it neglects the hunting phenomenon caused by the individual power control of each source on the common stable operating point. If the amount of asynchronous power goes up to say 20 % of the synchronous power, an unstable operating mode may occur and, may be, a collapsed system, depending on the degree of instability.

### 5.4.1 Topologies of Hydropower Connection

There are three main topologies of the induction generator (IG) operation: the direct-grid connected (DGC), the self-excited stand-alone (SEIG) and the doubly-fed (DFIG) or wound-rotor (WRIG). Every one of these types is more or less suitable for a given application, all depending on the power plant size and the technology available. The induction generator has economy of scale since it is just an induction motor used as an electrical generator. The induction squirrel cage (SC) machine has been introduced in connection with two gearboxes with different ratios for hydro and wind power, but each of these drive trains has a stiff speed-torque characteristic and mechanical problems with speed surges, volume and weight.

Two operating strategies can be used for the hydro power conversion. First, the maximum power point strategy searching for the maximal power, by exploiting the available input hydro energy. This control can be exerted over the source side or load side based on the maximum power output. It is suitable for medium and high-speed rivers. A power converter makes it possible to satisfy this partial speed-variable operation over a wide speed range with an overall high efficiency of power conversion. It is clear that the maximum power generation is more important than the maximum efficiency since if the water flow in nature is not used at the moment it is there, it will be wasted. The disadvantage of this strategy in non-smooth flowing rivers is that the generated electrical power will be strongly dependent on the changes of the hydro-input causing undesirable power fluctuations.

Second, the constant power strategy combines the rotor speed control and an active power regulation to obtain an approximately constant energy flow into the line-side. This strategy is not disadvantageous in a non-optimal power generation. The Doubly-Fed Induction Generator allows for improving the optimal efficiency points over a wide speed range with a partial speed variable converter as it is discussed below.

### 5.4.2 The Squirrel Cage Induction Generator (SCIG)

The direct-grid connected application of the squirrel cage induction generator (IG) is the simplest one demanding for only a minimum speed limiter to keep the induction machine turning at a speed  $n$  above the equivalent synchronous speed  $n_s$  of the mains grid, as depicted in Fig. 5.14. Voltage and frequency are controlled by the public network. The amount of power injected into the grid (usually no more than 500 kW) will be proportional to the difference between the local generator speed  $n$  and the synchronous speed  $n_s$ . A reasonable amount of reactive power is absorbed by these generators from the synchronous generation causing voltage drops if there is not any line reactive compensation and/or active filter.

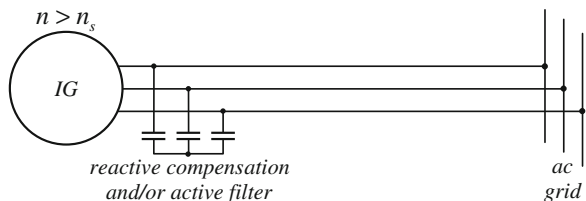
The stand-alone self-excited IG is used in low power applications (in general no more than 50 kW) just adequate for those loads not too sensitive to frequency oscillations  $\omega$ . It is an inexpensive and efficient solution for small stand-alone applications (see Fig. 5.15) [13, 14].

The main limitation of the self-excited induction generator is the cost of the capacitor banks for larger sizes. One way of decreasing the size of the capacitor bank is illustrated in Fig. 5.16. The reactive power in this case has to be supplied by a bank of capacitors or a power inverter connected to a battery bank that is able to produce a leading current to be supplied by the synchronous machine connected in parallel with the load. A competitive cost race in between the capacitor bank and the arrangement of battery bank plus power converters is something to be carefully considered for medium sized units.

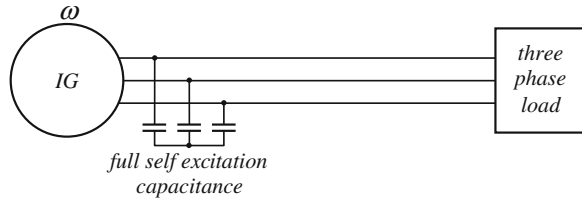
Other configurations are shown in Figs. 5.17 and 5.18. In Fig. 5.16 the generator frequency is decoupled from the synchronous speed and it can stay below or above it. The speed range of the hydro power generation is widened, increasing the possibilities for this generator. Figure 5.18 shows a configuration for which the capacitor bank is almost entirely replaced by power electronics [15]. This characteristic of being able to operate at variable-speeds of the primary machine without spare storage devices and a reduced capacitor bank is still a point of discussion for many studies.

Many disadvantages are apparent in the SC asynchronous grid connection topology: (1) The power converter is more expensive since it has to be designed for the full rate of the total power system; (2) Inverter output filters and EMI filters are rated for 1.0 p.u. output power, making filter design difficult and costly; (3) The converter efficiency plays an important factor in the total system efficiency over

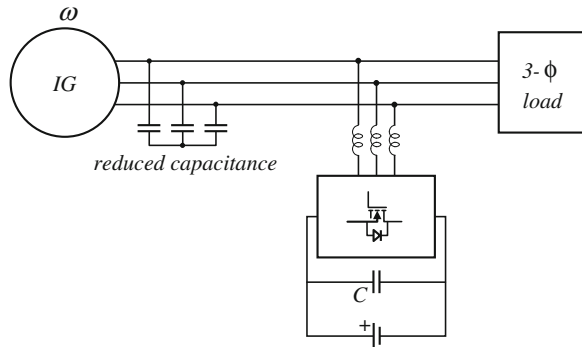
**Fig. 5.14** Direct-grid connection topology



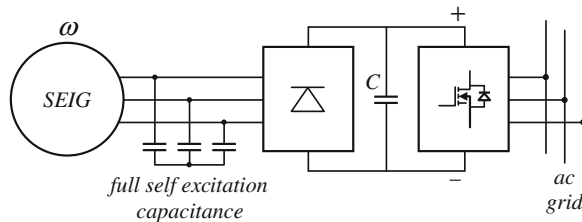
**Fig. 5.15** Squirrel cage stand-alone topology



**Fig. 5.16** SC battery excited stand-alone topology



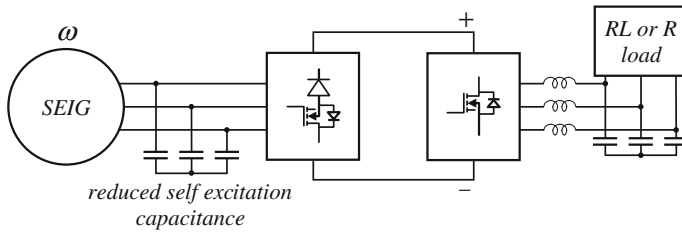
**Fig. 5.17** Self-excited squirrel cage asynchronous grid connection



the entire operating range. Even so, several units were built up to 1.5 MW all over the world [16–18].

### 5.4.3 Doubly-Fed Induction Generator (DFIG)

The brushless doubly fed induction machine is one type of generator whose stator and rotor can be externally or manually controlled by power electronics. It shows promising results for hydro power applications due to its poor rotor magnetic coupling and relatively high value of slip, and core loss. It plays an important role in affecting the steady state and dynamic performance of the next power generation machines. Although it is not common to see the wound rotor induction generator being used in the same way as the squirrel cage induction generator, it



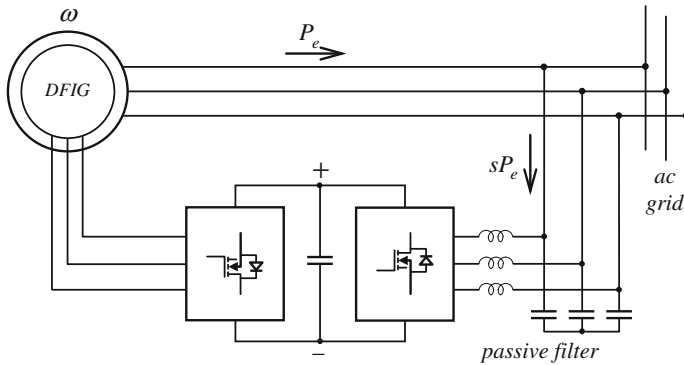
**Fig. 5.18** Sparse matrix converter for induction generator self excitation topology with RL or R load

presents some special features making it very attractive for high hydro or wind power plants.

DFIG is a more versatile induction generator and it has been strongly considered for many variable-speed applications, as is the case of the run-of-a-river, sea tide, sea wave, and wind power generation. In this generator, stator  $P_e$  and rotor  $sP_e$  powers are manipulated in such a way to allow the control over the pull-out torque, number of poles, load frequency, reactive power and other variables. It is specially suited for variable hydro and wind speed applications consisting of a DFIG based on a slip-ring wound rotor working in a partial speed variable mode, as illustrated in Fig. 5.19. An electronic inverter system based on a rotor side converter and a grid-side inverter connected by a dc-link allows the realization of a sub-synchronous mode of the generator for when the primary source cannot keep the synchronous speed [19–22].

The slip of the doubly-fed induction generator varies with a rotor converter and therefore the speed may be varied in a wide range. With short-circuited slip rings, the induction generator works within the natural speed–torque characteristic. However, an increase of water flow may lead the system beyond the stability limits. A solution could be a rotor side energy recovery through the speed slip and the machine will be operating in an over-synchronous mode. A decrease in the water flow will demand for additional electric power over the slip rings into the rotor, preventing the transition to the motor-driven mode, thus keeping it in the sub-synchronous mode. A quasi-speed-variable regime is optimally obtained within a  $\pm 30\%$  operating range with an equivalent power reduction in the converter rates. The increase in power rating with a variable-speed strategy brings some advantages such as reduced active power fluctuation, damped mechanical load steps and oscillations, adjustable power factor, optimal power points, better line-parallel and facilitate stand-alone solutions. Additional advantages expected from these systems include: precise synchronous operation over a wide speed range, adjustable displacement power factor, low harmonic distortion and the possibility of working as the main fed induction machine in case of power converter failure.

Among the various kinds of variable-speed hydro turbine technologies, DFIG is the most common since they are capable of decoupling the active and reactive



**Fig. 5.19** DFIG direct-grid connection topology

power control in both sub-synchronous and super-synchronous speed ranges. The associated inverter needs only to be rated for a fractional power of the machine, the fraction depending on rotor slip.

Many studies have been carried out in order to develop a machine which combines the great advantages of DFIGs with high reliability and low maintenance. Among other solutions, the use of the so-called brushless doubly fed machine (BDFM), also known as self-cascaded induction machine, could overcome high reliability and low maintenance. Although BDFM is slightly larger in size than DFIG due to poor magnetic design, its high reliability and low maintenance make it a good candidate for use in hydro power generation. The first attempts of creating such machines can be traced down to the machine proposed by Hunt in 1907 where wound rotor machines were used. But in the 1970s, Broadway and Burbridge proposed a new squirrel cage rotor for the BDFM, the nested loop rotor, which is very similar to the ones used today. There are a lot of papers considering steady-state and dynamic modeling of the BDFM. Several investigators have taken a BDFM virtually as the connection of two induction motors with different pole pairs with rotors electrically and mechanically connected in phase opposition [23–27].

#### 5.4.4 Modeling of the DFIG

The construction of a DFIG is similar to a wound rotor IM and comprises a three-phase stator winding and a three-phase rotor winding fed via slip rings as shown in Fig. 5.19. Figure 5.20 shows the equivalent models per phase of the IG.

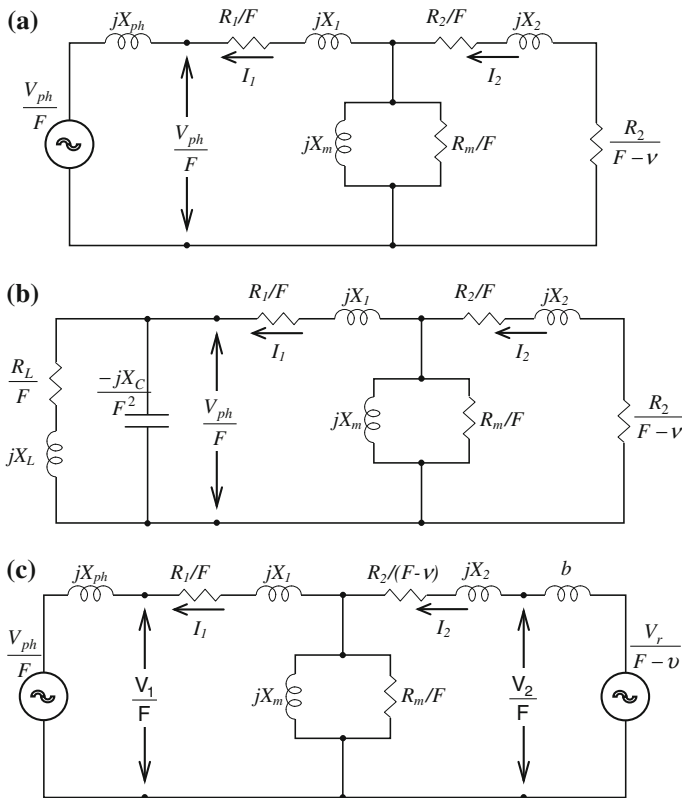
The stator  $v_{sk}$  and rotor  $v_{rk}$  voltages per phase and the electrical torque  $T_e$  equations of the DFIG in a stationary reference frame are related to the stator  $i_{sk}$  and rotor  $i_{rk}$  currents per phase by:

$$\begin{aligned}
 v_{sk} &= r_s i_{sk} + \frac{d\psi_{sk}}{dt} \\
 v_{rk} &= r_r i_{rk} + \frac{d\psi_{rk}}{dt} \quad k = a, b, c \\
 T_e &= \frac{p}{2} \sum_k i_k \frac{d\psi_k}{d\theta}
 \end{aligned}
 \tag{5.10}$$

where  $r_s$  and  $r_r$  are the stator and rotor resistances,  $p$  is the number of pole pairs.

The rotor quantities refer to the stator in these equations. Transforming these equations from three-phase to two-phase  $d$ - $q$  components and subsequently rotating all variables into a synchronous reference frame according to:

$$\begin{aligned}
 v_d &= \frac{2}{3} \left[ v_a \cos\theta + v_b \cos\left(\theta - \frac{2\pi}{3}\right) + v_c \cos\left(\theta + \frac{2\pi}{3}\right) \right] \\
 v_q &= \frac{2}{3} \left[ -v_a \sin\theta - v_b \sin\left(\theta - \frac{2\pi}{3}\right) - v_c \sin\left(\theta + \frac{2\pi}{3}\right) \right]
 \end{aligned}
 \tag{5.11}$$



**Fig. 5.20** IG Operating Technologies: **a** direct-grid operation; **b** stand-alone operation; **c** doubly-fed operation

where

$$\begin{aligned}
 \bar{v} &= v_d + jv_q & T_e &= -\frac{3}{2}p \cdot \text{Im}|\bar{\psi}_s, \bar{i}_s^*| \\
 \bar{v}_s &= r_s \bar{i}_s + \frac{\partial \bar{\psi}_s}{\partial t} + j\omega_s \bar{\psi}_s & \omega_r &= \omega_s - \omega_m \text{ (rotor slip frequency)} \\
 \bar{v}_r &= r_r \bar{i}_r + \frac{\partial \bar{\psi}_r}{\partial t} + j\omega_r \bar{\psi}_r & \omega_s &= \frac{2\pi \cdot pn_s}{120} \text{ (synchronous frequency)} \\
 \bar{\psi}_s &= L_s \bar{i}_s + L_m \bar{i}_r & \omega_m &= \text{mechanical angular frequency} \\
 \bar{\psi}_r &= L_m \bar{i}_s + L_r \bar{i}_r
 \end{aligned}$$

When dealing with variable-speed, the IG parameters of Fig. 5.19 have to be corrected for the frequency they will be working at and in this chapter the  $F$  parameter is used to define such correction as:

$$F = \frac{f}{f_{\text{ref}}} \quad (5.12)$$

where

$f$  is the operating frequency

$f_{\text{ref}}$  is the frequency with which the IG parameters were measured

$$\frac{R}{F_s} = \frac{R}{F \left(1 - \frac{n_r}{n_s}\right)} = \frac{R}{F - v}$$

The synchronous reference frame can be linked to the stator or rotor flux of the machine. However, a reference frame linked to the stator voltage space vector  $v_s$  is a convenient alternative because the DFIG operates as a generator maintaining or being fed with constant stator voltage. Hence, stator voltage and stator current are either given (line operation) or controlled (island operation) variables.

Two interpretations of the DFIG dynamic equations are possible depending on the state variables selected in the model. A synchronous machine model is obtained when selecting the flux linked to the rotor currents (or back-e.m.f. voltage) as a state variable. If the air gap flux (or magnetizing current) is chosen as a state variable, it will lead to a possible steady-state model of the induction machine for controlling purposes.

The active power delivered to the rotor by the 4-quadrant converter and the mechanical power delivered to the shaft of the generator can be calculated according to the well-know IM equations:

$$\begin{aligned}
 P_r &= sP_s \\
 P_m &= (1 - s)P_s
 \end{aligned} \quad (5.13)$$

Equations 5.13 describe clearly the power flow in the DFIG for over-synchronous and under-synchronous operation. Above synchronous speed the 4-quadrant converter operates as a generator of active power delivering power to the grid parallel to the DFIG. Below synchronous speed, the 4-quadrant converter bypasses active power from the grid into rotor circuit.

The stable operation and independent control of active and reactive power of the DFIG can use a vector controller because the synchronous reference frame in which the machine equations can be described is linked to the stator voltage space vector  $v_s$ , and not to the stator or rotor flux vector as is common in field oriented controllers for drives. All measured quantities, i.e., stator and rotor current  $i_s$  and  $i_r$  have to be transformed into the synchronous reference frame with a decoupling circuit calculating the desired active and reactive power signals for the rotor voltage command of  $v_{rd}$  and  $v_{rq}$ . A reverse vector rotation has to compute magnitude and phase of the rotor voltage commands in a stationary reference frame. Furthermore, the measured rotor current signals used for rotor current regulation can help to minimize the effects of parameter detuning and inverter gain errors [14].

The adjustable speed generators (ASG) concept consists of a DFIG with a 4-quadrant ac-to-ac converter connected to the rotor windings. Compared to the direct connected topology, the DFIG offers following advantages: (1) VAR control can be implemented at lower cost because the DFIG system (4-quadrant converter and induction machine) basically operates similar to a synchronous generator. The converter has to provide only excitation energy; (2) the DFIG dynamic model with 4-quadrant converter in the rotor circuit when compared to SCR based Kramer drives facilitates the development of a generator which has a control decoupled from its active and reactive power; (3) increases the system efficiency by about 15 % taking into account separately the losses in the power electronic devices, wire connections and the generator; (4) reduced inverter cost because inverter rating is typically 25 % of the total power system, while the speed range of the ASG is a third around the synchronous speed; (5) reduced cost of the inverter filters and EMI filters since filters are rated for 0.25 p.u. of total power system and inverter harmonics represent a smaller fraction of the total harmonics system [23–27].

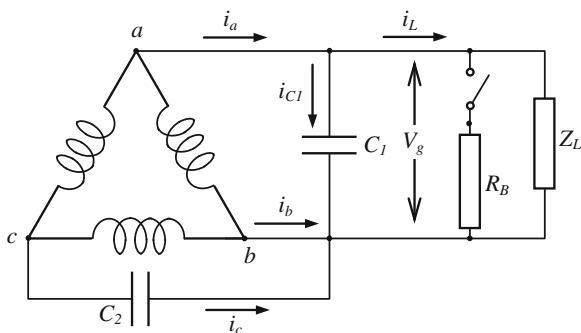
The main disadvantages of DFIGs are their brushes and slip rings which increase maintenance costs and fault rates. Also core losses in brushless doubly fed induction machines have not been extensively studied in the literature.

## 5.5 Power Electronic Controls for Three-Phase Generators Operating in Single-Phase Mode

A three-phase generator can be converted into a single-phase generator, which is usually derated to approximately 80 % of the nominal machine rating with the connection of two capacitors as shown in Fig. 5.21. The impedance  $Z_L$  represents the consumer load connected in parallel to the ballast load  $R_L$  which is used to



**Fig. 5.21** Single-phase output from a three-phase induction generator



maintain the total generator load at a constant value. The ballast load in fact is a variable load where its resistance is controlled so as to maintain the consumer load plus the ballast load at a constant value [28].

Of course such a single-phase connection suffers of poor voltage regulation, and the system is stable only for a limited range of resistive load. This is normally true for very small hydro schemes used to provide power for lighting, heating, cooking, and maybe ironing clothes. Using Eqs. (5.14) and (5.15) and assuming that the machine is operating as a balanced three-phase system, the phasor diagram can be constructed as shown in Fig. 5.22. As capacitor  $C_2$  is connected across phases  $b$  and  $c$ ,  $i_c$  is perpendicular to the voltage vector  $V_{bc}$ . In order to obtain a balanced operation the following two conditions must be satisfied:

$$\bar{i}_a = \bar{i}_L + \bar{i}_{C1} \quad (5.14)$$

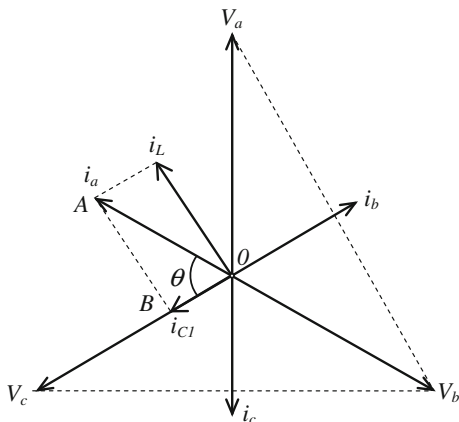
$$\bar{i}_b = -(\bar{i}_a + \bar{i}_c) \quad (5.15)$$

$$\theta = 60^\circ \text{ and } |\bar{i}_c| = |\bar{i}_a| \quad (5.16)$$

Following the analysis it is found that in order to obtain a balanced operation of the three-phase motor, capacitor  $C_1$  should be selected such that  $|\bar{i}_L| = \sqrt{3}|\bar{i}_{C1}|$  and also  $|\bar{i}_c| = 2|\bar{i}_{C1}|$  which leads to the result that capacitor  $C_2$  should be equal to  $2C_1$ . When an induction generator is used in this way, particular care must be taken over the connection of the capacitor  $C_2$ . If capacitor  $C_2$  is connected between phases  $a-c$  instead of  $c-b$ , then the resultant phasor diagram is shown in Fig. 5.22. In this case, the generator will run as an unbalanced system. It can be seen that the current through one of the windings of the induction generator becomes twice that of the other winding currents. Under this condition, the winding generator would overheat. Therefore, correct connection of the capacitor  $C_2$  is important.

In typical induction generator based small hydro schemes, the turbines used are run-of-the-river type, where the water input and thus the mechanical power into the generator cannot be controlled. For example a water-wheel as a turbine, or schemes where the generator operates under manual control of the sluice gate and, if the consumer load changes, then the generated voltage and the frequency will

**Fig. 5.22** Phasor diagram for the single-phase connection

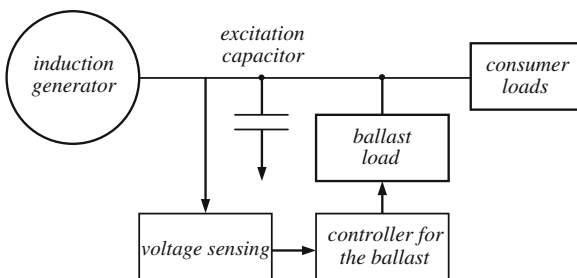


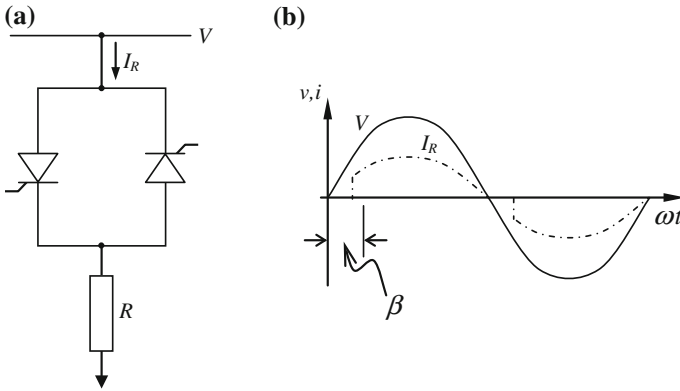
also vary. If the load is light the generator speed can increase, leading to runaway condition. The control technique used to maintain the generated voltage and frequency at their rated values is used to keep the total load connected to the machine at a near constant value using a ballast load as shown in Fig. 5.23. Since the terminal voltage under this condition is a constant value, voltage sensing is used to control the ballast load.

The ballast load can be implemented in several ways [28–32]. One way of obtaining a variable load is to use a resistor with two anti-parallel thyristors operating in phase control mode as shown in Fig. 5.24. By changing the firing angle  $\beta$ , the fundamental value of the current going through the resistor-thyristor circuit can be controlled. When  $\beta = 0^\circ$  there is a full current impressed through the resistor-thyristor circuit, i.e., maximum load. When  $\beta = 180^\circ$ , the current through the resistor-thyristor circuit is zero and a programmable ballast load is possible for values of  $\beta$  in between  $0^\circ$  and  $180^\circ$ .

Of course, as  $\beta$  is increased, the displacement factor of the resistor-thyristor circuit increases, thus absorbing reactive power. This circuit will draw a reactive current from the excitation capacitors, reducing the effective capacitance available to supply a magnetization current to the induction generator which causes a slight reduction in the output generator voltage. Another possible circuit, which does not absorb reactive power, uses a number of resistors with a switched thyristor

**Fig. 5.23** Typical small hydro scheme with a ballast load control



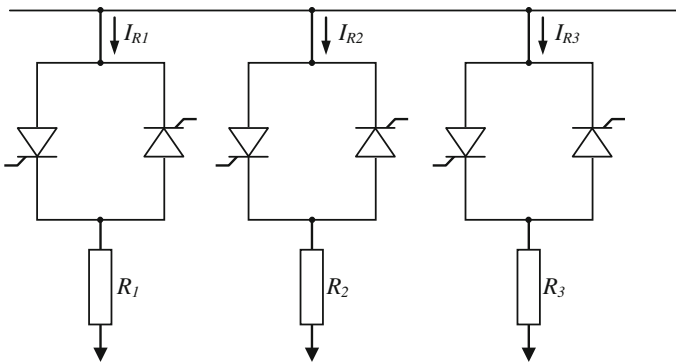


**Fig. 5.24** Thyristor phase controlled ballast load

scheme. The circuit is shown in Fig. 5.25 where the back-to-back thyristor pair operates either as a closed or open switch (on–off). Therefore, the load may be varied by controlling the number of parallel resistor–thyristor circuits, which are “on”. The variation of the load is in steps and smooth variation is not possible.

In order to get a better resolution from the circuit depicted in Fig. 5.25, resistors can be selected in a binary weighted configuration. If  $R_1 = R$ ,  $R_2 = 2R$  and  $R_3 = 4R$  then the load can be varied from 0 to  $7R$ , in steps of  $R$ . As indicated above, the thyristor-based circuits have some drawbacks.

A circuit that is very smooth in respect to a varying ballast load can be implemented with a full wave rectifier followed by a transistorized chopper operating at a high frequency as indicated in Fig. 5.26. If such frequency is at least 10 times higher than the fundamental induction generator frequency the system will be nearly at unit power factor for any pulse-width modulation (duty ratio) of the chopper.



**Fig. 5.25** Thyristor phase stepwise controlled ballast load

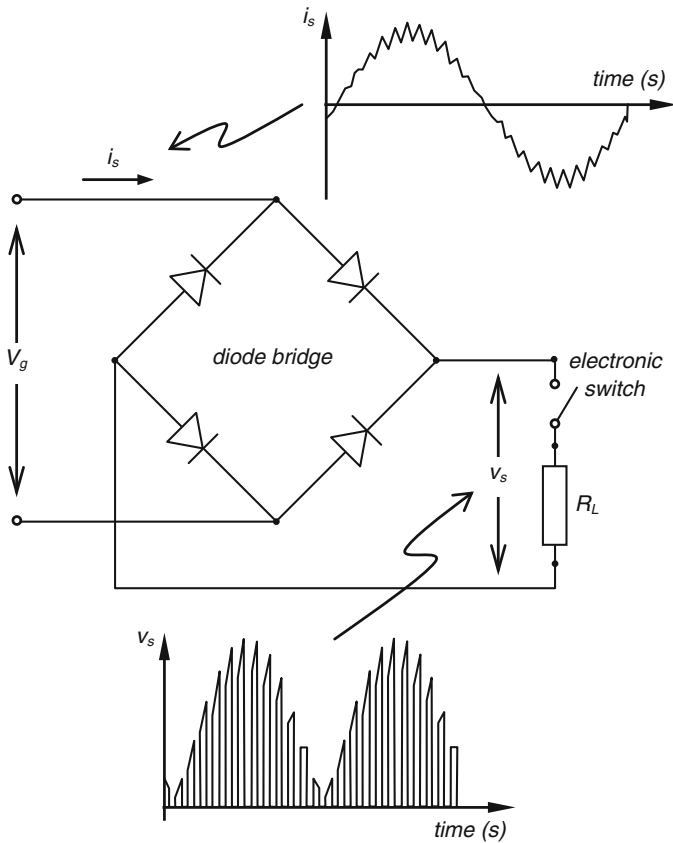
The effective resistance of the ballast load can be changed by varying the duty ratio of the switch. Figure 5.26 shows the voltage across the ballast load and the ac-side current when the consumer load is only 50 % of the rated load of the machine. Due to the inductance, the current drawn from the generator is nearly sinusoidal with a superimposed high-frequency ripple component.

In order to run the machine with a single-phase loading for minimum unbalance, the power output of the generator and the value of the excitation capacitor ( $C_1$ ) connected across the load should have the relationship depicted by Eq. (5.17):

$$P = V_g i_L = \sqrt{3} V_g i_{C1} = \sqrt{3} V_g^2 \omega C_1 \tag{5.17}$$

where  $V_g$  is the generate voltage,  $i_L$  is the load voltage, and  $i_{C1}$  is the current through the capacitor.

Power constraints of Eq. (5.17) assume that the induction generator is operating near to a balanced condition. Therefore, the family of curves of the terminal

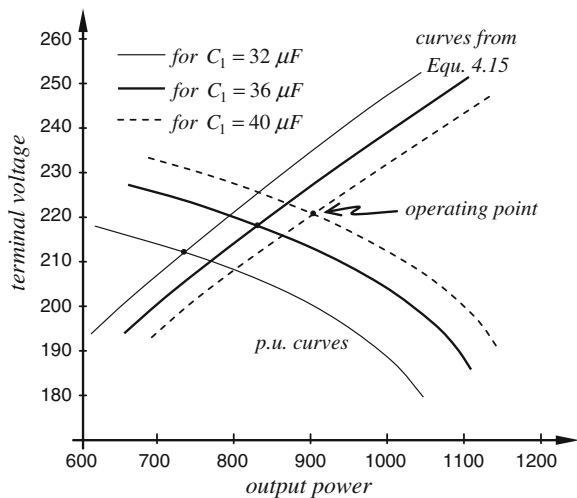


**Fig. 5.26** High-frequency ballast showing the voltage across the load and the supply side current for a 50 % loading in the machine

voltage which is a characteristic of the induction generator, and called Power–Voltage curves, can be found for different capacitor values by using the conventional induction generator steady-state equivalent circuit. This model includes the saturated magnetizing inductance of the generator besides considering the loading and operating speeds of the machine. The intersections of the terminal voltage characteristics and the information obtained using Eq. (5.17) give the operating points of the machine which satisfy both the steady-state machine equivalent circuit. This design method can be easily used in practice for dimensioning a small hydro scheme using an induction machine. Figure 5.27 shows a typical plot of characteristics for three different values of the excitation capacitor versus the supply voltage  $i_s$ . One can observe that if the value of the excitation capacitor  $C_1$  is  $40 \mu\text{F}$ , the generator produces 900 W at 220 V. Typically this is a derating of 80–90 % of the nominal machine power.

Under lightly loaded conditions or under no load, if the ballast load fails then only a small part of the mechanical power input is converted into the electrical power. Since the turbine is run-of-the river type, the mechanical power into the turbine cannot be controlled and therefore, the turbine and the generator will accelerate to runaway speed within a few seconds. The runaway speed depends on the turbine chosen. When runaway occurs, the torque-speed characteristic is mainly governed by the turbine, and the speed increases to that corresponding to the torque, which is just enough to overcome the friction and wind loss of the system. For the commonly used cross-flow turbine, runaway speed is around 175 % of the optimum speed. Under runaway conditions, the voltage of the generator will increase which can cause extensive damage to the generator (insulation failure), in addition to the connected loads and excitation capacitors. In order to prevent such overall damage an overvoltage protection circuit must be used. When the generated voltage rises above a certain threshold preset limit, the overvoltage protection isolates the excitation capacitors and the loads from the

**Fig. 5.27** Voltage versus power characteristics for variable  $C_1$



generator, thus allowing the induction machine to run freely without any current circulation.

## References

1. Inversin AR (1986) Micro-hydropower source book. National rural electric cooperative association (NRECA), International Foundation, Washington
2. Lauterjung H, Schmidt G (1989) Planning of water intake structures for irrigation or hydropower planning for intake structures, a publication of GTZ-postharvest project In: Deutsche Gesellschaft für Technische Zusammenarbeit (GTZ) GmbH, Eschborn. ISBN 3-528-02042-3
3. Lee HW (2003) Advanced control for power density maximization of the brushless dc generator. PhD Dissertation submitted to the office of graduate studies of Texas A&M University, Dec (2003)
4. Chalmers BJ, Wu W, Spooner E (1999) An axial-flux permanent-magnet generator for a gearless wind energy system. *IEEE Trans Energy Conversion*, 14(2):251–267
5. Anpalahan P, Soulard J, Nee HP (2001) Design steps towards a high power factor transverse-flux machine. In: Proceedings of European conference on power electronics and applications, Graz, Austria
6. Elevich LN (2005) Application note on 3-phase BLDC motor control with hall sensors using 56800/E digital signal controllers. Freescale semiconductor Inc, AN1916, Rev. 2.0
7. Boldea I (2005) Variable speed synchronous generators, electrical power engineering series. ISBN 0849357152, CRC Press, Boca Raton
8. Ortega C, Xavier del Toro AA (2005) Novel direct torque control for induction motors using short voltage vectors of matrix converters. *IEEE Trans Ind Appl*, pp 1353–1358
9. Afjei E, Hashemipour O, Saati MA, Nezamabadi MM (2007) A new hybrid brushless dc motor/generator without permanent magnet. *IJE Transactions B: Applications*, 20(1): 77
10. Svechkarenko D (2007) On analytical modeling and design of a novel transverse flux generator for offshore wind turbines. Licentiate Thesis, KTH Teknikringen, ISBN 978-91-7178-682-1, Stockholm, Sweden
11. Danielsson O, Thorburn K, Eriksson M, Leijon M (2003) Permanent magnet fixation concepts for linear generator. Division for electricity and lightning research, Department of engineering sciences, Uppsala University, Box 534, S-751 21, 5th European wave energy conference, Sweden
12. Dubois MRJ (2004) Optimized permanent magnet generator topologies for direct-drive wind turbines, M.Sc. Dissertation. Technische Universiteit Delft, Canada
13. Chapman JC (1999) Electric machinery fundamentals. WCB McGraw-Hill, Victoria. ISBN 0070119503
14. Godoy Simões M, Farret FA (2008) Alternative energy systems, design and analysis with induction generators, second edn. CRC Press, Boca Raton
15. Trapp JG, Parizzi JB, Farret FA, Serdotte AB, Longo AJ (2011) Stand alone self-excited induction generator with reduced excitation capacitors at fixed speed. In: Proceedings of the 11th Brazilian congress of power electronics. Natal, RN, Brazil v, 1:1–6
16. Marra EG, Pomilio JA (1999) Induction generator based system providing regulated voltage with constant frequency. In: *IEEE-Applied power electronics*, 14th annual conference and exposition. APEC '99. doi:10.1109/APEC.1999.749709, vol 1, pp 410–415
17. Szczesny R, Ronkowsky M (1991) A new equivalent circuit approach to simulation of converter—induction machine associations. European conference on power electronics and applications (EPE '91), pp 4/356–4/361, Firenze

18. La K-K, Schin M-H, Hyun D-S (2000). Direct torque control of induction motor with reduction of torque ripple. *IEEE Trans Ind Appl*, pp 1087–1092
19. Cadirici I, Ermis M (1992) Double-output induction generator operating at sub-synchronous and super-synchronous speeds: steady-state performance optimization and wind-energy recovery. *IEE Proc-B*, 139(5):429–441
20. Pena R, Clare JC, Asher GM (1996) Doubly-fed induction generator using back to back PWM converters and its application to variable-speed wind-energy generation. *IEE Proc Electr Power Appl*, no 3, pp 231–240
21. Hofmann W, Thieme A, Dietrich A, Stoev A (1997) Design and control of a wind power station with double fed induction generator. *EPE'97*, pp 2.723–2.728
22. Quang NP, Dittrich A, Thieme A (1997) Doubly-fed induction machine as generator: control algorithms with decoupling of torque and power factor. *Electr Eng* 80:325–335
23. Jahns T, De Doncker RW (1996) The control handbook, edition series “control of generators”. Editor-in-chief: William Levins, CRC Press, ISBN 084938570922
24. Muller S, Deicke M, De Doncker RW (2000) Adjustable speed generators for wind turbines based on doubly-fed induction machines and 4-quadrant IGBT converters linked to the rotor. *IEEE industry applications conference*, doi:[10.1109/IAS.2000.883138](https://doi.org/10.1109/IAS.2000.883138), vol 4, pp 2249–2254
25. Sen PK, Nelson JP (1997) Application guidelines for induction generators. department of electrical engineering, University of Colorado at Denver, Colorado 8040 1, pp WC1-5.1–wc1-5.3
26. Roberts PC (2005) A study of brushless doubly-fed (induction) machines: contributions in machine analysis, design and control. a dissertation submitted for the degree of doctor of philosophy, Emmanuel College, University of Cambridge, UK
27. Payam AF, Hashemnia N, Kashiha A (2010) A robust speed sensorless control of doubly-fed induction machine based on input-output feedback linearization control using a sliding-mode observer. *World Appl Sci J* 10 (11): 1392–1400, ISSN 1818-4952, IDOSI Publications
28. Ekanayake JB (2002) Induction generators for small hydro schemes, *Power Engineering Journal*, University of Cardiff, USA
29. Portolann CA, Farret FA, Machado RQ (1995) Load effects on DC–DC converters for simultaneous speed and voltage control by the load in asynchronous generation. First IEEE international caracas conference on devices, circuits and systems. doi:[10.1109/ICCDCS.1995.499159](https://doi.org/10.1109/ICCDCS.1995.499159), pp 276–280
30. Farret FA, Portolann CA, Machado RQ (1998) Electronic control by the load for asynchronous turbogenerators, driven by multiple sources of energy. Proceedings second IEEE international caracas conference on devices, circuits and systems, doi:[10.1109/ICCDCS.1998.705859](https://doi.org/10.1109/ICCDCS.1998.705859), pp 332–337
31. Smith OJM (1987) Three-phase induction generator for single-phase line. *IEEE transactions on energy conversion*, EC-2(3):382–387
32. Bhattacharya JL, Woodward JL (1988) Excitation balancing of a self-excited induction generator for maximum power output. *Generation, transmission and distribution*, IEE Proceedings C, 135(2):88–97

# Chapter 6

## Fuel Cell System

**Fei Gao, Mohammad Kabalo, Marek S. Rylko, Benjamin Blunier  
and Abdellatif Miraoui**

**Abstract** In this chapter, the fuel cell and fuel cell system basics and their associated power electronic converter topologies will be introduced. The first part focuses on the introduction of different fuel cell technologies. The fuel cell characteristic polarization curve and dynamic behavior will be discussed in general. Two control-oriented, ready-to-use models for proton exchange membrane fuel cell (PEMFC) and solid oxide fuel cell (SOFC) will be presented with detailed equations. The second part focuses on the introduction of different power converter topologies for fuel cell use. The power electronic particularity for a fuel cell system will be introduced. A state-of-art of different converter topologies and their highlights and drawbacks for a fuel cell system will be presented and discussed.

---

F. Gao (✉) · M. Kabalo · B. Blunier · A. Miraoui  
Institute for Transportation Research, Energy and Society,  
University of Technology of Belfort-Montbeliard, 90000 Belfort, France  
e-mail: fei.gao@utbm.fr

M. Kabalo  
e-mail: mohammad.kabalo@utbm.fr

B. Blunier  
e-mail: benjamin.blunier@utbm.fr

A. Miraoui  
e-mail: abdellatif.miraoui@utbm.fr

M. S. Rylko  
Research Laboratory, dtw sp. zo.o, Zabierzow, Poland  
e-mail: rylkoms@gmail.com



## 6.1 Introduction

The fuel cell is seen as a candidate for energy conversion in the future energy world. It converts directly the chemical energy into electrical energy without going through intermediate stages of conversion. Compared with the conventional electricity generation devices, the production of electricity from fuel cell systems has some major advantages, such as lesser CO<sub>2</sub> emission and higher efficiency.

However, the fuel cell is an open system. To ensure its proper operation, it requires auxiliaries, such as air compressor, cooling/heat exchanger, power electronic converter, etc. All those auxiliaries are strongly coupled and interdependent. To maintain its normal operation, an appropriate control strategy must be applied to the entire system. Among those auxiliaries, power electronic converter plays a key role in the overall efficiency of fuel cell systems: it is the final electric conversion stage in the fuel cell systems before the system power output.

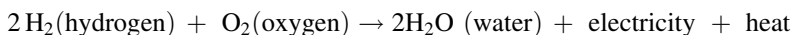
## 6.2 Fuel Cell Basics

This section introduces the principles of fuel cells. Different types of fuel cells and their area of applications will be presented in the following sections.

The output voltage of a fuel cell electrical varies significantly in respect to the output current load. Therefore, it is always required to have power electronic circuits for maintaining a constant DC or even AC voltage output for interaction with other systems. In order to understand how power converters must operate with fuel cells, it is important to know how their static and dynamic fuel cell characteristics perform under broad requirements and constraints.

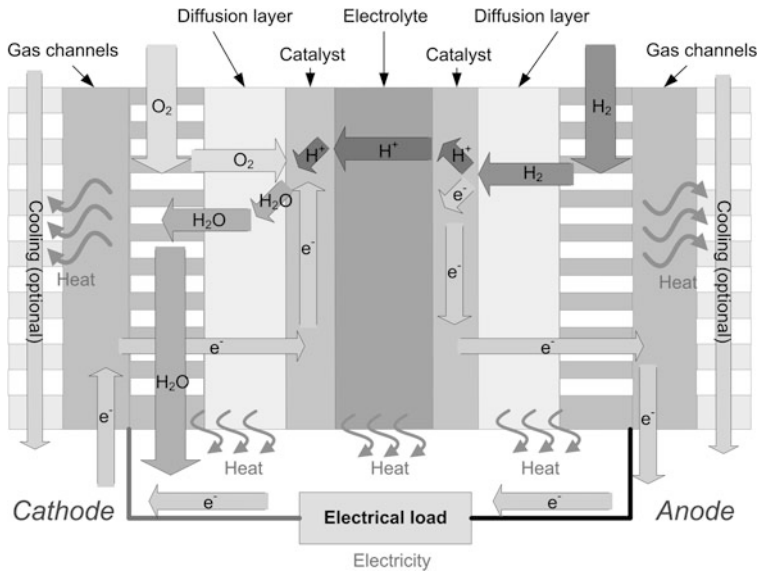
### 6.2.1 Fuel Cell Principles

The fuel cell is an energy conversion device that directly converts chemical energy stored in the fuel into electricity. A simple electrochemical equation that shows how hydrogen (supplied as a fuel) reacts is:



The hydrogen can be either produced from water electrolysis process, or from reformed fossil fuel. High temperature fuel cell may also directly use fossil fuel as fuel supply and the gas reform occurs inside those fuel cells as part of the conversion process.

Although there are several types of fuel cells, the operating principles are very similar. Figure 6.1 shows how a proton exchange membrane fuel cell (PEMFC) works. The following processes apply:



**Fig. 6.1** Diagram of operation of a proton exchange membrane fuel cell (PEMFC)

1. Hydrogen is supplied at the anode side and oxygen (ambient air) is supplied at the cathode side;
2. The two reactant gas (hydrogen and oxygen) flows in the supply channel of each side, and diffuses (through gas diffusion layers), to the catalytic layers;
3. At the anode catalytic layer, the hydrogen molecules (H<sub>2</sub>) are disassociated into protons (H<sup>+</sup>) and electrons (e<sup>-</sup>) by losing the electron that each molecule has;
4. The electron cannot pass through the fuel cell electrolyte, because the electrolyte material is nonpermeable to electrons. Thus, it takes the path of the external circuit from anode side to cathode side through the output load.
5. At the same time, the proton migrates through the fuel cell electrolyte, from anode to cathode;
6. At the cathode catalytic layer, the electrons from external circuit combine with the protons migrating through the electrolyte plus the oxygen molecule (O<sub>2</sub>): water molecules (H<sub>2</sub>O) are formed;
7. The water can be removed by the gas supply channels. Besides electricity, heat is also generated during this process (electrochemical reactions and joule effect). In order to facilitate the heat exchange, additional cooling channels can be added to fuel cell.

In other fuel cells, the major difference is the electrolyte used. Instead of proton (H<sup>+</sup>) migration in PEMFC, other fuel cells allow oxygen ions (O<sup>2-</sup>), hydroxide ions (OH<sup>-</sup>), or carbonate ions (CO<sub>3</sub><sup>2-</sup>) to migrate through their electrolytes (see Sect. 6.2.2). According to the electrolyte types of different fuel cells, water, the final electrochemical product, can be formed either at cathode side or anode side.

In a fuel cell, the following different functional layers can generally be presented:

#### 1. Gas supply channels:

The gas supply channels continuously provide fuel and oxidant to the reaction zone in the fuel cell, ensuring the continuity of the electrochemical reaction. The design and the geometrical channel shapes can be very distinct in different fuel cells, but with a common goal: to ensure a uniform distribution of the reactant gas in the gas diffusion layers. These channels also allow evacuating excess water produced by the electrochemical reaction.

#### 2. Gas diffusion layers (GDL):

The gas diffusion layer in the electrode is constructed from a porous material, which ensures many different functions: diffusion of reactants to the catalysts, evacuating the produced water and collecting the electrical current. The gas in the channel reaches the catalytic reaction sites through this porous layer. At the same time, water produced during the electrochemical reaction is partially drained to supply channels in the counter direction. This layer could either be an electronic conductor or with current collectors inside, in order to collect electrical current (e.g., electrons).

#### 3. Catalytic layers:

The gas passing through the diffusion layer arrives at the catalytic reaction sites, where the electrochemical reaction occurs (cathode and anode). The gas molecules are separated in this layer into ions and electrons. According to the technology of the fuel cell, the ion type could be different (see [Sect. 6.2.2](#)). Catalysts are used in this layer in order to accelerate the electrochemical reaction rates. This catalytic layer is associated with the porous electrode. The porous structure of the catalytic sites ensures good contact between the electronic conductor (current collector), the ionic conductor (electrolyte), reaction gas, and catalyst particles in an area 3D. This area is usually called “triple contact zone”.

#### 4. Electrolyte:

The electrolyte in fuel cells separates the anode and cathode and it is nonpermeable to electrons. The ions produced in electrochemical reactions migrate through the electrolyte from one side to another. This electrolyte layer could be in a solid state (like polymer membrane in PEMFC) or in a liquid state for different types of fuel cells. In order to achieve a good fuel cell performance, the electrolyte should be a very good ion conductor, and the electrolyte material should be chemically and mechanically stable under the fuel cell operation conditions.

5. Cooling channels:

Independent cooling channels are often used in medium and high power fuel cells. To ensure a stable temperature of fuel cell during operation, the heat generated by the reaction must be removed efficiently and continuously. This heat removal process can be achieved by a cooling circuit where the cooling channels are completely independent of the cathode and anode supply channels. Depending on the fuel cell power, air cooling or water cooling methods can be used.

Like a battery, the electrical voltage of a single fuel cell is relatively low. During fuel cell operation, this voltage is generally between 0.4 and 1.0 V. To deliver sufficient electrical power, the fuel cell is often composed of a dozen or a hundred individual cells connected electrically in series, forming a fuel cell stack. A fuel cell system generally consists of a fuel cell stack and a large number of auxiliaries, providing the fuel supply (hydrogen or fossil fuel), air (or pure oxygen) supply, gas humidification and compression, cooling, electrical power conditioning (power converter), and system control. A general fuel cell system diagram is shown in Fig. 6.2.

From this figure, different subsystems can be distinguished:

1. Fuel supply subsystem

Most of fuel cells use hydrogen as fuel. The hydrogen can be supplied either from hydrogen tank or external fuel reformer, depends on different application uses.

The use of a reformer increases the complexity of the fuel cell system, because the heat disposal or heat recovery from the reforming process and the produced gas evacuation must be managed. At the reformer outlet, hydrogen is not the only product. Other gases, such as carbon dioxide (CO<sub>2</sub>), carbon monoxide (CO), and

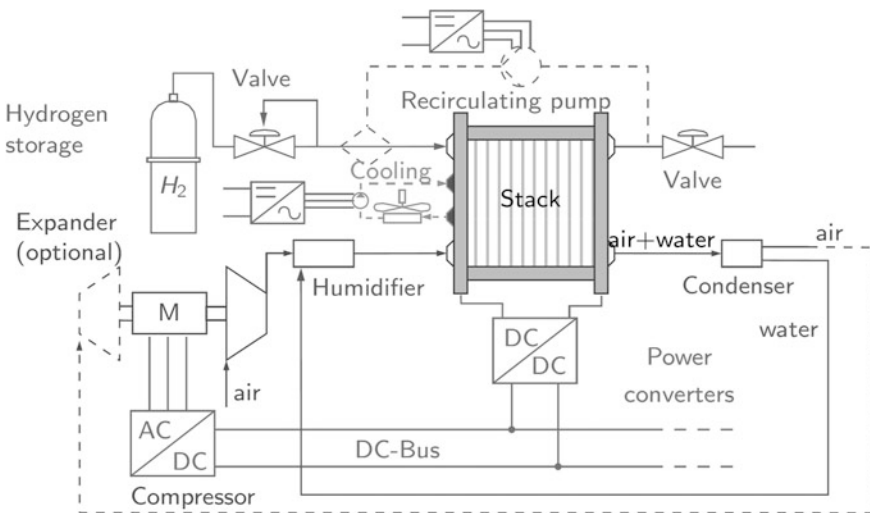


Fig. 6.2 Fuel cell system general schema

sulfur (S), could be generated at the same time in the reformer. For some types of fuel cell, CO and S are poisons gases. Thus, a gas purification process must be added between the reformer and fuel cell. The hydrogen in the tank can either be stored under high pressure, can be kept under liquid form, or stored as a metal hydride. Before enter into the fuel cell, the hydrogen pressure should be controlled by a pressure regulator.

## 2. Air (oxygen) supply subsystem

The air supplied to the fuel cell cathode is usually compressed via an air compressor. In some applications (PEMFC for example), the air is also be humidified before it enters the fuel cell. Depending on different type of fuel cell (pressure, temperature), the inlet air can be compressed by a motor-compressor or by a turbine-compressor (use of the fuel cell outlet gas). A heat exchanger could also be added in the air supply circuit, in order to preheat the inlet air. In some applications, the fuel cell can also be supplied with pure oxygen stored in compressed form. The use of pure oxygen allows to significantly increase the fuel cell performance and to get rid of the air compressor, which is an energy consumer device.

## 3. Cooling subsystem

The electrochemical reaction in fuel cell generates heat which must be removed in order to maintain a safe operating temperature of fuel cell stack. For small power fuel cells, surface natural convection or a cooling fan (forced convection) is sufficient for heat removal. In the case of high power fuel cells, other more complex cooling system, such as water cooling, should be used. In high temperature fuel cell applications, the heat removed from fuel cells could be reused for cogeneration purpose, forming combined heat and power (CHP) system, and the total energy efficiency becomes very attractive for a very large system application.

## 4. Power converter subsystem

The fuel cell output voltage varies as a function of output electrical current. In order to maintain a stable voltage output, power converters are used between the fuel cell and the load, where the load could be actually another power converter, energy storage components or electrical motors, and the power converter could also maximize the efficiency of the fuel cell, and interact with the balance of the system control. There exist different power converter topologies for fuel cell applications. Those topologies are discussed in [Sect. 6.4](#) “Power Electronic Topologies for Fuel Cells”.

## 5. Control subsystem

A fuel cell system has a large number of interconnected auxiliaries. Therefore, in order to ensure the proper operation of the system (performance, safety, monitoring and so on), it is necessary to have a control system capable to manage

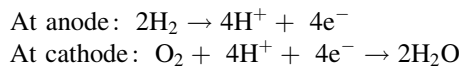
different subsystems. A well-designed control subsystem allows the fuel cell to operate in their optimal operating conditions.

## 6.2.2 Fuel Cell Commercial Technologies

The fuel cell commercial history dates back to 1950s when the first commercial PEMFC was developed by General Electric for a NASA space project [1]. Today, different fuel cell technologies are commercially available for different application uses, for a very large power range, from some watts (W) to more than Mega watts (1 MW =  $10^6$  W).

### 6.2.2.1 Proton Exchange Membrane Fuel Cell

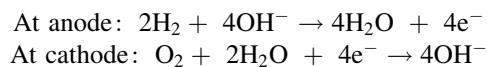
The PEMFC (or polymer electrolyte fuel cell) was invented in the 1950s. Currently, this type of fuel cell is used for transportation applications, such as electric vehicles or mobile systems, such as portable power supplies. In the PEM fuel cell, a very thin solid membrane is used as the electrolyte. One of the most widely used materials is Nafion (sulfonated tetrafluoroethylene-based fluoropolymer-copolymer). The electrodes are made of carbon paper or carbon cloth coated with fine particles of catalyst (usually platinum). The electrochemical half-reactions on the electrodes are:



The operation temperature of PEMFC is around 80 °C. Therefore, water in liquid form is presented in PEMFC during its operating and the system must dispose properly of such humidity.

### 6.2.2.2 Alkaline Fuel Cell

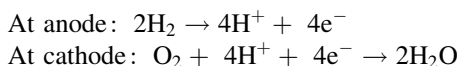
The alkaline fuel cell (AFC) is considered as the most developed fuel cell, because they have been widely used for space missions. They usually provide power source and the drinking water for space shuttles. The design of AFC resembles that of the PEMFC, but the electrolyte used in AFC is generally a porous matrix material saturated with an aqueous alkaline solution, such as the potassium hydroxide (KOH). The electrochemical half-reactions on the electrodes are:



The operating temperature of the AFC is very similar to that of PEMFC: about 80 °C. The required catalyst for electrodes can be chosen from many chemical products which are relatively inexpensive (compare to Platinum in PEMFC), but the current density is an order of magnitude smaller compared to the PEMFC.

### 6.2.2.3 Phosphoric Acid Fuel Cell

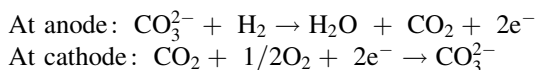
The phosphoric acid fuel cell (PAFC) is currently one of the most implemented fuel cell systems, generally used in stationary applications. As shown in its name, this type of fuel cell uses phosphoric acid as the electrolyte. One major advantage of this type of fuel cell is that the cell structure is simple and stable. The electrochemical half-reactions on the electrodes are:



The operating temperature of the phosphoric fuel cell is generally between 150 and 200 °C, the water is in vapor form, which makes easier to recycle the water in the environment. However, PAFC also need platinum as catalyst.

### 6.2.2.4 Molten Carbonate Fuel Cell

The molten carbonate fuel cell (MCFC) is working differently compare to those fuel cells described above. The electrolyte used consists of molten carbonate salts suspended in a porous and chemically inert ceramic matrix of beta-alumina solid electrolyte. Molten carbonate salts in electrolyte provide  $\text{CO}_3^{2-}$  ions migrating from cathode to anode, then form water with hydrogen particles. The electrochemical half-reactions on the electrodes are:

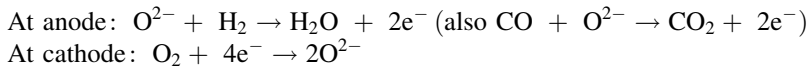


The operating temperature of MCFCs is above 650 °C. One advantage of this operating temperature is that nonprecious metals can be used as catalysts, contributing for reduced system costs.

### 6.2.2.5 Solid Oxide Fuel Cell

The solid oxide fuel cell (SOFC) is generally used in stationary applications with an output power from the order of several kilowatts (kW) to several megawatts (MW). This type of fuel cell uses dense ceramic materials as electrolyte, for example, yttrium-stabilized zirconia (YSZ), which separates the gas from anode and cathode, to block electrons and to conduct oxygen ion ( $\text{O}^{2-}$ ) from cathode to anode.

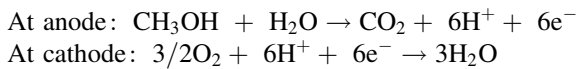
The electrochemical half-reactions on the electrodes are:



The operating temperature of SOFC is even higher than that of the MCFC. The typical value is around 700–1,000 °C. At this temperature, the CO in the reformed gas can be used directly as fuel. The high temperature nonconsumed fuel gas at the outlet of fuel cell can also be used to power a gas turbine, achieving increased overall system performance. In SOFC, Nickel (Ni) is generally used as an inexpensive catalyst.

### 6.2.2.6 Direct Methanol Fuel Cell

The direct methanol fuel cell (DMFC) is a derivation from the PEMFC. It uses directly methanol (CH<sub>3</sub>OH) as liquid fuel, where the CH<sub>3</sub>OH is first converted to CO<sub>2</sub> and hydrogen (H<sub>2</sub>) at the fuel cell anode, and the remaining reaction steps are identical to those of the PEMFC. The electrochemical half-reactions on the electrodes are:



The expected operating temperature for DMFC is about 120 °C. The disadvantages of DMFC are that, the conversion of CH<sub>3</sub>OH to H<sub>2</sub> requires a higher amount of platinum as catalyst than in PEMFC, and there are CO<sub>2</sub> (green house gas) emissions at the anode.

The different fuel cell technologies can be summarized in Table 6.1.

## 6.2.3 Power Characteristics

### 6.2.3.1 Static Characteristic (Polarization Curve)

The fuel cell static characteristic is presented by its polarization curve. Figure 6.3 shows an experimental voltage versus current curve of a low temperature single PEMFC at 60 °C. Other fuel cells polarization curve has a similar shape.

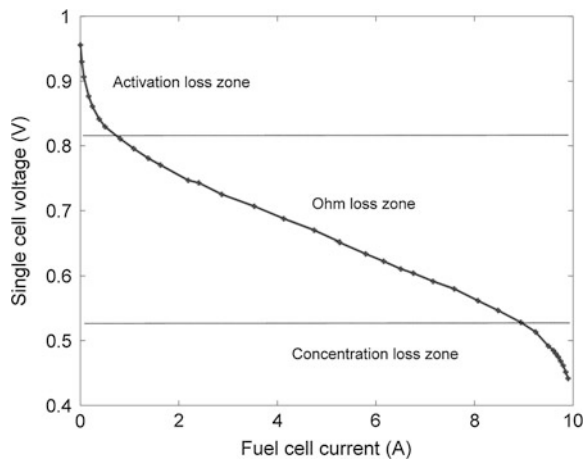
At zero current point, the voltage value represents the fuel cell open circuit voltage. In real fuel cells, this open circuit voltage is slightly lower than fuel cell theoretical thermodynamic voltage, especially in low temperature fuel cells. This difference is generally due to the internal losses in real fuel cells.

Depending on fuel cell type, its single cell thermodynamic voltage can vary from 0.8 to 1.5 V. This thermodynamic voltage depends also on the concentration



**Table 6.1** Different fuel cell technologies

Fuel cell type	Electrolyte	Operating temperature (°C)	Efficiency (stack only) (%)	Applications
Proton exchange membrane fuel cell (PEMFC)	Solid polymer membrane	Around 80	50–60	Transport Stationary Portable
Alkaline fuel cell (AFC)	Potassium hydroxide	Around 80	60–70	Transport (space)
Phosphoric acid fuel cell (PAFC)	Phosphoric acid	150–200	50–55	Stationary
Molten carbonate fuel cell (MCFC)	Molten carbonate salts	Around 650	50–55	Stationary
Solid oxide fuel cell (SOFC)	Dense ceramic	700–1,000	60–65	Transport Stationary
Direct methanol fuel cell (DMFC)	Solid polymer membrane	80–120	30–40	Transport Stationary Portable

**Fig. 6.3** An experimental proton exchange membrane fuel cell polarization curve

of the reactants at electrochemical reaction interface and fuel cell operating temperature (Nernst equation in electrochemical [2]).

During the fuel cell operating, three characteristic loss zones can be identified as indicated by the Fig. 6.3: activation loss zone, ohm loss zone, and concentration loss zone.

The fuel cell activation loss is due to the electrodes kinetics. During the electrochemical reactions, there is a voltage drop in order to provide continuous electrical current by giving necessary activation energy. This activation voltage loss depends logarithmically on fuel cell current value (Butler–Volmer equation [2]).

Thus, the activation loss is more significant compare to other losses when the cell current is small (at the beginning of the polarization curve).

The activation losses can be found in both cathode and anode side in fuel cell. Generally for a low temperature fuel cell (like a PEMFC), the cathode activation loss is some order of magnitude higher than that of anode. That is because the oxygen reduction is a slow electrochemical process and involves intermediate products, even with the platinum as catalyst. In a high temperature fuel cell (like a SOFC), the difference between the activation loss of cathode and anode is less significant. The high temperature can improve significantly the electrode kinetics.

At the fuel cell medium operating current range (ohm loss zone), ohm loss is the major cause of the voltage losses. However, in some fuel cells the activation loss contributes also an important part of the voltage losses in this zone. The ohm loss in a fuel cell is generally caused by two phenomena: the ionic resistance in electrolyte and the electronic resistance in electrodes (current collectors). The electrolyte ionic resistance is generally the main reason of the fuel cell ohm loss. This ionic resistance depends on many factors, like fuel cell temperature, humidity (especially in polymer membrane). This ohm loss obeys the ohm law (e.g., voltage = current  $\times$  resistance). Thus, the fuel cell polarization curve in this zone is in a linear form.

When the fuel cell is operated under high electric current, the voltage concentration loss becomes more important. As discussed above, the cell thermodynamic voltage and the activation loss is depending nonlinearly on the reactants concentration at electrode interface. At high current (thus high reaction rate), the reactants are consumed more quickly at electrode-catalyst interface, lead to a depletion of reactants. In addition, when reactant gases are supplied to the fuel cell, they need to be diffused to the electrode reaction interfaces. However, the reactants diffusion rate is limited by the electrode porosity, diffusion coefficient, electrode thickness, etc. Thus, at a very high reaction rate, the reactants concentration at electrode can decrease rapidly, lead to a significant cell voltage loss in concentration loss zone of polarization curve.

Due to these losses (activation, ohm, concentration), the real fuel cell operating voltage could be as low as 0.4 V.

### 6.2.3.2 Dynamic Behavior

When the fuel cell load current varies, its voltage takes always a transient period to reach the new operating point value. This fuel cell voltage dynamic behavior is due to different physical phenomena in different physical domains. The first important phenomenon in fuel cell is a double layer capacitance at the electrode interfaces (both anode and cathode). During the electrochemical reactions, the electrical charges in electrode and the ions in electrolyte form together two very thin electrical charge layers (+ for one layer and – for the other layer) which are equivalent to an electrical capacitor at electrode interface. The voltage on this capacitor is equal to the fuel cell activation loss voltage.

This double layer phenomenon behaves as an energy storage component. If the fuel cell current varies, the electrical charges on this double-layer capacitance need some time to increase or decrease. Thus, the fuel cell voltage, which is contributed by activation voltage losses, will not vary rapidly after a current change. This capacitance dynamic can be expressed by Corrêa et al. [3]:

$$\frac{d}{dt}V_{\text{act}} = \frac{i}{C_{dl}} \left( 1 - \frac{1}{\eta_{\text{act}}} V_{\text{act}} \right) \quad (6.1)$$

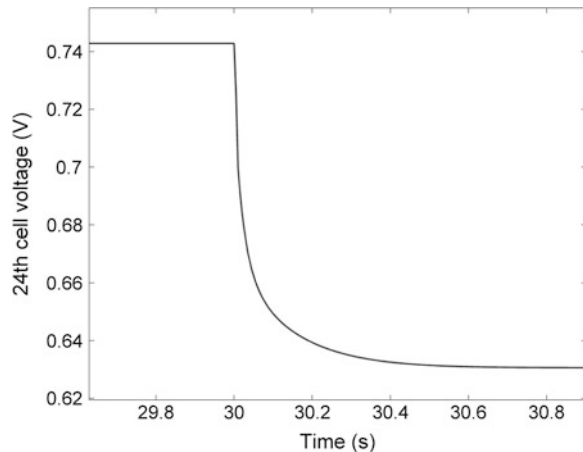
where  $V_{\text{act}}$  is the dynamic activation loss voltage (V),  $\eta_{\text{act}}$  the final steady-state activation loss voltage (V),  $C_{dl}$  the fuel cell double layer capacitance (F), and  $i$  the fuel cell current (A).

As the double layer capacitances are located at electrode reaction interface, the distance between two opposite charge layers is quite small: usually only a few nanometres ( $1 \text{ nm} = 10^{-9} \text{ m}$ ). For most of the fuel cells, its single cell double layer capacitance could reach to some Faraday (F).

The time constant of voltage dynamic (*remark: the first order dynamic transient time is about 4 times longer than its time constant*) due to this phenomenon depends on lots of factors, such as the double-layer capacitance value, the electrode exchange current value, etc. For example, Fig. 6.4 shows a PEMFC cell voltage dynamic due to this double layer capacitance effect, after a step current change at 30 s [4]. The voltage transient time due to its double layer capacitance effect is about 0.7 s.

It should be mentioned that, for different types of fuel cell, this transient time could be very different. As seen in Eq. 6.1, this voltage transient time is highly depending on the fuel cell steady-state activation loss value. In a high temperature fuel cell (for example a SOFC), the activation loss could be much smaller than that in a low temperature fuel cell (for example a PEMFC). Thus, for those fuel cells which have a good electrode kinetics, the transient time due to its double layer capacitance can take much less time.

**Fig. 6.4** PEMFC voltage response due to the double-layer capacitance effect



Another dynamic characteristic can be found in the fuel cell fluidic domain. During the fuel cell operating, the reactant gases are supplied to fuel cell by gas channels. The gas diffusion rate from gas channels to electrode is proportional to the fuel cell current demand. Under current changes, the gases mass balance (or the gas pressures) in supply channels volume will move to a new equilibrium point. Supposing the gases could be considered as perfect gas, the dynamic conservation equation for each gas component can be expressed by:

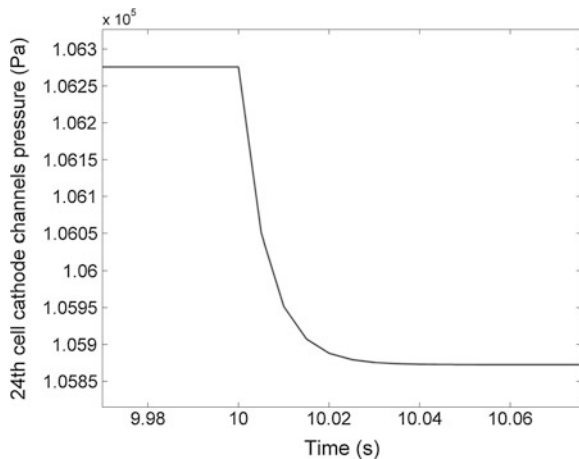
$$\frac{V_{\text{Ch}}}{R \times T} \left( \frac{d}{dt} P_{\text{gas}} \right) = \sum_{\text{in/out}}^{\text{Ch}} \dot{n}_{\text{gas}} \quad (6.2)$$

where  $V_{\text{ch}}$  is the supply channels volume ( $\text{m}^3$ ),  $P_{\text{gas}}$  the gas pressure (Pa),  $n_{\text{gas}}$  the corresponding gas molar flow rate entering or leaving the channels (mol/s),  $T$  the cell temperature (K), and  $R = 8.314$  the universal gas constant [J/(mol K)].

This gas pressure transient in supply channels leads to a gas concentration variation at electrode reaction interface, thus leads to a cell voltage transient. The time constant of this concentration variation is highly depending on supply channels geometry at anode and cathode. In a compact fuel cell stack, the cell channels volume is generally small. Thus, the gas pressure transient time in response to a diffusion rate change could be very fast. Figure 6.5 shows a cathode channel gas pressure dynamic of an air compressor supplied PEMFC cell, after a current step change at 10 s [4]. In this cell, the cathode pressure transient time is very short: about 40 ms to reach its steady-state pressure. However, in other fuel cells, this pressure transient time could be longer depending on their geometry.

In the most fuel cell applications, the fuel cell operating temperature is well regulated and remains quasi-constant during its operation. However, in some cases, the cell operating temperature is regulated in a wide range (as high as 50 °C difference) or isn't regulated at all, especially for those low power, low

**Fig. 6.5** PEMFC cathode gas pressure response due to the gas channels volume effect



temperature fuel cells. In this case, the cell temperature variation takes effect on the cell voltage which is dependant on cell temperature.

Under a current step, the heat produced by a fuel cell changes due to its internal resistance (ionic and electronic) under Joule effect and its electrochemical reaction loss (entropy, activation). The transient time for the fuel cell to reach its new temperature depends on its cooling method and its thermal capacity. The dynamic equation can be approximated by:

$$C_{p,\text{cell}} \frac{dT_{\text{cell}}}{dt} = hA(T_{\text{coolant}} - T_{\text{cell}}) + \sum \dot{Q}_{\text{internal}} \quad (6.3)$$

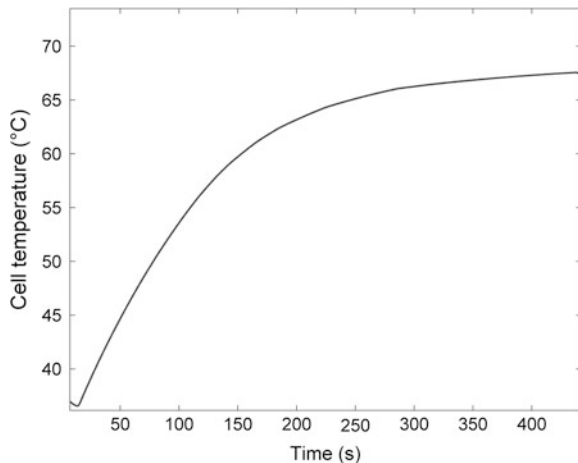
where  $C_{p,\text{cell}}$  is the fuel cell thermal capacity (J/K),  $T_{\text{cell}}$  the cell temperature (K),  $T_{\text{coolant}}$  the coolant (usually the ambient air in low power fuel cells) temperature (K),  $hA$  a heat transfer coefficient (W/K) and  $\dot{Q}_{\text{internal}}$  the internal heat sources in fuel cell (W).

Depending on fuel cell stack size and its cooling system (forced cooling or natural cooling), the time constants of fuel cell temperature dynamic could vary from seconds to minutes. That means, if a fuel cell stack is not regulated in a quasi-constant operating temperature, it may take minutes for the fuel cell output voltage to reach its steady-state value after a step current change.

In an experimentation of a commercial 1,200 W, 47 cells PEMFC stack (Ballard Nexa stack), the temperature transient time is measured: about 450 s following a step current change, as shown in Fig. 6.6 [4]. As a consequence of this stack temperature variation, the stack voltage difference between the beginning and the end of transient period could reach to some volts (for a total of 47 cells) while maintaining the same electrical current value.

The Table 6.2 summarizes the different dynamic phenomena mentioned above in fuel cells. The magnitude order of these dynamic transient times in a commercial PEMFC is also given for Ref. [4].

**Fig. 6.6** PEMFC temperature response due to cell thermal capacity effect



**Table 6.2** Dynamic phenomena in fuel cells

Phenomenon	Physical domain	Influence factors	Example: transient time for a Ballard Nexa 1.2 kW fuel cell stack after a step current change
Double-layer capacitance effect	Electrical (voltage)	Double-layer capacity Activation loss	Around 0.7 s
Supply channels gas volume effect	Fluidic (concentration or pressure)	Gas flow rate Channels geometry	Some milliseconds
Fuel cell thermal capacity effect	Thermal (temperature)	Fuel cell thermal capacity Cooling heat transfer coefficient	Some minutes

### 6.3 Fuel Cell Modeling for Integration with Power Electronics Controls

In this section, a fuel cell electrical equivalent circuit and related physical equations will be introduced. Both fuel cell static behavior (thermodynamic voltage, activation loss, ohm loss) and dynamic behavior (double-layer capacitance) will be mathematically considered and the overall fuel cell performance will be discussed.

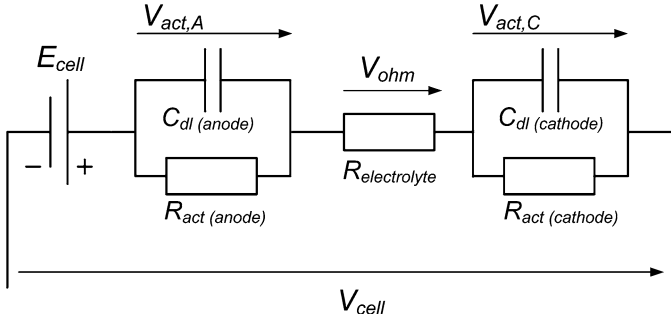
As presented in the Sect. 6.2.2, there exist different types of fuel cell technologies. In order to represent the most commercially used fuel cells, two different fuel cell models will be presented in the following section: a planar PEMFC model (low temperature, polymer electrolyte) and a tubular SOFC model (high temperature, ceramic electrolyte).

#### 6.3.1 Fuel Cells Electrical Equivalent Circuit

A typical fuel cell can be represented by an electrical equivalent circuit, as shown in Fig. 6.7.

The  $E_{\text{cell}}$  is the fuel cell thermodynamic voltage (electromotive force),  $V_{\text{act},A}$ ,  $V_{\text{act},C}$  are, respectively, the anode and cathode activation losses associated to their double-layer capacitance  $C_{dl}$ ,  $V_{\text{ohm}}$  is the ohm loss in fuel cell electrolyte, and eventually  $V_{\text{cell}}$  is the fuel cell output voltage.

It should be noted that, the concentration losses in electrode do not explicitly show in this equivalent circuit. As mentioned in previous section, the concentration losses are due to the mass transport limitation from gas supply channels to catalytic reaction interfaces through diffusion layers of fuel cell. If the *reactant concentrations at catalytic interfaces* are known a priori, there is no need to include



**Fig. 6.7** Typical fuel cell electrical equivalent circuit

“concentration losses” components in the circuit. However, usually only the concentrations in the gas supply channels are measurable, so if it is used directly such *reactant concentrations in gas channels* as the gas concentration values for modeling purpose, additional resistive “concentration losses” components must be added next to each “activation resistance” in the equivalent circuit (in the same branch), in order to “correct” the voltage deviations due the concentration differences between gas channels and catalytic interfaces. But will be seen in the modeling examples below, the *reactant concentrations (pressures) at catalytic interface* can be calculated from the *reactant concentrations (pressures) in gas channels* by diffusion law equations in electrodes. If it is used these *reactant concentrations (pressures) at catalytic interface* as the concentration values for model, the “concentration losses” are implicitly included in the components ( $E$  et  $R$ ) of the fuel cell equivalent circuit.

### 6.3.2 PEMFC Modeling

Low temperature PEMFC has very slow reduction kinetics at cathode side and because the cathode activation loss is an order of magnitude higher than the anode activation loss  $V_{act,A}$  [5]), the anode effects can be neglected in a PEM fuel cell model for the sake of simplification purposes. The single PEM fuel cell output voltage can be then expressed from the equivalent circuit:

$$V_{cell} = E_{cell} - V_{act,C} - V_{ohm} \quad (6.4)$$

The PEM cell thermodynamic voltage  $E_{cell}$  (V) can be modeled from the Nernst equation [6]:

$$E_{cell} = 1.229 - 0.85 \times 10^{-3}(T - 298.15) + \frac{R \times T}{2F} \ln(\sqrt{P_{O_2}} \times P_{H_2}) \quad (6.5)$$

where  $T$  is the temperature of the cell (K),  $P_{O_2}$  the oxygen pressure (atm) at *the cathode catalytic interface*,  $P_{H_2}$  the  $H_2$  pressure (atm) at *the anode catalytic interface*,  $R = 8.314$  the universal gas constant (J/mol K), and  $F = 96,485.3$  the Faraday constant (C/mol).

The dynamic cathode activation losses voltage  $V_{act,C}$  (V) due to the “double layer capacitance” can be expressed:

$$\frac{d}{dt} V_{act,C} = \frac{i}{C_{dl,C}} \left( 1 - \frac{1}{\eta_{act,C}} V_{act,C} \right) \quad (6.6)$$

where  $C_{dl,C}$  is the single fuel cell cathode double-layer capacitance (F),  $i$  is the fuel cell current (A), and  $\eta_{act,C}$  is the cathode steady-state activation loss (V), which is related to the cathode activation resistance  $R_{act,C}$  ( $\Omega$ ) in fuel cell equivalent circuit:

$$R_{act,C} = \frac{\eta_{act,C}}{i} \quad (6.7)$$

The cathode steady-state activation loss  $\eta_{act,C}$  value can be obtained from the well-known Tafel equation [5]:

$$\eta_{act,C} = \frac{R \times T}{2 \times \alpha \times F} \ln \left( \frac{i}{j_{0,C} \times A_{cata}} \right) \quad (6.8)$$

where  $A_{cata}$  is the fuel cell catalytic layer geometric surface area ( $m^2$ ),  $\alpha$  the electrochemical reaction symmetry factor (usually between 0.2 and 0.5), and  $j_{0,C}$  the cathode exchange current density ( $A/m^2$ ).

The PEM fuel cell cathode exchange current density can be calculated by an empirical equation:

$$j_{0,C} = \gamma_C \times (P_{O_2})^{\beta_C} \times e^{-\frac{E_C}{RT} \left( 1 - \frac{T}{298.15} \right)} \quad (6.9)$$

where  $\gamma_C$  and  $\beta_C$  are 2 empirical parameters need to be identified through fuel cell experimental tests,  $E_C$  is the oxygen activation energy at electrode platinum interface (J/mol), and  $P_{O_2}$  is the oxygen pressure (atm) at *the cathode catalytic interface*.

As discussed in previous section, in order to take into account the fuel cell concentration losses in electrodes, the reactant pressures ( $P_{O_2}$  and  $P_{H_2}$ ) used in Eqs. 6.5 and 6.9 must be the pressures at *electrode catalytic interfaces*. The differences between the gas supply pressures and the electrode interface pressures are due to the gas diffusion phenomenon through the porous electrodes in a PEM fuel cell, which can be modeled by Fick law:

$$P_{x,ch} - P_{x,cata} = \frac{N_{x,GDL} \times \delta_{GDL} \times R \times T}{D_{x-H_2O,eff} \times A_{GDL}} \quad (6.10)$$

where  $D_{x-H_2O,eff}$  is the gas effective diffusion coefficient to water vapor (product of electrochemical reaction) through the porous diffusion layer ( $m^2/s$ ),  $P_{x,ch}$  is the



reactant gas supply pressure in the channels (Pa),  $P_{x,\text{cata}}$  is the reactant gas pressure at *electrode catalytic interfaces* (Pa),  $N_{x,\text{GDL}}$  is the reactant molar flow rate through the diffusion layer (mol/s),  $\delta_{\text{GDL}}$  is the gas diffusion layer thickness (m), and  $A_{\text{GDL}}$  is the gas diffusion layer surface area (m<sup>2</sup>).

The reactant gas molar flow rates are directly related to the fuel cell current:

$$N_{\text{H}_2} = \frac{i}{2F} \text{ and } N_{\text{O}_2} = \frac{i}{4F} \quad (6.11)$$

The effective gas diffusion coefficients can be obtained using the Slattery-Bird formula and the Bruggemann correction [7, 8]:

$$D_{x-\text{H}_2\text{O},\text{eff}} = D_{x-\text{H}_2\text{O}} \times \varepsilon^\tau \quad (6.12)$$

where  $D_{x-\text{H}_2\text{O}}$  is the binary gas diffusion coefficient (m<sup>2</sup>/s) between the reactant (H<sub>2</sub>, O<sub>2</sub>) and product (H<sub>2</sub>O) given in the Refs. [7, 8],  $\varepsilon$  is the corresponding gas diffusion layer porosity and  $\tau$  is the corresponding gas diffusion layer tortuosity. It is important to remind that the concentration losses become significant only at high fuel cell operating current. If the concentration losses do not necessarily need to be included in a fuel cell model, we can use directly the gas supply pressures (in atm) in Eqs. 6.5 and 6.9 in order to simplify the model equations.

The PEM fuel cell ohm losses  $V_{\text{ohm}}$  is due to the electrolyte ionic resistance. The proton (H<sup>+</sup>) conductive Nafion membrane from DUPONT Company is commonly used as the electrolyte in PEM fuel cells. The ion (proton) conductivity  $\sigma_{\text{mem}}$  (S/m) of Nafion is highly related to the water content of the membrane. Its value can be calculated by Springer et al. [9]:

$$\sigma_{\text{mem}} = (0.5139 \times \lambda_{\text{mem}} - 0.326) e^{[1268 \times (\frac{1}{303} - \frac{1}{T})]} \quad (6.13)$$

where  $\lambda_{\text{mem}}$  is the membrane water content:  $\lambda_{\text{mem}} \approx 7$  for a dry membrane,  $\lambda_{\text{mem}} \approx 14$  for a well-humidified membrane, and  $\lambda_{\text{mem}} \approx 22$  for a flooded membrane.

Thus, the PEM fuel cell ohm loss can be calculated from the membrane conductivity:

$$V_{\text{ohm}} = R_{\text{electrolyte}} \times i = \frac{i \times \delta_{\text{mem}}}{\sigma_{\text{mem}} \times A_{\text{mem}}} \quad (6.14)$$

where  $R_{\text{electrolyte}}$  is the membrane resistance ( $\Omega$ ),  $\delta_{\text{mem}}$  is the membrane thickness (m), and  $A_{\text{mem}}$  is the membrane surface area (m<sup>2</sup>).

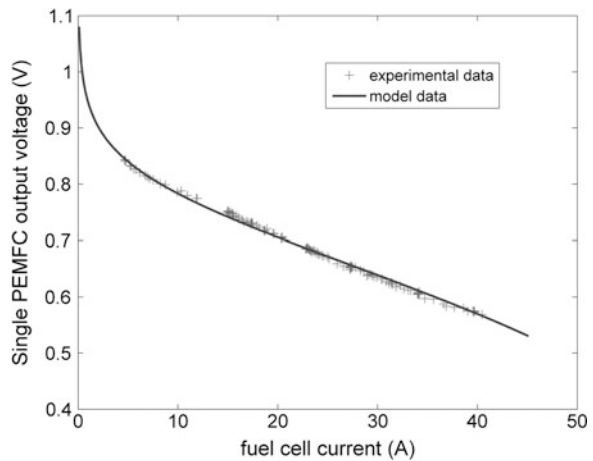
The PEM fuel cell model using the above equations is experimentally validated against to a H<sub>2</sub>-air supplied commercial fuel cell. The parameters used in the model are summarized below in Table 6.3.

The model simulation results are compared to the experimental polarization curve of the modeled fuel cell in Fig. 6.8.

**Table 6.3** PEM fuel cell model parameters

Parameter	Value	Units
$P_{O_2, ch}$	0.21	atm
$P_{H_2, ch}$	1.6	atm
$T$	60	°C
$C_{dl}$	2.2	F
$E_C$	66	kJ/mol
$\alpha$	0.25	–
$\gamma_C$	2.48	A/m <sup>2</sup>
$\beta_C$	2.42	–
$D_{O_2-H_2O}$	0.3246	cm <sup>2</sup> /s
$D_{H_2-H_2O}$	1.0323	cm <sup>2</sup> /s
$\epsilon$ (cathode and anode)	0.224	–
$\tau$ (cathode and anode)	2.62	–
$\lambda_{mem}$	10.97	–
$A_{cata}, A_{GDL}, A_{mem}$	147.58	cm <sup>2</sup>
$\delta_{GDL}$ (cathode and anode)	400	μm
$\delta_{mem}$	127	μm

**Fig. 6.8** Simulation-experimentation PEM fuel cell polarization curve



### 6.3.3 SOFC Modeling

While a PEMFC is a low temperature device, the SOFC operates at a much higher temperature (700–1,000 °C), and because at this temperature, the activation losses at cathode and anode have almost the same magnitude, they must be both considered for modeling purposes. Thus, the single tubular SOFC output voltage can be calculated from:

$$V_{cell} = E_{cell} - V_{act,C} - V_{act,A} - V_{ohm} \tag{6.15}$$

At such high temperature, the water produced from the electrochemical reaction is in vapor form. The cell thermodynamic voltage is defined by the Nernst equation as a function of the Gibbs free energy change during the electrochemical reaction [6]:

$$E_{\text{cell}} = -\frac{\Delta G^0}{2F} + \frac{R \times T}{2F} \ln \left( \frac{P_{\text{H}_2} \times \sqrt{P_{\text{O}_2}}}{P_{\text{H}_2\text{O}}} \right). \quad (6.16)$$

where  $\Delta G^0$  is the Gibbs free energy change from reactants to products (J/mol),  $F = 96,485.3$  is the Faraday constant (C/mol),  $R = 8.314$  is the gas constant [J/(mol K)],  $T$  is the reaction temperature (K), and  $P_{\text{H}_2}$ ,  $P_{\text{O}_2}$ ,  $P_{\text{H}_2\text{O}}$  are the gas pressures (atm) of  $\text{H}_2$ , oxygen, and vapor at *the electrode catalytic interfaces*, respectively.

The Gibbs free energy change is calculated from the Gibbs free energies of species involved in electrochemical reaction:

$$\Delta G^0 = G_{\text{H}_2\text{O}}^0 - \left( G_{\text{H}_2}^0 + \frac{1}{2} G_{\text{O}_2}^0 \right) \quad (6.17)$$

where  $G_{\text{H}_2\text{O}}^0$ ,  $G_{\text{H}_2}^0$ ,  $G_{\text{O}_2}^0$  are, respectively, the Gibbs free energies (J/mol) of vapor,  $\text{H}_2$ , oxygen, which can be calculated by:

$$G_{\text{specie}}^0 = H_{\text{specie}}^0 - T \times S_{\text{specie}}^0 \quad (6.18)$$

where  $H_{\text{specie}}^0$  is the corresponding enthalpy (J/mol) of each specie and  $S_{\text{specie}}^0$  is the corresponding entropy [J/(mol K)] at a given temperature.

Some values of enthalpy  $H^0$  and entropy  $S^0$  for  $\text{H}_2$ ,  $\text{O}_2$ , and  $\text{H}_2\text{O}$  in a SOFC operating temperature range of 750–850 °C (1,023.15–1,123.15 K) are given in the Table 6.4.

The steady-state activation losses in the SOFC can be modeled by the Butler-Volmer equation in electrochemical field:

$$i = A_{\text{cata}} \times j_0 \left( e^{\frac{\alpha \times n_e \times F}{R \times T} \eta_{\text{act}}} - e^{-\frac{(1-\alpha) \times n_e \times F}{R \times T} \eta_{\text{act}}} \right) \quad (6.19)$$

where  $i$  is the cell electrical current (A),  $A_{\text{cata}}$  is the electrode catalytic surface area ( $\text{m}^2$ ),  $j_0$  is the corresponding exchange current density ( $\text{A}/\text{m}^2$ ) at the cathode or the anode side,  $\eta_{\text{act}}$  is the corresponding activation losses (V) at the cathode or the anode,  $\alpha$  is the symmetry factor, and  $n_e = 4$  or 2 is the number of electrons involved in the half-reactions of the cathode or the anode, respectively.

Because the activation losses in both cathode and anode should be considered in the model, their current density can be approached by the following empirical equations [10]:

$$j_{0,C} = \gamma_C \times P_{\text{O}_2}^{0.25} \times e^{\left(-\frac{E_C}{RT}\right)} \quad (6.20)$$

$$j_{0,A} = \gamma_A \times P_{\text{H}_2} \times P_{\text{H}_2\text{O}} \times e^{\left(-\frac{E_A}{RT}\right)} \quad (6.21)$$

**Table 6.4** Gas enthalpy and entropy values

	H <sub>2</sub> O	H <sub>2</sub>	O <sub>2</sub>
<b>T = 750 °C</b>			
$H^0$ (kJ/mol)	-214.9	21.4	23.5
$S^0$ (J/(mol · K))	233.5	166.8	244.4
<b>T = 800 °C</b>			
$H^0$ (kJ/mol)	-212.8	22.9	25.3
$S^0$ (J/(mol · K))	235.5	168.3	246.0
<b>T = 850 °C</b>			
$H^0$ (kJ/mol)	-210.7	24.5	27.0
$S^0$ (J/(mol · K))	237.4	169.7	247.6

where  $P_{(\text{specie})}$  is the pressure (atm) of the corresponding specie at *the electrode catalytic interfaces*,  $E_C$  and  $E_A$  are the activation energies (kJ/mol) at the cathode and the anode, respectively.

In Eqs. (6.20) and (6.21),  $\gamma_C$ ,  $\gamma_A$  are, respectively, two empirical parameters for the cathode and the anode that should be adjusted from experimental tests.

The corresponding activation resistances  $R_{\text{act},A}$  and  $R_{\text{act},C}$  in equivalent circuit model can be then calculated by:

$$R_{\text{act}} = \frac{\eta_{\text{act}}}{i} \quad (6.22)$$

The activation losses of a SOFC can be modeled with the Tafel equation (6.8). In fact, this equation can be deduced directly from the Butler–Volmer equation when electrical current is relatively high. The disadvantage of the Butler–Volmer equation is that the activation loss is in an implicit form (exponential at right side), and it must be solved by iteration. But the use of Butler–Volmer equation can give more accurate results, especially at low electrical current.

The SOFC cathode and anode dynamic activation losses can be calculated in the same way from the Eq. (6.6). However, while a PEMFC can be used for fast variable load, a SOFC is usually used in stationary applications where stable power output (base power) is maintained. Therefore, the implementation of the double layer dynamic phenomena due to a current change in a SOFC is rare in the literature models. Thus, if the modeled SOFC has a stable output power (which is most often the case), the double layer capacitances in the equivalent circuit (Fig. 6.7) could be removed in order to simplify the SOFC model.

As discussed in previous section, if we want to take into account the concentration losses in the SOFC model, the reactant gas pressure at *the electrode catalytic interfaces* should be used for cell thermodynamic voltage and activation losses computations. The pressure drop due to the diffusion phenomena of species through the porous diffusion layer can be modeled in a same way by the Eqs. (6.10–6.12).

The electrolyte used in a SOFC is an oxygen ion ( $O^{2-}$ ) conductive ceramic material. One commonly used ceramic is the Ytria-stabilized zirconia (YSZ). Its ion conductivity  $\sigma_{YSZ}$  (S/m) can be calculated from (Colclasure et al. [11]):

$$\sigma_{YSZ} = \frac{\sigma_0}{T} e^{\left(-\frac{E_{YSZ}}{RT}\right)} \quad (6.23)$$

where  $\sigma_0 = 3.6 \times 10^7$  (S  $\times$  K/m) is the reference YSZ ion conductivity and  $E_{YSZ} = 80$  (kJ/mol) is the YSZ electrolyte activation energy.

Thus, the SOFC electrolyte resistance and ohm loss can be obtained by:

$$V_{ohm} = R_{electrolyte} \times i = \frac{i \times \delta_{electrolyte}}{A_{electrolyte} \times \sigma_{YSZ}} \quad (6.24)$$

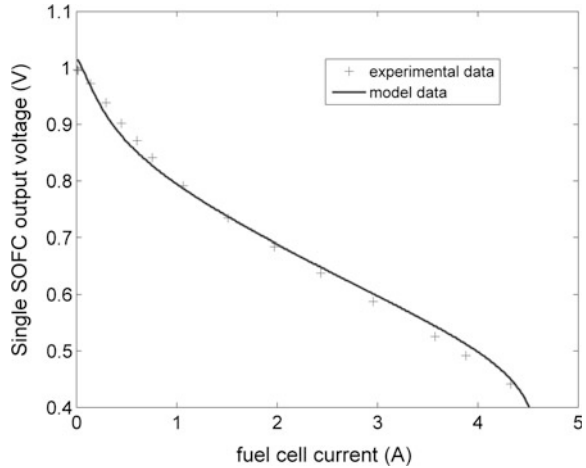
where  $\delta_{electrolyte}$  is the YSZ electrolyte thickness (m) and  $A_{electrolyte}$  is the YSZ electrolyte surface area ( $m^2$ ).

The presented SOFC model (double layer capacitances neglected) has been experimentally validated to a single air- $H_2$  supplied tubular SOFC. The  $H_2$  is supplied into the tube channel of the tubular cell, and the air is supplied to the outer surface of the cell (tubular SOFC of anode inside and cathode outside). The parameters used in the model are summarized below in Table 6.5.

**Table 6.5** A solid oxide fuel cell model parameters

Parameter	Value	Units
$P_{O_2, cathode}$	0.173	atm
$P_{H_2, tube}$	0.295	atm
$P_{H_2, tube}$	0.164	atm
$T$	850	$^{\circ}C$
$E_C$	120	kJ/mol
$E_A$	100	kJ/mol
$\gamma_C$	$7.0 \times 10^7$	$A/m^2$
$\gamma_A$	$20.0 \times 10^8$	$A/m^2$
$\alpha$	0.33	–
$D_{O_2-H_2O}$	6.6703	$cm^2/s$
$D_{H_2-H_2O}$	33.941	$cm^2/s$
$\varepsilon$ (cathode)	0.17	–
$\tau$ (cathode)	4.06	–
$\varepsilon$ (anode)	0.33	–
$\tau$ (anode)	2.39	–
$A_{cata} A_{GDL}$ (cathode)	764.98	$mm^2$
$A_{cata} A_{GDL}$ (anode)	761.84	$mm^2$
$A_{electrolyte}$	763.41	$mm^2$
$\delta_{GDL}$ (cathode)	30	$\mu m$
$\delta_{GDL}$ (anode)	1 000	$\mu m$
$\delta_{electrolyte}$	20	$\mu m$

**Fig. 6.9** Simulation-experimentation solid oxide fuel cell polarization curve

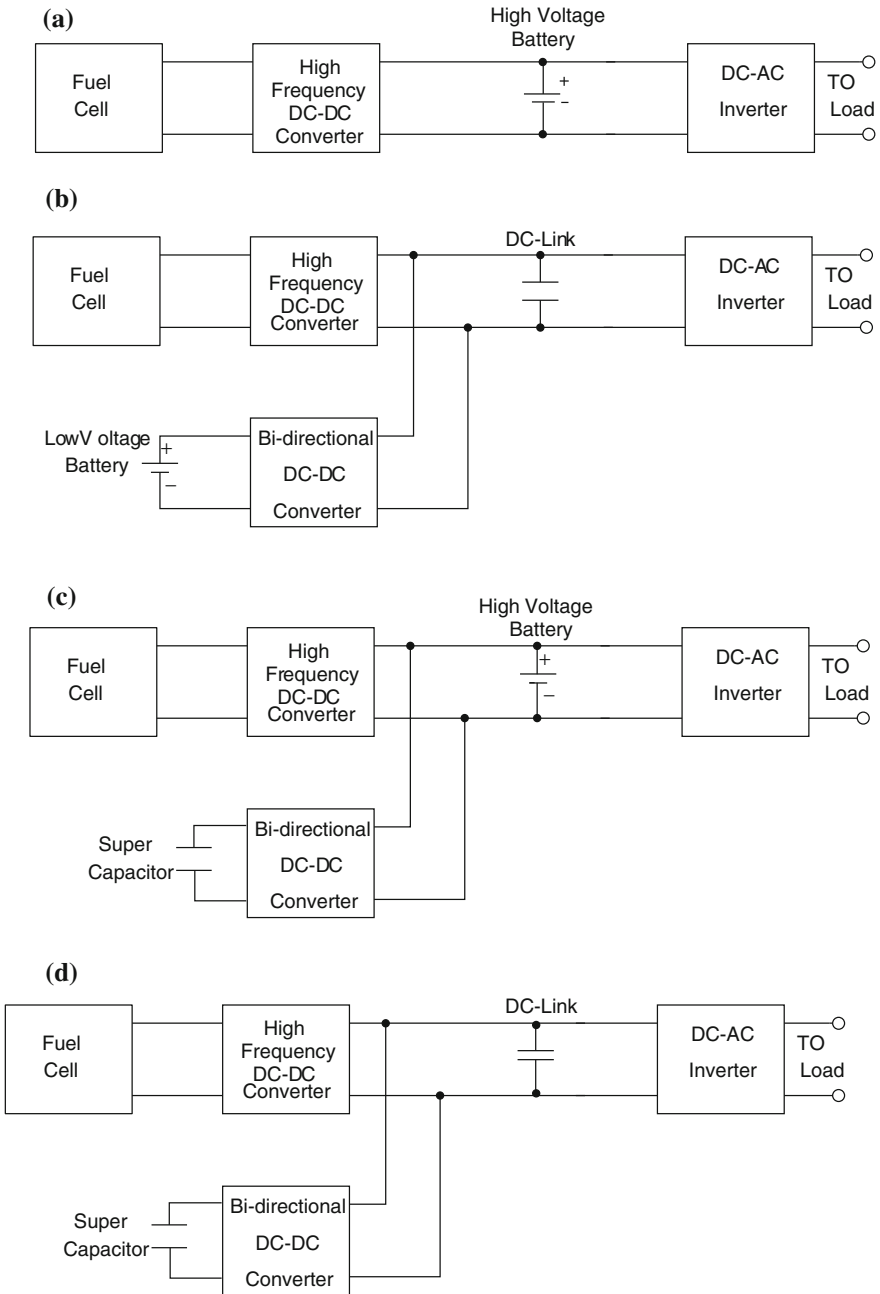


The model simulation results are compared to the experimental polarization curve of the modeled fuel cell in Fig. 6.9. From the current is about 4.5 A, the concentration loss zone can be seen in polarization curve.

## 6.4 Power Electronic Converter for Fuel Cell

A fuel cell (FC) is usually a low voltage device with hybrid voltage/current source characteristics. A single cell produces voltage approximately 1 V or less. Therefore, several cells must be stacked in order to achieve high voltage output. The FC's stacking has a reduced reliability and lifetime and dependent on the weakest cell, since it is a series string. In order to maintain reliability and lifetime within reasonable range, the FC stack output voltage is limited to approximately 100 V. When used for transportation applications such as electric vehicles, the powertrain dc-bus is usually a high voltage of a few hundred volts. Therefore, a DC–DC converter is required to interface a FC stack with the powertrain dc-bus voltage. Such a DC–DC converter is required not only for the voltages boost, but also for the voltage conditioning as the FC output voltage varies strongly with the load. Additionally, due to the slow dynamic response of the FC, a battery or a supercapacitor is required to handle any high power transients during acceleration or deceleration, and to store braking energy as FCs do not absorb power back. A bi-directional DC–DC converter is necessary to manage this kind of peak power sources (PPS). Although there are many variations of DC–DC converters, bi-directional DC–DC converters, and DC–AC inverters, they can be generally grouped into three main categories shown in Fig. 6.10 [12–14].

For the configuration of Type 1 a high voltage battery is connected directly to the high voltage dc-bus. The battery is used to provide the low and high frequency peak power demand. The FC is designed to work in its optimal zoon by controlling



**Fig. 6.10** Basic configurations of power conversion system (PCS) for FC. **a** Type 1. **b** Type 2. **c** Type 3. **d** Type 4

its current by means of high frequency DC–DC converter. The battery output voltage varies upon the state of charge; thus, Type 1 allows for some variability of the high voltage dc-bus. Similar to the FC, the battery pack is comprised of series chain of the battery cells; thus, the reliability decreases with the output voltage as more cells are connected. In order to increase the total reliability, in Type 2, the battery is no longer connected directly to the high voltage dc-bus, it is connected through a bi-directional DC–DC converter. In both Type 1 and Type 2, it is assumed that the battery provides the low and high frequency peak power demand. For Type 3, a super capacitor is used to provide the high frequency peak power demand. This configuration permits to decrease the charge–discharge cycles of the battery and consequently increase its lifetime. For Type 4, the low and high voltage battery is avoided to increase the system compactness. In this configuration the high voltage dc-bus is controlled through the bi-directional DC–DC converter. This chapter presents various topologies of unidirectional, bidirectional DC–DC converters suitable for FC interface for FCVs. Isolated and nonisolated soft and hard-switched topologies are compared and contrasted and general overview is given. Finally, the chapter provides some indications to the designer in order to improve the most optimum topology selection in terms of compactness, efficiency, and cost.

### ***6.4.1 DC–DC Power Converter***

A DC–DC converter is a common sub-system of several residential and commercial applications such as personal computers, power supplies, office equipments, telecommunication, appliances, and DC motor drives. The DC–DC power converter plays an important role in FC-based power systems. The FC converters input DC voltage is unregulated as FC voltage characteristic is load depended, while the output is a regulated DC voltage of usually higher voltage and possibly different polarity. The main characteristics required by these converters are Song [16]:

- 1 High efficiency.
- 2 High power density.
- 3 Small size and light weight.
- 4 Low electromagnetic interference (EMI).
- 5 Reduced ripple current to avoid the FC damage and increase its lifetime.
- 6 Low cost.
- 7 If possible, soft-switching for the high efficiency and low EMI.

There are many DC–DC converter topologies that are suitable for FC-powered vehicles comprising of isolated and nonisolated topologies [17–19].



### 6.4.2 Nonisolated DC–DC Converter

A common topology is a classic step-up boost converter shown in Fig. 6.11. The boost ratio indicated in Fig. 6.11b is valid for steady state in continuous conduction mode (CCM).

The principles of inductor volt-second and capacitor charge balance state that the average values of the periodic inductor voltage and capacitor current waveforms are zero, when the converter operates in steady state.

$$\begin{aligned}\langle v_L \rangle_T &= 0 \\ \langle i_C \rangle_T &= 0\end{aligned}\quad (6.25)$$

The boost converter conversion ratio, inductor current ripple, and output voltage ripple could be obtained using the previous principles:

$$M(D) = \frac{1}{1-D} \quad (6.26)$$

$$\Delta i_L = \frac{D(1-D)V_o}{Lf} \quad (6.27)$$

$$\Delta v_o = \frac{DV_{in}}{(1-D)RCf} \quad (6.28)$$

where  $D$  is the duty cycle,  $f$  is the switching frequency and  $R$  is the load. The current and the voltage stress of the power electronic devices could be calculated as following:

$$\text{Diode}_{\text{currentstress}} = \text{Switch}_{\text{currentstress}} = \frac{I_o}{1-D} + \frac{D(1-D)V_o}{2Lf} \quad (6.29)$$

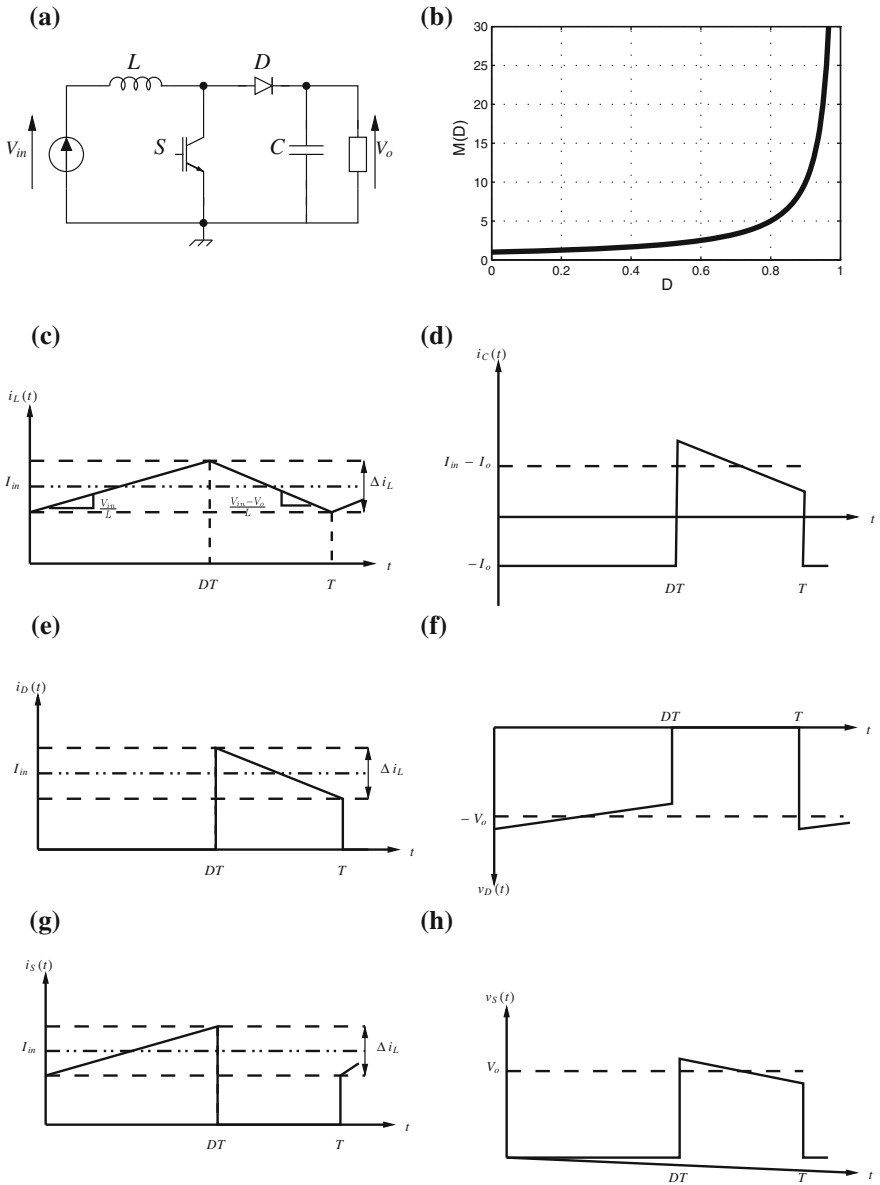
$$|\text{Diode}_{\text{voltagestress}}| = \text{Switch}_{\text{voltagestress}} = \frac{V_{in}}{1-D} + \frac{DV_{in}}{2(1-D)RCf} \quad (6.30)$$

A similar topology to the boost converter is a step-down buck converter and it is obtained by interchanging the switch with the diode. The power is converted from high voltage to the low voltage side, so the converter produces an output voltage lower than its input voltage and unlike to the boost converter, the source current is discontinuous. Figure 6.12 presents buck converter, its conversion ratio, and the steady-state waveforms in CCM.

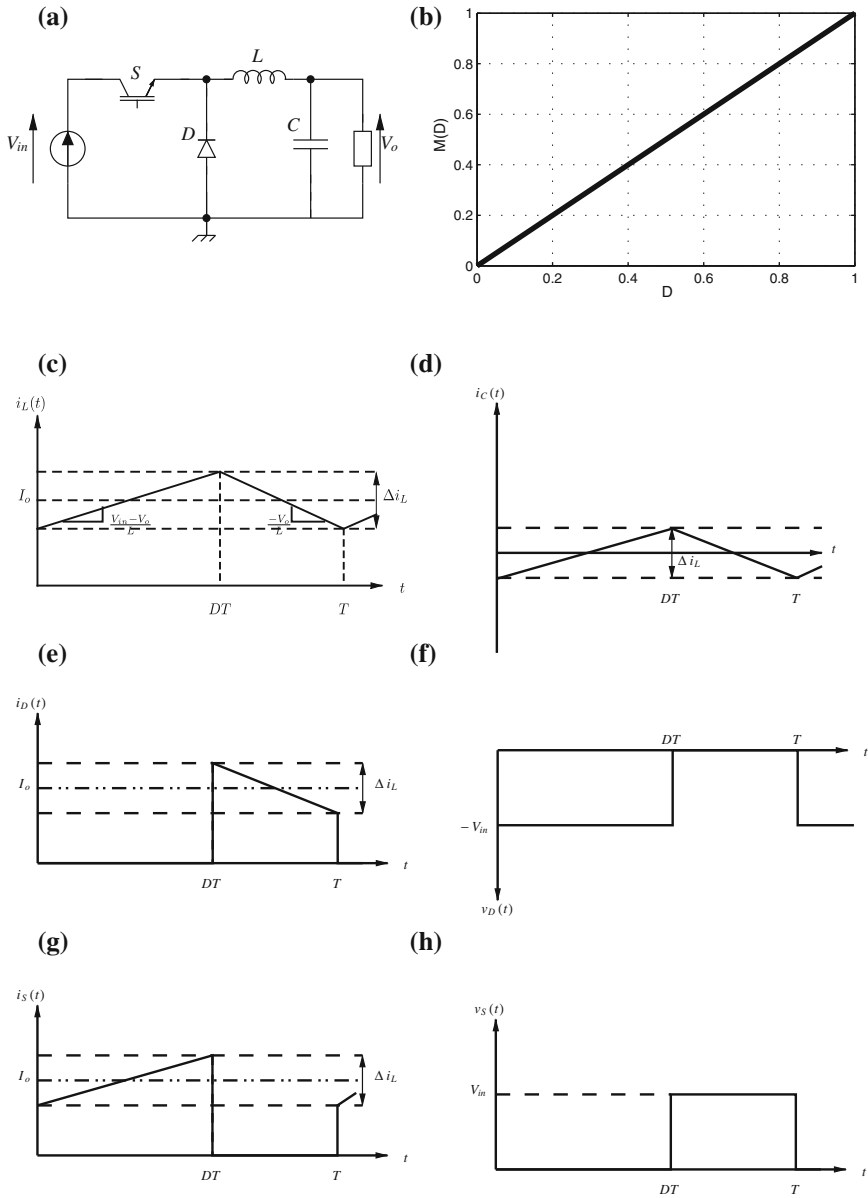
Similar to the boost converter, the buck conversion ration, inductor current ripple, and output voltage ripple could be determined by the following equations:

$$M(D) = D \quad (6.31)$$

$$\Delta i_L = \frac{(1-D)V_o}{Lf} \quad (6.32)$$



**Fig. 6.11** Boost steady-state waveforms in CCM. **a** Boost converter. **b** Boost ratio. **c** Inductor current. **d** Capacitor current. **e** Diode current. **f** Diode voltage. **g** Switch current. **h** Switch voltage



**Fig. 6.12** Buck steady-state waveforms in CCM. **a** Buck converter. **b** Buck ratio. **c** Inductor current. **d** Capacitor current. **e** Diode current. **f** Diode voltage. **g** Switch current. **h** Switch voltage

$$\Delta v_o = \frac{(1-D)V_o}{8LCf^2} \quad (6.33)$$

The voltage and current stress on the diode and the switch could be calculated as following:

$$\text{Diode}_{\text{currentstress}} = \text{Switch}_{\text{currentstress}} = \frac{I_{\text{in}}}{D} + \frac{(1-D)V_o}{2Lf} \quad (6.34)$$

$$|\text{Diode}_{\text{voltagestress}}| = \text{Switch}_{\text{voltagestress}} = V_{\text{in}} \quad (6.35)$$

The third converter is known as the buck-boost converter, similar to the buck converter the source current is also discontinuous. Figure 6.13 shows buck-boost converter, its conversion ratio, and the steady-state waveforms in CCM.

The output voltage can be regulated in a full voltage range from 0 to ideally infinite voltage and it is function of duty cycle  $D$  as follows:

$$M(D) = \frac{D}{1-D} \quad (6.36)$$

The inductor current ripple and the output voltage ripple are determined as following:

$$\Delta i_L = \frac{(1-D)V_o}{Lf} \quad (6.37)$$

$$\Delta v_o = \frac{D^2 V_{\text{in}}}{(1-D)RCf} \quad (6.38)$$

The current and the voltage stress on the diode and the switch for the buck-boost converter:

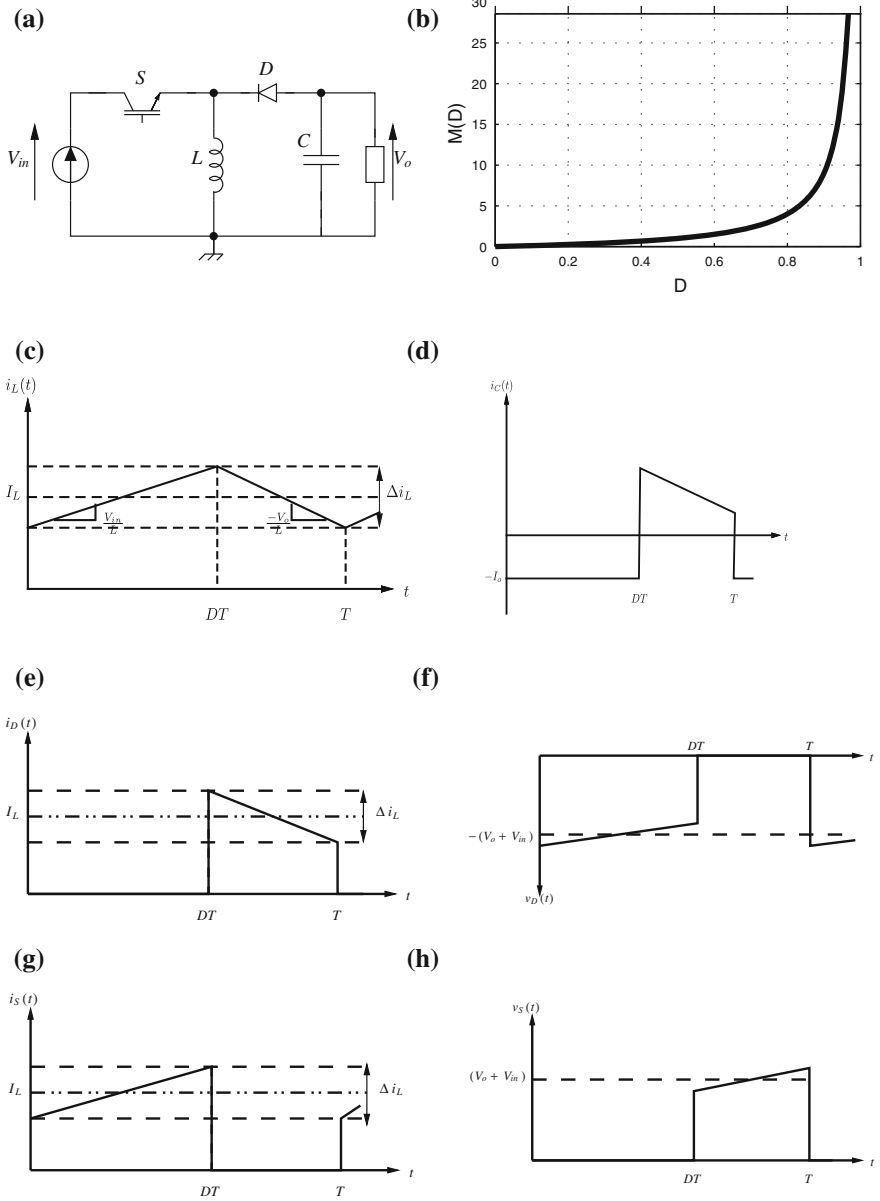
$$\text{Diode}_{\text{currentstress}} = \text{Switch}_{\text{currentstress}} = \frac{I_o}{1-D} + \frac{(1-D)V_o}{2Lf} \quad (6.39)$$

$$|\text{Diode}_{\text{voltagestress}}| = \text{Switch}_{\text{voltagestress}} = V_{\text{in}} + V_o + \frac{D^2 V_{\text{in}}}{2(1-D)RCf} \quad (6.40)$$

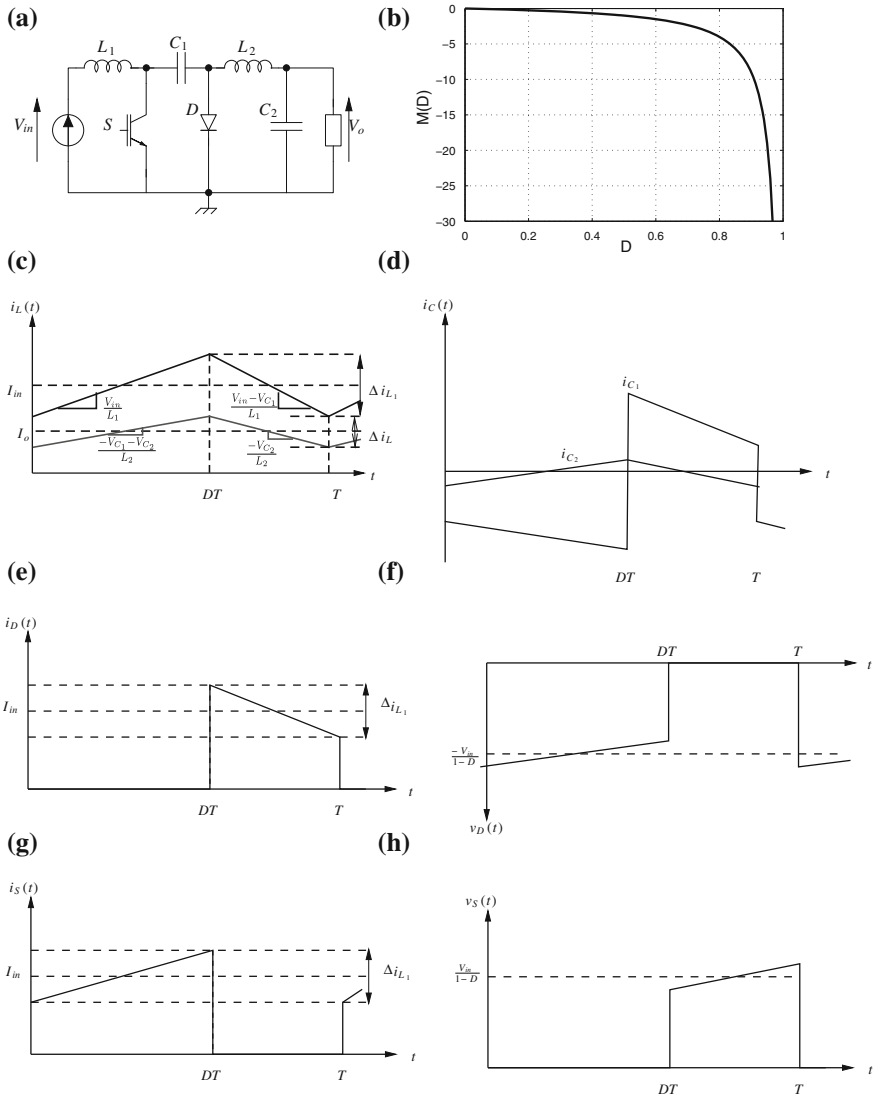
The Cuk converter, contains an inductor in series with the input and the output, thus it produces a smooth current at both sides of the converter. The Cuk converter conversion ratio is identical to that of buck-boost converter with inverted polarity. Figure 6.14 shows cuk converter, its conversion ratio, and the steady-state waveforms in CCM.

Cuk conversion ratio, input and output inductor current ripple, input capacitor voltage ripple, and output voltage ripple are given by the following equations:

$$M(D) = \frac{-D}{1-D} \quad (6.41)$$



**Fig. 6.13** Buck-boost steady-state waveforms in CCM. **a** Buck-boost converter. **b** Buck-boost ratio. **c** Inductor current. **d** Capacitor current. **e** Diode current. **f** Diode voltage. **g** Switch current. **h** Switch voltage



**Fig. 6.14** Cuk steady-state waveforms in CCM. **a** Cuk converter. **b** Cuk ratio. **c** Inductor current. **d** Capacitor current. **e** Diode current. **f** Diode voltage. **g** Switch current. **h** Switch voltage

The inductor current ripple and the output voltage are determined as following:

$$\Delta i_{L1} = \frac{DV_{in}}{L_1 f} \tag{6.42}$$

$$\Delta i_{L2} = \frac{D(D-1)V_{in}}{(1-D)L_2 f} \tag{6.43}$$

$$\Delta v_{C1} = \frac{D^2 V_{in}}{(1 - D)RC_{1f}} \tag{6.44}$$

$$\Delta v_o = \frac{D(D - 1)V_{in}}{8(1 - D)L_2 C_2 f^2} \tag{6.45}$$

The current and voltage stress on the power electronic devices:

$$\text{Diode}_{\text{currentstress}} = \text{Switch}_{\text{currentstress}} = I_{in} + \frac{DV_{in}}{2L_1 f} \tag{6.46}$$

$$|\text{Diode}_{\text{voltagestress}}| = \text{Switch}_{\text{voltagestress}} = \frac{V_{in}}{1 - D} + \frac{D^2 V_{in}}{(1 - D)RC_{1f}} \tag{6.47}$$

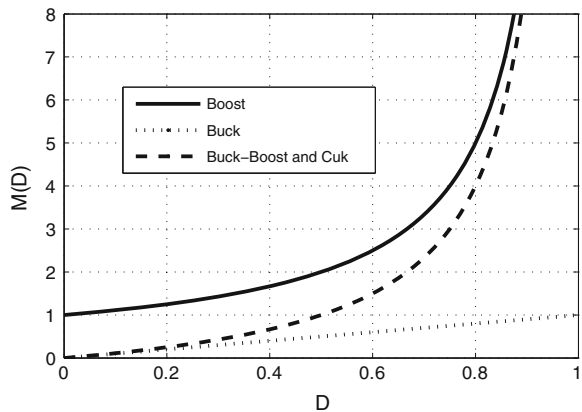
To increase the reliability of the FC, it is recommended that the number of the cells to be limited. This tradeoff between the FC reliability and its stack voltage (which is the sum of each cell voltage) is a key issue for FC applications. The FC stack voltage is rather low; therefore, it has to be boosted to several hundreds of volts required for the FCVs dc-bus or for grid-connected application. From this point of view, one of the most important features expected from the FC DC–DC converter is a high voltage ratio. Figure 6.15 shows that between the most common DC–DC converters the boost converter shows a higher voltage ratio.

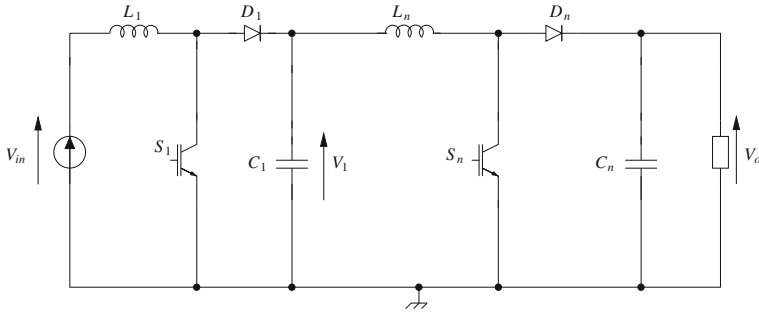
It is possible to increase the boost conversion ratio by connecting several boosts in series as shown in Fig. 6.16. This topology is well-known as cascade boost converter.

Equation (6.48) gives the conversion ratio of such topology. This topology still requires a large inductor value to decrease the FC current ripple. However, using several boosts in series decreases the overall system reliability.

$$M(D) = \prod_{i=1}^n \frac{1}{1 - D_i} \tag{6.48}$$

**Fig. 6.15** Voltage ratio comparison





**Fig. 6.16** Cascade boost converter

Where  $n$  is the number of boosts connected in series.

Another important feature expected from the FC DC–DC converter is a low input current ripple as high-current ripple may reduce lifetime of the FC [20]. From the Eq. (6.3) which gives the FC current ripple for the boost converter as a function of the system parameters, it can be seen that small current ripple requires a large inductor value, and consequently large inductor size, which drives the converter total volume to be large. However, the inductance requirement may be reduced if the switching frequency will increase, but this may be limited as semiconductor switching losses are increasing with frequency.

From the current and voltage stress equations that are discussed before, it can be seen that, for the boost converter, the current and voltage stress are the FC current which is a high current and the dc-bus voltage which is also a high voltage. From this point of view, high power application requires more silicon quantity and consequently high cost and size of the power electronic devices. This will limit the benefits of the boost converter as a low number of components and simple structure. Another problem of the basic boost converter is that for a high conversion ratio ( $>5$ ), the boost efficiency decreases drastically as a function of duty cycle.

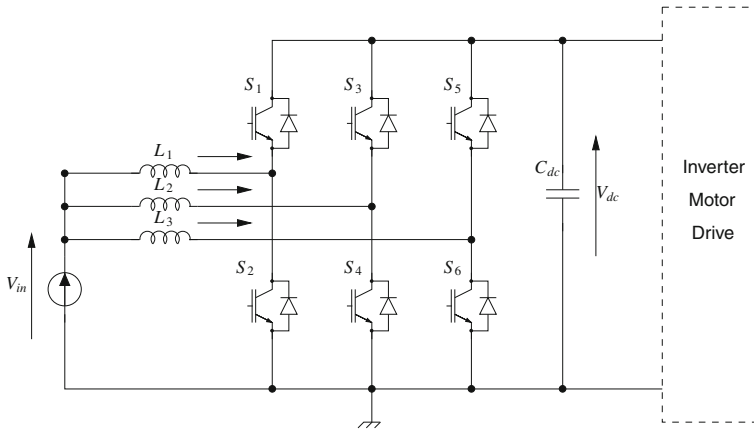
In order to decrease the current stress of the power electronic devices and the FC current ripple, the concept of interleaving is introduced. Figure 6.17 shows three-phase bidirectional interleaved boost converter. More details about this converter can be found in Ref. [21–23].

The conversion ratio of a such topology is similar to that of the boost converter. The number of phases can be increased as much as desired.

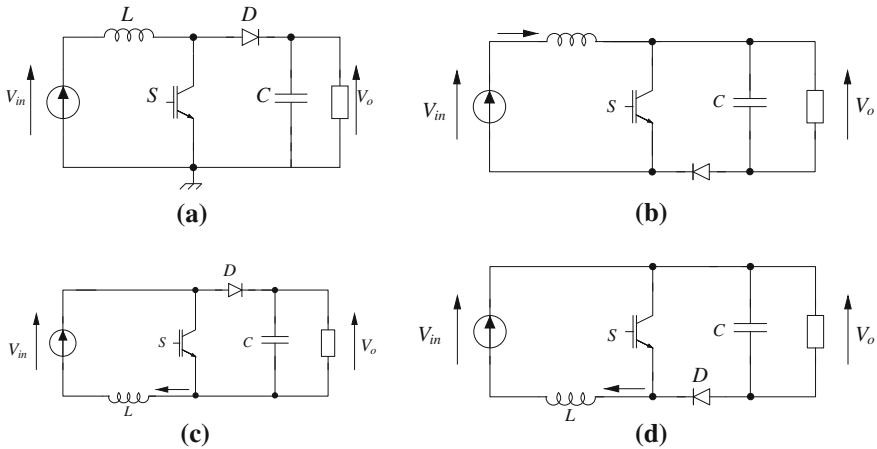
Several topologies based on the basic boost configuration are proposed in order to improve voltage gain, compactness, and efficiency. Basic variations of a conventional boost converter are shown in Fig. 6.18.

The floating interleaved boost converter (FIBC) topologies have many advantages for high conversion ratio applications. Similarly to the conventional boost converter, the topologies shown in Fig. 6.9 allows for interleaving in order to reduce input current ripple taken from the FC [24, 25]. Such FIBC allows for the voltage gain improvement over the traditional boost converter. Therefore, FIBC





**Fig. 6.17** Three-phase interleaved bi-directional DC-DC converter

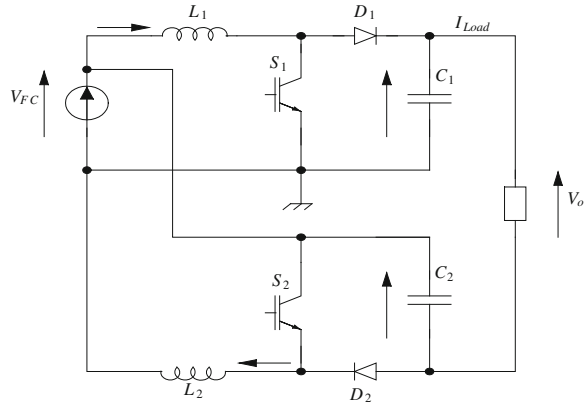


**Fig. 6.18** Basic boost converters: **a** Nonfloating boost. **b** Floating boost (FB) and inductor placed on the positive rail. **c** Floating boost (FB) and inductor placed on the negative rail. **d** Floating boost (FB) and inductor placed on the negative rail

topologies are found to be suitable for FC applications. The two-phase FIBC is shown in Fig. 6.19.

The two-phase FIBC is built of floating (lower) and nonfloating boost (upper) powered from the same voltage source. The parallel connection at the input and the series connection at the output of the floating and nonfloating boost converter allows for the input current ripple reduction with respective phase shift between the parallel converters  $S_1, S_2$  and for a following voltage gain improvement:

Fig. 6.19 2-phase FIBC



$$\frac{V_o}{V_{in}} = \frac{1 + D}{1 - D} \tag{6.49}$$

where  $D$  is the duty cycle of all switches.

Like the classic boost interleaved, the number of floating and nonfloating version can be increased as much as desired. The four-phase FIBC is shown in Fig. 6.20. More details about these topologies can be found in Ref. [26].

The principle of the floating interleaving and the cascade connection is used to obtain another topology called floating interleaved cascade boost converter FIC-BC. This topology is shown in Fig. 6.21.

The chain connections of the converters allow for a high voltage gain and reduces the output voltage ripple. The FICBC voltage gain is given as follows:

$$\frac{V_o}{V_{in}} = \frac{2}{(1 - D_1)(1 - D_2)} - 1 \tag{6.50}$$

where  $D_1, D_2$  are the duty cycle of the first and second stage, respectively.

In order to decrease the FC current ripple, the FICBC converter still requires a large inductor value and consequently increasing the overall converter volume. Another problem is the converter reliability as this last decreases by using the cascade connection principle. The FICBC converter may be further improved by interleaving, but it would increase system complexity.

It is possible to increase the FC output voltage without using extra power electronic devices by using a Z-source inverter. Such a system is presented in Fig. 6.22. The major problem related to this topology is that it requires an adequate control of the inverter to achieve the desired dc-bus voltage, because the boost action happens during modulation of the dead-time of the transistors, further details about this converter can be found in Refs. [27–32].

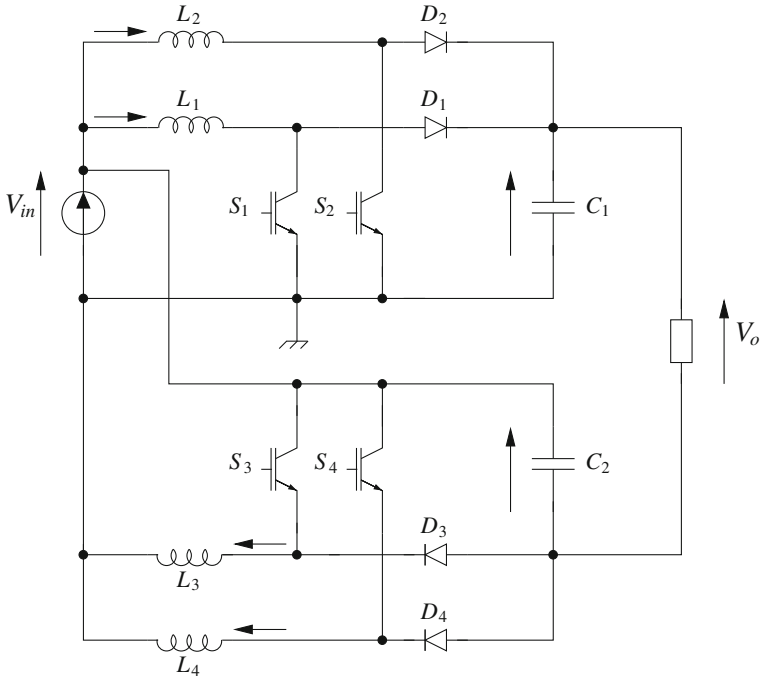


Fig. 6.20 4-phase FIBC

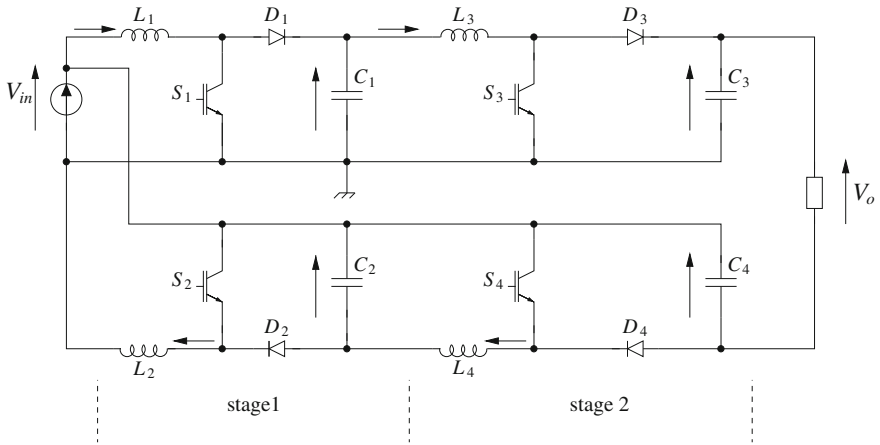


Fig. 6.21 FICBC converter

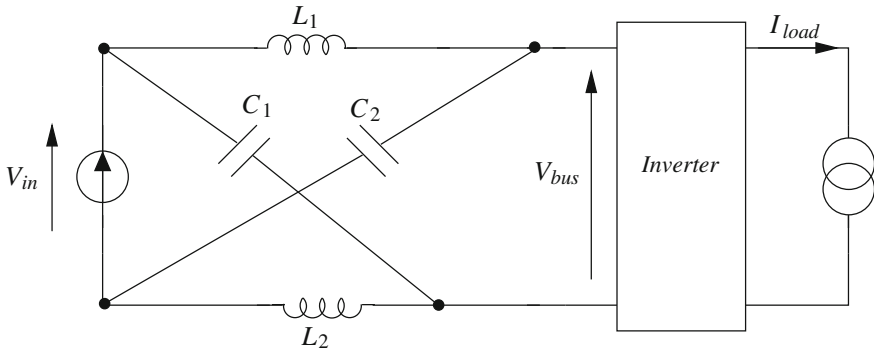


Fig. 6.22 Z-source inverter

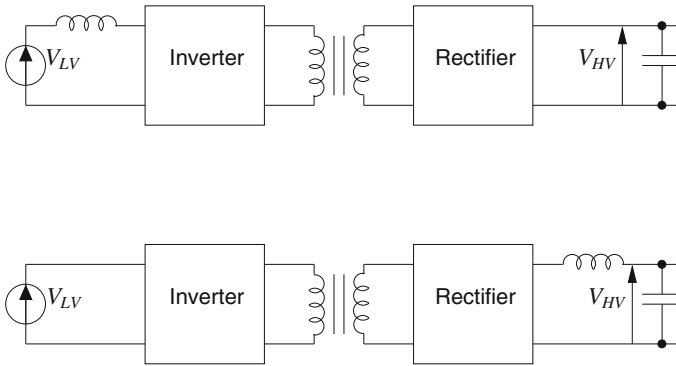


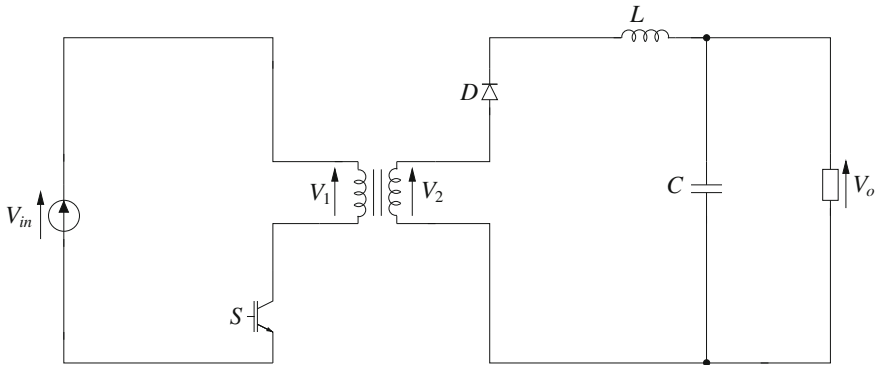
Fig. 6.23 Basic isolated DC-DC converter configurations

### 6.4.2.1 Isolated DC-DC Converter

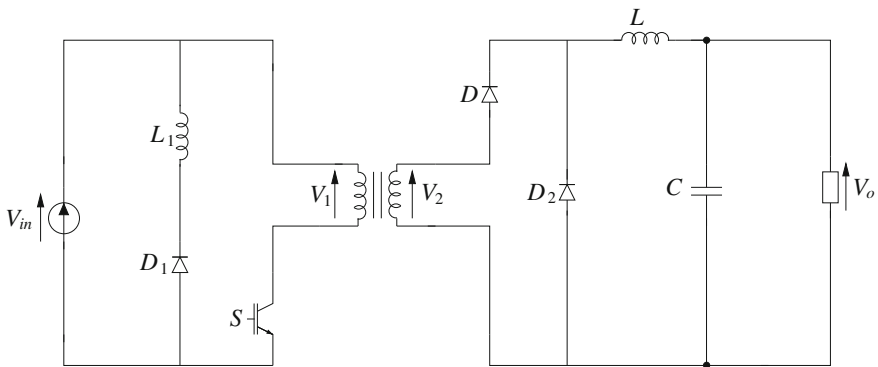
Some application requires an electrical isolation between the converter input and output. Such converter uses a high frequency circuits with a transformer for the galvanic separation. The high frequency operation of 10–100 kHz allows for the transformers size reduction. However, the high frequency operation may be penalized by the increased eddy current effects as wire thickness becomes to be larger than the magnetic field penetration depth. This may be a limiting factor for a high power system; however, it may be solved by a multiphase operation as shown in Ref. [33].

The transformer allows for a high step-up or step-down conversion ratio without the efficiency compromise. By an appropriate choice of the transformer turns ratio, the current or voltage stresses imposed on the transistors and diodes can be minimized and may lead to an improved efficiency and lower cost.

In general, an isolated DC-DC converter voltage ratio is usually fixed and additional circuitry is required for the output voltage regulations. The isolated



**Fig. 6.24** Flyback converter



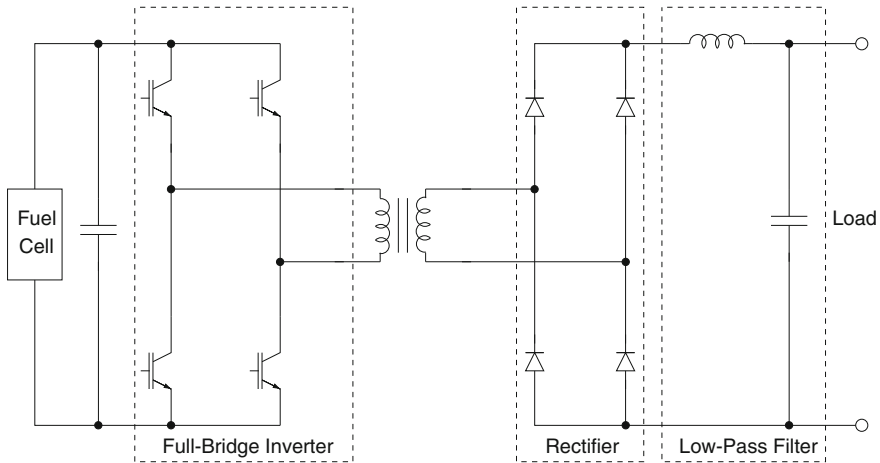
**Fig. 6.25** Forward converter

converters with incorporated regulation stage are often penalized by a lower efficiency.

There are many circuit configurations of isolated DC–DC converter. Figure 6.23 [34] shows two basic configurations of the isolated DC–DC converters. The inductor that serves as a current source can be placed either on low or high voltage side. The inductor placed at the low voltage side requires a large current in the magnetic component, but at the high voltage side it increases voltage stress on the semiconductor devices. It is also possible to embed the inductor in the leakage inductor of the transformer.

The inverter may be a voltage source with an input capacitor or a current source converter with an input inductor. In practice, the topologies of voltage source and current source are combined for high efficiency and high performance [12].

Figures 6.24 and 6.25 show two types of isolated DC–DC converter, the first known as flyback and the second as forward. The flyback converter has a low number of components and a simple structure. The main drawbacks of this



**Fig. 6.26** Isolated full-bridge converter

topology are high input current ripple, current and voltage stress on the power electronic devices, and discontinuous source current. However, such a topology is suitable for low power applications.

For the forward topology a third winding ( $L_1$ ) is placed on the transformer core allowing for the demagnetization of the transformer due to any remaining energy in the core which may lead to saturation problems. This topology has also a low number of components and a simple structure. Its main drawbacks are the presence of two magnetic components, misuse of the magnetic circuit of the transformer, and similar to flyback, current and voltage stress on the power electronic devices, and discontinuous source current. From this point of view, this converter is also suitable for low power applications.

The most popular isolated converter referred as a full-bridge converter is shown in Fig. 6.26.

The main advantage of the full-bridge converter is reasonable device voltage ratings, which is overshadowed by high switching losses due to hard commutation, high number of components, current mode control due to transformer saturation and last, fixed voltage ratio but no least a low efficiency.

The switching power loss issue is addressed in a series-resonant full-bridge converter shown in Fig. 6.27. The resonant converter provides a soft-switching for the transistors; thus, frequency can be increased and the passive associated components can be reduced. The resonant converter allows for a very high efficiency, but still suffers an increased component count.

A half-bridge converter is shown in Fig. 6.28. The number of the active components is reduced, but the semiconductor devices have to handle twice of the current. Also a split capacitors may cause some balancing issues. If the FC full-load voltage is 30 V, and output power is 10 kW, then the transformer sees 15 V assuming that the power devices do not have voltage drop. The transformer, and

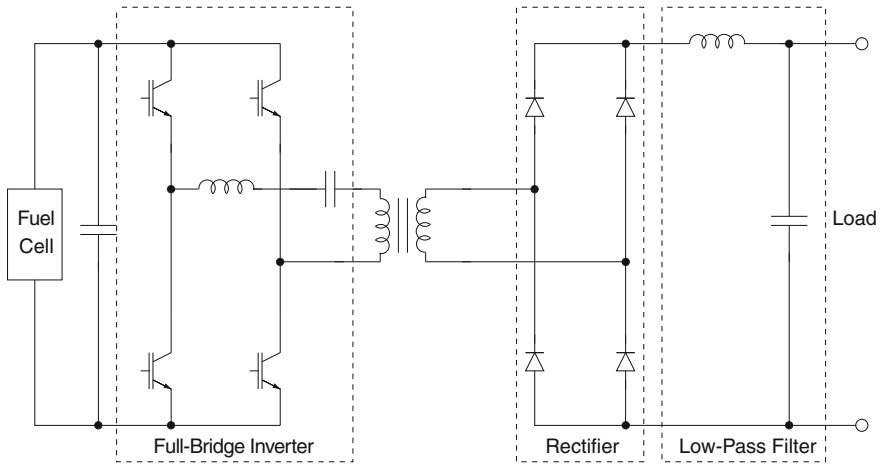


Fig. 6.27 Isolated series-resonant full-bridge converter

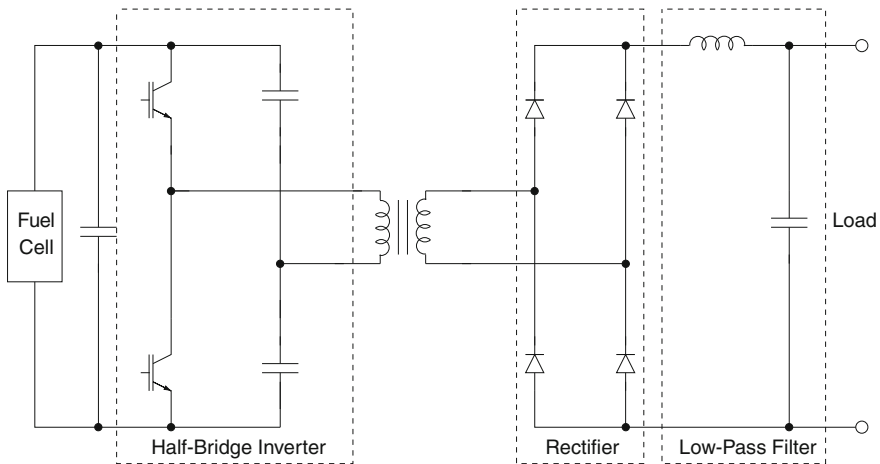
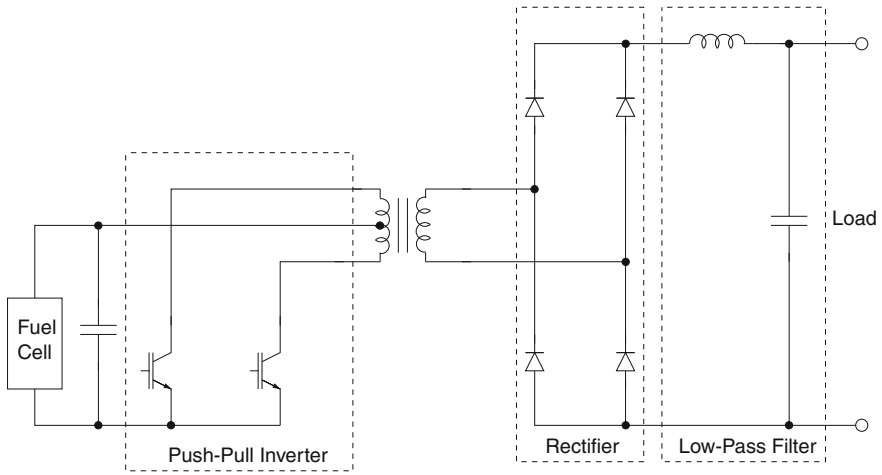


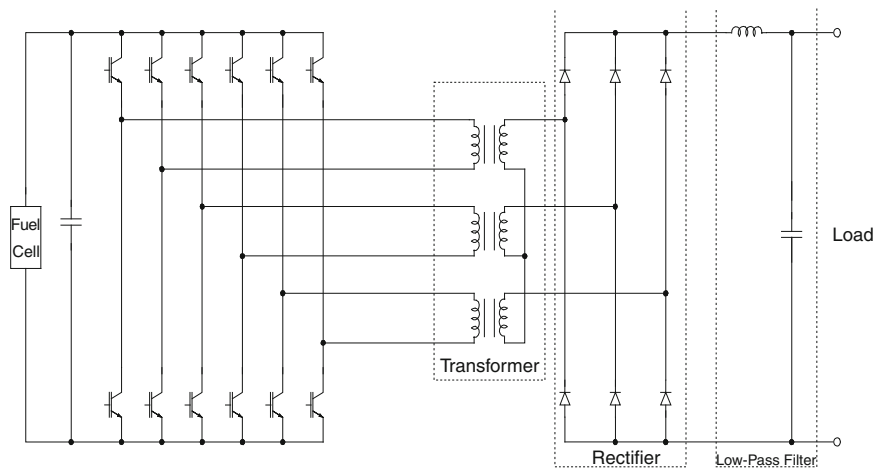
Fig. 6.28 Isolated half-bridge converter

thus the power devices current will exceed 600 A. Such a current is nontrivial for any single silicon device or transformer to handle. In addition, interconnect and parasitic inductances will further induce significant  $i^2R$  and  $Li^2$  losses, which decrease the converter's efficiency.

While the isolated converters presented above suffers fixed voltage ratio the one of the topologies suitable for the FC applications is the push-pull converter shown in Fig. 6.29. This converter is suitable for a low voltage and low power applications. The major issue of the push-pull converter is that the device handles twice of the input voltage, thus, a high voltage device (MOSFET or IGBT) is required.



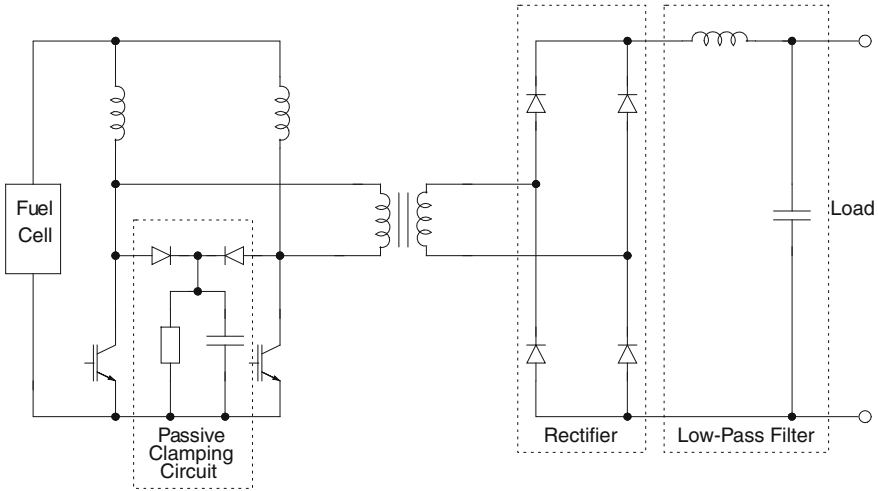
**Fig. 6.29** Isolated push-pull converter



**Fig. 6.30** Isolated  $V_6$  converter

The main challenge for the FCV powertrain designer is to reduce the converters size while the FC current and voltage ripples are as small as possible. Similar to the nonisolated converters, a multiphase design is introduced. A three-phase six-leg converter is thus proposed, as shown in Fig. 6.30 [35]. This converter is known as  $V_6$ . The phase-shift modulation (PSM) can be preserved to achieve soft-switching [36, 37]. Three phases are controlled with  $120^\circ$  apart, thus the ripple can cancel each other. More details about the operating mode analysis can be found in [38].





**Fig. 6.31** Isolated  $L$ -type converter

The  $V_6$  converter has several advantages:

- 1 Reducing of the root mean square (RMS) current per phase, thus reducing the  $I^2R$  conduction losses.
- 2 Secondary voltage over-shoot reduction, thus cost and size reduction with elimination of voltage clamping circuit.
- 3 Soft-switching over a wide load range.
- 4 High efficiency.

Nevertheless, the  $V_6$  employs large number of the active devices, the voltage transformation is fixed and it may require a complex transformer design.

The isolated DC–DC current source  $L$ -type converter with a series inductor is shown in Fig. 6.31 [34]. The input inductor volume may be reduced and the converter eliminates the current ripple.

An auxiliary clamping circuit is employed to reduce main device voltage stress due to the discharge of inductors during the commutation. The auxiliary circuit increases complexity and introduces additional losses as inductors energy is lost in the clamping circuit. On the other hand, the design of the converter shows that the volume of the inductor remains dominating and the converter's efficiency is not satisfactory [39, 40]. The full-bridge current source converter is shown in Fig. 6.32. It reduces the number of the input inductors at the expense of additional active switches. The input inductor requires active voltage clamping circuit in order to avoid excessive voltage stress of the main switches during the commutation.

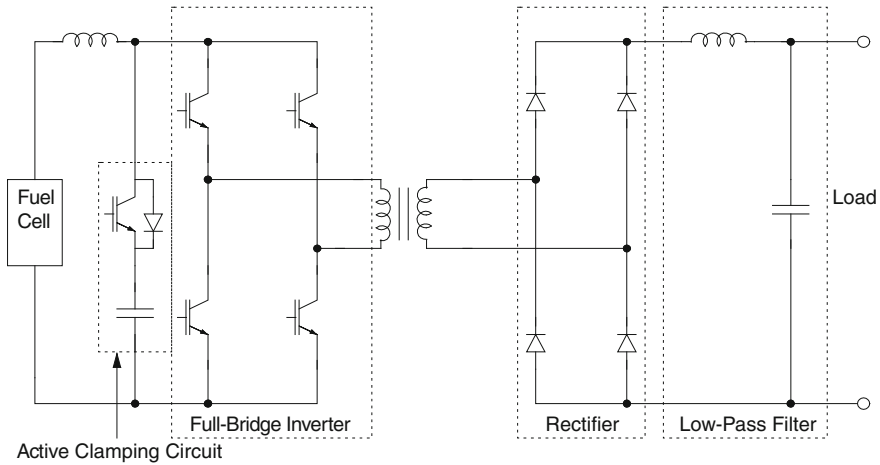


Fig. 6.32 Isolated full-bridge current source converter

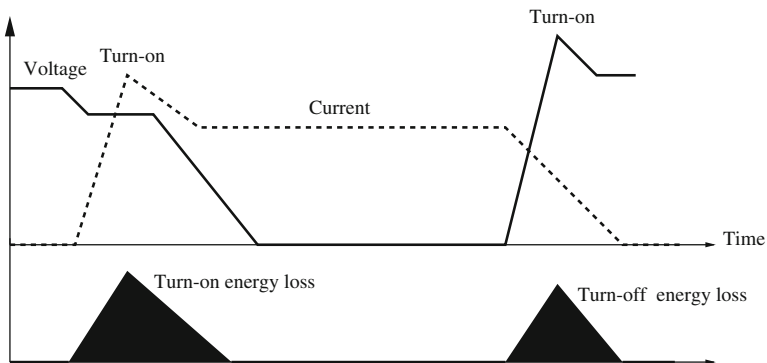
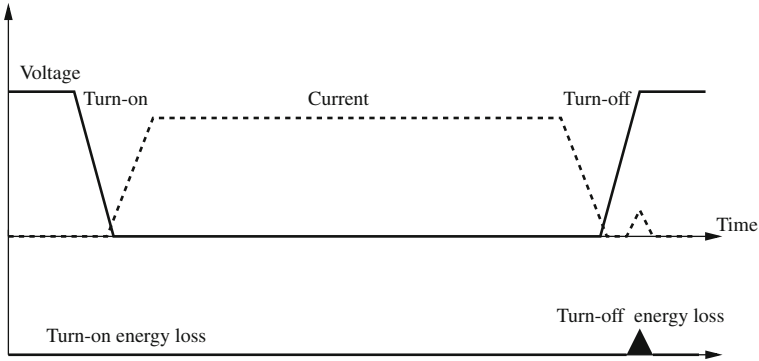


Fig. 6.33 Hard-switched transistor operation

### 6.5 Soft-Switching Topologies

Hard switching transistor operation has power loss due to turn-on and turn-off transients and in addition one of the major contributors to the switching power loss in nonisolated DC–DC converters is the diode reverse recovery charge. Switching power losses during transient in a hard-switched converter is shown Fig. 6.33.

The power loss is equal to the product of current and voltage across the switch, as it can be seen the diode is a significant power loss contributor during transistor turn-on transient. The energy lost during a single switching period limits the maximum energy transferred through the switch and limits the switching frequency and may affect converters efficiency. The switching power losses set the



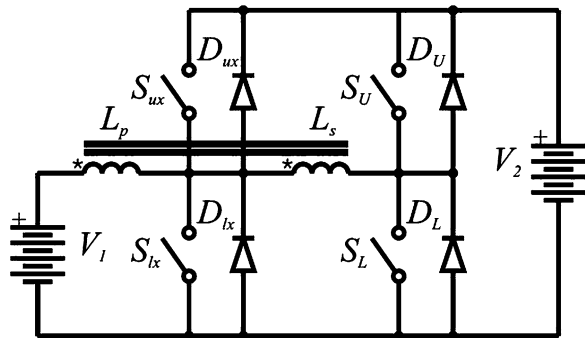
**Fig. 6.34** Soft-switched transistor operation

operating frequency area for the switch as the switching power losses become substantial as frequency increases.

As noted earlier, the silicon-based diode suffers significant power loss due to reverse recovery. The reverse-recovery power loss depends on several factors such as temperature, initial current, and switching current rate of change. Due to reverse recovery, the diodes power loss is usually significant contributor to the total semiconductor losses. Some low recovery power loss alternative diodes exist as SiC and GaN or low voltage range Si-based Schottky diodes, but this is beyond the scope of this work due to high cost and availability of a high current dies at the time of writing this chapter; however, SiC and GaN diodes are foreseen as a natural succession of traditional silicon diodes.

The switching power loss phenomenon is well-known and recognized as in Ref. [41]. A number of snubber circuits were developed throughout the years in order to reduce switching power losses. The snubber circuitry softens the voltage and current transients and allows for so called soft-switching. A typical voltage and current soft-switching waveforms for the IGBT transistor are illustrated in Fig. 6.34.

**Fig. 6.35** Buck-boost with tapped inductor



As it is shown, at turn-on the current rise may be delayed, e.g., by the inductive snubber or auxiliary soft-switching cell, while turn-off is usually assisted by the capacitive snubber. The diode turn-off process is usually softened by the controlled rate of change of current descend. Please note that reverse recovery charge is linked with the diode turn-off current fall rate. Severns (41) is a very extensive source of knowledge on snubbers. The IGBT tail-current power loss under soft-switching usually shows lower power loss reduction than anticipated due to charge recombination.

In general, the soft-switching allows for semiconductors switching loss reduction at the expense of increased circuit complexity and some power loss in the snubber itself. The snubber circuit requires design compromises between: cost, complexity, reliability, power loss, and circuit performance. Note that waveforms and associated energy loss shown in Figs. 6.33 and 6.34 are of same scale.

Soft-switching techniques are employed in a nonisolated DC–DC converter in order to limit power loss during switching transients. The DC–DC converter usually requires snubber in order to achieve soft-switching condition. In general, soft-switching circuitry provides zero current ZCS or zero voltage ZVS transients during switching or both. The converters efficiency is improved at the expense of additional circuitry as switching power losses from the main devices are shifted to somewhat smaller power loss in the auxiliary devices.

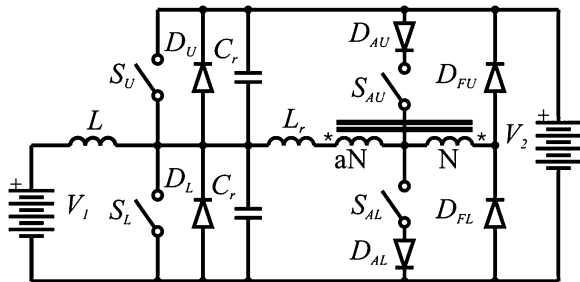
Basic DC–DC nonisolated hard-switched converters are presented previously, but there is a great variety of the soft-switching cells (snubbers) that may be applied to the basic topologies.

Figures 6.35 and 6.36 show two boost converters with tapped inductor [42] and auxiliary soft-switching cell [43, 44], respectively.

The topology with tapped inductor shown in Fig. 6.35 allows for efficiency improvement with low auxiliary component count. This topology allows for a significant efficiency increase, but at the expense of control circuit complexity as it requires inductor current sensing in order to trigger main switch. Also the tapped inductor leakage inductance take part in the commutation for current fall rate control, note that high voltage converter may require relatively large leakage. This topology is a practical example of application of the active soft-switching cells.

The converter with soft-switching cell shown in Fig. 6.36 allows for soft-switching of the main transistors in the entire range of operation and allows for

**Fig. 6.36** Buck-boost with auxiliary soft-switching



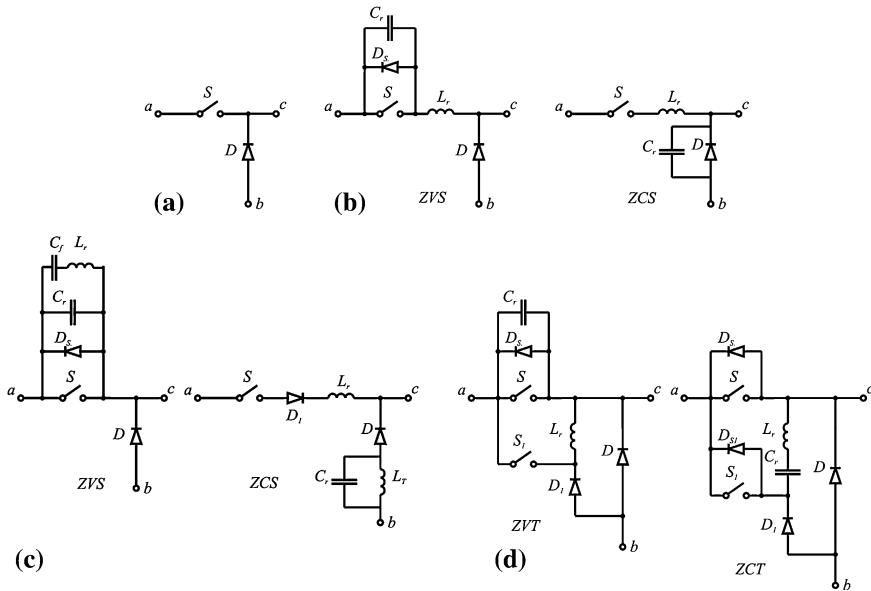


Fig. 6.37 Switching cells

ZCS turn-on of the auxiliary transistors with a very small turn-off current. This topology is very easy to control and it shows high robustness with a good efficiency gain, but it requires five additional components. Note that this circuitry is quasi-resonant with an auxiliary voltage. The main advantage of this solution over the others is low stress on the components, bi-directional operation, ZVS, and ZCS for main switch transient and high part-load efficiency. It is worth of note that auxiliary cell is rated for approximately 15 % of the main power and thus, the auxiliary components are relatively small. The generalized analysis of soft-switching DC–DC converters is presented in Ref. [45].

Selected switching cells are shown in Fig. 6.37. As it is seen, the basic hard-switched cell shown in Fig. 6.37a is extended by additional components in order to achieve soft-switching. The additional circuitry may create quasi-resonant cell (QRC), voltage- or current-clamped quasi-square wave cell (QSW CV or CC), or PWM active cell (ZVT- or ZCT-PWM) as shown in Fig. 6.37b, c and d, respectively.

The high-current ripple converters may use a natural commutation or zero-crossing conduction mode for 2-quadrant converters and the switching frequency may be modulated in order to improve efficiency and provide soft-switching conditions. This type of converters may have some limitation in respect to the maximum transferred power and thus may require multiphase system.

The general characteristic of soft-switched topologies is presented in Table 6.6. Additional components increase conduction power loss, but switching power loss is reduced. Due to resonant cell, soft-switched converters are usually optimized for

**Table 6.6** Comparison of soft-switched topologies

Item	Hard switched	Quasi-resonant	Quasi-square wave	PWM	Auxiliary cell with voltage source
Conduction losses	Lowest	High	Moderate	Low	Moderate
Switching losses	High	Low	Low	Low	Very low
EMC behavior	Poor	Good	Good	Good	Good
Control complexity	Very low	Low	Moderate	High	Low
Control range	Very good	Good	Poor	Moderate	Good
Converter size	Largest	Medium	Small	Small	Small
Converter complexity	Low	Low	Medium	High	High

high efficiency at given operating point and low load efficiency is typically lower than for hard-switched converters. Soft-switched converters are appreciated by improved EMC behavior. The control range of the soft-switched converters is reduced due to pole's average voltage reduction and for some converters it is limited by resonant operation of the cell. Soft-switching converter is expected to have smaller size than the hard-switched in terms of lower silicon use, which is the most expensive part of the converter. The benefits of soft-switched converters are penalized by increased complexity.

Due to development of the new wide band gap semiconductors, the existence of soft-switching cells may be at question, especially if silicon diodes are replaced with low recovery charge SiC or GaN diodes. It is foreseen, that soft-switched converters are likely to be limited to some specific high power application while low and medium power will be dominated by wide band gap devices.

## 6.6 Conclusion

The topology selection is not an easy process as it requires many constraints to be considered. This chapter gives a brief overview of the available topologies. Since the vehicle powertrain does not require an electrical isolation, the nonisolated converters are of the prime interest. The nonisolated converters allows for the minimum size design. The vehicle operation is a very specific as the vehicle average power is much lower than a peak power during accelerating or braking. Therefore, the converter must provide a high efficiency over the wide load range and maintain a high efficiency during acceleration when a high boost ratio is expected at full power as FC output characteristic is nonlinear.

The isolated converters are recommended for all applications where electrical isolation is required for a safety reason. It would be the automotive charging units or any grid-connected high power system. The isolated DC–DC converters are

usually not considered for a vehicle powertrain as they require additional voltage conditioning systems.

In general, high power converters tend to be multiphase for current sharing. Also, multiphase structure allows for an increased part-load efficiency. The non-isolated converter is the most optimal solution for a low size converter in a low to medium voltage gain range. If a high voltage gain is required, the floating or transformer-based converters are the most optimum solution. The lowest input current ripple is available from multiphase converters due to current ripple cancelation.

## References

1. NASA (2004), The Gemini Program, available from NASA history website. <http://www-pao.ksc.nasa.gov/history/gemini/gemini.htm>
2. Carl HH, Andrew H, Wolf V (2007) *Electrochemistry*, 2nd edn. Wiley-VCH Verlag GmbH. ISBN-10: 352731069X, ISBN-13: 978-3527310692
3. Corrêa JM, Farret FA, Canha LN, Simões MG (2004) An electrochemical-based fuel-cell model suitable for electrical engineering automation approach. *IEEE Trans Ind Electron* 51(5):10
4. Gao F, Blunier B, Miraoui A, El-Moudni A (2010) Proton exchange membrane fuel cell multi-physical dynamics and stack spatial non-homogeneity analyses. *J Power Sources* 195(22):7609–7626
5. O'Hayre R, Cha S-W, Colella W, Prinz FB (2005) *Fuel cell fundamentals*, 1st edn. Wiley, New York, p 409
6. Larminie J, Dicks A (2003) *Fuel cell systems explained*, 2nd edn. Wiley, Chichester
7. Gao F, Blunier B, Miraoui A, Moudni AE (2010) A multiphysics dynamic 1D model of a proton exchange membrane fuel cell stack for real time simulation. *IEEE Trans Ind Electron* 26:184–194
8. Bird R, Stewart W, Lightfoot E (2002) *Transport phenomena*, 2nd edn. Wiley, New York
9. Springer TE, Zawodzinski TA, Gottesfeld S (1991) Polymer electrolyte fuel cell model. *J Electrochem Soc* 138(8):9
10. Costamagna P, Selimovic A, Del Borghi M, Agnew G (2004) Electrochemical model of the integrated planar solid oxide fuel cell (IP-SOFC). *Chem Eng J* 102:61–69
11. Colclasure AM, Sanandaji BM, Vincent TL, Kee RJ (2010) Modeling and control of tubular solid-oxide fuel cell systems. I: physical models and linear model reduction. *J Power Sources*. doi:<http://dx.doi.org/10.1016/j.jpowsour.2010.06.074>
12. Choi D, Lee B, Choi S, Won C, Yoo D (2005) A novel power conversion circuit for cost-effective battery-fuel cell hybrid systems. *J Power Sources* 152:245–255
13. Lee BK, Fahimi B, Ehsani M (2011) Overview of reduced parts converter topologies for ac motor drives. In: *IEEE power electronics specialist conference*, pp 2019–2024
14. Lee B, Hong J, Ehsani M (2003) Generalized design methodology of reduced parts converters for low cost bldc motor drives. In: *IEEE applied power electronics conference*, pp 277–280
15. Erickson R, DC–DC power converters” *Wiley Encyclopedia of Electrical and Electronics Engineering DC–DC Power Converters*, pp 80 309–0425 15 JUN 2007. doi:[10.1002/047134608X.W5808.pub2](https://doi.org/10.1002/047134608X.W5808.pub2)
16. Song Y (2004) *Analysis and design of high frequency link power conversion systems for fuel cell power conditioning*. PhD dissertation, Texas A&M University, Texas
17. Middlebrook R (1988) Small-signal modeling of pulse-width modulated switched-mode power converters. *Proc IEEE* 76(4):343–354

18. Uzunoglu M, Alam M (2007) Dynamic modeling, design and simulation of a PEM fuel cell/ultra-capacitor hybrid system for vehicular applications. *Energy Convers Manage* 48(5):1544–1553
19. Middlebrook RD (1981) Power electronics: topologies, modeling, and measurement. *Proc IEEE Int Symp Circ Syst PEL-1*:76–89
20. Fontes G, Turpin C, Astier S, Meynard T (2007) Interactions between fuel cells and power converters: Influence of current harmonics on a fuel cell stack. *Power Electron, IEEE Trans* 22(2):670–678
21. Tipton C, Urciuoli D, Porschet D (2004) Development of a 90 kW, two-phase, bi-directional DC–DC converter for power dense applications, Dec 2004, 3p. <http://www.ntis.gov/search/product.aspx?ABBR=ADA433112>
22. Li H, Peng F, Lawler J (2001) A natural ZVS high-power bi-directional DC–DC converter with minimum number of devices. In: Conference record of the IEEE industry applications conference, vol 3, pp 1874–1881
23. Eckardt B, Hofmann A, Zeltner S, Marz M (2006) Automotive powertrain DC/DC converter with 25 kW/dm<sup>3</sup> by using SiC diodes. In: Proceedings of 4th international conference on integrated power systems, pp 7–9
24. Zhang M, Jiang Y, Lee F, Jovanovic M (1995) Single-phase three-level boost power factor correction converter. In: Applied power electronics conference and exposition, APEC'95, vol 1, pp 434–439
25. Teodorescu R, Kjaer S, Munk-Nielsen S, Blaabjerg F, Pedersen J (2001) Comparative analysis of three interleaved boost power factor corrected topologies in DCM. In: IEEE 32nd annual power electronics specialists conference, 2001. PESC, vol 1
26. Kabalo M, Blunier B, Bouquain D, Miraoui A (2011) Comparison analysis of high voltage ratio low input current ripple floating interleaving boost converters for fuel cell applications. In: Vehicle Power and Propulsion Conference (VPPC). IEEE, pp 1, 6, 6–9 Sept. doi:10.1109/VPPC.2011.6043101
27. Peng F (2003) Z-source inverter. *Ind Appl, IEEE Trans* 39(2):504–510
28. Rajakaruna S, Jayawickrama Y (2005) Designing impedance network of z-source inverters. In: Power engineering conference. IPEC the 7th international. IEEE, pp 962–967
29. Fang X, Qian Z, Peng F (2005) Single-phase z-source pwm ac–ac converters. *Power Electron Lett, IEEE* 3(4):121–124
30. Peng F, Joseph A, Wang J, Shen M, Chen L, Pan Z, Ortiz-Rivera E, Huang Y (2005) Z-source inverter for motor drives. *Power Electron, IEEE Trans* 20(4):857–863
31. Loh P, Gajanayake C, Vilathgamuwa D, Blaabjerg F (2008) Evaluation of resonant damping techniques for z-source current-type inverter. *Power Electron, IEEE Trans* 23(4):2035–2043
32. Shen M, Peng F (2005) Operation modes and characteristics of the z-source inverter with small inductance. In: Industry applications conference, 2005. Fourteenth IAS annual meeting. conference record of the 2005, IEEE, vol 2, pp 1253–1260
33. De Doncker R, Jacobs J, Averberg A (2004) A novel three-phase dc–dc converter for high-power applications. *PESC* 3:1861–1867
34. Lai J, Nelson D (2007) Energy management power converters in hybrid electric and fuel cell vehicles. *Proc IEEE* 95(4):766–777
35. Lai J (2005) A high-performance V6 converter for fuel cell power conditioning system. In: IEEE conference vehicle power and propulsion, p 7
36. Sabate J, Vlatkovic V, Ridley R, Lee F, Cho B (1990) Design considerations for high-voltage high-power full-bridge zero-voltage-switched pwm converter. In: Applied power electronics conference and exposition, 1990. APEC'90, conference proceedings, fifth annual. IEEE, 1990, pp 275–284
37. Hua G, Lee F, Jovanovic M (1993) An improved full-bridge zero-voltage-switched pwm converter using a saturable inductor. *Power Electron, IEEE Trans* 8(4):530–534
38. Liu C, Johnson A, Lai J (2007) A novel three-phase high-power soft-switched dc–dc converter for low-voltage fuel cell applications. *IEEE*, 2005 vol 41(6), pp 1691–1697



39. Wang K, Lin C, Zhu L, Qu D, Lee F, Lai v (1998) Bi-directional dc to dc converters for fuel cell systems. *Power Electron Transp*, pp 47–51
40. Lai J, Peng F (1996) Multilevel converters-a new breed of power converters. *IEEE Trans Ind Appl* 32(3):509–517
41. Severns R (2008) *Snubber circuits for power electronics*. Rudolf Severns
42. Lee D, Lee F (1997) Novel zero-voltage-transition and zero-current-transition pulse-width-modulation converters. In: *Power electronics specialists conference. PESC'97 record*. 28th annual IEEE, vol 1, pp 233–239
43. Martins D, de Seixas F, Brilhante J, Barbi I (1993) A family of dc-to-dc pwm converters using a new zvs commutation cell. In: *Power electronics specialists conference. PESC'93 record*, 24th annual IEEE, pp 524–530
44. Rylko M, Egan M, Hayes J, Power D (2007) A soft-switched bi-directional dc–dc converter. In: *Power electronics and applications, European conference on IEEE*, pp 1–10
45. Abu-Qahouq J, Batarseh I (2000) Generalized analysis of soft-switching dc–dc converters. In: *Power electronics specialists conference. PESC IEEE 31st annual IEEE*, vol 1, pp 185–192

# Chapter 7

## Variable-Speed Power Generation

Włodzimierz Koczara and Grzegorz Iwanski

**Abstract** Theory of the variable (adjustable) speed generation systems is described. The main part is related to island (autonomous) operation. Variable speed means an additional degree of freedom of the generation system. Moreover, it provides higher speed than conventional system based on wound rotor synchronous generator. The higher speed results in higher power of driving engine. Adjustable speed provides reduction of fuel consumption. To reduce the engine fuel use, its speed is adjusted to areas of low specific fuel consumption. Two basic topologies are presented. First topology is based on application of the permanent magnet generator, whereas second on the slip-ring induction machine. Power flow drawn from the engine via generator is controlled by power electronic converters. In case of use of permanent magnet generator, the applied power electronic converter is built on the basis of the intermediate DC link voltage. The generator voltage of variable frequency and amplitude is rectified and then converted to the AC voltage. This concept is realized by application of several different rectifier and inverter topologies. The power electronics converter controls the rectified current and in this way adjusts the load torque produced by the generator. Speed control systems of the driving engine are presented. The variable speed power generation with slip-ring induction machine system uses a control method based on space vector theory. According the reference stator voltage vector, the rotor current amplitude, frequency, and phase are adjusted to provide sinusoidal three-phase stator voltage.

---

W. Koczara (✉) · G. Iwanski  
Warsaw University of Technology, Koszykowa 75, 00-662 Warszawa, Poland  
e-mail: koczara@isep.pw.edu.pl

## 7.1 Introduction

### 7.1.1 Goals of Variable Speed Technology

The electricity supply system, that is in present electric power used commonly in the whole world, is based on wound rotor synchronous generator (WRSG) operating with fixed speed. The synchronous generator fulfills simultaneously two main requirements. The first requirement is a conversion of mechanical into electrical power, while the second requirement is production of high quality electrical power. The high quality electrical power means stable amplitude of AC voltage, instantaneous voltage values that correspond to sine function and stable, strictly standardized, frequency. During the last 100 years, the WRSG was significantly developed and improved. Its power did reach 1,000 MVA and tens of years reliable operation. Low power units, from few kilowatts to several Megawatts are produced in hundreds of thousands units a year. Moreover, brushless excitation and sophisticated cooling were introduced. However, the advantage of construction simplicity, combining conversion of energy and power quality, limits rotational speed  $n_{gm}$ , determined by output frequency  $f_g$

$$n_{gm} = \frac{60f_g}{\left(\frac{p}{2}\right)} \quad (7.1)$$

where speed  $n_{gm}$  is expressed in rpm and  $p$  means number of poles.

The generator mechanical angular speed  $\omega_{gm}$  is expressed in rad/s

$$\omega_{gm} = \frac{2\pi f_g}{\left(\frac{p}{2}\right)} \quad (7.2)$$

Hence the generators and prime movers were designed, built, and optimized mainly to fixed speeds 3,000 or 1,500 rpm for 50 Hz loads and 3,600 or 1,800 rpm for 60 Hz loads.

The mechanical power  $P_{de}$  delivered to generator by prime mover depends on its speed and driving torque  $T_{de}$ . For speed  $n_{de}$  expressed in rpm

$$P_{de} = \frac{2\pi}{60} n_{de} T_{de} \quad (7.3)$$

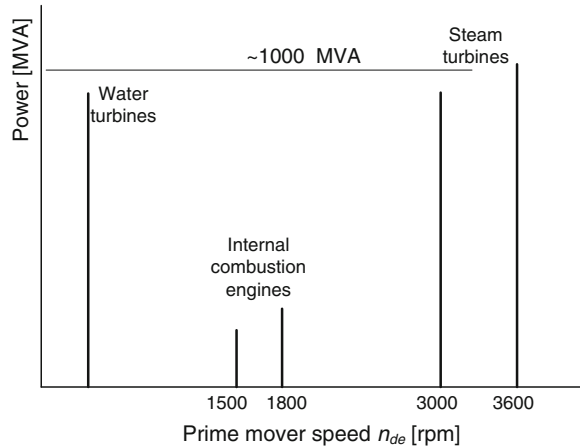
or for speed expressed in angular mechanical speed  $\omega_{de}$

$$P_{de} = \omega_{de} T_{de} \quad (7.4)$$

Figure 7.1 shows an example of prime mover available power as a function of speeds (7.1).

Therefore, power variation is caused only by driving torque. So the progress in generating technology improvement was frozen, i.e., only operation with synchronous speed was permitted.

**Fig. 7.1** Power of prime movers for the case of fixed speed operation



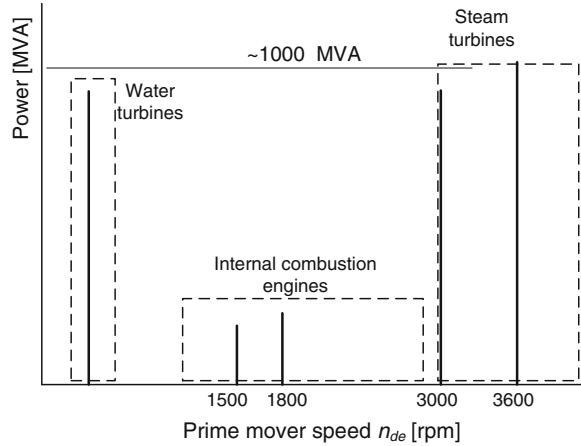
Prime movers have their highest efficiency area which usually does not overlaps with required fixed synchronous speed. The efficiency of commonly used prime movers is low and it has significant influence on power losses in electricity production.

Synchronous generators have tendency to unstable operation. Any electromechanical perturbations as instantaneous speed variation produces frequency variation. To avoid disconnection of swinging unit great number of generators are connected together creating high power robust electrical system. So the generating set is coupled to grid with very limited degrees of freedom.

Any increase of speed results in size and mass reduction of prime movers and generators. Increase of produced frequency also brings generator size and weight diminution. Directly grid connected WRSG does not permit speed to be varied, because it combines function of energy conversion and voltage quality. Hence by splitting these functions to different devices, it is possible to provide decoupled generation. This may be achieved using any generator as only energy converter and power electronic converter as source of electricity, i.e., voltage or current. The variable amplitude and frequency generator voltage is conditioned by power electronic system which produces high quality standardized voltage. In this way, prime mover and generator gain additional degree of freedom in speed. Figure 7.2 shows simplified speed range for different prime movers.

The generating system may operate in variable speed mode or fixed but not conventional speed. The method of decoupled generation opens the research in generation system development especially in the field of prime energy savings, size, and weight reduction, stability and power quality improvement [1–5]. When speed rises over conventional speed then the prime mover and generator rated power increases too.

**Fig. 7.2** Areas of prime movers speed variation of decoupled generation



### 7.1.2 Features of Wound Rotor Synchronous Fixed Speed Generation

The synchronous generator has been used and tested since more than 100 years. It did result in high efficiency, reliability, low cost of manufacturing, and especially in common knowledge providing easy maintenance and exploitation. The synchronous generator is a source of active and reactive power. Therefore for the variable speed generation, the conventional generation technology may be a reference. There are two modes of the synchronous generator operation: autonomous (island) and grid connection. Figure 7.3 shows generating set supplying directly loads, i.e., in island mode operation. The prime mover PMo drives the synchronous generator producing torque  $T_{de}$ . There are two basic topologies of the synchronous generator. First, presented in Fig. 7.3a shows conventional generator with excitation windings supplied through slip rings (WRSG) and second (Fig. 7.3b) is brushless (WRNSG). The brushless excitation system (BES) may be powered from AC or DC source. Prime mover PMo drives WRSG with speed  $n_{gm}$  (or angular speed  $\omega_{gm}$  providing  $V_{sg}$  rms. Voltage with frequency

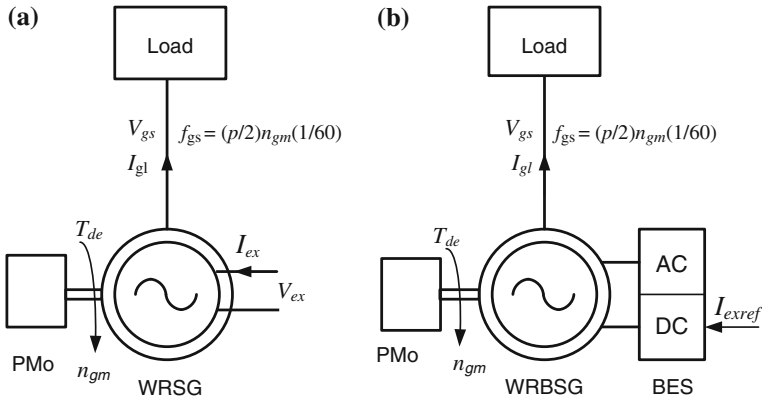
$$f_{gs} = \frac{1}{60} n_{gm} \frac{p}{2} = \frac{1}{2\pi} \omega_{gm} \frac{p}{2} \quad (7.5)$$

Block diagram of the synchronous generator producing instantaneous voltage  $v_{gs}$

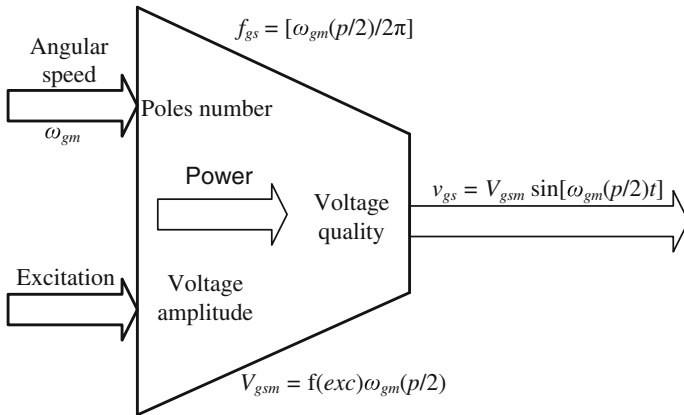
$$v_{gs} = V_{gsm} \sin \left[ \omega_{gm} \left( \frac{p}{2} \right) t \right] \quad (7.6)$$

is presented in Fig. 7.4.

The peak output voltage  $V_{gsm}$  is a function of excitation and angular rotor speed.



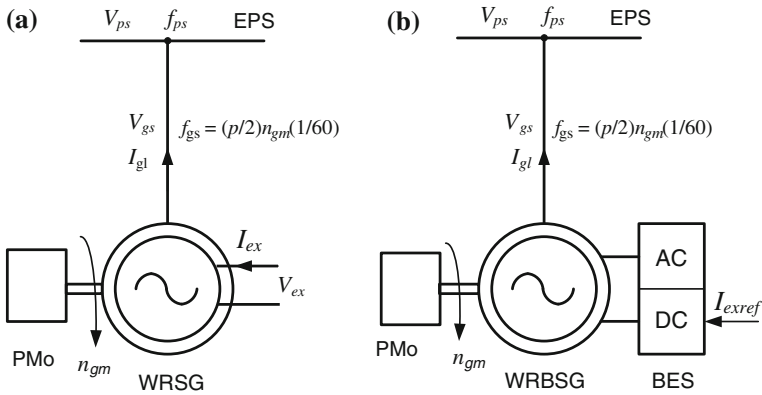
**Fig. 7.3** Generating set with wound rotor synchronous generator: **a** excitation through slip rings, **b** brushless excitation



**Fig. 7.4** Block diagram of the wound rotor synchronous generator producing sinusoidal voltage (7.6)

During island operation any changes of load produces transient frequency variation.

Power grid connected generator (Fig. 7.5) operates with stable frequency and voltage  $V_{gs} = V_{ps}$  provided by an electrical power system EPS. A driving engine PMo keeps generator fixed speed  $n_{gm}$  corresponding to grid voltage frequency  $f_{ps}$ . However, in case of step load small transient frequency changes, caused by variation of load angle  $\delta_{gs}$ , may happen. In steady state condition, generator frequency  $f_{gs}$  is equal to frequency  $f_{ps}$  of power system EPS. Produced active power  $P_{gs}$  is function of load angle  $\delta_{gs}$  generator electromotive  $E_{gs}$ , generator reactance  $x_{gs}$ , and grid voltage  $V_{gs}$



**Fig. 7.5** Grid-connected synchronous generator: **a** excitation through slip rings, **b** brushless excitation

$$P_{gs} = V_{gs} E_{gs} \sin(\delta_{gs}) \frac{1}{x_{gs}} \tag{7.7}$$

Reactive power delivered by the generator

$$Q_{gs} = V_{gs} E_{gs} \cos(\delta_{gs}) \frac{1}{x_{gs}} - V_{gs}^2 \frac{1}{x_{gs}} \tag{7.8}$$

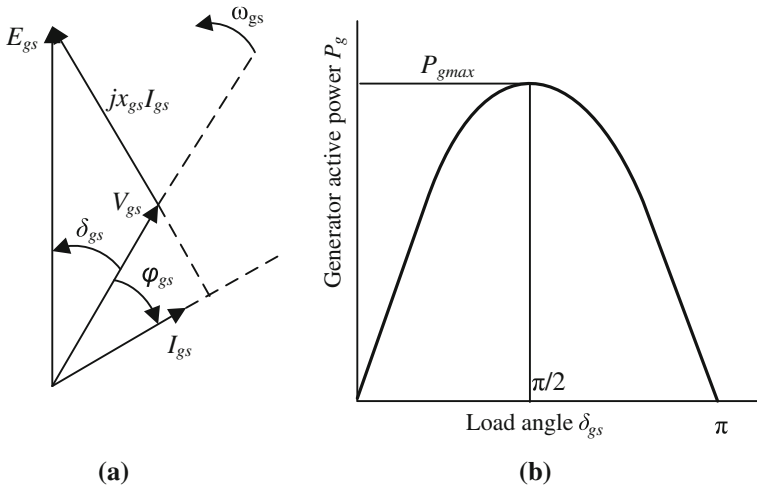
The reactive power is controlled through the generator excitation adjusting emf.  $E_{gs}$  is sensitive to active power changes. Figure 7.6 illustrates grid-connected generator operation.

The active power is controlled by driving torque  $T_{de}(t)$  but reactive power by emf.  $E_{gs}$ . Safe generator operation responds to load angle  $\delta_{gs} < (\pi/2)$ . The load angle variation is caused by driving torque  $T_{de}(t)$  and the generator load torque  $T_{ge}(t)$

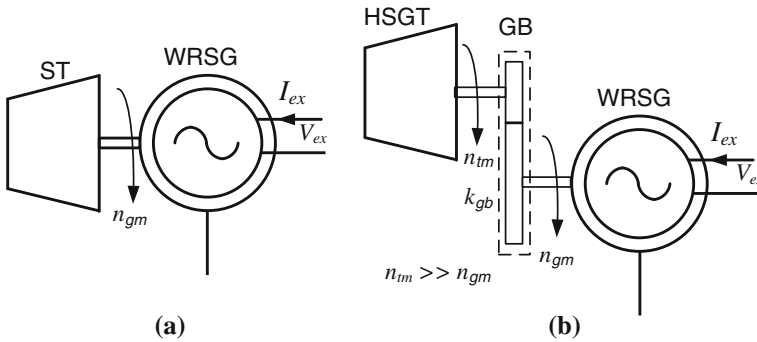
$$\delta_{gs} = \delta_{gsi} + \int_{t_1}^{t_2} \frac{T_{de}(t) + T_{ge}(t) p}{J_{dg} 2} dt \tag{7.9}$$

where  $\delta_{gsi}$  means initial load angle. In steady state condition  $T_{de}(t) + T_{ge}(t) = 0$ .

The steam turbine ST drives turbogenerator WRSB directly (Fig. 7.7a) whereas external combustion gas turbine HSGT (Fig. 7.7b) operates with very high speed  $n_{tm}$  (more than 10,000 rpm.) and to get 50 or 60 Hz voltage a reduction gearbox GB is required.



**Fig. 7.6** Wound rotor synchronous generator connected to power grid: **a** phasor diagram, **b** active power as a function of load angle



**Fig. 7.7** Wound rotor synchronous generator WRSNG driven by turbines: **a** direct drive by steam turbine ST, **b** gear box application for high speed gas turbine HSGT

### 7.1.3 Non-conventional Decoupled Generation Strategy

Decoupled generation provides output voltage data independent of the generator motion in range of speed and voltage [1–3]. It is achieved by splitting generation process into two blocks by application of decoupling power electronic converter as is shown in Fig. 7.8. There are two input quantities: “Rotational speed” and “Excitation”. The generator data are represented by “poles number” and result is “Voltage amplitude”. The “Decoupling converter” produces voltage with demanded quality. There are two stage of generation. At first a generator converts mechanical power to electrical. Produced voltage frequency  $f_{elm}$  and amplitude  $V_{gm}$  are dependent on speed. This voltage is, in second block, adjusted to reference



voltage  $v_{eld}$  by power electronic decoupling converter. In this way, the stage of mechanic–electrical conversion has additional degrees of freedom related to speed, voltage frequency amplitude, and phase. These additional degrees of freedom give opportunity to select different prime movers and optimize their operation especially in relation of primary energy consumption. Moreover used generators may have variable, not standard frequency and amplitude. So they have to be decoupled from load or grid.

The generator voltage is a function of its speed and excitation. Any AC or DC generator can be used. In case of AC generator, the peak of produced voltage is a function of excitation  $f(exc)$

$$V_{gsm} = f(exc)\omega_{gm}\left(\frac{p}{2}\right) \tag{7.10}$$

and frequency

$$f_{elm} = \omega_{gm}\left(\frac{p}{2}\right)\frac{1}{2\pi} \tag{7.11}$$

The number of poles is not limited and the generator frequency may be higher than in generator used in conventional coupled generation. The output voltage, produced by generating system, is independent to the generator motion. In case of sinusoidal output voltage, the output voltage is expressed as

$$v_{eld} = V_{mref} \sin(\omega_{ref}t + \gamma_{ref}) \tag{7.12}$$

and frequency

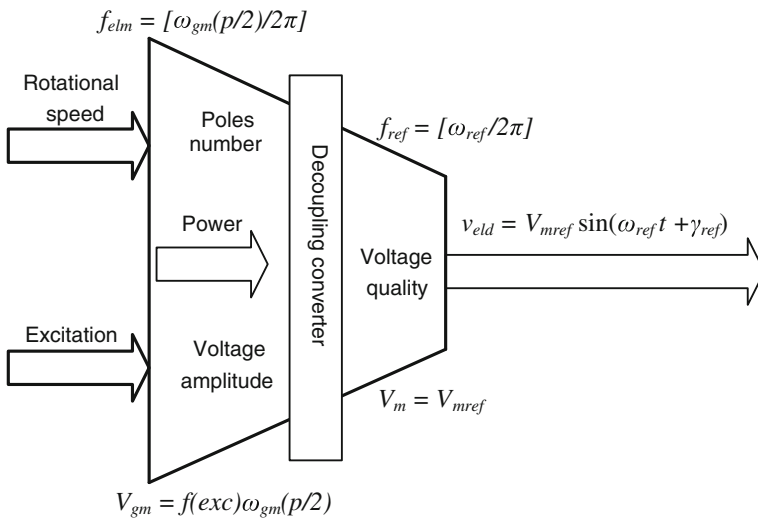


Fig. 7.8 Block diagram of decoupled generation

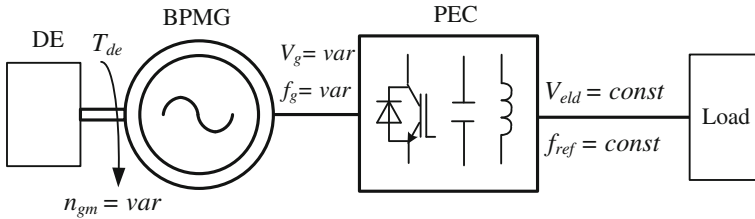


Fig. 7.9 Decoupled generation system—case of island operation

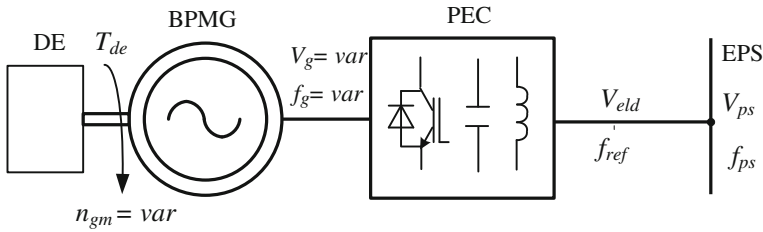


Fig. 7.10 Decoupled generation system—case of power grid connected operation

$$f_{ref} = \omega_{mref} \frac{1}{2\pi} \tag{7.13}$$

where  $V_{mref}$  is adjusted reference peak voltage delivered by power electronic converter,  $\omega_{ref}$  is adjusted angular electrical speed, and  $\gamma_{ref}$  is adjusted arbitrary reference phase angle. Therefore, the decoupled generating system provides fully controllable instantaneous voltage or current.

There are a great number of topologies presenting decoupled generation [4–6]. Figures 7.9 and 7.10 show basic topologies of decoupled generation. Figure 7.9 responds to island whereas Fig. 7.10 to power grid connected operation. The decoupled generation system consists of driving engine DE, brushless permanent magnet generator BPMG Load (Fig. 7.9) or electrical power grid EPS (Fig. 7.10).

A brushless permanent magnet generator BPMG, driven by prime mover DE producing driving torque  $T_{de}$ , operates with variable frequency  $f_g$ , and voltage  $V_g$ , delivers power to power electronic converter PEC. The converter PEC provides demanded quality output voltage  $V_{eld}$  to a separate load (Fig. 7.9) or to electrical power grid EPS (Fig. 7.10).

Grid-connected operation requires frequency  $f_{ref}$  produced by the converter PEC to be equal to power grid frequency  $f_{ps}$ .

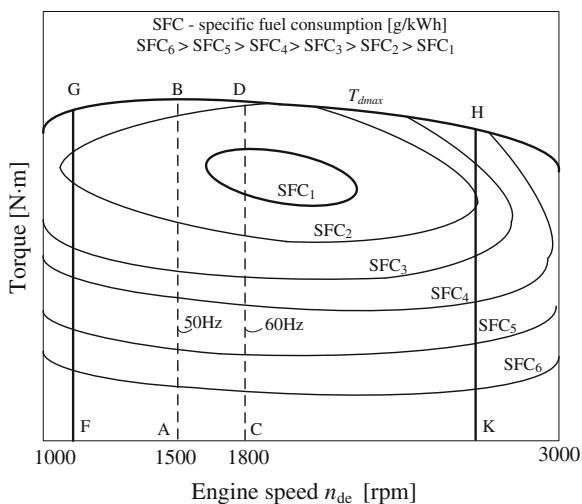
## 7.2 Features of Internal Combustion Engines

### 7.2.1 Torque and Power of Diesel Engines (Specific Fuel Consumption as Function Torque and Speed)

Industrial Internal Combustion Engines (IICE) are used commonly as prime movers of low and medium power fixed speed systems with WRSG. There are two basic groups of Diesel engines. First is dedicated to automotive application. These light weight engines combine high dynamics and fuel savings. Another group is used by industry. They are heavy and robust. Especially, diesel engines that have high efficiency and long life cycle did find wide application in electric power generation. Another great advantage of industrial diesel engine is the ability to produce high driving torque in wide speed range. Therefore, the Diesel engine finds application in variable speed generation systems. Figure 7.11 shows an example of engine maximal driving torque  $T_{dmax}$  as a function of engine speed  $n_{de}$ . Moreover, there is map of specific fuel consumption SFC (g/kWh). The available maximum torque  $T_{dmax}$  is limited by environmental regulations. Here are also presented cases of fixed speed generation responding 50 Hz (1,500 rpm—dot line AB) and 60 Hz (1,800 rpm—dot line CD).

Low specific fuel consumption is a response to the high torque area. When driving torque is low then specific fuel consumption increases significantly. The case of 1,800 rpm (60 Hz) generation is more economical than the case of 1,500 rpm (50 Hz) because it reaches minimum fuel consumption  $SFC_1$ . The variable speed generation has a wide area of operation from low speed (line FG) and below line  $T_{dmax}$  (line GH). According to Eq. (7.3), the given delivered power may be produced by great number of pairs  $n_{de}T_{de}$ . So in the case of variable speed, the pair selection is provided according to low specific fuel consumption.

**Fig. 7.11** Simplified example of maximum torque as function of speed of diesel engine and specific fuel consumption



**Fig. 7.12** Torque, specific fuel consumption, and power of the diesel engine

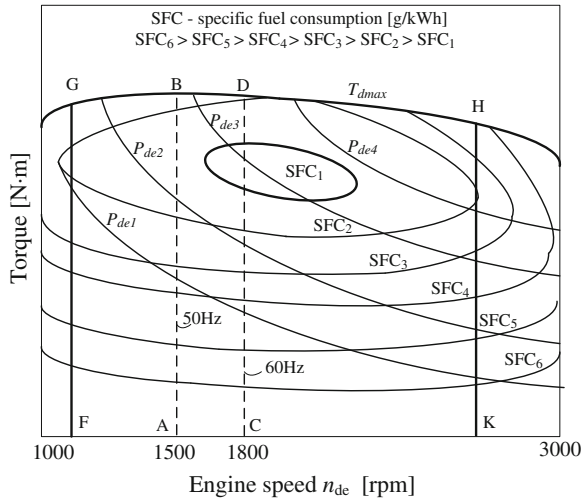


Figure 7.12 shows torque as a function of speed for case of fixed power  $P_{de1} - P_{de4}$ . Depending on the point of operation, the same power needs different amount of fuel. For instance, the power  $P_{de2}$ , at low speed, may be delivered consuming per engine low rate of fuel per kWh (area  $SFC_2$ ) and at high speed high rate of fuel (area  $SFC_3 - SFC_4$ ).

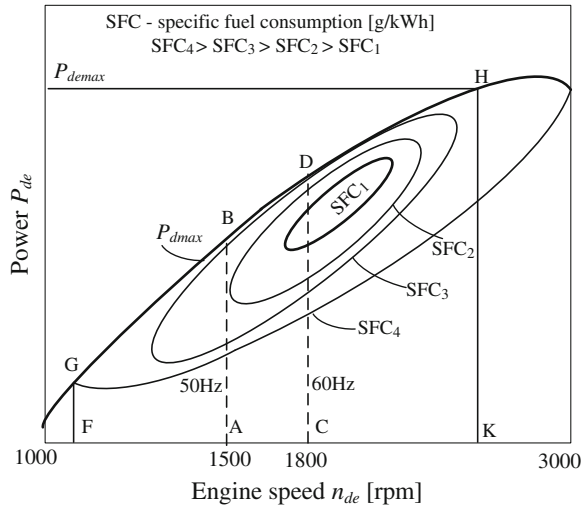
The engine maximum power is proportional to speed (Fig. 7.13). The same engine operating with 1,800 rpm (dot line CD) is producing higher maximum power than at 1,500 rpm (dot line AB). Moreover, when variable speed generation is applied then maximum power  $P_{dmax}$  reaches point H. So the engine is better used than in fixed speed technology because it provides higher power.

The variable speed generation area is marked by lines FGH. Hence, inside this field are low and high fuel consumption areas. Figure 7.14 shows a case when using developed algorithm of speed control technology (dot line STH) delivered power is produced in very economical way.

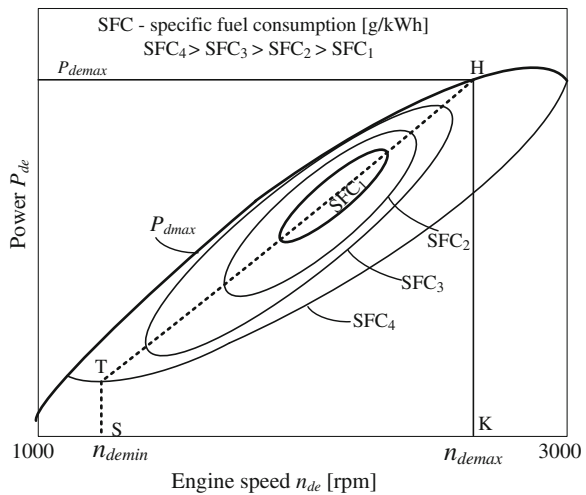
### 7.2.2 Dynamic Features of Internal Combustion Engine

The internal combustion engine ratings are related to well-warmed body and cooling liquid. When cold engine starts, given time is required for the engine to be able to produce torque and power. This delay is important in case of emergency operation, i.e., when instant power is required. The engine torque is produced by burning fuel in piston chamber. Injection of the fuel requires given time. Moreover, the fuel in four stroke engine is burned only in given piston position, i.e., when a mixture of air and fuel get high pressure. The delay in action depends on number of pistons. The worst case appears in a single cylinder engine. In four cylinder engine, this delay time is four times shorter. Controllable speed variation

**Fig. 7.13** Simplified example of maximum power as function of speed of diesel engine and specific fuel consumption



**Fig. 7.14** An example of efficient production of mechanical power by diesel engine

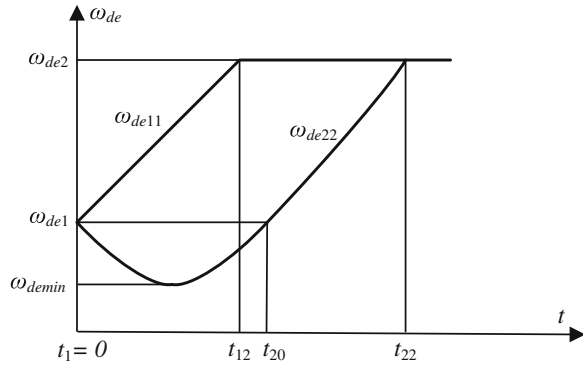


requires the engine torque to be higher than load generator current, i.e.,  $T_{de}(t) + T_g(t) > 0$ . The shaft angular acceleration is a function of the sum of torques and total equivalent inertia  $J_{dg}$  of the engine and the generator

$$\frac{d\omega}{dt} = \frac{T_{de}(t) + T_g(t)}{J_{dg}} \tag{7.14}$$

Both torques are function of time but increase of load torque, produced by generator load, is very short whereas speed response of the engine is much slower. The speed of generating set

**Fig. 7.15** Engine speed response in case of sudden increase in driving torque and when the engine torque building process is longer than zero



$$\omega_{de} = \omega_{de1} + \int_{t_1}^{t_2} \frac{T_{de}(t) + T_{ge}(t)}{J_{dg}} dt \tag{7.15}$$

where  $\omega_{de1}$  is speed at initial state, i.e., for time  $t_1$ . Figure 7.15 shows speed  $\omega_{de11}$  of the engine in theoretical case of sudden increase of engine torque and transient speed  $\omega_{de22}$  when the engine torque building process is longer than zero. Initially, the engine torque is low and the speed  $\omega_{de22}$  drops to  $\omega_{demin}$ . A total time  $t_{22}$  of speed change from  $\omega_{de1}$  to  $\omega_{de2}$  is longer than time  $t_{12}$  responding to case of instant rising torque of engine.

### 7.3 Variable Speed Generation System with Permanent Magnet Generators

#### 7.3.1 Basic Topologies of Generating System

The variable speed generation systems (Figs. 7.16 and 7.17) consists of driving engine DE, brushless permanent magnet generator BPMG, and power electronic converter PEC. The driving engine DE produces driving torque  $T_{de}$  resulting in variable speed  $n_{gm}$ . Figure 7.16 shows a case of autonomous operation whereas the Fig. 7.17 shows grid connected mode.

The power electronic voltage source converter PEC is based on intermediate DC link voltage  $V_{dcg}$  with capacitor  $C_{de}$  as DC energy storage. The generator BPMG produces variable amplitude  $V_{gm}$  and frequency  $f_g$  voltage, which is rectified by input converter Re. The converter Re has to provide the intermediate DC voltage of value higher than peak value of output AC voltage  $V_{acm}$ , i.e.,  $V_{dcg} > V_{acm}$ . A DC-to-AC converter In (i.e., inverter) produces modulated single or three-phase voltage  $V_{pwm}$  with high content of fundamental component. A low pass LC filter Fi removes majority of high frequency of voltage components

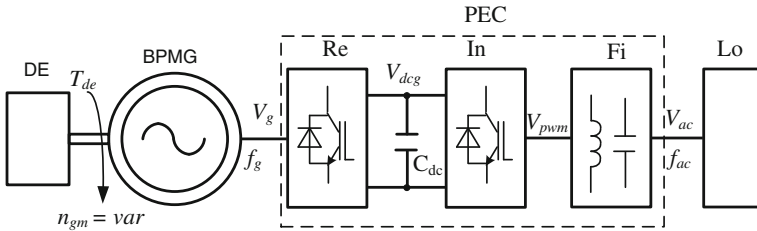


Fig. 7.16 Block diagram of autonomous variable speed generation system

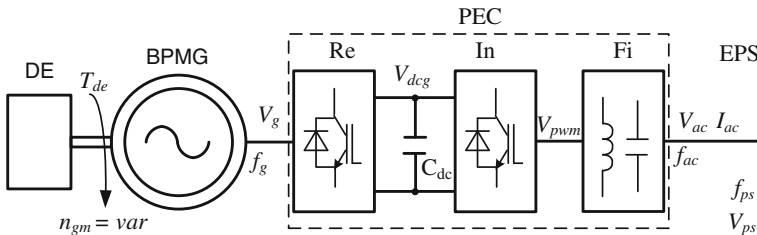


Fig. 7.17 Block diagram of grid-connected variable speed generation system

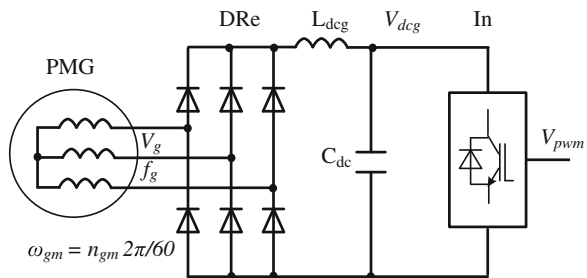
produced by the inverter In. The output AC voltage  $V_{ac}$  (Fig. 7.16) has constant frequency  $f_{ac}$  which is independent of the generator voltage. In the case of grid-connected current controlled mode (Fig. 7.17), the output filter is used to remove harmonics from current delivered to electrical power system EPS [7].

### 7.3.2 Input Rectifier of the Generating System

The DC link output voltage  $V_{dcg}$  of the rectifier DRe (Fig. 7.18) depends on input voltage and applied topology. Figure 7.18 shows very simple diode three-phase bridge rectifier supplied from three-phase generator PMG. This figure is also showing a filter  $L_{dcg} - C_{dc}$  and inverter In.

The generator line-to-line voltage

Fig. 7.18 Topology of the simple diode rectifier supplying inverter



$$v_{ge} = V_{gem} \sin(\omega_{ge}t) = V_{gem} \sin\left(\omega_{gm} \frac{p}{2} t\right) \quad (7.16)$$

or

$$v_{ge} = V_{gem} \sin\left(n_{gm} \frac{2\pi p}{60} t\right) \quad (7.17)$$

where  $V_{gem}$  represents maximum line-to-line voltage,  $\omega_{gm}$  is angular mechanical speed of the generator,  $p$  is number of generator poles, and  $n_{gm}$  is generator mechanical speed.

The voltage

$$V_{gem} = \sqrt{2}k_{\psi}\omega_{ge} = \sqrt{2}k_{\psi}n_{gm} \frac{2\pi p}{60} \quad (7.18)$$

is proportional to the equivalent linkage stator flux factor  $k_{\psi}$ , calculated from generator ratings: rated induced voltage  $V_{gen}$  and rated angular speed  $\omega_{gen}$

$$k_{\psi} = \frac{V_{gen}}{\omega_{gen}} \quad (7.19)$$

The stator rectified DC voltage passes through  $L_{deg} - C_{dc}$  filter and its value varies approximately from

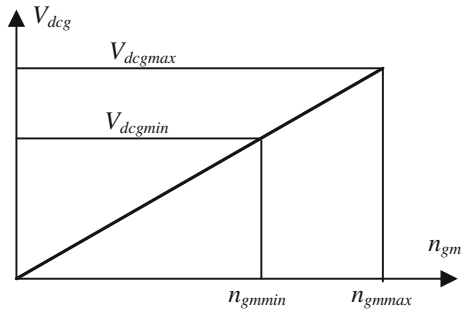
$$V_{dcg} = \frac{3}{\pi} \sqrt{2}k_{\psi}\omega_{ge} = \frac{3}{\pi} \sqrt{2}k_{\psi}n_{gm} \frac{2\pi p}{60} \quad (7.21)$$

to

$$V_{dcg} = V_{gem} \quad (7.22)$$

The rectified DC link voltage  $V_{dcg}$  is proportional to rotational speed  $n_{gm}$  as is shown in Fig. 7.19. The speed varies from  $n_{gmmin}$  to  $n_{gmmax}$  and then at the minimum speed the rectified voltage has to be  $V_{dcgmin} > V_{acm}$  where the  $V_{acm}$  means maximum of output inverter AC voltage.

**Fig. 7.19** Rectifier output voltage supplying inverter





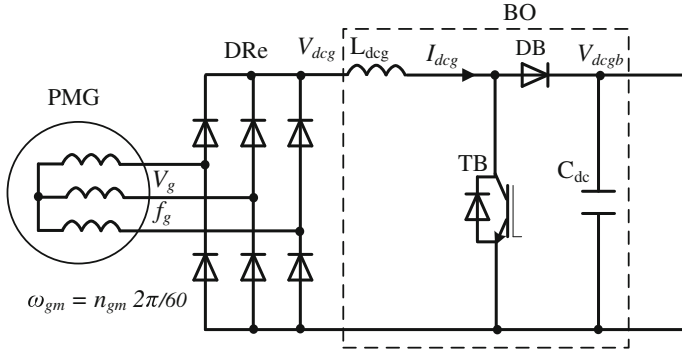


Fig. 7.20 Rectifier—booster supplying the inverter

Any increase of speed results in rising DC link voltage over demanded  $V_{dcmin}$  level. Therefore such topology may be applied to low voltage sources and not to wide speed range. For instance, in low single phase voltage say  $120 V_{rms}$ , the minimum DC link voltage is close to 200 V. Then increase of speed even twice, in relation to minimum speed, results in DC link voltage  $V_{dcgmax}$  increase to 400 V. In such topology can be used low voltage transistors. However in a three-phase  $400 V_{rms}$ , the double increase of speed brings DC link voltage  $V_{dcgmax}$  from 650 to 1,300 V and it requires high-voltage inverter transistors. This makes generation system practically very expensive and then not economical.

When the three-phase rectifier is equipped in an additional DC-to-DC converter BO operating as a booster (Fig. 7.20) then rectified input minimum voltage  $V_{dcg}$  may be lower than minimum voltage  $V_{dcgb}$  required by the inverter.

The booster BO operates very efficiently when the ratio (Fig. 7.21) output to input voltage

$$2 \geq \frac{V_{dcgb}}{V_{dcg}} > 1 \tag{7.23}$$

According to Eq. (7.23), the efficient speed range as ratio maximum to minimum speed is approximately 2.

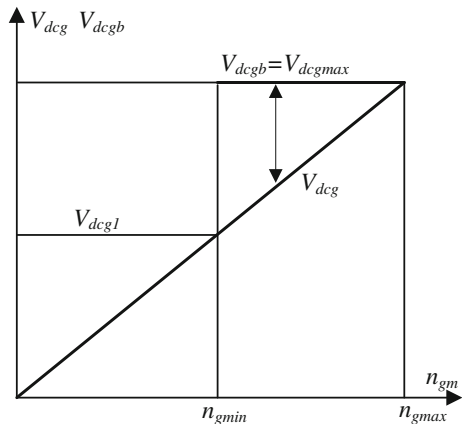
In case of continuous generator rectified load current  $I_{dcg}$ , the generator current has trapezoidal waveform and the generator current fundamental component is displaced, versus generator-induced phase voltage, by angle

$$\varphi_g = \arccos\left(1 - \frac{I_{dcg}}{2I_{gsc}}\right) \tag{7.24}$$

where  $I_{gsc}$  is maximum value of line-to-line generator short circuit current.

Usually, in the range below generator rated current  $I_{dcgn} \ll I_{gsc}$  generator power factor  $\cos\varphi_g \cong 1$  and the displacement may be neglected. For such a case, the generator produces load torque  $T_{ge}$  proportional to the rectified current.

**Fig. 7.21** Rectifier and output boosted voltage supplying inverter



$$T_{ge} = \sqrt{2} \frac{3p}{\pi} k_{\psi} I_{dcg} \tag{7.25}$$

Therefore, the DC-to-DC converter BO controls not only DC link voltage but also generator torque. By setting maximum generator current, the generator torque is limited.

The six-pulse rectifier Re produces square wave generator current, which besides the fundamental, comprises also higher frequency components as 5, 7, 13, and 17 harmonics. Applying a three-phase AC-to-AC booster ACB, as is shown in Fig. 7.22, instead of the DC booster, it is possible to provide sinusoidal waveform of the generator current. There are three bidirectional switches ACB1, ACB2, and ACB3 [6] made with diode bridge and controlled transistors T1, T2, and T3. Each switch operates as AC voltage booster and AC generator current controller. The boosters are dedicated to given generator phase operated independently.

If the generator inductance is very low, then to assure low components of switching harmonics, another inductive filter  $L_{acg}$  is required. The generator current is practically in-phase with the generator phase voltage. Therefore, the torque produced by the generator is proportional to the generator current. The booster ACB is used to control the generator current and to provide sufficient DC link voltage required by the inverter.

The diode rectifiers (Figs. 7.18, 7.20, 7.22) transfer the power from AC-to-DC side. So there is no option for generating system to absorb the transient power coming from DC load and AC side.

The variable speed generating systems represent energy storage in moving parts of the generator and driving engine. In case of rotating parts with moment of inertia  $J_{dg}$  and angular speed  $\omega_{gm}$ , stored energy  $W_{dg}$  is

$$W_{dg} = \frac{J_{dg} \omega_{gm}^2}{2} \tag{7.26}$$

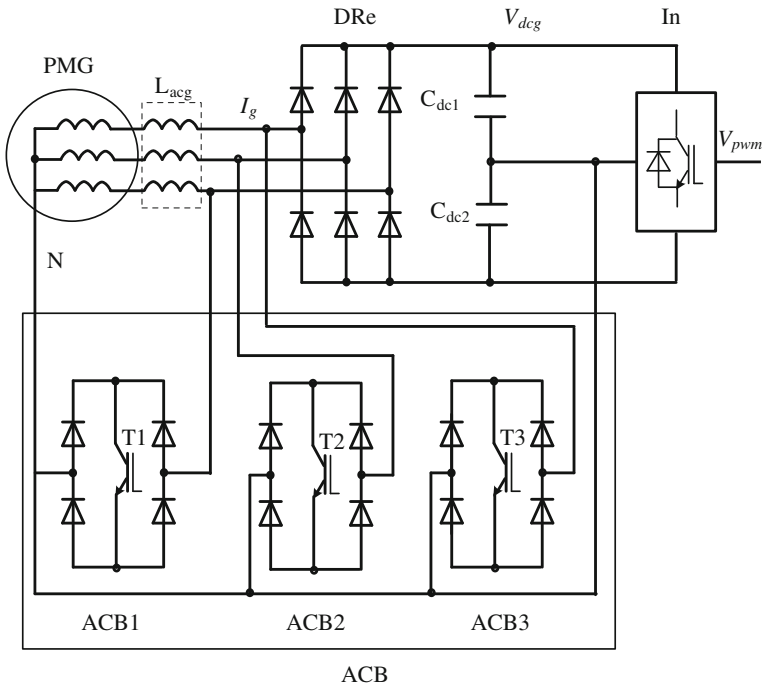


Fig. 7.22 Controlled rectifier providing sinusoidal generator current

When the mechanical speed of generation system changes from  $\omega_{gm1}$  to  $\omega_{gm2}$ , the energy stored in moving parts varies as follows:

$$\Delta W_{dg} = \frac{J_{dg}(\omega_{gm2}^2 - \omega_{gm1}^2)}{2} \tag{7.27}$$

If the generator speed increases, then stored energy is rate is positive. As in diode-based rectifiers (Figs. 7.18, 7.20, 7.22) provide unidirectional power flow from generator to DC link the speed increase may be caused only by driving engine.

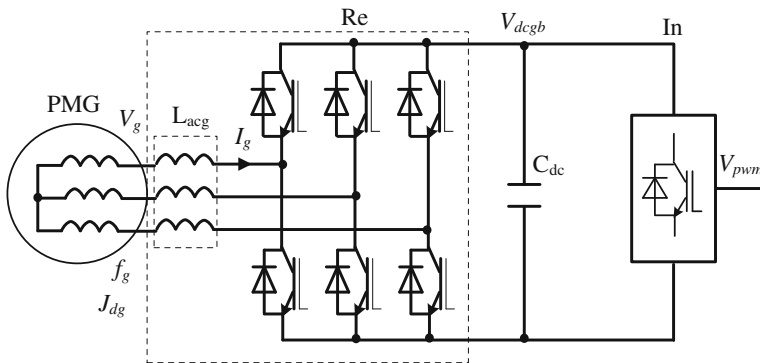
Generation system, using commonly known active bridge rectifier shown in Fig. 7.23, controls bidirectional power flow between generator and DC link.

Power  $P_g$  delivered by the generator

$$P_g = \sqrt{3}V_g I_g \cos \varphi_g \tag{7.28}$$

is controlled by the transistor converter, which adjusts generator current  $I_g$  and its phase angle  $\varphi_g$ .

The transistor converter Re draws a sinusoidal current from the generator and maintains DC link voltage  $V_{dcgb}$  on the level required by the inverter In. An additional option of the bidirectional rectifier application is motor operation of the



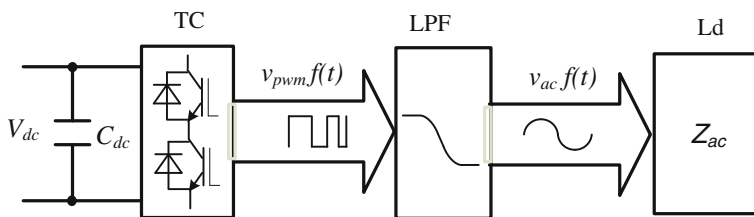
**Fig. 7.23** Bidirectional rectifier providing sinusoidal generator current

PMG machine. This ability may be used for instance for diesel engine or gas turbine starting facility. Another application of bidirectional converter Re is pumping storage where the electrical machine has to operate as motor or generator. Operation of the rectifier Re with sinusoidal current of the generator results in low power losses in the generator. However, the stator inductance of the permanent magnet generator is usually very low and then the PWM control of the current results in significant content of harmonics. Therefore to reduce these harmonics, an additional choke  $L_{acg}$  is used.

### 7.3.3 Conversion DC-to-AC Sinusoidal Voltage

The DC voltage produced by the rectifier Re (Fig. 7.16) is converted to AC by the DC-to-AC inverter In and filter Fi. The inverter comprises of power electronic switches TC (Fig. 7.24) and the low pass filter LPF built with inductor and capacitor.

The converter TC produces square wave high frequency pulse width modulated (PWM) AC voltage  $v_{pwm}f(t)$  and then the low pass filter LPF reduces switching frequency components and delivers sinusoidal voltage  $v_{ac}f(t)$ . A load  $L_d$  is a common load of impedance  $Z_{ac}$ . Examples of single-phase converters with filters



**Fig. 7.24** Block diagram of the voltage source inverter with output low pass filter

and loads are shown in Figs. 7.25 and 7.26. Half-bridge topology (Fig. 7.25) is very simple but requires DC supply system containing two DC voltage sources  $V_{dc1}$  and  $V_{dc2}$  that additionally have to fulfill condition  $V_{dc1} = V_{dc2}$ .

When only one DC voltage source is available then full bridge topology (Fig. 7.26) is used.

The PWM controlled converter TC (Fig. 7.26) [8] provides voltage, whose fundamental component is a function of modulation index  $m_{ac}$  and DC link voltage  $V_{dc}$

$$V_{acm} = m_{ac} V_{dc} \tag{7.29}$$

where amplitude modulation index is defined as

$$m_{ac} = \frac{V_{acref}}{V_c} \tag{7.30}$$

and  $V_{acref}$  is amplitude reference signal and  $V_c$  is amplitude of carrier signal.

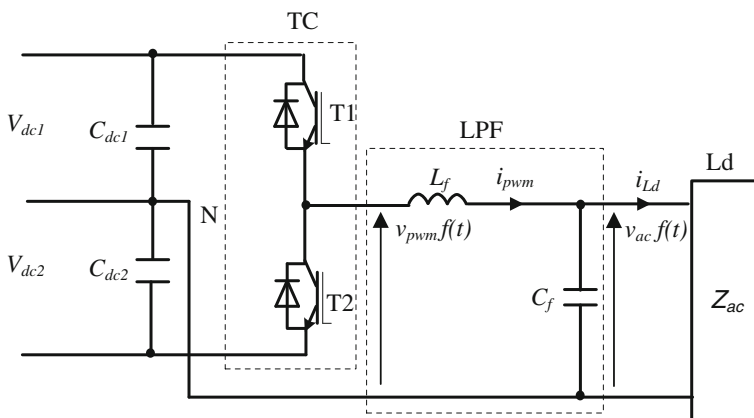
When the PWM method, based on symmetrical triangle wave as the carrier and sinusoidal reference is applied, then output voltage  $v_{pwm}$  contains components:

- fundamental frequency  $f_{ac1}$ ,
- high frequency harmonic, that result from the switching carrier frequency  $f_{sc}$ ,
- sideband harmonics  $f_{sb}$ ,
- very high frequency harmonics at MHz range.

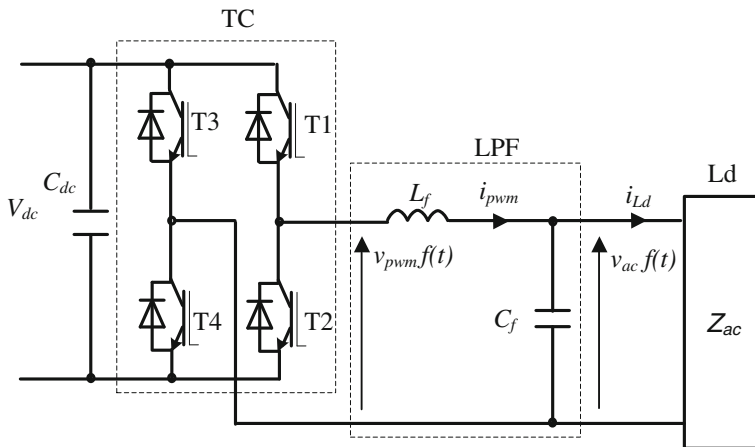
The sideband harmonics with frequency  $f_{sb}$  are function of switching carrier frequency  $f_{sc}$

$$f_{sb} = nf_{sc} \pm mf_{ac1} \tag{7.31}$$

where  $m = 0, 2, 4 \dots$  and  $n = 1, 3, 5 \dots$



**Fig. 7.25** Single-phase half-bridge transistor converter TC and second order LC low pass filter LPF



**Fig. 7.26** Single-phase H-bridge power electronic switches and second-order low pass LC filter LPF

The second-order low pass filter voltage transfer function

$$G_{Vtf}(s) = \frac{V_{ac}(s)}{V_{pwm}(s)} \tag{7.32}$$

and for fixed filter inductance  $L_f$ , resistance  $R_f$ , and capacitance  $C_f$

$$G_{Vtf}(s) = \frac{Z_{ac}(s)}{s^2 L_f C_f Z_{ac}(s) + s[C_f R_f Z_{ac}(s) + L_f] + R_f + Z_{ac}(s)} \tag{7.33}$$

In case of no load operation, i.e., for  $Z_{ac} \rightarrow \infty$  the transfer function

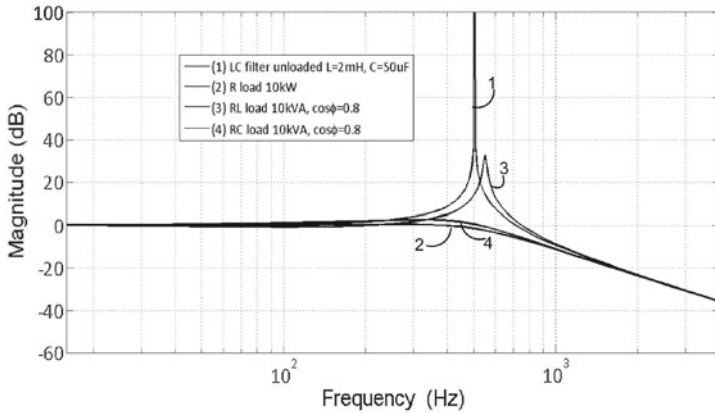
$$G_{Vtf}(s) = \frac{1}{s^2 L_f C_f + s R_f C_f + 1} \tag{7.34}$$

The filter resonance frequency

$$f_{ire} = \frac{1}{2\pi\sqrt{L_f C_f}} \tag{7.35}$$

The load  $Z_{ac}(s)$  has significant impact on the transfer function and then on stability of the output voltage. Frequency characteristic is obtained for  $s = j\omega$ . Figure 7.27 shows an example of characteristics described by transfer function (7.33) of different types of loads (calculated case is related to 10 kW and 10 kVA load and resonant frequency 503.55 Hz).

The resistive R or resistive-capacitive RC loads result in characteristic flattening and they improve voltage stability.



**Fig. 7.27** An example of transfer function characteristic of 10 kW/10 kVA load and filter resonant frequency 503.33 Hz

The  $L_f$ – $C_f$  filter is second order unit (7.38) that has own oscillation frequency  $f_{\text{fire}}$  (7.35) which may deform the output voltage. Considering not loaded filter amplitude characteristic (Fig. 7.27 trace 1), then three frequency bands are distinguished: a low frequency pass band from 0 to approximately  $0.1f_{\text{fire}}$ , filter resonance proximity from  $0.1f_{\text{fire}}$  to  $10f_{\text{fire}}$ , and damping band (40 dB/decade at frequencies higher than  $10f_{\text{fire}}$ ). In order to ensure stable operation of the inverter, the demanded output fundamental frequency  $f_{\text{ac1}}$  must be placed in the pass band but all other harmonics must be placed in the damping band.

Therefore to keep stability of the output voltage, operating with frequency  $f_{\text{ac1}}$  (for instance 50 or 60 Hz), the resonance  $f_{\text{fire}}$ , and carrier (switching) frequency  $f_{\text{sc}}$  of the two-level inverter must fulfill conditions

$$f_{\text{ac1}} \ll f_{\text{fire}} \ll f_{\text{sc}} \pm 2f_{\text{ac1}}. \quad (7.36)$$

In practice, the resonance frequency  $f_{\text{fire}}$  is set more than a decade above fundamental frequency produced AC voltage. The switching frequency  $f_{\text{sc}}$  has to be more than a decade over resonance frequency. Hence the filter resonance frequency, selected as 505.33 Hz (in Fig. 7.27), is almost suitable for 50 Hz but is too low for 60 Hz output. Thus the filter is suitable for two voltage systems. The filter inductance is produced by a choke made from coil and high frequency material core. In case of the core saturation, the inductance decreases. It results in increase of resonant frequency (7.35).

Topology of the inverter providing three-phase three-wires power supply is shown in Fig. 7.28. The inverter is made from three-phase transistor bridge PT3 and three filters.

When the inverter is dedicated to three-phase four-wires distribution system, then neutral wire is required. In such a case, the three-phase system is made from three independent single-phase inverters as is shown in Fig. 7.29.

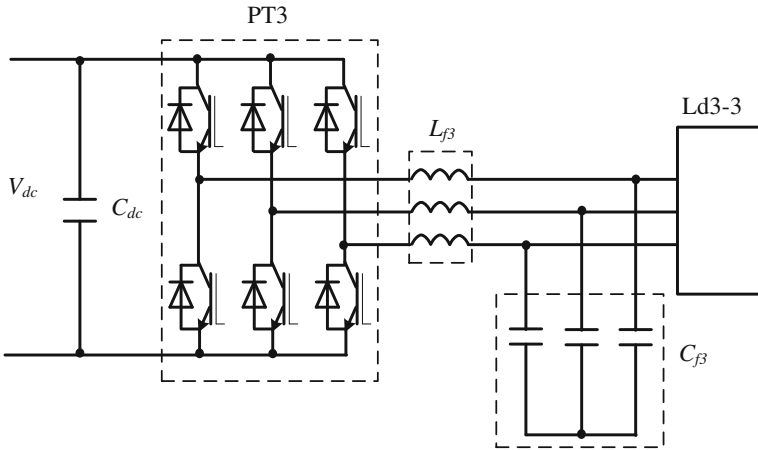


Fig. 7.28 Three-phase three-wires two-level bridge inverter

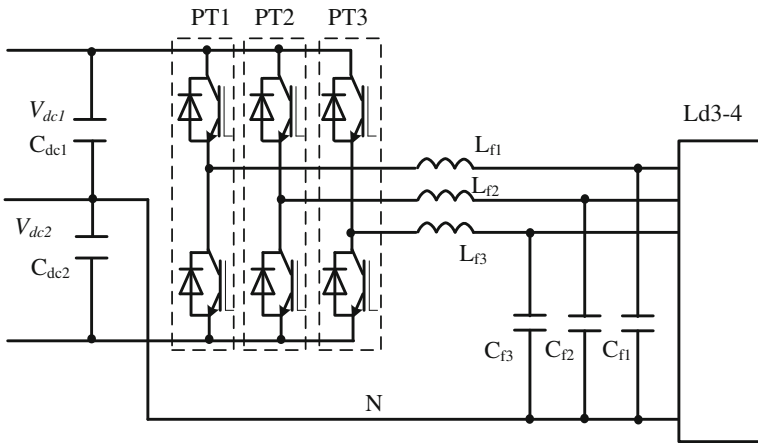


Fig. 7.29 Three single-phase two-level inverters (four wires output)

The three converters PT1, PT2, and PT3 operate independently providing AC voltage in case of symmetrical and asymmetrical loads. There are two DC voltage sources and it is required  $V_{dc1} = V_{dc2}$ . The DC supply voltages equality is demanded in rated and overload conditions.

The two-level converters produce PWM voltage  $v_{pwm}$  which has positive and negative components even of creating positive amplitude. Three-level converter provides positive pulses for positive sign of amplitude and negative for opposite sign. So the three-level converters have lower content of harmonics, better efficiency, and may operate with lower switching frequency. Figures 7.30 and 7.31 shows topology examples of three-level DC-to-AC converters. The conventional single-phase converter, made from transistors T1 and T2 (Fig. 7.30) is equipped in



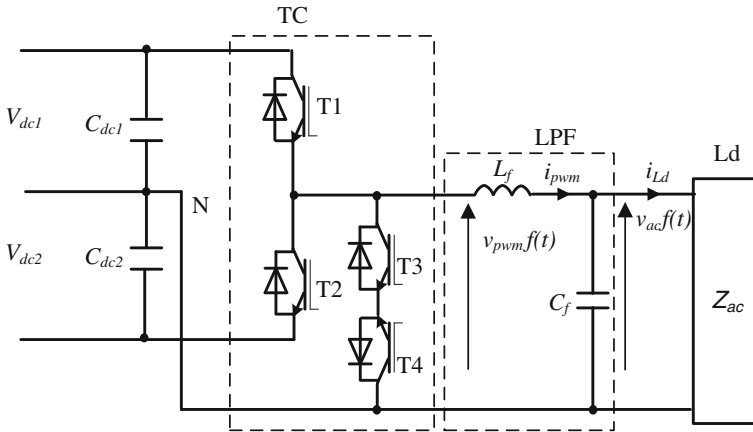


Fig. 7.30 Single-phase bidirectional switch neutral point clamped (BSNPC) three-level inverter

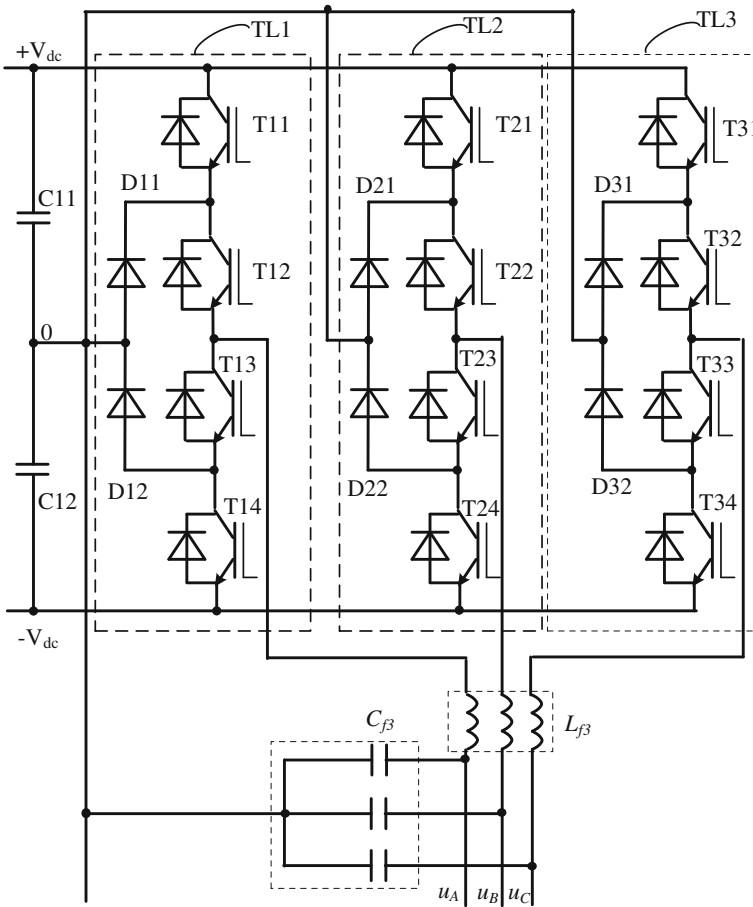
transistors T3 and T4 operating as a bidirectional switch [8]. The bidirectional switch acts as a freewheel system.

Figure 7.31 shows three-phase bidirectional switch neutral point clamped (BSNPC) three-level inverter. It consists of three legs TL1, TL2, and TL3 supplying load through three-phase LC filter. The neutral voltage (0 voltage) is made only by capacitor divider (capacitors C11 and C12). There is a strong impact of the loads on the capacitors voltage and usually  $|+V_{dc}| \neq |-V_{dc}|$ . Such a system is dedicated for low and high voltages but only to symmetrical loads arrangements [8].

### 7.3.4 Control of Variable Speed Generation Systems with Permanent Magnet Generator

Strategy of fuel saving speed control of diesel engine [9] is shown in Fig. 7.32. At no load operation, the speed of engine and coupled generator is set to minimum  $n_{gmin}$  (point A). Load increase results initially in passing the generator load torque  $T_g$  from point A toward its maximum marked by point B. Such increase of load torque moves engine point of operation from high specific fuel consumption  $SFC_6$  to low  $SFC_2$ . Therefore, efficiency of the engine increases significantly. To keep low fuel consumption, the load torque  $T_g$  has to follow line  $T_g = T_{gmax}$  (from B to C), i.e., to pass the region  $SFC_1$  of the lowest specific fuel consumption. To provide this high efficiency operation, the engine-generator set has change its speed from  $n_{gmin}$  to  $n_{gmax}$ . The load torque is kept below maximum engine torque, i.e.,  $T_{dmax} + T_{gmax} > 0$ .

The transient speed change depends on engine torque  $T_{dmax}(t)$ , generator torque  $T_{gmax}(t)$ , and moment of inertia of moving components  $J_{dg}$



**Fig. 7.31** Three-phase bidirectional switch neutral point clamped (BSNPC) three-level inverter

$$\omega_{gm} = \omega_{gm1} + \int_{t_1}^{t_2} \frac{T_{dmax}(t) + T_{gmax}(t)}{J_{dg}} dt \tag{7.37}$$

(The generator torque is negative but to make easy torques comparison the Fig. 7.32 graphic presentation usually shows  $T_{gmax}$ ).

Figure 7.33 shows basic topology of the variable speed generation. The Diesel engine DE drives brushless permanent magnet generator BPMG that produces variable frequency and amplitude  $V_g$  voltage. The rectifier Re transfers energy from the generator to the DC link and stabilizes voltage  $V_{dcgb}$ . The inverter In converts the DC voltage to PWM AC voltage  $V_{PWM}$  which is smoothed by the filter Fi. A generator system controller SCS is produced using digital signal processor DSP.

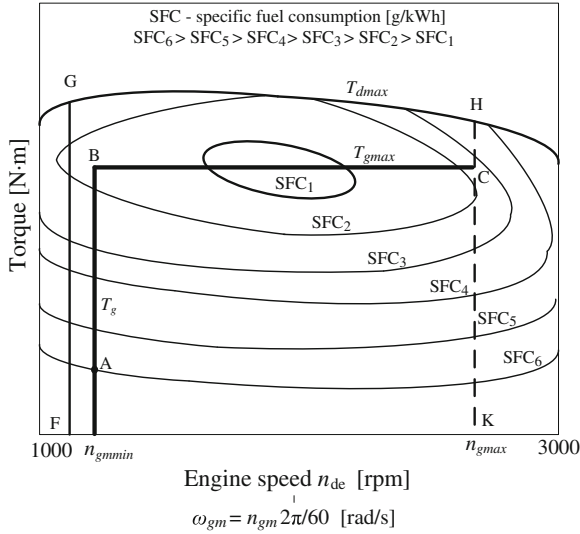


Fig. 7.32 Speed-torque control strategy

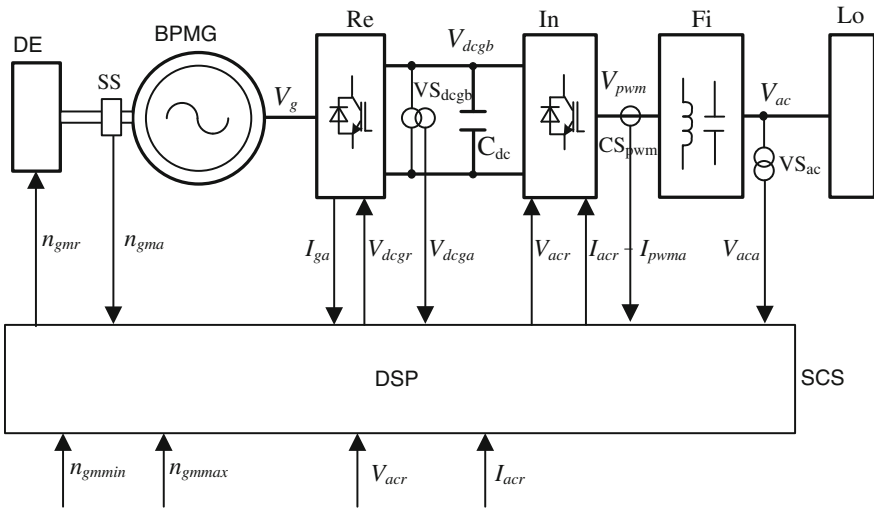


Fig. 7.33 Main blocks and control of variable speed generation

To provide variable speed operation (Fig. 7.33), according to concept shown in Fig. 7.32 a number of information signals is required. The speed sensor SS delivers actual speed signal  $n_{gma}$ . To control of the load torque, the generator actual current signal  $I_{ga}$  is needed. This signal is usually obtained from DC rectified current sensor. The DC link stable voltage is required to produce PWM AC voltage with low harmonics content. So the voltage sensor  $VS_{dcgb}$ , which

delivers actual DC voltage  $V_{dcgba}$ , is applied. To protect transistors of the inverter In against overload, a feedback signal  $I_{pwm}$ , representing load current, is produced by current sensor  $CS_{pwm}$ . The control of the output symmetrical AC voltage requires very precise voltage sensor  $VS_{ac}$ , which delivers feedback signal of the actual voltage  $V_{aca}$ . An example of simple variable speed generation system topology and control is shown in Fig. 7.34 [1]. The system operates according the concept of fuel saving presented in Fig. 7.32 (lines ABC) and Fig. 7.14 (lines STH). The generator torque is controlled by adjusting rectified generator current  $I_{dcg}$  (7.25) by current controller  $RI_{dcg}$ . The DC link voltage  $V_{dcgb}$  is controlled by voltage regulator  $RV_{dcb1}$  and by a voltage regulator  $RV_{dcb2}$ . The controller  $RV_{dcb1}$  provides generator reference current  $I_{dcgr}$  to current regulator  $RI_{dcg}$ . The rectified generator current  $I_{dcg}$  is adjusted by switching the TB transistor of the DC-to-DC boost converter. Another voltage regulator  $RV_{dcb2}$  keeps DC link voltage by adjusting speed of the engine. The  $RV_{dcb2}$  regulator produces reference speed signal  $n_{gmr}$  to speed regulator  $Rn$ . The regulator  $RV_{dcb1}$  receives reference signal  $V_{dcg1r}$  and actual voltage signal  $V_{dcgba}$  whereas the regulator  $RV_{dcb2}$  receives reference signal  $V_{dcg2r}$  and actual voltage  $V_{dcgba}$ . The two DC link voltage reference signals are different and  $V_{dcg1r} > V_{dcg2r}$ . This gives priority operation of the voltage regulator  $RV_{dcb1}$ . The  $RV_{dcb1}$  regulator produces reference signal  $I_{dcgr}$  delivered to the current regulator  $RI_{dcg}$ . In case of high load, the current regulator  $RI_{dcg}$  produces maximum rectified current of the

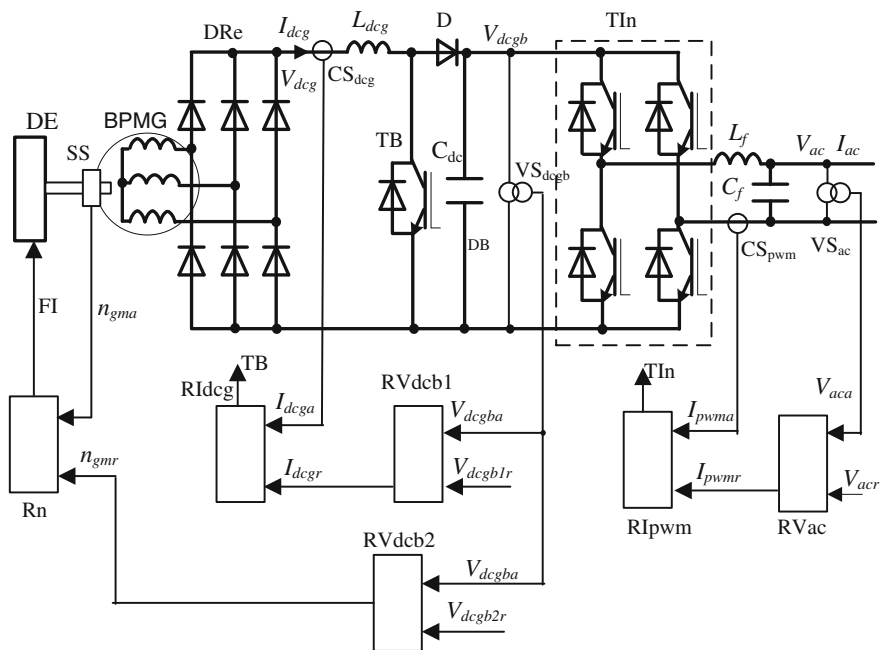


Fig. 7.34 Control of the variable speed generation system with permanent magnet generator

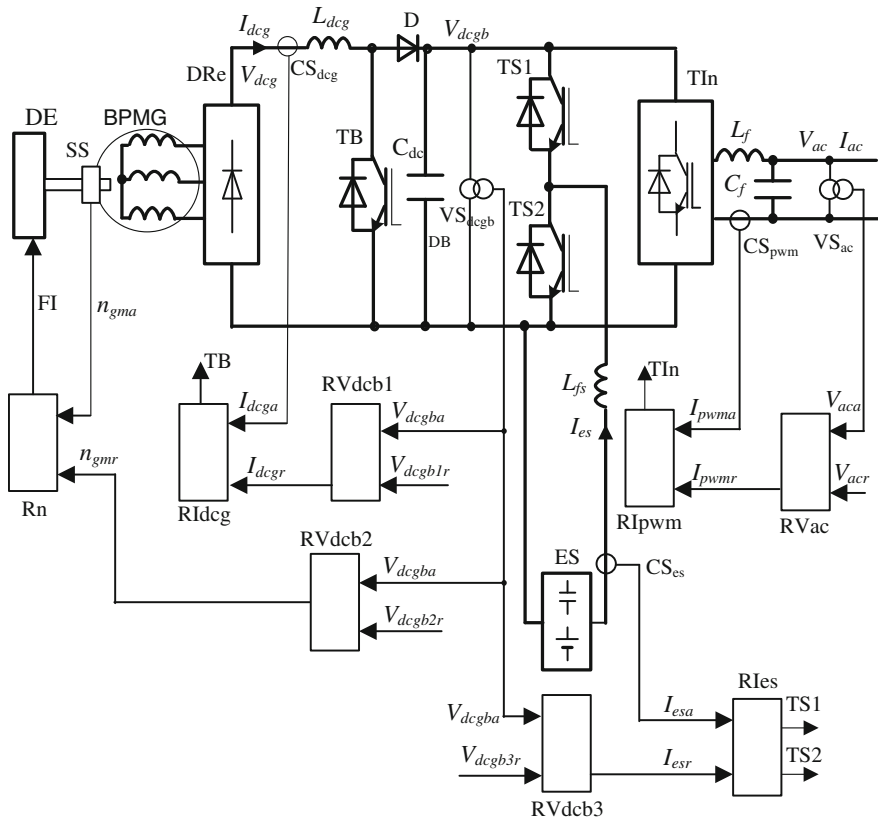
generator. When the load still increases, the DC link voltage drops to value responding reference voltage  $V_{dcg2r}$  and the voltage regulator RVDCb2 produces reference signal  $n_{gmr}$  resulting in speed increase. Therefore in case of low load, the speed of the generating set is low and constant. This load is depicted by line AB on the Fig. 7.32. When increasing load results in maximum reference current  $I_{dcgrmax}$  the DC link voltage drops and is maintained according to reference signal  $V_{dcgb2r}$  by the engine acceleration. This state of operation is shown in the Fig. 7.32 by the line BC. The maximum speed reference signal  $n_{gmr}$  is set to  $n_{gmrmax}$  that responds to maximum speed  $n_{demax}$  on the Fig. 7.14. At the point H (Fig. 7.14), the engine produces highest power that is not available by conventional generation systems operating with 1,500 or 1,800 rpm.

The AC output voltage  $V_{ac}$  is controlled by voltage regulator RVac and the inverter current regulator RIpwm. The maximum load current is limited by reference signal  $I_{pwmr}$ . The output voltage is sensed by a voltage sensor VS<sub>ac</sub> but the inverter actual current signal is provided by current sensor CS<sub>pwm</sub>. The power produced by the generating set, operating with variable speed, is proportional to speed. However, the speed does not rise instantly whereas changes of load may have step nature. So in case of significant step load, the DC link voltage drops and results in AC voltage fluctuation. To improve quality of the produced AC voltage, an additional energy storage is applied as is shown in Fig. 7.35 [9]. The energy storage ES (supercapacitor or battery) is connected to the DC link through DC-to-DC reversible converter made from transistors TS1-TS2. The energy storage delivers power to the DC link in case of low DC link voltage, i.e., below the reference  $V_{dcgb3r}$ . The three reference DC link voltages fulfil condition

$$V_{dcgb3r} < V_{dcgb2r} < V_{dcgb1r}. \quad (7.38)$$

A voltage regulator RVdcb3 keeps the DC link voltage on the level close to  $V_{dcgb3r}$  producing reference current  $I_{esr}$ . The current regulator Rles receives actual current signal  $I_{esa}$  from current sensor CS<sub>es</sub>. When the DC link voltage is higher than  $V_{dcgb3r}$ , then the energy storage ES is charged from the DC link.

Another advantage of the generation system, shown in Fig. 7.35, is case of application of energy storage as only energy source [1]. When the load is low or generator requires maintenance the battery delivers power. This option may be treated as UPS (Uninterruptible Power Supply) facility. When the generation system supplies regenerative loads, then energy is transferred from AC-to-DC link and then the energy storage is charged. In case of regenerative loads connected to generating system shown in Fig. 7.34, the energy is delivered to the DC link and its voltage increases and may destroy switches and capacitors. To avoid unwanted increase of the DC link voltage a discharging resistor RB is applied as is shown in Fig. 7.36. To control the DC link voltage by discharging system another regulator RVdcb4 is used. So if the DC link voltage  $V_{dcgba}$  is higher than reference  $V_{dcgb4r}$ , the voltage regulator RVdcb4 activates transistor TB and then a conducting resistor RB dissipates the DC link energy.



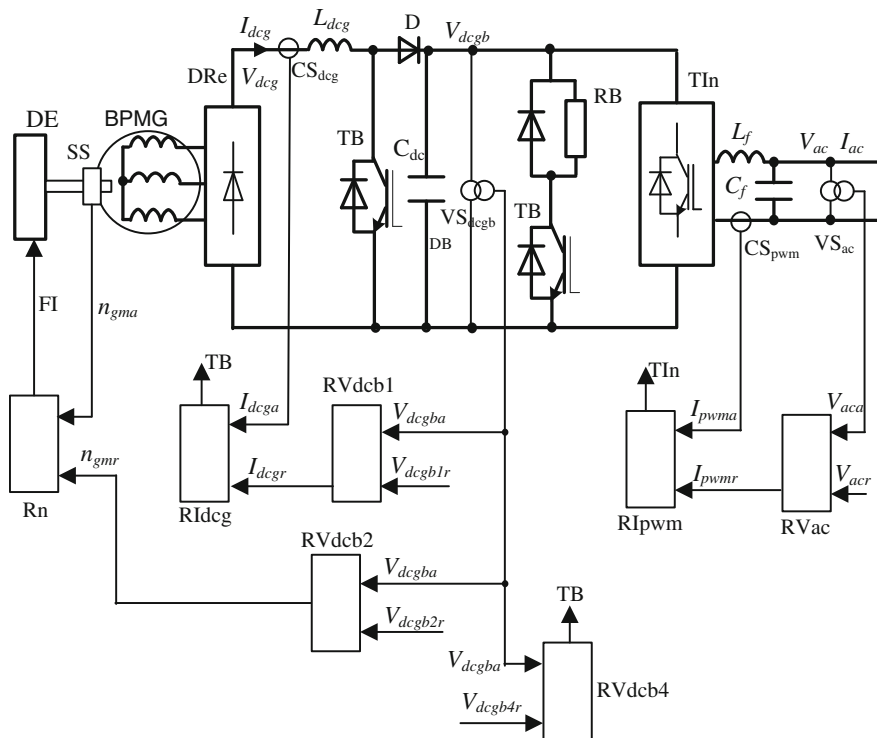
**Fig. 7.35** Control of the variable speed generation system with permanent magnet generator and energy storage

Hybrid system combining discharging resistor (Fig. 7.36) and energy storage (Fig. 7.35) damps transient oscillations of the energy systems, accept regenerative energy, provides UPS features, and then it results in high reliability.

### 7.3.5 Grid Connection of Variable-Speed Generation Systems with Permanent Magnet Generator

The variable-speed generation system, shown in Fig. 7.37, has two mode of operation: autonomous (island) or grid connected [7]. The island operation is described in Sect. 7.3.4. Connection to electrical power system EPS requires different method of control of the output inverter In.

The island operation is based on production of output AC voltage with arbitrary selected amplitude, frequency and phase. To get grid connected mode, a current



**Fig. 7.36** Control of the variable speed generation system with permanent magnet generator and discharge circuit

control is required. In single or three phase with neutral cable, the current is “injected” to each phase separately (Fig. 7.37). For the grid single voltage

$$v_{ps} = V_{psm} \sin(\omega_{ps}t) \tag{7.39}$$

where  $V_{psm}$  is voltage amplitude and  $\omega_{ps}$  is voltage angular speed, the current delivered by generating system is oriented to the grid voltage by adjustable phase angle  $\varphi$

$$i_{ac} = I_{acm} \sin(\omega_{ps}t + \varphi) \tag{7.40}$$

and the current amplitude  $I_{acm}$  is fully adjustable also.

A voltage-current controller RViac receives two reference signals  $V_{acr}$  and  $I_{acr}$ . When the voltage signal  $V_{acr}$  is active, then the system operates in island mode. For the case of active current reference signal  $I_{acr}$  starts grid-connected mode. A voltage sensor  $VS_{ps}$  produces signal for a process of synchronization that is provided by the RViac controller. The input current reference signal  $I_{acr}$  responds to Eq. (7.40) and is converted to current controller RIpwm reference signal  $I_{pwmrg}$ . There is a significant difference between power flow control by the inverter

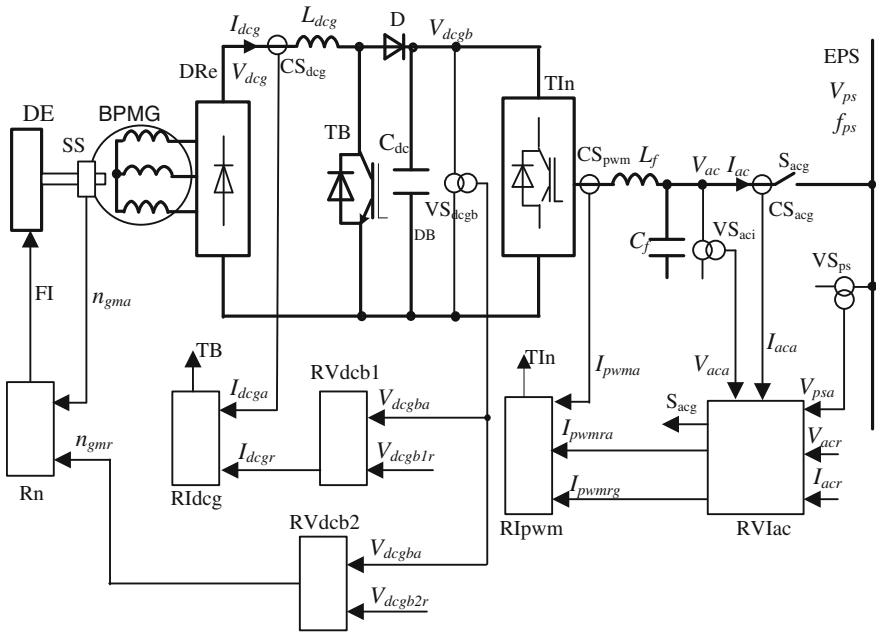


Fig. 7.37 Control of the variable-speed generation system connected to electrical power system EPS

(Fig. 7.37) and synchronous generator (Fig. 7.6) and Eq. (7.9). The inverter control is instant whereas the conventional synchronous generator has to change speed caused by the driving torque. Control (production) of demanded reactive power is also instant. However, the variable speed generation system to produce more active power needs to accelerate or to draw energy from energy storages.

## 7.4 Variable-Speed Generation Using Doubly Fed Induction Generator

### 7.4.1 Basic Topologies of Grid Connected and Standalone DFIG

Doubly fed induction generator (DFIG) is a rotating three-phase transformer, whose stator side is connected to the electric power system EPS (Fig. 7.38a) or supplies an isolated load (Fig. 7.38b). The rotor side is supplied by the electronic converter of rated power reduced in relation to the rated power of the machine and to the total power of the whole system. Rotor converter RC is responsible for control of the stator current  $i_s$ , or voltage  $u_s$ , depending on the grid connection or



standalone operation, through the adjustment of the amplitude and frequency of the three-phase rotor current  $i_r$ . The grid side converter GC is responsible for stabilization of the voltage in a DC link capacitor  $C_{dc}$  in both operation modes. The direction of stator current  $i_s$  in Fig. 7.38 agrees with the widely accepted mathematical model, in which the magnetization current equals the sum of the rotor and stator currents flowing into the machine. This assumption originates from the motor operation of the machine used at first in a drive systems, and for generator operation the stator current has a negative sign. This is the reason of direction of other currents marked in Fig. 7.38, such as grid current  $i_g$ , stator seen load current  $i_o$ , or the generator load current  $i_{ld}$ .

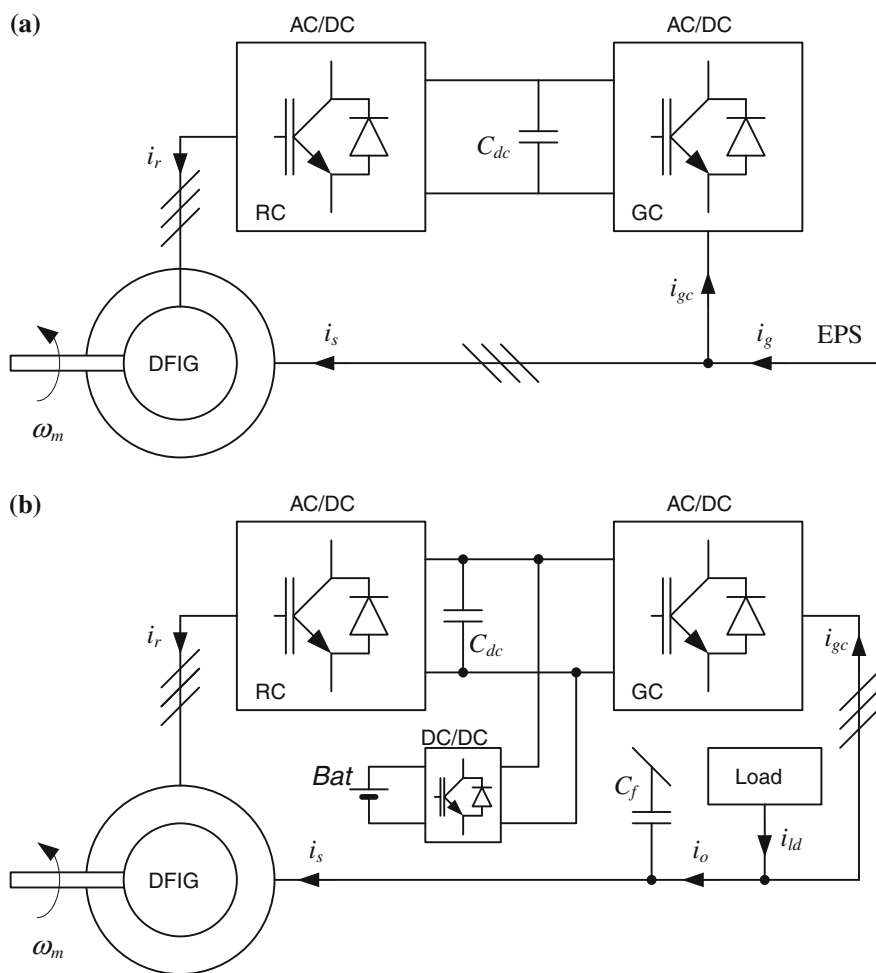


Fig. 7.38 DFIG-based variable-speed power systems, **a** grid connected and **b** standalone

To obtain autonomous operation of induction generator, the initial excitation is needed. In the case of internal combustion engine, the initial energy for preliminary charging of the DC link of converter can be taken from the engine starting battery Bat (Fig. 7.38b).

The main advantage of the DFIG system is related to the speed limitation of the prime mover. In a limited range of speed, the slip power, for which the power converter is designed, is reduced proportionally to the speed range around the synchronous speed. In the case of internal combustion engine, a limited range of the mechanical speed is natural, therefore the application of DFIG is justified. The rotor terminal rms voltage  $U_r$  is proportional to the speed range and its value equals to

$$U_r = |s| U_m \quad (7.41)$$

where  $U_m$  is a rated rotor voltage specified for motionless rotor, while  $s$  is the slip.

If the rotor to stator voltage ratio equals

$$\eta = \frac{1}{|s|_{\max}} \quad (7.42)$$

the maximum value of the rotor terminals voltage, in the limited speed range, is equal to the stator terminals voltage. This way, the rotor and stator converter current and voltage parameters are equal, and symmetrical back-to-back converter can be applied. For the limited speed range, the rated power of converter equals

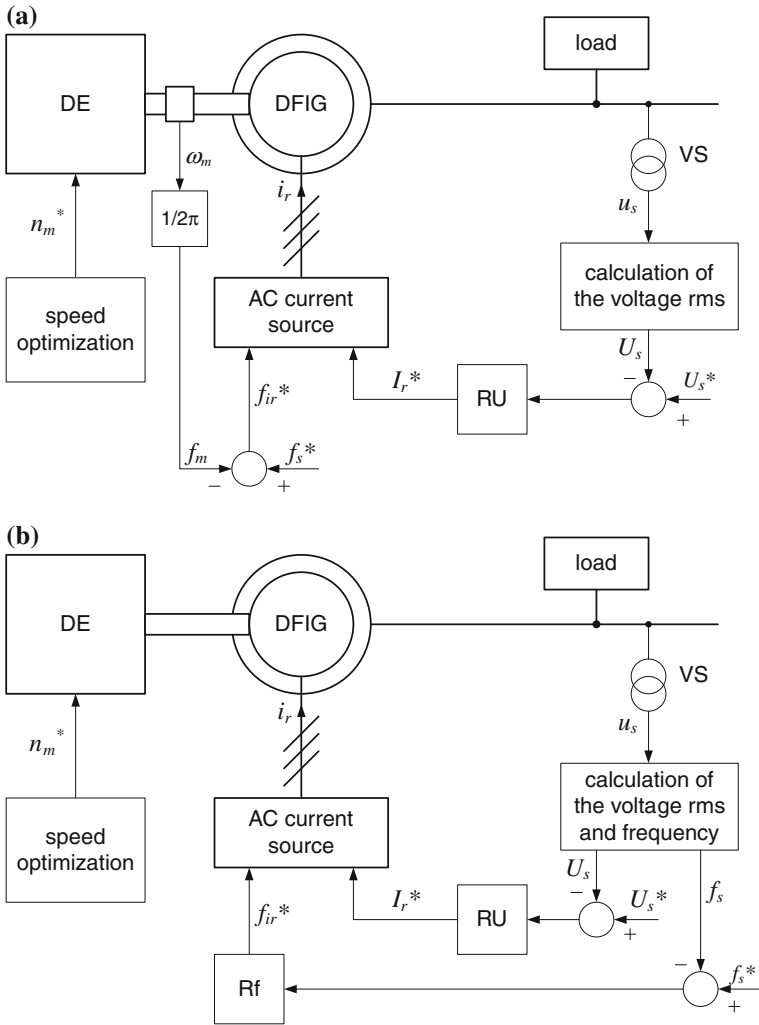
$$P_r = |s|_{\max} P_{s \max} \quad (7.43)$$

The narrower speed range around synchronous value means lower rated power of rotor converter. For wind turbines, typical range is  $\pm 0.33$  of synchronous speed, what means the rated power of back-to-back converter equals 0.33 of stator rated power, that is 0.25 of the total power of the DFIG system. For multi-MW range hydropower generation systems, with DFIG supplied from the rotor side by thyristor cycloconverter, the speed range equals to  $\pm 0.1$  around synchronous value and the converter power equals to 10 % of the stator power.

Operation principles of the doubly fed induction machine are analogous to the principles of DC excited wound rotor synchronous machine [10]. The exception, which determines the advantages of the DFIG and allows the variable speed operation, is that the rotor has three-phase windings. The sum of frequency  $f_m$ , connected with the mechanical speed  $\omega_m$ , and frequency  $f_{ir}$  of the rotor current  $i_r$ , equals the stator voltage frequency  $f_s$ . Adjustment of the rotor current frequency  $f_{ir}$  to the instantaneous mechanical speed  $\omega_m$  to obtain fixed sum of the frequencies, introduces the control of the driving engine speed to be independent on the output voltage frequency.

The idea of stator voltage frequency control by the use of speed sensor is shown in Fig. 7.39a. The frequency of the stator voltage is controlled in the open loop, through the rotor current frequency  $f_{ir}$  obtained as a difference between reference stator voltage frequency  $f_s^*$  and the frequency  $f_m$  connected with a mechanical

speed. Controller RU of the stator voltage rms value  $U_s$  provides a reference signal of the rms value  $I_r^*$  of the rotor current  $i_r$  to obtain reference rms value  $U_s^*$  of the stator voltage  $u_s$ . A very simple idea of the stator voltage rms control without the speed and rotor position is shown in Fig. 7.39b. The method is similar to the control of the stator voltage of standalone WRSG, where frequency controller adjusts the rotor speed to maintain fixed stator frequency. The actual stator voltage frequency  $f_s$  can be calculated based on the zero crossing of the stator voltage sine waveform.



**Fig. 7.39** Simple idea of stator voltage control in standalone DFIG power system, **a** with a rotor speed sensor and **b** with a frequency controller

The difference in relation to the synchronous generator is, that the frequency controller Rf provides a reference signal for the rotor current frequency  $f_{ir}^*$  instead of the reference mechanical speed like in a synchronous generator. Thus, the mechanical speed can be controlled independently. In both cases, shown in Fig. 7.39, a stator voltage phase is not controlled.

Similarly to the scalar control, a sensor-based and sensorless vector control methods of the stator voltage can be obtained. Vector control provides better features of power electronics systems due to the control of instantaneous value of the controlled variables. In the case of DFIG, the control system may require some parameters of the machine, to obtain high quality of the generated voltage or delivered power. Therefore, the space vector model of the doubly fed induction machine and the synthesis of the control method based on this model are described in the next subsections.

### 7.4.2 Doubly Fed Induction Generator Model

Mathematical model of doubly fed induction machine is described by the following equations

$$\vec{u}_s = R_s \vec{i}_s + \frac{d\vec{\psi}_s}{dt} + j\omega_x \vec{\psi}_s \quad (7.44)$$

$$\vec{u}_r = R_r \vec{i}_r + \frac{d\vec{\psi}_r}{dt} + j(\omega_x - \omega_m) \vec{\psi}_r \quad (7.45)$$

$$\vec{\psi}_s = L_s \vec{i}_s + L_m \vec{i}_r \quad (7.46)$$

$$\vec{\psi}_r = L_r \vec{i}_r + L_m \vec{i}_s \quad (7.47)$$

where  $\vec{u}$ ,  $\vec{i}$ ,  $\vec{\psi}$  represent the voltage, current, and flux vectors, respectively,  $R$  and  $L$  represent the resistance and inductance, “s” and “r” indexes describe the variables and parameters of the stator and rotor side, respectively,  $L_m$  represents magnetizing inductance,  $\omega_x$  is an angular speed of the frame, in which the vector model is described, and  $\omega_m$  is the rotor angular speed scaled by the number of poles pairs. Mechanical equation is neglected, as not important in the stator voltage and stator power control design. In the case of standalone operated system, additional equation of stator equipped with filtering capacitors  $C_f$  is introduced:

$$\vec{i}_s = -C_f \frac{d\vec{u}_s}{dt} + \vec{i}_o - j\omega_x C_f \vec{u}_s \quad (7.48)$$

where  $\vec{i}_o$  is a current vector of the load seen on the stator side, representing the sum of physical load current  $\vec{i}_{ld}$  and the current taken or delivered by the grid side converter  $\vec{i}_{gc}$ . Taking into account the resistive character of the physical load,

which is enough assumption for the control design of fundamental harmonics of the stator voltage, and the sinusoidal stator voltage and grid converter current, it can be written the Eq. (7.49)

$$i_o = -\frac{u_s}{R_o} \quad (7.49)$$

in which the  $R_o$  is a resistance representing equivalent resistive load seen from the stator side.

Voltage-current steady state equations of DFIG, with a rotor current as the variable decided about the machine behavior, can be derived:

$$\bar{U}_s = R_s \bar{I}_s + j\omega_s L_s \bar{I}_s + j\omega_s L_m \bar{I}_r \quad (7.50)$$

$$\bar{I}_s = \bar{I}_o - j\omega_s C_f \bar{U}_s \quad (7.51)$$

where  $\bar{U}_s, \bar{I}_s, \bar{I}_r, \bar{I}_m$  are the phasors of the stator voltage, stator current, rotor current, and magnetizing current, respectively, and the  $\omega_s$  is an angular synchronous speed, which is a speed of rotation of the vector variables. Neglecting the stator resistance, the relation between currents phasors in a steady state can be described by Eq. (7.52)

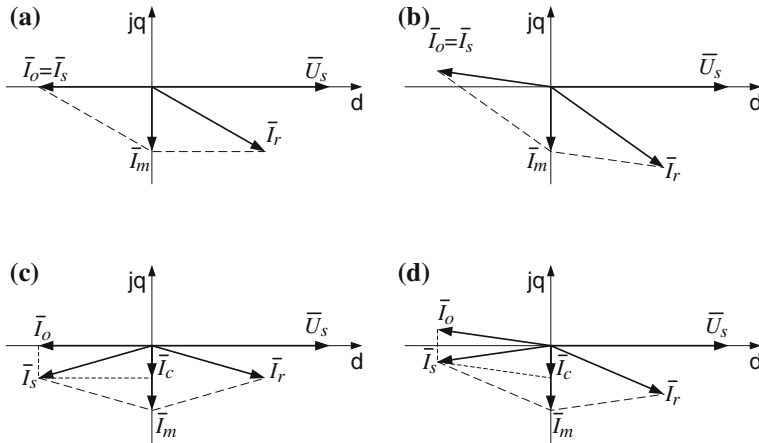
$$\bar{I}_r = \bar{I}_m (1 - \omega_s^2 L_s C_f) + \frac{L_s}{L_m} \bar{I}_o \quad (7.52)$$

Neglecting the stator leakage inductance, it can be seen in Eq. (7.52), that the rotor current  $\bar{I}_r$ , needed to obtain the reference stator voltage, equals the sum of load current  $\bar{I}_o$ , and part of magnetizing current uncompensated by stator-connected filtering capacitors. Neglecting the stator resistance and leakage inductances, the simplified vector diagram can be used for representation of the machine steady state.

Stator output voltage is perpendicular to the magnetizing current. Figure 7.40 presents the machine vector diagram without (Fig. 7.40ab) and with (Fig. 7.40cd) the stator connected filtering capacitors  $C_f$ . For the cases without stator side filtering capacitors, stator current equals the load current, and the magnetization current is fed from the rotor side. For the case of inductive load (Fig. 7.40bd), higher negative  $q$  component of the rotor current vector is required to compensate the inductive load current.

Stator-connected filtering capacitors  $C_f$  compensating part of the magnetization current by  $i_c$  current, provide reduction of  $q$  component of the rotor current. The filtering capacitor  $C_f$  should not overcompensate the machine's reactive power, calculated for the frequency  $f_m$  related to the maximum possible mechanical speed  $\omega_{\text{mmax}}$ :

$$C_f < \frac{1}{4\pi^2 f_m^2 L_s} \quad (7.53)$$



**Fig. 7.40** Stator voltage and rotor current vector diagrams of DFIG system **(ab)** without and **(cd)** with filtering capacitor, and loaded by **(ac)** resistive and **(bd)** inductive load

Simplified method of filtering capacitor selection can be verified on the basis on the mathematical model. Based on the model Eqs. (7.44–7.48), the dynamic model equations of a double fed induction generator can be derived. A general model of a dynamic system is described by set of Eq. (7.54)

$$\begin{cases} \dot{x} = Ax + Bu \\ y = Cx + Du \end{cases} \quad (7.54)$$

in which  $u$ ,  $x$ , and  $y$  are the vectors of input, state, and output variables, respectively, and  $A$ ,  $B$ ,  $C$ , and  $D$  are the state, input, output, and transition matrices. For a model of standalone DFIG the vectors and matrices are described by Eqs. (7.55–7.62) derived from (7.44 to 7.48)

$$x = [i_{sd} \quad i_{sq} \quad i_{rd} \quad i_{rq} \quad u_{sd} \quad u_{sq}]^{-1} \quad (7.55)$$

$$u = \begin{bmatrix} u_{rd} \\ u_{rq} \end{bmatrix} \quad (7.56)$$

$$y = \begin{bmatrix} u_{sd} \\ u_{sq} \end{bmatrix} \quad (7.57)$$

$$A = \frac{1}{k} \begin{bmatrix} -R_s L_r & k\omega_s + \omega_m L_m^2 & R_r L_m & \omega_m L_r L_m & L_r & 0 \\ -k\omega_s - \omega_m L_m^2 & -R_s L_r & -\omega_m L_r L_m & R_r L_m & 0 & L_r \\ R_s L_m & -\omega_m L_s L_m & -R_r L_s & k\omega_s - \omega_m L_r L_s & -L_m & 0 \\ \omega_m L_s L_m & R_s L_m & -k\omega_s + \omega_m L_r L_s & -R_r L_s & 0 & -L_m \\ -\frac{k}{C_f} & 0 & 0 & 0 & -\frac{k}{R_o C_f} & k\omega_s \\ 0 & -\frac{k}{C_f} & 0 & 0 & -k\omega_s & -\frac{k}{R_o C_f} \end{bmatrix} \quad (7.58)$$

$$B = \frac{1}{k} \begin{bmatrix} -L_m & 0 \\ 0 & -L_m \\ L_s & 0 \\ 0 & L_s \\ 0 & 0 \\ 0 & 0 \end{bmatrix} \quad (7.59)$$

$$C = \begin{bmatrix} 0 & 0 & 0 & 0 & 1 & 0 \\ 0 & 0 & 0 & 0 & 0 & 1 \end{bmatrix} \quad (7.60)$$

$$D = \begin{bmatrix} 0 & 0 \\ 0 & 0 \end{bmatrix} \quad (7.61)$$

$$k = L_s L_r - L_m^2 \quad (7.62)$$

The other type of description of the dynamic system with the use of the A, B, C, and D matrices from the model is a matrix of transmittances  $G(s)$  calculated in general way with Eq. (7.63).

$$G(s) = [C(sI - A)^{-1}B + D] \quad (7.63)$$

in which  $G(s)$  is a matrix of transmittances describing the influence of the rotor voltage vector components on the stator voltage vector components, in a frame rotating with an angular speed  $\omega_s$ ,  $s$  is a Laplace operator, and  $I$  is an identity matrix.

Selecting a rotor voltage vector components as the input signals and the stator voltage vector components as the output, a four elements  $G(s)$  matrix ( $2 \times 2$ ) can be derived (7.64), in which the elements correspond to the adequate transmittances

$$G(s) = \begin{bmatrix} G_{dd}(s) & G_{dq}(s) \\ G_{qd}(s) & G_{qq}(s) \end{bmatrix} = \begin{bmatrix} \frac{u_{sd}(s)}{u_{rd}(s)} & \frac{u_{sd}(s)}{u_{rq}(s)} \\ \frac{u_{sq}(s)}{u_{rd}(s)} & \frac{u_{sq}(s)}{u_{rq}(s)} \end{bmatrix} \quad (7.64)$$

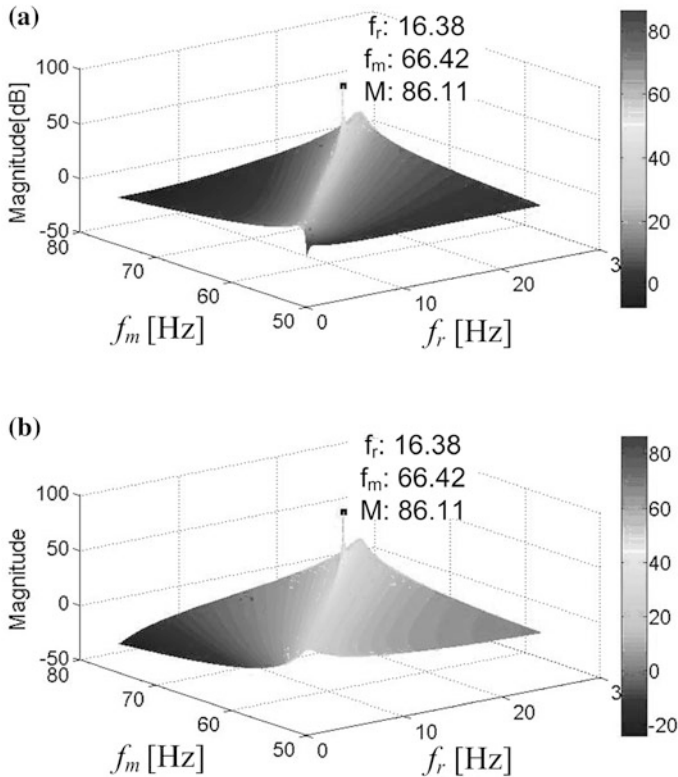
The transmittances placed on the same diagonal are, in this particular case, identical. Based on the matrix of transmittances, a Bode characteristics can be drawn and the resonant frequencies can be determined similarly to the LC filter characteristics shown in the Fig. 7.27.

The basic selection of the capacitor should be done for unloaded system, similarly to the case of power inverter with the LC filter, because, neglecting the case of energy return from the load, this is the worst case of operation due to the smallest damping ratio of the system. In this case, the equivalent load resistance  $R_o$  goes to infinity.

The parameters of 2.2 kW slip-ring induction generator used for laboratory verification, described in a next sections, are as follows:  $R_s = 1.7 \Omega$ ,  $R_r = 2.72 \Omega$ ,  $L_s = 230 \text{ mH}$ ,  $L_r = 230 \text{ mH}$ , and  $L_m = 210 \text{ mH}$ . For filtering capacitor  $C_f = 25 \mu\text{F}$ , a three-dimensional Bode plots made in a Matlab-Simulink have been

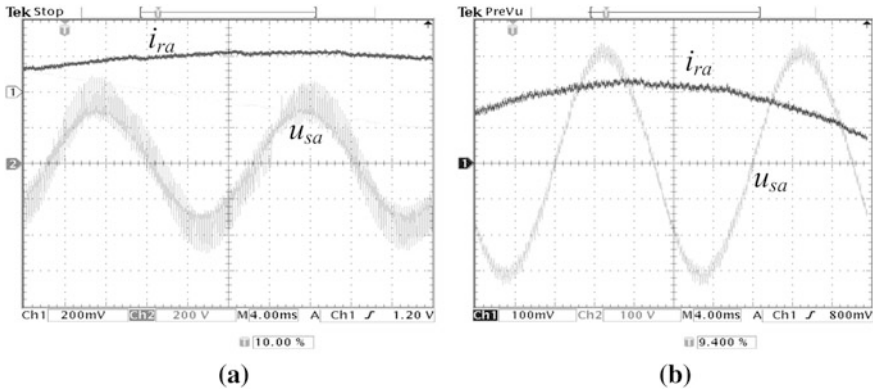
obtained. A capacitance of filtering capacitors was selected on the basis of Eq. (7.53) for maximum assumed rotor speed, that is 1.33 of the synchronous speed  $\omega_s$ . The Bode characteristics, for above parameters, are shown in Fig. 7.41, where simultaneous dependence of the magnitude from the rotor voltage frequency and from the frequency corresponded to the mechanical speed, is presented. In the Fig. 7.41a,b, a resonant peak is observed at the maximum mechanical frequency ( $1.33 f_s$ ) for the rotor voltage frequency equal to 16.6 Hz ( $0.33 f_s$ ). A resonance, seen in the characteristics, at the assumed maximum rotor speed proves that the simplified method of capacitor selection is sufficiently accurate.

In a synchronously rotated dq frame, in which the mathematical model of standalone DFIG is described, such a frequency of the rotor current (16.67Hz) is related to the force rotating together with a rotor. In practice this force, even if it is not intentionally generated by the control system, may originate from the remanence flux, responsible for uncontrolled excitation, and the DC component of the rotor current caused by DC offsets of the current sensors. At such a visible



**Fig. 7.41** A three-dimensional magnitude characteristics of the stator voltage vector components showing the resonance points for **a** transmittances  $G_{dd} = G_{qq}$ , **b** transmittances  $G_{dq} = G_{qd}$





**Fig. 7.42** Oscillograms presenting stator voltage and rotor current waveforms of **a** unloaded, and **b** fully loaded standalone operated DF IG without filtering capacitor—laboratory tests

resonance, even small amount of DC component in the rotor flux may cause instability of the system and the capacitor has to be selected adequately, to move the resonance point beyond the assumed range of the rotor speed.

Figure 7.42 presents the rotor current and voltage waveforms of the standalone DF IG without filtering capacitors. It can be seen, that the stator voltage is distorted by the switching frequency harmonics. The distortions are higher for no load operation (Fig. 7.42a), than for loaded generator (Fig. 7.42b). The stator voltage with improved quality will be shown in the Sect. 7.4.4, where stator voltage control method of standalone DF IG is described.

### 7.4.3 Power Flow Control of Grid-Connected DF IG

DF IG structure is known mainly from wind energy conversion systems, in which control of the stator voltage is usually used only for synchronization. The reason is, that the wind turbines, are almost always connected to the grid and are poor standalone power sources. Several methods, which has been analyzed for grid-connected operation, including grid voltage oriented vector control, stator flux oriented vector control [11], direct power control DPC [12], and direct torque control DTC [13] were described detail [14]. Basic control method of grid-connected DF IG in the frame connected with stator (grid) voltage is shown in Fig. 7.43. Stator power is controlled using an instantaneous power theory, where  $p$  and  $q$  power components are calculated using stator voltage and current vectors (7.65–7.66)

$$p = \frac{3}{2} (u_{sz}i_{sz} + u_{s\beta}i_{s\beta}) = \frac{3}{2} (u_{sd}i_{sd} + u_{sq}i_{sq}) \tag{7.65}$$

$$q = \frac{3}{2} (-u_{sz}i_{s\beta} + u_{s\beta}i_{sz}) = \frac{3}{2} (-u_{sd}i_{sq} + u_{sq}i_{sd}) \tag{7.66}$$

where  $u_{sz}$ ,  $u_{s\beta}$ ,  $i_{s\beta}$ , and  $i_{sz}$  are the stator voltage and current vectors represented in a stationary frame, whereas  $u_{sd}$ ,  $u_{sq}$ ,  $i_{sd}$ , and  $i_{sq}$  are the same vectors represented in a rotating frame.

According to the standard assumption, the stator current flowing to the machine has positive value. The positive value of  $p$  stator power component means, that power is consumed by the machine, while the negative value of this component means power generation. Opposite situation concerns the  $q$  component of instantaneous power. A positive value means, that the machine generates reactive power, while negative value means, that reactive current is consumed by the machine for magnetization. Output signals from  $R_p$  and  $R_q$  power controllers are responsible for the signals of the rotor current vector components  $i_{rd}^*$  and  $i_{rq}^*$

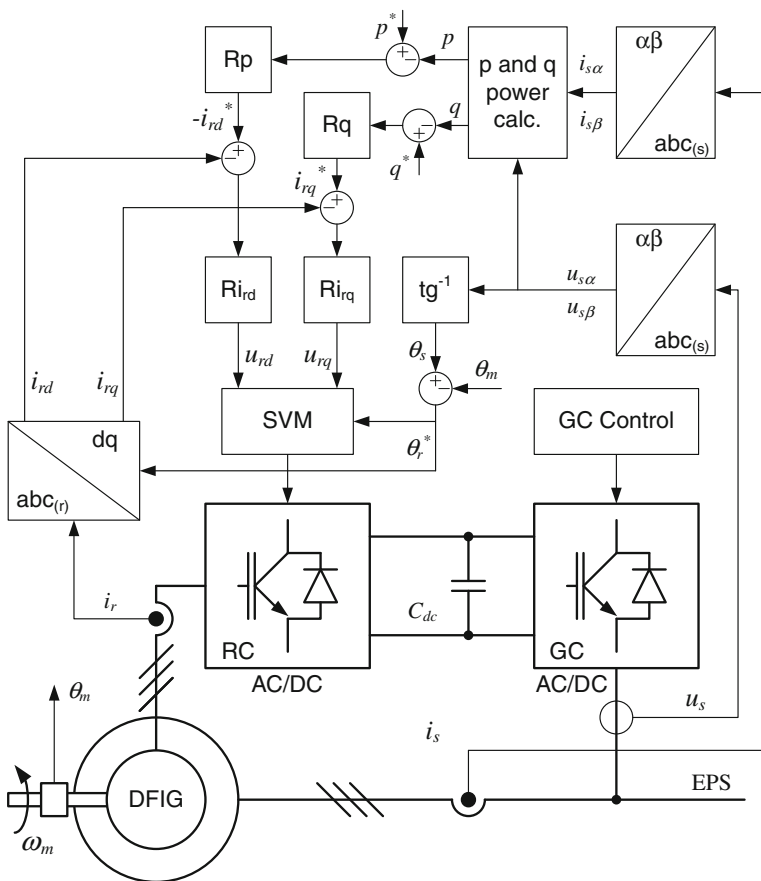


Fig. 7.43 Stator voltage oriented control method of rotor converter in grid connected DFIG

respectively, fed as a reference for the controllers  $Ri_{rd}$  and  $Ri_{rq}$  of the rotor current components. From the vector diagram (Fig. 7.40), and with consideration of Eqs. (7.65–7.66), it can be concluded, that positive value of the rotor current vector  $i_{rd}$  causes generation of active power, that means negative value of  $p$  component. Decrease of  $i_{rq}$  component of the rotor current causes the  $q$  component of stator power to be decreased, therefore  $Rq$  controller output signal with positive sign is used as a reference signal  $i_{rq}^*$  of  $Ri_{rq}$  controller.

Transformation angle  $\theta_r^*$  is needed to calculate the actual values of rotor current components  $i_{rd}$  and  $i_{rq}$  from the three-phase signals, as well as for transformation of dq components of the rotor voltage vector  $u_{rd}$  and  $u_{rq}$  to the signals required by space vector modulator SVM. This angle is obtained as a difference between the angle of stator voltage vector  $\theta_s$  and rotor position angle  $\theta_m$  detected by the position sensor, with consideration of the number of poles.

$$\theta_r^* = \theta_s - \theta_m \quad (7.67)$$

In the stator voltage oriented synchronously rotated dq frame, it can be assumed, that in the steady state, the stator flux components occurs only in q axis. Then, the decomposed Eq. (7.46) provides the following formulas:

$$\psi_{sd} = i_{sd}L_s + i_{rd}L_m = 0 \quad (7.68)$$

$$\psi_{sq} = i_{qs}L_s + i_{qr}L_m = -j\frac{u_{sd}}{\omega_s} \quad (7.69)$$

Using (7.65–7.66) and (7.68–7.69), the power components in the stator voltage oriented frame can be calculated

$$p_s = -\frac{3}{2} \cdot u_{sd} \frac{L_m}{L_s} \cdot i_{rd} \quad (7.70)$$

$$q_s = \frac{3}{2} \cdot u_{sd} \left( \frac{L_m}{L_s} \cdot i_{rq} - \frac{u_{sd}}{\omega_s L_s} \right) \quad (7.71)$$

where

$$-\frac{u_{sd}}{\omega_s L_s} \approx i_m \quad (7.72)$$

and  $i_m$  is a magnetizing current, which is close to the current consumed by the grid-connected machine at opened rotor circuit.

Formulas (7.70–7.71) can be used for elimination of power controllers and reference the rotor current components directly, based on the required values of  $p$  and  $q$  power components.

The angle  $\theta_s$ , as the angle of reference frame, calculated from the stator voltage components, may not assure high quality power during distorted grid as the angle of transformation includes oscillations. To eliminate this problem, different methods can be proposed. One of them is a connection of the reference frame with

the d component of the first harmonics stator voltage vector obtained by PLL structure. Another solution is a filtration of the harmonics signals from the d and q components of the stator voltage vector by the low pass filters applied in each of the voltage vector dq components. The next one is orientation of reference frame along the d axis of stator flux (Fig. 7.44), which can be calculated by integration of stator voltage in stationary coordinates (7.73). A DC component caused by the integration, has to be eliminated by the use of the high pass filter.

$$\psi_{sz\beta} = \int (u_s - R_s i_s) dt \quad (7.73)$$

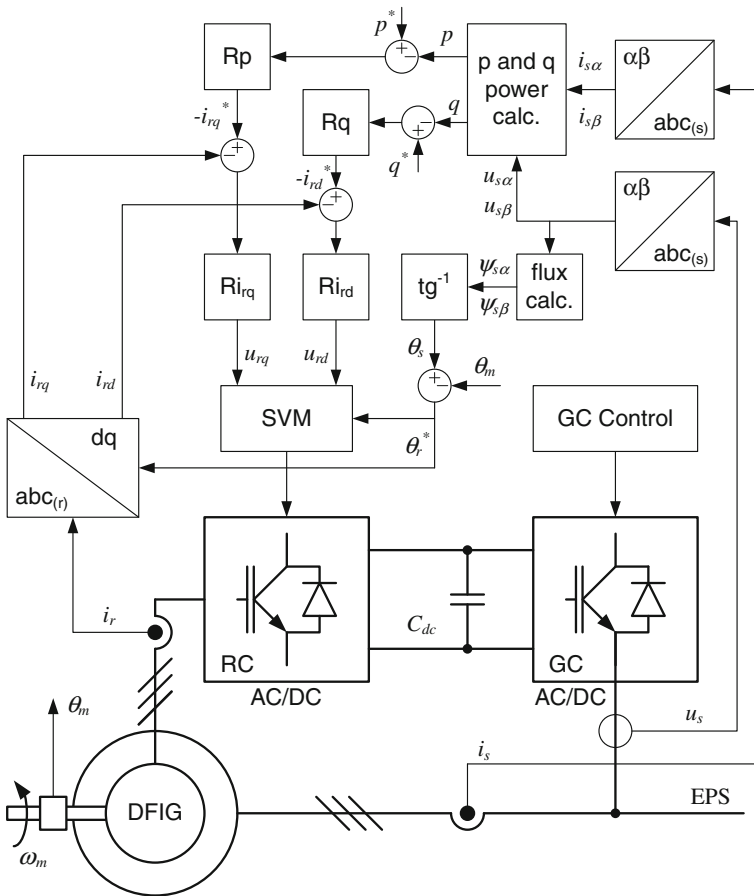
Next, based on the  $\alpha\beta$  stator flux vector components  $\psi_{sz}$  and  $\psi_{s\beta}$ , the  $\theta_s$  is calculated as an angle of the coordinates frame, in which the control method is realized.

Integration of the voltage provide natural filtration of higher harmonics in the signal obtained from the stator voltage. In the stator flux oriented frame, the stator voltage occurs only in q axis, stator flux only in d axis, and the power equations are as follows (7.74–7.75):

$$p_s = -\frac{3}{2} \cdot u_{sq} \frac{L_m}{L_s} \cdot i_{rq} \quad (7.74)$$

$$q_s = \frac{3}{2} \cdot u_{sq} \left( \frac{u_{sq}}{\omega_s L_s} - \frac{L_m}{L_s} \cdot i_{rd} \right) \quad (7.75)$$

To eliminate the rotor position sensor, a method of rotor position estimation can be used. One of the method, described as a model reference adaptive system MRAS, is based on the synchronization of the measured and estimated variable. As a pair of variables there can be used a stator flux vector calculated as an integration of stator voltage, which is treated as a reference and the stator flux vector calculated on the basis of the machine model, which is treated as an estimated one. A variant of this method is the synchronization of the measured rotor current  $i_{rz\beta}$  and the estimated current  $i_{rz\beta}^{\text{est}}$  obtained from the machine model [15]. The estimated rotor current  $i_{rz\beta}^{\text{est}}$  is obtained by the calculation of the stator flux  $\psi_{sz\beta}$  in stationary frame based on Eq. (7.73) and next determination of the rotor current vector from the model Eq. (7.46). A PI controller is responsible for elimination of displacement between the vectors, which is calculated with the use of cross product of the measured and estimated rotor current. A cross product is divided by the product of the vectors magnitudes obtained from the vectors components in the stationary  $\alpha\beta$  frame. Then, the error of PI controller is the sine function of the displacement angle. The error has a periodic character during transients states when the rotor speed is searched, as the unsynchronized vectors have a different rotational speeds. Output signal from this controller is the estimated rotor speed  $\omega_m^{\text{est}}$ , which is integrated to obtain estimated rotor position  $\theta_m^{\text{est}}$ , needed for transformation of the measured rotor current to the  $\alpha\beta$  stationary frame. The structure of

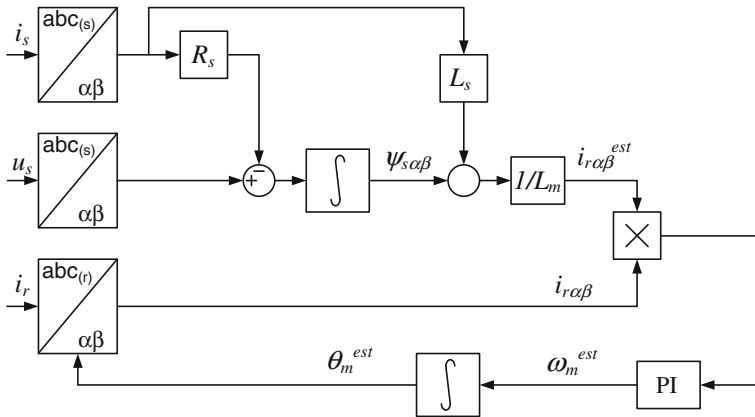


**Fig. 7.44** Stator flux oriented control method of the rotor converter in grid-connected DFIG

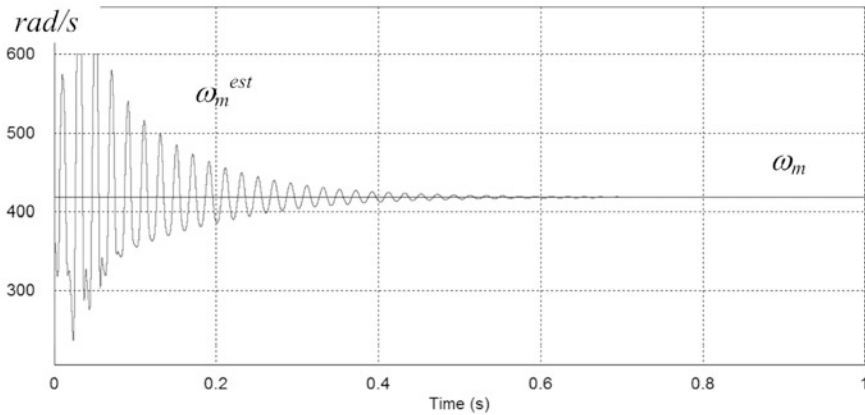
rotor position estimator based on the synchronization of the estimated and measured rotor current vectors is shown in the Fig. 7.45.

Figure 7.46 presents the speed estimation during start up of grid-connected double fed induction generator of parameters used for filtering capacitors selection in the standalone DFIG. It can be seen, that the time of speed search during start up can be shorter than 1 s, but relatively high oscillations of the estimated speed  $\omega_m^{est}$  are observed.

The described method of the rotor position estimator can be modified, to eliminate the sine function of the error of PI controller responsible for vectors synchronization. The modification bases on both, cross and dot product, which ratio equals the tangent of the displacement angle between the vectors (Fig. 7.47). The displacement angle in the range from  $-\pi$  to  $\pi$  can be calculated using adequate inverse function, and this angle is fed as the error for the PI controller. In this form, the error has periodical character, similarly to the previous estimator, what is



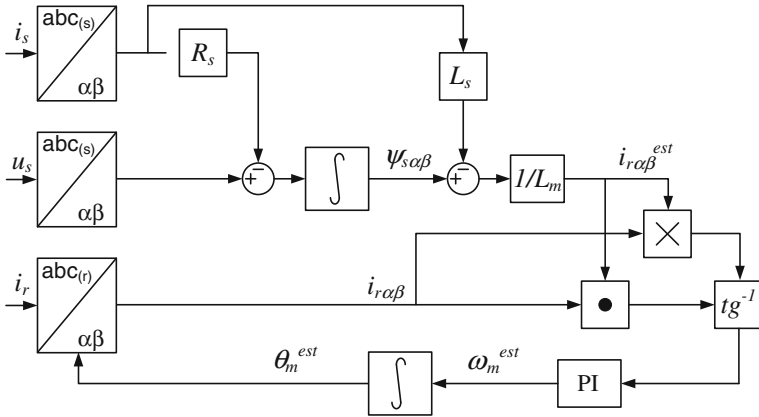
**Fig. 7.45** Rotor position estimation based on the synchronization of the estimated and measured rotor current vectors with the use of cross product of the vectors



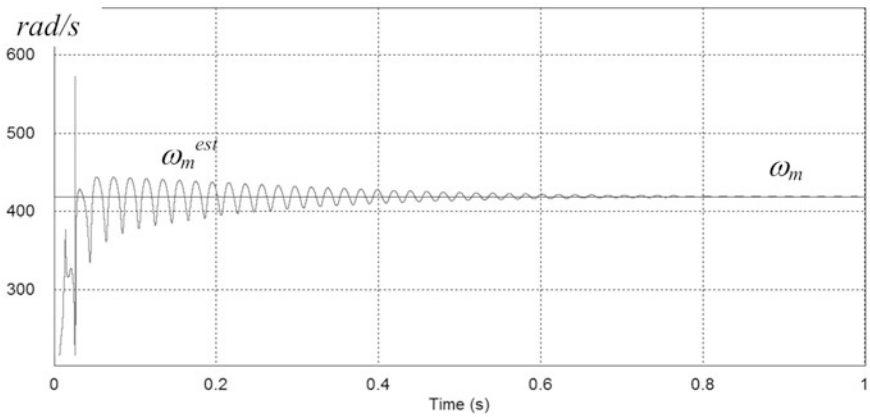
**Fig. 7.46** The waveforms of the actual and estimated rotor speed during start up of the grid connected DFIG with the use of estimator based on the measured and estimated rotor current—simulation results

adverse for the PI controller. However, the signal of the controller error, which is in the range from  $-\pi$  to  $\pi$ , with a rapid change from  $-\pi$  to  $\pi$  or from  $\pi$  to  $-\pi$ , can be modified to obtain the error signal as a monotonic function of the displacement angle. This way, a periodic character of the error signal is eliminated. Details about modification of the controller error has been described in [16] on the example of the phase locked loop PLL.

Figure 7.48 presents the speed estimation during start up of grid-connected double fed induction generator using the estimator based on the cross and dot products, with the parameters of PI controller set to obtain similar time of speed



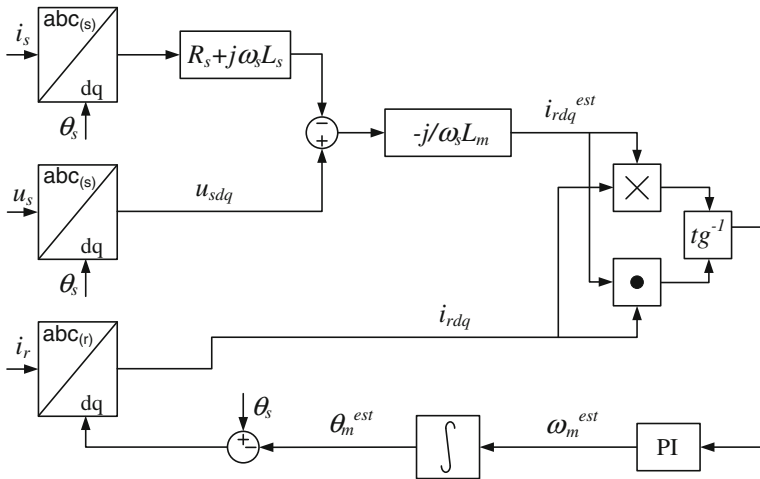
**Fig. 7.47** Rotor position estimation based on the synchronization of the estimated and measured rotor current vectors with the use of cross and dot products of the vectors



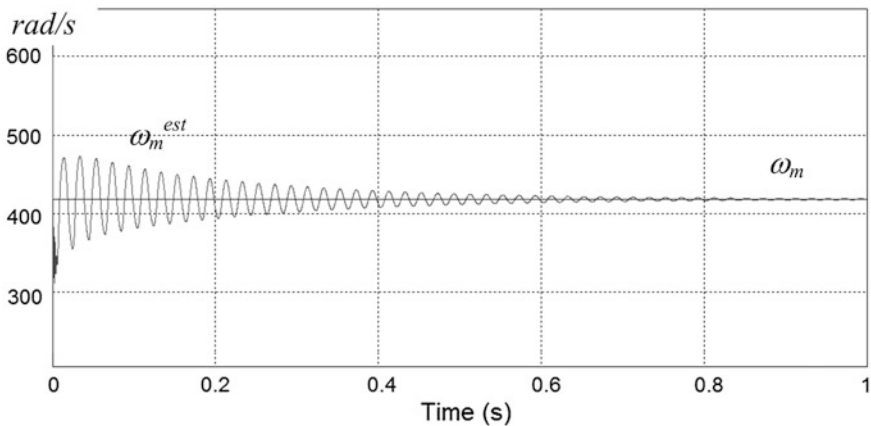
**Fig. 7.48** The waveforms of the actual and estimated rotor speed during start up of the grid-connected DFIG with the use of estimator based on the cross and dot products of the vectors—simulation results

search. It can be seen significant reduction of the estimated speed oscillations in comparison to the case of estimator with cross product.

Similarly to the estimator based on the flux model equations, synchronizing the measured and estimated rotor current vectors, other structure can be used for the rotor position estimation. In the new estimator, the estimated rotor current vector is derived from the stator circuit Eq. (7.44), in which the stator flux equation is replaced according to the Eq. (7.46). Using a steady state model in a synchronously rotated frame (by neglecting of stator and rotor current derivatives, which in steady state are equal to zero), a new model of rotor position estimator can be



**Fig. 7.49** Rotor position estimator with the use of cross and dot products of the estimated and measured rotor current vectors and current–voltage equations of the stator circuit

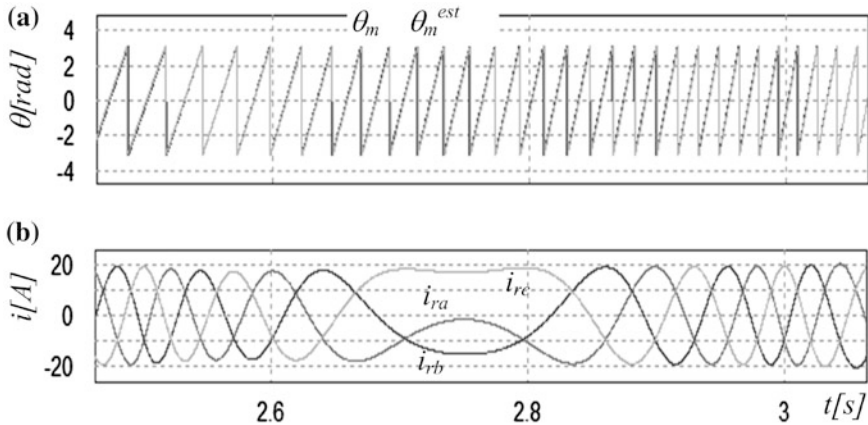


**Fig. 7.50** The waveforms of the actual and estimated rotor speed during start up of the grid connected DFIG with the use of estimator based on the cross and dot products of the vectors—simulation results

proposed (Fig. 7.49). The waveforms of actual and estimated rotor speed using the voltage-current steady state equation of the stator circuit is presented in Fig. 7.50.

The features of the new estimator based on the current–voltage stator equation are close to the properties of estimator based on the stator flux equation, presented in the Fig. 7.47. With the same PI controller parameters, set to achieve similar time of the rotor speed search, oscillations of the estimated speed are on similar level. However, the advantage of the new structure is, that the problems of a stator flux determination are avoided.





**Fig. 7.51** The waveforms of **a** the actual and estimated rotor position, and **b** three phase rotor current of the grid connected DFIG, with the use of estimator based on the cross and dot products and voltage–current stator equation—simulation results

Figure 7.51 presents a simulation results of the variable speed grid connected double fed induction generator with rotor position estimator from the Fig. 7.49. The rotor position needed for variables transformation are estimated with negligible error (Fig. 7.51a) in wide range of the rotor speed change in both, subsynchronous and oversynchronous range of operation. It allow to appropriate control of the rotor current in the variable speed operation (Fig. 7.51b).

#### 7.4.4 Conventional and Sensorless Control of the Stator Voltage

The DFIG is an attractive solution not only for wind energy systems but for other applications also. For the large hydropower stations or internal combustion engines, standalone operation may increase significantly the advantages of DFIG application. In the wind energy conversion systems, besides the initial energy for the excitation, an additional energy source or long-term energy storage is required to obtain high reliability of the power system. Basic control method of the output stator voltage of DFIG is shown in the Fig. 7.52. The stator voltage is controlled by the outer loop controllers  $Ru_{sd}$  and  $Ru_{sq}$  of the stator voltage vector components  $u_{sd}$  and  $u_{sq}$ , represented in a synchronously rotated frame. Reference signal  $u_{sd}^*$  equals to the voltage amplitude, whereas reference signal  $u_{sq}^*$  equals zero. Thus, the stator voltage vector is oriented to the d axis of the arbitrarily set coordinates frame. Output signals of the voltage vector controllers  $Ru_{sd}$ ,  $Ru_{sq}$  are responsible for reference rotor current vector components represented in the same synchronously rotated frame. Actual values of the dq stator voltage components are calculated using the transformation angle  $\theta_s^*$ , obtained by integration of reference

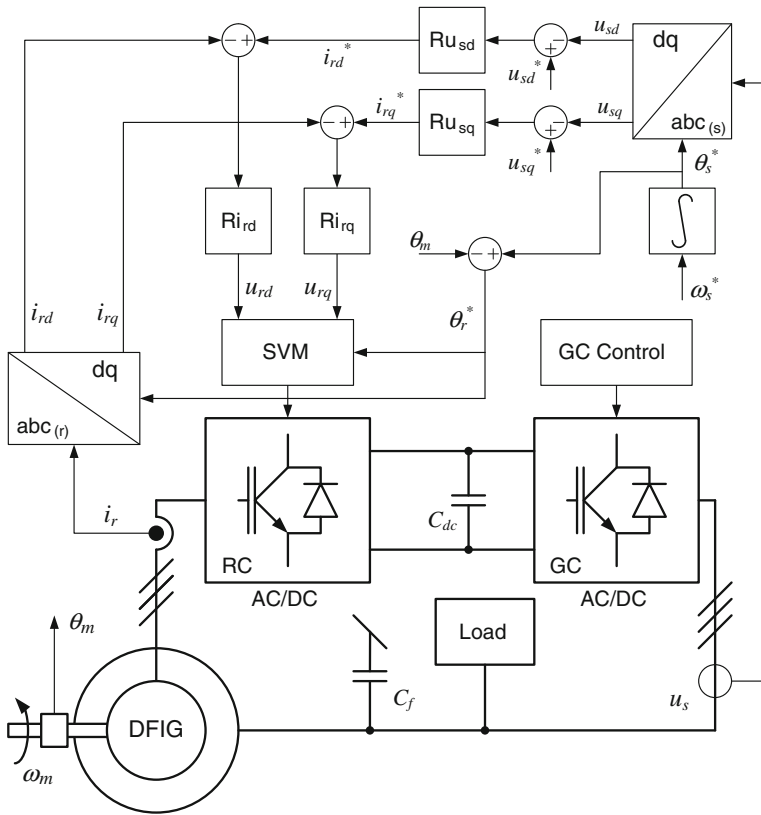


Fig. 7.52 Stator voltage control of standalone DFIG with the rotor position sensor

angular synchronous speed  $\omega_s^*$  corresponding to the reference frequency of the generated voltage. Actual values of rotor current components are calculated using the transformation angle  $\theta_r^*$ , obtained as a difference between reference angle  $\theta_s^*$  and rotor position angle  $\theta_m$  detected by the position sensor with consideration of the number of poles.

Output signals from the rotor current controllers,  $Ri_{rd}$  and  $Ri_{rq}$ , are responsible for the rotor voltage vector components represented in a dq frame. It is necessary to transform of the obtained rotor voltage components  $u_{rd}$ ,  $u_{rq}$ , to the frame connected with rotating rotor, in which the rotor converter RC is directly controlled. Thus, the rotor voltage dq components are transformed by space vector modulator SVM with the transformation angle  $\theta_r^*$ .

Fixed stator voltage and frequency can be obtained by the control of stator voltage itself or indirectly by the control of stator flux. Independently on the selected orientation of the control system, the critical issue in the control of DFIG is the determination of adequate rotor current vector. Instead of use of rotor

position sensor, the mathematical structures can be used for determination of the rotor current vector position.

The rotor current vector can be controlled in synchronously rotated frame dq connected with the stator voltage vector, as well as in the rotating frame xy connected with the rotor current vector itself. In this second frame, the x component of the rotor current vector is identical with the rotor current vector magnitude, whereas y component equals zero. These values are referenced for the rotor current controllers, where x component is an output signal of stator voltage vector magnitude whereas y component is referenced arbitrarily. Stator voltage is controlled in the polar frame, whereas rotor current in the xy frame connected with the rotor current vector (Fig. 7.53). The angle between both coordinates frames  $\gamma_{usir}$  (Fig. 7.54) is considered naturally in the transformation angle  $\theta_r^*$ .

Polar control of the stator voltage vector, has an advantage in relation to the control of the vector components in the Cartesian dq frame. Stator voltage

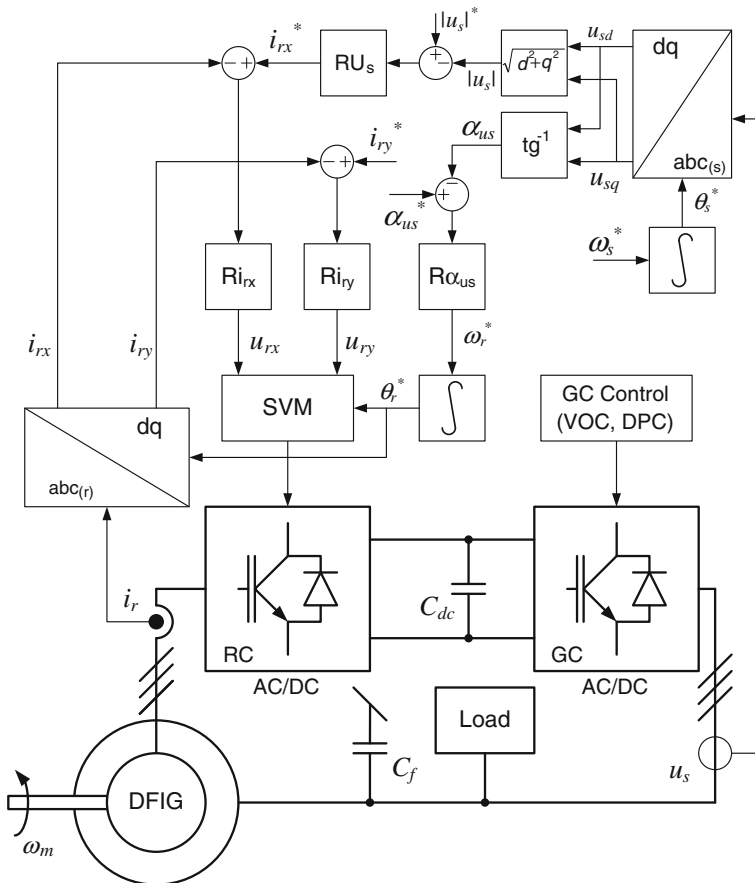
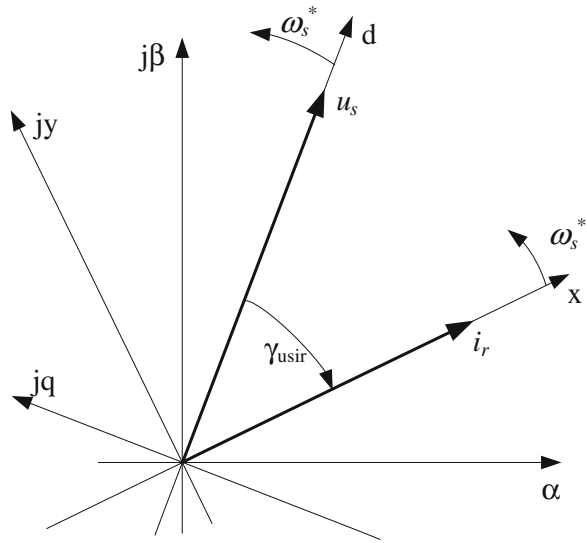


Fig. 7.53 Sensorless stator voltage control of standalone DFIG with the use of PLL

**Fig. 7.54** Vector diagram presenting the orientation of stator voltage and rotor current frames



amplitude is proportional to the magnitude of the rotor current vector, and it is true even if the actual stator voltage vector is displaced from the steady state position. It is true also for any relative positions of the rotor current polar frame and stator voltage polar frame, which are different for different load. The polar frame control of the rotor current can also be realized, but the dynamics is much worst.

Rotor current control is much faster than stator voltage control, therefore it can be assumed, that the rotor current vector always overlaps the x axis of xy frame. Thus, the  $i_{rx}$  component can be treated as rotor current vector magnitude and the reference value  $i_{rx}^*$  of this component is produced by the controller of stator voltage vector magnitude.

Additional control loops can be used for the stator voltage asymmetry [17] and harmonics [14] compensation in the cases of unbalanced or nonlinear load supply. A variant of the asymmetry correction method is shown in Fig. 7.55. An unbalanced-three phase voltage in the three-wire system consists of the positive and negative sequence vector components rotating with the same angular speeds, but in opposite directions. In a positively rotated frame  $dq_{(p)}$ , each of the d and q voltage vector components consists of the DC signal representing positive sequence, and 100 Hz signal representing negative sequence. In the negatively rotated frame, a DC signal represents negative sequence, whereas 100 Hz signal represents positive sequence. Elimination of the negative sequence by the use of classical PI controllers, require extraction of the negative sequence vector components  $u_{sdn}$  and  $u_{sqn}$  in the negatively rotated frame  $dq_{(n)}$ . A 100 Hz component, in this frame, is eliminated by the use of low pass filters with much lower cut-off frequency (e.g. 10 Hz). However, a typical second-order low pass filter may not be strong enough to eliminate 100 Hz signal, because of the high amplitude of this signal as a consequence of high value of positive sequence. To improve the elimination of the

100 Hz signal in the negatively rotated frame  $dq_{(n)}$ , additional operation are applied. First, a negative sequence signals of the stator voltage vector components are eliminated in a positively rotated frame  $dq_{(p)}$ , and as a result a positive sequence DC signal  $u_{sdp}$ ,  $u_{sqp}$  is obtained. Second, the DC signals representing positive sequence are transformed to the frame rotating in the negative direction  $dq_{(n)}$  to be represented by 100 Hz. Next, these 100 Hz signals are subtracted from the signal obtained from a direct transformation of stator voltage vector  $u_s$  to the negatively rotated frame  $dq_{(n)}$ . This way, a 100 Hz signal representing a positive sequence in a  $dq_{(n)}$  frame, is significantly reduced and can be further efficiently filtered by second order LPF. The reference negative sequence components of the stator voltage vector are set to zero to obtain symmetrical voltage, and separate controllers of each component produces adequate output signals as additional references of the rotor current negative sequence components  $i_{rdn}^*$ ,  $i_{rqn}^*$  in a negatively rotated frame  $dq_{(n)}$ . These reference current components have to be transformed back to the xy frame of the rotor current control, as an additional components of the rotor current vector  $i_{rn}^*$  responsible for stator voltage unbalance elimination.

Similarly to the case of voltage unbalance elimination, a harmonics elimination can be also implemented. Figure 7.56 presents a control scheme for reduction of the stator voltage negative sequence 5th harmonics and positive sequence 7th harmonics as typical for the standard three-phase nonlinear loads. The stator voltage vector  $u_{sdq}$  represented in a synchronously rotating frame is transformed to the frames rotating with angular speeds corresponding with the eliminated harmonics. Next a vector components are filtered by the low pass filters. For 5th and 7th harmonics, the filtered signals includes DC components representing the

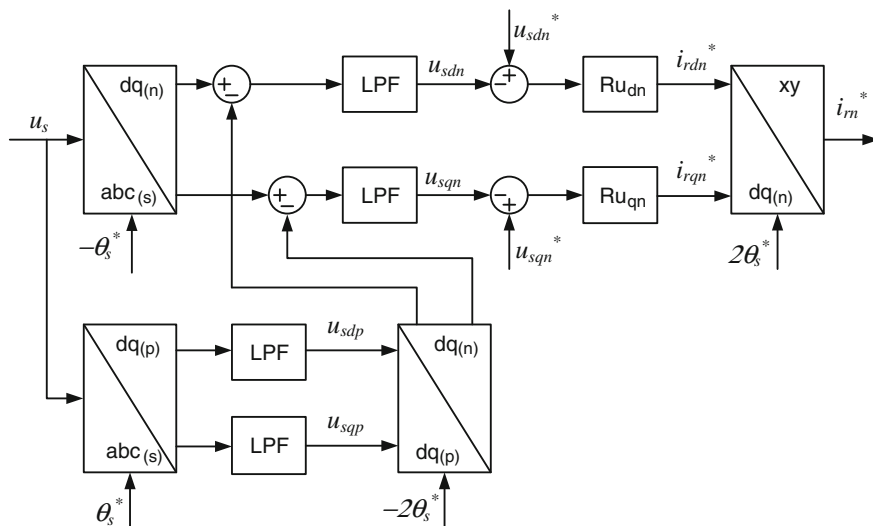


Fig. 7.55 Control of the rotor side converter for the stator voltage unbalance elimination

respective harmonics and 300 Hz signal representing positive sequence components of fundamental frequency (50 Hz). The second-order low pass filter LPF of cut-off frequency equal to 10 Hz is strong enough to eliminate 300 Hz component from the filtered signals. Therefore, an additional calculations, improving the process of negative sequence extraction in the case of unbalance elimination, can be neglected in the case of harmonics components extraction. After filtration, the signals  $u_{sd5}$ ,  $u_{sq5}$ ,  $u_{sd7}$ , and  $u_{sq7}$ , representing harmonics components, are the feedbacks for the PI controllers  $Ru_{d5}$ ,  $Ru_{q5}$ ,  $Ru_{d7}$ , and  $Ru_{q7}$  with a reference values of this components equal to zero. Output signal of the PI controllers are responsible for the reference values of the rotor current harmonics components  $i_{rd5}^*$ ,  $i_{rq5}^*$ ,  $i_{rd7}^*$ , and  $i_{rq7}^*$  for 5th and 7th harmonics, respectively, which are transformed to the xy frame connected with control of the rotor current, to create a common reference signal of the rotor current component  $i_{rh}^*$  responsible for the stator voltage harmonics elimination.

Figure 7.57a presents a signal waveforms recorded during laboratory tests with unbalanced load, for which the voltage asymmetry is eliminated. Similarly for the nonlinear load, 5th and 7th harmonics are eliminated using a presented control methods (Fig. 7.57b). A PI rotor current controllers used in the tests, provide a steady state errors in the control of the rotor currents, as the rotor current vector components responsible for unbalance and harmonics elimination are sinusoidal in the frame xy. It, however, does not have negative impact in the control of the stator voltage, as the rotor current control is in the inner control loop, and the steady state errors of all the applied stator voltage controllers are zero.

Presented method allows to obtain fixed amplitude and frequency of the stator voltage as well as its controlled phase. It is useful for synchronization of the

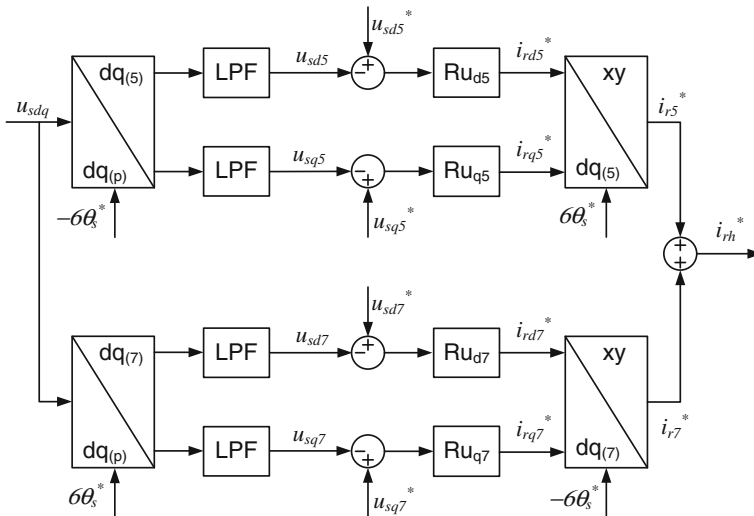
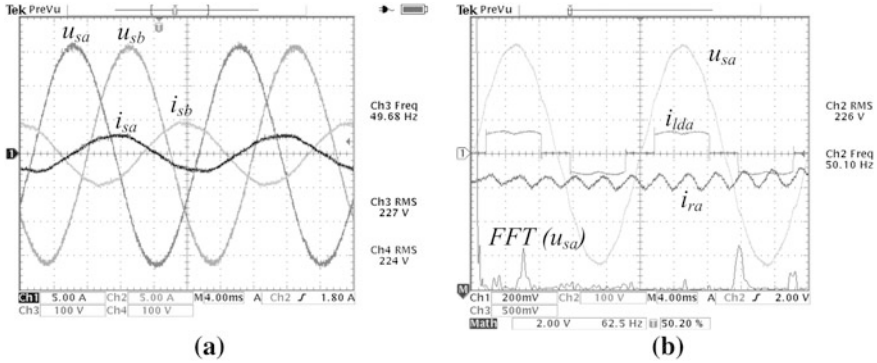
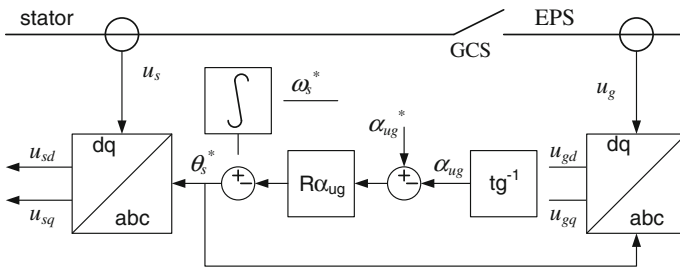


Fig. 7.56 Control of the rotor side converter for the stator voltage harmonics elimination



**Fig. 7.57** The waveforms of **a** stator voltage and current during unbalanced load supply and **b** stator voltage, rotor and load currents during nonlinear load supply—laboratory tests

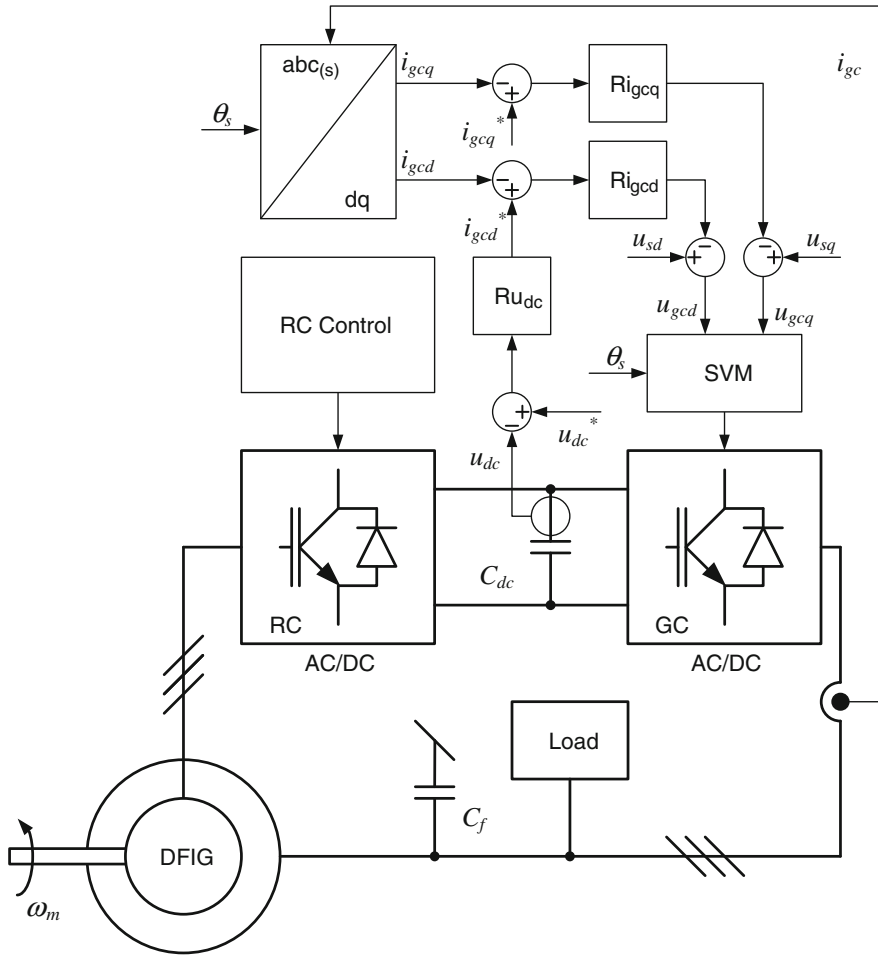


**Fig. 7.58** Control scheme of the grid synchronization method of the standalone DFIG

generator before its connection to the power grid. To obtain synchronization, it is required additional controller  $R\alpha_{ug}$  [18] of the grid voltage angle  $\alpha_{ug}$  calculated in the frame connected with the stator voltage based on the grid voltage vector components  $u_{gd}$ ,  $u_{gq}$  (Fig. 7.58).

### 7.4.5 Control of the Grid Side Converter

Grid side converter, shown as a GC box in the Figs. 7.42, 7.43, 7.44, and 7.45, is an AC-to-DC converter, which the main function is stabilization of the DC link voltage. Besides the power electronics devices, the GC box also includes an inductors between converter and stator terminals. Basic control of the grid side converter GC is in fact independent on the operation mode. In both—standalone and grid connected—modes, this converter is a current controlled voltage source and the control method can be oriented to the stator voltage vector, which is controlled by the rotor converter in the standalone mode, and imposed externally in a grid connected mode. Typical voltage oriented control VOC method [19] can



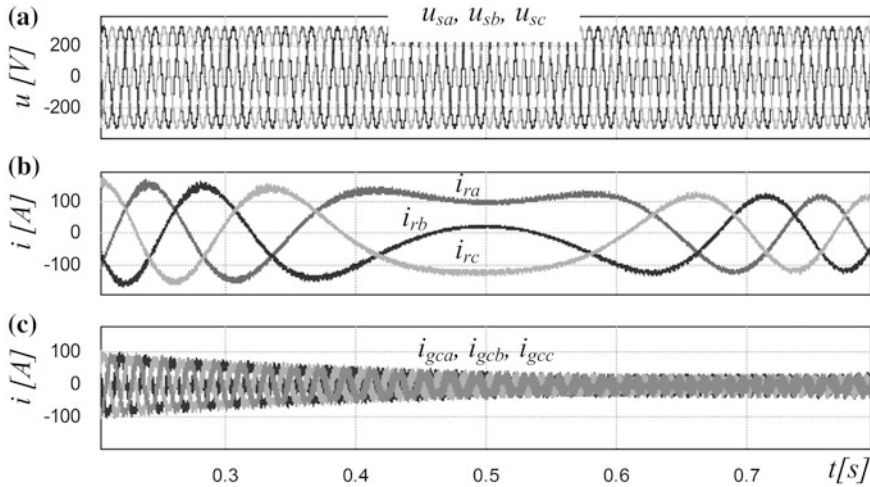
**Fig. 7.59** Scheme of the stator voltage oriented control of grid side converter of DFIG

be used (Fig. 7.59) to achieve stabilization of the DC link voltage and sinusoidal current taken or delivered to the AC line.

The transformation angle for grid side converter current stator voltage and the converter voltage consider the synchronous transformation angle  $\theta_s$  calculated on the basis of the stator voltage vector  $\alpha\beta$  components, in the same way like it is shown in Fig. 7.43. Active current is referred by outer controller of the DC link voltage, whereas typically q component of current vector equals zero, when unity power factor of the grid side converter current is required.

The results, shown in the Fig. 7.60, are obtained by simulation of 250 kW slipping machine model equipped with rotor connected back-to-back converter controlled with the methods presented in Figs. 7.53 and 7.59. The waveforms of currents and voltages of standalone operated DFIG are obtained for linear change





**Fig. 7.60** Waveforms of **a** stator voltage, **b** rotor currents, and **c** grid converter currents during linear change of speed of standalone DFIG system—simulation results

of the rotor speed from  $0.66 \omega_s$  to  $1.33 \omega_s$  and for acceleration equal to 2,000 rpm/s.

Stator voltage amplitude and frequency is speed independent thanks to the adjusting of the rotor current frequency to the rotor speed. The load power  $P_o$  is a sum of stator  $P_s$  and rotor  $P_r$  power (7.76) and power distribution depends on the slip  $s$  (7.76–7.78).

$$P_o = P_s + P_r = P_s + sP_s \tag{7.76}$$

$$P_s = \frac{P_o}{1 + s} \tag{7.77}$$

$$P_r = \frac{sP_o}{1 + s} \tag{7.78}$$

It can be seen in the Fig. 7.60b, that rotor current amplitude decreases with the increased speed. At the low speed (subsynchronous range), the grid side converter consumes the energy and this energy has to be generated by the machine on the stator side. It causes higher rotor current. Oppositely, at the high rotor speed (oversynchronous range), the slip power is negative, and the grid side converter delivers the energy to the load. Then the stator of the machine is less loaded and it requires smaller (reduced) rotor current. Consequently, for the same load, the grid side converter current has higher amplitude for minimum speed (Fig. 7.60c).

In the case of standalone operated system, a grid side converter control can be extended in the cases of unbalance and nonlinear load supply. Asymmetry and harmonics compensation through the rotor side control causes the electromagnetic torque ripples, what may be disadvantageous for the electric machine. Grid side

converter, besides its main function, which is stabilization of the DC link voltage, may partially operate as an active filter and be the source of the load demanded unbalance and harmonics current. Additional control parts may be responsible for the reference signals of the grid side converter currents obtained from the controllers providing balancing and elimination of harmonics of the stator current.

Variant of the additional part of the grid side converter control method during unbalanced load supply is presented in Fig. 7.61. The method is fully analogous to the method of voltage harmonics elimination presented in the Fig. 7.55. An unbalanced stator current consists of the positive and negative sequence components, and the negative sequence signals  $i_{sdn}$ ,  $i_{sqn}$  are extracted as a DC component in a negatively rotated frame  $dq_{(n)}$ . Next, two PI controllers  $Ri_{dn}$ ,  $Ri_{qn}$  are applied to produce the reference signals of the grid side converter current components  $i_{gcdn}^*$ ,  $i_{gcqn}^*$ , responsible for elimination of the stator current negative sequence. Obtained signals are transformed as  $i_{gcn}^*$  vector component to the positively rotated frame  $dq$ , in which the grid side converter current control is realized. Compensation of the unbalances and harmonics of the stator current, does not require additional current sensors like in the case of active filtering operation based on the load current measurement.

Similarly to the case of stator voltage harmonics elimination, a stator current harmonics elimination can be also implemented. Figure 7.62 presents a control scheme for reduction of the stator current negative sequence 5th harmonics and positive sequence 7th harmonics during nonlinear load supply. The stator current vector  $i_{sdq}$ , represented in a synchronously rotating frame, is transformed to the frames rotating with angular speeds corresponding with the eliminated harmonics. Next, the stator current vector components are filtered by the low pass filters. The

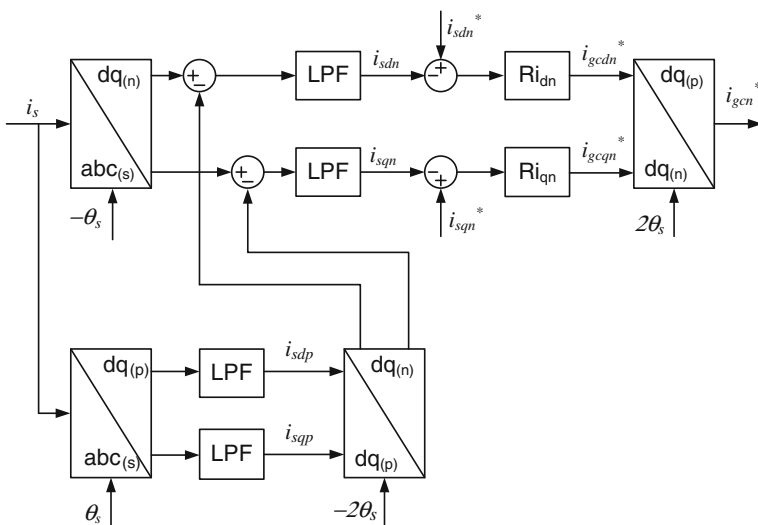


Fig. 7.61 Control of the grid side converter for the stator current unbalance elimination

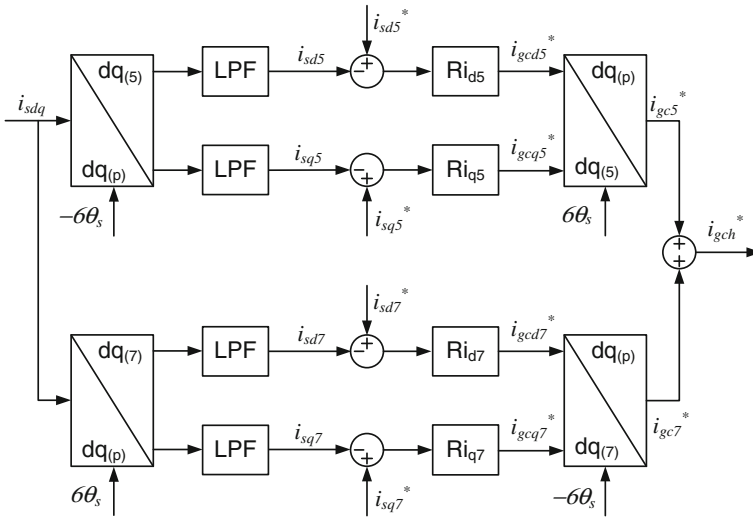


Fig. 7.62 Control of the grid side converter for the stator current harmonics elimination

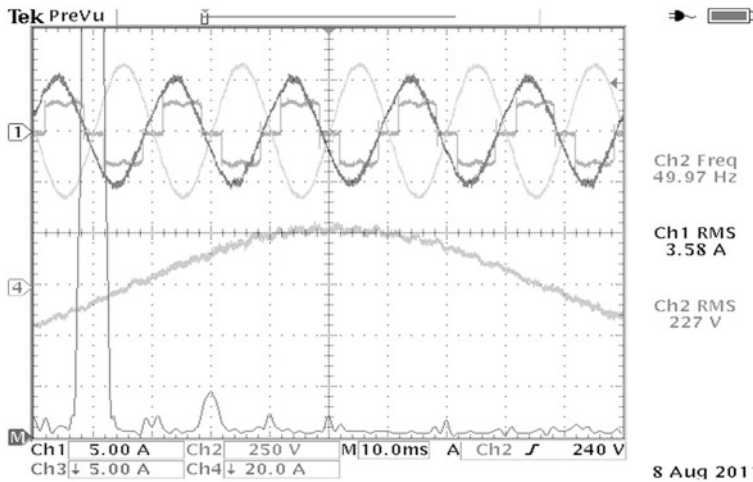


Fig. 7.63 The waveforms of stator voltage, rotor, stator, and load current, and FFT spectrum of the stator current during nonlinear load supply—laboratory tests

2nd order low pass filters LPF of cut-off frequency equal to 10 Hz eliminate 300 Hz component from the filtered signals. After filtration, the signals  $i_{sd5}$ ,  $i_{sq5}$ ,  $i_{sd7}$ , and  $i_{sq7}$ , representing stator current harmonics, are the feedbacks to the PI controllers  $Ri_{d5}$ ,  $Ri_{q5}$ ,  $Ri_{d7}$ , and  $Ri_{q7}$  with a reference values of this components equal to zero. Output signal of the PI controllers are responsible for the reference values of the grid side converter current components  $i_{gcd5}^*$ ,  $i_{gcq5}^*$ ,  $i_{gcd7}^*$  and  $i_{gcq7}^*$  for

5th and 7th harmonics, respectively. Next, the reference signals are transformed to the positively rotated  $dq_{(p)}$  frame, in which the control of the grid converter current is realized. This way, the harmonics needed by the load are fed by the grid side converter instead of the stator of the machine.

From the machine point of view, the stator current is symmetrical and sinusoidal (Fig. 7.63), therefore the rotor current is also sinusoidal and torque oscillations are avoided. It can be seen on the spectrum of fast Fourier transformation FFT, that 5th and 7th harmonics is completely eliminated in the stator current by the use of described control method.

## References

1. Da Ponte M, Grzesiak L, Koczara W, Pospiech P, Niedzialkowski A (1996) Hybrid generator apparatus. Patent US 6175217 (B1)
2. Koczara W (2008) Adjustable speed power generation. In: Srzelecki R, Benysek G (eds) Power electronics in smart electrical energy networks. Springer, London
3. Al-Khayat N, Seliga R, Koczara W, Krasnodebski A, Kaminski B (2002) DSP control of variable speed generator. IEEE international symposium industrial electronics '02, L'Aquila, Italy, pp 970–974
4. Bolognani S, Venturato A, Zigliotto M (2000) Novel control technique for high-performance diesel-driven AC generator-sets. Power electronic and variable speed drives conference, pp 518–523
5. Tolbert LM, Peterson WA, Scudiere MB et al (2001) Electronic power conversion system for an advanced mobile generator set, vol 3. IEEE industrial applied conference—IAS'01, pp 1763–1768
6. Kaminski B, Wejrzanowski K, Koczara W (2004) An application of PSIM simulation software for rapid prototyping of DSP based power electronics control systems, vol 1. IEEE power electronic specialists conference '04, Aachen, Germany, pp 336–341
7. Koczara W, Ernest E, Al-Khayat N et al (2004) Smart and decoupled power electronic generation system. IEEE power electronic specialists conference '04, Germany, pp 1902–1907
8. Kaminski B, Koczara W, Al-Khayat N (2006) Increased efficiency three-level inverter topology for low voltage applications. International PCIM'06 conference, Nurnberg, Germany
9. Chlodnicki Z, Koczara W, Al-Khayat N (2008) Laboratory simulation of the variable speed generation system. EPE J 17(4) pp 37–49
10. Jiao L, Ooi BT, Joos G, Zhou F (2005) Doubly-fed induction generator (DFIG) as a hybrid of asynchronous and synchronous machines. Electr Power Syst Res 76:33–37
11. Pena R, Clare J, Asher G (1996) Doubly-fed induction generators using back-to-back PWM converters and its applications to variable-speed wind energy generation. Proc Inst Electr Eng B 153:231–241
12. Datta R, Ranganathan VT (2001) Direct power control of grid connected wound rotor induction machine without rotor position sensors. IEEE Trans Power Electron 16:390–399
13. Seman S, Niiranen J, Kanerva S et al (2006) Performance study of a doubly fed wind-power induction generator under network disturbances. IEEE Trans Energy Convers 21:883–890
14. Abad G, Lopez J, Rodriguez MA, Marroyo L, Iwanski G (2011) Doubly fed induction machine: modeling and control for wind energy generation. IEEE press series on power engineering, Wiley, Boca Raton

15. Pena R, Cardenas R, Proboste J, Asher G, Clare J (2008) Sensorless control of doubly-fed induction generators using a rotor-current-based MRAS observer. *IEEE Trans Ind Electron* 55:330–339
16. Iwanski G, Koczara W (2011) Standalone double fed induction generator. In: Irwin JD, Wilamowski BM (eds) *The industrial electronics handbook. Power electronics and motor drives*, vol 4. CRC Press, New York
17. Iwanski G, Koczara W (2007) Sensorless direct voltage control of the stand-alone slip-ring induction generator. *IEEE Trans Ind Electron* 54:1237–1239
18. Iwanski G, Koczara W (2008) DFIG based power generation system with UPS function for variable speed applications. *IEEE Trans Ind Electron* 55:3047–3054
19. Malinowski M, Kazmierkowski MP, Trzynadlowski AM (2003) A comparative study of control techniques for PWM rectifiers in AC adjustable speed drives. *IEEE Trans Power Electron* 18:1390–1396

# Chapter 8

## Microturbines

Stephen Gillette and Mark Gilbreth

**Abstract** Microturbines are a relatively new power generation technology, and usually include integrated control and power electronics. They are extremely versatile, and can be used in many different applications that take advantage of their unique characteristics. This chapter provides basics of microturbine operation including the key components and how they are controlled. Some unique characteristics of microturbines are defined along with several application examples. Different power delivery topologies are reviewed, along with discussions of control, synchronization, fault handling, and circuit protection.

### 8.1 Introduction

Microturbines are a relatively new technology for generation of electric power, and are commercially available in ratings from 30 kW up to 1 MW or more. This chapter will describe how microturbines perform, and how they differ from other more traditional forms of electric power generation. Emphasis is placed on the power electronics and control features of typical microturbines. Figure 8.1 shows several 65 kW microturbines installed in a combined heat and power (CHP) installation. There are several manufacturers of commercially available microturbines, as well as companies developing new designs. Information contained in this section is from published manufacturer's specifications as of the time of writing, which information may not be error-free or directly comparable between manufacturers. Therefore, most of the examples and descriptions in this chapter will be from the authors' company, Capstone Turbine Corporation.

---

S. Gillette (✉) · M. Gilbreth  
Capstone Turbine Corporation, 21211 Nordhoff Street, Chatsworth, CA, USA  
e-mail: sgillette@capstoneturbine.com

M. Gilbreth  
e-mail: mgilbreth@capstoneturbine.com

**Fig. 8.1** Installation of several 65 kW microturbines



## 8.2 Microturbine Basics

Not all microturbines are constructed in the same way. However, most commercially available microturbines provide electrical output using a generator with an integrated control system so that end-use customers and design engineers do not need to be concerned with many of the details of how to manage their operation. This [Sect. 8.2](#) provides an overview of the microturbine generator functionality and characteristics, while [Sect. 8.3](#) Power Electronics Topologies for Microturbines and [Sect. 8.4](#) Controls for Microturbine Power Electronics provide additional details.

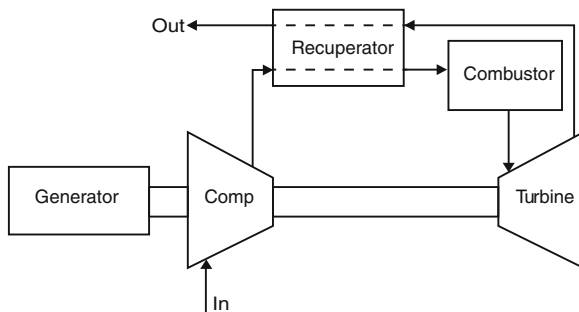
### 8.2.1 Energy Generation

This subsection describes how microturbines take combustible fuel as an input and efficiently convert it to useable electrical power as an output, either AC or DC. Some unique characteristics are also discussed, as well as how the clean exhaust energy can be used to increase net system efficiency.

#### 8.2.1.1 Recuperated Brayton Cycle

Microturbines are a simple form of gas turbine, usually deploying radial compressor and turbine rotors and often using just one stage of each. They typically utilize exhaust energy to preheat compressed inlet air, thereby increasing electrical efficiency compared to a simple cycle machine. The air-to-air heat exchanger is

**Fig. 8.2** Major components in recuperated Brayton cycle



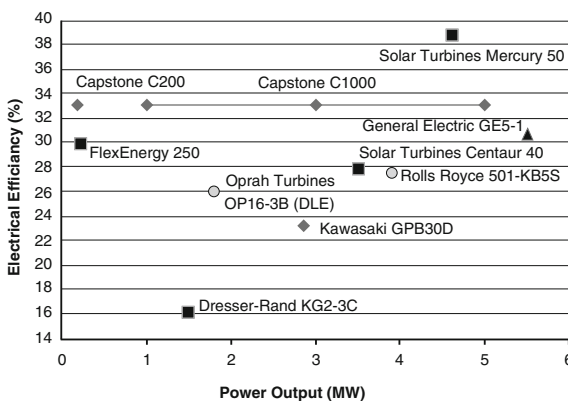
termed a “recuperator”, and the system is typically called a recuperated Brayton cycle. Figure 8.2 shows an example of the major components in a typical microturbine system using one compressor, one turbine, a recuperator, and an electric generator.

The recuperated Brayton cycle can achieve net electrical efficiencies above 30 %, and microturbines have the highest electrical efficiencies of any gas turbine up to about 5 MW. Figure 8.3 shows a comparison of electrical efficiencies of several gas turbine models.

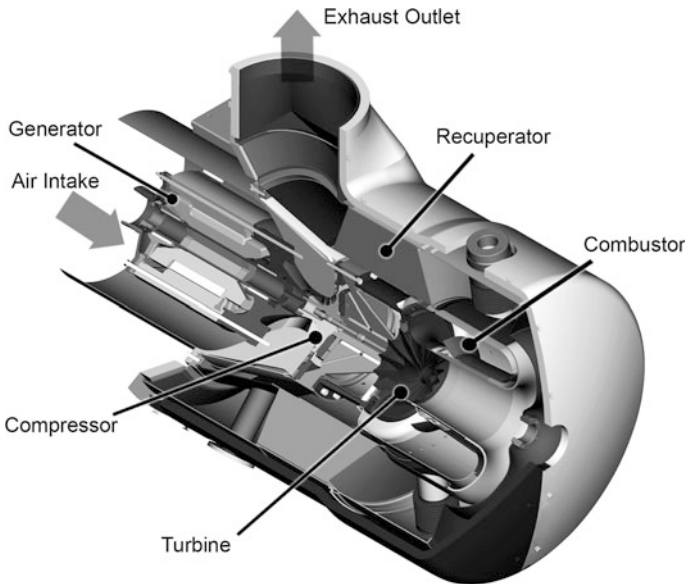
### 8.2.1.2 Rotating Components

Figure 8.4 shows a cutaway view of a typical 65 kW microturbine illustrating how these major components are arranged in a commercial product. The assembly in Fig. 8.4 is often called the “turbogenerator (TG)”, as it includes all the gas turbine components plus the generator. The single assembly of turbine, compressor, and generator is rotating at high speed—96,000 rpm in the case of this 65 kW turbogenerator. The output of this type of TG is therefore high frequency AC, which must be conditioned using power electronics to provide a useable 50 or 60 Hz electrical output, as will be described in more detail in Sect. 8.3 Power Electronic

**Fig. 8.3** Comparison of electrical efficiencies of several gas turbines







**Fig. 8.4** Cutaway view of microturbine showing major components

Topologies for Microturbines. Split-shaft microturbines have been offered commercially, and more are under development. A discussion of these is included in several sections below.

### 8.2.1.3 Fuels

Microturbines are able to burn a wide range of fuels in terms of both energy content as well as contaminants. Most manufactures offer models that are able to operate on at least some of the fuels listed in Table 8.1. Some microturbines are able to operate with hydrogen sulfide content up to 70,000 ppm [1]. This makes microturbines a good choice for waste fuel applications, including oil production where associated gasses are uncontrolled. All systems have their limits, however,

**Table 8.1** Typical fuel capabilities of microturbines

Fuel type	Fuel designations	Comments
Gaseous	Natural gas, propane, LNG, landfill gas, digester gas, flare gas, associated gas, syngas	Requires gas compression, either as an integrated option installed in the microturbine or as an external component
Liquid	Diesel, kerosene, aviation fuels, biodiesel, and other liquid biofuels	Consult manufacturer for proper application of liquid biofuels

and equipment manufacturer's fuel requirements specifications should be consulted for each specific fuel stream.

Microturbines need to boost fuel pressure in order to inject it into the combustion chamber. Typical required fuel inlet pressures are 75–80 psig, and future microturbines may require higher pressures. All known microturbine manufactures as of the date of this publication provide natural gas compression capability, either integrated into the microturbine or as an accessory designed for the specific microturbine [2–8]. These gas boosters represent a parasitic load that should be accounted for in the net output of the system. Manufacturers provide data for this either as a net electrical output of the microturbine or as an electrical load required by the gas booster that may be subtracted from the gross output of the microturbine when making financial and load calculations.

In addition to the use of combustion to provide energy, several microturbine manufacturers have been able to adapt their systems to receive heat energy from external energy sources, such as concentrated solar or heat from a fuel cell stack [9]. This can provide a high efficiency power system, with the ability to also operate on traditional fuels when renewable sources are not available. Examples are provided in Sects. 8.5.4 and 8.5.5 later in the chapter.

#### 8.2.1.4 Useable Waste Heat

Microturbines provide a large amount of clean exhaust flow that is ideal for heat recovery. The sensible heat energy available in the exhaust stream ( $kW_t$ ) is represented by Eq. 8.1. In this equation,  $T$  is the exhaust gas temperature,  $c_p$  is the specific heat of the exhaust gas, and  $dm/dt$  is the exhaust mass flow.

$$kW_t = \int_{T_1}^{T_2} c_p \frac{dm}{dt} T \quad (8.1)$$

Since the exhaust is mostly heated air with a relatively small quantity of the products of combustion, the exhaust has two characteristics:

- The specific heat coefficient  $c_p$  is almost constant over the useable temperature range, so the recoverable heat energy is essentially linear with temperature.
- The dew point is relatively low. For example, one manufacturer's 65 kW microturbine with an electrical efficiency of 29 % operating on natural gas produces exhaust with a water content of 150 grains per pound of air which equates to a dew point of about 80 °F [10]. This means that its total exhaust energy can be practically used in a heat recovery system down to an exit temperature of 100 °F without concern for condensation, resulting in high overall system efficiencies.

The heat recovered from the microturbine's exhaust can be used for heating water (often referred to as Combined Heat and Power, or CHP), or used with an absorption or adsorption chiller system to produce chilled water (often referred to as Combined Cooling, Heating and Power, or CCHP). The effectiveness of air conditioning equipment such as chillers can be measured in terms of a coefficient of performance (COP), which is calculated as chilled water output divided by electrical or thermal input. Since double-effect chillers have a high COP approaching 1.3, the chilled water output can actually be greater than the useable exhaust heat energy input. Table 8.2 provides example performance for a hot water heat recovery (CHP) and double-effect chiller system (CCHP). Some applications have also been able to directly use the microturbine's exhaust for process heating and drying.

### 8.2.1.5 Unique Characteristics

Microturbines offer some unique features compared with other generation technologies, as summarized in Table 8.3. Not all microturbines offer every one of these characteristics.

## 8.2.2 Microturbine Control

Microturbines typically have digital controls integrated into their power electronics, as will be described in detail in Sect. 8.4 later in the chapter. This section provides an overview of the functional control requirements for microturbines.

### 8.2.2.1 Start/Stop Sequences

Microturbines require a prescribed sequence of steps for starting and stopping under normal operating conditions.

For starting, the generator can typically act as a starting motor by taking power from the utility grid or battery pack. The turbine will then be spun up to a preset rotating speed before introducing fuel and ignition. Once flame temperatures are detected, additional fuel is added and the system is allowed to increase speed and

**Table 8.2** Example efficiencies of CHP and CCHP applications

Manufacturer/type	Electrical efficiency (%)	Total efficiency (%)	Notes
Capstone C65 ICHP [11]	29.0	80.6	60 °C inlet water
UTC PureComfort 240 CCHP [12]	29.0	89.4	142RT cooling

**Table 8.3** Some unique microturbine characteristics and associated benefits

Feature	Benefits
Ultra low exhaust emissions—meets strict CARB standards	Eliminates need for air permit in some cases, simplifies air permitting when required
UL 1741 listed—meets IEEE 1547 utility Interconnection requirements	Expedites utility interconnection, eliminates need for fault current mitigation
UL 2200 listed	Complies with national electric code, satisfies local building codes and standards
Oil-free air bearings	Avoids costly periodic oil changes, eliminates hazardous material disposal, assures clean exhaust for critical applications
Essentially no vibration	Eliminates costly isolation mounting
High reliability and high availability	Maximizes valuable uptime, reduces unscheduled maintenance costs
Durable construction—can operate 24/7	Minimizes scheduled maintenance costs, maximizes valuable uptime
Integrated heat recovery system—includes automatic thermal controls	Reduces field connections, simplifies site engineering and design, eliminates additional thermal control hardware

start generating power to meet the load requirement. The total process can take several minutes, depending on microturbine size and whether it is starting from a cold or warm condition. During this startup sequence, some amount of external electrical energy will be required, and fuel consumption will be higher than under steady-state conditions until the recuperator and other internal components are brought up to operating temperature. Note that some of this additional fuel energy required to bring components up to temperature is actually recovered during a normal stop sequence.

A stop sequence will also typically use the generator as a motor during a portion of the sequence. First fuel is shut off, and the generator will continue providing some net electrical output to a grid connected load, or to recharge a battery. The electrical power will continue as a net output while turbine speed decreases until the thermal energy stored in the recuperator and other components is no longer sufficient to power the compressor section. At this point, the generator will become a motor and take power back from the connected utility grid or battery pack to keep the air flowing through the system until measured temperatures reach a preset limit. The turbine may then be stopped quickly by simply shorting the generator terminals momentarily. This normal stop sequence is often called a “cooldown,” as it is designed to bring key components to a safe temperature and avoid damage due to uncontrolled hot soaking. A cooldown can take 10–20 min, depending on the microturbine size and manufacturer.

A turbine may also be required to stop outputting power immediately, either as a result of a fault or commanded operation. A “brake resistor” is often included in the microturbine system to absorb any excess energy that cannot be accommodated by a utility grid or a battery pack. As long as there is control power available, the system will still proceed through a normal cooldown as described above.

However, if there is complete loss of control function or an emergency stop command has been given, the microturbine may simply coast to a stop with any excess power being absorbed by the brake resistor. Such an uncontrolled stop sequence is often called a “warmdown,” since internal temperatures cannot be controlled to desired limits.

### 8.2.2.2 Speed and Power Control

The controls built into microturbines are optimized to reduce sensing hardware costs. Typical sensors include turbine exhaust temperature (TET), ambient air inlet temperature, and ambient air pressure. Most microturbines have a generator fixed directly to the turbine shaft, in which case turbine speed can be monitored by the generator output frequency. In all cases, power output is measured as well.

Several control strategies can be used for fuel, power, and turbine speed. Fuel control systems often include a map of flow versus commanded valve position, or in the case of liquid fuel a commanded pump speed. This calibration data can be referenced by the microturbine fuel metering module to provide an initial command that relates to a desired fuel flow level. The system controller can also read ambient temperature and pressure to estimate what fuel flow is needed for a desired output power level. Finally, the measured output power and TET may be used to provide closed loop control of the system to fine tune fuel flow. Turbine speed can also be managed by taking power into or out of the generator to prevent over speed and regulate speed changes.

Changes in turbine generator power output are typically limited to some slew rate that is dependent on the associated speed changes in the turbine, and are in the range of 5–10 % per second. For applications where the microturbine is the only power source, an energy storage system, such as a battery pack, is typically used to provide fast response to load changes. This allows output power to remain stable in frequency and voltage while the turbine generator adjusts to the new average power requirement. A more detailed description of how the Capstone microturbines operate in Grid Connect and Stand Alone modes is provided below.

In Grid Connect operation, power can be provided from the microturbine system to the utility interface on an as needed basis for peak shaving or load following. A power demand is requested, either manually from the user, via a power meter, or from a building management system. The utility provides a stiff voltage source on the output power lines allowing the output inverter to maintain the DC-Link voltage by regulating current in phase with the utility voltage. Current may be sourced from the utility during generator start up. Current will be delivered to the utility once the microturbine engine is able to produce power. Microturbine speed is increased or decreased based on ambient operating conditions to meet the user power demand. The generator inverter varies current in phase with the microturbine generator to control speed. Fuel is provided to meet the predetermined temperature setpoint for the microturbine engine. Injectors are further staged to maintain combustion stability and meet emissions requirements.

In the Grid Connected mode of operation the output inverter is configured to regulate the DC-Link voltage by varying AC current in phase with the utility frequency. A desired DC-Link voltage is determined to provide adequate voltage margin for the output inverter IGBT's to generate the 480VAC or 400VAC output. The DC-Link voltage feedback is sensed by the output inverter controller and compared to the desired DC-Link voltage to determine a DC-Link voltage error. A closed loop algorithm adjusts the desired output current proportional to the DC-Link voltage error. For example, as the DC-Link voltage error increases, the desired output current is increased at a proportional rate. The output current feedback is sensed by the output inverter controller and compared to the desired output current and further used to calculate the output IGBT switching voltage. Utility phase voltages are sensed by the output inverter controller and converted to a utility frequency and phase angle. Using the output IGBT switching voltage and utility phase angle, the controller can then calculate the output IGBT duty cycle for each output inverter phase. Output current feedback, utility voltage feedback, and utility phase angle are used to calculate the output power feedback for other system controls.

Desired engine speed of the microturbine is determined using either proportional or model-predictive control algorithms based on the difference between the requested power demand and the output power feedback provided from the DC-Link voltage control. Most often these controls will use ambient pressure and ambient temperature to correct for variations in ambient operating conditions to more accurately select the desired engine speed. The desired engine speed is then communicated to the generator inverter controller.

The generator inverter controller uses the desired engine speed setting from the power control to regulate current into the microturbine generator. Generator current feedback is sensed by the generator inverter controller to calculate generator current magnitude, generator frequency or engine speed feedback, and generator phase angle. The generator current command is calculated based on the proportional difference between the desired engine speed and the engine speed feedback. Further, a generator IGBT switching voltage is calculated based on the proportional difference between the generator current command and the generator current feedback. Using the generator IGBT switching voltage and generator phase angle, the controller can then calculate the generator IGBT duty cycle for each generator inverter phase. Generator current, voltage, and phase angle are used to calculate the generator power feedback for other system controls.

A temperature controller is used to determine the desired TET setting and regulate the fuel control valve position to maintain the desired setting. Generator power feedback is gathered from the speed control to determine the desired TET setting. Additional considerations are made in selecting the desired TET based on ambient operating conditions and material limits within the microturbine engine. The desired TET is ideally selected to provide maximum operating efficiency and emissions for the microturbine engine. The desired TET setting is compared with the TET feedback sensed in the temperature controller to set the fuel control valve position. It can be advantageous to include additional sensors to monitor the fuel

supply given variations in fuel energy content, temperature, pressure, density, lubricity, and other fuel properties that the microturbine system may be exposed to. These sensors can then be used by the temperature control to compensate for variations in performance to provide more robust control.

Controls for sequencing multiple injectors on and off are required in order to provide optimal combustion performance over the engine speed, ambient conditions, and varying fuel flow. The injector control uses the feedback signals from the temperature and speed controls to determine the number and sequence of manifold solenoids that are enabled to deliver fuel to the injectors. Enabling the correct injector configuration is essential to ensure microturbine parameters such as stability, flashback, metal temperatures, and emissions limits are achieved. Better control resolution can be achieved by using more injectors, however increasing the number of injectors must be balanced with system complexity and design costs.

A simplified diagram for the Grid Connect control scheme described above is given in Fig. 8.5.

For operation in Stand Alone mode, the user sets the desired output frequency and voltage (typically either 50 or 60 Hz and 400 or 480 V). The system must regulate the output voltage and frequency into the customer load since there is no Utility power. The output inverter adjusts the output current to maintain output voltage and frequency to the desired user settings. The energy storage device provides current to maintain the DC-Link voltage. A state-of-charge (SOC) management algorithm is required to determine long term energy storage requirements for recharging. The output inverter and energy storage power demand requirements are combined to determine the microturbine power requirements. Microturbine speed is increased or decreased based on ambient operating conditions to meet total system power demands. The generator inverter varies current in phase with the turbine generator to regulate speed. Fuel is provided to meet a predetermined temperature setpoint for the microturbine engine. Injectors are staged to maintain combustion stability and meet emissions requirements.

In the Standalone mode of operation the output inverter is configured to regulate the AC output voltage by varying AC current in phase with the user output frequency and voltage settings. With no Utility available to provide desired output AC voltage and frequency reference signals, the system must provide output power at user requested values. The output AC voltage feedback is sensed by the output inverter controller and compared with the desired output AC voltage set by the user. A closed loop algorithm adjusts the desired output current proportional to the output AC voltage error. For example, as the output AC voltage error increases the desired output current is increased at a proportional rate. The output current feedback is sensed by the output inverter controller and compared to the desired output current and further used to calculate the output IGBT switching voltage. The user output frequency setting is integrated over time to calculate an instantaneous output phase angle that will be used for sequencing the output IGBT's. Using the output IGBT switching voltage and output phase angle, the controller can then calculate the output IGBT duty cycle for each output inverter phase.

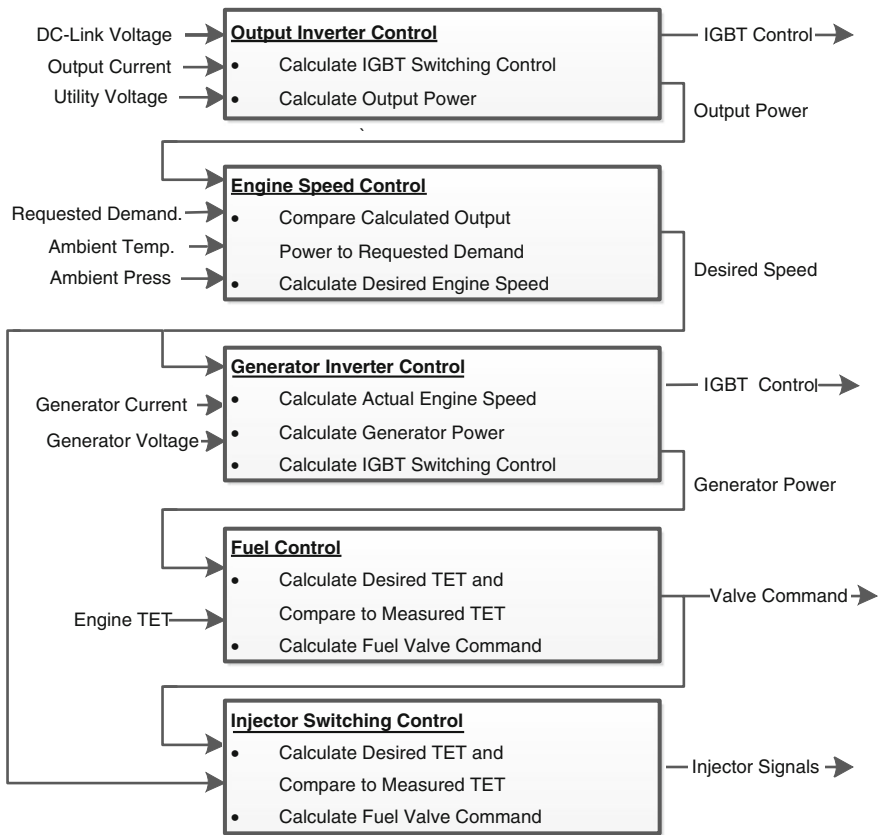


Fig. 8.5 Example grid connect microturbine control scheme

Output current feedback, output voltage feedback, and output phase angle are used to calculate the output power feedback for other system controls.

A separate energy storage system must be employed in this type of system to provide responsive DC-Link control as the microturbine engine is not able to quickly respond to changes in required output. A desired DC-Link voltage is determined to provide adequate voltage margin for the output inverter IGBTs to generate the 480VAC or 400VAC output. Generally, with an energy storage system such as a battery, flywheel, or ultra-capacitor which has unique discharge and charging requirements, the DC-Link voltage is not controlled to a constant value. Typically, a window of operation is allowed such that the energy storage system may be drawn upon below a lower DC-Link voltage and above a higher DC-Link voltage. A closed loop algorithm adjusts the desired energy storage current proportional to the DC-Link voltage error. For example, as the DC-Link voltage falls below the lower DC-Link voltage setting, the energy storage inverter IGBT's will be enabled to deliver energy storage current to the DC-Link.



When the DC-Link voltage feedback is between the lower and the higher DC-Link voltages, the energy storage inverter IGBT's are disabled, thereby delivering no energy storage current between the DC-Link and the energy storage system. The energy storage inverter IGBT's are enabled to deliver energy storage current from the DC-Link to the energy storage system when the DC-Link voltage is greater than the higher DC-Link voltage. Energy storage current and voltage feedback are used to calculate the energy storage power feedback for other system controls.

A SOC management control is required to evaluate the energy storage device condition to determine longer term energy storage power requirements. Energy is delivered and absorbed by the energy storage device to support the demands of the DC-Link control in this mode of operation. Left unregulated, the energy storage device could deplete all of its energy capability, ultimately collapsing the entire system with no energy to support the DC-Link control. Conversely, the energy storage device could absorb too much energy, creating an overcharge condition that results in overheating or failure of the energy storage device. Energy storage power feedback is therefore integrated over time to monitor how much energy has been delivered and absorbed by the energy storage device. Energy delivered reduces the SOC, while energy absorbed increases the SOC. A desired energy storage power is calculated based on the energy storage SOC and is further adjusted to support the charging profiles required to optimally maintain the energy storage device.

Desired output power and desired energy storage power are combined to determine the required power demand that must be delivered from the microturbine engine. Desired engine speed for the microturbine is determined using either proportional or model predictive control algorithms based on the difference between the power demand and the sum of the output power feedback provided from the output voltage control and the energy storage power feedback provided from the DC-Link control. Most often these controls will use ambient pressure and ambient temperature to correct for variations in ambient operating conditions to more accurately select the desired engine speed. The desired engine speed is then communicated to the generator inverter controller.

For the Stand Alone mode of operation, the system is able to take advantage of the same speed, temperature, and injector controls that are used in the Grid Connected mode.

### **8.2.2.3 Data Recording and Fault Handling**

A variety of data and fault conditions are monitored continuously and actions taken depending on severity levels. For example, if the measured TET falls below a preset limit for a set time, a "flameout" alarm condition is declared. This condition can cause an attempt to restart by reintroducing fuel and ignition. If several repeated attempts to relight are unsuccessful, the system can automatically shut down and indicate the cause.

As another example, if measured output voltage drops below preset limits for a set time period, output power may be immediately disconnected and a fault condition logged. This may also result in an attempted reconnection to the load, depending on the severity level and how the microturbine was configured by the user for the specific application.

Most microturbines have the ability to not only log fault status with a time stamp, but also record key operating parameters prior to and after the event to assist with diagnosing the problem. Software for a personal computer (PC) is generally available to view these logs and events, as well as configure the microturbine for the specific installation. Figure 8.6 shows an example of data from one manufacturer’s monitoring software with key parameters displayed in the form of a strip chart. This example shows a turbine starting event, with engine speed, TET, output power, fuel flow, and injector state over a 6 min period. Note that engine speed is well controlled, and passes through several preset levels before arriving at full speed of 96,000 rpm. TET is also well controlled after the initial introduction of fuel. At the start of the sequence, output power is negative, and is required from the utility grid for the power electronics and to accelerate the turbine/generator assembly to a “light-off” state. When sufficient fuel energy has heated the turbine and recuperator assembly, generator speed is increased to develop the 60 kW power demand and fuel increased to maintain the desired TET.

### 8.2.3 Power Characteristics

The microturbine has several important output power characteristics as described in the following subsections.

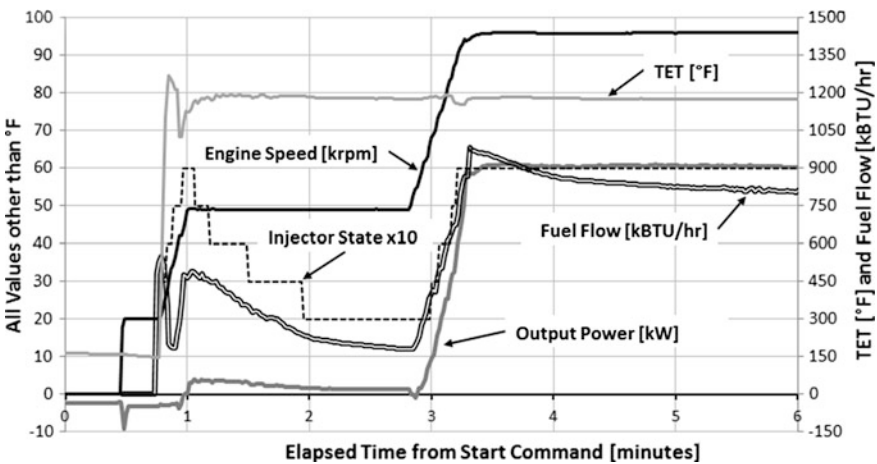


Fig. 8.6 Data monitoring during 60 kW microturbine start

### 8.2.3.1 Operating Modes

Depending on the manufacturer and model, the output electrical power can be either AC or DC, and can operate in several modes. Table 8.4 provides a summary of several modes of operation. Not all microturbine manufacturers offer products that are able to operate in all modes.

Switching between a current source and a voltage source operating mode typically requires shifting between operating software modules, and therefore takes some amount of time without any output power at all. Some manufacturers offer a “fast transfer” system that will allow shifting between Grid Connect and Stand Alone modes within 10 s [13]. The Hybrid UPS mode allows seamless transfer between utility and microturbine power sources, as well as allowing them to operate in parallel.

### 8.2.3.2 Power Quality

Power quality is a general term that often refers to the waveform of the output current or voltage under specified conditions, as well as the reliability or availability of that power output. IEEE 519 [14], IEC 62040 [15], and other similar international standards provide guidance on specific criteria and measurement techniques. Microturbines typically use power electronics with appropriate filtering to condition their electrical outputs. As a result, steady state power output

**Table 8.4** Microturbine operating modes

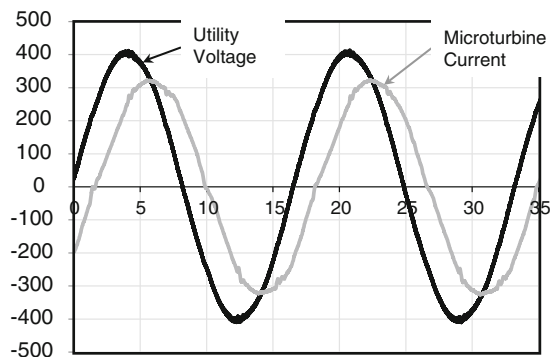
Operating mode	Description
Grid connect	A current source operating mode where the microturbine is connected to a utility voltage source. Voltage is measured and current is injected into the utility grid and is controlled to meet a set electrical power demand
Stand alone	A voltage source operating mode where the microturbine is the only power source. Voltage is maintained at a preset amplitude and current follows the load. Typically requires an integrated energy storage system, such as a battery pack, to provide fast response to changing load conditions
Thermal load following	A current source operating mode where the microturbine is connected to a utility voltage source. Voltage is measured and current is injected into the utility grid to meet a power demand that is determined by the thermal output of the microturbine
Hybrid UPS	A voltage source operating mode where the power source can be the microturbine, a utility grid, or a combination of both. Voltage is maintained at a preset value and current follows the protected load. When the utility grid is present and stable, the output voltage to the protected load is also synchronized with the utility within a few degrees of phase shift
Hybrid electric vehicle	A current source operating mode where the microturbine is connected to a DC energy storage system in a hybrid electric vehicle drivetrain. Voltage is measured and current provided to the energy storage system to follow a power demand command from the vehicle control system

closely matches a sine wave and manufacturers provide output specifications according to recognized standards. Figure 8.7 shows the current output of one manufacturer's microturbine operating in grid connect mode. In the figure, one phase of the microturbine's three-phase current output is shown, along with the respective utility phase voltage reference. The example also shows that the current can be shifted to a preset phase angle relative to the utility voltage in order to provide both real and reactive power.

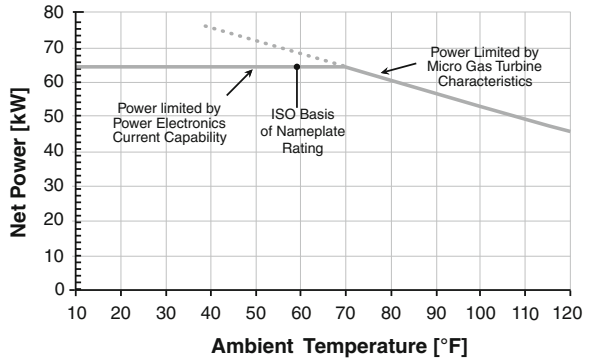
### 8.2.3.3 Temperature and Elevation Factors

Microturbines are often called “mass flow devices” due to the fact that they take in significantly more air than is required for stoichiometric combustion. Microturbine systems have been designed with this characteristic in mind, and the size and capability of the generator and associated power electronics are matched to the microturbine output. Manufacturers typically publish their outputs based on International Organization for Standardization (ISO) conditions at sea level, 59 °F, and 60 % relative humidity [16]. Several microturbine manufacturers take the high frequency output of the generator that is connected to a common shaft with the gas turbine power section and use power electronics to rectify it to DC, and then invert back to useable AC power at 50 or 60 Hz. Since the generator windings and power electronics outputs are limited by their current carrying capacity, the net microturbine power output is typically controlled not to exceed some maximum level as temperature decreases, even though the gas turbine engine could produce additional power. Figure 8.8 shows an example of the published power output of a 65 kW microturbine system as a function of temperature [17]. Derating factors apply to changes in elevation, electrical efficiency, and useable waste heat as well. Consult the microturbine manufacturer for their published performance curves based on temperature and elevation.

**Fig. 8.7** Microturbine current output waveform



**Fig. 8.8** Power output performance versus temperature for a 65 kW microturbine



### 8.2.3.4 Overcurrent Capability

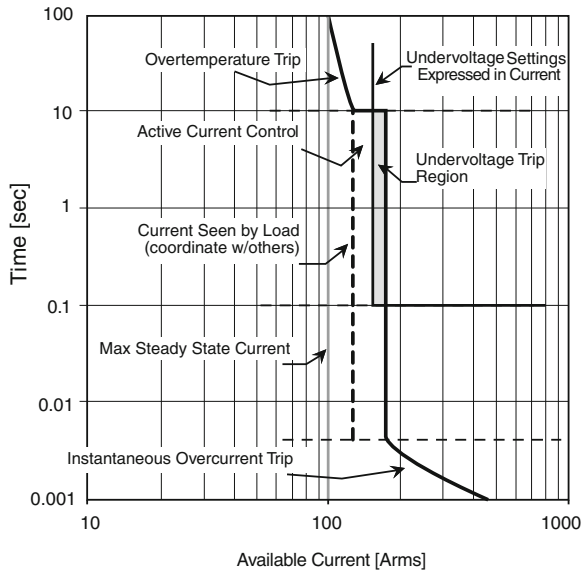
Microturbines using power electronics to condition their output characteristics have some unique overload current characteristics.

When operating in a Grid Connect mode, the microturbine is acting as a current source, and therefore current output will automatically increase to maintain the power demand setting as grid voltage drops. This will happen relatively slow compared to an abrupt change in grid voltage due to a fault. In addition, the current that can be provided is limited, and voltage drops below the microturbine’s internal protective settings will quickly disconnect power. For these reasons, microturbines with power electronics outputs are generally not considered to contribute fault current in a utility network. This is in contrast to a synchronous generator, where fault current contributions of six to ten times rated current are possible, and this additional current may exceed utility circuit protective device capacities.

When operating in a Stand Alone or Hybrid UPS mode, the microturbine is acting as a voltage source, and therefore will immediately adjust current in response to any abrupt load change. Each microturbine’s power electronics will have a maximum allowable steady state current output that is related to the maximum power output rating. Currents above this steady state limit typically fall into three different zones of operation, as shown in Fig. 8.9 and discussed below:

- **Overtemperature Trip**—For moderate overloads, the thermal protection within each IGBT module will shut off power if temperatures reach potentially damaging limits.
- **Active Current Limit Control**—For heavier overloads, the inverter controls will actively adjust output voltage to maintain current at some threshold level. This is often termed “Active Current Limit Control”. The resulting reduced output voltage (and current) may be somewhat distorted, as the inverter constantly makes adjustment to maintain active current limit control. This controlled current condition is not directly limited in time, but can indirectly cause a

**Fig. 8.9** Time-overcurrent curve for a 65 kW microturbine



shutdown if over temperature limits are reached or the reduced output voltage drops below any protective relay undervoltage settings.

- **Instantaneous Overcurrent Trip**—If short circuit currents try to exceed a set peak current for any reason, the inverter may immediately shut down on an instantaneous overcurrent trip condition.

For purposes of coordination with other protective devices, the time-overcurrent curve in Fig. 8.9 uses a log/log scale and shows these three zones of operation for a 65 kW microturbine [18]. The dashed line at the left edge of the active current limit control zone should be used for coordinating with other circuit protection devices.

Note that undervoltage settings can be expressed in equivalent fault current based on the performance of any active current limit control function. For example, the voltage versus available current in Fig. 8.10 is based on the performance of a 65 kW microturbine operating at 480 V nominal output. In this example, the active current limit control will reduce output voltage to try to maintain a current of 127 Arms resulting in increasing voltage drop as the available fault current increases. An undervoltage setting of 400 V corresponds to about 152 Arms available fault current using Fig. 8.10, which is then shown in Fig. 8.9 as the “undervoltage settings expressed in current” line.

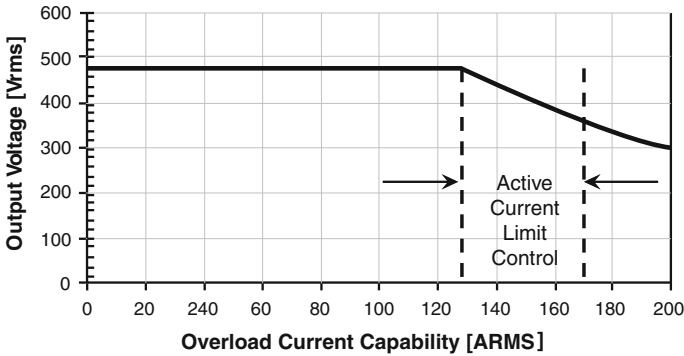


Fig. 8.10 Voltage versus overload current for a 65 kW microturbine

### 8.2.4 Standards and Certifications

There are currently no published standards specifically for microturbines. However, there are many recognized national and international standards that can be applied. Meeting selected standards can facilitate installation and permitting of microturbines, especially when independent third parties like Underwriters Laboratories (UL) and the California Air Resources Board (CARB) have certified the results. Table 8.5 summarizes some relevant standards.

#### 8.2.4.1 Utility Interconnection (IEEE 1547)

Utilities typically require any onsite generator be permitted by them before being allowed to be connected to their grid. There are multiple reasons for this, including safety concerns for utility linesmen, potential impact on the quality of utility power, and capacity of the existing utility system. The international standard IEEE 1547 was developed with participation from utilities and equipment manufacturers to provide guidance on the technical requirements for inverters to be connected to a grid. UL adopted this in UL 1741, and can now certify equipment to this standard.

Offering a microturbine that is certified to UL 1741 is extremely useful, but not sufficient by itself to acquire a local utility permit. The utility must review many

Table 8.5 Benefits of meeting recognized international standards

Standard	Description	Benefit
UL 2200 [19]	Engine generator sets	Expedites building Approval
UL 1741/IEEE 1547 [20, 21]	Inverters for utility grid connection	Simplifies utility interconnection
CARB [22]	California air resources board DG standard	Eliminates or simplifies air permitting

factors before deciding that a particular microturbine at a given site can be permitted. For example, California took a leading role to simplify utility interconnection permitting in an effort to remove barriers to installing distributed generation. The result is termed “Rule 21”, which created an eight question screening guide. If the answers to all questions meet specific criteria, the generator qualifies for a simplified interconnection agreement that avoids costly and time consuming engineering review. Figure 8.11 shows the Rule 21 recommended review process flow chart [23]. Note that Screen 3 is the only question where prior equipment certification helps expedite the process. As of this printing, a new working group is updating this interconnection process. Other local authorities have similar requirements.

#### **8.2.4.2 Safety Requirements (UL & CE)**

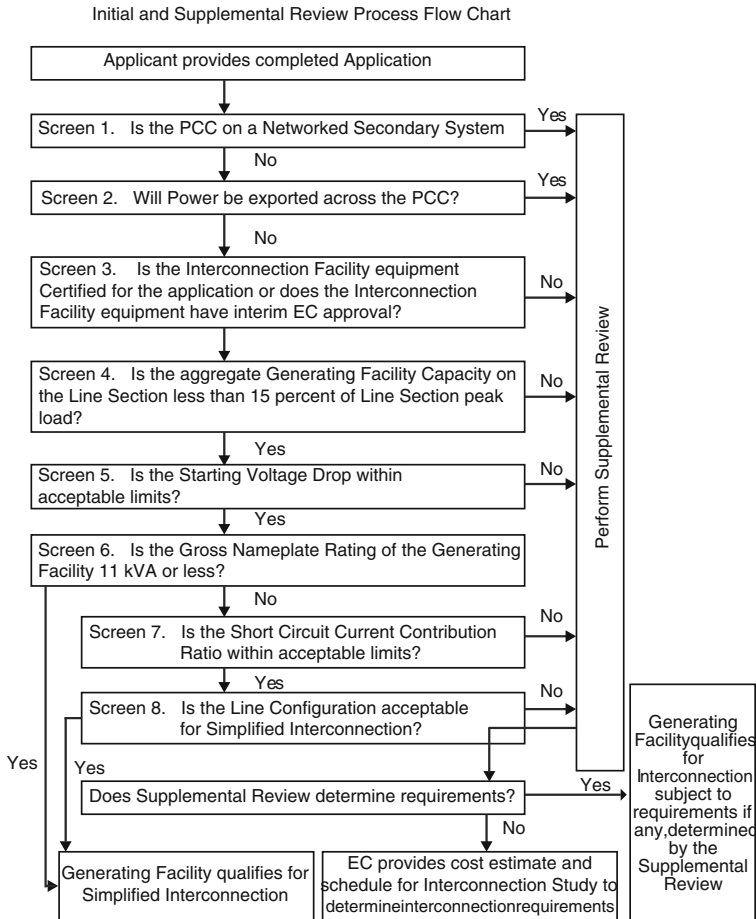
As with any distributed generation equipment, microturbines will typically require local building authority approval before installation and operation is permitted. Equipment that meets relevant local equipment standards, or better yet is certified by a recognized third party, will have a much easier time gaining approval. Building inspectors are not experts in the details of every piece of equipment, especially a relatively new type of generator such as a microturbine. Standards like UL 2200 for generators, or the many Conformité Européene (CE) directives, such as the Low Voltage Directive (98/79/EC) and Safety of Machinery Directive (98/37/EC), help local authorities to address their safety concerns. However, as with utility grid interconnection, there may be additional local requirements to be adhered to. For example, the New York City Department of Buildings has a process called the materials and equipment acceptance (MEA) index [24], which lists specific equipment that has been pre-certified by them, along with application and operational requirements that the installation must adhere to. Microturbine manufacturers can receive approval under MEA for their products, which includes the requirement for adherence to UL standards as well.

#### **8.2.4.3 Exhaust Emissions (CARB)**

Local air districts and/or national environmental protection agencies will often require permitting or certification before allowing microturbine operation in stationary or mobile applications. Because of their continuous lean combustion processes, microturbines can typically meet the strictest criteria pollutant standards in the world, including those of the CARB. Typical criteria pollutants of concern include oxides of nitrogen (NO<sub>x</sub>), unburned hydrocarbons or volatile organic compounds (VOC's), carbon monoxide (CO), and for liquid fuels particulate matter (PM).

As an example, the CARB standard for distributed generation was set using current state-of-the-art natural gas fired central power plant emissions as the



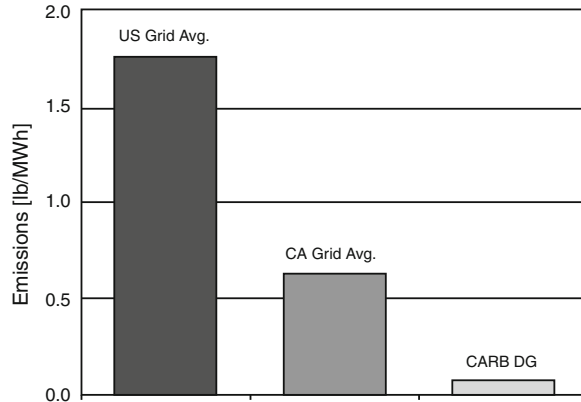


**Fig. 8.11** California rule 21 utility interconnection review process

reference. Several microturbine manufacturers have achieved certification to this low level, and have done so without requiring any active exhaust after-treatment. To put this achievement in perspective, Fig. 8.12 provides a comparison of the relative NO<sub>x</sub> emissions from an equivalent amount of electrical energy output from the average US power grid, the California power grid, and the CARB requirement for microturbines used as distributed generation. References for the grid NO<sub>x</sub> values were taken from the US EPA Power Profiler website [25], while the CARB DG level is taken as the 2007 natural gas certification requirement [22].

Microturbines can also be used in mobile applications such as hybrid electric vehicles. Emissions standards for this application are often higher than for stationary distributed generation since the state-of-the-art reference is small reciprocating gasoline or diesel engines. Figure 8.13 compares emissions results from certification of two 30 kW microturbines to the CARB 2010 Heavy Duty Diesel

**Fig. 8.12** Utility NOx emissions versus CARB distributed generation standard



Engine standard [26, 27]. The manufacturer of these microturbines designates them C30. Note that the 30 kW microturbines exhibit emissions significantly lower than the standard, and that they achieve similar low emissions results whether operating on natural gas or diesel fuel.

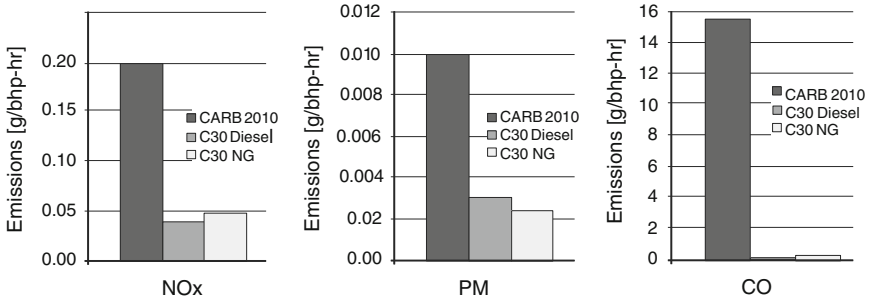
### 8.3 Power Electronic Topologies for Microturbines

Most commercial microturbines use power electronics with insulated gate bipolar transistors (IGBT's) as the switching elements. One manufacturer uses a high speed gearbox connected to the turbine output to drive a conventional synchronous generator. Several topologies are discussed in the subsections below.

#### 8.3.1 Stationary Power Topologies

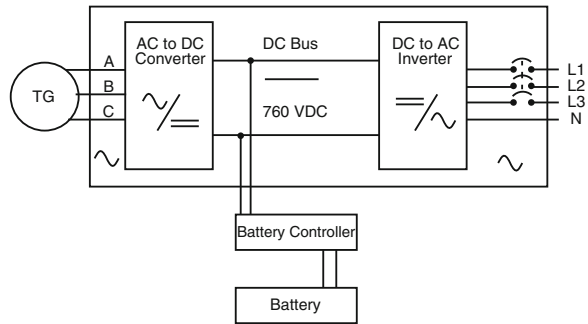
The topology in Fig. 8.14 is the most common configuration for stationary power generation, and is often referred to as a DC-Link Topology. The microturbine TG on the left provides high frequency AC power output that is typically variable in frequency with speed. Commercial microturbines are currently in the operating speed range of 30,000–100,000 rpm, and use a two pole permanent magnet three phase generator design. This results in generator output frequencies of about 500–1,600 Hz.

The high frequency AC output from the microturbine generator is first rectified to DC using an active rectifier with bi-directional pulse-width modulation. The generator inverter IGBT switching frequency is typically in the range of 7.5–20 kHz depending on resolution of control required to match the speed range of the microturbine generator, IGBT switching loss optimization, and optimization



**Fig. 8.13** Emissions of 30 kW microturbines versus CARB 2010 engine standard

**Fig. 8.14** Typical microturbine DC-link topology



of magnetics costs. Power is then transmitted to the output using a bi-directional pulse-width modulated DC to AC inverter, typically providing three phase AC voltage at 400–480 V line-to-line and frequency at 50 or 60 Hz. The output inverter IGBT switching frequency is typically in the range at 5–15 kHz depending on resolution of harmonics required on the AC output, IGBT switching loss optimization, and optimization of magnetics costs. Nominal output voltage and frequency are configurable by the user for Stand Alone application. For a Grid Connected application, the output inverter controls the DC-Link voltage by sourcing and sinking current from the connected utility which determines the AC voltage and frequency. Grid Connected applications have the additional advantage of providing start power for the microturbine system from a connected utility.

For a Stand Alone application, starting power is required from an energy storage system, typically a battery pack integrated into the microturbine package. In this case, an additional bi-directional pulse-width modulated DC to DC converter (or Battery Controller) is used to connect to a battery. Such a Battery Controller is required since the battery pack will typically have a lower voltage than the DC bus, and will also exhibit voltage swings depending on power draw and state of charge. The battery is not only used for starting, but can source or sink

power during load changes so that the output AC remains stable while the microturbine generator adjusts its power output.

Suitable filtering is included in all the IGBT switching modules to achieve acceptable levels of voltage and current distortion. The switching modules are typically designed to attain efficiencies in the 95–97 % of full power range so that overall fuel-to-electric conversion efficiencies remain high.

### 8.3.2 Hybrid Vehicle Topologies

For use in hybrid electric vehicle drive systems, a DC output version of the microturbine is required. The microturbine generator provides high frequency AC output that is typically variable in frequency with speed. The first conversion stage is essentially the same as the AC to DC converter shown in Fig. 8.14. Again, the high frequency AC output from the microturbine generator is first rectified to DC using an active rectifier with bi-directional pulse-width modulation. It is the vehicle energy storage system that will dictate the actual DC bus voltage, which will depend on SOC, power draw, and other factors. Current vehicle energy storage systems typically use lithium ion batteries, although ultra-capacitors and flywheels are finding some limited applications.

Figure 8.15 shows a typical series hybrid electric topology where energy to recharge the batteries can come from three sources: the microturbine at any time, an electric utility grid when the vehicle is parked, and regenerative braking energy through the traction electric motor and its vehicle drive system when the vehicle is slowing down. Typical DC bus voltages are in the 300–400 V range for automotive and light duty trucks, and 600–700 V for heavy duty truck and bus applications.

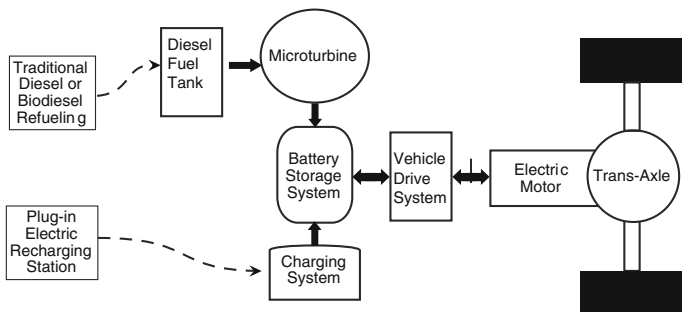


Fig. 8.15 Series hybrid vehicle topology

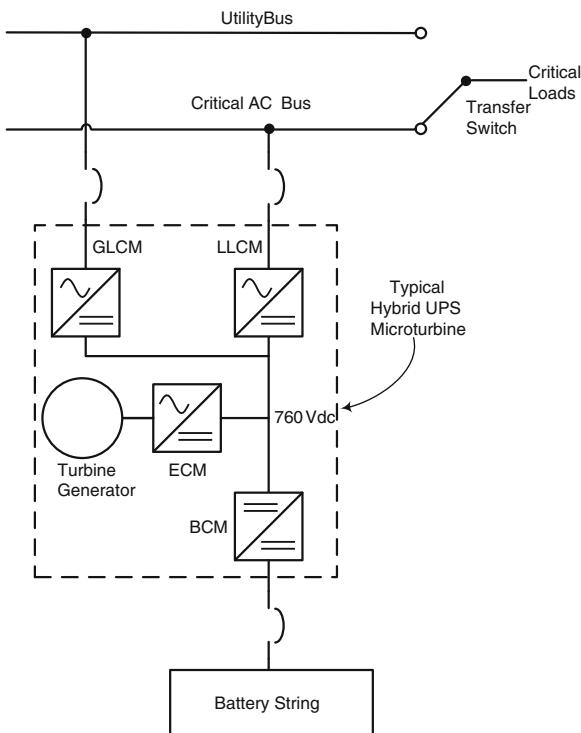
### 8.3.3 Hybrid Topologies

The inverter modules used in microturbines are typically bi-directional and flexible enough to be combined into different system topologies. One example is the Hybrid UPS design of one manufacturer, as shown in Fig. 8.16.

Comparing this topology to that in Fig. 8.14, a second DC to AC Inverter is added. One of these two DC to AC Inverters is connected to the utility bus (noted as GLCM in the figure). The second DC to AC Inverter module is connected to the critical AC bus (noted as the LLCM). The topology also includes the AC to DC Converter (noted as ECM in the figure), and the Battery Controller (noted as BCM in the figure).

Power can now flow in several directions, depending on both the condition of the utility bus power as well as commanded operating mode from the user. Table 8.6 summarizes the operating modes and sources of power to the critical AC bus. One capability of this topology is that the LLCM output to the critical AC bus can be automatically synchronized with the GLCM input from the utility bus within a few electrical degrees so that the transfer switch in Fig. 8.16 can be immediately connected to the utility source when required. Typically the transfer switch would be of the make-before-break type, so there would be no disturbance

**Fig. 8.16** Hybrid UPS topology



**Table 8.6** Hybrid UPS operating modes

Mode	Power source	Power flow
UPS normal	Utility	From utility to critical load
High efficiency	Utility plus microturbine	From microturbine to critical load with difference imported from or exported to the utility
Emergency	Microturbine and/or battery	From microturbine and/or battery to critical load

to the critical AC bus when transferring back and forth between direct utility connection and the hybrid UPS microturbine.

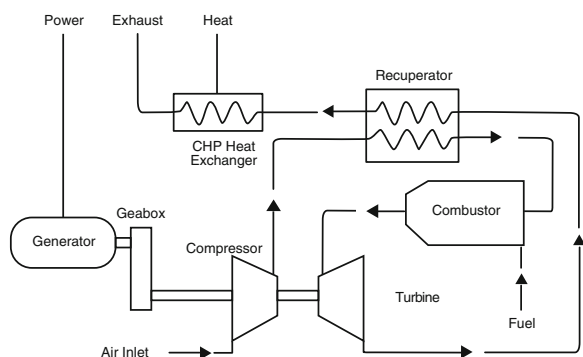
### 8.3.4 Direct Conversion Topologies

One microturbine manufacturer does not use IGBT-based electronics to convert turbine power to useable electrical output, but instead uses a gear reduction to drive a traditional synchronous generator [7]. Figure 8.17 shows a block diagram of the major components for this type of construction.

### 8.3.5 Advanced Topologies

Alternative electronics topologies have been proposed for future microturbines. One concept, termed a “High-Frequency Link Converter”, uses high frequency conversion between the microturbine generator and the connection to the utility. This has the advantage of galvanic isolation between the output inverter and the rest of the power electronics, but requires additional components. Another concept uses direct AC to AC conversion called a cycloconverter or matrix converter. This has the advantage of potentially smaller size and weight, but makes connection to an energy storage element more difficult. Both of these advanced topologies are

**Fig. 8.17** Microturbine using gearbox to generator output



discussed in more depth in a National Renewable Energy Laboratory Technical Report NREL/TP-581672 [28].

### 8.4 Controls for Microturbine Power Electronics

Figure 8.18 shows one manufacturer’s block diagram of the individual modules and how they are interconnected. The figure shows power as well as digital communications connections. In Fig. 8.18 there are digital signal processors (DSP’s) embedded in the Fuel Metering Module, Generator Control Module, Load Control Module (LCM), and Battery Controller Module. The DSP’s in each module have specific functions to perform, and are coordinated by the computer in the System Control Board. The subsection below will describe each module in more detail.

#### 8.4.1 Internal Control Modules

Referring to Fig. 8.18 and the topology in Fig. 8.14, the major control modules and their functions are summarized in Table 8.7. Not all commercial microturbines use this exact module functional breakdown, but it is provided here as one practical example.

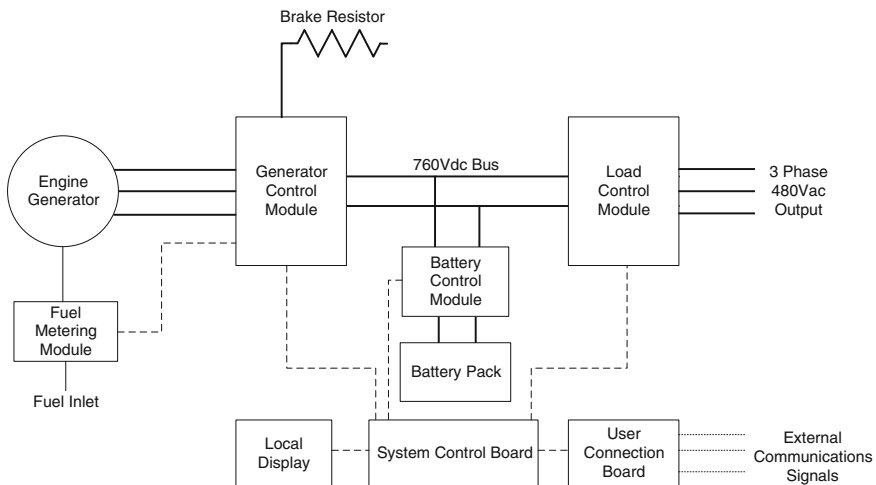


Fig. 8.18 Block diagram of major microturbine components

**Table 8.7** Summary of internal control modules and their primary functions

Control module	Primary functions
Generator control module	Passes power to/from engine generator and DC bus using PWM control of its IGBT's, provides commands to fuel metering module, directs power to brake resistor module when load control module or battery control modules cannot accept it, acts as the 24VDC control power source for all modules
Fuel metering module	Converts commands from generator control module to fuel flow, monitors engine temperatures, controls fuel injectors, activates igniter during start and injector switching, controls safety shutoff valves
Load control module	Passes power from the DC bus to/from the 3 phase AC output using PWM control of its IGBT's, provides control in grid connect or stand alone mode, measures output voltage, current, frequency, and power and provides protective relay logic
Battery control module	Passes power to/from battery pack using PWM control of its IGBT's, manages battery pack
System control board	Manages overall microturbine operation, communicates with all control modules to send commands and receive operating data and status, interfaces with user through display and user connection board interfaces

### 8.4.2 Synchronization and Load Sharing

When more than one microturbine is installed at a site, one of the microturbines can act as a master to coordinate operation of the group. A digital communications link between each microturbine is used to pass synchronization information between them so that they share the connected load equally and provide one common interface to the user to simplify monitoring and control.

For more sophisticated control, an external accessory is typically available to coordinate multiple microturbine groups, provide higher level logic, and interface with other equipment. Figure 8.19 shows a connection diagram for one such accessory controller—in this example the UPS Controller [29] which is designed to interface with the Hybrid UPS microturbine described above.

This type of master controller can start and stop individual microturbines to balance run times, meet customer load requirements, and improve total system efficiency. Figure 8.20 shows one example of how such a controller can turn microturbines on or off to match the customer load to provide improved efficiency over the full power range. This type of control can also include a minimum spinning reserve setting so that sufficient microturbines are maintained in a load state to accommodate an abrupt load increase.



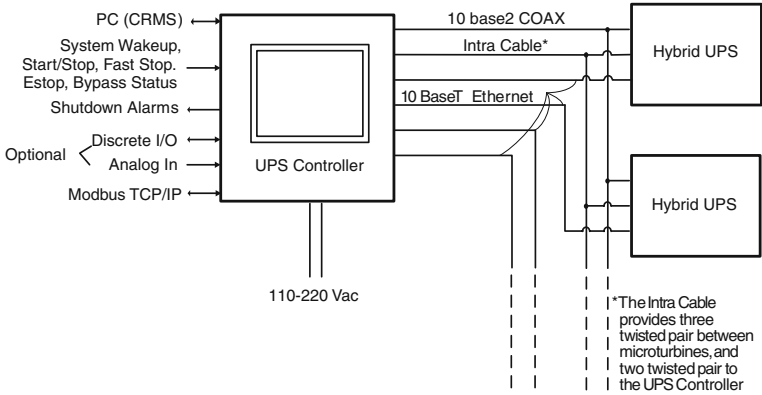


Fig. 8.19 Master controller to coordinate multiple microturbines

### 8.4.3 Protective Relaying

Information about the AC voltage, current, and frequency is constantly monitored in each microturbine, typically in what is shown as the LCM in Fig. 8.18. One of the functions of the LCM is to automatically trip the system based on measured values and preset time and threshold levels. This will typically include traditional protective relay functions such as over and under voltage, over and under frequency, and overcurrent. IEEE 1547 and UL 1741 prescribe requirements for these settings, and Fig. 8.21 provides an example time–voltage plot for one manufacturer’s microturbine.

Since microturbines are power generation sources, they are also able to provide active protective functions that traditional protective relays cannot. For example, in Fig. 8.21 there are two regions of voltage and time duration where the

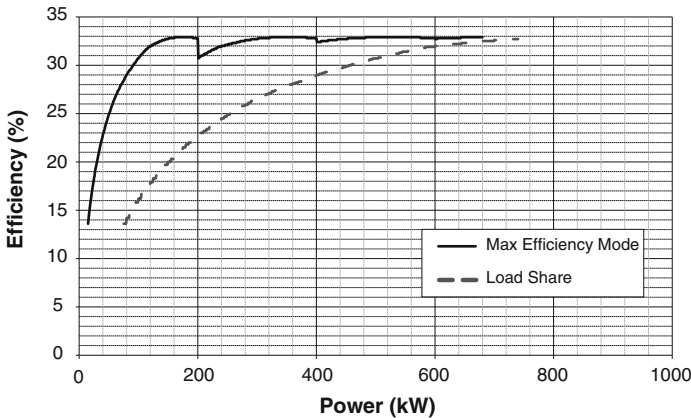


Fig. 8.20 Maximum efficiency control versus simple load sharing

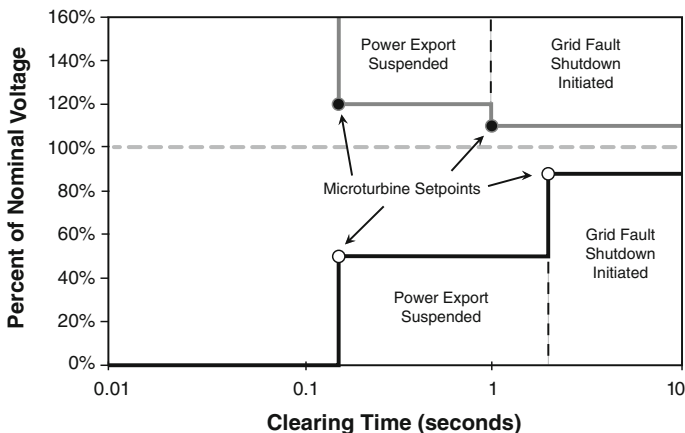


Fig. 8.21 Voltage protection function

microturbine will momentarily stop exporting power until conditions return to within preset limits.

Another important active function is called “Anti-Islanding”. This function is designed to detect a condition where the utility grid has been disconnect from part of the load, but the remaining load is matched to the output of the microturbine such that there would be little voltage or frequency change, creating a so called “unintentional island”. The microturbine protects against this condition by constantly changing its power output frequency slightly and measuring the system frequency response. If the utility grid is present, any attempted change in microturbine output frequency will result in no change in the measured grid frequency. However, if the utility is disconnected, an attempt to change frequency will result in some measureable shift, which can then be used to automatically trip the microturbine on a fast underfrequency setting and stop producing power. Response times can be very quick, typically less than 2 s.

### 8.4.4 External Communications

The computer in the System Control Board of Fig. 8.18 not only communicates with each internal module, but also has the capability to communicate externally with other microturbines and control equipment. In addition, external master control accessories such as shown in Fig. 8.19 have the ability to communicate with building management or other control systems using industry standard protocols. Typical digital communications capabilities include Ethernet, RS485, CANbus, and RS232 using proprietary as well as standard Modbus or Internet protocols. Discrete I/O and 4–20 mA analog inputs are also available with various microturbines.

One of the important advantages of using integrated power electronics is the ability to remote monitor microturbine status, read historical and real time data to help diagnose problems, and even download software or configuration files to improve performance. Manufacturers typically offer software that can be loaded onto a PC and remotely connected to their microturbines using the Internet or other communications network. Figure 8.22 shows an example screen for one such PC software.

### 8.5 Examples of Microturbine Integration

Several examples of how microturbines can be integrated into complete systems are provided in the subsections below. These cover stationary as well as mobile applications, and provide some insights into the performance as well as communications and control interfaces.

#### 8.5.1 Combined Cooling, Heating, and Power Example

Microturbines provide clean exhaust energy that can be recovered using thermal processes like heating water and driving an absorption chiller. This means there are two or three useful outputs from one fuel input, and the overall system efficiency can be significantly higher than using traditional separate conversion process for electricity, heat, and cooling. All commercial microturbine manufacturers have multiple examples of such installations, and there are various approaches to

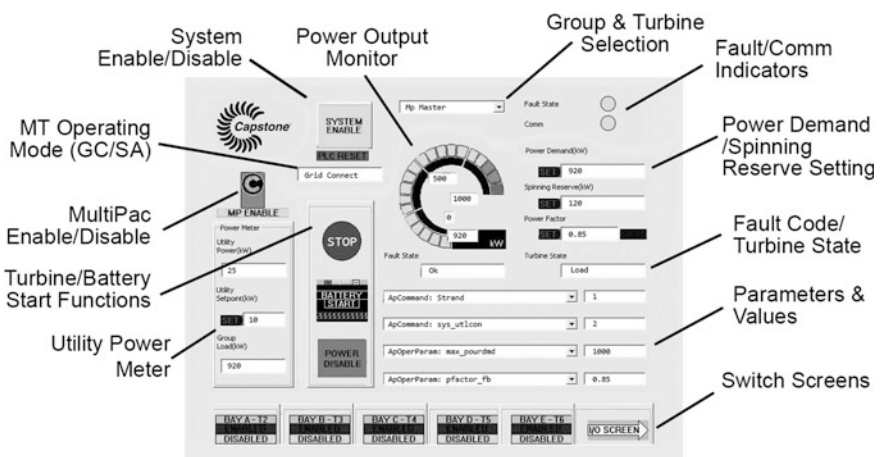


Fig. 8.22 PC software displaying microturbine information

putting such a system together. The example in this subsection is one practical application that has been in operation 24/7 since 2005 at the Ronald Reagan Presidential Library in Simi Valley, California.

The installed system consists of three UTC PureComfort™ packages, each with four 60 kW microturbines and a Carrier absorption chiller. The system also includes four additional 60 kW microturbines with integral hot water heat recovery modules. In addition to producing 960 kW of electricity, the direct exhaust-fired absorption chillers capture thermal energy to provide 387 tons of refrigeration for cooling, and the four heat recovery modules can produce 480,000 BTU/h of hot water. Figure 8.23 shows a photograph of the installed microturbines and chillers, with exhaust ducting to the chillers.

The microturbines in this installation are controlled by the chiller management system, which measures and responds to the thermal needs of the building.

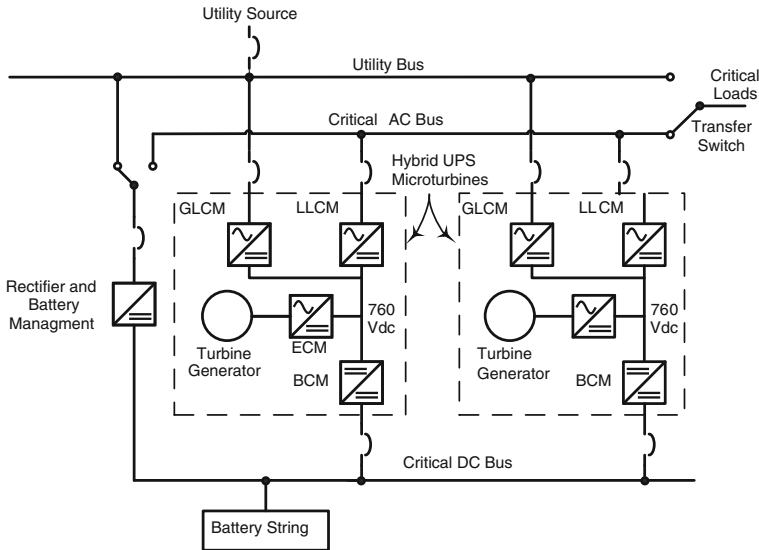
### 8.5.2 Hybrid UPS Example

Syracuse University, in partnership with IBM and others, set some high objectives for a new data center they were building that included a targeted 50 % energy reduction compared to deploying traditional design approaches. Some of the contributors to achieve this target included using water cooled heat exchangers installed directly inside data servers and distribution of some of the power using DC rather than AC. However, the biggest contributor to efficiency improvement was to replace traditional double-conversion UPS systems and electric chillers with a combined cooling, heating, and power system based on the Hybrid UPS microturbine topology described in Sect. 8.3.3.

Figure 8.24 shows a simplified electrical diagram of part of this installation that includes six Hybrid UPS microturbines, transfer switches, and connections to a

**Fig. 8.23** Microturbine CCHP installation





**Fig. 8.24** Electrical diagram of hybrid UPS installation

common battery bank. A building management system controls the microturbines through a microturbine master controller using Ethernet with Modbus protocol. The microturbine master manages commands from the building management system and using its own control logic directs each microturbine to start or stop and at what power level to operate. For example, the building management system monitors the thermal requirements of the facility, and estimates what microturbine power level is needed to support operation of the absorption chiller or heat recovery module. It then sends this information to the microturbine master controller as a desired total electrical output. The microturbine master uses this requested power demand to determine how many microturbines are required, which microturbines should run based on their operating hours, and what power level to run at. It then monitors them for proper operation and readjusts as needed to track any changes in the requested total electrical output.

If the utility grid experiences an outage, each connected Hybrid UPS microturbine will automatically switch to emergency mode operation. In this mode, power can be immediately taken from the battery bank as needed to maintain uninterrupted power to the critical loads. If a microturbine's engine is not already running at the time of the utility disturbance, the microturbine will wait a preset amount of time before starting its engine. This is to avoid unnecessary starts and stops due to short duration utility disturbances. If that microturbine's engine is already running, it will adjust its power level to meet the critical load demand rather than the power demand that came from the building management system. The microturbine master controller coordinates the transitions to and from

emergency mode by indicating status to the building management system and bringing the microturbines back to the appropriate state when the utility power returns.

This is one example of how control responsibilities can be divided between a third party building management system, a microturbine master control accessory, and the microturbines themselves.

### 8.5.3 Hybrid Electric Vehicle Example

There is growing interest in hybrid electric vehicles and microturbines are well suited for this application. In this case, the microturbine is typically acting as a battery charger, or “range extender” for what is otherwise a battery powered electric vehicle. Figure 8.25 shows a simplified diagram of the major components in a series hybrid system.

Energy for vehicle propulsion comes from an on-board battery pack. Most of them use lithium-ion batteries, with individual 2.4–3.8 V cells put in series to achieve the required system voltage. Automobile applications may be 300–400 VDC, while heavier duty truck and bus applications may use 550–650 VDC to gain efficiency and reduce conductor and motor sizes. Many applications use permanent magnet AC traction motors driven by a variable frequency DC to AC inverter, very much like the technology used in the microturbine itself. Output from the motor drives the vehicle wheels using appropriate gear reduction. A multi-speed transmission may be included, but can often be avoided due to the wide speed range of the traction motor and its high torque at low rpm.

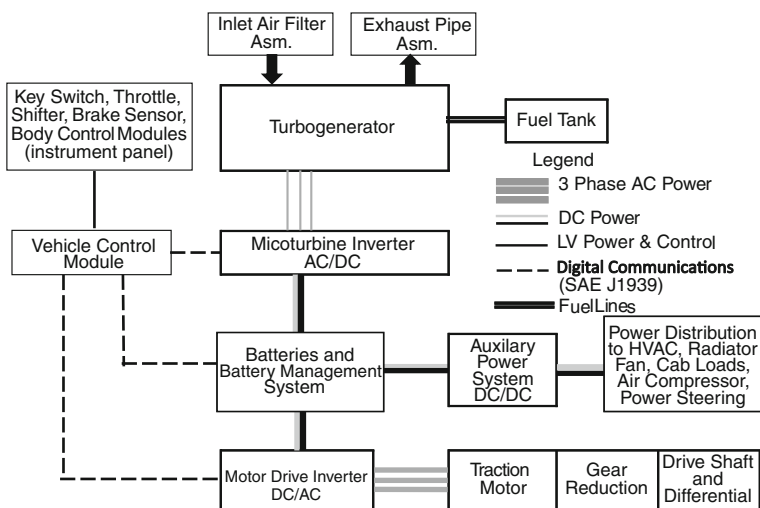


Fig. 8.25 Block diagram of series hybrid electric vehicle components

A vehicle control module interfaces with the chassis components such as the key switch, accelerator, and brake pedal, and converts operator inputs to commands for the major components. An industry standard CANbus is normally used to communicate data and commands to and from the traction motor's inverter, a battery management system, and the microturbine. SAE J1939 defines standard CANbus communications protocols for vehicles, however there are unique messages for a series hybrid design that require more standardization. In the meantime, proprietary data packets are being used to deal with the increased amount of information available in hybrid designs.

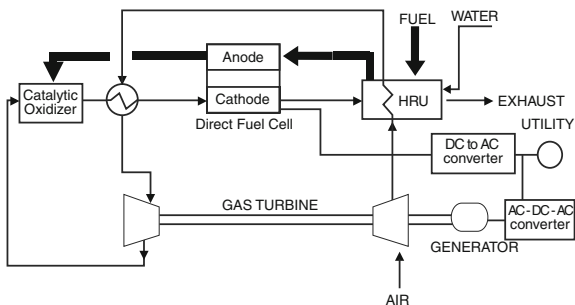
The role of the microturbine in this application is to recharge the battery pack when needed. The vehicle control module monitors battery SOC, as well as vehicle power requirements, and determines when to turn the microturbine on or off, and at what power to operate. The microturbine responds to these commands by monitoring the DC bus voltage, and then injecting current to meet the requested power demand. The simplest control scheme is to turn the microturbine on at its maximum power output when battery SOC reaches a low limit, then turn it off when the SOC has reached a high limit. More sophisticated control schemes can be used that adjust the microturbine's output power to track the average vehicle power so that the batteries are not charged and discharged so frequently or deeply in order to extend battery life. Other control schemes may even use feed-forward logic to assure that batteries are at an optimum SOC for the next intended operation—for example to fully charge them if a large increase in load is predicted or to discharge them at the end of daily use so they can accept a maximum recharge from an electric utility when power rates are low.

#### ***8.5.4 Hybrid Microturbine/Fuel Cell Example***

Commercial fuel cells for stationary power applications typically use high temperature stack technologies such as solid oxide or molten carbonate. These stacks may need to be pressurized to achieve highest efficiency, and are also exothermic. Microturbines can be used in combination with such fuel cells to create a hybrid system to increase electrical efficiencies and lower capital cost compared with a fuel cell by itself. Figure 8.26 shows a block diagram of one application.

In this particular application, incoming air is first sent through the microturbine's compressor section where it is pressurized and becomes heated. It then passes through a heat recovery unit (HRU) where it picks up additional heat energy from the exhaust of the fuel cell stack. Passing through a second heat exchanger, it picks up additional heat energy from the output of the catalytic oxidizer section of the fuel cell. That heated air is then able to drive the microturbine's turbine section to extract enough energy to both power the compressor section as well as supply additional electric output from its generator. The exhaust from the turbine exits back through the catalytic oxidizer and then through the stack itself and finally out to the atmosphere. In this example the stack is not being pressurized by the

**Fig. 8.26** Block diagram of hybrid microturbine/fuel cell system

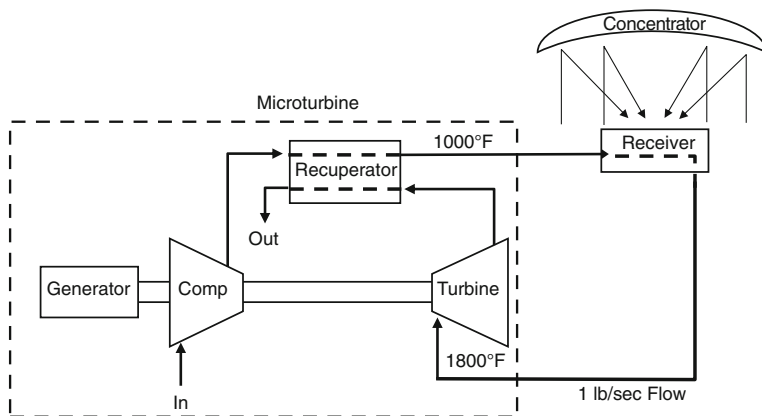


microturbine, however sufficient waste energy is captured to achieve an overall efficiency of 58 % [9].

Microturbine control for this application comes from the fuel cell controller, which must monitor stack temperatures and sequence power up and down slowly to manage thermal stresses. The microturbine starts out being driven by the connected utility grid to provide the air flow necessary to start the fuel cell stack. As the fuel cell stack comes up to operating temperature, sufficient energy becomes available to achieve a net positive electrical output. The microturbine uses speed control to maintain stable operation.

### 8.5.5 Solar Energy Example

Microturbines can be driven by essentially any high temperature heat source, and one emerging application is using concentrated solar energy. Figure 8.27 shows a block diagram of how such a system works. Sunlight is focused onto a receiver using a concentrator such as a dish or tower with individual heliostats. The



**Fig. 8.27** Block diagram of solar energy system



receiver is constructed to pass this high intensity radiated energy into a heat exchanging chamber and minimize reradiation back out. A quartz window can be used along with high temperature materials such as ceramics inside the receiver to absorb the radiant energy and heat the flow of air from the microturbine.

The solar collector system has a master controller that tracks the sunlight, focuses the concentrator to adjust radiant power levels at the receiver, and provides commands to the microturbine for starting, stopping, and speed adjustment. For example, during start-up the microturbine will be commanded to a speed point to get air flow to the receiver. The microturbine generator will automatically take power from the connected utility grid to do this. The master controller will then focus light onto the receiver, which will result in net power output from the microturbine. Microturbine speed can be adjusted to maintain a set turbine exhaust temperature or a receiver temperature. When the system goes off sun, the reverse process can be used to manage critical temperatures—both in the receiver as well as the microturbine itself. A combustor can be added in series with the output of the receiver to supplement solar energy and guarantee power output during conditions of low or no sunlight.

## References

1. C30 MicroTurbine Oil & Gas datasheet (Capstone P/N 331034E)
2. Product Specification, Model C30—Capstone MicroTurbine (460000 RevJ)
3. Capstone Gas Pack Technical Reference (410058 RevA)
4. Product Specification, Model C200—Capstone MicroTurbine (460045 RevD)
5. Product Specification, Models C600, C800, and C1000 Capstone MicroTurbine (460051 RevD)
6. TA100 Natural Gas datasheet (Capstone P/N 331064A)
7. Turbec T100 International datasheet. [http://www.turbec.com/pdf/Turbec%20brochure%202005%20eng\\_Email%20version.pdf](http://www.turbec.com/pdf/Turbec%20brochure%202005%20eng_Email%20version.pdf)
8. FlexEnergy MT250 G3 technical sheet. [http://www.flexenergy.com/wp-content/uploads/2012/03/Flex-MT250\\_G3-Specs\\_3-12.pdf](http://www.flexenergy.com/wp-content/uploads/2012/03/Flex-MT250_G3-Specs_3-12.pdf)
9. Ghezel-Ayagh H, Walzak J, Patel D, Jolly S, Lukas M, Michelson F, Adriani A (2008) Fuel cell seminar and exposition abstract 1807. [http://www.fuelcellseminar.com/assets/pdf/2008/wednesdayPM/RDP33-2\\_HGhezel.Ayagh.ppt.pdf](http://www.fuelcellseminar.com/assets/pdf/2008/wednesdayPM/RDP33-2_HGhezel.Ayagh.ppt.pdf)
10. Avallone E, Baumeister T III, Sadegh A (2007) Marks' standard handbook for mechanical engineers, 11th edn. McGraw-Hill, New York
11. Capstone Application Guide, Model C65 Integrated CHP (480014 RevA)
12. Morrow A, Savarino P, UTC PureComfort 240, Ritz-Carlton San Francisco. [http://www.ornl.gov/sci/de\\_materials/Day2/Morrow.pdf](http://www.ornl.gov/sci/de_materials/Day2/Morrow.pdf)
13. Capstone Technical Reference, Dual Mode System Controller (410071 RevD)
14. IEEE-519 (1992) Recommended practices and requirements for harmonic control in electrical power systems
15. IEC 62040-3 (2011) Uninterruptible power systems (UPS)—part 3: method of specifying the performance and test requirements
16. ISO 3977-2 (1997) Gas turbines—procurement—part 2: standard reference conditions and ratings
17. Capstone Technical Reference, Model C65 Performance (410048 RevB)

18. Capstone Application Guide, Model C65 Hybrid UPS (480049 RevA)
19. Stationary Engine Generator Assemblies, UL 2200
20. Inverters, Converters, Controllers and Interconnection System Equipment for Use With Distributed Energy Resources, UL 1741
21. IEEE 1547 (2003) IEEE standard for interconnecting distributed resources with electric power systems
22. Final Regulation Order, Amendments to the Distributed Generation Certification Regulation. <http://www.arb.ca.gov/energy/dg/2006regulation.pdf>
23. California Interconnection Guide Book, Overdomain LLC, P500-03-083. [http://www.energy.ca.gov/reports/2003-11-13\\_500-03-083F.PDF](http://www.energy.ca.gov/reports/2003-11-13_500-03-083F.PDF)
24. NYC Department of Buildings, Materials and Equipment Acceptance (MEA). [http://www.nyc.gov/html/dob/html/codes\\_and\\_reference\\_materials/mea\\_index3.shtml#distr](http://www.nyc.gov/html/dob/html/codes_and_reference_materials/mea_index3.shtml#distr)
25. US Environmental Protection Agency, How clean is the electricity I use?—Power Profiler. <http://www.epa.gov/cleanenergy/energy-and-you/how-clean.html>
26. CARB Executive Order A-338-0009. [http://www.arb.ca.gov/msprog/onroad/cert/mdehdehdv/2011/capstoneturbine\\_ubh\\_a3380009\\_0d20-0d01\\_cng.pdf](http://www.arb.ca.gov/msprog/onroad/cert/mdehdehdv/2011/capstoneturbine_ubh_a3380009_0d20-0d01_cng.pdf)
27. CARB Executive Order A-338-0007. [http://www.arb.ca.gov/msprog/onroad/cert/mdehdehdv/2010/capstoneturbine\\_ubh\\_a3380007\\_0d20-0d01.pdf](http://www.arb.ca.gov/msprog/onroad/cert/mdehdehdv/2010/capstoneturbine_ubh_a3380007_0d20-0d01.pdf)
28. Kramer W, Chakraborty S, Kroposki B, Thomas H (2008) Advanced power electronic interfaces for distributed energy systems, part 1: systems and topologies. NREL Technical Report NREL/TP-581-42672. <http://www.nrel.gov/docs/fy08osti/42672.pdf>
29. Capstone User's Manual, Hybrid UPS Controller (400028 RevA)

# Chapter 9

## Battery Energy Storage System

Stan Atcitty, Jason Neely, David Ingersoll, Abbas Akhil  
and Karen Waldrip

**Abstract** This chapter discusses the various technical components of battery energy storage systems for utility-scale energy storage and how these technical components are interrelated. The introduction lists the basic types of large-scale storage and how storage can be used to mitigate the variability associated with renewable generation. It also provides an overview of how to define storage applications as primarily “power” or “energy” based. A basic description of how battery energy storage works is provided with several examples to illustrate how battery energy storage can be used in large-scale applications. A brief discussion of the various battery chemistries that are suited to large-scale applications is provided, as well as guidance on what factors to look for when trying to select an appropriate chemistry for a given application. An overview of how the storage system’s power electronics work is followed by a more detailed description of possible power electronic topologies and power electronic controls that are used to ensure that the system can be properly integrated with the generation source and, if necessary, the load. Battery management and battery monitoring via the power electronic controls is discussed briefly. This chapter concludes with a detailed example of battery energy storage system integration that is summarized with data obtained in the field.

### Acronym List

BES	Battery energy storage
BESS	Battery energy storage system
BEWAG	Berliner Kraft- und Licht
BMS	Battery management system
CAES	Compressed air energy storage
CREW	Continuous Reliability Enhancement for Wind
CSI	Current-source inverter

---

S. Atcitty (✉) · J. Neely · D. Ingersoll · A. Akhil · K. Waldrip  
Sandia National Laboratories, 5800, MS0734 Albuquerque, NM 87185, USA  
e-mail: satcitt@sandia.gov

DQ	Direct/quadrature
EC	Electrochemical capacitor
EMI	Electromagnetic interference
EPRI	Electric Power Research Institute
FACTS	Flexible AC transmission systems
FESS	Flywheel energy storage system
GNB	Gould National Battery
GTO	Gate turn-off thyristor
GVEA	Golden Valley Electric Association
HVDC	High voltage direct current
IGBT	Insulated-gate bipolar transistor
LCL	Inductance-capacitance-inductance
LCR	Inductance-capacitance-resistor
ORAP	Operational reliability analysis program
PCC	Point of common coupling
PCS	Power conversion system
PH	Pumped hydro
PI	Proportional integral
PREPA	Puerto Rico Electric Power Authority
PSOC	Partial state of charge
PV	Photovoltaic
PWM	Pulse-width modulation
RMS	Root mean square
SCR	Silicon-controlled rectifier
SLI	Starting, lighting, and ignition
SMES	Superconducting magnetic energy storage
SOC	State of charge
SOH	State of health
VAR	Volt-ampere reactive
VRB	Vanadium redox flow
VSI	Voltage-source inverter

## 9.1 Introduction

### 9.1.1 Overview

Energy storage is a valuable tool for mitigating the temporal and often geographic differences between energy generation and consumption that can be particularly difficult to manage when generation is provided by variable renewable sources such as wind and solar energy. Variable generation sources must typically be converted and conditioned using power electronics to serve a typical AC load

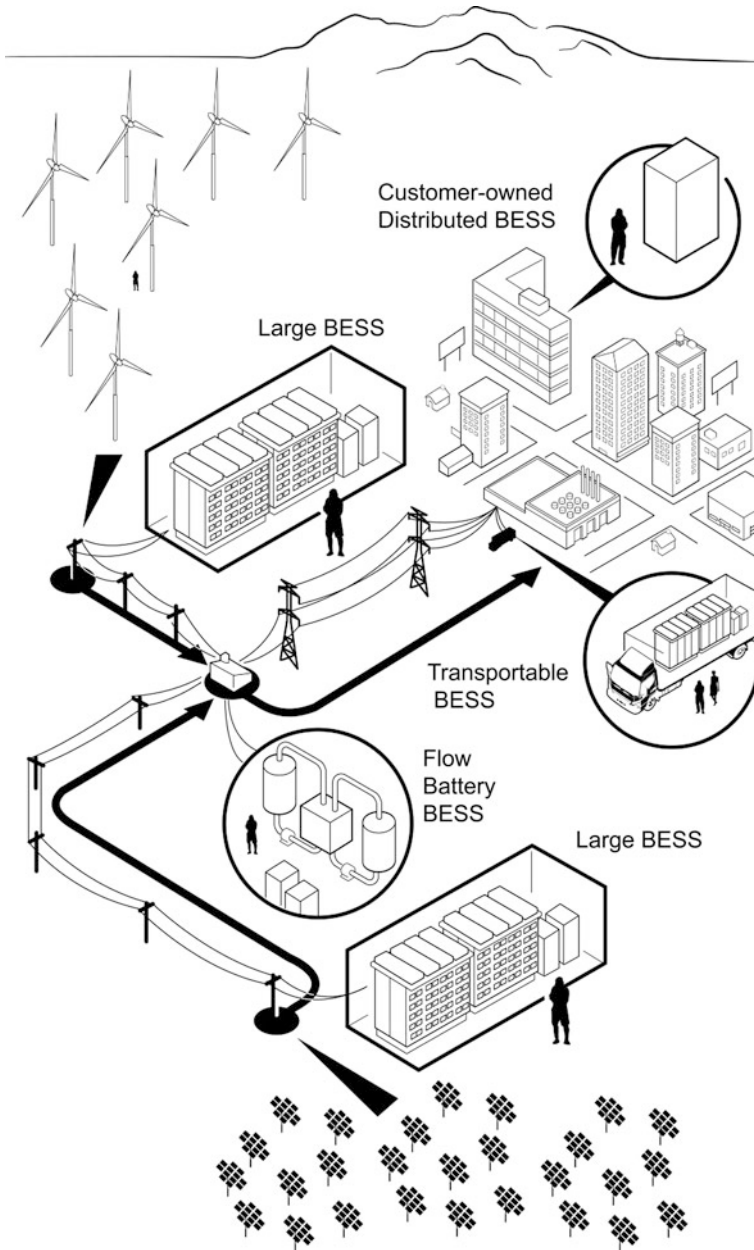
either on the utility grid or in smaller, distributed networks. The vast majority (>99 %) of today's energy storage is in the form of pumped hydro (PH). While PH is a cost-effective storage strategy and is used worldwide, further PH development is limited by the number of remaining available geographic sites, arduous permitting processes, large capital investment, and high environmental impact on existing wildlife. Other forms of energy storage gaining in popularity are (1) electrochemical energy storage supplied by either batteries or electrochemical capacitors (ECs); (2) mechanical energy storage such as flywheel energy storage systems (FESS) and compressed air energy storage (CAES); and (3) electromagnetic energy storage, such as superconducting magnetic energy storage (SMES). Battery energy storage (BES) is a versatile technology that offers advantages for both power and energy applications by selecting from a variety of electrochemical couples (anode and cathode materials) to meet the needs of the specific application.

There are numerous benefits to energy storage for wind applications, with the largest being load-shifting in time and firming [1]. The latter is a *power* application, while the former requires larger capacity (i.e., it is an *energy* application). A battery energy storage system (BESS) can be used independently or can be integrated into a hybrid system (e.g., with ECs) to provide both energy and power responses in a given application as diagrammatically depicted in Fig. 9.1.

### 9.1.2 Power Versus Energy

In general, electric energy storage is categorized based on function—to provide *power* or to provide *energy*. Although certain storage technologies *can* be used for applications in both categories, most technologies are not practical and/or economical for both power *and* energy applications. For example, *energy* applications use storage to decouple the timing of generation and consumption of electric energy, while *power* applications use storage to ensure continuity, quality, and proper frequency of delivered power in real time. In general, energy applications involve (relatively) long-duration discharge and power applications involve short-duration discharge. Table 9.1 shows the suitability of some of the more common technologies (battery and others) for various applications.

An assortment of battery technologies is represented in Table 9.1 along with other forms of energy storage (flywheels, CAES, and PH). This helps to illustrate the diversity of energy storage needs that BESS can serve. More detail on the chemistries is provided below, and further information on each specific technology can be found in detail elsewhere [2]. New technologies are being explored in the laboratory with the goal of meeting performance requirements at the required cost targets. In some applications (e.g., wind firming), BESS is already cost-competitive with combustion turbines, while in other applications (e.g., load shifting), the economic targets have yet to be reached.



**Fig. 9.1** Schematic representation of the use of BESS in integrating renewable energy at various locations on the utility grid

**Table 9.1** BESS applications by category (power or energy) [Electricity Storage Association and Sandia National Laboratories 2010]

Technology	Advantage	Disadvantage	Power applications	Energy applications
Flywheels	High power	Low energy density	Fully capable and reasonable	N/A
Electrochemical capacitors (ECs)	Long cycle life	Very low energy density	Fully capable and reasonable	N/A
Traditional Lead-acid	Low capital cost	Limited cycle life	Fully capable and reasonable	Feasible but not practical
Advanced lead-acid with carbon-enhanced electrodes	Low capital cost	Low energy density	Fully capable and reasonable	Fully capable and reasonable
Sodium sulfur (Na/S)	High power and energy density	High cost and restrictive operating parameters (high-temperature operation)	Fully capable and reasonable	Fully capable and reasonable
Lithium-ion (Li-ion)	High power and energy density	High cost and extensive control circuitry	Fully capable and reasonable	Reasonable
Zinc bromine (Zn/Br)	Independent power and energy	Medium energy density	Reasonable	Fully capable and reasonable
Vanadium redox	Independent power and energy	Medium energy density	Reasonable	Fully capable and reasonable
CAES	High energy, low cost	Special site requirements	N/A	Fully capable and reasonable
Pumped hydro	High energy, low cost	Special site requirements	N/A	Fully capable and reasonable

Electricity Storage Association and Sandia National Laboratories 2011, Technology Comparison Chart, 2010, accessed July 2011. [http://www.electrictystorage.org/images/uploads/static\\_content/technology/technology\\_resources/comparison\\_large.gif](http://www.electrictystorage.org/images/uploads/static_content/technology/technology_resources/comparison_large.gif)

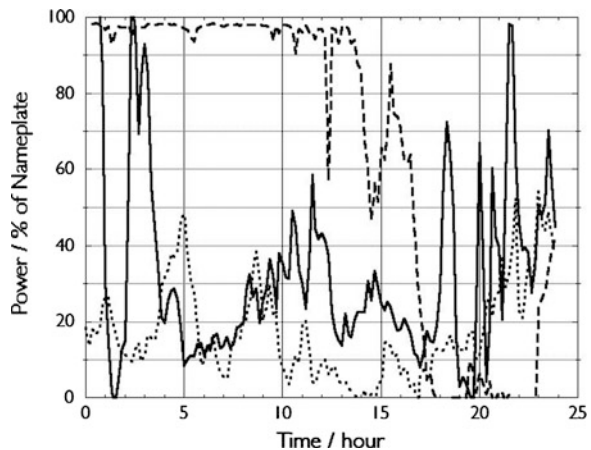
### 9.1.3 BESS Applications

The two categories described above (energy or power) can be refined based on how frequently BESS is expected to be used (frequent use or infrequent use) in a given application. In general, long-duration storage (i.e., energy management applications) means a discharge duration of up to hours or more. Frequent discharge for long-duration storage implies almost daily use throughout the year. Infrequent discharge of long-duration storage implies discharge between one and two times per month over the course of a year. Actual frequency of use will depend on both the specific application and the specific needs the storage system is expected to meet. Short-duration discharge (used for power management applications) can be any discharge from a few fractions of a second up to about 15 minutes, depending on the application. In general, frequent discharge of short-duration storage implies hundreds of discharges over the course of a year. Infrequent discharge of short-duration storage implies between one and two discharges per month averaged over the course of a year. Again, actual system use will vary with application and needs.

An additional distinction can be drawn between capacity applications and energy applications. In this case *capacity* applications use the BESS to defer or reduce the need for additional equipment (e.g., transmission and distribution or generation). *Energy* applications use the BESS to store a large amount of electric energy to offset the need to purchase or generate electricity to serve load.

The variability of renewable generation, illustrated in Fig. 9.2, represents a significant challenge toward integrating large amounts of renewable energy onto the grid. Represented in this graph are wind energy data collected over the course of 24 h from several different wind turbines. The large-scale changes in output as a function of time are evident in all three curves. At low penetration levels on large-scale utility grids this can be mitigated by a variety of mechanisms involving deviating the operating conditions of the combustion turbines from their optimized

**Fig. 9.2** Wind generation output as a percent of nameplate over the course of 24 h for several locations. *Source* sandia's continuous reliability enhancement for wind (CREW) database, collected by operational reliability analysis program (ORAP<sup>®</sup>) for Wind





values, resulting in excess carbon emissions and accelerated wear and tear on the generators. A similar situation exists for solar energy. As the amount of renewable penetration on the utility grid increases to substantial values ( $> \sim 15\%$  of the connected load), this will become increasingly problematic for ensuring the stability of the grid. BESS and hybrid BESS can help make renewables dispatchable because of their ability to meet power and energy requirements.

## 9.2 BESS Basics

Battery energy storage systems have characteristics that are quite different from the traditional power sources that electric utilities are most familiar with. In the first instance, there is no rotating mass. Consequently, as an energy source a BESS has electrical characteristics that are quite different from a more traditional, mechanical generator with a rotating mass that has a finite up- and down-ramp rate. The absence of inertia allows the BESS to respond to load fluctuations orders of magnitude faster than any fast start engine or combustion turbine in an electric utility system.

There are operational differences as well. A steam or combustion turbine-driven generator that is the workhorse of the electric grid is a firm dispatchable energy source as long as there is an unlimited supply of fuel—which there always is. In contrast, BESSs are limited in their available energy depending on their state of charge (SOC) at any given point in time. Practical size considerations and inherent characteristics of most battery chemistries generally limit the maximum energy storage times to between two and six hours for deep discharges. Despite this energy limitation, BESSs have operational advantages that make them a desirable resource. These advantages include the absence of point-of-use emissions, silent operation and the ability to perform multiple tasks in the grid such as voltage and frequency control and load shifting. Nevertheless, the idea of using a battery system for multiple applications did not emerge until the late 1980s. Before that, battery energy storage systems were regarded as a useful resource for a single application—load leveling. The rationale was that the BESS would be charged at night when the electric grid is lightly loaded and discharged during late afternoon and evening hours when the electric grid needs energy to serve peak loads. This was the classical load-leveling or peak-shaving application.

In the late 1980s this single-application concept was revisited, and researchers at Electric Power Research Institute (EPRI) and Sandia National Laboratories began proposing that BESSs could indeed perform multiple functions in both the transmission and distribution sides of the electric grid. The Berliner Kraft- und Licht (BEWAG) battery system in Berlin, which performed spinning reserve and frequency regulation duty, was a successful demonstration of this dual-benefit capability. The BEWAG system was followed by the 20-MW Puerto Rico Electric Power Authority (PREPA) BESS commissioned in 1996 that replicated the same

dual-function capability of the BEWAG battery for Puerto Rico's island grid. Several reports have discussed the multiple benefits in detail. The most recent is [3].

While multiple uses of energy storage offer several benefits, the stacking of benefits has to be chosen carefully because practical size and control considerations limit the number of benefits or applications that can be stacked. Additionally, depending on the regulatory structure or market, there may not be a policy mechanism to derive financial value for each application. Generally, an application that requires a shallow discharge or a series of shallow charge/discharges over a sustained period can be successfully combined with a deep discharge application, as long as controls are in place to reserve the capacity needed for the deep discharge as and when needed. This is the case for the frequency regulation application combined with the deep discharge required for spinning reserve application. In this case there is a control to ensure that the frequency regulation duty does not push the battery below a set SOC, such as the 70–75 % SOC level for lead-acid batteries. Thus, the remaining energy capacity of the battery is always available as spinning reserve, as required by any spinning reserve duty source.

An example of a relatively modest size BESS is shown in the photograph in Fig. 9.3. This system is located in the island community of Metlakatla, Alaska, and was originally intended to mitigate the large voltage and frequency fluctuations caused by intermittent motor loads at the local lumber mill. These fluctuations were caused because the hydro power generating units that form the backbone of the village power grid could not ramp up as the large 400 and 600 hp motors

**Fig. 9.3** A portion of the BESS at Metlakatla, Alaska that uses GNB ABSOLYTE IIP 100A75 modules. Seen is one bank of a back-to-back row



driving the lumber mill machinery came online randomly on a 24-hour basis. The village had installed a 3-MW diesel engine in an attempt to mitigate the effects of these fluctuations, but it was an expensive solution, costing the village about \$400,000 per year (then-year dollars) in diesel fuel and maintenance. The BESS offered not only a cost-effective solution that was recovered in 3 – 4 years, but also eliminated the diesel's carbon footprint.

The battery system was originally designed to respond exclusively to voltage/frequency fluctuations, but soon after it was installed it was also used to supply spinning reserve, which it did during unscheduled outages on the hydro units.

The Metlakatla system uses lead-acid battery chemistry in a valve-regulated cell design manufactured by Gould National Battery (GNB), now Exide Battery, using their Model 100A25 ABSOLYTE<sup>®</sup> cell. Three cells connected in parallel comprise a single module (the GNB ABSOLYTE IIP 100A75 module), and 378 of these modules are connected in a single series string in two back-to-back rows to form the 756 V battery. This system is rated at 1 MW and has a nominal discharge capacity of 1.4 MWh at the 60-minute discharge rate. A General Electric power conversion system (PCS) based on gate turn-off thyristors (GTOs) is used, and is designed for rapid bi-directional four-quadrant operation. The battery is operated in a partial state-of-charge (PSOC) mode to maximize battery lifetime as well as to optimize grid performance. In this operating mode the battery SOC is maintained between 70 and 90 %, with recharge being provided primarily by hydroelectric sources or by using a diesel generator in the event of insufficient hydroelectric power.

The initial lifetime projection for this system was 8 years based on GNB's calculated end-of-life for the battery. However, good battery management, including regular equalization charging and effective thermal management (air conditioned battery housing building), allowed the battery to last 12 years in active duty—well beyond its expected life. The system was renovated in 2008 with removal and replacement of all 378 modules. Subsequent in-depth analysis and characterization of 36 of the used cells indicate that even longer life might have been achieved had conditioning charging been more frequently employed.

On the other end of the size spectrum is the large, 46-MW BESS that was commissioned by Golden Valley Electric Association (GVEA) in Fairbanks, Alaska, in late 2003. The battery is comprised of 13,760 Saft SBH 920 rechargeable nickel–cadmium cells and an ABB converter. (The ABB-built converter can support a 46-MW discharge for five minutes, which it did during an unscheduled event in December 2003; its normal operating limit is 27-MW for 15 min).

The cells are arranged in four parallel strings, with a nominal voltage of  $\pm 2,500 V_{DC}$  and a storage capacity of 3,680 Ah. Not only is the battery a significant engineering milestone because of its size, it also represents one of the few cases where five use-cases were stacked to justify its cost and operation. During its 8 years of operating history the battery has successfully operated in all of the use scenarios at one time or another. Most BESSs that have been installed by electric utilities usually have one, or at most two, use cases (e.g., frequency regulation stacked on top of spinning reserve duty). The specific use cases of GVEA system

include (1) black start, a duty that is essential if the transmission line between Fairbanks and Anchorage goes down and Fairbanks becomes an island; (2) voltage support under steady state and emergency conditions; (3) transmission line stabilizing; (4) automatic scheduling; (5) scheduled load increases; (6) automatic generation control; and (7) charging.

Another BESS is the S&C PQ2000 shown in Fig. 9.4, which is also the first production model of a modular, transportable BESS. This 2-MW BESS was specifically designed to provide up to 2 MVA for 30 s or less where power quality is imperative for continued operation. This system continuously monitors grid voltage and, when a disruption is observed (e.g., electrical storm derived transients), switches in the PQ2000 to replace the grid power with power supplied by the BESS. The switching speed for the system is relatively fast ( $\frac{1}{4}$  of one cycle in this case), which is essential for this type of application.

The system comprises several battery strings, each with its own integrated PCS. A separate isolation transformer to step up the PCS output voltage is also present, as well as a 2-MVA electronic selector device with additional switchgears. The system employs 384 Delco deep discharge batteries (48 batteries in eight modules). (The current PureWave<sup>®</sup> System is designed around the operating characteristics of the Group 31 deep-cycle sealed lead-acid battery.) Because of the relatively low frequency of occurrence of these grid power transients, the batteries are usually on float service. As with the Metlakatla battery system, the container housing the batteries is conditioned to ensure long operational lifetime of the cells.

The PureWave<sup>®</sup> and Metlakatla BESSs span a fairly broad temporal response domain and use the same battery chemistry, specifically lead-acid. This is possible by tailoring the cell design and cell configuration for the specific application. Another interesting feature of the PureWave<sup>®</sup> system is that it is intended not only for utility applications, but also for the consumer side as well. In fact, one of the early demonstrations of this system was done at a semiconductor manufacturing



**Fig. 9.4** AC Battery PQ2000 system on a truck slated for delivery. The PQ2000 is the forerunner of the current S&C Electric Company PureWave<sup>®</sup> system

plant, where power interrupts to manufacturing lines can have significant consequences. While the lead-acid battery chemistry used in these two systems is a mature technology whose modes of operation and control are well known and characterized, the system being installed on the Lanai, Hawaii, grid for photovoltaic (PV) renewable integration (see Fig. 9.5) will be based on a new battery chemistry.

PV arrays are inherently variable generation devices, with the level of variability depending on seasonal solar variations and local weather patterns. A properly designed battery can mitigate variability. Figure 9.6 shows how a BESS can be used for ramp-rate support during a short duration (40 s) period of variability resulting from cloud cover. In this example the load demand is 5.5 MW, with 1.2 MW of the load being supported by the PV plant and the balance (4.3 MW) being supported by generators. As clouds move across the array, the PV generation capacity drops precipitously (for a few seconds), and the generators ramp up to provide sufficient power to support the demand. The ramp rate on the generators is slow compared to the power loss rate from the PV plant, tens of seconds versus seconds. Batteries, however, respond instantaneously and can provide the necessary load support, which slowly tapers off as the generators continue to ramp up. A similar situation exists as the clouds clear, where more power is being generated than required, and during which time the generators are ramping down. The batteries can be used to store this excess capacity.

The PV plant on Lanai has been in operation since late 2008 without a battery. Since that time several engineering studies have been completed in order to identify a suitable battery chemistry. Rather than use one of the mature battery chemistries already evaluated (e.g., vanadium redox, sodium sulfur, or lead-acid) a

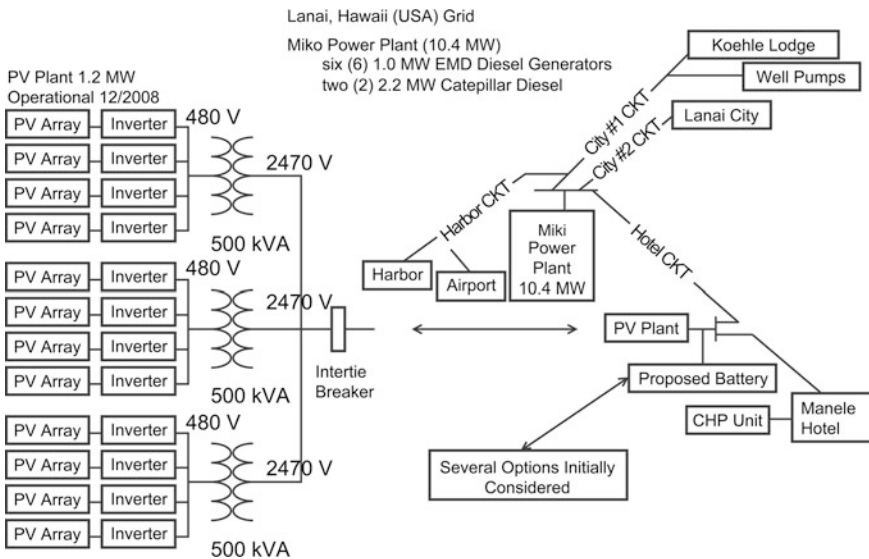
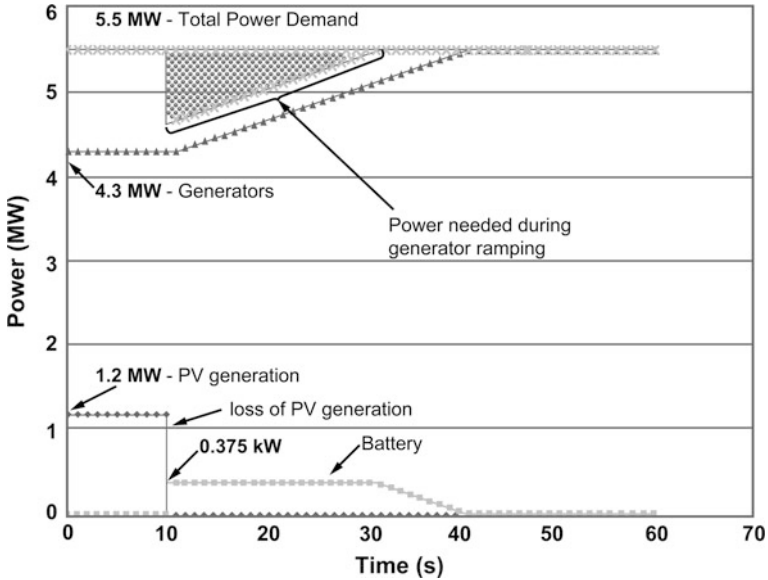


Fig. 9.5 Diagram of the Lanai, Hawaii power grid and the 1.2 MW PV array



**Fig. 9.6** Simplified example of BESS as a means of providing ramp-rate support during PV variability

relatively new battery chemistry was selected and funds allocated for its acquisition. The system selected was a turnkey battery system from Xtreme Power rated at 1.125-MW and 500 kWh. The fundamental chemistry of this battery is not known outside the company. As a turnkey system this is not necessarily a disadvantage or an impediment to deployment or operation since sufficient information for its operation and maintenance is provided by the manufacturer.

As with most engineering decisions, there are a number of trade-offs that must be considered when deciding which battery chemistry to use in a BESS installation. In general, however, the application for which the BESS will be used will dictate the choice of battery chemistry.

### 9.2.1 Batteries and Battery Chemistries

An optimized battery solution for an application is developed by balancing the intrinsic and extrinsic cell characteristics (e.g., choice of cell chemistry and internal cell design) and the battery design (e.g., how the cells are interconnected).

When properly designed and monitored, batteries can provide nearly instantaneous power and switching speeds, and can be easily scaled in size to provide the requisite energy. However, the intrinsic and extrinsic cost and performance characteristics of the different battery chemistries factor heavily into their suitability for a particular application.

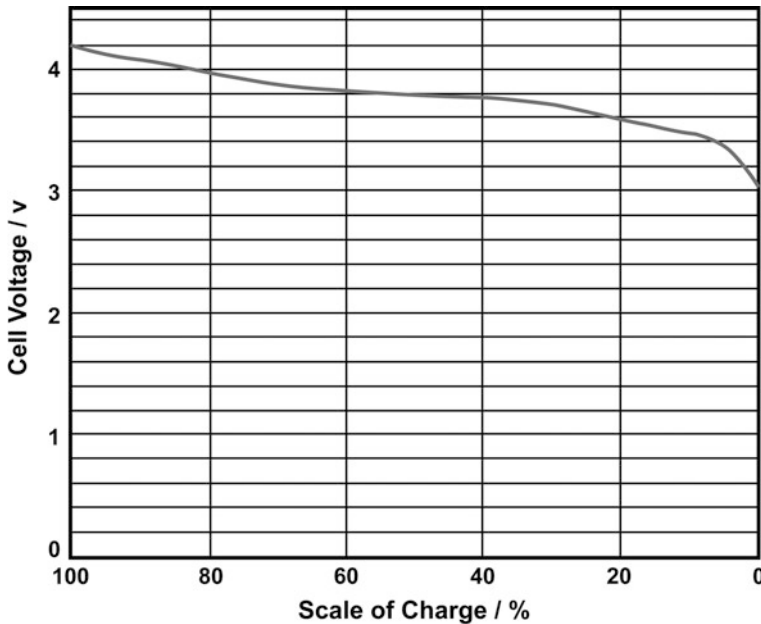
**Table 9.2** Common battery chemistries and nominal voltages

Battery chemistry	Nominal cell voltage (V)
Lead acid	2.1
Nickel cadmium	1.2
Nickel metal hydride	1.2
Lithium-ion	2, 3.5, 3.6
<i>High-temperature batteries</i>	
Sodium sulfur (NaS)	2
Zebra	2.35, 2.58
<i>Flow batteries</i>	
VRB (vanadium redox flow battery)	1.4
Zinc bromine	1.8
Zinc chlorine	2.12

Table 9.2 provides a short list of some battery chemistries considered for or used in large-scale applications, and also identifies descriptive categories into which these chemistries can be placed, including high-temperature and flow batteries. In the case of the high-temperature batteries shown, the intrinsic material characteristics (e.g., the melting point of sodium metal anode) necessitate high temperature operation, which in turn impose operational constraints on the batteries. Since the battery inefficiencies and the associated Joule heating during charge and discharge provide some of the energy necessary for maintaining operational temperature, and since freeze–thaw cycling can be problematic, those applications necessitating continuous charge and/or discharge are best suited for these chemistries.

In the case of flow batteries, the active electrode materials are generally liquids, and these are held in separate storage reservoirs and pumped through the electrochemical cell during charge and discharge. Since the storage reservoirs can be resized independently from the electrodes and cell stack, the energy and power of these battery chemistries can be independently controlled, unlike virtually every other battery chemistry having fixed cell geometry with a single compartment for both the active materials and electrodes. Although categorized as flow batteries, it must be mentioned that the charged anode in zinc-bromine and zinc-chlorine cells is zinc metal that is deposited onto the electrode structure, and as such provides a practical limit to the independence of power and energy.

Also shown in the table are nominal cell voltages for the different chemistries, and these are dictated by the battery chemistry itself, specifically by the anode and cathode materials used—their chemical compositions, chemical structures, etc. A single value is listed for *most* of the battery chemistries because there is only a single combination of electrode materials available. However, in some cases multiple values are listed because different combinations of cathode and/or anode materials can be used. For example, several alternative cathodes are available for lithium-ion cells (e.g.,  $\text{LiFePO}_4$ ,  $\text{LiCoO}_2$ ,  $\text{LiNiO}_2$ , and  $\text{LiMn}_2\text{O}_4$ ) and these provide different nominal cell voltages. Furthermore, while a single nominal value is



**Fig. 9.7** Voltage as a function of SOC for the room-temperature, low-rate discharge (five hours) of a Kokam lithium-polymer cell

listed, it is more often the case that a range of voltages will be observed over the entire SOC. For example, Fig. 9.7 shows the discharge curve for a Kokam lithium-polymer battery discharged at a low rate. As seen, this particular cell chemistry exhibits a sloping discharge curve over its entire SOC, from 4.2 V (100 % SOC) to 3 V (0 % SOC). Further complicating this relationship is the internal cell impedance, which leads to both higher nominal voltages during charge and lower nominal voltages during discharge, and which is functionally dependent on cell age and SOC in some cases. Furthermore, as in the case of cell impedance, the nominal voltage is typically not a constant value, but is instead dependent on a number of factors, such as temperature, cycle-life, SOC, and cell design. These issues must be considered when determining how many cells to use in a series string to attain the requisite voltage.

The other cell constituents (e.g., electrolyte solution, separator, current collectors, etc.) are also specific to each battery chemistry and, together with the electrode materials, impose cell-level design and performance constraints that can be balanced against one another to develop an optimized cell design for the application. Some of these constraints, such as the need for high-temperature operation in the case of the NaS and Zebra (Na-NiCl<sub>2</sub>) battery chemistries, leave little room for design/performance trade-offs. Other performance needs, such as higher power and energy, can be more easily accommodated through design changes. For example, altering the electrode structure (e.g., using high-surface-area electrodes) will provide higher



power; using thicker electrodes (or, for flow batteries, increased tank volume to accommodate more active material) will provide higher energy.

Beyond cell design, the battery itself can be engineered and optimized to the power and energy requirements through the seemingly straightforward process of engineering the battery stack. This is typically accomplished by altering the series and parallel combination of cells making up the stack, or in the case of redox flow batteries, adjusting the quantity of stored fluid to control the system energy.

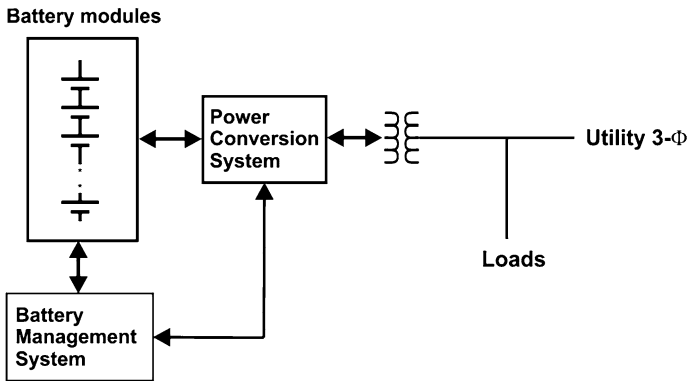
Regardless of how the system is designed and engineered, a primary consideration during operation is to ensure that every cell in the battery stack stays within the operational performance limits defined by the manufacturer, such as the high and low voltage limits of the cell or the upper temperature limit. Operation outside of the manufacturer's performance envelope can lead to irreversible degradation of the cell, and possibly even catastrophic battery failure. Maintaining the proper limits can be accomplished by monitoring and controlling each cell in the stack or by monitoring at the module level and assuming that the cells within any given module are behaving uniformly. The control circuitry can also allow for cell balancing, help to identify problematic cells, and help to identify cells in need of maintenance. To ensure that the cells are maintained within their respective performance envelope, other ancillary equipment may be necessary, such as that required for thermal management when high charge/discharge rates are employed or where the ambient temperature will lead to significant cell degradation. Some examples include the conditioned facilities in which the lead-acid batteries of the Metlakatla and PureWave<sup>®</sup> systems are housed, and actively pumped cooling for lithium-ion systems. When properly designed and monitored, batteries can provide instantaneous power and switching speed and provide one more option for storing electrical energy, as described in the remaining sections.

## 9.2.2 BESS Power Electronics

Two principle power electronic-based systems are at work in the BESS: the PCS and the battery management system (BMS). In general, the PCS manages the flow of power between the source (or sources), the battery storage, and the load (or loads). To accomplish this, the PCS may connect directly to the utility, the load, the energy storage, and even a renewable source. This chapter focuses on *grid-connected parallel configurations* of the PCS, in which the BESS is connected in parallel with the utility to the load [4] (see Fig. 9.8).

### 9.2.2.1 Power Conversion Systems

Power flow in the PCS must be bidirectional; that is the PCS must be able to convert DC power from the battery into AC power to supply the utility (inversion) and also be able to convert AC power into DC power (rectification) to recharge the



**Fig. 9.8** Basic representation of how power electronics are configured with a BESS

batteries. Power conversion in the PCS is accomplished using high-power switching circuits that can synthesize the sinusoidal currents or voltages at a fixed frequency (typically 60 Hz) needed on the AC side. The relationship between current and voltage determines the direction and quantity of real and reactive power flow (see Eqs. 9.1–9.8). However, power electronic components are typically sized according to the *apparent power*, which is given by the product of the current and voltage magnitudes in volt-amperes (see Eq. 9.9).

In most fielded systems (750 kVA and below) the PCS uses insulated-gate bipolar transistors (IGBTs) which are both gated on *and* gated off (hard switched) and often switched at several kHz. At 10 MVA and above, PCSs typically use silicon-controlled rectifiers (SCRs) and GTOs. These devices are only gated on *or* off and are typically switched in the hundreds of Hz range [4]. The range from 750 kVA and 1 MVA remains a grey area, but most systems still use IGBTs. In the range from 1–10 MVA, there are few fielded systems [4]. Some PCS circuit topologies are presented in Sect. 9.3. Some control schemes are presented in Sect. 9.4.

### 9.2.2.2 Battery Management Systems

The BMS monitors the condition of the batteries, aids in balancing batteries during charge/discharge, and communicates critical information to the PCS. Monitoring is done using measurements of cell temperature, voltage, and current. The BMS can estimate the battery SOC or state-of-health (SOH) by using these measurements and information such as the battery age and the number of charge/discharge cycles. The BMS may also protect the battery by disconnecting it from the PCS in the event of an over voltage, under voltage, over temperature, or over current. The BMS may also include a thermal management or active cooling system.

Through connections made to individual cells or modules connected in series, the BMS may redirect currents to ensure that charging or discharging of series-

connected cells or modules is balanced. These currents used for balanced charging/discharging are typically a small percentage of the overall charge/discharge current maintained by the PCS. The consequence of unbalanced charging is the potential over voltage of a cell or module. The consequence of unbalanced discharge is under voltage or even reverse voltage on a cell or module.

The BMS communicates critical information about the battery to the PCS, including measured quantities such as battery bus voltage and battery temperature, and also computed quantities such as maximum charge/discharge current, SOH, and SOC. Additional details on the role of the BMS, as well as the determination of SOH and SOC, are provided in Sect. 9.4.

### 9.3 Power Electronic Topologies for BESS

Of considerable importance to any BESS is the design of the power electronics and the formulation of the control scheme used to regulate the flow of power between the batteries and the utility. The power electronics and the controls comprise the PCS. Select topologies for the PCS are presented here, followed by an outline of control schemes based on pulse-width modulation (PWM) that can be used to regulate power flow.

This section focuses on power electronic topologies that have two interfaces: (1) a DC interface to a battery bank and (2) an AC interface to a utility. Figure 9.9 shows a basic configuration for a grid-tied BESS. In this case, both a DC/DC preregulator block and a DC/AC converter block are present, making the PCS in the figure a *multi-stage topology*. The DC/DC converter may be necessary either to provide additional regulation for battery charge/discharge control or to regulate a specific DC voltage/current for the DC/AC converter [4]. If such design considerations are not necessary, the DC/DC converter is omitted and the battery modules may be directly connected to the DC/AC converter, comprising a *single-stage topology*. It must be noted that for BESS applications, the DC/DC and DC/AC converters must be bi-directional.

On the output, a filter consisting of passive components (inductors, high voltage capacitors, and resistors) is used to mitigate high-frequency harmonics in the currents delivered to the transformer. Finally, an isolation transformer is used to

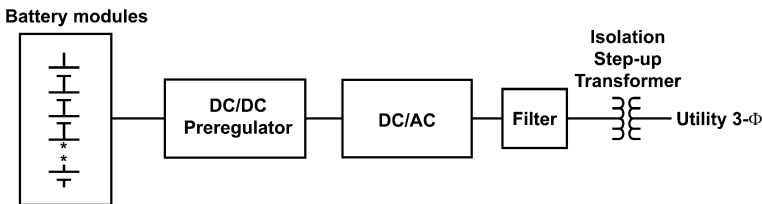


Fig. 9.9 Building blocks of the BESS PCS

step up the AC voltage and to provide isolation between the utility and the BESS. A typical filter topology is the LCL filter which is a third-order, low-pass filter connected between each phase. Other topologies such as LCR notch filters may be used to eliminate specific harmonics. Filter design is not considered in this chapter.

### 9.3.1 Single-Stage Bi-Directional Topologies

Figure 9.10 shows a practical single-stage bi-directional power converter. In this circuit, the DC-link bus is directly connected to  $N$  series-tied battery modules. Assuming the DC-link capacitance is sufficiently high, the DC side appears as a constant voltage; thus, the DC/AC converter is referred to as a *voltage source inverter* (VSI). The DC/AC conversion takes place through switching the six fully controlled semiconductor switches, which are shown in the figure as IGBTs with anti-parallel flyback diodes.

IGBTs may be turned *on* or *off* via a signal applied to the device's gate (gate commutation). The ability to directly turn these switches on and off allows for the use of PWM techniques that will be presented in the next section. However, because the switches are typically conducting when they are gated off, switching loss due to the transition between the on and off states may affect efficiency considerably. In contrast, a line-commutated converter uses SCRs or thyristors. The SCR or thyristor does not conduct when reverse-biased. When the device is forward biased, conduction is delayed until a gating signal is applied and the device then conducts until it is again reverse biased. Comparing the gating signal delay to the cycle period gives the *firing angle*. Because the switch turn-off occurs at a zero-crossing, switching losses are mitigated. Line-commutated converters are thus favored at higher power levels.

A line-commutated converter may be built by replacing the IGBTs in Fig. 9.10 with thyristors and replacing the DC link capacitance with a series inductance to create a *current source inverter* (CSI). However, line-commutated converters only allow control of the *firing angle*, resulting in AC currents with higher harmonic

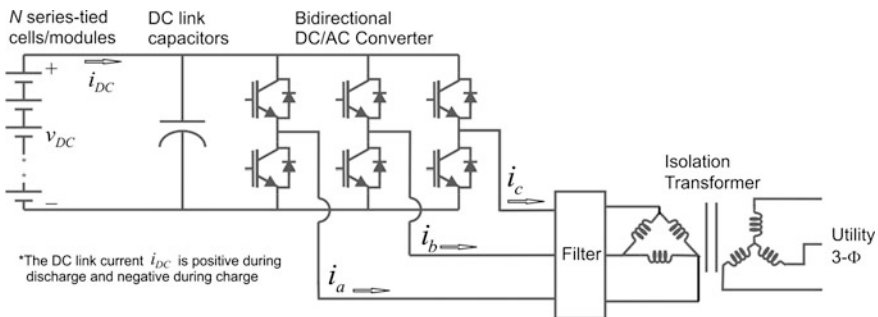


Fig. 9.10 PCS using a single 3-phase, 6-pulse bridge converter

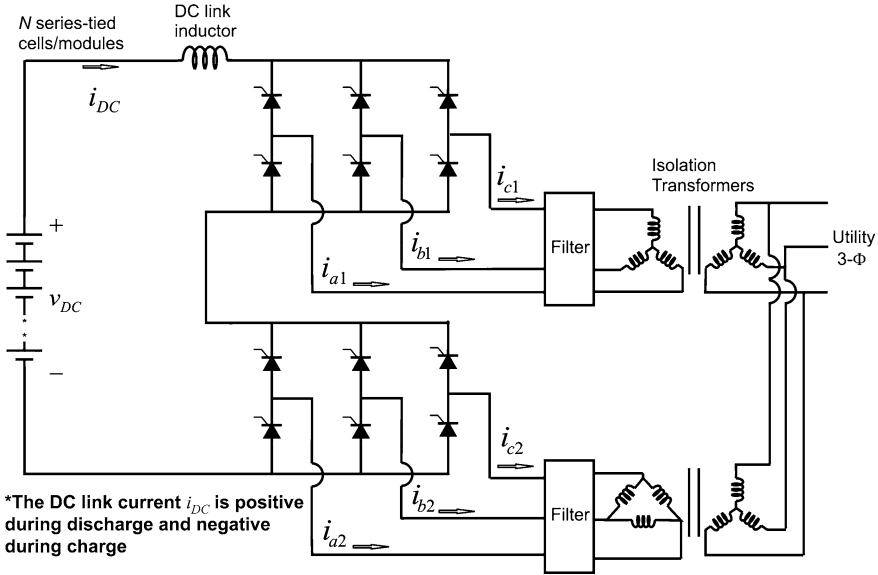


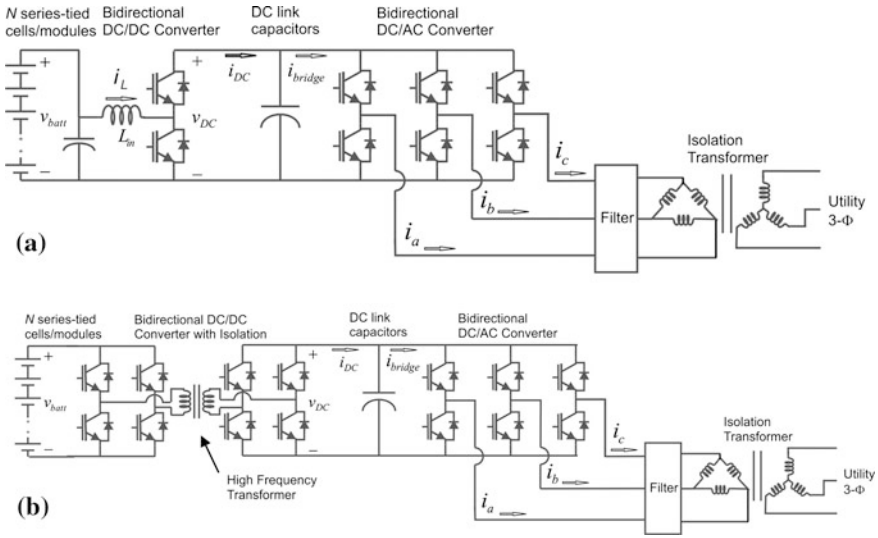
Fig. 9.11 PCS using 3-phase, thyristor-based, 12-pulse converter

distortion than PWM-controlled converters and thus requiring larger filters [4]. To reduce the harmonic distortion, it is common to employ multi-pulse converter topologies. Figure 9.11 shows a 12-pulse, thyristor-based converter topology. In this topology, the DC sides of two 6-pulse bridge converters are connected in series and the outputs of the bridge converters are connected to the utility through wye-wye and delta-wye transformers [4,5]. Voltages produced on the secondary side of the top and bottom bridge are phase shifted by  $30^\circ$  with respect to one another. This shift provides a staggered voltage/current contribution from each converter and results in harmonic cancellation and thus a lower harmonic output than the 6-pulse line-commutated converter.

An alternative to using *multi-pulse* topologies for harmonic mitigation is to use *multi-level* topologies where the voltages/currents generated at each phase leg have more than two levels. Multi-level topologies are not considered here; see [6] for a thorough discussion of multi-level converter topologies.

### 9.3.2 Multi-Stage Bi-Directional Topologies

Figure 9.12 shows two two-stage power conversion systems having a bi-directional switch-mode DC/DC converter connected between the battery and inverter. In Fig. 9.12a, the DC/DC converter performs as a boost (step-up) converter when the battery is discharging ( $i_{DC} > 0$ ) and a buck (step-down) converter when the battery is charging ( $i_{DC} < 0$ ). If the top switch of the DC-DC converter is assigned



**Fig. 9.12** Two-stage power converters each with a 6-pulse inverter and **a** a non-isolated bidirectional DC/DC converter and **b** isolated bidirectional DC/DC converter

a duty cycle  $d$ , and the bottom switch is assigned a duty cycle  $(1-d)$ , then the current through the inductor  $i_L$  increases when  $v_{batt} > dv_{DC}$  and decreases when  $v_{batt} < dv_{DC}$ . Thus,  $d$  may be controlled to manage the flow of power in the bidirectional DC–DC converter.

In Fig. 9.12b, the DC/DC conversion takes place through a high-frequency isolation transformer using inversion and then rectification and filtering. For discharging the battery using the bidirectional DC–DC converter, the primary-side H-bridge configuration (on the left) drives the primary of the high-frequency transformer with an alternating voltage; the secondary-side H-bridge configuration (on the right) rectifies the voltage generated on the secondary and produces a DC voltage/current for the DC/AC converter. When charging the battery using the bidirectional converter, the power flow is reversed; the primary-side H-bridge configuration rectifies and drives a DC current into the battery.

### 9.4 Power Electronic Controls for BESS

In this section, popular control methods are presented for regulating the DC/DC converters and DC/AC inverters presented in Sect. 9.3. Because a complete presentation cannot be made of all the control methods employed in regulating BESS power electronics, this section will focus on two general PWM-based control approaches. Specifically, for DC/AC converters, open-loop and closed-loop current controls with user-supplied power and reactive power commands are

presented; for DC/DC bi-directional converters, a voltage feedback current-regulation control is presented.

### 9.4.1 Regulation of Bi-Directional DC/AC Converters

Before the PWM control schemes are presented, it is convenient to define some relevant quantities that allow for a proper motivation for the desired converter operation.

#### 9.4.1.1 Overview of Control Objectives and Applications

For grid-tied cases, control of the converter assumes the phase voltage of the utility is unaffected by the power that is added or subtracted by the BESS. Thus, for a root-mean-square (RMS) phase voltage  $V_{\text{rms}}$ , frequency  $f$ , and time  $t$ , the time-varying phase voltages are given by

$$v_a(t) = \sqrt{2} V_{\text{rms}} \cos(2\pi ft) \quad (9.1)$$

$$v_b(t) = \sqrt{2} V_{\text{rms}} \cos\left(2\pi ft - \frac{2\pi}{3}\right) \quad (9.2)$$

$$v_c(t) = \sqrt{2} V_{\text{rms}} \cos\left(2\pi ft + \frac{2\pi}{3}\right) \quad (9.3)$$

For an RMS phase current  $I_{\text{rms}}$  and phase angle  $\phi_i$  the desired phase currents are expressed in the form

$$i_a(t) = \sqrt{2} I_{\text{rms}} \cos(2\pi ft + \phi_i) \quad (9.4)$$

$$i_b(t) = \sqrt{2} I_{\text{rms}} \cos\left(2\pi ft - \frac{2\pi}{3} + \phi_i\right) \quad (9.5)$$

$$i_c(t) = \sqrt{2} I_{\text{rms}} \cos\left(2\pi ft + \frac{2\pi}{3} + \phi_i\right) \quad (9.6)$$

For the voltages and currents expressed above, it is easily verified that the *real power*  $P$  delivered to the utility is given in watts (W) by

$$P = i_a v_a + i_b v_b + i_c v_c = 3 I_{\text{rms}} V_{\text{rms}} \cos(\varphi_i) \quad (9.7)$$

It is noted that for a balanced 3-phase system having constant  $V_{\text{rms}}$ ,  $I_{\text{rms}}$ , and  $\phi_i$  the power delivered to the utility is constant (i.e., it does not oscillate).

The *reactive power*  $Q$  delivered to the utility is given in volt-amperes reactive (VAR) by

$$Q = 3I_{\text{rms}}V_{\text{rms}}\sin(\phi_i) \quad (9.8)$$

The *apparent power*  $S$  is given in volt-amperes by

$$|S| = (P^2 + Q^2)^{1/2} = 3I_{\text{rms}}V_{\text{rms}} \quad (9.9)$$

By controlling  $P$  and  $Q$  the BESS can provide power and VAR support to the grid. Specifically, for frequency regulation, the grid frequency may be increased by providing positive  $P$  (discharging the battery) or decreased by providing negative  $P$  (charging the battery) [7]. To maintain voltage stability, a negative  $Q$  may be supplied to the grid to compensate for highly inductive loads [7]. It is noteworthy that, in general, a battery is not necessary to provide VAR support; a VSI with sufficiently large DC-link capacitance will suffice.

The controller is given a commanded power  $P^*$  and a commanded reactive power  $Q^*$ , and the objective of the control is to generate a PWM control policy that drives the errors  $|P - P^*|$  and  $|Q - Q^*|$  to zero. This may be done by regulating the AC currents. Specifically, from Eqs. 9.7 and 9.8, a commanded real power  $P^*$  and a commanded reactive power  $Q^*$  allows computation of a commanded current amplitude  $I_{\text{rms}}^*$  and phase  $\phi_i^*$  using

$$I_{\text{rms}}^* = \frac{\left((P^*)^2 + (Q^*)^2\right)^{1/2}}{3V_{\text{rms}}} \quad (9.10)$$

$$\phi_i^* = \tan^{-1}\left(\frac{Q^*}{P^*}\right) \quad (9.11)$$

From Eqs. 9.4–9.6, 9.10, and 9.11, it follows that commanded  $i_a^*$ ,  $i_b^*$ ,  $i_c^*$  may be synthesized. The control, however, is subject to system limits. For a converter efficiency of  $\eta$ , which accounts for losses in the inverter, the steady-state battery current is given by

$$i_{\text{DC}} = \frac{P}{\eta v_{\text{DC}}} \quad (9.12)$$

It is noted that, as battery voltage falls during discharge, the battery current must increase to maintain a given  $P^*$ .

When charging the battery, the commanded current  $i_{\text{DC}}^*$  is negative and thus the commanded power  $P^* = \eta v_{\text{DC}} i_{\text{DC}}^*$  is negative. In this mode of operation, the DC–AC converter is an active rectifier. It is noted that only the angle  $\phi_i$  given by (9.11) changes when  $P^*$  changes sign.



### 9.4.1.2 Current-Regulated Voltage Source Inverter with Hysteresis Control

Hysteresis current control is applicable for a 6-pulse inverter with fully controlled switches. For reference currents  $i_a^*$ ,  $i_b^*$ ,  $i_c^*$  and some hysteresis band  $h$  (in amps), the control provides a simple bang–bang regulation scheme to keep each phase current within  $h$  amps of its reference. Consider, for example, the  $a$ -phase. If the measured phase current  $i_a > i_a^* + h$ , then the top switch is turned off, and the bottom switch is turned on ( $S_a = 0$ ) so that  $i_a$  decreases. Likewise, if the measured phase current  $i_a < i_a^* - h$ , then the top switch is turned on, and the bottom switch is turned off ( $S_a = 1$ ) so that  $i_a$  increases. This same control scheme is applied to the  $b$  and  $c$  phases. The control scheme is summarized in Fig. 9.13 [8].

As the hysteresis band is contracted (smaller  $h$ ), the phase current tracks the reference with greater fidelity and thus with less harmonic distortion; however, this comes at the cost of greater switching frequency and switching losses. An additional disadvantage of this control is that the switching frequency varies with DC voltage, line voltage, and even throughout the cycle. This can be troublesome when electromagnetic interference (EMI) issues must be considered.

An example of a commercial system that employs hysteresis current control is the PQ2000 by Omnion Power Engineering Corporation. The system is a 30-second or less, 2-MW battery energy storage system that uses IGBTs and hysteresis current control [4].

### 9.4.1.3 Current-Regulated, Voltage-Source Inverter with Sinusoidal PWM

A triangle waveform  $Tri$  is created that oscillates between  $-1$  and  $1$  at the desired switching frequency, and control of switching in each phase leg of the inverter is determined through comparison of  $Tri$  and a phase-specific duty cycle. Specifically, for some commanded RMS voltage, the modulation index  $d$  ( $0 \leq d \leq 1$ ) is defined as

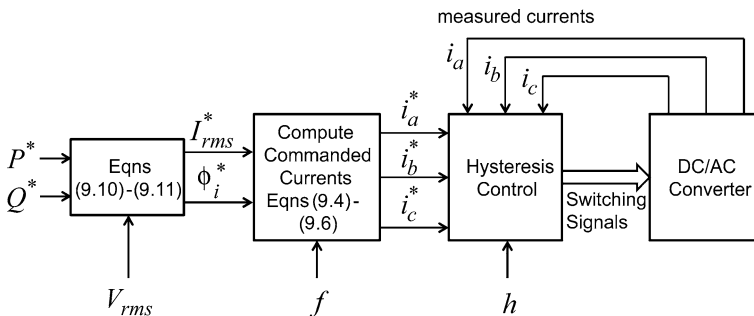


Fig. 9.13 Hysteresis current-regulated inverter control

$$d = 2\sqrt{2} \frac{V_{rms}^*}{v_{DC}} \quad (9.13)$$

and an electrical angle  $\phi_v$  (relative to some reference such as the grid) is selected. These quantities provide the following definitions for sinusoidally varying duty cycles assigned to each phase [5,8].

$$d_a = d \cos(2\pi ft + \phi_v) \quad (9.14)$$

$$d_b = d \cos\left(2\pi ft - \frac{2\pi}{3} + \phi_v\right) \quad (9.15)$$

$$d_c = d \cos\left(2\pi ft + \frac{2\pi}{3} + \phi_v\right) \quad (9.16)$$

For each phase, the assigned duty cycle is compared to the signal  $Tri$ . Consider the  $a$ -phase. When  $d_a \geq Tri$ , the top switch of the phase-leg is on and the bottom switch is off ( $S_a = 1$ ), thus setting the phase-to-ground voltage to  $v_{DC}$ . When  $d_a < Tri$ , the top switch of the phase-leg is off and the bottom switch is on ( $S_a = 0$ ), setting the phase-to-ground voltage to zero. This same procedure is repeated for the  $b$  and  $c$  phases. Figure 9.14 illustrates this operation. The top plot shows the triangle waveform  $Tri$  and  $d_a$  with  $d = 0.75$ . The center plot shows the switch signal  $S_a$  that results from comparing  $Tri$  and  $d_a$ . The bottom plot shows the resulting  $a$ -phase line-to-neutral voltage on a balanced 3-phase output where  $V_{DC} = 2000V$ .

Current regulation is accomplished by adjusting the duty cycles (9.14)–(9.16) using a feedback controller (e.g., a proportional plus integral, or PI, controller). Fig. 9.15 shows a feedback control for use with sine-triangle modulation. It is noted that in practice, the PI control scheme shown in Fig. 9.15 is used to command quantities in the  $q$ - $d$  reference frame [8]. In particular, two separate PI controllers would be used to manipulate the  $q$ -axis and  $d$ -axis currents by generating commands for  $q$ -axis and  $d$ -axis voltages. These  $q$  and  $d$  axis voltages would then be converted to phase voltages. A proper discussion of reference frame methods is beyond the scope of this chapter. Additional details of this control are available in [8].

As noted in the earlier sections, the control in Fig. 9.15 accomplishes the rectifier mode of operation when  $P^*$  is negative.

## 9.4.2 Regulation of Bi-Directional DC–DC Converters

Consider again Fig. 9.12. In Sect. 9.4.1, two control schemes were presented for regulating the AC currents generated by the DC/AC converter assuming  $v_{DC}$  was constant. In this section, control schemes are presented for regulating the DC bus voltage about some reference value. For the voltage-source inverter configuration, the DC bus voltage may be modeled with the following differential equation:

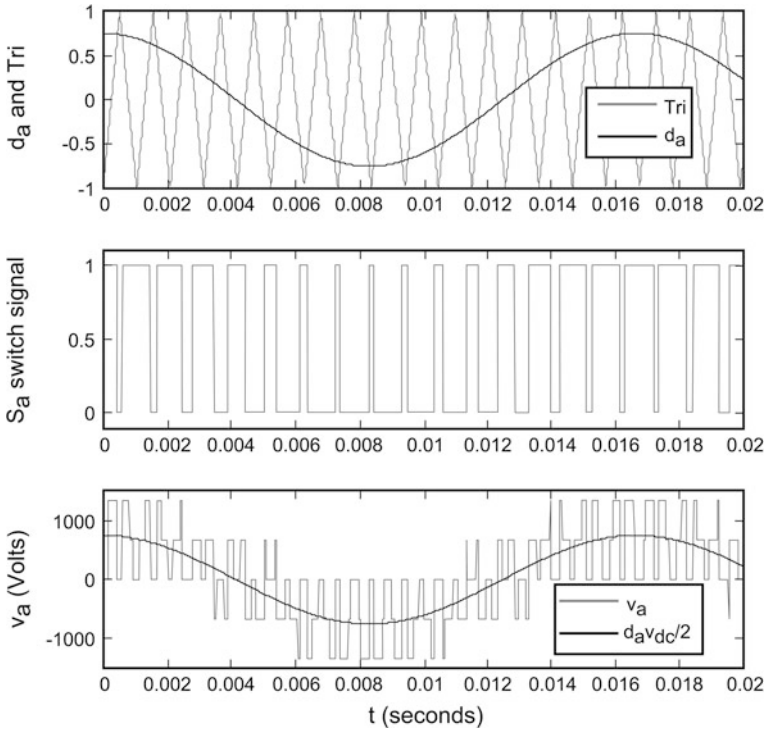


Fig. 9.14 Sine-triangle PWM waveforms

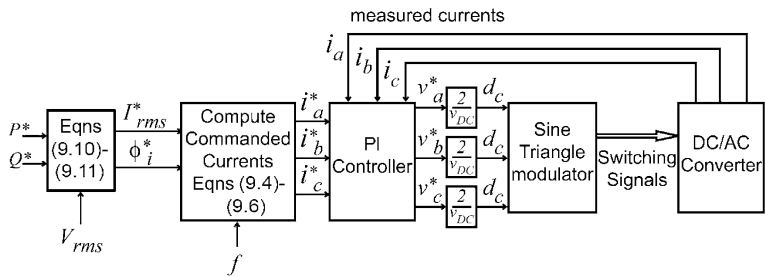


Fig. 9.15 Sine-triangle current-regulated inverter control

$$\frac{dv_{DC}}{dt} = \frac{1}{C_{link}} (i_{DC} - i_{bridge}) \tag{9.17}$$

For a DC-link voltage reference  $v_{DC}^*$ , the objective of the DC/DC controller is to determine a control policy that drives the error  $|v_{DC} - v_{DC}^*|$  to zero. Since  $v_{DC}^*$  is constant, this implies that the control will also drive  $\frac{dv_{DC}}{dt}$  to zero (whereby  $i_{DC} = i_{bridge}$ ) in steady state.

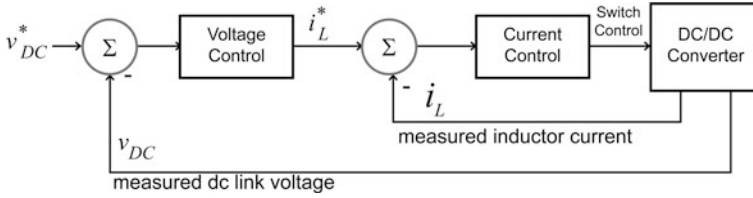


Fig. 9.16 Feedback control scheme for non-isolated DC/DC converter

9.4.2.1 Non-isolated DC/DC Converters

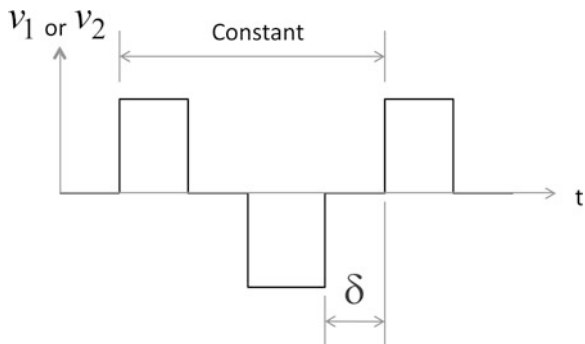
For regulating the DC/DC converter in Fig. 9.12a, a typical control method includes two feedback loops: (1) an outer voltage-control loop that determines an  $i_L^*$  to drive  $|v_{DC} - v_{DC}^*|$  to zero and (2) an inner current-control loop that provides a switch control to drive  $|i_L - i_L^*|$  to zero with a control response much faster than that of the outer loop. This control is illustrated in Fig. 9.16. A common configuration uses a PI compensator for the voltage control and a hysteresis controller to regulate the inductor current.

9.4.2.2 Isolated DC/DC Converters

A control structure similar to that used with the non-isolated converter is used for regulating the isolated DC/DC converter in Fig. 9.12b. In this case, however, the PWM control is used to drive the high-frequency transformer with a particular voltage waveform; a DC voltage is then attained on the other side through rectification. Specifically, the switch control is determined by controlling the interval  $\delta$  in Fig. 9.17 [5]. As  $\delta$  decreases, the fundamental voltage (and thus the energy transfer) increases. Likewise, as  $\delta$  increases, the energy transfer decreases.

The bidirectional DC–DC converter discharges the battery when  $i_L^*$  is positive and charges the battery when  $i_L^*$  is negative

Fig. 9.17 PWM scheme for driving the high-frequency transformer



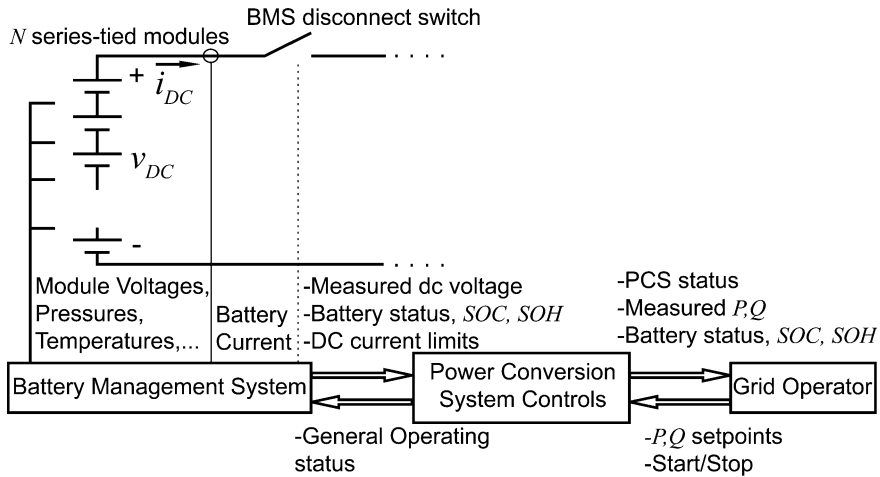


Fig. 9.18 Basic BMS

### 9.4.3 Battery Management

The BMS uses measured data from the battery to ensure balanced charging/discharging of the modules, that charge or discharge current is within specified limits, that cell voltages are within limits, that system failures are detected, and to provide estimates of the battery state-of-charge (SOC) and state-of-health (SOH). When operated outside the accepted operating region, the BMS is able to disconnect the battery from the system and notify the operator.

A basic BMS is shown in Fig. 9.18. In this system, the DC-link current is monitored on a string of  $N$  series-connected cells or modules. The BMS also monitors individual module voltages. The connections used for voltage monitoring may also be used as additional current paths for balanced charging. Additionally, the BMS communicates the battery voltage, the BMS/battery status, the charge and discharge current limits, and battery SOC to the PCS control. The PCS control uses information from the BMS to determine a control policy that is consistent with the operating abilities of the battery.

#### 9.4.3.1 SOC Monitoring

Battery SOC is typically defined as some percentage where  $0 \leq SOC \leq 100$  and  $SOC = 20$  represents a 20 % SOC. The battery SOC is not directly measurable; instead, an estimate of SOC is calculated by continuously monitoring battery current, voltage, and other parameters, such as internal pressure or electrolyte acidity.

It is assumed that the battery SOC is primarily a function of the charge/discharge schedule but it is also affected by time or battery temperature. Thus,

battery SOC may be estimated by continuously monitoring the battery current, voltage, and temperature and by using a function that is developed through laboratory study of the battery, to estimate the actual SOC characteristics.

The simplest method for estimating SOC is the *Coulombic* or *Integrated Current* approach wherein it is assumed the battery terminal voltage is constant, and SOC is estimated according to

$$\text{SOC}(t) = 100 \left( \frac{Q_{\text{batt}} - \int_{t_0}^t i_{\text{DC}}(\tau) d\tau}{Q_{\text{batt}}} \right) \quad (9.18)$$

where  $Q_{\text{batt}}$  is the total available charge in a full battery, and  $\text{SOC}(t_0) = 100$ . Equation (9.18), however, is an idealization; in practice, an accurate online estimate of SOC requires a more detailed model of the battery condition and charge/discharge schedule. The estimated SOC may instead be updated according to a function that is developed by matching empirical data to candidate functions that are identified primarily by trial and error. Because of the labor intensive nature of this development, SOC monitoring methods are often proprietary and not published. In Reference 9, however, an empirically validated run-time model is presented for a utility-scale carbon-enhanced valve regulated lead-acid battery. In this model, the electrical dynamics of the battery and the SOC were related analytically; parameters in the analytical models were then determined such that simulation results matched measured data with an RMS error below 1 %. Although this model is intended to support dynamic simulation efforts, it may also be used to improve SOC estimates from measured electrical characteristics.

Finally, to avoid inaccurate SOC values that arise from the accumulation of numerical error during integration, the SOC value must be allowed to periodically reset. This requires a scheme for detecting full charge on the battery, thus identifying an accurate initial condition  $\text{SOC}(t_0)$ .

#### 9.4.3.2 SOH Monitoring

Battery SOH is a subjective metric used to quantify a battery's condition or ability to perform. The SOH is determined by measuring or tracking certain characteristics that mark aging or degradation. Indicators of a reduced SOH include but are not limited to the following:

- Greater charge/discharge cycle count
- Increased float current
- Increased battery impedance
- High cell voltage variance
- Reduced ability to accept charge

If the cycle life of a battery is known a priori, then the simplest (but not necessarily the easiest) method for estimating SOH is to keep track of the number of charge/discharge cycles that have been performed since the battery was manufactured. As the number of cycles increases, the SOH estimate decreases. However, this method of SOH determination assumes the battery is used under normal operating conditions and that the depth of charge/discharge is consistent from cycle to cycle.

An alternative method for determining SOH is to measure the *float current* on the battery pack; the float current is the current that is applied at the conclusion of a charge cycle to maintain the battery at full charge. An increased float current can indicate a reduced SOH as this indicates a higher self-discharge rate. This approach is simple; however, it fails to identify individual faulty cells in a series-connected configuration.

As a battery ages, the battery impedance, given as the relationship between voltage and current at the terminals, increases. Thus, another method for SOH monitoring is to apply a small sinusoidal voltage  $\Delta v_{\text{batt}}$  to the battery and to measure the resulting sinusoidal current  $\Delta i_{\text{batt}}$ . As the impedance  $\Delta v_{\text{batt}} / \Delta i_{\text{batt}}$  increases, the estimated SOH will decrease. If the cell voltages are monitored independently, this method may assign an SOH value to individual cells.

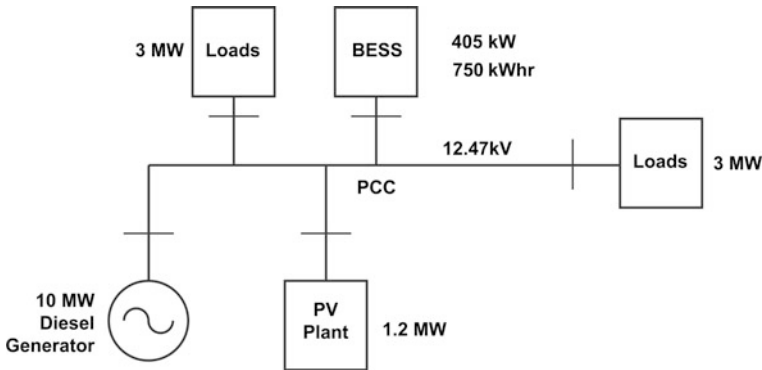
Similarly, if cell voltages are monitored independently, the SOH may be estimated for individual cells by quantifying cell voltage statistics, in particular the variance, during a normal charge/discharge cycle. If a particular cell has a voltage that is very different from the others during the cycle, this would indicate that an individual cell is bad or has a lower SOH than the others.

Finally, while an estimate of SOC may require knowledge of  $Q_{\text{batt}}$ , the value of  $Q_{\text{batt}}$  will reduce as the battery degrades. By developing an estimator that updates the value of  $Q_{\text{batt}}$  each cycle, the SOH may be determined by comparing the latest value of  $Q_{\text{batt}}$  to that of a new battery.

It should be noted that most BMSs will use more than one method to characterize the battery SOH and/or the SOH of individual cells, and the above list of monitoring methods is certainly not complete. For a more complete survey, the reader is directed to Fregosi et al. [9].

## 9.5 Example of BESS Integration

Currently, there are a number of value-added electric utility applications for the BESS such as frequency regulation, renewable firming or smoothing, power quality management, ramp-rate control, and spinning reserve. In the example below, a specific system integration scenario is used to summarize the information in this chapter. The example system consists of an isolated 12.47 kV radial power system powered by a central 10-MW diesel power plant and a 1.2-MW PV farm.



**Fig. 9.19** Simplified one-line diagram of a BESS installation at an isolated power system

The system's resulting renewable penetration is high and the system serves two major load centers each rated at 3 MW peak. System frequency is maintained by the diesel generators which are sensitive to load changes. If the load increases, the system frequency will drop and if the load decreases, the system frequency will increase. The generators' speed control is typically used to maintain an average system frequency of 60 Hz. The BESS in the example system has a combined power capacity of 405 kW and a useable energy capacity of 750 kWh. The BESS is integrated near the PV plant to provide ramp-rate mitigation for the diesel generators. The point of common coupling (PCC) is defined between the BESS and the PV plant. A one-line diagram of the example system and a close-up view of the PV plant and BESS are shown in Figs. 9.19 and 9.20, respectively.

Diesel generators consist of the diesel engine (or the prime mover), an electrical generator, and various other devices such as circuit breakers and generator controls. The generator controls are typically implemented using a droop controller that constantly adjusts the fuel intake as the electrical load changes to keep the frequency output of the generator constant. When the load increases, the fuel intake to the combustion system increases. Likewise, when the load decreases, the fuel intake to the combustion system decreases. For this example, a sudden change in PV output power would result in a generator frequency deviation that, in severe cases, could fall so far outside system operating parameters that load shedding would be required to prevent total blackout. It is for this reason that ramp-rate limits are imposed on systems with generators. The limits are even more important to systems with a high penetration of variable generation sources, such as PV or wind farms, especially when they are located near the system's diesel generators. For this example, the interconnection requirement for the PV power ramp rate is limited to a maximum of 60 kW/s to keep the frequency deviation on the system within acceptable limits. The BESS and a ramp-rate controller are used to keep the ramp rate within limits, as described below.



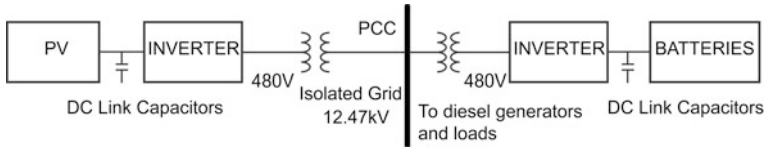


Fig. 9.20 Close-up view of the PV plant and BESS

### 9.5.1 PCS for the BESS

The BESS control system consists of ramp-rate controller, a real and reactive power controller, and a current controller (see Fig. 9.21). The BESS control system measures the power output of the PV plant and smooths it by either injecting or absorbing power from the system. The inverter operates as a voltage source in current-control mode using direct-quadrature ( $D-Q$ ) current control. The voltage-source converter in current-control mode is typical of most installations. The PV plant’s measured power is fed into the ramp-rate controller. The ramp-rate controller provides the  $P$  and  $Q$  commands to the  $P-Q$  power controller which then feeds the current references to the current controller. The current controller provides gating signals to the inverter to control BESS power output. The primary objective is to keep the ramp-rate out of the PV plant within limits; the secondary objective is to maintain the batteries at a particular SOC. The measured SOC of the battery is fed into the ramp-rate controller where it is compared to a reference or desired SOC. If the SOC reference is too high or too low, the batteries will not be capable of delivering or absorbing power for ramp-rate control [11]. The SOC reference is application specific and depends on the battery type. Lead-acid systems are known to operate anywhere from 20 to 80 % SOC for cycling applications [12].

The ramp-rate controller in this example is implemented using a moving-average filter algorithm. The moving-average filter is a simple and robust way to control ramp rates [13, 14]. This implementation provides a maximum ramp rate given a step change in power output of the variable source, in this case the PV output power. It samples the PV power output at low rates (10 to 100 Hz), thus keeping the length of the output filter manageable. A simplified graphical description of the ramp-rate controller is shown in Fig. 9.22.

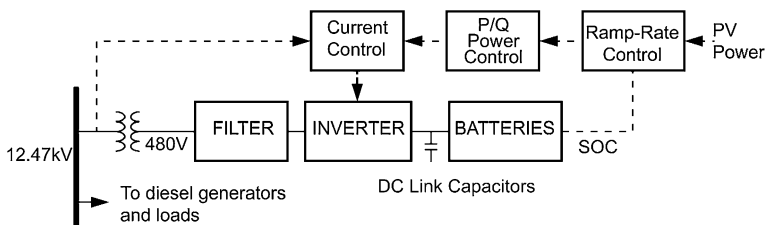
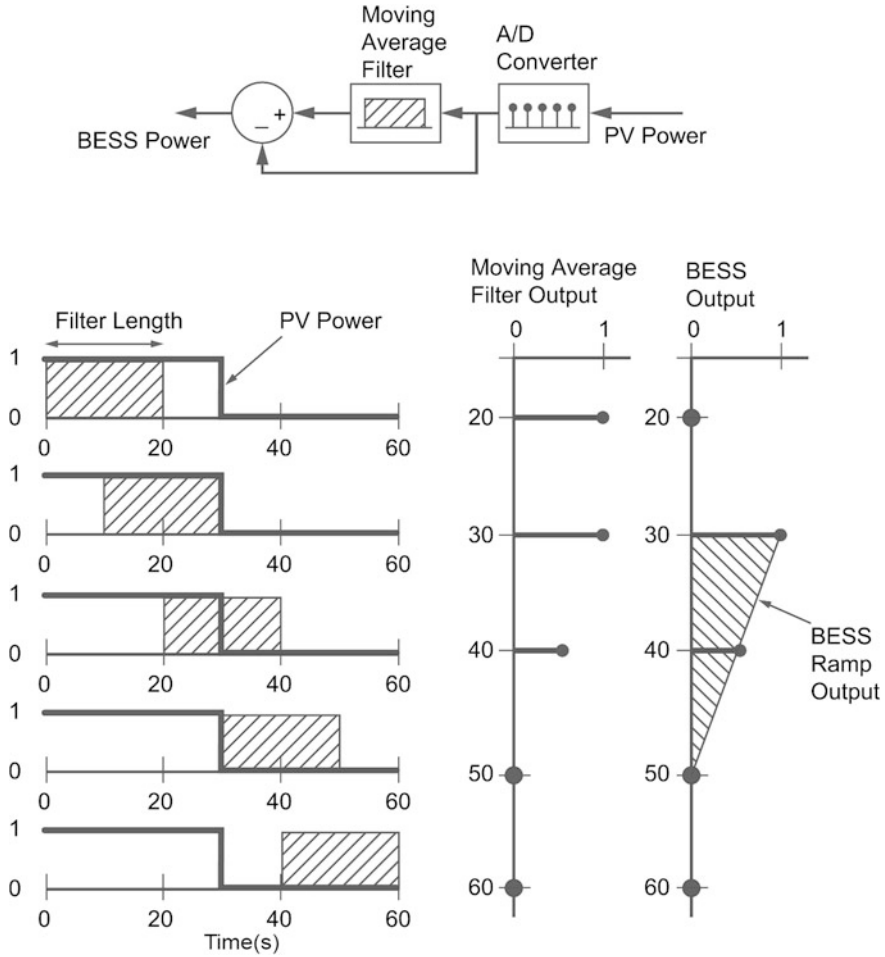
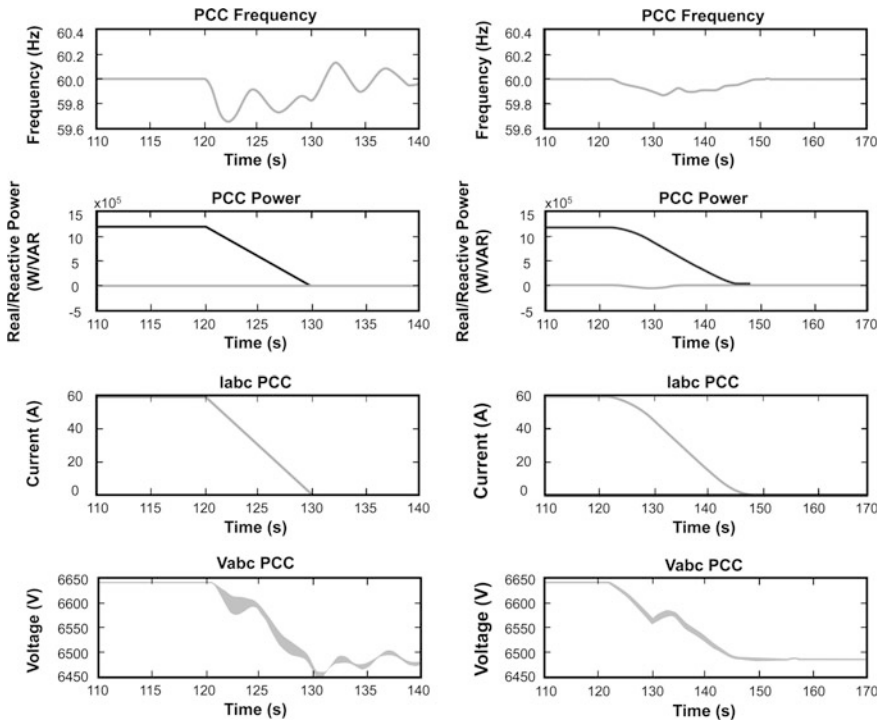


Fig. 9.21 Basic block diagram of the BESS control for ramp-rate control



**Fig. 9.22** Graphical representation of a moving-average filter control

The figure shows an ideal step change in PV power output. A more likely scenario would occur when passing clouds cause the PV output power to drop quickly. The figure shows how at 30 s the PV power output goes from a unit power of one to zero and BESS power output (dotted lines) ramps from a unit power of one to zero in 20 s. The filter length is directly proportional to how much energy is required from the battery. In other words, the longer the filter length the longer it would take the BESS output to ramp to zero, thus requiring more energy to accommodate the ramp. The shorter the filter length, the shorter the ramp time to zero, thus requiring less energy to accommodate the ramp. Care must be taken in selecting the filter length of the ramp-rate controller. The filter length should be such that the BESS power output does not exceed the power rating of the inverter. Detailed system studies have to be made to determine the optimal filter length and battery size.



**Fig. 9.23** Dynamic response curves for ramp-rate control without (*left plots*) and with (*right plots*) integrated BESS

### 9.5.2 BESS Performance and Field Data

The one-line diagram shown in Fig. 9.19 was simulated using MATLAB/Simulink SimPowerSystems© toolbox. The objective of the simulation was to show the frequency response at the PCC, with and without a BESS, using ramp-rate control. The results are shown in Fig. 9.23. The PV output ramp rate was set to 120 kW/s, which represents the worst case scenario, where the PV output drops from maximum output to zero in 10 s. As can be seen from the left plot, the frequency output at the PCC drops to 59.65 Hz during the time the ramp is decreasing. When the ramp ends, the frequency reaches a maximum of 60.14 Hz. This type of frequency swing may cause sensitive loads to go off-line. In the right plot, which shows a system implemented with a BESS at full rated capacity of 405 kW and 750 kWh, the PV ramp rate at the point of common coupling (PCC) was reduced to about 44 kW/s. As a result, the frequency output at the PCC drops to 59.86 Hz during the ramp down with no frequency overshoot when the ramp ends. Also shown on the plots are single-phase current and voltage at the PCC. This clearly shows that the ramp rate can be reduced by active power support by the BESS and proper ramp-rate controls.

**Acknowledgments** The authors gratefully acknowledge support for this work from Dr. Imre Gyuk and the Energy Storage Program in the Office of Electricity Delivery and Energy Reliability at the US Department of Energy.

Sandia National Laboratories is a multi-program laboratory managed and operated by Sandia Corporation, a wholly owned subsidiary of Lockheed Martin Corporation, for the U.S. Department of Energy's National Nuclear Security Administration under contract DE-AC04-94AL85000.

## References

1. EPRI (2003) Handbook for T&D applications wind application supplement
2. Linden D (2010) Linden's handbook of batteries, 4th edn. McGraw-Hill, New York
3. Eyer J, Corey G (2010) Energy storage for the electricity grid: benefits and market potential assessment guide. Sandia National Laboratories, New Mexico
4. Atcitty S, Ranade S, Gray-Fenner A (1998) Summary of state-of-the-art power conversion systems for energy storage applications. Sandia National Laboratories, New Mexico
5. Mohan N, Undeland T, Robbins WP (2003) Power electronics: converters, applications, and design, 3rd edn. Wiley, New York
6. Rodriguez J, Lai JS, Peng FZ (2002) Multilevel inverters: a survey of topologies, controls, and applications. *IEEE Trans Ind Elec* 49(4)
7. Hannemann H (2010) Innovative solutions for grid stabilization and support. ABB power electronics napier
8. Krause PC, Wasynczuk O, Sudhoff SD (2002) Analysis of electric machinery and drive systems, 2nd edn. Wiley, New York
9. Fregosi D, Bhattacharya S, Atcitty S, Empirical battery model characterizing a utility-scale carbon-enhanced VRLA battery. Energy conversion congress and exposition (ECCE), IEEE, pp 3541–3548, 17–22 Sept. 2011
10. Cox DC, Perez-Kite R (2000) Battery state of health monitoring, combining conductance technology with other measurement parameters for real-time battery performance analysis. Telecommunications energy conference
11. Hund T, Gonzalez S Barrett K (2010) Grid-Tied PV system energy smoothing. 35th IEEE Photovoltaic specialists conference
12. Rand DAJ, Mosely PT, Garche J, and Parker CD (2004) Valve-regulated lead-acid batteries
13. Kakimoto N, Satoh H, Takayama S, Nakamura K (2009) Ramp-rate control of photovoltaic generator with electric double-layer capacitor. *IEEE Trans Ener Conv* 24(24):465–473
14. Kasem AH, El-Saadany EF, El-Tamaly HH, and Wahab M (2008) Ramp rate control and voltage regulation for grid directly connected wind turbines. Power and energy society general meeting—conversion and delivery of electrical energy in the 21st century

# Chapter 10

## Fast Response Energy Storage Systems

Juan M. Carrasco, Eduardo Galván, Sergio Vázquez,  
Luis García-Tabarés and Marcos Lafoz

**Abstract** Fast Response Energy Storage describes several technologies characterized by the ability to provide or to absorb a high amount of electrical energy in a short period of time without diminishing the life time of the storage device. Major technologies discussed in this chapter are: Electric Double Layer Capacitors (EDLC) that store energy in the electrical field of a capacitor; Flywheels that do it as kinetic energy and Superconducting Magnets (SME) where energy is kept in the magnetic field of a lossless inductor. All these technologies can develop a wide range of different applications. In this way, they can support an increasing level of renewable energy sources penetration in the conventional grid by providing the necessary features. The most important are: Power quality issues, including grid frequency regulation and grid voltage stability; Smart grids development, including hybrid energy storage systems, like EDLC plus batteries, that support short-term and long-term necessities of the grid and electrical and hybrid vehicles as distributed energy storage systems. In this chapter, the basics for these technologies are presented, addressing information about the power converters needed to manage the energy of these devices. Besides, the most important applications regarding renewable energy integration are described, providing information about implemented real systems.

---

J. M. Carrasco (✉) · E. Galván · S. Vázquez  
Department of Electronics Engineering, University of Seville, Avd. Camino de los  
Descubrimientos s/n 41092 Seville, Spain  
e-mail: jmcarrasco@us.es

L. García-Tabarés · M. Lafoz  
CIEMAT, Av Complutense 40, 28040 Madrid, Spain

## 10.1 Introduction

Storing energy is a way of modifying the basic equation of the electrical energy production which states that the energy produced must equal the consumed one. If an energy storage device is present in the network the equation is modified; the produced energy is now the sum of the consumed and the stored energy with its corresponding sign: “plus” when storing and “minus” when pumping back. This means that storing is a way of “decoupling” the offer and the demand at a certain moment [1].

This idea is quite old and good examples are hydro-pumping or massive storage heaters. In both cases, the cheaper energy produced during the night was stored and released during the day.

Ensuring that a storing term is always present in the energy equation is usually challenging, especially for high levels of energy and power. The presence of this term would guarantee generation under the best possible conditions or, that less energy would be wasted, especially in renewable systems.

Nevertheless, even for small grids where the involved levels of energy and power are modest, the availability of the storage term can be very helpful to manage that grid in the most efficient way (maximizing the produced energy, minimizing the dimensions of the grid, or improving its robustness to energy cuts or faults). To be able to take advantage of some of these potential benefits, the storage devices need to be fast: they must be able to deliver full power in the shortest possible time [2].

Instead of conventional storage devices such as hydro-pumping or batteries, this chapter will focus on the applications of three alternative Energy Storage Devices (ESD) which, although well known for many years, advances in materials development along with new power electronics topologies, have broadened their applications and capabilities and also have enhanced them to be the best candidates for fast ESD.

These ESD are Electric Double Layer Capacitors (EDLC), Flywheels (also called Kinetic Energy Storage Systems-KESS), and Superconducting Magnetic Energy Storage (SMES).

In the first case, the energy is stored in the electrical field of a capacitor, in the second as kinetic energy in a rotating flywheel and finally, in the third one, in the magnetic field of a lossless inductor (superconducting). All forms of storage are dual and can be expressed as half the product of a parameter given by the geometry of the device, times the square of a state variable (see Table 10.1).

**Table 10.1** Energy equations for three fast ESD

ESD	Geometrical parameter	State variable	Energy
EDLC	Capacitance (C)	Voltage (V)	$\frac{1}{2} CV^2$
KESS	Moment of inertia (J)	Angular speed ( $\omega$ )	$\frac{1}{2} J\omega^2$
SMES	Self-inductance (L)	Current (I)	$\frac{1}{2} LI^2$

This duality easily allows representing them by its equivalent circuit, including flywheels, where the inertia can be associated to an inductor and the angular speed to the current flowing through it or, alternatively, to a capacitor and the voltage across it, respectively.

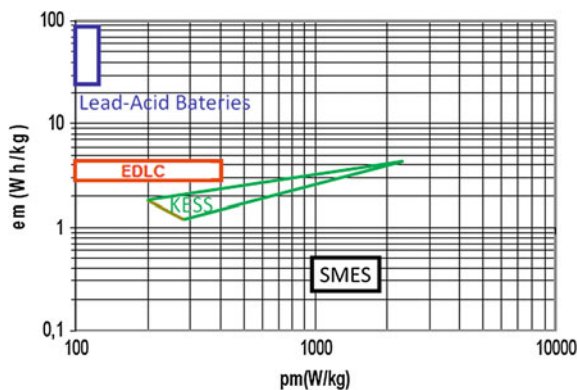
Any ESD can be defined by two basic parameters, the power and the energy. Usually both are independent resembling, somehow, the flow rate and the volume of a water tank: One can image for instance, a big deposit (high energy) with a small drain (low power) or any other combination of these two variables. It is also very common to speak in terms of energy and power densities, normalizing with the mass or the volume of the device.

In general, achieving high power is a matter of the power capability of the “driving device”: A power source for EDLC and SMES and an electrical machine for KESS, while attaining high energy depends, exclusively, on the device where the energy is stored: It is usually a combination of geometrical design (to achieve an optimum capacitance, self-inductance, or moment of inertia) and material properties (to withstand breakdown voltage, critical current, or stresses associated to high speeds).

A very intuitive and helpful way of comparing different ESD is the so-called Ragone Plot (Fig. 10.1) where the x-axis represents mass power density ( $pm$ ) while the y-axis is associated to mass energy density ( $em$ ) (usually a log–log scale is used) [3]. Every family of ESD has its typical location in this energy-power diagram. In general terms, EDLC or Ultracapacitors have a higher energy density, SMES, on the contrary exhibit a higher power density while Flywheels are somewhere in the middle with intermediate values. For comparison, Lead-Acid batteries have also been included in the plot.

In the last years renewable energies have grown very quickly because they present several benefits. However, the development of renewable energies has manifested new challenges and issues regarding their integration in the grid [4]. These energy resources, like wind or PV, have unique characteristics that made different to conventional ones. Specifically, there are concerns on how they should be included in a mature and sometimes inflexible utility framework [5]. Several

**Fig. 10.1** Ragone plot for several ESD



topics related with renewable energy systems have been the object of research activities in the past years: Control strategies to achieve maximum profits from these energy resources, control techniques to satisfy technical connection requirements (national standards and codes), research about the most suitable power converter topologies for each application, modulation techniques and control algorithms to reduce switching losses or reduce passive components, etc. [6]. One of the most worrying aspects regarding renewables is their variability. This issue has given rise to several studies about the effect of this variability over the grid reliability [4]. For instance, new forecast techniques have been developed and in the future it is expected new ones will be even more accurate to increase the information of the availability of these resources. These studies also pointed out energy storage systems will have an important role in the integration of renewables into the grid [7, 8]. Two main aspects are considered. In one hand, renewables are not dispatchable in the sense of “wind blows when it blows” or “sun shines when it shines”. This means, that sometimes renewables produce more energy than the actual load or sometimes less than necessary. Currently, these problems are solved by curtailment of renewable resources or making use of the spinning or non-spinning reserves by the independent system operator (ISO). However, long-term energy storage system can improve the system by shifting the energy production curve [9]. On the other hand, renewable resources have high short-term variability and high ramping production rate. As a consequence, increasing the penetration of renewable in the utility requires high flexibility of the system. This means, that operating reserves of the system, as regulation and contingency spinning reserves, should have the suitable features to accommodate the renewable resources. Fast response energy storage systems fit very well with these new necessities, providing even improvements to the system because they can achieve faster time responses than conventional systems used for operating reserves [10].

## **10.2 Technology Basics**

### ***10.2.1 EDLC***

#### **10.2.1.1 Introduction to the Technology**

Electrochemical double-layer capacitor (EDLC) works in much the same way as conventional capacitor in that there is no ionic or electronic transfer resulting in a chemical reaction (there is no Faradic process), [11, 12]. In other words, energy is stored in the electrochemical capacitor by simple charge separation. Therefore, the energy stored in the electrochemical capacitor can be calculated using the same well-known equation that is used for conventional capacitors:



$$Q = C \cdot V = \frac{A \cdot \epsilon}{d} V \quad (10.1)$$

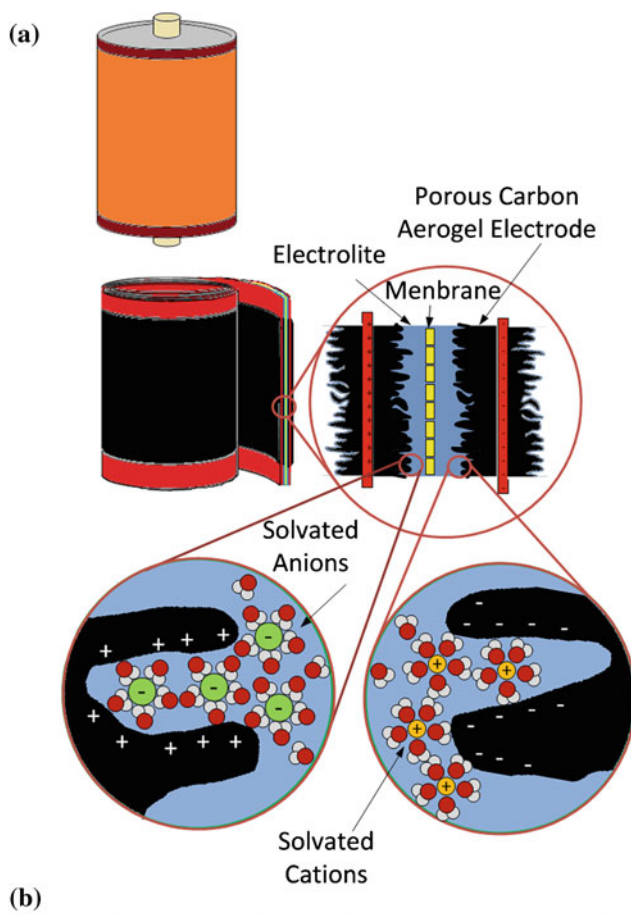
As for the conventional capacitor, the capacitance  $C$  is proportional to the area  $A$  of the plates and the permittivity of the dielectric  $\epsilon$  and is inversely proportional to the distance  $d$  between the plates. EDLCs are designed to have a very high electrode surface area and use high permittivity dielectric. The electrode surface area is maximized by using porous carbon as the current collector allowing a relatively large amount of energy to be stored at the collector surface. Therefore EDLC attain very high capacitance ratings (kilo-Farads versus mili- and micro-Farads for conventional capacitors). The two electrodes are separated by a very thin porous separator and immersed in an electrolyte such as propylene carbonate. Due to the high permeability and close proximity of the electrodes, EDLCs have a low voltage withstand capability (typically 2 V–3 V).

EDLC stores energy by physically separating unlike charges. This has profound implications on cycle life, efficiency, energy, and power density. EDLCs have a long cycle life due to the fact that (ideally) there are no chemical changes on the electrodes in normal operation. EDLCs have superior efficiency: it is only a function of the ohmic resistance of the conducting path. EDLCs also provide exceptional power density, since the charges are physically stored on the electrodes. Conversely, energy density is low since the electrons are not bound by chemical reactions. This lack of chemical bonding also implies that the EDLC can be completely discharged, leading to larger voltage swings as a function of the state-of-charge.

### 10.2.1.2 Constructive Blocks

The minimum constructive EDLC element is a cell. This cell can be built as a classical capacitor that could be piled or rolled up as shown in Fig. 10.2a. In this device, the charge is stored as the solvated ions reach the so-called Helmholtz double layer region, close to the porous carbon electrodes. When a voltage is applied, solvated anions are accumulated at the positive layer and solvated cations are accumulated at the negative layer. These ions are always solvated, that is, rounded by water or other solvent molecules and isolated from carbon electrode by an extremely short distance, in the range of several angstroms. The electrodes are built by porous activated carbon. After activation, carbon is a highly porous material and offers a surface over 2,000 m<sup>2</sup> per gram. These two geometric characteristics, high surface, and small dielectric distance, produce a very high capacitance, in the range of several hundred farads.

The voltage and capacitance of an elementary cell is very low, typically 2.5 V and 10F respectively. To increase these parameters, cells are arranged in series and parallel constituting a stack. Cells and stacks also operate as ideal capacitors and so, voltage is linear and drops evenly from full voltage to zero volt with constant current discharge. Because this, a dc/dc converter is needed to connect the

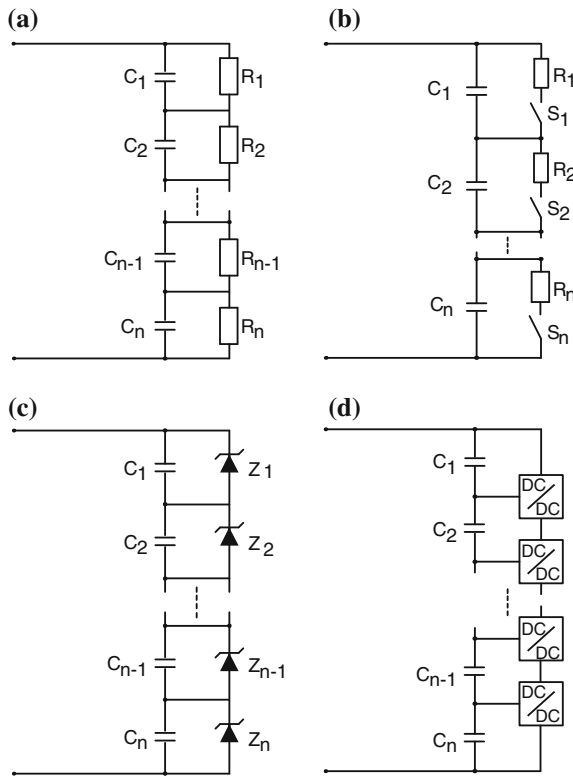


**Fig. 10.2** EDLC technology. **a** Basic cells structure. **b** 18F/380 V EDLC stack under test at the ESD-Lab sited in the Engineering School of Seville's University

capacitor stack to a constant voltage to get the maximum efficiency of the overall system.

Connecting several cells in series requires equalization of the overall system because, as cells are cycled, voltages are different for each cell. This effect is produced because the capacitance, efficiency, and leakage current of each cell are different.

The balancing techniques are classified in two types, energy consume type and energy transfer type [13]. Figure 10.3 shows some equalization circuits. Circuit in Fig. 10.3a uses equalization resistors,  $R_i$ . In this circuit, all resistors are adjusted to the same value to get the same voltage in all EDLC connected in series. The circuit in Fig. 10.3b uses switches to reduce auto-discharge effect. When voltages are balanced, the switches are off and this reduces the auto-discharge effect produced by these resistors. Similar functionality can be gotten by circuit in Fig. 10.3c using Zener diodes. The Zener diode switches on only when unbalance occurs. Circuits shown in Fig. 10.3a–c consume energy dissipating in resistors and Zener diodes at least during balancing process. An example of energy transfer circuit is depicted in



**Fig. 10.3** Balancing circuits. **a** Using equalizing resistors. **b** Using resistors and switches. **c** Using Zener diodes. **d** Using DC/DC converter

**Table 10.2** Technical characteristics of a typical EDLC stack

Characteristic	Units	Value
Nominal operating voltage	V	390
Maximum operating voltage	V	394
Surge voltage	V	406
Nominal capacitance	F	17.8
Tolerance capacitance	%	+20 %/- 0 %
DC series resistance	mΩ	65.0
Maximum continuous current assuming 15 °C temperature rise above ambient temperature	A	150
Self-discharge 30 days RT 100 V; 12 h charge and hold Voltage	% of initial	5,000 %
Energy available $(0.5C (V_{nom}^2 - (0.5V_{nom})^2)/3600)$	Whr	282
Isolation voltage	V	3,500
Maximum string operating voltage	V	1,500
Lifetime 390 V, RT (End of life characterized as -20 % C from nominal C, or increase of 100 % in ESR)	hr	15,0000
Cycles 390 to 62.5 Vdc, RT	Cycles	100,0000

Fig. 10.3d. In this figure, the DC/DC converter transfers energy from a capacitor to the adjacent one and no energy is dissipated during this energy transfer. Energy consume type has the disadvantage of lower efficiency, but also slower voltage balance speed. In opposite, these have the advantage of a simpler circuitry.

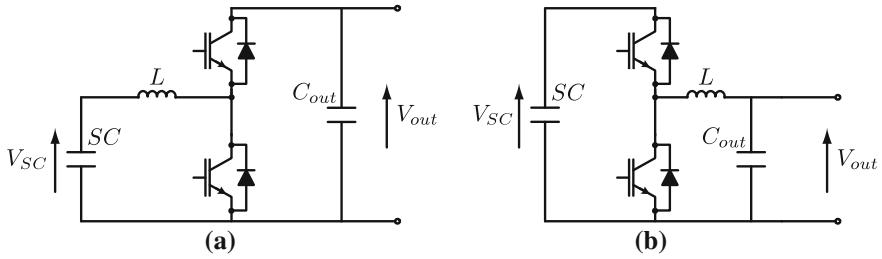
Table 10.2 shows the technical characteristics of the 18F/380 V EDLC stack shown in the photo of Fig. 10.2b. This photo shows an EDLC under test at the ESD-Lab located at the Engineering School of Seville's University.

### 10.2.1.3 Power Converters

EDLCs are devices that store energy in an electric field. To put in or to get out energy is necessary a power convert that adapts the actual dc voltage output of the EDLC to the connection point of the energy storage system. Different options can be chosen as the power converter topology. It mainly depends on the specific application and the voltage level in the connection point. In any case, the power converter should provide bi-directional energy flow capability.

#### *dc-dc Buck-Boost Converter*

The most common power converter interface used for EDLC is the dc-dc buck-boost converter [14–18]. Two different scenarios can be considered. The first one, when voltage level in the connection point ( $V_{out}$ ) is higher than the maximum voltage achieved by the EDLC ( $V_{SC}$ ) device. The second case, when the minimum

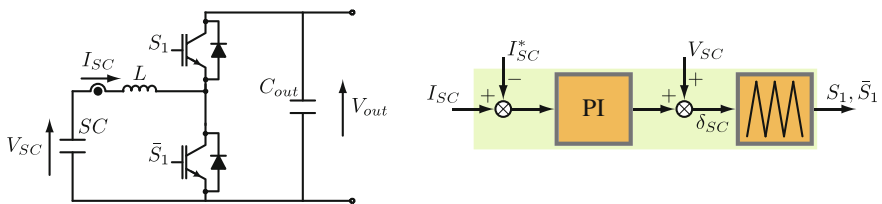


**Fig. 10.4** Buck-boost converter for EDLC applications **a**  $V_{out} > V_{SC}$  **b**  $V_{SC} > V_{out}$

voltage allowed to the EDLC stack is higher than the voltage level in the connection point. This converter can be used in both situations as it is shown in Fig. 10.4. In both cases the EDLC module (SC) is connected to the output capacitor  $C_{out}$ . It should be noticed that in Fig. 10.4 only a single dc–dc stage has been considered. However it is possible to use several stages if they are needed to achieve the desired voltage level.

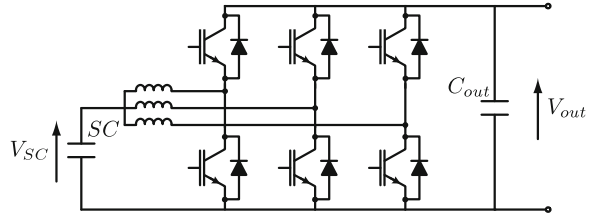
The control of the current supplied by the EDLC ( $I_{SC}$ ) can be done using conventional techniques. Figure 10.5 shows the control scheme when the converter in Fig 10.4a is used. The controller is performed by a simple PI over the error between the measured current  $I_{SC}$  and its reference  $I_{SC}^*$ . The final control signal ( $\delta_{SC}$ ) is calculated adding the voltage of the EDLC to the output of the PI block. Finally, the firing pulses for the power switches are calculated comparing the control signal  $\delta_{SC}$  with a PWM carrier. The method to calculate the reference current for the EDLC ( $I_{SC}^*$ ) depends on the application. But usually it is related to the power that should be supplied or absorbed by the module [17].

In some cases there are technical restrictions over the current ripple that can be provided by the EDLC device. In these circumstances the interleaved dc–dc buck-boost power converter topology is a good option [19, 20]. This converter is composed by several two power switches leg connected in parallel to the storage device as it is shown in Fig. 10.6. Each leg supplies part of the total current drawn from the EDLC stack. If the PWM carriers used to generate the switching pulses of each leg are suitable shifted then the ripple of each leg current are canceled in the total current provided by the module. To control this current the same algorithm as for the conventional dc–dc buck-boost converter can be used.



**Fig. 10.5** Control scheme for the EDLC current when a dc–dc buck-boost converter is used

**Fig. 10.6** Interleaved dc–dc buck–boost power converter with three legs

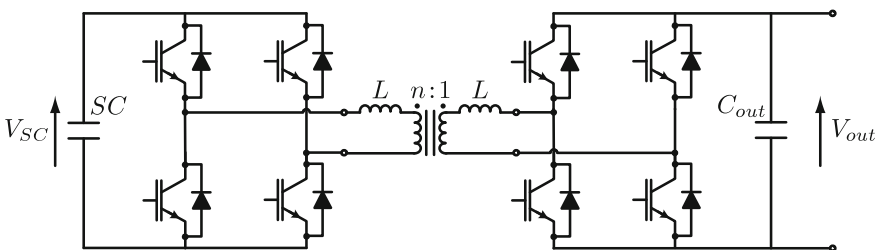


*Other Topologies*

Although the dc–dc buck–boost power converter is the most common topology used for EDLC systems. Other power converter topologies have been considered regarding the application characteristic or the voltage level in the connection point [21,22].

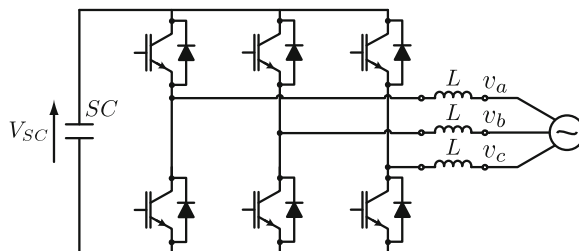
For instance, if the voltage steps between the EDLC device and the output is too large then an option is to use dc–dc converters with transformer as presented in Fig. 10.7 [23,24]. This topology allows higher operating range than conventional buck–boost converter. Besides, if high frequency transformers are used then it permits to build converters with reduced weight and volume. Also, it is possible to use zero voltage switching (ZVS) or zero current switching (ZCS) modulation strategies that increase the efficiency of the system.

On the other hand, for grid connection it can be adopted a conventional two-level three-phase converter (Fig. 10.8). This choice usually requires a large number of series and parallel connection of EDLC cells. This structure is not normally optimal. For this reason, the use of multilevel converters, like neutral point clamped (NPC) or cascaded H-bridge converter (CHB), is also a good option for grid connected applications [25–27].



**Fig. 10.7** Bi-directional energy flow dc–dc converter with isolated transformer

**Fig. 10.8** Three-phase two-level converter



## 10.2.2 SMES

### 10.2.2.1 Introduction to Superconductors

Superconductivity is a physical property that some materials exhibit below a certain temperature (called critical temperature). The best known consequence of superconductivity is the absence of electrical resistance. Nevertheless, two other effects are also associated with this phenomenon: a finite reduction of the specific heat of the material below critical temperature and the presence of the so-called Meissner-Ochsenfeld effect with the expelling of any magnetic field inside the superconductor regardless the way of applying that field (first establishing the field and then cooling the material below critical temperature, or first cooling the material in the absence of any field and then applying the field). Nevertheless, beyond a certain value of the applied magnetic field (called critical field), superconductivity is destroyed. Meissner-Ochsenfeld effect cannot be explained by Maxwell equations (considering a perfect conductor with no resistance) and allows superconductivity to be considered as a thermodynamic phase transition [28].

Superconductivity was discovered in 1911 by Kamerling-Ones and during many years the first known superconductors (type I), which were usually metals, had a very low critical field and no practical applications were found for them. At the end of the 1930s in the past century, it was predicted the existence of another type of superconductors (type II), usually binary or ternary alloys, which were able to allow the penetration of the magnetic field up to very high fields which finally destroyed the superconducting state. Critical fields for type II superconductors are much higher than for type I and this makes them suitable for industrial applications, particularly for the fabrication of high field magnets, like those required for SMES. Not only temperature and magnetic field define the superconducting state, but also the current density that flows in the material. Beyond a certain value, which is called critical current density, the superconductor is driven to the normal state.

From all the materials that show the superconducting property, just very few have significant values of critical field and current density for applications. If technological aspects are also included to consider the ability of the material for producing wires which can easily be wound into magnets and coils, just two of

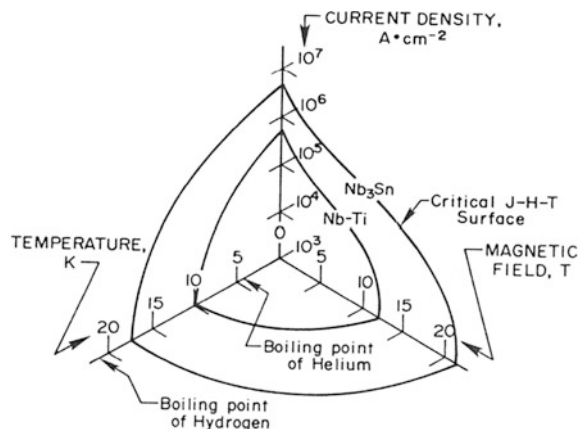
them can be considered as really commercial in the group of the so-called low critical temperature superconductors (LTc): The NbTi and the Nb<sub>3</sub>Sn.

Figure 10.9 shows the Superconducting Critical Surface for these two materials. This surface separates the superconducting and the normal states as a function of the temperature, the magnetic field, and the transport current density. Intersections of this surface with the axes define the corresponding critical values for the current density ( $J_c$ ), the magnetic field ( $B_c$ ), and the temperature ( $T_c$ ). As it can be noticed Nb<sub>3</sub>Sn, presents a much better behavior (higher values of the critical values), but it is a fragile material with much worse technological properties.

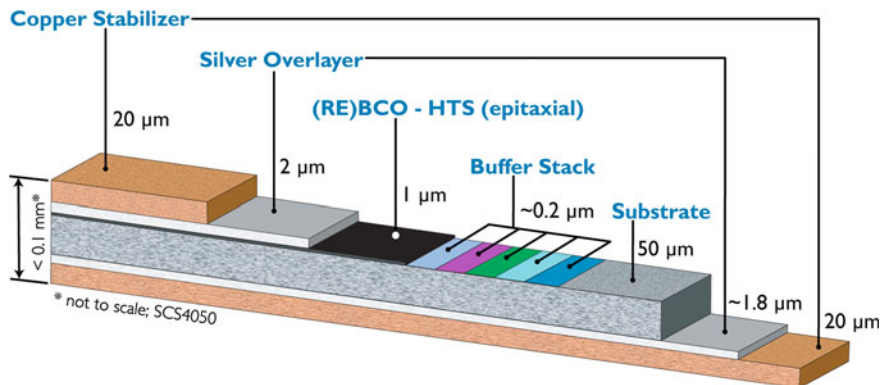
In 1986, the so-called high critical temperature superconductors (HTc) were discovered. While critical temperatures for LTc were below 20 K, for HTc the critical temperature could be above 140 K. HTc superconductors are ceramic and brittle materials and since they were discovered, much scientific and technological effort has been done to develop reliable and robust wires with commercial applications. Presently there are, basically, two technologies [29]: first one is the so-called first generation BiSCO wires which are based on the traditional wire drawing technology on the compound Bi<sub>2</sub>Si<sub>2</sub>Ca<sub>2</sub>O<sub>7</sub> ( $T_c = 112^\circ\text{K}$ ) in a silver alloy matrix. The second one, called second generation YBCO wires, relies on thin film technology to deposit flexible layers of YBa<sub>2</sub>Cu<sub>3</sub>O<sub>7-X</sub> ( $T_c = 93^\circ\text{K}$ ) on a metallic foil. A critical issue for the performance of this wire is the buffer layer between the foil substrate and the HTS coating. These wires have a very high current carrying capacity at liquid nitrogen temperature and an excellent ductility.

Finally, in 2001 the last element of the presently competing materials was announced, the MgB<sub>2</sub>. Although still considered as a Low  $T_c$  superconductor, it has a very high critical temperature (39 K). Superconducting magnesium diboride wires can be produced by two methods: (a) Conventional wire drawing of a metal tube in which a mixture of boron and magnesium is poured. The wire is then heated to the reaction temperature to form MgB<sub>2</sub> inside (b) Filling the tube with MgB<sub>2</sub> powder, drawing, and sintering at 800–1,000 °C.

**Fig. 10.9** Critical surface for NbTi and Nb<sub>3</sub>Sn







**Fig. 10.10** Lay out of a second generation HTc tape (courtesy of SuperPower Inc.)

Although bulk superconductors find some applications like magnetic bearings, when winding magnets they must be used in the form of tapes or wires. A commercial superconducting wire must include some features to achieve a proper operation. There are two main concerns: Time varying field losses and thermal stabilization. Finite critical current density in a superconductor is responsible for magnetization losses when working under a.c. fields [30]. The way to reduce them is subdividing the superconductor in small filaments. On the other hand, superconductors need to be thermally stabilized with a high conductivity (thermal and electrical) metal matrix to guarantee no thermal overrun. Figure 10.10 shows the layout of a second generation HTc superconducting tape.

### 10.2.2.2 SMES Configurations

A Superconducting Magnetic Energy Storage is basically a lossless inductor (with inductance  $L$ ) connected to a source of  $V$  volts. Storing and discharging the SMES has three different stages: (1) When the inductor is connected to the source the magnet starts to charge at a rate  $V/L$ . (2) Once the nominal current is achieved, the inductor is short-circuited with the aid of a so-called superconducting switch, the current can flow through the magnet without losses and full energy is stored in its magnetic field. (3) For releasing that energy and pumping it back, the magnet is connected again to the source reversing its polarity. It starts, then, to discharge at a rate  $-V/L$  until all the energy has been transferred back to the voltage source.

Performing the previous process with a normal conducting magnet would lead to an inadmissible efficiency: the only way to overcome the problem is to use a superconducting magnet which, in theory, allows storing of the energy for an infinitely long time without losses.

There are many topologies of superconducting magnets which can be found in power applications; nevertheless, most of them can be classified according to

**Table 10.3** Magnet topologies for power applications

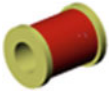


	Geometry	Magnetic field shape
	Solenoid	Dominant along the magnet axis
	Dipole	Dominant along a perpendicular axis to the magnet mid-plane
	Toroid	Practically constant along the circular magnet axis

Table 10.3, which also provides their magnetic field shape. Basically they are solenoids, dipoles, and toroids [31]. By far, the simplest magnets to manufacture are solenoids, since they can be easily wound turning a wire around a simple bobbin. The other two types require more complicated movements to wind the coil. Since the aim of an SMES magnet is to store energy in a magnetic field regardless its shape, solenoids, in principle, appear as the preferable option.

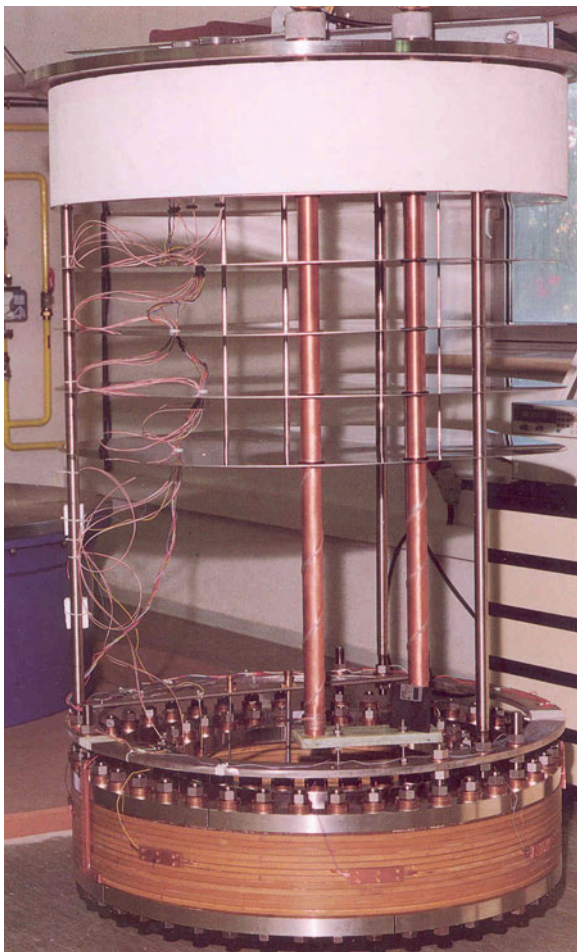
For a conventional resistive magnet, the optimum solution to build an SMES is the so-called Brooks Coil, a solenoid with the same values of height, thickness, and inner radius achieves the maximum possible self-inductance for a given length of wire [32].

In the case of a superconducting magnet, things are much more complicated as the allowable current density depends on the magnetic field, and hence on the magnet shape. Final solution will strongly depend on the superconductor's critical current density properties, but in any case it will be a flat and thick solenoid rather than a slender one. Figure 10.11 shows an optimized solenoid for a SMES built for a Spanish Utility Association in the late 1990s, hanging from the supporting structure to place it in a cryostat [33].

Although solenoids are the simplest topologies, they suffer from two big drawbacks: high stray fields and big stresses in the coils induced by electromagnetic forces. This problem is especially severe in SMES solenoids, because they are thick and develop radial tensile stresses induced by the electromagnetic pressure, which also induces huge hoop stresses in the superconducting wire. Since superconducting coils should never work under radial traction and positive hoop stresses should be limited, a pre-compression structure must be added to the magnet, increasing its size, cost, complexity, and operational cost as it also has to be cooled down [31].

Stray fields can also be a problem, especially for big and flat solenoids as they can create significant magnetic fields very far away from the magnet. To avoid these two drawbacks, SMES based on toroids have been proposed and built [34]. The simplest way of building a toroid is by arranging solenoids in a circular way as it is shown in the toroid figure in Table 10.3. If the solenoids are very close, the stray field is negligible and the main field is confined inside the torus volume.

**Fig. 10.11** Solenoid Magnet for a SMES



Since in this case the solenoids are thin, radial stresses are small and compressive and supporting structures can be simpler than for the SMES solenoidal solution. Moreover there have been some developments of toroidal SMES wound in helical shape in such a manner that the poloidal and toroidal components of the current are balanced to reduce or eliminate some stresses [35].

Regardless the type of magnet used in a SMES, there are other components which are common to all of them: basically those related to the cryogenic aspects and those to the power electronics converters.

The way the magnet is cooled down is closely related to the type of superconductor and its critical temperature, While for LTc superconductors, working at boiling helium temperature at atmospheric pressure (4.2 K) is mandatory (GE Industrial Systems and American Superconductors [36], for HTc superconductors temperatures as high as 20 or 30 K can be feasible. In both cases, the magnet

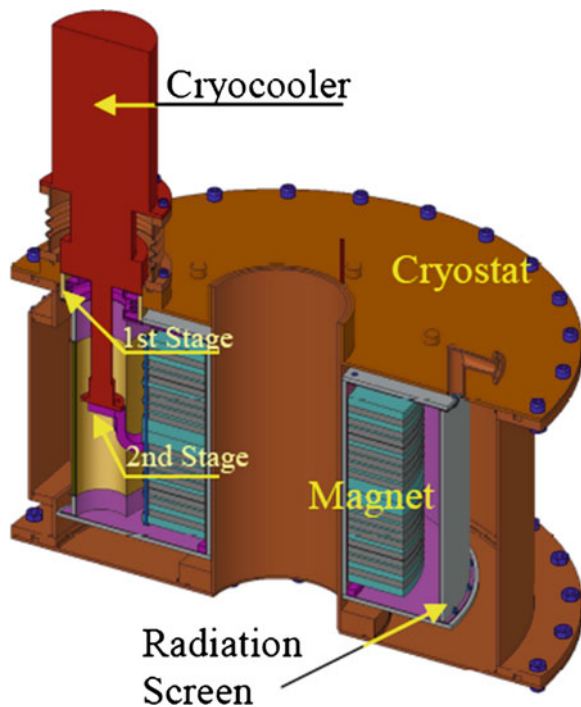
should be immersed in a vessel thermally isolated from the outside world (cryostat). In the first case this cryostat is usually filled with liquid helium that cools down the coil. The gas is evaporated and then recondensed in a close loop.

When working at 20 or 30 K there is the possibility of using a “dry” scheme where all the heat losses of the system are extracted by conduction using a cryocooler which is a device to achieve low temperature by cycling certain gases [37]. Depending on the thermodynamic cycle there are different types like the Stirling, the Gifford-McMahon, or even the Pulse-Tube refrigerators [38].

Figure 10.12 shows a diagram of a complete HTc magnet system inside its cryostat, which is refrigerated using a cryocooler. Since it normally has two stages, the hottest one is connected to a thermal shield that reduces radiation losses, while the coldest one is anchored to the magnet to extract losses by conduction.

Current is injected to the magnet from the power converter through the so-called current leads which need to be carefully designed balancing the conduction losses that introduce in the cryostat and the Joule losses generated when flowing the current through them. HTc magnets are usually wound in “pancakes”, which are finally series-connected in order to overcome the problems of a conventional winding procedure with such fragile wires.

**Fig. 10.12** HTc Magnet System



### 10.2.2.3 Power Converters

In superconducting energy storage systems (SMES), it is the power converter or power conditioning system (PCS) that manages the power transfer between the superconducting coil and the a.c. system. There are three different topologies that can be used [39]: (a) thyristor-based converter, (b) voltage source converter (VSC), and (c) current source converter (CSC).

#### *Thyristors Topology*

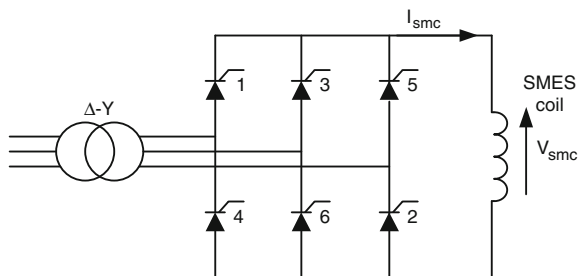
Figure 10.13 presents the thyristor-based SMES. Charge and discharge of the superconducting coil are controlled by the firing angle  $\alpha$  of the thyristors. If  $\alpha$  is less than  $90^\circ$ , the converter charges the coil, operating as a rectifier. If  $\alpha$  is greater than  $90^\circ$ , the converter discharges the coil and operates as an inverter. The bridge current  $I_{smc}$  is not reversible, so as the active power is only a function of the angle  $\alpha$ . This topology has a little ability to control reactive power and its control depends on the active power level since firing angle ( $\alpha$ ) affects the power factor. This solution will not be used in applications where reactive power regulation is required [40, 41]. Thyristors were a very common technology in the past [42], currently it is still used in low performance and low-cost electric drives and applications.

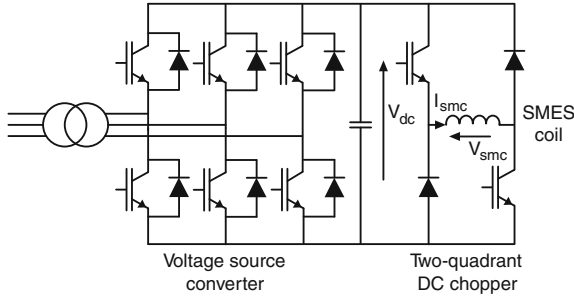
#### *Voltage Source Converter Topology*

The VSC configuration is composed by a six-pulse width modulation converter and a two-quadrant DC–DC chopper, linked by a DC-link capacitor. In the 1990s, when this technology started for SMES applications, GTO was the most common semiconductor used for the PCS because of their high voltage and current ratings. Currently, IGBTs that offers a simplified gate drive circuitry with high levels of current and voltage and good thermal and safe behavior, ensure a better reliability. Figure 10.14 shows VSC topology based on IGBTs.

Voltage source converter (VSC) is preferred in case of reactive power requirements of the utility. That is because better continuous voltage control can be provided.

**Fig. 10.13** Thyristor-based topology for SMES

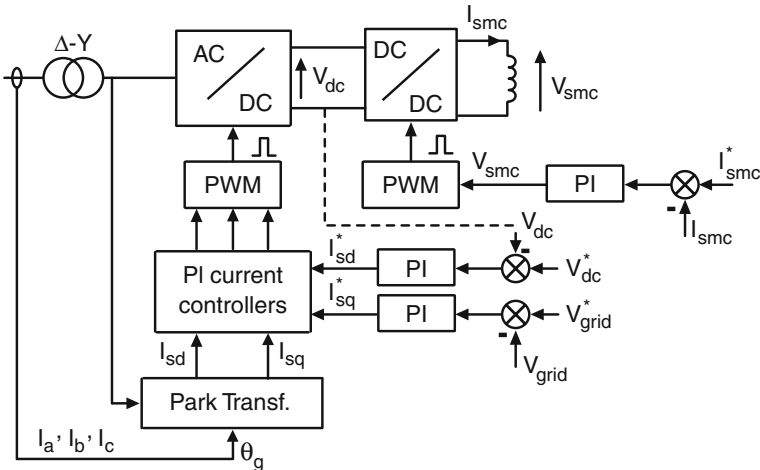




**Fig. 10.14** VSC topology for SMES using IGBTs

Nevertheless, a second stage of a two-quadrant DC chopper is required due to the high inductance of the dc load and the control becomes more complex. The topology presented ensures the control of the voltage applied to the superconducting coil, maintaining the direction of the current [39]. By adjusting the duty cycle of the chopper IGBTs larger than 0.5 or less than 0.5, the voltage applied over the coil  $V_{smc}$  can be increased or reduced, keeping constant the DC-link voltage  $V_{dc}$ , and charging or discharging the superconducting coil (increasing or decreasing  $I_{smc}$ ) depending on the application requirements. The chopper IGBTs pulses are generated by comparison of the duty cycle signal with a triangular carrier.

On the other hand, the VSC is in charge of keeping constant the  $V_{dc}$  voltage exchanging power with the grid. Moreover, is able to control the reactive power independently, so this topology can be used for active and reactive power applications. Figure 10.15 shows the regulation control scheme. It is a current control based on a d-q reference frame created from the grid voltage. d-axis produces the



**Fig. 10.15** Control scheme of a VSC and dc chopper for SMES application

current component to control the dc-link voltage while q-axis component is in charge of providing the reactive power to control the voltage module at the grid. PI controllers are used to generate the voltage reference for a PWM module that provides the switching pulses to the converter.

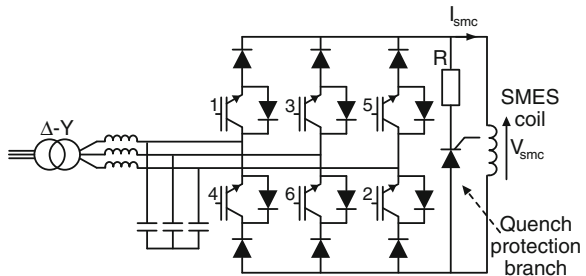
*Current Source Converter Topology*

The topology of current source converter (CSC) is provided specially for DC loads where the current is non-interruptible. A superconducting coil (SCC) is intrinsically a current source and therefore a suitable application for this topology. The difference with a VSC is that CSC does not commute voltage but current and can be a direct interface between the superconducting coil and the ac side. GTO topology was used some years ago but nowadays IGBT can manage high currents and it is more commonly used. In case of very large currents, IGCT modules would be used. Figure 10.16 presents the CSC topology with IGBTs. CSC topology used for SMES requires a bypass switch to maintain the current flowing through the dc circuit when converter is not exchanging power to the electric grid, as Fig. 10.16 shows.

It is also critical to add at the dc part of the power electronic converter a quench detector branch at the inverter. The quench phenomena occurs when the coil stop being superconducting due to an internal problem with the superconducting material. As a consequence, the resistance increases, producing a voltage run up if maintained the current level by the control. In this case the energy stored in the SCC will be delivered in a dissipation resistance.

A bank of capacitors is connected to the grid terminal in order to buffer the energy stored in all line inductances during the process of ac line current commutation. This resonance frequency of the filter is usually set to the 9th harmonic, reducing the high order harmonics in line current. The simplest control is based on a current control with a current reference, a PI controller, and the modulation index as a result of it. Conventionally a static commutation pattern can be used [43] to

**Fig. 10.16** CSC topology for SMES with IGBTs



minimize the low order harmonics (5th, 7th, 11th, and 13th). However, during transients of current variation, firing angle distorts the switching pattern exciting the resonance modes of the LC filter. That produces unacceptable over-currents. As a first solution is to slow down the current variation but it reduces the fast response of the SMES. A dynamic commutation pattern based on space vector modulation (SVM) is preferred to improve the dynamic behavior [44], avoiding such a problem since the switching frequency is controlled during the transient of the current variation and reducing the requirements of the LC filters.

The SVM strategy used for a CSC is based on the well-known strategy used for VSC [45]. A hexagon is formed by six active vectors as Fig. 10.17 shows, corresponding to the nine possible combinations of switches in the CSC. Besides, there are other three combinations that produce zero output current.

Current space vector is defined as Eq. (10.2). The current reference to be injected into the electric grid is referred as this current space vector.

$$\vec{I}_s = \sqrt{\frac{2}{3}} \left( I_a(t) + I_b(t) \cdot e^{j\frac{2\pi}{3}} + I_c(t) \cdot e^{-j\frac{2\pi}{3}} \right) \tag{10.2}$$

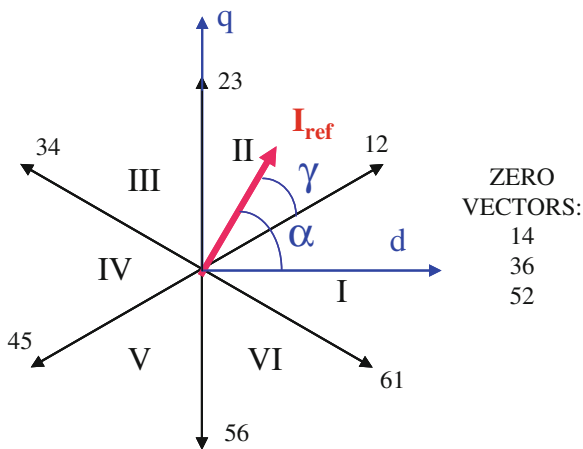
Considering a d-q reference based on the grid voltage position, a  $\gamma$  angle is calculated by Eq. (10.2) from the angle  $\alpha$ , determining the sextant where is the reference current space vector.

$$\gamma = \alpha - \left[ (k-1) \frac{\pi}{3} - \frac{\pi}{6} \right] \tag{10.3}$$

Three vectors compose the sextant  $k$ , as presented in Eq. (10.4), two active vectors and one zero vector.

$$\vec{i}_{s1} = \frac{2}{\sqrt{3}} I_{dc} e^{j[(k-1)\frac{\pi}{3} - \frac{\pi}{6}]} \quad \vec{i}_{s2} = \frac{2}{\sqrt{3}} I_{dc} e^{j[k\frac{\pi}{3} - \frac{\pi}{6}]} \quad \vec{i}_{s0} = \vec{0} \tag{10.4}$$

**Fig. 10.17** Space Vector Modulation (SVM) for a CSC





The current reference vector can be expressed as a linear combination of the three previous vectors, as described in (10.5) and (10.6) equations.

$$\vec{I}_{\text{ref}} = \frac{t_1}{T_s} \vec{i}_{s1} + \frac{t_2}{T_s} \vec{i}_{s2} + \frac{2t_0}{T_s} \vec{i}_{s0} \quad (10.5)$$

$$\vec{I}_{\text{ref}} = \frac{t_1}{T_s} \frac{2}{\sqrt{3}} I_{\text{dc}} e^{j[(k-1)\frac{\pi}{3} - \frac{\pi}{6}]} + \frac{t_2}{T_s} \frac{2}{\sqrt{3}} I_{\text{dc}} e^{j[k\frac{\pi}{3} - \frac{\pi}{6}]} \quad (10.6)$$

On the other hand, the current reference  $I_{\text{ref}}$  is nonvariable during the sampling period  $T_s$ .

$$I_{\text{ref}} = \frac{t_1}{T_s} \frac{2}{\sqrt{3}} I_{\text{dc}} e^{j[\frac{\pi}{3} - \gamma]} + \frac{t_2}{T_s} \frac{2}{\sqrt{3}} I_{\text{dc}} e^{j[\gamma]} \quad (10.7)$$

Defining the modulation index  $m$  as follows:

$$m = \frac{I_{\text{ref}}}{I_{\text{dc}}} \quad (10.8)$$

Separating into real and imaginary parts and solving the equations, the application time of the active vectors are obtained in Eq. (10.9)

$$t_1 = T_s \cdot m \cdot \sin\left(\frac{\pi}{3} - \gamma\right) \quad t_2 = T_s \cdot m \cdot \sin(\gamma) \quad (10.9)$$

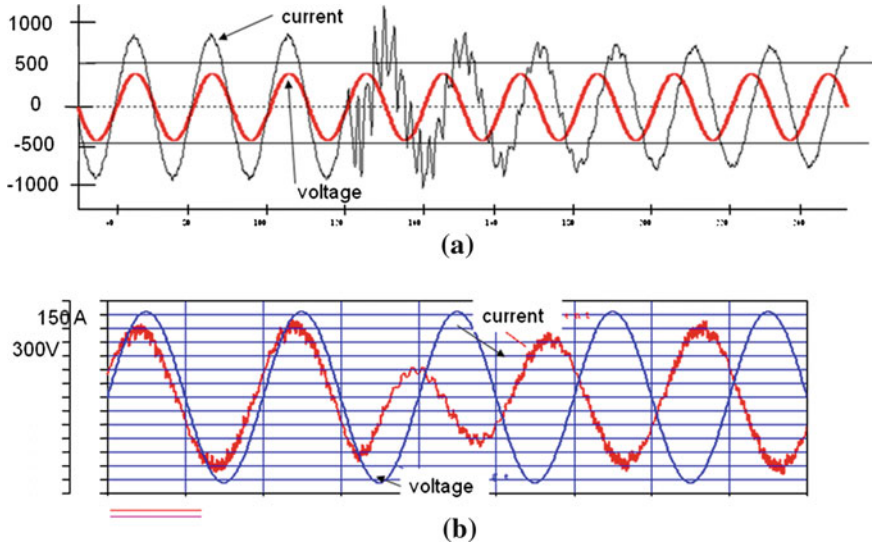
The remaining time,  $t_0$ , is allocated to zero vectors. This recirculating period should be equally distributed during the sampling time  $T_s$ , half at the beginning and half at the end of  $T_s$ , to control the voltage across the smoothing capacitors. Therefore is calculated as Eq. (10.10).

$$2t_0 = T_s - t_1 - t_2 \quad (10.10)$$

Figure 10.18 shows the comparison between using a static pattern and a dynamic strategy based on SVM.

### *Twelve-Pulse Converter Topology*

In the case of using GTOs as semiconductors, the GTO switching-on time cannot be reduced below a minimum (120  $\mu\text{s}$  in the case study described in Sect. 10.3.2.). If current is increased (high modulation index) the current harmonic distortion increases too, achieving unacceptable values of THD, greater than 15 %. Therefore a twelve-pulse topology with two six-pulse converters connected in parallel would be a better option [46, 47]. Providing a delta-wye ( $\Delta$ -Y) power transformer at the output of a twelve pulses harmonics of  $6(2n-1) \pm 1$  are removed. So, harmonics 5th and 7th are suppressed. An additional advantage is obtained with twelve-pulse converter: reduces the voltage ripple at the superconducting coil and therefore the a.c. component, minimizing the possibilities of producing a quench in



**Fig. 10.18** Transient current variation with a static pattern (a) and dynamic SVM strategy (b)

the coil produced by the a.c. losses. An extended explanation of the twelve-pulse converter application to SMES will be described in [Sect. 10.3.2](#), where a real study case will be presented.

## 10.2.3 Flywheels

### 10.2.3.1 Flywheel Mechanics

A kinetic Energy storage system is simply a flywheel driven by an electrical machine, able to work as a motor or a generator. When the machine (acting as a motor) exerts a positive torque  $T$  to a flywheel with moment of inertia  $J$ , it increases its speed at a rate  $T/J$ , until it reaches maximum velocity, storing a given kinetic energy. At this stage the energy can be maintained constant by just supplying the idle losses with the motor. For releasing the energy, the electrical machine (acting as a generator) applies a negative torque  $-T$  to the flywheel, braking at a rate  $-(T/J)$  and pumping the energy back to the source to where it is connected.

In a similar way to the SMES and in order to achieve an efficient charging/discharging processes, flywheel losses should be kept to a minimum. Basically, there are two sources of losses: aerodynamic friction between the wheel and the gas surrounding it and mechanical friction in the bearings that support and guide the wheel. The roundtrip efficiency of flywheel modules is in the 80–85 % range, Depending on bearing and winding losses and cycle time. During the power

exchange the efficiency is relatively high, and it depends on the type of electric machine used. However, the time on standby (no power exchange) affects very much this value depending on the aerodynamic friction. The way of reducing them is by decreasing the pressure and using advance bearing systems with low losses. Ideally the flywheel should work in vacuum, but sometimes a residual pressure is left to help evacuating any heat which is generated inside. Concerning the bearings, most of the flywheels use either magnetic or even superconducting bearings and in many cases magnetic levitation is required.

Regarding the mechanical design of a flywheel for a KESS, in principle, things are simpler than for the magnet of a SMES, since the energy is concentrated in the flywheel volume and not spread all over an infinite volume like for the SMES magnet.

For a rotating disk, there are some useful and simple mechanical expressions that allow making interesting considerations on its size and speed. On the one hand, the kinetic energy stored in a spinning disk will be proportional to its mass times the square of the tip speed, while centrifugal stresses will be proportional to the material density times the tip speed, hence the specific energy (per unit mass “ $e_m$ ” or volume “ $e_v$ ”) can be expressed as:

$$e_m = \frac{\xi \sigma}{\rho} \quad (10.11a)$$

$$e_v = \xi \sigma \quad (10.11b)$$

where  $\sigma$  is the maximum stress level in the disk,  $\rho$  its density, and  $\xi$  a form factor that only depends on the disk shape [48]. For a cylinder its value is 0.6, for a ring 0.3 (even if it is a thick-wall cylinder), and 0.87 for an optimized geometry with the highest possible value for  $\xi$ . Obviously, mechanical stresses in the flywheel during operation must be below the yield strength of the material.

Equations (10.11a) and (10.11b) allow making considerations on how an optimum flywheel should be designed. First, it is important to distinguish whether volume or mass restrictions are more important. In general, for stationary applications volume is more a concern than the mass, while for moving applications mass optimization is mandatory. In any case, to achieve high energy densities, a high value of  $\xi$  is required. Ring-shaped flywheels should be avoided. Optimum-shaped ones provide a high value for  $\xi$  but are difficult to fabricate. Cylindrical flywheels are usually the preferable option.

Regarding the material, there are also two choices: for high mass energy density, high strength and light materials should be used, while for high volume energy density, only the high strength of the material is a concern. Table 10.4 shows the mechanical properties of some selected materials and their ideal energy storage capability for a disk-shaped flywheel.

It can be inferred from Table 10.4 that the best choice for making an “energetic” and light flywheel is using carbon fiber, while using high strength steel will allow to make “energetic” and small machines but much heavier. Nevertheless

**Table 10.4** Mechanical properties of some selected materials

Material	$\sigma$ (MPa)	$\rho$ (Kg/m <sup>3</sup> )	$e_m$ (kJ/kg)	$e_v$ (kJ/m <sup>3</sup> )
Steel (AISI 4340)	1,800	7,800	140	1.092.000
Alloy (AlMnMg)	600	2,700	135	364.500
Titanium (TiAl62r5)	1,200	4,500	162	729.000
Fiberglass (60 %)	1,600	2,000	485	970.000
Carbon fiber (60 %)	2,400	1,500	970	1.455.000

carbon fiber is usually wound for making ring-shaped flywheels leading to a very anisotropic behavior, with poor properties in the radial direction. For a fair comparison between materials, this fact should be taken into account [48]. Steel rotors have specific energy up to around 5 Wh/kg, while high speed composite rotors have achieved specific energy up to 100 Wh/kg.

A very interesting point to consider is the required speed to achieve a given energy. Apparently, once the flywheel material is chosen, Eqs. 10.11a and b state that a certain amount of mass is required regardless the rotational speed: it does not matter how slow or fast the wheel turns. The reason is that the material is supposed to work at a certain level of stress and this automatically imposes the speed as a function of the density: Light materials will rotate fast while heavy ones will be slow [49].

A crucial aspect when designing a flywheel is its dynamical behavior. The flywheel shaft, the bearings, and the housing, constitute an elastic structure prone to oscillate in two typical modes: conical and cylindrical (Fig. 10.19). The problem is that gyroscopic effects must be taken into account leading to the fact that the natural frequencies for those two modes depend on the rotating speed [50].

A typical way of representing the solution is using the so-called Campbell diagram in which the natural frequency is plotted against the rotating speed. Intersection with the line frequency equal to speed, will give the natural frequencies which should be avoided for both cases.

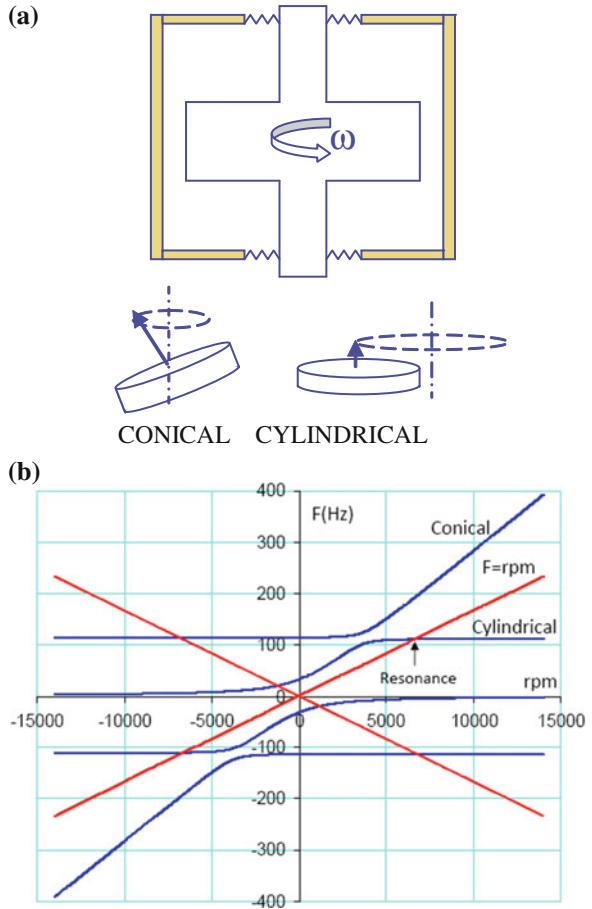
The interesting fact is that below a certain flywheel aspect ratio (Height/Radius) both lines will never intersect for the conical mode, and this is the reason why flywheels are usually flat, resembling, somehow, SMES magnets.

### 10.2.3.2 Flywheel Electromagnetics

Two electromagnetic systems are the basis for operating flywheels: Electrical machines and in some cases electromagnetic bearings.

There are many types of machines with very good performances in terms of efficiency, robustness, or reliability, among others. Nevertheless, not all the electrical machines are good candidates for driving a flywheel. Those of them with wound rotors should be avoided. This includes dc machines, conventional synchronous machines and induction motors (although some successful applications for flywheels have been done with asynchronous machines or with modified synchronous ones [51]). The reason is that when spinning at such speeds, brushes,

**Fig. 10.19 a** KESS mechanical structure and oscillating modes.  
**b** Campbell Diagram



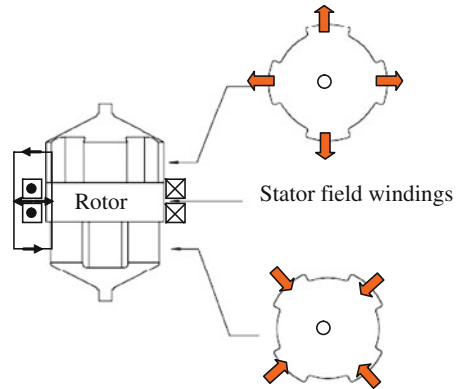
or slip rings should be avoided and even for the case of squirrel-cage induction machines where none of those elements are present, the heat generation in the rotor windings is inadmissible, since heat is difficult to extract.

Presently, there are three families of electrical machines that fulfil the previous conditions for driving flywheels: Homopolar, Reluctance, and Permanent Magnet machines [52].

In fact, practically all of them can be considered as special cases of a synchronous machine with three corresponding windings in the equivalent d-q model: two d-q windings in one side and one D excitation winding in the other (which can be present or replaced by a permanent magnet). Rotor dumping rings are not present.

The first group corresponds to Homopolar machines. The term homopolar comes from the fact that all the magnetic flux crosses the armature windings in the same radial direction everywhere. There are different types of homopolar machines, even dc with brushes, but the type which is used for KESS is the so-called synchronous homopolar motor or homopolar inductor motor .

**Fig. 10.20** The homopolar machine

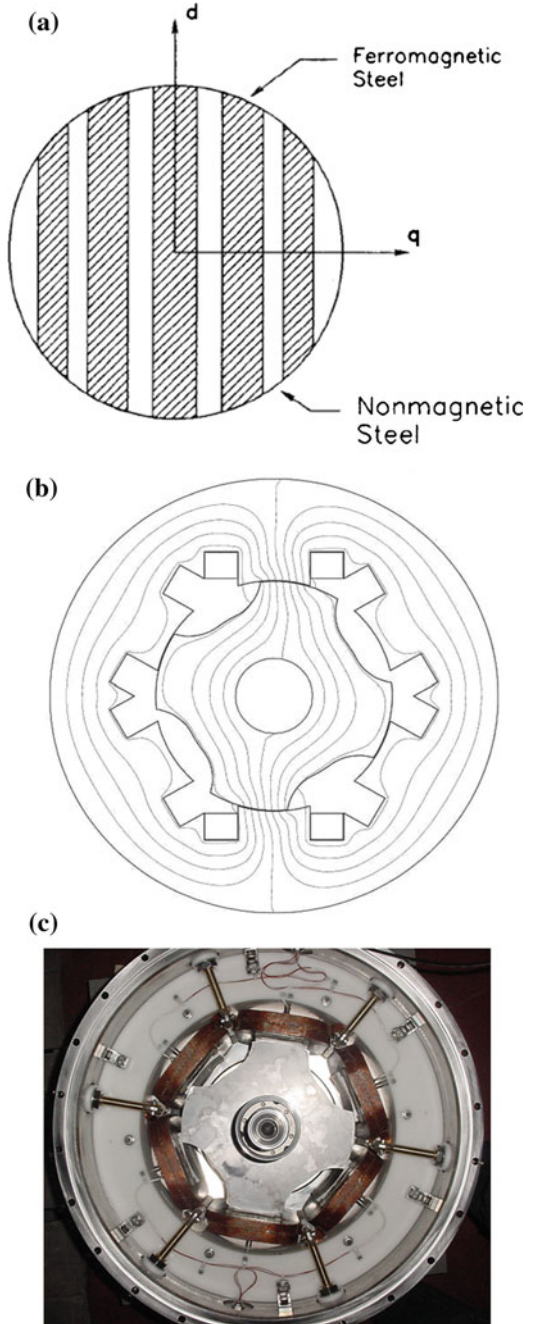


The main characteristic of this machine is that the magnetizing D-winding in charge of creating the magnetic field is now fixed in the stator and encircles the rotor rather than being placed in the rotor like in conventional synchronous machines [53]. The rotor is a massive piece of high-strength magnetic steel, the poles are conveniently machined in its periphery and the stator windings are distributed to achieve a sinusoidal magneto-motive force distribution, thus avoiding rotor heating due to harmonic content in the field. Some commercial developments have been done using this type of machine [54]. Figure 10.20 shows a scheme of a homopolar motor, including the magnetic flux direction in the rotor poles. This type of machine is very robust and suitable to run at very high speeds since rotor losses can be very small, even at high frequencies.

The second group is Reluctance machines which again can be divided into two groups, Synchronous and Switched Reluctance machines. The first one is like a conventional synchronous machine with no magnetizing D-winding, only d and q windings in the stator. The way of producing torque in this case is ensuring that the corresponding inductances of the stator windings ( $L_d$  and  $L_q$ ) are very different. This can be achieved by two ways. One is with poles in the rotor that vary the air gap lengths in the d and q axes and hence the values of each inductance. The other is introducing different magnetic permeability in each axis (Fig. 10.21a). In a two-pole machine this is easier to attain; the rotor uses a magnetic anisotropic material made from alternating magnetic and non-magnetic laminations [55]. This type of machines is also suitable for high speeds due to the low losses in the rotor if the magneto-motive force distribution is sinusoidal. On the other hand, since big differences in the values of  $L_d$  and  $L_q$  are not easy to achieve, power density of the machine is usually low.

Switched Reluctance Machines (SRM) are conceptually very different, especially from the stator side. The rotor is laminated and has no windings. It is shaped in a certain number of poles  $N_r$ . Stator is also laminated and has concentrated windings around a number of stator poles  $N_s$  which are connected in pairs separated 180 electrical degrees. The coils are made from Litz wire to minimize eddy current losses. Every group of pole pairs connected in series constitutes one of

**Fig. 10.21** a Anisotropic rotor in a synchronous machine b Magnetic field lines in a SRM c Top view of a real SRM for flywheel applications



each  $m$  stator phases [56]. Each phase is switched on and off sequentially and normally individually so that, usually, there is only one phase active. Every time a stator pole is energized, the closest rotor pole will try to align with it to minimize the reluctance of the magnetic circuit. There are different combinations of stator and rotor poles numbers. In general, the rotor angular stroke,  $\theta_d$ , every time a new phase is switched on is given as:

$$\theta_d = \frac{2\pi}{mN_r} \quad (10.12)$$

Ideally,  $\theta_d$  should be maximum in order to work with the lowest possible commutation frequency, which implies the minimum values for  $m$  and  $N_r$ .

From the magnetic point of view, SRM can work fully saturated or in the linear mode. Working in saturation means that the relative magnetic energy to magnetise the circuit is smaller, thus reducing the dimensions of the power supply for a given machine power. On the contrary, not all rotor topologies are allowed if the machine is saturated.

By far, the most common SRM topology is the 6/4 (6 Stator poles and 4 Rotor poles). Figure 10.21b shows the geometry of a 6/4 poles machine with the field lines when the upper and lower poles are energized while Fig. 10.21c shows a top view picture of the same machine for a flywheel application [57].

The SRM is very robust and simple to fabricate, since the concentrated stator winding is much simpler than the distributed one for synchronous machines. Negative aspects are the acoustic noise due to the presence of high electromagnetic radial forces and higher losses in the iron induced by the commutation of the phases. Several topologies have been proposed to reduce the iron path and hence these losses [58].

Finally, the last type of machine that has also been used for flywheel applications is the Synchronous Permanent Magnet (SPM) Machine, basically a conventional synchronous machine where the magnetizing D-winding has been substituted with an array of permanent magnets.

The main two issues in this type of machine are the magnetic material for the magnets and the topology in which they are arranged [59].

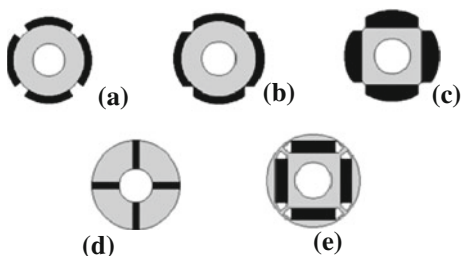
Regarding the material, Neodymium Iron Boron (NdFeB) and Samarium Cobalt (SmCo) are the only competing candidates since their remanence and coercitivity are much higher than for any other alternative. Although NdFeB has better values than SmCo its temperature stability is not so good and since rotor heating can be a problem in flywheels, SmCo is usually the preferable option.

Concerning the topology there are, generally speaking, two options: external or internal magnet arrangement. Figure 10.22 shows different alternatives for placing the magnets (in black) in the rotor: Alternatives (a), (b), and (c) are different options for the so-called surface mounted magnets, (d) is the spoken topology, while (e) represents the buried magnet solution.

Normally, surface mounted topology achieves a higher power density with a smaller harmonic content than any other alternative, but for flywheel applications a



**Fig. 10.22** Magnet topologies in SPM



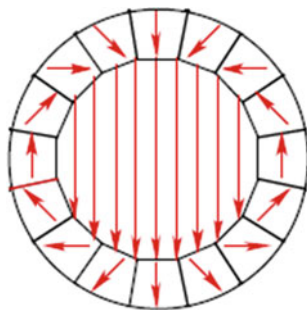
special concern must be considered: The high centrifugal stresses induced in the magnets and their poor mechanical properties [60]. The way to overcome this problem is to precompress the magnets by some procedure like shrink fitting or by means of a carbon fiber bandage around them. The distribution of the permanent magnets can be oriented to produce a dipole field aligned across the bore of the rotor as Fig. 10.23 shows in the so-called “Halbach array”.

The SPM is also a good candidate for driving a flywheel. It is a high performance machine with a very good efficiency. The main drawbacks are the cost and the potential demagnetization of the magnets due to armature reaction or to temperature increase. A particular problem for this type of machine is the “cogging torque”, which is due to the attraction of the magnets against the stator slots, producing an undesired ripple. For high speed machines like those used for KESS, it is not a major concern. There is also another drawback for the PM machines which is the iron losses when the machine is not exchanging power with the load, since there is always an emf present.

The other aspect where electromagnetism plays a key role in KESS is in the guidance of the flywheel. Either in high mass energy density machines or in high volume energy density ones, conventional bearings are limited. In the first case, because their weight is small, but the speed is very high (>50,000 rpm). In the second one, speed is admissible (<10,000 rpm) but not the weight. Even if high speed precision bearings can be used, the loads they are subjected are huge and their life is significantly reduced making maintenance very expensive.

In the case of low speed flywheels there is a simple solution: alleviating the weight of the flywheel using magnetic suspension. Usually, a set of permanent

**Fig. 10.23** Halbach array for a SPM

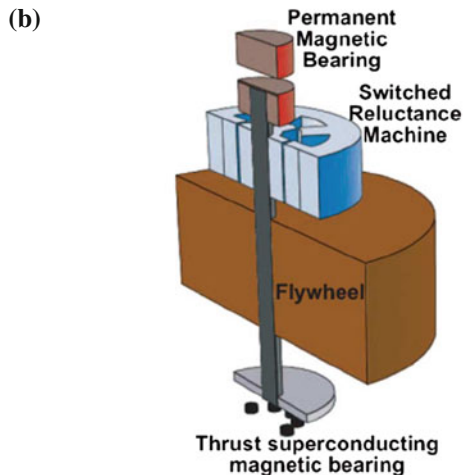
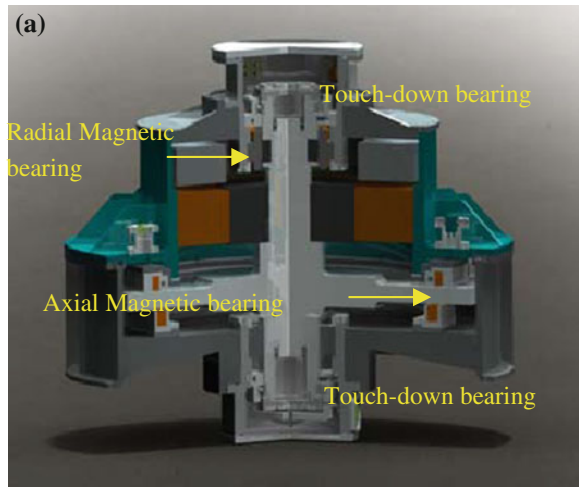


magnets is placed in the upper cap of the housing. Since the wheel is generally made from a magnetic material, an attraction force will pull upwards compensating its weight and reducing static loads on the bearings [59].

A step forward is replacing the conventional bearings with active magnetic bearings [61]. They are based on the use of coils exerting forces on the axis to be guided. Since this type of levitation is intrinsically unstable a feedback is required: a sensor measures the axis position and a power amplifier feeds the coils to keep the axis rotating in its position. Finally, some prototypes of flywheels use HTc superconducting bearings, as Fig. 10.24 shows.

They are usually based on the interaction between bulk superconductors and permanent magnets. A superconductor in front of a permanent magnet behaves like a magnetic mirror: it is equivalent to place another magnet in front of the real

**Fig. 10.24** **a** Flywheel based on SRM and magnetic bearings (courtesy of Tekniker). **b** Scheme of a flywheel based on SRM and superconducting bearings Kangwon et al. [40]



one, thus exerting a force. This force appears when the superconductor is cooled below critical temperature and is intrinsically stable: The superconductor will react to any change in its relative position to the magnet trying to maintain the initial magnetic flux [62].

Most of the developments using this technology take profit of the stable levitation force between the magnets (usually placed in the flywheel) and the superconductor (placed in the housing). Nevertheless it is very usual that conventional bearings are still used to enhance radial stability as well as a touch-down system in the event of a failure [63–65].

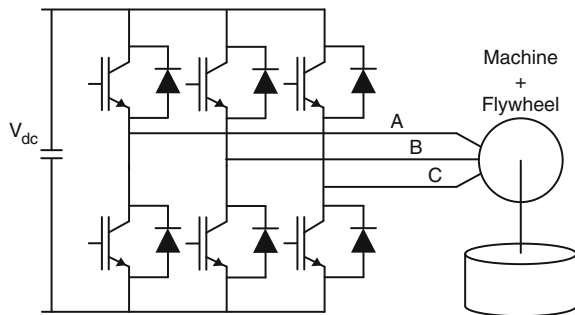
**10.2.3.3 Power Converters**

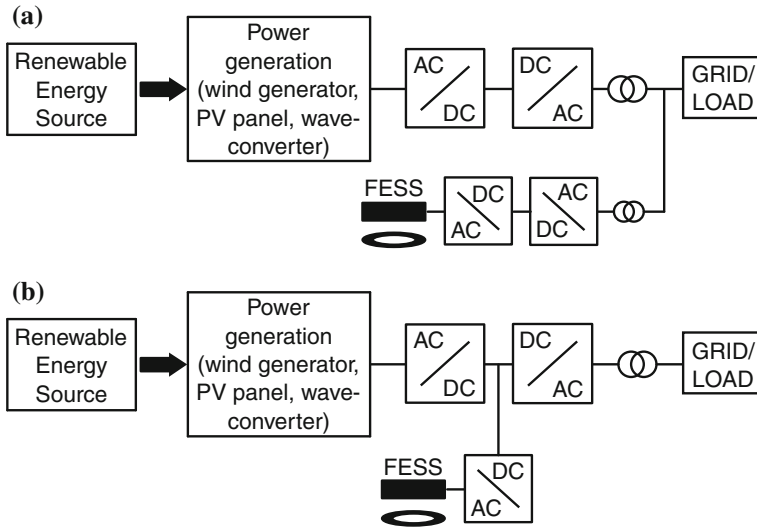
The power electronic converter used as interface between a flywheel and the load or the electric grid is usually a pulse width modulated (PWM) bi-directional converter that uses insulated-gate bipolar transistor (IGBT) technology, as Fig. 10.25 shows, and depends on two different topics: the connection point to exchange the power with the load and the type of electric machine used for driving the flywheel.

*Connection Point*

Most of the renewable applications where a flywheel is suitable to be installed are composed by a back to back converter with a common dc-link. The dc voltage is maintained constant by one of those converters. The connection to it ensures a faster response, a lower cost for the whole system and a better energy management due to the integration with the generation device. Many times the owner of the generation power system does not permit the access to the already installed power converter because it implies several design and operation modifications and responsibilities in the system behavior. That is not only the case of connecting flywheels but any other type of energy storage device. Figure 10.26 presents the

**Fig. 10.25** PWM Power converter connecting a flywheel





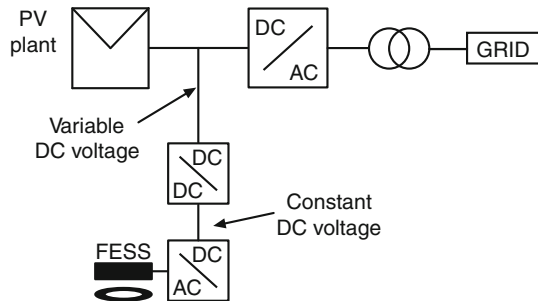
**Fig. 10.26** Possibilities of FESS connection to a renewable generation plant

two connection possibilities, (a) for AC connection and (b) for DC connection. The recommendation is to connect the smallest power converters to increase the reliability of the system.

For instance, in wind energy and wave energy converters, the FESS can be connected to the dc-link easily. However, in the case of solar PV-plants, if the FESS is connected directly to the inverter at the PV-panels side, the dc voltage depends on the optimum operation point and it will change continuously, so the flywheel-machine might have variable voltage and an extra dc/dc converter could be required, as presented in Fig. 10.27.

Considering the previous limitations related to the modifications in the control, it would be better option to connect after the PV inverters, using a grid-side converter (GSC).

**Fig. 10.27** PV-solar plants with FESS



One important factor to be taken into consideration is the voltage level at the connection point. When the connection voltage level is the same as the flywheel-machine voltage (supported by commercial IGBTs) a conventional dc/ac converter should be used. IGBTs technology permits to achieve a dc-link of 4 kV using 6.6 kV IGBTs with currents of 1 kA and a switching frequency of around 500 Hz. Only in the case of necessity of improvement of current quality or even higher voltages, a multilevel converter results a better option. However, machines for flywheels with voltages higher than 1 kV are not common.

In case of dc connection, a dc/dc converter should be used. When power level and the voltage ratio are low a boost-buck topology results appropriate; for other options it is better to select a topology with intermediate ac link using a medium frequency transformer. See [Sect. 10.3.3](#) for further details.

In case of ac connection, the voltage adaptation is usually carried out with a power transformer. This solution might appear more expensive—since an extra converter is required—but the FESS adds value to the system through its grid-side converter (GSC), which permits controlling the reactive power supplied to the grid. Currently, many of the inverters used in renewable energies do not provide the possibility to adjust power factor or protection against voltage sags.

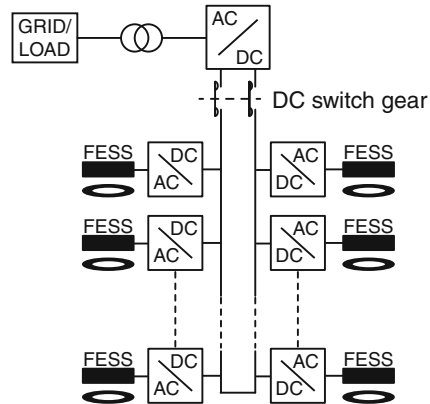
### *Modularity and Integration of FESS*

Large power machines have not been developed for flywheel application but usually the applications, like frequency regulation, require an important amount of power and energy. Usually there will be a matrix of FESS [48] to accomplish the power regulation problem with higher level of power and energy, as presented in [Fig. 10.28](#). Using just one GSC, all the units of this matrix can be connected to the same converter using single power transformer and electric grid protections for the whole system. Modularity is an important issue because it reduces the total cost of the elements (especially the flywheels), increasing the reliability of the system. Moreover, it results convenient to package the FESS together with the power electronics in a similar way of a dc battery to increase the integration and robustness of the FESS.

### *Typologies of Machines and Converters*

The most important electric machines used for flywheels are: the synchronous homopolar machine (SHM), the permanent magnet synchronous machine (PMSM), the synchronous reluctance machine (SYNRM), and the switched reluctance machine (SRM). From the point of view of power electronics particular differences can be considered, especially related to rotational speed, number of poles, and switching frequency, all connected to each other. The energy depends on the square of rotational speed. So high speed is mainly considered (range from 5,000 to 50,000 rpm) and therefore a low number of poles are always preferred.

**Fig. 10.28** Matrix connection of FESS



The rotational frequency of the machine will be in the range of 2–20 kHz. Moreover, the power converter has to commute at least to this frequency, considering the switching pattern selected. The efficiency, which is mainly dependent on the mechanical losses, is also affected by the power converters in terms of switching and conduction losses. The main challenge is to reduce the power converter losses in order to simplify the cooling system and to reduce the total cost.

On the other hand the switching frequency affects the quality of the power supplying the machine. Harmonic distortion in the machine currents and torque oscillations depend on the switching pattern and the switching frequency selected. Those variables in this type of load do not result as a critical issue since the torque is just applied to accelerate or decelerate an inertia. However, they had to be taken under control because mechanical behavior (flywheel and bearings) depend on the torque dynamics.

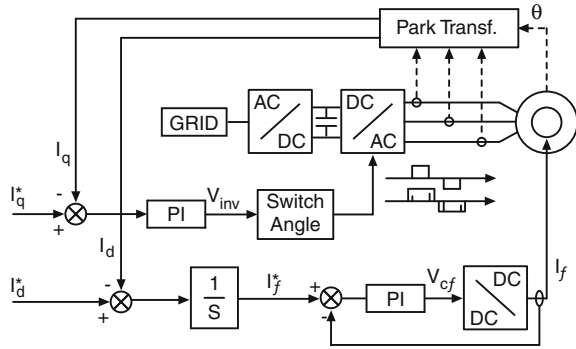
As a result, an agreement between power quality and the switching frequency has to be achieved.

*Synchronous Homopolar Machine*

The power converter used for synchronous homopolar machine (SHM) is the six-step converter [53, 66]. The main benefit of six-step operation is that switching losses are considerably lower than for PWM, since the maximum switching frequency for any one switching element is the machine’s electrical frequency, in this case between 3.3 and 6.6 kHz. This frequency is relatively low for modern IGBT technology.

Figure 10.29 shows the switching pulses for the upper IGBT of every phase, the line voltage applied and one of the phase currents produced. Figure 10.29 also presents the control scheme for a SHM used for a flywheel. It is very similar to a conventional synchronous machine. A d-q frame has been selected, with the d-axis in the direction of the machine excitation flux. Several control criteria can be determined for the machine (optimum torque/ampere or unity power factor).

**Fig. 10.29** Power converter control for a SHM



The optimal control will ensure the maximum torque per ampere. That is achieved when the current vector is located in the  $q$ -axis. The switching angle to perform the inverter voltage ( $V_{inv}$ ) is obtained from the control of the  $q$ -axis current component. On the other hand the  $d$ -axis current component affects to the magnetic flux of the machine. An integral controller provides the current command  $I_f$  and a PI controller ensures that a DC/DC converter is providing the voltage that produces the current  $I_f$ . The  $q$ -axis loop provides the torque while the  $d$ -axis ensures the flux in the machine providing a certain power factor. Six-step power converter has a frequency equals to the electrical speed.

*Synchronous Reluctance Machine (SynRM)*

A synchronous reluctance machine is a low cost and simple configuration compared to other machines due to nonexistence of magnets and rotor windings. Magnetic saliency produces torque under the effect of stator current, as shown in Eq. (10.13)

$$T = k(L_d - L_q)i_{sd}i_{sq} \tag{10.13}$$

where  $k$  depends on the number of poles and some constant related to the reference frame transformation.

There is no concern about demagnetization, losses with no load, or field weakening requirements. However, the reluctance machine has a poor power factor. The SynRM has a power factor that depends on the ratio of direct to quadrature inductances  $L_d/L_q$ . Higher  $L_d/L_q$  ratios yield higher power factors, corresponding with lower copper losses and reduced voltage to current ratings at the power converter [52, 67]. Again, a PWM three-phase power converter can be used to drive this type of machine.

Figure 10.30 shows the control scheme for this type of machine.  $d$ -axis in a reference frame is coincident with the saliency of the rotor. The maximum torque per ampere control criteria is achieved in this type of machine when the  $d$  and

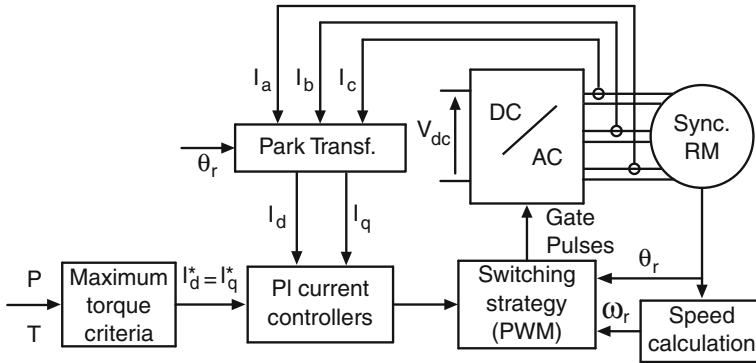


Fig. 10.30 Control scheme for a SynRM

$q$  current components are equal. In order to improve the dynamic response of the currents and therefore the torque, it is important to consider nonlinear magnetics and flux dynamics [68].

### Switched Reluctance Machine (SRM)

The electromagnetic torque in a SRM does not depend on the current sign. As a result, a unidirectional power converter is enough to drive it. Since concentrate and separated windings are used in SRM, conventional PWM converters are not suitable and other topology is required. Although many attempts to drive a SRM can be considered [56, 69], actually two different types of topology are discussed to be used in SRM driving flywheels: H-bridge asymmetrical converter (a) and H-bridge symmetrical converter (b), presented in Fig. 10.31. The asymmetrical is the basic topology to drive a SRM and it is good enough since the current flows in the same way during both motor and generator operation. Nevertheless, it can be important from the point of view of the iron losses. If current is applied with the same sign, the magnetic orientation in every rotor pole is changing from crossing under the phase winding A to the phase winding A', increasing the hysteresis losses. However if current sign is changed from winding A is applied to winding A', the magnetization sign is maintained and the hysteresis losses are reduced. This effect is even higher in the case of saturated machines. Figure 10.32 shows both symmetrical and asymmetrical topology results.

This improvement is important when heat generated in the rotor is important to be reduced at maximum, especially when very low pressure around the rotor-flywheel is provided.

The electrical time constant of a phase winding and the back emf vary strongly depending on current and rotor position, therefore a robust current control is required. The current closed-loop control can be achieved with a hysteresis control, delta modulation or PWM. Hysteresis-band (Fig. 10.33a) has the higher dynamics



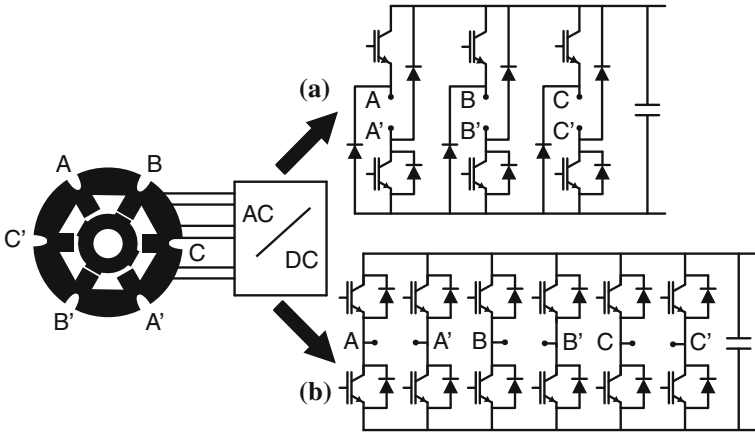


Fig. 10.31 SRM power converter topologies

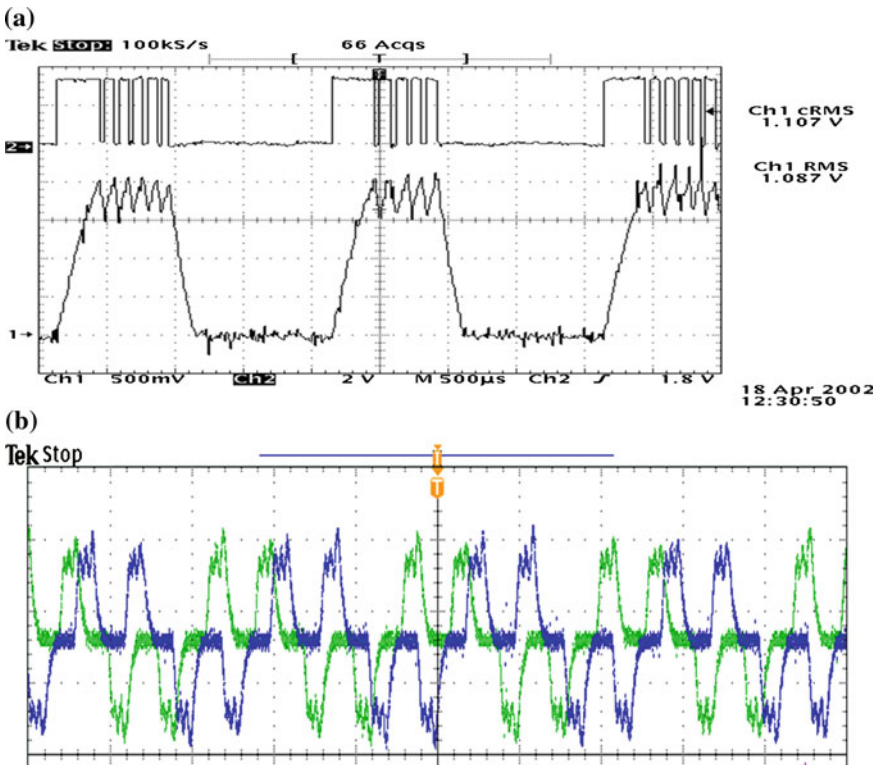


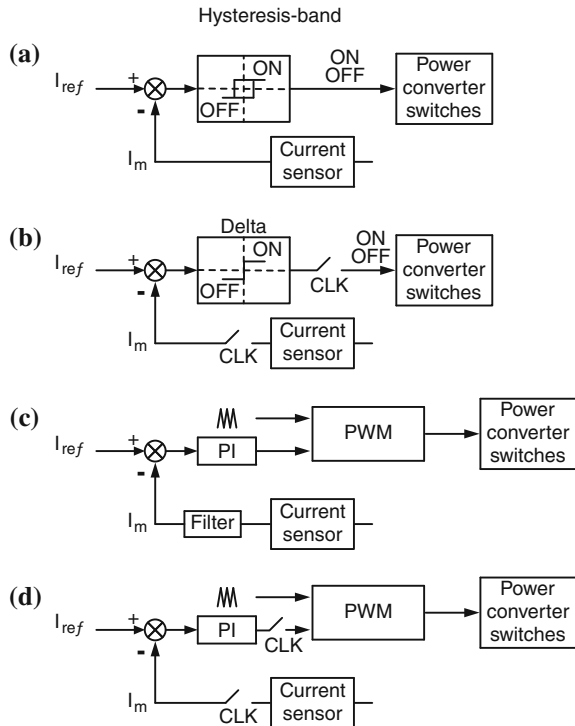
Fig. 10.32 a Unidirectional current using asymmetrical H-bridge. b Bidirectional current using a symmetrical H-bridge

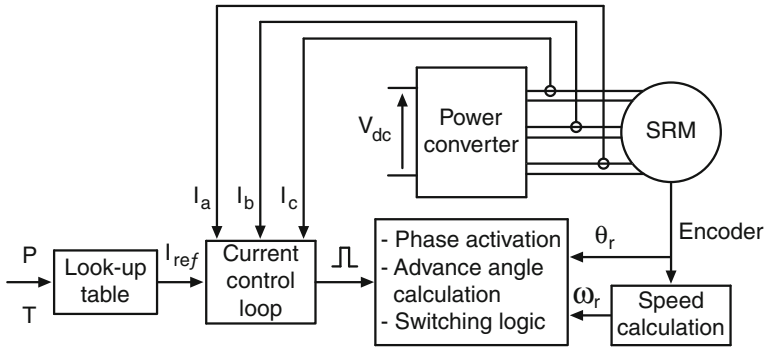
and it is easier to implement. However it has the important drawback of a varying switching and a high switching frequency requirement. Sometimes the switching frequency could exceed the limits of the switching devices or lead to high commutation losses [69]. Some adaptations of the hysteresis-band current control have been done [70–72] to adjust the hysteresis band width to achieve constant or at least controlled switching frequency while maintaining the dynamic response. Delta modulation (Fig. 10.33b) is close to hysteresis-band current control but the implementation uses digital devices (microcontroller, DSP, or FPGA) and permits fixed frequency. However, fixed commutation frequency results in a higher current ripple and some current peaks in the low inductance area. Finally, PWM technique (Fig. 10.33c) allows operating with constant switching frequencies and sampling time. The dynamics of the current loop are limited by the sampling time and the filter used to smooth the current ripple. By the use of symmetrical sampling and symmetrical modulation in the current control loop, a true average current may be sampled and no filters are necessary [73] (Fig. 10.33d).

Soft-switching commutation should be used to reduce the acoustic noise and losses in the inverter. The control implementation requires a fast sampling device. FPGA devices demonstrate a good performance level.

The control scheme used for a SRM in a flywheel application is shown in Fig 10.34 [73–76]. Power or torque reference is supplied as the system command.

**Fig. 10.33** Current control strategies to be applied to SRM





**Fig. 10.34** Control scheme for a SRM used as a flywheel

That reference variable comes from an upper level control, as further detailed at the end of the chapter. Since nonlinear approach is usually considered for the machine design, the relation between power (or torque) and current ( $I_{ref}$ ) has to be obtained by previous machine analysis or experimentally; as a result a look-up table will be provided to the control system. Once the current reference is generated for every phase, measuring the phase currents, the switching pulses for the power converter will be obtained (hysteresis or PWM techniques). On the other hand, a logic circuit will determine what phase should be activated every moment depending on the rotor position ( $\theta$ ). A switching logic routine will be also in charge of determining when soft or hard commutation is required in the machine to ensure the minimum switching frequency and the current control at the same time. Moreover, some advances to the on and off activation times are required to maximize the torque or minimize the rotor mechanical vibration.

The SRM is very dependent of the rotor position measure. That reduces the reliability of the application. Applying sensorless techniques the rotor position signal gets redundant, providing a higher robustness to the system.

*Permanent Magnet Synchronous Machine (PMSM)*

When using surface mounted magnets, inductance is usually very low. As a result the torque ripple is high. Since the rotational speed usually is very high and the magnets always produce flux, iron losses happen continuously even when the flywheels is not exchanging power with the load.

When designing an electric machine to drive a flywheel, the important issue usually is to provide a constant power during the rotational speed range. That means a torque-speed curve with a constant power area, as the one shown in Fig. 10.35. It implies that between rated speed ( $\omega_r$ ) and maximum speed ( $\omega_{max}$ ) the machine has to operate in field weakening mode. In the case of PMSM, magnets provide the main flux density. In order to reduce the flux, the  $i_{sd}$

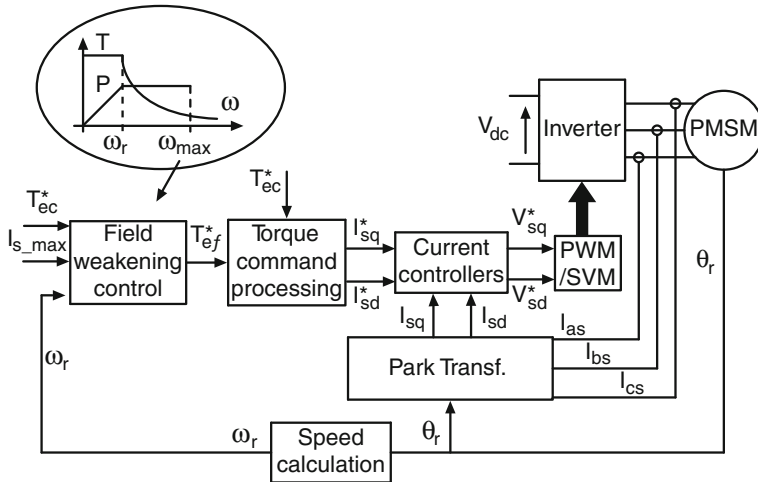


Fig. 10.35 Control scheme for a PMSM for flywheel applications, including field weakening

component that is maintained to zero when  $\omega < \omega_r$ , needs to be increased. This current component produces a flux opposite to the magnets flux. That is included in Fig. 10.35. Moreover, considering the power electronics operation, it is also important to maintain back emf. under control to ensure the correct operation of the inverter with the ratio  $V_{dc}/E_{max} > 1.7$ , being  $V_{dc}$  the DC-link voltage and  $E_{max}$  the maximum back emf provided by the machine. This number is calculated as presented in Eq. (10.14).

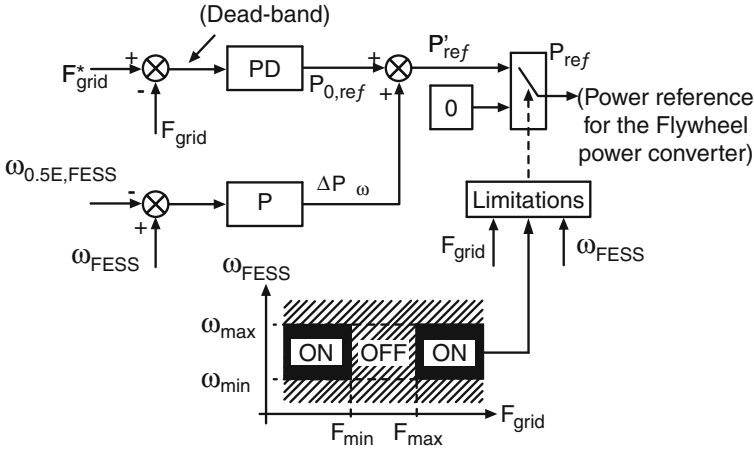
$$\frac{V_{dc}}{2} \geq \hat{E}_{max,ph-n}$$

$$V_{dc} \geq \frac{2\sqrt{2}}{\sqrt{3}} E_{max,ph-ph} = 1.63 \cdot E_{max,ph-ph} \cong 1.7 \cdot E_{max,ph-ph} \quad (10.14)$$

Same torque-speed characteristic is required in other machine types. In the case of SHM the back emf can be adjusted with the field winding. In SynRM and SRM saturation of the magnetic circuit produces a natural behavior in constant power mode once the saturation speed is over passed.

### Power Converter Control

Operation of a flywheel system depends on the connection to the rest of the system, as mentioned above. When the FESS is connected to the dc-link, the usual regulation scheme is based on the regulation of the dc voltage using a dead-band control scheme. The flywheel charges when the voltage exceeds the top of the dead-band and discharges when the voltages drops to the lower limit. The width of



**Fig. 10.36** Regulation scheme for frequency stabilization with Flywheels

the dead-band is adjusted depending on the application and the response time of the frequency at the electric grid.

The control scheme for reducing the grid frequency variation [77] by using FESS is presented in Fig. 10.36. The electric grid frequency ( $F$ ) is measured with an appropriate method [78]. A PD controller determines a primary output active power reference ( $P_{0,ref}$ ); When the frequency decreases, the FESS supplies power to the grid. When the frequency increases, the FESS absorbs power. This power value is modified by a term named  $\Delta P_w$  that depends on how far is the flywheel speed from the speed related with the half of the maximum stored energy, denoted by  $\omega_{0.5E,FESS}$ . The value of  $P_{0,ref}$  is modified to a lower value when the rotor speed is under  $\omega_{0.5E,FESS}$  or to a higher value when the speed is over  $\omega_{0.5E,FESS}$ . That way, the flywheel increases the charging power level when is more discharged and the discharging power level when is more charged. The new reference is  $P'_{ref}$  would have some limitations due to boundary speeds,  $\omega_{max}$  and  $\omega_{min}$ , as included in Fig. 10.36.

### 10.3 Applications and Control of Fast Response Energy Storage Systems

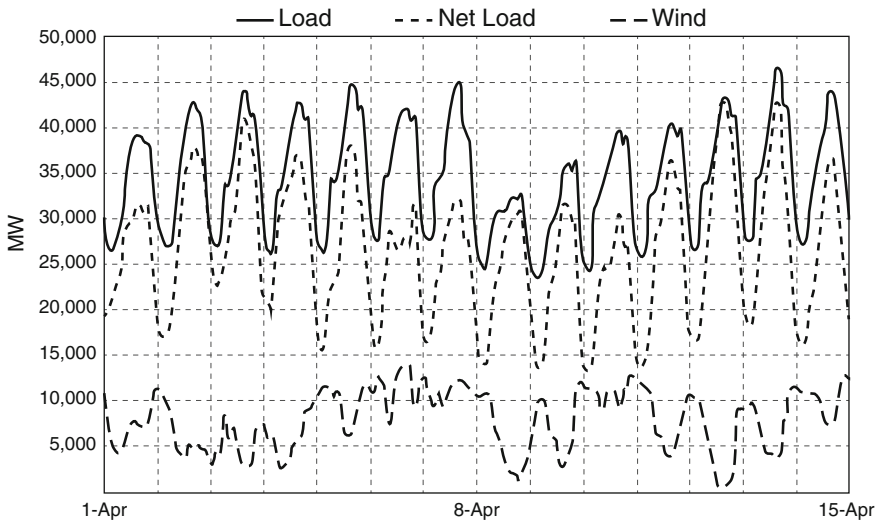
#### 10.3.1 Peak Shaving Application (Grid Frequency Regulation)

Peak shaving application concerns in reducing peaks power demand that should be supplied by the grid during small times. These power peaks are usually due to connection or disconnection of loads such as heavy motor drives [79]. As it is not

possible to know when these loads are going to be connected or disconnected, these peaks are not included in the power production schedule. For this reason, the power peaks produce unbalance between the power supplied and the power consumed leading to variation of the grid frequency that can destabilize the utility system. To solve this problem the independent system operator (ISO) has the regulation operating reserves. The objective of the frequency regulation reserves is to respond fast enough increasing or decreasing generation to respond to random, unpredictable variations in demand. Frequency regulation units must act in the order of seconds to minutes, having a discharge time of minutes and being a net zero energy service when extended time periods are considered. Typically, the frequency regulation units are hydroelectric generators (in pumped hydro systems) or natural gas or oil plants [9].

Renewable energy resources (RES) have great interest to the society because they present several advantages. For instance, they have no greenhouse gas emissions; reduce dependence from fossil fuel resources; etc. On the other hand, integration of RES in the current utility requires solving several new technical challenges associated to the nature of these resources. One of the problems is the variability of the RES. Due to this ISO sometimes thinks about RES systems, like wind power farms, as non-dispatch units. To understand more easily the effect of RES integration over the utility performance it is better to consider their generation like a reduction in load. In this case, conventional unit have to meet the net load, defined as the normal load demand minus the power produced by RES.

Figure 10.37 shows the waveform of net load over certain time period. In this case the RES penetration is around 10 % of the total average load in the network. It can be noticed that inclusion of RES to this level does not affect to the variability of the net



**Fig. 10.37** Effect of RES variability over the utility system

load compare to the normal demand. However, the ramp rate and the ramp range both increase respect to the operation without RES. This effect is also larger when higher level of RES penetration is considered. As a consequence, inclusion of RES affect to the frequency regulation reserves needed to maintain the system stability.

Development of new RES systems to high penetration levels will require new frequency regulation units. Although these units can be developed using conventional systems, some studies show that this application is especially appropriate to fast respond energy storage systems [4, 7, 10]. Moreover, it is particularly suitable to flywheel energy storage systems (FESS). The main reasons are:

- Compared to conventional systems, FESS provides faster response. This reduces the time needed to act and consequently reduce the amount of reserves needed to ensure system stability.
- Compared to batteries energy storage systems, FESS can have more number of discharging cycles without affecting the life time of the device. This supposes lower maintenance cost.
- To know the state of charge (SOC) of a battery usually require complex systems. In contrast, for a flywheel unit it is possible to know the exact SOC, because it only depends of the rotational speed that can be easily measured.

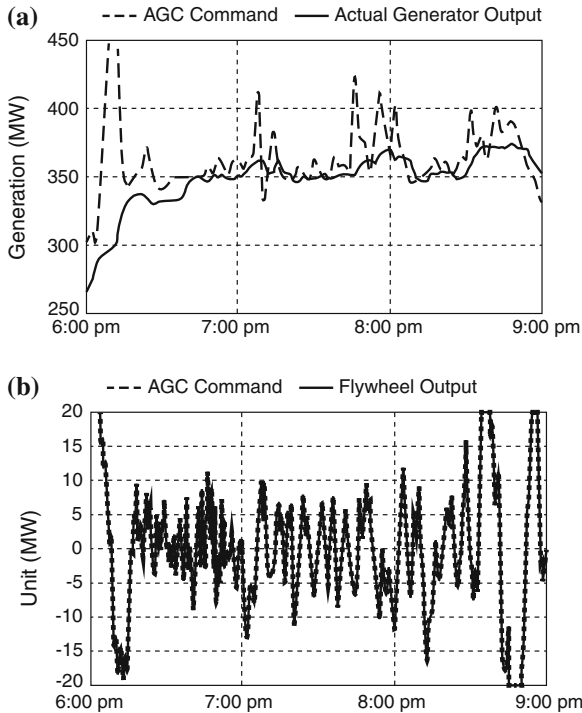
### 10.3.1.1 A Practical Case

FESS cannot be considered as a mature technology yet. However, practical implementation of this technology for frequency regulation has been tested. Besides, it is possible to find available commercial products in the market to perform this task. The company Beacon Power Corporation (<http://beaconpower.com/>) offers a 20 MW frequency regulation plant, Table 10.5 summarizes the specifications of the product bid by the company [80].

The development of this product and its inclusion in the market can be considered as the conclusion of an important research effort performed by companies and ISOs. Both have tried to figure out what are the best choices to solve the frequency regulation problem when high penetration level of RES is under concern. To develop this research, a pilot plant using FESS was tested by ISO New England (ISO-NE) from 2008 [81, 82]. After that, other ISOs, like California ISO (CAISO), New York ISO (NYISO), Midwest ISO (MISO), or Pennsylvania-New

**Table 10.5** 20 MW frequency regulation plant specifications

Characeristic	Value
Output power	20 MW maximum for 15 min
Power range	40 MW (20 MW up or down)
Rated output energy	5 MWh
Response time	<4 s (to rated power)
Flywheel design life	20 years



**Fig. 10.38** Response of a coal fire plant (*top*) and FESS (*bottom*) to an AGC command

Jersey-Maryland (PJM) interconnection operator, have evaluated the benefits of this technology and even are developing or planning to develop their own plants to perform field test and contribute to the study of the best alternatives for RES integration [83].

Some of the results of these studies are summarized here:

- The 1 MW pilot plant in NE-ISO performed 6,300 charging–discharging cycles per year. This means that for 20-year-life it requires around 125,000 cycles. This number of cycles supports flywheel technology as a good choice for frequency regulation service [81, 82].
- FESS can provide frequency regulation reserve with zero greenhouse gas direct emissions [84].
- Fast response of FESS is a valuable feature. Compared with coal fire plant it can provide almost instantaneous response (Fig. 10.38-Data extracted from [81–83]).
- FESS is more effective than conventional plant for frequency regulation task (Fig. 10.39-Data extracted from [81–83]). According to [81, 82] faster responsive resources can reduce CAISO’s regulation procurement by up to 40 %.
- The FESS system can correct more area control error (ACE) as compare to a conventional generator with a 5 min ramp. Besides, it contributes more



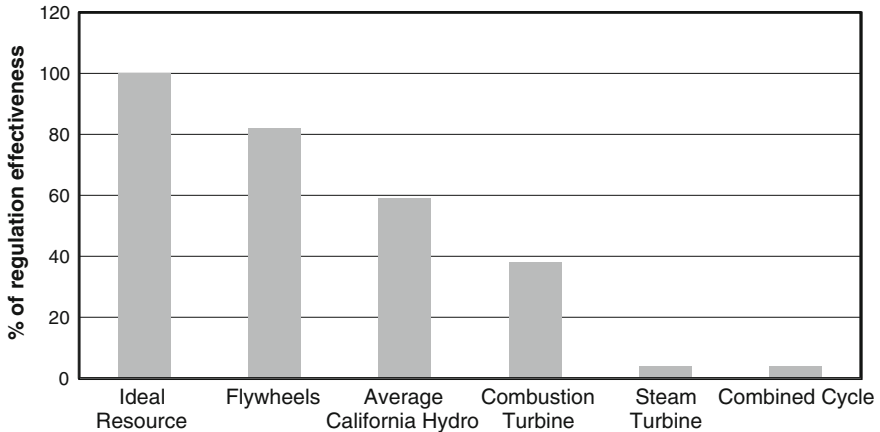


Fig. 10.39 Comparison between different technologies to provide frequency regulation services

effectively to the stability of the system, because the slow ramping resources sometimes work against the ACE (Fig. 10.40-Data extracted from [81–83]).

## 10.3.2 Grid Voltage Stability

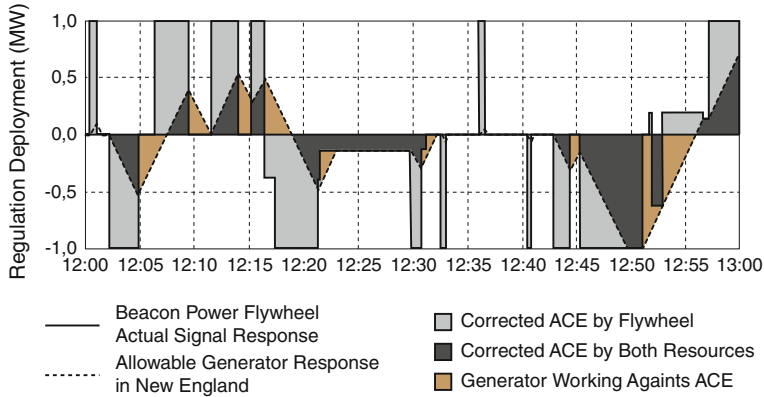
### 10.3.2.1 The Project AMAS500

In March 1993, the AMAS500 prototype was developed in Spain, a superconducting magnet energy storage system (SMES) to be used in grid stability applications. The project was participated by some electricity utilities as Iberdrola and Unión Fenosa, the Electric System Operator (REE), research centers like CEDEX, ICMA, Polytechnic University of Madrid and IIT, and finally the industry with the companies ELIOP, ENERTRON, and ANTECSA [45].

The objective of project AMAS500 was the design and development of a superconducting magnet and a power converter of 500 kVA and 1 MJ to improve the power quality at the electric grid by compensating voltage and frequency oscillations.

### 10.3.2.2 The Superconducting Coil

The superconducting coil was based on Niobium-Titanium working at 4.2 K. Although toroidal geometry has a higher magnetic confinement, solenoid geometry was selected for this project because of: the energy density is higher, so less superconductor cable is required; the mechanical design for the coil is able to



**Fig. 10.40** Comparison of ACE correction between FESS and a conventional generator with 5 min ramp

support high forces and the cryocooler for this geometry can be smaller and the coil fabrication is easier. Two superconducting coil prototypes were developed in this project: the AMAS50, a 50 kW, 25 kJ coil with a self-inductance of 3.14 H, designed for 167 A; and the AMAS500, a 500 kW, 1 MJ, 2 H coil, working at a maximum current of 1 kA. The maximum operation voltage at the dc side was 500 V and the power to exchange 500 kW. The superconducting coil is presented in Fig. 10.41 and its characteristics are summarized in Table 10.6.

The superconducting cable for the coil fabrication had the structure shown in Fig. 10.42. Each cable is composed by a strand of 20 wire elements (Fig. 10.42a). Every wire (Fig. 10.42b) is composed by an external copper filament ring, a cell matrix of the superconducting NbTi filaments with a diameter of 5 μm in the middle to reduce the ac losses and a copper-nickel core in the inner part. The ratio Cu/Cu-Ni/NbTi is 5/5/1.

Cooled with liquid helium, the magnet is contained inside a vacuum-cooled cryostat 4.2 K. Evaporated helium could be recondensed back to the system. The heat introduced into the system due to the leak at the vacuum chamber and through the current leads, helium valves and measurement probes has to be calculated.

### 10.3.2.3 Power Electronics

Current source converters (CSC) were considered as the best option to get a fast transfer of both active and reactive power into the electric grid. Two different options of GTO-based CSC were considered (six-pulse and twelve-pulse).

Figure 10.43 shows the six-pulse GTO current source converter. The main bridge switches are composed of a GTO and a Power Diode in series. This is because asymmetric GTOs with a very low reverse voltage (17 V) have been used to increase the power rating and reduce the final cost. Power converter presented in

**Fig. 10.41** AMAS500 at the testing lab



**Table 10.6** AMAS500 superconducting coil characteristics

Characteristic	Value
Interior diameter	734 mm
External diameter	992 mm
Height	193 mm
Maximum magnetic field density	4.14 T
Number of terms	1392
Number of pancakes	12
Length of superconducting cable	3774 m

**Fig. 10.42** Superconducting cable used for the construction of the SMES AMAS500. **a** Cable section. **b** Wire section

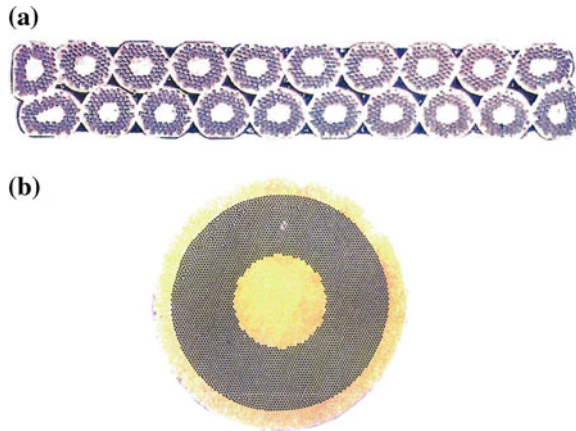


Fig. 10.43 also includes a bypass branch to permit the current circulation during the waiting mode, when the power exchange to the grid is not produced, and quench protection branch that connects a resistor in parallel to reduce the current through the SMES coil.

When compensating electric grid oscillations, the SMES had to be capable of injecting the active and reactive power demanded by the control system. A fast variation of the set points has to be provided by the SMES by means of varying modulation index ( $m$ ) and phase angle ( $\alpha$ ). This rapid variation of both parameters could produce transient effects that have to be considered.

Figure 10.44a shows the resonant effects produced by a sudden variation of switching angle  $\alpha$ . This increases of ac line currents and capacitor voltages to unacceptable values. By using an adequate strategy of varying linearly from  $\alpha_0$  to  $\alpha_1$  during a complete grid period (20 ms) the current response improves as presented in Fig. 10.44b.

The twelve-pulse GTO CSC option is presented in Fig. 10.45 Two sets of currents  $30^\circ$  shifted are generated by the converter. As explained in Sect. 10.2.2.3, the minimization of 5th, 7th, 11th, and 13th harmonics is only possible for low GTO minimum on-time values. Increasing the power, this time becomes more important, resulting in unacceptable THD values. Therefore, in high power applications a twelve-pulse topology is more appropriate because the elimination of 5th and 7th harmonics is achieved by means of the input transformer.

The 500 kW twelve-pulse power converter constructed to supply both AMAS50 and AMAS500 superconducting coils during this project is presented in Fig. 10.46.

Figure 10.47 shows experimental results with the twelve-pulse CSC. The figure shows the current obtained from both CSC modules, shifted  $30^\circ$ , and the total current, addition of them, after the power transformer, when most of the harmonics are suppressed. Moreover, an LC filter set to compensate the 19th harmonic has been also connected.

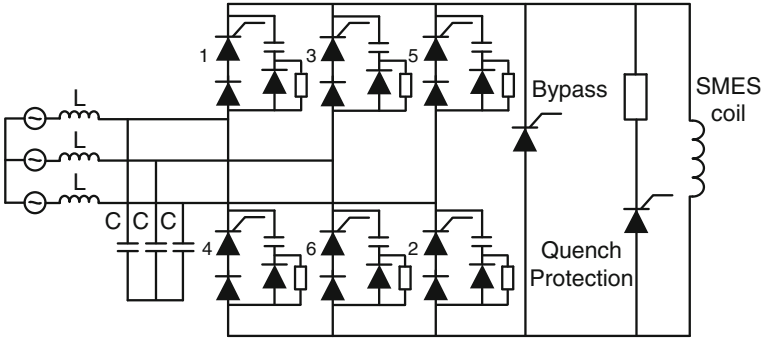


Fig. 10.43 GTO 6-pulse current source converter (CSC) for the SMES

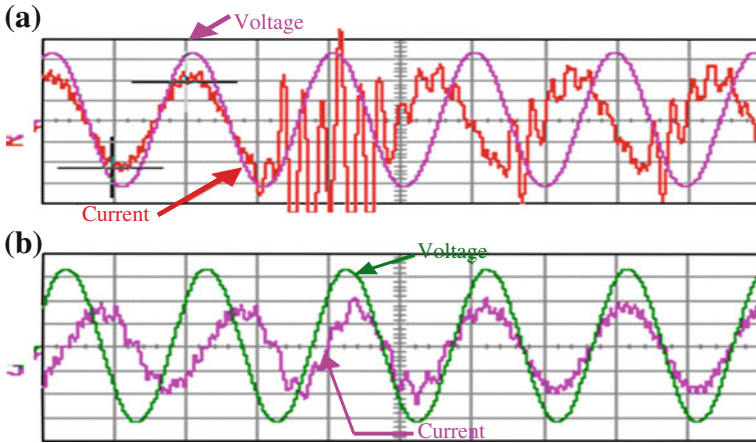


Fig. 10.44 a Sudden variation of angle  $\alpha$ . b Soft variation of angle  $\alpha$

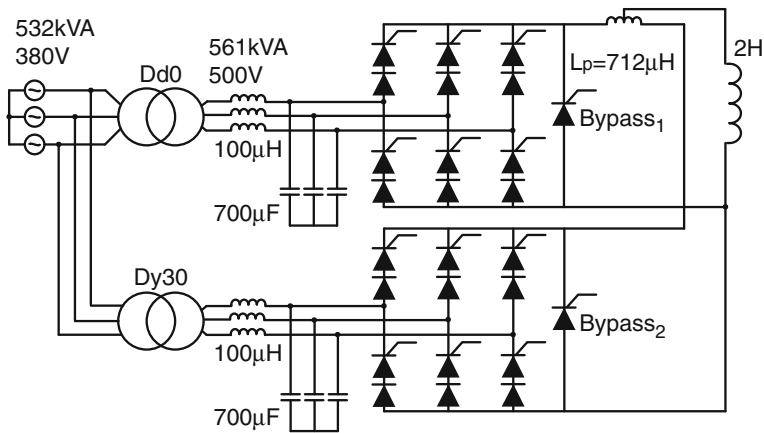


Fig. 10.45 Twelve-pulse CSC with two parallel modules

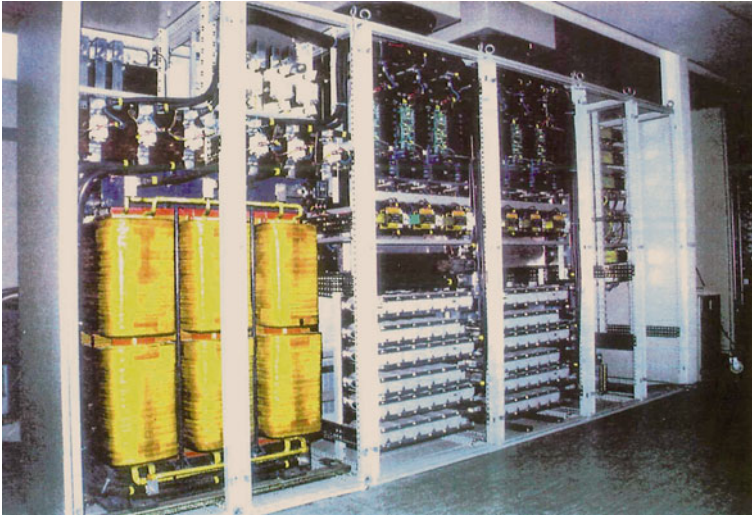


Fig. 10.46 500kVA 12-pulse current source converter

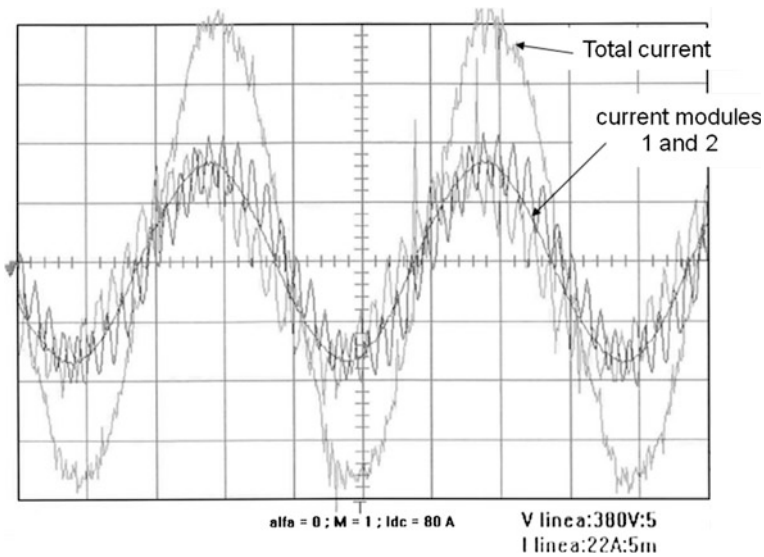
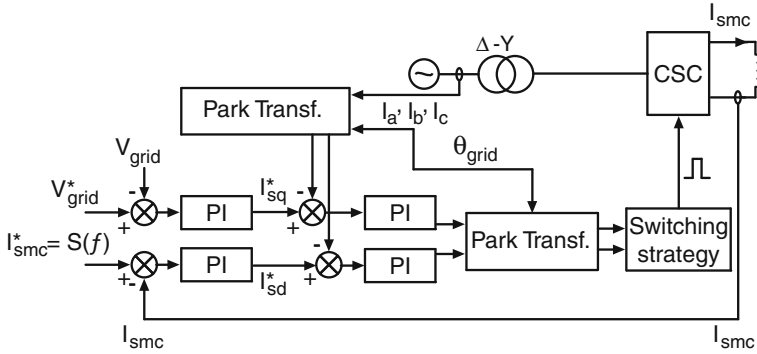


Fig. 10.47 Experimental results of current output in a 12-pulse CSC

SMES control scheme for frequency and voltage stabilization.

Network frequency is regulated through active power (P) while voltage amplitude at the connection point is regulated through reactive power (Q). Two PI controllers will be provided to establish the P and Q requirements to be injected by



**Fig. 10.48** Control scheme for network stabilization with SMES

the CSC (Fig. 10.48). A full controlled converter (IGBTs) is required if P and Q control is necessary since only this type permits two variables to be controlled. d-q reference based on the concepts explained in Sect. 10.2.1.3 has been used for this control scheme. The grid voltage is aligned to the *d*-axis, so the voltage is controlled by means of *q* current component. On the other hand, a reference for the SMES current is obtained as a function of the grid frequency.  $I_{scm}$  is controlled by means of *d* current component, as the same way of the  $V_{dc}$  voltage is controlled in a VSI.

An important issue is that the SMES system will be able to compensate the network frequency whether the current  $I_{scm}$  is high enough, that means the SMES is properly charged. If  $I_{scm}$  is greater than a minimum value  $I_{scm\_min}$  and lower than  $I_{scm\_max}$  the system is permitted to exchange active power and therefore to manage frequency regulation (there is an analogy with the voltage operation range of a battery). Talking about the reactive power, the system is able to operate with reactive power without using any amount of the stored energy (as the same as in batteries), operating the system as an STATCOM. Therefore, the network voltage compensation can be done at any time.

The AMAS50 project was tested connecting it to the electric grid to compensate voltage fluctuations. Figure 10.49 shows a 12 % voltage fluctuation compensated by the SMES in 0.1 s. Moreover, the dynamic response of the CSC has been tested. Figure 10.50 presents the transition between a firing angle of 40° and a firing angle of 270°.

Due to the high cost of the tests, especially because of the helium, a first prototype of superconducting coil was developed first, named AMAS50, in order to test with a lower amount of coolant and lower power (50 kW). The experimental results shown in Fig. 10.50 correspond to the AMAS50 superconducting coil.

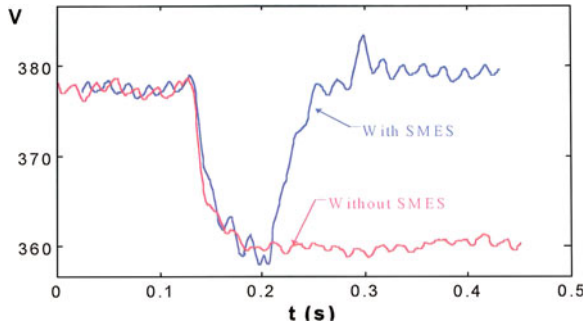


Fig. 10.49 Network voltage response without and with a SMES

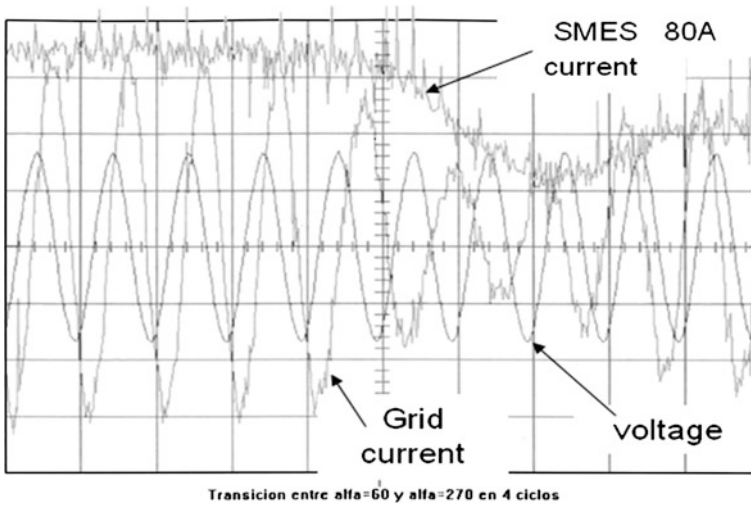


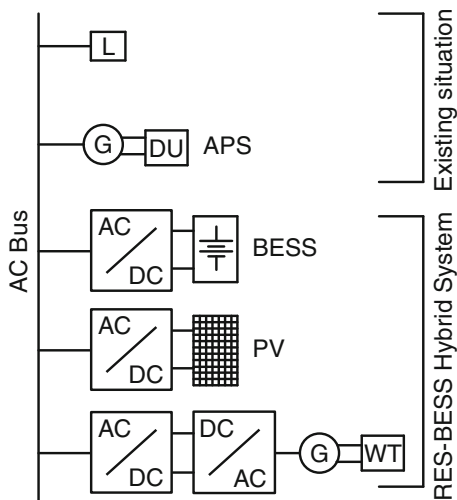
Fig. 10.50 Voltage and current in the grid and current at the superconducting coil

### 10.3.3 Hybrid Energy Storage Systems for Renewable Integration

Most remote rural communities use diesel to generate electricity. But the recent rapid development of a commercial wind and solar industry, along with the rise in diesel fuel prices, has increased interest in renewable energies in rural areas, both to reduce energy costs and to provide local, renewable, sustainable energy. Wind and solar resources are abundant in many places, and a growing number of rural communities are building wind-solar diesel systems, integrating wind and sun into isolated diesel power plants. These systems have moved from the initial demonstration phase a decade ago toward a technology available for many communities [85].



**Fig. 10.51** Typical system configuration of a standalone wind-solar diesel system



The percentage of electricity wind and solar power supplies in a wind-solar diesel system is known as renewable energy penetration. Wind-diesel systems can be classified into low, medium, and high penetration systems. The amount of wind power on the grid determines what ancillary equipment is needed for power control and energy storage.

Although a favorable renewable energy source (RES) potential might exist, the classical technical constraints introduced by the conventional generators result in relatively low RES penetration levels, typically up to 15–20 % of the annual energy demand. To overcome such limitations, introduction of energy storage is necessary. In the case of small and medium standalone systems, lead-acid or NiCd batteries energy storage systems (BESS) constitute a technically mature solution with considerable application potential. Achieving significantly higher RES penetrations calls for the introduction of energy storage systems, which counter-balance the inherent intermittency of RES power supply and permit its adaptation to the load profile. [86–88]. Besides, a fast response storage system (ultracapacitors or flywheel) can be included in order to improve the frequency control of the grid and the reliability of the different components of the generation system [89].

Figure 10.51 outlines the simplified structure of a standalone system. It includes conventional diesel units (DU) supplying the load demand as an autonomous power station (APS). A hybrid station is considered, consisting of wind turbines (WT) and solar Photovoltaic (PV) generators, as the primary energy source, and a battery energy storage system (BESS) system to balance the intermittent RES supply. Alternative architectures are possible for the electrical interconnection of the components, including the possibility for dc interconnection of photovoltaic stations (PV) to the battery inverters. In Fig. 10.51, the ac interconnection alternative is assumed, in which all components are connected to the ac distribution network of the island, due to its superior flexibility, but there are other possible system configurations.

To achieve high RES penetration levels, the system must be capable of operating in “RES-only” mode, i.e., with the diesel unit (DU) out of operation. For this purpose, the BESS inverter should provide frequency and voltage regulation, while additional technical requirements may also exist, including the provision of sufficient short-circuit capacity for proper operation of the network overcurrent protection. For this purpose, additional devices, such as ultracapacitor banks or flywheels may also be used for primary frequency regulation.

There are many papers and research works regarding operating policies for standalone power systems. In [86] a specific operating strategy is proposed. In this case, the system relies on a basic decision making interval of 1 h. Unit commitment decisions are taken half an hour before each hourly interval, based on the short-term forecasting of load demand over the next interval, to provide enough time for the start-up of the diesel systems. While the maximization of RES penetration is a primary objective, the reliability of supply to the load needs to be ensured, i.e., loss-of-load events due to the intermittency and uncertainty of RES power availability must be excluded.

The renewable resources are intermittent therefore its availability is not always ensured, a diesel generator is sometimes required to achieve the power demand. But a diesel generator lifetime can be reduced when it is used to compensate all fluctuating current provided by the renewable resource. So, storage devices can be added to the hybrid system for more efficiency, but the technology choice depends on the storage process capability. Batteries provide a small number of charge/discharge cycles (around 2,000 cycles). The best way to improve their lifetime is to prevent them from fast dynamic currents and high number of cycles. On the opposite, fast response energy storage systems (flywheels and ultracapacitors) are able to absorb currents with fast dynamics and to provide a significant number of cycles (around 50,000 cycles) [8, 89]. But the fast response energy system is not only included to improve the lifetime of the different subsystems of the standalone power generation plant, but it is also required to be used as a frequency voltage regulation to guaranty the stability of the grid.

### ***10.3.4 Electrical Vehicles and Fast Rechargeable System Applications***

Many cities and regions have taken very active approaches to developing public infrastructure to support electric vehicles. A second place to charge during the day, typically at work, could effectively double the electric range of the EV. As the public charging infrastructure develops over the next few years, many areas will have sufficient locations for electric vehicles to charge when necessary, alleviating concerns about range.

Electric vehicles can be charged from a standard one phase outlet, 120 V in US or 240 V in EU market. If fast charging is required, it is necessary to install a

dedicated two or three phase charger, rated to 240 V for US or 400 V for the EU market. Medium and fast charging power is above 3 kW. With this power range, about the same power draw as clothes dryer or an air conditioning system, the car could be fully charged in 3–8 h.

Fast response storage system is very useful for rechargeable station in electro-mobility application and distributed generation systems. An EDLC stack could be used alone or in parallel with a battery to increase the system energy capability. This parallel configuration improves also the efficiency and increase the life time of the battery [90].

The fast charging infrastructures could be arranged as a distributed energy resource, that needs a very high peak power and energy in a short period of time. Distributed power supplies are expected to increase with the deregulation of electric power business [21].

To fulfil this new peak power demand, some alternatives are possible: increase the capacity of the infrastructure, use a fast response storage system or a combination or both in several percentages options, for example, 80 % existing infrastructure, 20 % new needed capacity delivered by the storage system.

From the point of view of the infrastructure, fast charging station require a fast response storage system if a high current is required at a high cycling rate, where standard batteries cannot be operated. The main problem is peak power and charge efficiency.

Charging efficiency  $\eta$  of an EDLC by a dc voltage source can be defined by following equation [91]

$$\eta = \frac{E_c}{E} = \frac{1}{2} \frac{V_c - V_c(0)}{V_c} \quad (10.15)$$

where  $E_c$  is the charged energy,  $E$  is the supplied energy, and  $V_c(0)$  is the initial voltage of the EDLC. When the initial voltage  $V_c(0)$  is equal to 0, the efficiency is 50 %. The efficiency charging by a voltage source is low and is independent from the series resistance  $R$  in opposition to charge by a current source as will be shown just below.

If the EDLC is charged by a current source  $I$ , the efficiency is obtained as follows:

$$\eta = \frac{E_c}{E} = \frac{V_c(0) + \frac{IT}{2C}}{R \cdot I + V_c(0) + \frac{IT}{2C}} \quad (10.16)$$

where  $T$  is the charging time,  $C$  is the capacitance and  $R$  the series resistance.

From Eq. (10.16), the efficiency becomes 100 % when the internal resistance  $R$  of the EDLC is small enough. This result shows that the EDLC should be charged by a constant current. The constant current charger can be built by a dc–dc converter to get this constant current. These formulas are useful to have a first calculation of system efficiency of the system knowing the parameters of the EDLC.

In order to calculate the capacitance of an EDLC bank, the following equation can be used:

$$C = \frac{2E_c}{V_{\text{nom}}^2 - (0.5V_{\text{nom}})^2} \quad (10.17)$$

Here  $V_{\text{nom}}$  is the nominal voltage of the stack and  $E_c$  is the stored energy.

For example, let us analyze a dc fast charging infrastructure rated to 400 V. From Eq. (10.1), it would be required 60 F/kWhr. Suppose that the overall system has to deliver 60 kW during 15 min and so, a 15 kWhr energy storage system is required. It is assumed that the electrical infrastructure installed power can deliver 80 % of required power and so, 80 % of total energy. Then, the capacity of the stack will be 20 % of the total capacity, which is 3 kWh, thus  $C$  will be equal to 180 F.

Using 560F, 2.5 V basic cell, the system is compounded by 160 units in series and the capacitance of each EDLC string becomes 560 F/160 = 3.5 F. Then, the number of parallel string will be 52 (180 F/3.5 F) and 8320 (160×52) cells will be required for this storage system.

In a fast charging infrastructure, power converters can be tightly controlled and exhibit constant power character. In the sense from the small signal point of view, constant power converter exhibits negative impedance viewed from the input port [92, 93]. That is, though its impedance is positive at every moment, the increment of impedance is always negative. As a result, when the input voltage of constant power load increases, the current of the load decreases, vice versa.

The current and the equivalent impedance of the constant power load are given, respectivel, as

$$i_{\text{pc}}(P, V) = \frac{P}{V} \quad (10.18)$$

$$Z_L = \frac{\partial V}{\partial i_{\text{pc}}(P, V)} = \frac{-V^2}{P} \quad (10.19)$$

Since  $P$  is always larger than zero, the impedance of the constant power load is smaller than zero. That is, it has negative impedance viewed from the input port which will make system stability deteriorate or even unstable. This characteristic have to be taken into account to avoid instabilities of a distributed dc charging station connected to the same dc bus.

## References

1. Ter-Gazarian A (1994) Energy Storage for Power Systems, IEE Energy Series. Peter Peregrinus, Hitchin
2. Ribeiro PF, Johnson BK, Crow ML, Arsoy A, Liu Y (2001b) Energy storage systems for advanced power applications. Proc IEEE 89(12):1744–1756
3. Christen T, Carlen MW (2000) Theory of Ragone Plots. J Power Sources 91:210–216
4. CAISO, Energy GE (2010) Integration of renewable resources—Operational requirements and generation fleet capability at 20% RPS. Available via <http://www.caiso.com/2804/2804d036401f0.pdf>

5. Milligan M, Lew D, Corbus D, Piwko R, Miller N, Clark K, Jordan G, Freeman L, Zavadil B, Schuerger M (2009) Large-scale wind integration studies in the United States: preliminary results. In: Proceeding of the 8th international workshop on large-scale integration of wind power and transmission networks for offshore wind farms, Bremen, Germany, 14–15 Oct 2009
6. Carrasco JM, Franquelo LG, Bialasiewicz JT, Galvan E, Guisado RCP, Prats MAM, Leon JI, Moreno N (2006) Power-electronic systems for the grid integration of renewable energy sources: a survey. *IEEE Trans Ind Elect* 53(4):1002–1016
7. Denholm P, Ela E, Kirby B, Milligan M (2010) The role of energy storage with renewable electricity generation. Available via [www.nrel.gov/docs/fy10osti/47187.pdf](http://www.nrel.gov/docs/fy10osti/47187.pdf)
8. Vazquez S, Lukic SM, Galvan E, Franquelo LG, Carrasco JM (2010) Energy storage systems for transport and grid applications. *IEEE Trans Ind Elect* 57(12):3881–3895
9. Kirby B, (2007) Ancillary services: technical and commercial insights. Available via [www.consultkirby.com/files/Ancillary\\_Services\\_Technical\\_And\\_Commercial\\_Insights\\_EXT\\_.pdf](http://www.consultkirby.com/files/Ancillary_Services_Technical_And_Commercial_Insights_EXT_.pdf)
10. Makarov YV, Ma J, Lu S, Nguyen TB (2008) Assessing the value of regulation resources based on their time response characteristics. Tech. Rep. PNNL-17632, Pacific Northwest National Laboratory, Richland, WA, Jun 2008
11. Ribeiro FP, Johnson BK, Crow ML, Arsoy A, Liu Y (2001a) Energy storage systems for advanced power applications. *Proc IEEE* 89(12):1744–1756
12. Lukic SM, Jian C, Bansal RC, Rodriguez F, Emadi A (2008) Energy storage systems for automotive applications. *IEEE Trans Ind Electron* 55(6):2258–2267
13. Iwasawa K, Inoue T, Koizumi K (2010) A novel voltage equalizer using series/parallel switching capacitors. In: proceeding of the IEEE international conference on digital sustainable energy technologies (ICSET), Sri Lanka, 6–9 December 2010
14. Thounthong P, Raël S, Davat B (2007) Control strategy of fuel cell and supercapacitors association for a distributed generation system. *IEEE Trans Ind Elect* 54(6):3225–3233
15. Muyeen SM, Takahashi R, Murata T, Tamura J (2009) Integration of an energy capacitor system with a variable-speed wind generator. *IEEE Trans Energy Convers* 24(3):740–749
16. Samosir AS, Yatim AHM (2010) Implementation of dynamic evolution control of bidirectional dc–dc converter for interfacing ultracapacitor energy storage to fuel-cell system. *IEEE Trans Ind Elect* 57(10):3468–3473
17. Fakhm H, Di L, Francois B (2011) Power control design of a battery charger in a hybrid active PV generator for load-following applications. *IEEE Trans Ind Elect* 58(1):85–94
18. Liyan Q, Wei Q (2011) Constant power control of DFIG wind turbines with supercapacitor energy storage. *IEEE Trans Ind Appl* 47(1):359–367
19. Sang-Min K, Seung-Ki S (2006) Control of rubber tyred gantry crane with energy storage based on supercapacitor bank. *IEEE Trans Power Electron* 21(5):1420–1427
20. Joon-Hwan L, Seung-Hwan L, Seung-Ki S (2009) Variable-speed engine generator with supercapacitor: Isolated power generation system and fuel efficiency. *IEEE Trans Ind Appl* 45(6):2130–2135
21. Monai T, Takano I, Nishikawa H, Sawada Y (2004) A collaborative operation method between new energy-type dispersed power supply and EDLC. *IEEE Trans Energy Convers* 19(3):590–598
22. Kinjo T, Senjyu T, Urasaki N, Fujita H (2006) Output leveling of renewable energy by electric double-layer capacitor applied for energy storage system. *IEEE Trans Energy Convers* 21(1):221–227
23. Inoue S, Akagi H (2007) A Bidirectional dc–dc converter for an energy storage system with galvanic isolation. *IEEE Trans Power Electron* 22(6):2299–2306
24. Haimin T, Kotsopoulos A, Duarte JL, Hendrix MAM (2008) Transformer-coupled multiport ZVS bidirectional dc–dc converter with wide input range. *IEEE Trans Power Electron* 23(2):771–781
25. Maharjan L, Inoue S, Akagi H (2008) A transformerless energy storage system based on a cascade multilevel PWM converter with star configuration. *IEEE Trans Ind Appl* 44(5):1621–1630

26. Grbovic PJ, Delarue P, Le Moigne P, Bartholomeus P (2010) A bidirectional three-level dc-dc converter for the ultracapacitor applications. *IEEE Trans Ind Elect* 57(10):3415–3430
27. Vilathgamuwa M, Jayasinghe S, Madawala U (2011) Diode-clamped three level inverter based battery/supercapacitor direct integration scheme for renewable energy systems. *IEEE Trans Power Electron* 26:3720–3729
28. Ginsburg VL (1991) Superconductivity, superdiamagnetism, superfluidity. MIR Publishers, USSR, Moscow
29. Chu CW (1997) High-temperature superconducting materials: a decade of impressive advancement of T<sub>c</sub>. *IEEE Trans Appl Supercond* 7(2):80–89
30. Iwasa Y (1994) Case studies in superconducting magnets. Plenum Press, New York
31. Wilson MN (1987) Superconducting Magnets. Oxford University Press, USA
32. Boom RW, Peterson H (1972) Superconductive energy storage for power systems. *IEEE Trans Magnetics* 8(3):701–703
33. Bautista A, Esteban P, Garcia-Tabares L, Peon G, Martinez E, Sese J, Camon A, Rillo C, Iturbe R (1997) Design, manufacturing and cold test of a superconducting coil and its cryostat for SMES applications. *Trans Appl Supercond* 7(2):853–856
34. Juengst KP, Komarek P, Maurer W (1994) Use of superconductivity in energy storage. World Scientific, Singapore
35. Tsutsui H, Kajita S, Ohata Y, Nomura S, Tsuji-Iio S, Shimada R (2004) FEM analysis of stress distribution in force-balanced coils. *Trans Appl Supercond* 14(2):750–753
36. GE Industrial Systems & American Superconductors (2001) D-SMES. Available via [www.amsc.com](http://www.amsc.com)
37. SuperPower (2010) Superconducting magnetic energy storage. Available via <http://www.superpower-inc.com/content/superconducting-magnetic-energy-storage-smes>
38. Ackermann RA (1997) Cryogenic regenerative heat exchangers (International cryogenics monograph series). Plenum Press, New York
39. Ali MH, Wu B, Dougal RA (2010) An overview of SMES applications in power and energy systems. *IEEE Trans on Sust Ener* 1(1):38–47
40. Karasik V, Dixon K, Weber C, Batchelder B, Campbell G, Ribeiro P (1999) SMES for power utility applications: a review of technical and cost considerations. *Trans Appl Supercond* 9(2):541–546
41. Ham WK, Hwang SW, Kim JH (2008) Active and reactive power control model of superconducting magnetic energy storage (SMES) for the improvement of power system stability. *J Elect Eng Tech* 3(1):1–7
42. Rogers J, Boenig H, Schermer R, Hauer J (1985) Operation of the 30 MJ superconducting magnetic energy storage system in the bonneville power administration electrical grid. *IEEE Trans Magn* 21(2):752–755
43. Iglesias IJ, Acero J (1995) Comparative study and simulation of optimal converter topologies for SMES. *IEEE Trans Appl Supercond* 5(2):254–257
44. Zelaya H, Iglesias IJ, González O, Tamarit J (1997) Modulation and control of current source converters for high dynamic performance of induction motors. In: *Proceeding of the european power electronics conference (EPE)*, Trondheim, 8–10 Sept 1997
45. Van der Broeck HW, Skundelny HC, Stanke GV (1988) Analysis and realization of a pulsewidth modulator based on voltage space vectors. *IEEE Trans Ind Appl* 24(10):142–150
46. Iglesias IJ, Bautista A, Visiers M (1997) Experimental and simulated results of a SMES fed by current source inverter. *IEEE Trans Appl Supercond* 7(2):861–864
47. Iglesias IJ, Acero J, Bautista A (1995) Comparative study between six and twelve pulse current source converter for SMES. In: *Proceeding of the European power electronics conference (EPE)*, Sevilla, 19–21 Sept 1995
48. Genta G (1985) Kinetic energy storage: theory and practice of advanced flywheel systems. Butterworths, London
49. Active Power (2008) Understanding flywheel energy storage: does high speed really imply a better design? Available via [www.activepower.com](http://www.activepower.com)
50. Genta G (1999) Vibration of structures and machines. Springer, New York

51. Piller Power Systems (2010) UNIBLOCK UBT. Rotary UPS. Available via [www.piller.com](http://www.piller.com)
52. Nasar SA, Boldea I, Unnerwher LE (1993) Permanent Magnets, Reluctance and Self-Synchronous Motors. CRC Press, USA
53. Tsao P (2003) An integrated flywheel energy storage system with homopolar inductor motor/generator and high frequency drive. *IEEE Trans Ind Appl* 39(6):1710–1725
54. Active Power (2008) Integrated flywheel based uninterruptible power supply for broadcast applications. Available via [www.activepower.com](http://www.activepower.com)
55. Hofmann H, Sanders SR (1996) Synchronous reluctance motor/alternator for flywheel energy storage systems. In: *Proceeding of the IEEE power electronics in transportation (PET)*, Dearbon, 24–25 Oct 1996
56. Miller TJE (1993) Switched reluctance motors and their control. Magna Physics Publishing & Clarendon Press, Ohio
57. Lafoz M, Calero J, Garcia-Tabares L, Ugena D, Portillo S, Vazquez C, Gutierrez JL, Tobajas C, Iglesias J, Martinez JC, Lucas J, Echeandia A, Echeandia J, Zuazo C (2007) The ACE2 system: A kinetic energy storage for railway substations. In: *Proceeding of the electrical energy storage applications and technologies (EESAT)*, San Francisco, 23–26 Sept 2007
58. Powell JP, Jewell GW, Calverley SD, Howe D (2005) Iron loss in a modular rotor switched reluctance machine for the “More-Electric” aero-engine. *IEEE Trans Magn* 41(10):3934–3936
59. Hanselman DC (1994) Brushless permanent-magnet motor design. McGraw-Hill, New York
60. Nagomy A, Dravid NV, Jansen RH, Kenny BH (2005) Design aspects of a high speed permanent magnet synchronous motor/generator for flywheel applications. In: *Proceeding of the IEEE international conference on electric machines and drives (ICEMD)* San Antonio, 15 May 2005
61. Etxaniz I, Izpizua A, San Martin M, Arana J, Perez I (2007) Levitation techniques applications. *Sens Lett* 5(1):323–328
62. Moon FC (1993) Superconducting Levitation. John Wiley & Sons, New York
63. Strasik M, Johnson PE, Day AC, Mittleider J, Higgins MD, Edwards J, Schindler JR, McCrary KE, McIver CR, Carlson D, Gonder JF, Hull JR (2007) Design fabrication and test of a 5kWh/100 kW flywheel energy storage utilizing a high-temperature superconducting bearing. *IEEE Trans Appl Supercond* 17(2):2133–2137
64. Kangwon L, Bongsu K, Junseok K, Sangkwon J, Seung L (2007) Advanced design and experiment of a small-size flywheel energy storage system using a high-temperature superconductor bearing. *Supercond Sci Technol* 20(7):634–639
65. Goncalves G, Andrade R, Ferreira AC (2007) Magnetic bearing sets for a flywheel system. *IEEE Trans Appl Supercond* 17(2):2150–2153
66. Tsao P, Senesky M, Sanders S (2002) A synchronous homopolar machine for high-speed applications. In: *Proceeding of the IEEE 37th IAS annual meeting conference record of the industrial applications society (IAS)* Pittsburgh, 13–18 Oct 2002
67. Lipo TA, Vagati A, Malesani L, Fukao T (1992) Synchronous reluctance motors and drives—a new alternative. In: *Proceeding of the IEEE 26th IAS annual meeting conference record of the industrial applications society (IAS)* Houston, 4–9 Oct 1992
68. Park JD, Kalev C, Hofmann H (2008) Modeling and control of solid-rotor synchronous reluctance machines based on rotor flux dynamics. *IEEE Trans Magn* 44(12):4639–4647
69. Krishnan R (2001) Switched reluctance motor drives. Modeling, simulation, analysis, design and applications. CRC Press, USA
70. Malesani L, Tenti P (1990) A novel hysteresis current method for current-controlled voltage source inverters with constant modulation frequency. *IEEE Trans Ind Appl* 26(1):88–92
71. Elliott CR (1999) Hysteresis current controller for a reluctance machine. US patent No. 5, 998, 945
72. Gallegos-Lopez G, Rajashekara K (2002) Peak PWM current control of switched reluctance and AC machines. In: *Proceeding of the IEEE 37th IAS annual meeting conference record of the industrial applications society (IAS)* Pittsburgh, 13-18 Oct 2002

73. Blaabjerg F, Kjaer PC, Rasmussen PO, Cossar C (1999) Improved digital current control methods in switched reluctance motor drives. *IEEE Trans Power Electron* 14(3):563–572
74. Vazquez C, Lafoz M, Ugena D, Garcia-Tabares L (2007) Control system for the switched reluctance drive of a flywheel energy-storage module. *Euro Trans Electr Power* 17(6):537–553
75. Lafoz M, Vazquez C, Iglesias JI (2009) DC railway catenary regulation based on KESS. In: *Proceeding of the electrical energy storage applications and technologies (EESAT)* Washington, 4–7 Oct 2009
76. Lafoz M, Vazquez C, Garcia-Tabares L (2008) Efficiency considerations of a kinetic energy storage system used for railway applications. In: *Proceeding of the international conference on electrical machines (ICEM)* Vilamoura, 6–9 Sept 2008
77. Takahashi R, Tamura J (2007) Frequency stabilization of small power system with wind farm by using flywheel energy storage system. In: *Proceeding of the IEEE international symposium on diagnostics for electric machines, power electronics and drives (SDEMPED)* Cracow, 6–8 Sept 2007 (IAS) Houston, 4–9 Oct 1992
78. Akamatsu M, Tsukada M, Itoh D (1998) A novel PLL and frequency detecting method suited for the abnormal voltages under fault conditions in the power system. *IEEJ Trans Power Electron* 118-B(9):955–961
79. Flynn MM, McMullen P, Solis O (2008) Saving energy using flywheels. *IEEE Ind Appl Mag* 14(6):69–76
80. Beacon Power Corporation (2010) Smart energy matrix™ 20 MW frequency regulation plant (June 2010). Available via [www.beaconpower.com/files/SEM\\_20MW\\_2010.pdf](http://www.beaconpower.com/files/SEM_20MW_2010.pdf)
81. Lazarewicz ML, Ryan T (2010) Grid-scale frequency regulation using flywheels. Available via <http://www.beaconpower.com/files/ISO-NE-performance-paper-2010.pdf>
82. Cleary J, Lazarewicz ML, Nelson L, Rounds R, Arsenault J (2010) Interconnection study: 5 MW of Beacon Power flywheels on 23 kV line—Tyngsboro, MA. In: *Proceeding of the IEEE conference on innovative technologies for an efficient and reliable electricity supply (CITRES)*, USA, 27–29 Sept 2010
83. Lazarewicz ML, Ryan TM (2010) Integration of flywheel-based energy storage for frequency regulation in deregulated markets. In: *Proceeding of the IEEE power and energy society general meeting*, USA, 25–29 July 2010
84. KEMA corporation (2007) Emissions comparison for a 20 MW flywheel-based frequency regulation power plant. Available via <http://beaconpower.com/products/presentations-reports.asp>
85. Fay G, Schwörer T (2010) Alaska isolated wind-diesel systems: performance and economic analysis. Available via [www.iser.uua.alaska.edu](http://www.iser.uua.alaska.edu)
86. Vrettos EI, Papatthanassiou SA (2011) Operating policy and optimal sizing of a high penetration RES-BESS system for small isolated grids. *IEEE Trans Energy Convers* 26:744–756
87. Abbey C, Joos G (2008) Sizing and power management strategies for battery storage integration into wind-diesel systems. In: *Proceeding of the 34th annual conference of IEEE industrial electronics society (IECON)*, Orlando, 10–13 Nov 2008
88. Sebastian R, Peña R (2009) Simulation of a high penetration wind diesel system with a Ni-Cd battery energy storage. In: *Proceeding of the 35th annual conference of IEEE industrial electronics society (IECON)*, Porto, 3–5 Nov 2009
89. Tankari MA, Camara MB, Dakyo B, Nichita C (2010) Attenuation of power fluctuations in wind diesel hybrid system—using ultracapacitors and batteries. In: *Proceeding of the international conference on electrical machines and drives (ICEMD)* Rome, 6–8 Sept 2010
90. Urasaki N, Iwasaki M (2010) Hybrid power source with electric double layer capacitor and battery in electric vehicle. In: *Proceeding of the international conference on electrical machines and systems (ICEMS)* Incheon, 10–13 Oct 2010
91. Nagaoka N, Miyamoto A, Ametani A (2004) New EDLC charging system for photovoltaic generation part 1: numerical simulation. In: *Proceeding of the 39th international universities power engineering conference (UPEC)*, Bristol, 6–8 Sept 2004



92. Wildrick CM, Lee FC (1995) A method of defining the load impedance specification for a stable distributed power system. *IEEE Trans Power Electron* 10(3):280–285
93. Liang Y, Hu Z, Chen Y (2003) A survey of distributed generation and its application in power system. *Power Syst Technol* 12:72–75

# Chapter 11

## Modular Power Electronics

Sudipta Chakraborty

**Abstract** In this chapter, the basics of modular power electronics such as power electronics building block (PEBB) and integrated power electronics module (IPEM) are discussed first followed by a review of common power electronics topologies for different renewable and distributed energy systems. Generalized power electronic topologies are formalized based on such applications that can be used to design modular power electronics interfaces. Those modular power electronics will be flexible to work with different sources, scalable to meet various power requirements, incorporating lower cost and improved reliability, and such modular power electronics can eventually improve the overall life-cycle cost for renewable and distributed energy systems.

### 11.1 Introduction

As evident from several chapters in this book, all renewable and distributed energy generations and storages need power electronics to convert the generated power into useful energy that can be directly interconnected to the utility grid and can be used for consumer applications. The power electronics can account for significant costs to the overall energy system; therefore, improvement of the renewable and distributed energy economics strongly requires decreased costs for the power electronics.

Another important aspect to the life-cycle cost of the renewable and distributed energy systems is reliability. Many of the power electronics used for such

---

Views expressed in this chapter are personal with no implied endorsement of the same by NREL/DOE.

---

S. Chakraborty (✉)  
National Renewable Energy Laboratory, 15013 Denver West Parkway, Golden,  
CO 80401, USA  
e-mail: sudipta.chakraborty@nrel.gov

applications have a low reliability and typically consumer has to replace them even before the energy sources reach their end-of-life.

A survey conducted by Navigant Consulting under the California Energy Commission Public Interest Energy Research (PIER) initiative had found that from the commercialization perspective, the key business needs for renewable and distributed energy power electronics are reducing costs and improving reliability [1]. Associated with these cost and reliability issues, three major technology challenges exist when discussing power electronics for such energy applications [1].

- There is a lack of standardization and interoperability among power electronics components and systems. This increases the cost of manufacturability and reduces volume and reliability.
- Power electronics devices must be modular and scalable. This will simplify applications and designs, leading to increased use; higher production volumes will lower costs and improve performance.
- Current research focuses on power electronics subsystems and component rather than the distributed energy system package. Improvements in the system package are urgently needed for distributed energy.

This chapter summarizes power electronics topologies for different distributed energy systems in order to support generalized topologies that can be used for different distributed energy applications, with very small or almost no modifications. The objective for such generalized power electronics topologies is to apply a building block concept into designing a power electronics interface that is flexible to work with different sources, scalable to meet various power requirements, incorporating modular design, lower cost and improved reliability, and further improving the overall life-cycle cost of the renewable and distributed energy systems.

## 11.2 Basics of Modular Power Electronics

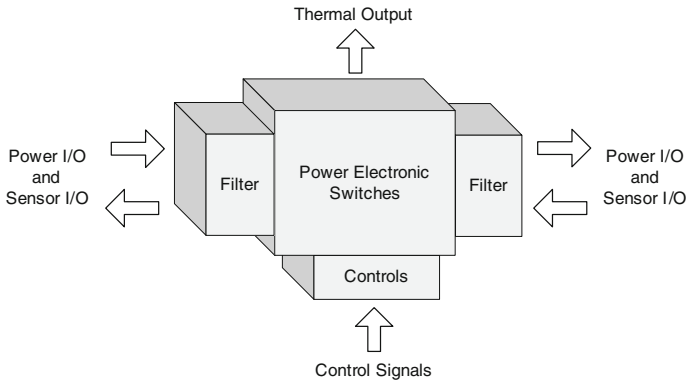
The modular power electronics design revolves around two main concepts, namely power electronics building block (PEBB) and integrated power electronics module (IPEM). Though researchers often use these two terms interchangeably, IPEM is a term used to describe a new generation of power electronic devices that includes power electronic switches along DC filtering, various electrical and thermal sensors, gate drivers, heat sink, and a digital controller all into a single highly optimized package. IPEMs are typically designed for low to medium power applications. On the other hand, PEBB encompasses broader domain to include functional building blocks for both the power electronics and controller for high power applications. Using these standard functional blocks along with some standardized control and communication interfaces, various power electronics converters can be developed for multiple applications, and therefore have the potential to reduce the cost of the power converters.

## ***11.2.1 Power Electronics Building Blocks***

### **11.2.1.1 Background and Concept of PEBB**

The concept of PEBB has been supported by the U.S. Government sponsored research and development program initiated in late 1994 by the U.S. Office of Naval Research (ONR) [2]. The program's main goal was to reduce the cost by changing the design and manufacturing paradigm for high power electronics and control. It was envisioned that the PEBB concept would convert the typical approach of designing the complete system for each application from scratch to a better system design approach achieved by selecting from a small set of standard building blocks or modules thus reducing the design and manufacturing cost [2]. As the U.S. Government does not manufacture products, it was very critical for the ONR program that the new concept got acceptance by the power electronics manufacturing industry and by various commercial and military users of these products. To achieve this, ONR created a large team that included academia, a U.S. Navy laboratory, U.S. Government laboratories, industrial manufacturers, and system integrators for commercial and military customers. The group tackled various challenges such as implementation of PEBB using several available techniques, public demonstration of interim product, and technology review workshops [2]. The ONR was the developer and primary sponsor of all PEBB and PEBB-related R&D [2]. The PEBB developed under this program was demonstrated in various commercial applications such as electric vehicles, utility distribution systems, motor controllers, and some renewable energy systems. In addition, various military applications like high-power propulsion and auxiliary power system for ships, submarines, aircraft also utilized the PEBB-based power conversion systems.

According to the definition provided in the literature [3, 4], PEBB is a concept that incorporates progressive integration of power devices, gate drives, programmable processor, and other components into building blocks with specific functionalities and interfaces in order to serve multiple applications. Based on functional specifications of PEBBs that relate to the performance requirements of intended applications, the PEBB designer addresses the details of the device stresses, stray inductances and switching speed, losses, thermal management, protection, measurements of required variables, control interfaces, and potential integration issues at all levels [3]. The advantages of this approach lies in various fronts. First of all, by adopting the same functional building blocks for various applications, the cost of the power conversion systems become lower due to high-volume production. Also the engineering effort, design testing, commissioning, and development risk of such building blocks are much less which in turn significantly reduces the time to market and R&D cost [3, 5]. Various technological aspects such as advanced devices, integrated packaging and progressive integration from device level to system level makes the PEBB more reliable than the discrete component based power electronics. Finally, with standardized interfaces,



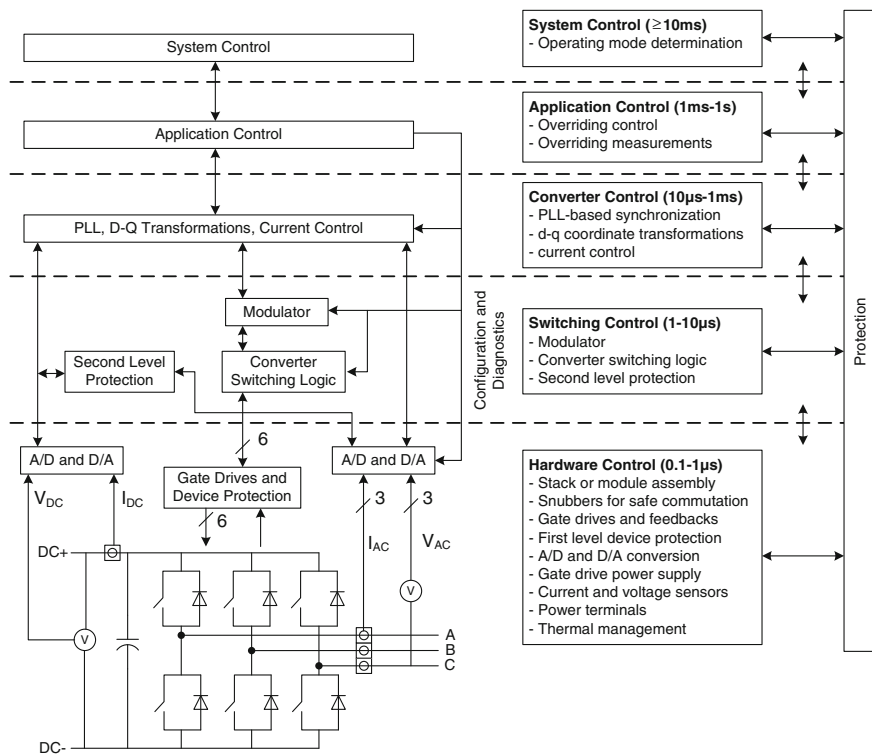
**Fig. 11.1** Building block concept in power electronics

the PEBB enables the power electronics to become plug-and-play devices where every manufacturer produce a product that can be easily integrated in every other manufacturer's product [2]. The concept of PEBB as shown by IEEE Power and Energy Society is given in Fig. 11.1 [5].

To add plug-and-play capability to the PEBB, overall control architecture must have the inherent capability to support the integration of these PEBBs, regardless of how they are configured together. In 2010, IEEE has released a Standard 1676–2010 titled “IEEE Guide for Control Architecture for High Power Electronics (1 MW and Greater) Used in Electric Power Transmission and Distribution Systems”. Within this standard, hierarchical control architecture for the PEBB-based high power systems is discussed that can lead to multiple vendors to design and manufacture components, subassemblies, and software that can be used in a large variety of power electronic products or systems [6].

A generic control architecture applicable to PEBB is shown in Fig. 11.2 [6]. In this figure, various control layers are shown that is common to different applications. Also shown in the figure are functions that need to be handled within each layer, parameters that need to be communicated between the layers and the required speed range [6]. In this case, the power hardware subsystem is composed of a three-phase bridge assembly with the functions of switching and primary device monitoring and protection, as well as the various voltage and current sensing. However, the modularization of a power electronic system does not depend on the power module configuration. It is important to note that partitioning hardware modules will not change the basic function of the hardware control layer and will be transparent to higher control layers [6].

In Fig. 11.2, the converter control system is shown to have five hierarchical layers: a system control layer, an application control layer, a converter control layer, a switching control layer, and a hardware control layer. The system control layer determines the overall mission of the system and determines the operational mode. The application control layer maintains the overall functions of the power electronics system. The converter control layer implements many common



**Fig. 11.2** Control architecture for PEBB [6]. (This figure is adapted from Fig. 1 of the IEEE Standard 1676–2010 titled “IEEE guide for control architecture for high power electronics (1 MW and greater) used in electric power transmission and distribution systems”)

functions of converters such as synchronization, transformation. The switching control layer that handles the switching logic and sequence, and the hardware control layer manages everything specific to the power hardware. Each layer has characteristic processing and communication speed requirements, irrespective of the final applications.

It is recognized in the IEEE Standard 1676–2010 that an application may have more than one piece of power electronics hardware and the converters may be remote from each other and linked together through transmission or distribution lines. The proposed architecture recommends that each converter must have their own independent switch control to serve their hardware control. The proposed architecture further suggests that there may be a common converter control to serve multiple switching controls. Also, one application control may serve more than one converter control. The function of protection is to take the necessary action as fast as required; therefore, the function of protection may go to any of the layers [6].

### 11.2.1.2 Example Applications of PEBB: Marine and High Power Systems

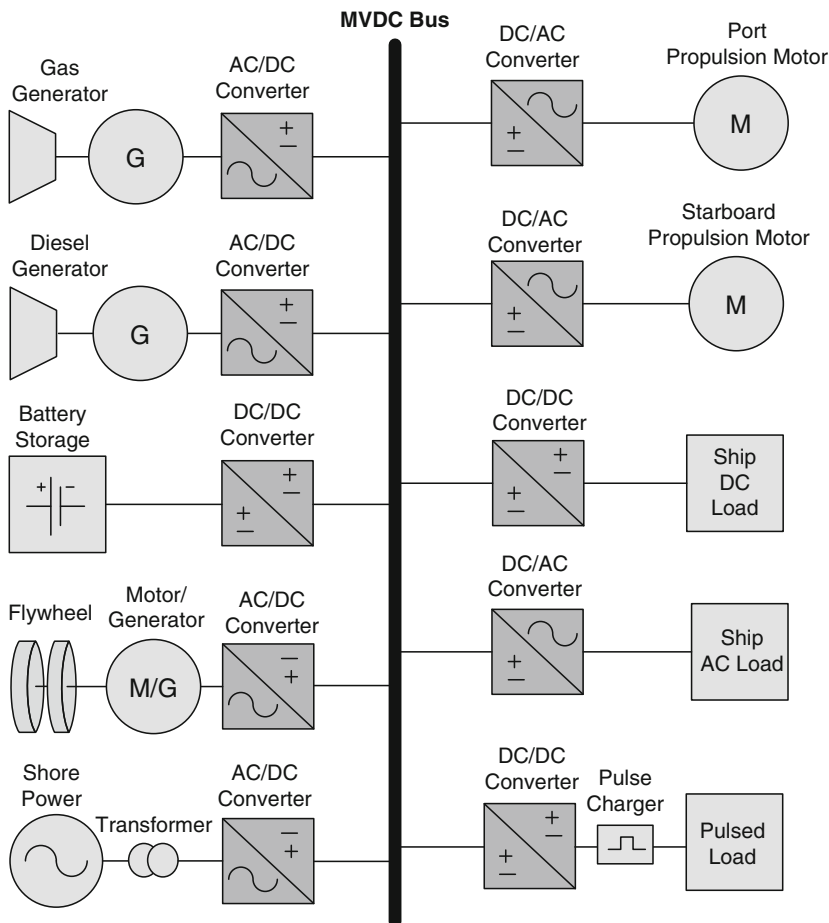
In marine applications, PEBB is an enabler for the medium voltage DC distribution systems (MVDC). A MVDC conceptual system for the ship power is shown in Fig. 11.3. In that system all generators, loads, and storage are connected to the DC bus via power electronics converters, DC–AC, DC–DC, or AC–DC. Such an approach allows limiting fault currents and provides relatively easy connection of different size generators, storage, and loads [7]. Commercially available PEBBs are used in such a MVDC system where each PEBB with built-in intelligence are programmable and self protecting [7, 8].

During the ONR’s PEBB program, ABB has developed a highly compact PEBB that is based on Integrated Gate-Commutated Thyristor (IGCT) technology to serve multiple medium-voltage applications [9]. The maximum output power of the ABB’s water-cooled PEBB in a three-phase configuration is in the range of 9–27 MVA at a system voltage of 3300 VAC. The PEBB has been designed to serve highly demanding medium-voltage drives for various applications including rolling mills and marine [10]. A picture of the 9MVA PEBB is shown in Fig. 11.4 along with its circuit configuration.

Advances in power conversion technologies based on PEBB technology also created market for high-power converters capable of handling medium to high voltage for power system applications, mainly at the power distribution level. Examples of such systems can be found in the literatures [6, 11–13]. This chapter briefly discusses two of the high power electronic system next that is developed with PEBB for power systems.

When the voltage sags in the transmission is caused by faults, the injection of voltage combined with the supply of active power is necessary. The custom power device called dynamic voltage restorer (DVR) can be used to mitigate this power quality issue. Very high reliability is a necessary for high-tech manufacturing plants such as semiconductor plants which can be severely affected by fluctuating voltages [13]. The basic idea of the DVR is to inject a dynamically controlled voltage generated by a forced-commutated converter in series to the bus voltage by means of a booster transformer. The same IGCT-based PEBB as shown in Fig. 11.4 is used by ABB to develop the DVR. In Fig. 11.5 a, diagram of DVR operating principle is shown followed by the picture of a commercial 22 kV, 22.5 kVA PEBB-based DVR [13].

Another application for high power PEBB for power systems can be found in the form of static transfer switch (STS). An STS is a power electronic system that can transfer a customer’s load from one distribution source to another within a subcycle upon power system disturbances [12]. In Fig. 11.6a, a thyristor-based STS is shown. In this configuration, during normal operation, the switch (SW1) is kept closed thus supplying power to the load from Source 1. Upon a power disturbance at Source 1, the conducting solid–state switch (SW1) is turned-off and the alternate switch (SW2) is turned on, so that the load is transferred to Source 2. This transfer takes place in less than a cycle, so that the vast majority of customer



**Fig. 11.3** PEBB-based marine power system

load remain powered. Static transfer switches can operate at both low- and medium-voltage levels.

As discussed in [12], the STS with various system configurations can be developed by using thyristor PEBBs. The AC switch PEBB is designed with the anti-parallel phase controlled thyristors. In addition to thyristors, the PEBB also includes a snubber circuit, varistor, diagnostic circuit, and gate drive unit as shown in Fig. 11.6b [12]. This PEBB-based STS is manufactured by the Silicon Power Corporation, Exton, PA, and can operate from 5 to 38 kV with load current ratings range from 400 to 1200 A [12]. The more recent products developed by the same company utilizes super gate turn-off thyristor (SGTO) based PEBB for the STS that is capable of transferring loads in hundred of microseconds [14].



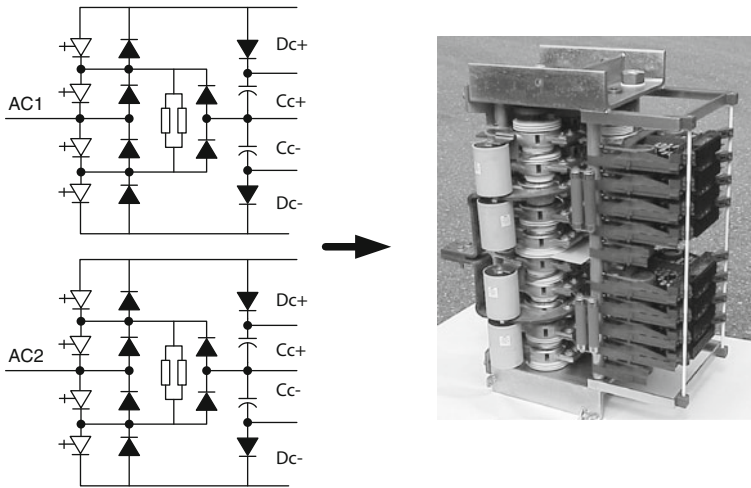


Fig. 11.4 PEBB with IGCT for MVDC applications [13]

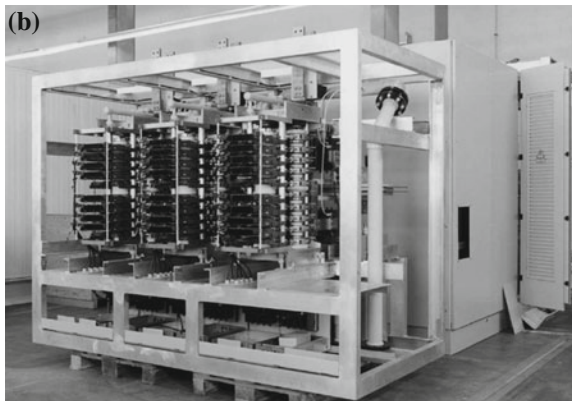
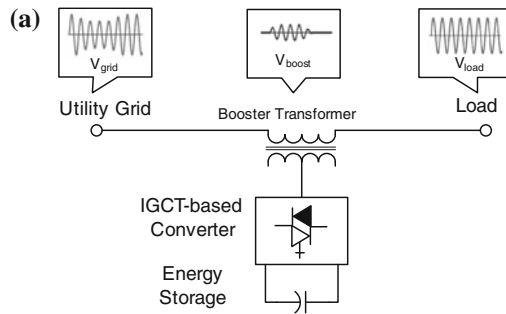


Fig. 11.5 a DVR operating principle, b picture of PEBB-based DVR from ABB [13]

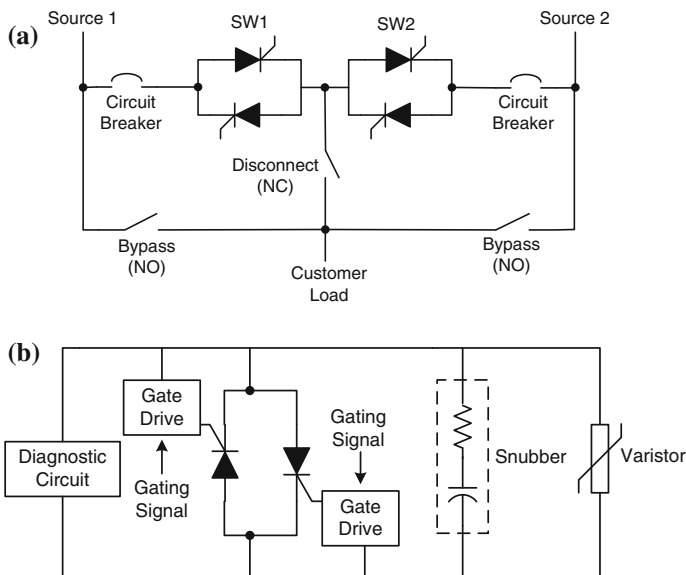


Fig. 11.6 a Thyristor-based STS, b AC switch PEBB circuit

## 11.2.2 Integrated Power Electronics Modules

### 11.2.2.1 Basics of IPEM

The IPEM can be regarded as the modular power electronics part of the PEBB paradigm. The typical power level for the IPEM is lower than that of the PEBB modules [11]. The term IPEM was made popular by the Center for Power Electronics Systems (CPES) in Virginia Tech in order to describe their concept of an integrated system approach for power electronic systems. The underlying goal for IPEM concept is similar to that of PEBB, in which the IPEM is considered as a solution to reduce the cost of power electronics [15]. The advanced packaging of a new generation of devices, innovative circuits, and functions in the form of standard functional building blocks and the integration of these building blocks into application-specific system solutions is the cornerstone of IPEM. The IPEM approach enables dramatic improvement in performance, reliability, and cost-effectiveness of power electronic systems [15].

In last few decades, the power electronic devices have evolved tremendously from their familiar plastic package form toward integrating more components into a module. The module package initially combined discrete switching devices to form a half bridge, then evolved to include H-bridge circuits, three-phase bridges (six-packs), and more recently gate drives and sensors. As noted in [15], for reducing the cost of power electronics, the packaging, control, thermal management, and system integration issues becomes as important as the advancement of

semiconductor devices. IPEMs, such as the Semikron SKAI modules or PM1000 by American Superconductor, have appeared in the market to address these issues [16]. In this approach, the IPEM consists of power electronic devices, DC bus filter capacitors, current and temperature sensors, gate drivers, heat sink, and the digital controller into a single highly optimized module. The digital controller can communicate with a higher level controller through different communication interfaces [16, 17].

The power electronics devices can be configured in different ways inside the IPEM. Some manufacturer products based on half-bridge power modules, where each of the half-bridge can be considered as the PEBB with their own hardware controller and sensors [18]. Also IPEM with three leg, six switches configurations is also available in the market [19, 20]. In any case, it is important to note that the IPEM concept typically beyond just power electronic switches and it also includes integration of sensing and control. The structure of a representative IPEM is shown in Fig. 11.7 [16]. This particular IPEM consists of six IGBT switches arranged in three-phase bridge format. The DC bus filter capacitor, electrical and thermal sensors, auxiliary power supply, and gate drivers are all included inside the IPEM having a common heat sink. A local digital controller can also be included inside IPEM depending on the user's preference for application level of control [16].

When designing power electronics systems, IPEMs allow designers to use a building-block approach with hardware and software, defining the function of each identical block similar to PEBB. The versatility of the module for different applications also facilitates the economics of production. Additionally, the fact that the module integrates many of the subcomponents means that the user is getting a fully integrated and tested package that is already qualified to meet some of the stringent specifications, and therefore highly reliable [16]. Although the modules are highly integrated, if the integration is done using commercial-off-the-shelf products, IPEM lends itself to the development of several standard configurations easily using say different heat sinks, additional output sensors, and a wide selection of switching devices to populate the module [16].

### 11.2.2.2 Advanced Integration Techniques

It has been discussed in various papers by the CPES researchers [15, 21–23], a real paradigm shift in integration technology for power electronics can only evolve from the development of a technology that uses appropriate planar electromagnetic materials in conjunction with metalization for all interconnects, planar layers for dielectrics and magnetics and their interconnects, and stacking of these planar layers in a quasi-3D fashion for high density. It is expected that this low profile construction will have the power processing to conform to the form factor of the applications it drives and will increase the surface-to-volume ratio very favorably for thermal management [22].

To achieve such high level of integration that is compatible with an integrated production, the IPEM-based converters can be partitioned into active IPEMs for

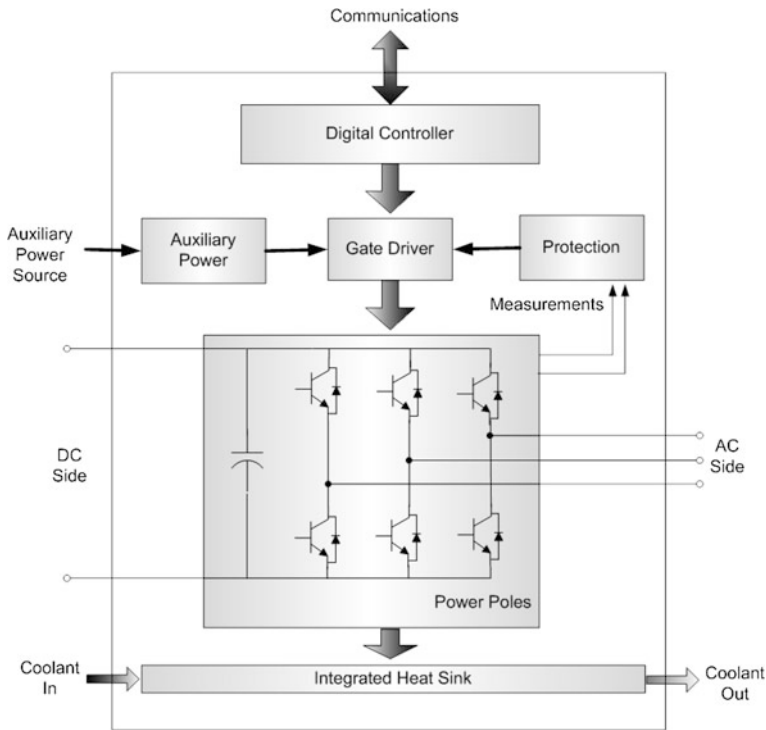
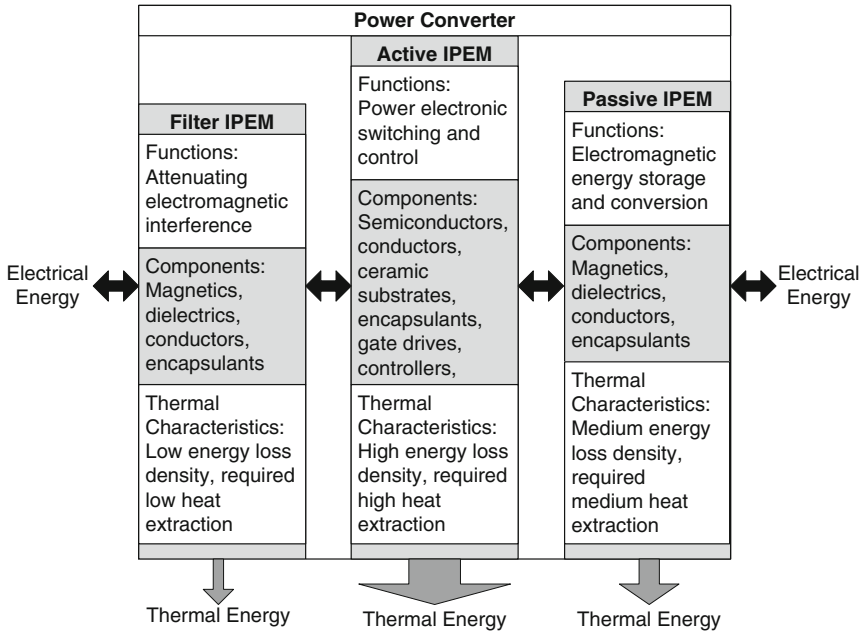


Fig. 11.7 Typical IPED structure [16]

the power switching stages, passive IPEDs for the electromagnetic energy storage and conversion, and filter IPEDs for the electro-magnetic interference (EMI) filters, as shown in Fig. 11.8 [22]. The power processing function and thermal considerations should be taken into considerations in the IPED partitioning. For example, while the energy loss density in the switching devices in active IPED is high, the same is much lower in the passive IPED. Therefore, different thermal design approaches are required for optimum IPED performance [15].

Embedded power technology can be used for the packaging of active IPEDs which are usually comprised of power switches and associated electronics circuitry [21]. It typically consists of three levels, electronic components, a multiple embedded power chip stage, and a base substrate. These three parts are soldered together to build a final module. The electronic circuitry includes a gate driver, control, and protection components. The base substrate provides electrical interconnection and cooling of power chips. The embedded power stage consists of ceramic frame, power chips, isolation dielectrics, and metalized circuit [21].

It is typical to have around 50–60 % of the power converter volume occupied by the power passive components such as inductors, capacitors, and transformers. The development of passive IPED is therefore very important for reducing the size of the power converters. Integrated magnetics technology, planar magnetics, and

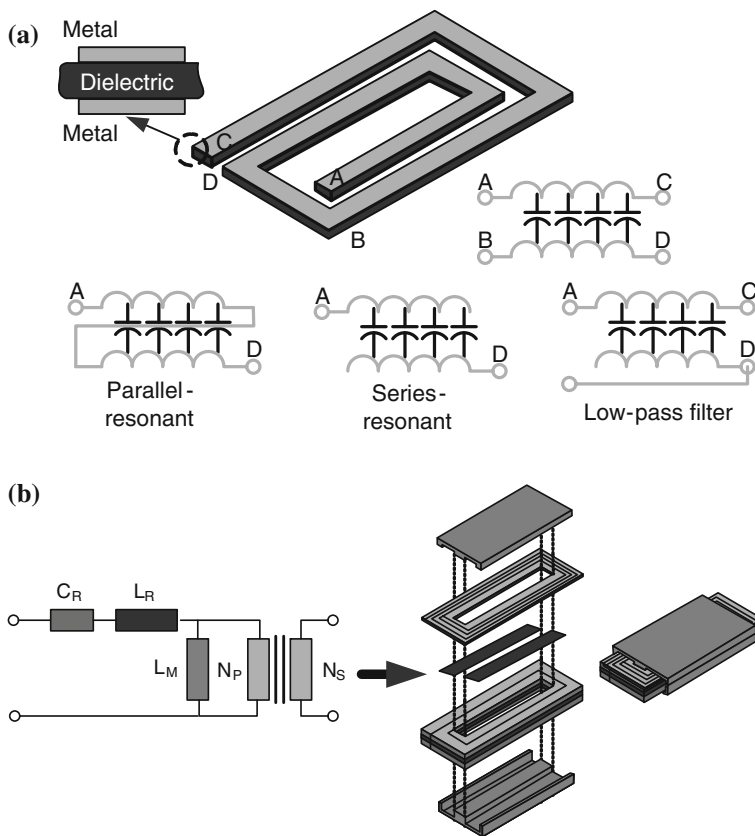


**Fig. 11.8** Partitioning of power converter into active, passive and filter IPEMs

new integration technology are among the approaches developed for passive IPEM [22, 24]. One example of such integration technology for power passives can best be described by first considering a simple bifilar spiral winding as shown in Fig. 11.9a that consists of two windings (A–C and B–D), separated by a dielectric material [21, 22]. This resultant structure creates distributed inductance and capacitance and behaves as an electromagnetically integrated L–C resonant structure for which equivalent circuit characteristics depend on the external connections as shown in Fig. 11.9a. Even more complex integrated structures can be realized by adding more winding layers. This has been demonstrated with an integrated resonant transformer structure (L–L–C–T) as shown in Fig. 11.9b [21, 22, 24].

The integration of an EMI filter into a filter IPEM can be done using the similar concepts as discussed for the passive IPEMs. In this approach, applying the low-pass filter configuration of the planar integrated L–C structure, as illustrated in Fig. 11.9a, an EMI filter can be integrated into a single planar module [15, 23]. But the functions and requirements for the EMI filters is different than the passive IPEMs. Whereas the passive IPEMs need to be designed to reduce losses for thermal limits, the EMI filters need to attenuate, instead of propagate, and electromagnetic energy at switching frequency. Consequently, the high-frequency characteristic is the major concern for EMI filters [23].

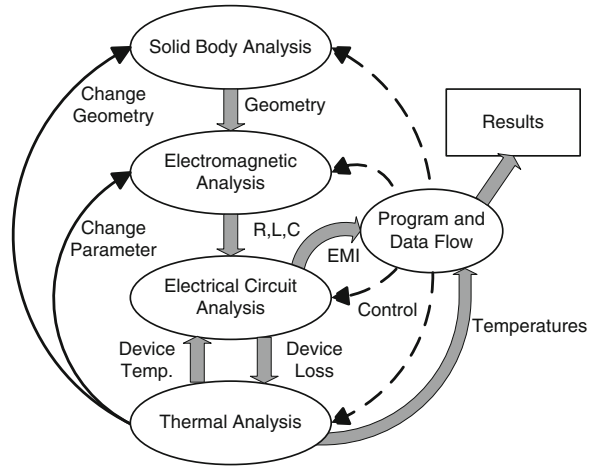
A multidisciplinary approach to optimize materials utilization, packaging, and thermal management is necessary to realize an IPEM design. An example of



**Fig. 11.9** Passive IPER. **a** spiral integrated L-C structure. **b** Exploded view of L-L-C-T integrated resonant transformer [22]. This figure is adapted from Fig. 9 of the paper by Boroyevich [22]

integrated analysis used for design optimization of the active IPER is shown in the flowchart in Fig. 11.10 [21]. It can be observed that the entire analysis procedure for designing an IPER requires integration of various software tools such as mechanical CAD software, electromagnetic analysis software, electrical circuit analysis software, and thermal analysis software. All these analyses enable the designer to evaluate the tradeoffs between the electrical and thermal performance at the component, sub-system, and system levels. The user can then change the relative layout, size, and material of the structural parts, or even select different heat sink sizes or fluid flows, to achieve satisfactory results [21].

**Fig. 11.10** Typical design process for active IPEM [21]

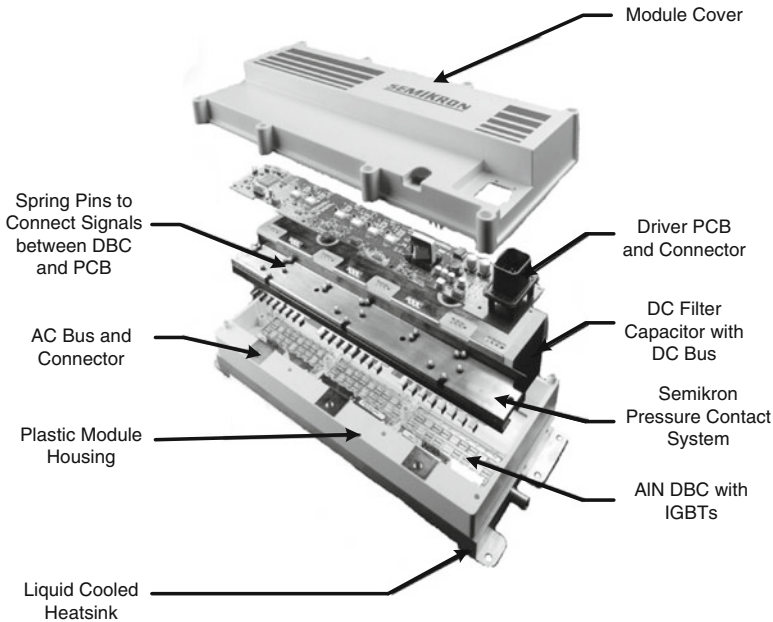


### 11.2.2.3 Commercial Products

The manufacturers often markets their integrated power electronic products using various terms such as Integrated/Intelligent Power Module (IPM) by Semikron or PEBB by American Superconductor, but the construction and functionality of these products are based on the IPEM concept.

Incorporating some of the desirable IPEM characteristics mentioned in the previous sections Semikron developed a first-generation power module for the automotive industry named Semikron Advanced Integration (SKAI) module [25]. The module integrates the power stage with the air/liquid cooled heat sink, gate drivers, controller, and protection logic to provide a ready solution to the automotive suppliers. The block diagram of the SKAI module is very similar to the typical IPEM structure shown in Fig. 11.7.

An exploded view of the first-generation SKAI module is shown in Fig. 11.11. In the figure, a high level of integration is visible inside the SKAI module. Each Direct Bonded Copper (DBC) AlN ceramic substrate contains 600 V NPT or 1200 V trench IGBTs, matching diodes and a positive coefficient thermistor (PTC) [25]. The bus structures (AC and DC) and the populated DBCs are all held together using Semikron's SKiiP technology, a proprietary pressure contact system. Using the SKiiP technology, reliability can be greatly improved as the pressure system eliminates the large solder interfaces typically seen between the DBC and the module base plate [25]. The pressure system is shown to be superior to traditional power modules by a factor of 10 in power cycling tests. The use of AlN substrate also improves reliability compared to typical  $\text{Al}_2\text{O}_3$  substrate. Bus filtering is included with a 1 mF metalized polypropylene film capacitor which is also closely integrated with the bus bars. The magnetoresistive current sensors are included with the AC bus bars which are attached to the control board via flexible cables. The control board interfaces with the DBCs via spring pins and includes



**Fig. 11.11** Semikron SKAI/SKIIP with exploded view [25]

the power supply, gate drives, digital signal processor (DSP), communications hardware, and protection circuitry [25].

Recently, Semikron has developed the second-generation SKAI, named as SKAI 2 with improved design. In this design, new technologies are used to eliminate all solder interfaces [26]. The most significant problem caused by higher temperatures and larger swings of temperature is de-lamination of soldered joints. This problem has been eliminated in the SKAI 2 systems by using sinter technology to join the semiconductor chips to the ceramic substrate. Therefore, the SKAI 2 can operate at higher temperatures with increased reliability. In addition, the temperature related fatigue of the wire bonds has been minimized by changing the geometry of welded joints and the by introduction of novel stress-relief techniques [26]. The thermal and electrical contacts of the power semiconductors are established by pressure contact technology similar to earlier SKAI. The high-voltage SKAI 2 is available as a water-cooled 600/1200 V IGBT system with outputs up to 250 kVA, and has been optimized for use in applications such as full electric or plug-in hybrid cars and electric buses [26].

Another example of commercially available IPEM is American Superconductor's Power Module PM1000 power converter architecture that is modular and can be quickly configured to meet both the hardware and software needs of different applications. The PM1000 includes printed circuit board (PCB) design with state-of-the-art IGBTs, control algorithms and air or liquid cooling [27]. Due to the integration of an embedded controller and an application-specific interface board,



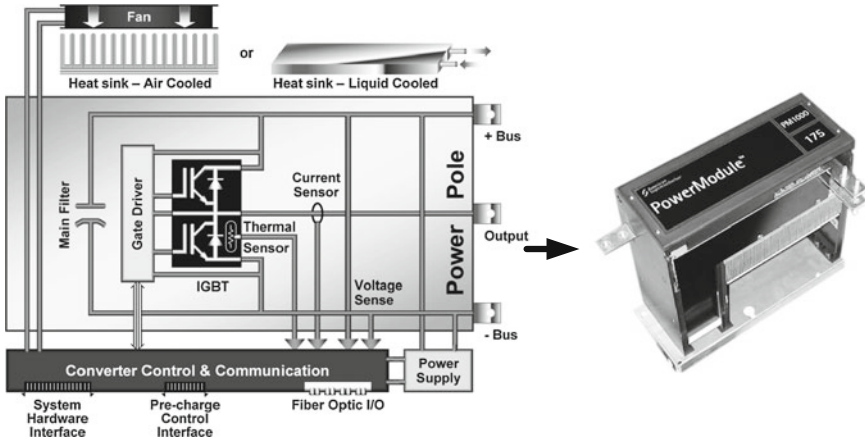


Fig. 11.12 American Superconductor PM1000 power pole

along with the modular and scalable power pole design, this power module is termed as PEBB by the manufacturer [18].

The PM1000 unit is made up with a phase leg, termed as power pole. A modular, configurable power converter is constructed by assembling two to eight power poles (phase legs). A single power pole with all the components is shown in Fig. 11.12. The power module provides its own control power and incorporates a dual DSP controller. These controllers can also be used to incorporate user's control algorithms. The power module can be regarded as a fully self-supportive, high-density power converter which is loaded with one of four standard software applications (active rectifier; DC–DC converter; AC voltage source or motor control). The programming environment utilizes a fiber optic link to communicate between the modules and a graphical user interface (GUI) [18].

Several PM1000 converters can be configured in series and/or in parallel for higher voltage and higher power-rated converters and systems. Also the power module provides user the ability to rapidly configure hardware and software for new applications. User determined parameters allow quick customization of performance and can be changed in real time [28].

### 11.3 Modular Power Electronics for Renewable and Distributed Energy Systems

Previous chapters in this book show that the power electronic converters are essential for converting generated/stored power by renewable and distributed energy into useful power that can be directly interconnected to the utility grid. In this section, we will briefly summarize common power electronics topologies for

each of the renewable and distributed energy systems that can lead to generalized and modular power electronic topologies.

### 11.3.1 Review of Power Electronics Topologies for Renewable and Distributed Energy

A centralized converter-based PV system as shown in Fig. 11.13a is the most common type of PV installation for the sizes typically over 50–100 kW. PV modules are connected in series and parallel to get the required voltage and current and then the output of the PV array is connected across a filter capacitor. The output of the capacitor connects to the input of a voltage source three-phase inverter. A three-phase transformer is then used to connect the inverter to the utility providing voltage boost and galvanic isolation [29, 30].

To avoid the bulky low-frequency transformers, which are regarded as poor components mainly due to their relatively large size and low efficiency, the multiple-stage conversion systems are widely used in residential scale PV

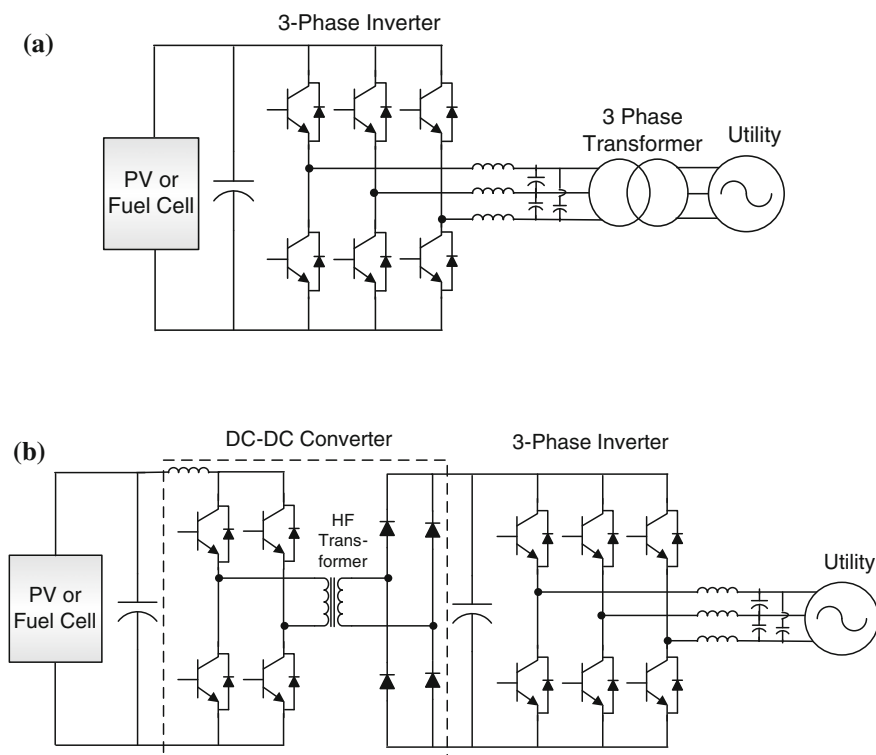


Fig. 11.13 PV/fuel cell power converters a single stage, b dual stage

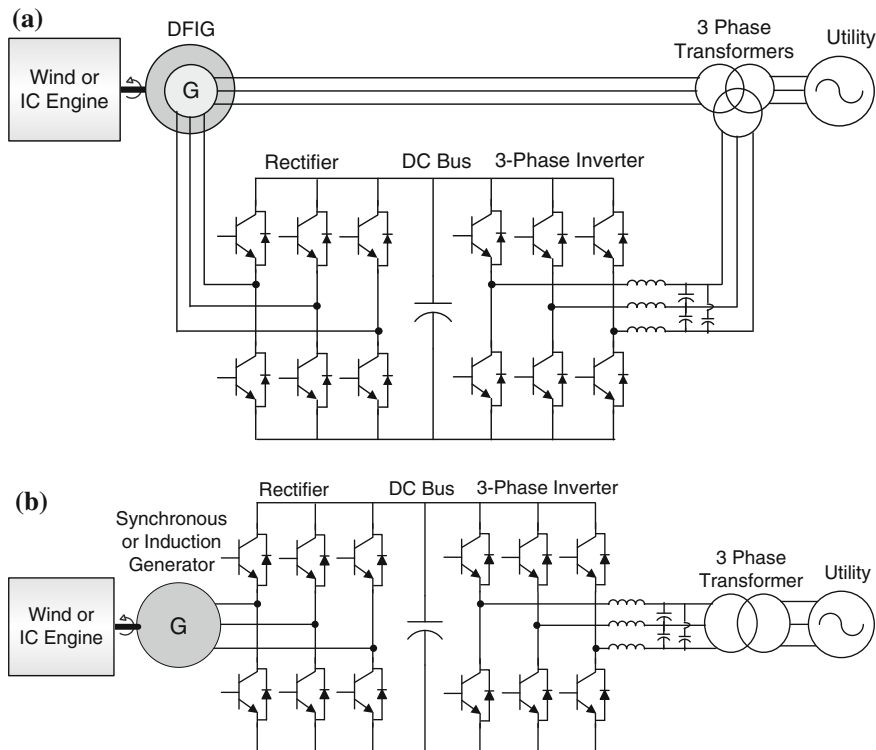
applications. The most common topology consists of a DC–AC grid-connected voltage source inverter along with a PV connected DC–DC converter. A simple design for a multiple-stage PV inverter is shown in Fig. 11.13b, which utilizes a high frequency transformer included in the DC–DC converter [30]. In general, the maximum power point tracking (MPPT) and voltage boost are done by the DC–DC converter controller and the power flow control to the utility as well as the sinusoidal unity power factor current injection to the utility are obtained by the DC–AC inverter controller [30].

Power generated by the fuel cell is also DC, similar to a PV system, therefore the power conditioning systems, including inverters are required in order to supply normal customer load demand or send electricity into the grid. The simplest form of power electronics for the fuel cell can be single stage DC–AC inverter or can be of multiple stages where the DC–DC inverter precedes the DC–AC inverter similar to the configurations shown in Fig. 11.13 [31]. The DC–DC converter performs two functions, one is the DC isolation for the inverter, and the second is to produce sufficient voltage for the inverter input, so that the required magnitude of the AC voltage can be produced [31].

The modern wind power systems can fundamentally be divided into three categories: the systems without power electronics, the systems with partially rated power electronics, and the systems with full-scale power electronics for interfacing wind turbines [30].

For the partially rated power electronics based wind system, a wound rotor induction generator, known as doubly fed induction generator (DFIG), is used as the electrical generator. The power electronics required for the DFIG consists of AC–DC–AC converters also known as back-to-back converters. The stator winding is connected directly to the 60 Hz grid while the rotor is fed at a variable frequency through the AC–DC–AC converter [32, 33] as shown in Fig. 11.14a. This design does allow the wind turbine to have some amount of variable speed operation. If the generator is running super synchronously, the electrical power is delivered through both the rotor and the stator. If the generator is running sub-synchronously the electrical power is delivered into the rotor from the grid. This partially rated power electronics provides various advantages such as lowering the safety margin of gear, having reactive power compensation/production and capturing more energy from the wind. This arrangement allows the generator stator winding to be undersized by about 25 % with the power electronics making up the power difference from the rotor power [16, 30].

Full-scale power electronics based wind system uses conventional or permanent magnet synchronous generator or induction generator to convert the wind turbine power to a variable voltage, variable frequency output that varies with wind speed. The AC–DC–AC converter or back-to-back rectifier–inverter system, as shown in Fig. 11.14b, are then used to convert the full-rated output of the machine to 60 Hz AC. This output is then boosted using a transformer to voltage levels required by the utility's AC system power. Unlike the partially rated power electronics based system; this system requires power converters rated to handle the whole wind generator output. The design allows the wind turbine to operate in a variable speed



**Fig. 11.14** Wind/IC engine power system with **a** partially-rated power converters, **b** full-scale power converters

mode which can allow more of the energy of the wind to be captured. Though diode bridges are often used as the rectifiers, due to cost considerations, self-commutated active rectifiers provide more flexible control [30].

The power electronics systems for variable speed IC engines are similar to the wind energy systems. Typically, most IC engines are interconnected to the utility through a fixed speed synchronous generator that has protective relays. In automotive application, it has been shown that the torque curve of a diesel engine is optimized for high power versus speed performance over the range 1000–3600 rpm. But for power generation and direct utility connection, the generator speed must be constant for 60 Hz systems, depending on the number of generator poles. Therefore, conventional IC engines do not utilize the full speed range of the engine when the electrical load changes. Using a power electronics interface with an IC engine offers the advantage of having variable speed operation of the IC engine which in turn optimizes fuel usage for varying loads [34].

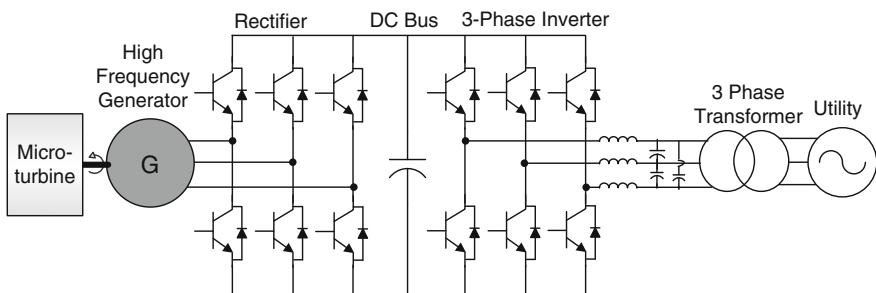
The variable speed IC engine-generator configuration can be of different types depending on the generator. For synchronous generator or cage induction generator, variable voltage, variable frequency output is converted into the 60 Hz utility

compatible AC by using back-to-back rectifier–inverter configurations, similar to Fig. 11.14b [34]. Also the DFIGs and associated power electronics can also be used similar to Fig. 11.14a [35].

The shaft construction defines many important characteristics of the microturbine that influence the required power electronics and control system. There are mainly two types of shaft construction, single shaft and split shaft [36]. In a high-speed single-shaft design, the compressor and turbine are mounted on the same shaft and the alternator rotates at speeds of 90,000–120,000 revolutions per minute (rpm). The microturbine drives a high-frequency generator that may be either synchronous or asynchronous type [37]. The split-shaft microturbines are very different in terms of design and electrical power output. This system typically employs the two-pole generator sets running at 3600 rpm. Although the manufacturer claims that this type of microturbine does not need power electronics, it requires synchronizing equipment and relays for connection to the utility grid [36].

The most common power converter topology that is used for connecting high-speed microturbines to the grid is the AC–DC–AC or back-to-back rectifier–inverter systems [37]. The high-frequency power from the generator must be converted to DC first either by using diode-bridge passive rectifier or by self-commutated active rectifier. The DC-link is then used to construct three-phase voltages at 60 Hz using DC–AC inverter. Figure 11.15 shows a microturbine generator feeding power to the utility by AC–DC–AC converters.

The main shortcomings of the AC–DC–AC conversion unit are large physical dimensions, high weight, and excessive volume/foot-print of the DC-link component, i.e., the DC capacitor (and if applicable the inductor) and the low reliability of the DC capacitor. To overcome these problems, a direct AC–AC converter such as cycloconverter or matrix converter can be used to connect microturbine generator to the grid [38]. The disadvantages of these converters are that they have higher number of switches compared to the DC-link approach, and they do not have a DC or AC link to store energy. Without energy storage in the converter, any fluctuations at either side of the converter directly influences the other side. They are not yet commercial due to cost and technological issues associated with them [37].



**Fig. 11.15** Microturbine power converters

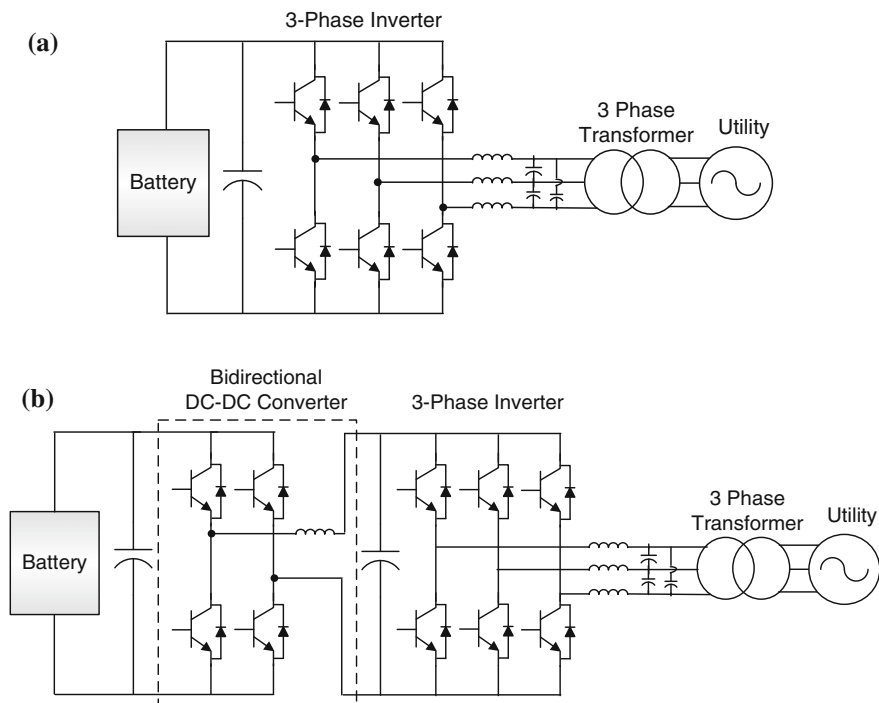


Fig. 11.16 Battery energy storage power converters **a** single stage, **b** dual stage

The battery energy storage systems (BESS) produce DC power that must be converted to AC power to connect to the utility. The individual battery cells are generally connected in different configurations in series and parallel to achieve the required voltage and current outputs. The most unique aspect to power electronics for BESS is that they must be bidirectional, that is both taking power (during charging) and providing power (during discharge) from/to the grid. Unlike PV and fuel cell inverters; however, BESS inverters are not expected to consider the peak power operations. They only provide the power level demanded by the system that can be sustained by the battery [36].

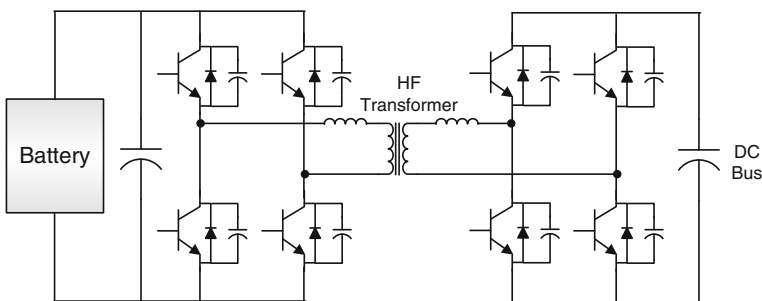
The simplest form of battery system configuration, as shown in Fig. 11.16a, consists of a BESS followed by DC–AC converter. The DC output of the battery system is connected across a filter capacitor to limit the harmonic currents in the battery. The output of the capacitor connects to a voltage-source inverter. Such converter is inherently bidirectional so the power can flow in/out of the battery. If the isolation or a high-voltage conversion ratio is required, a line-frequency transformer is usually integrated into the system [39].

The most common two-stage topology for the BESS consists of a DC–AC inverter with a bidirectional DC–DC converter. A simple design for a two-stage power electronics topology is shown in Fig. 11.16b. In that figure, a full-bridge DC–DC converter is used that can operate with any voltage and current polarity [40].

All the BESS power electronics topologies discussed so far has no isolation present in them. For utility connection, therefore, a line-frequency transformer is used for galvanic isolation. To avoid the bulky line-frequency transformers, several bidirectional isolated DC–DC converter topologies have been developed [41, 42]. One such DC–DC topology is given in Fig. 11.17 that can galvanically isolate the output terminals from the input terminals, and can step up and down its output voltage by using a high-frequency transformer [41]

Flywheels are getting popular as energy storage due to the simplicity of storing kinetic energy in a spinning mass. Conversion from kinetic to electric energy is accomplished by electromechanical machines. The key is to match the decreasing speed of the flywheel during discharge and the increasing speed during charging with a fixed frequency electrical system [36]. The primary purpose of the power electronics system is to couple the fixed-frequency AC-electrical grid with the variable-speed flywheel as well as to invert, regulate, and provide the proper wave form for providing power to the grid. By reversing the process, the power electronics are also able to draw power from the AC utility connection and drive the flywheel motor to spin up and recharge the flywheel [16].

The most common power electronics topology for the flywheel energy storage consists of a DC–AC grid-connected converter and a bidirectional AC–DC flywheel-connected converter, having a common DC bus [43]. During discharge, the flywheel converter works as the rectifier and the grid converter works as the inverter to send stored power to the utility grid. During charging, the rectification and inversion processes are reversed and the power flows from the utility grid to the flywheel. Depending on the utility connection, the utility converter can be of single phase or three phase. A simple design for a back-to-back converter topology is shown in Fig. 11.18. Galvanic isolation is provided by the three-phase transformer connected to the utility converter.



**Fig. 11.17** Isolated bidirectional converter with battery storage

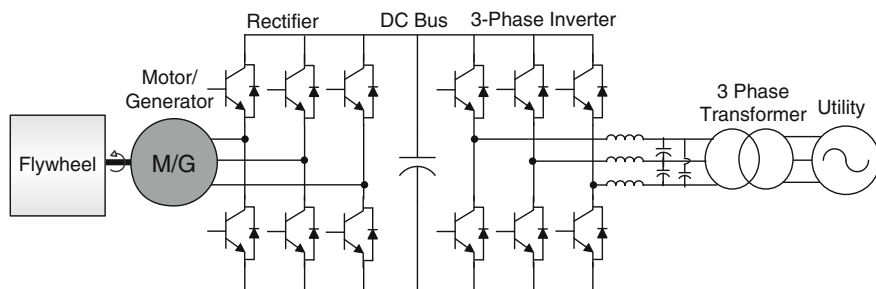


Fig. 11.18 Flywheel energy storage power converters

### 11.3.2 Topologies for Modular Power Converters

From the discussions presented in the previous section, it can be observed that the most generalized power electronics topology for photovoltaic (PV) and fuel cell systems is the isolated DC–DC converter cascaded with DC–AC inverter.

The wind and microturbine systems generate variable frequency AC output which needs to be converted into 60 Hz AC for utility connection. The use of back-to-back converter is the most efficient way to utilize the generated power from wind and microturbine systems. Typically, most internal combustion (IC) engines are interconnected to the utility through a fixed speed synchronous generator, but as discussed before, using a back-to-back voltage source converter with an IC engine offers the advantage of having variable speed operation which in turn optimizes fuel usage for varying loads.

Depending on the type of storage, different bidirectional power electronics converters are required for utility connection. For BESS, a bidirectional DC–DC converter followed by a DC–AC inverter is the most general choice, whereas for the flywheel system a back-to-back converter can be utilized for utility connection.

A diagram showing the use of modular power electronics with different renewable and distributed energy systems is given in Fig. 11.19. In this figure, IPEMs are used. Each of the IPEMs includes six IGBTs along with gate drivers and sensors as discussed in the previous subsection. In some cases, additional hardware components are required for designing the converter. Also, three power interfaces are shown in Fig. 11.19 that are essential for the operation of the complete system. The source interface (I1) for such systems typically consists of EMI filters and in some cases a boost inductor for DC–DC converters. The utility interface (I3) includes the output filters and in some cases the line frequency transformer. Additional DC bus filter may also be required in the DC bus interface (I2) if the capacitor inside the IPEM is not sufficient for the application [16, 17].

For the isolated DC–DC converters with PV and fuel cell systems, the IPEM-based solution with three-phase bridges is not optimal, as one-third of the switches are not used in that configuration. However, the IPEMs offer cost savings due to the commonality of the hardware and short development time for the system [16].



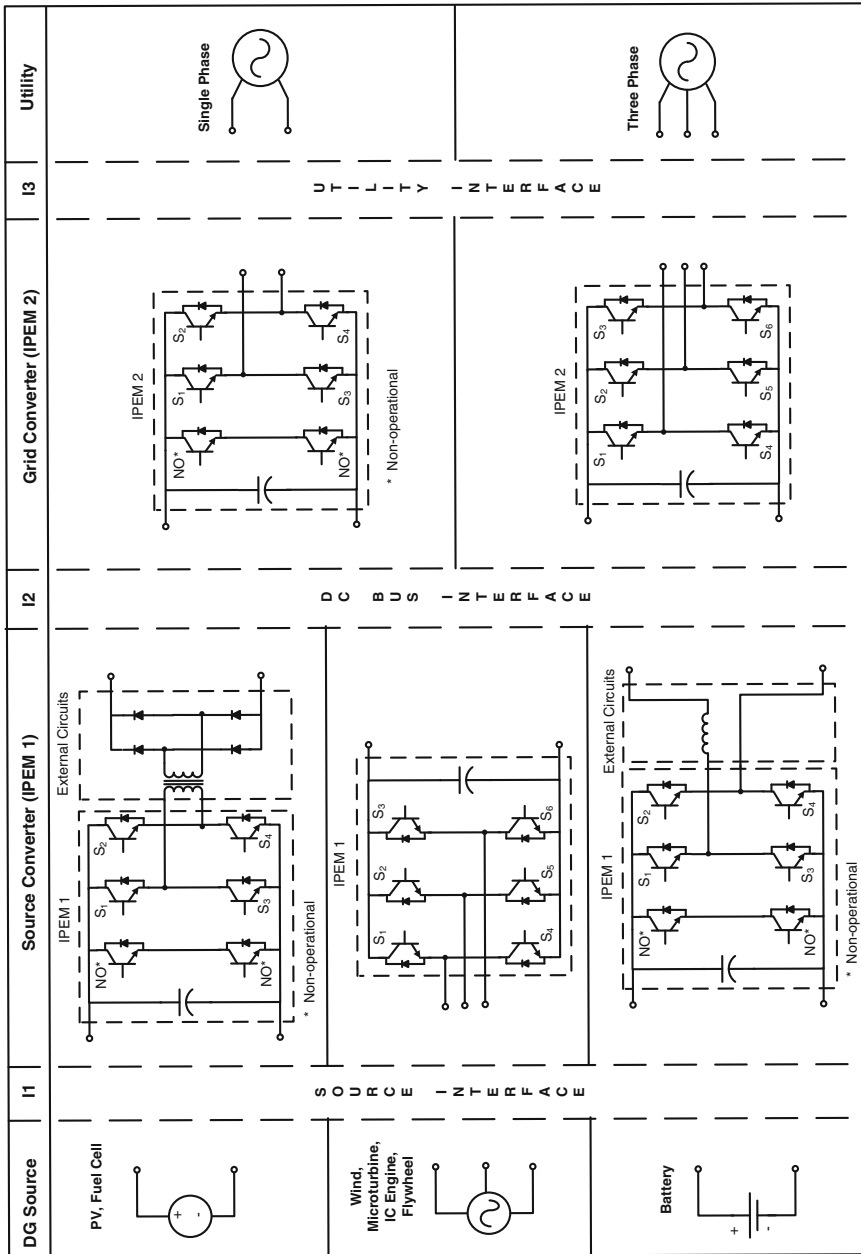


Fig. 11.19 Generalized IPEM-based power electronics for different renewable and distributed energy systems

For the power electronics topologies with wind, microturbines, IC engine and flywheel systems, the high-frequency isolation is not feasible. Hence, the line-frequency transformers are often included in utility interface for galvanic isolation [16]. The power electronics for the BESS consists of a full-bridge DC–DC converter can operate with any voltage and current polarity. In this topology, a line-frequency transformer is included for galvanic isolation [16].

The most common power electronics part of each of the renewable and distributed energy systems is the utility connected inverter. Depending on utility connection type, this inverter can be of single phase or three phase. As can be observed from Fig. 11.19, the single-phase inverter uses only four IGBT switches out of six available ones, hence not optimized. Again the IPEMs offer cost savings due to the commonality of the hardware [16].

### ***11.3.3 Controllers for Modular Power Converters***

Use of dual converters for the renewable and distributed energy systems as shown in Fig. 11.19 provides the flexibility of designing different control objectives. The function of the source converter (the converter directly connected to the renewable or distributed energy sources) can be different depending on the type of generator. The function of the grid converter, connected directly to the grid, is typically same for all the sources and storages. They are used to maintain active power and in some cases reactive power to the grid.

In PV systems, the source DC–DC converter provides galvanic isolation between the PV string and the grid; the PV strings can be easily system grounded and compatible with the National Electric Code (NEC) requirements. This converter is often controlled to achieve MPPT from the PV [29]. Over the years, many MPPT methods have been developed and implemented. These methods vary in complexity, required sensors, convergence speed, cost, range of effectiveness, implementation hardware, popularity, etc., as discussed in the PV chapter of this book.

In wind systems, depending on the type of generators (permanent magnet, synchronous, induction, or doubly fed induction) and type of power electronics (partially rated or full scale) various control objectives can be achieved for the source converter. For example, in a wind system with full-scale power electronics, the source converter can be used for controlling generator speed, current, and flux as well as to maintain the DC bus voltage [44]. Also the source converter can generate programmable excitation for the induction generator and can help in improving quality of the generator current waveform [44].

For the microturbine system, the source converter control loop can work as the DC bus voltage regulator. A reference DC bus voltage is set and the rectifier is controlled to follow the set-point [45]. An additional control loop can be utilized to control the fuel governor's response with respect to generator speed and temperature. The total efficiency of the microturbine system is optimal at a certain speed

and temperature [36]. The purpose of the control system is to produce the demanded power while maintaining the optimal speed and temperature characteristics [36].

The isolated DC–DC converter as shown in Fig. 11.19 is used to regulate DC bus voltage of the fuel cell power conversion system. When the active power reference is increased, drawing more power from the fuel cell with constant hydrogen flow rate reduces the fuel cell output voltage, which in turn decreases the DC bus voltage [46]. The DC voltage regulator tries to maintain the constant DC voltage by changing the switching pattern of the single-phase high-frequency inverter embedded in the DC–DC converter. For the steady-state power adjustment, power changes must be followed by a proper hydrogen flow rate control using a fuel flow controller. It is important to remember that the response of the fuel cell is much slower than electric load response, especially when the load power changes abruptly. The chemical reaction of the fuel cell cannot keep up with the fast changes of the load demand. The use of power electronics converters mitigates this problem to some extent. Employing high-power density ultracapacitors and/or battery storage system is required in some cases, especially when the fuel cell is used for supplying power in the islanded mode to some local loads [31].

In the IC engine system, the AC–DC converter connected to the generator maintains the DC bus voltage. In addition, a speed control loop for an IC engine operates by changing the throttle angle, so that the engine runs in its optimized fuel usage point for varying loads [47]. Whenever there is a change in the output power supplied by the inverter, that power comes from the DC bus and changes the DC bus voltage. The DC bus voltage regulator tries to maintain that voltage fluctuation by changing switching of the controlled rectifier. The input power for the rectifier comes from the generator, which is powered by the IC engine; therefore, any fluctuations in the power demand also causes change in the speed of the generator, and the IC engine may run outside its optimized fuel usage region due to the speed variation. The speed control loop maintains the generator speed based on the load demand, DC bus voltage and current speed to define the power-speed characteristics of the IC engine–generator system, so that the fuel usage is optimum [16].

There are two different modes of operation for the battery BESS connected to the utility as the BESS can either send power to the utility by discharging or it can receive power from the utility to charge itself. The operation mode controller is typically required to decide the charging/discharging operation for the BESS. The control goals for power electronic systems are different for charging and discharging modes. When the mode of operation for the BESS is charging, the power flows from the utility to the battery system through power electronic converters. The DC–DC source converter controller can be used to control the charging current, so that battery charges within its safe operating limits. The DC–AC converter works as the controlled rectifier and the controller maintains the DC bus voltage at a preset value. During discharge mode, the power flows from the BESS to the utility. In this mode, the DC–DC converter maintains the DC bus voltage for

**Table 11.1** Typical control functions with IPEM-based power electronics for distributed energy systems

Energy systems	Control functions		
	Source converter (IPEM 1)	Grid converter (IPEM 2)	Additional
PV	MPPT	Power flow to grid	NA
Wind	Generator speed, current, flux	Power flow to grid	NA
Microturbines	DC bus voltage	Power flow to grid	Governor response
Fuel Cell	DC bus voltage	Power flow to grid	Fuel flow
IC engine	DC bus voltage	Power flow to grid	Fuel Usage
BESS-charge	Charging current	DC bus voltage	Operational mode
BESS-discharge	DC bus voltage	Power flow to grid	Operational mode
Flywheel	Generator flux, DC bus voltage	Power flow to grid	NA

the inverter, and the grid connected inverter controls the active and reactive power flow [16].

For flywheel energy storage with induction motor/generator, the bidirectional source converter maintains the DC bus voltage. In addition, the generator flux can be controlled using the source converter [48].

There are two basic control modes for the grid converters: constant current control and constant power control. It is debatable whether an inverter should be allowed to regulate voltage during grid-connected operation. The current IEEE 1547 Standard does not allow distributed generation to actively regulate voltage, while some people in the energy industry suggest that the voltage regulation may have some positive impact on the grid [49]. In the constant current control, the current injected to the utility grid is controlled based on a predefined current reference. For the constant power control, the active and reactive power output of the inverter is controlled. In some cases, the reactive power reference could be a power factor reference. In a variation of the constant power control, instead of using the active power reference, DC bus voltage can be regulated [49]. Also in some advanced applications, the grid converter can be controlled to regulate the voltage at the point of common coupling [50].

In Table 11.1, some typical control functions are shown for different distributed energy systems. These control functions can be implemented for the modular power converters by either using the local embedded controller or by utilizing a higher level controller with fast communications.

## 11.4 Standardization of Interfaces

In traditional centralized digitally controlled power electronics systems, construction, debugging, and maintenance of the power converters are complicated and difficult due to lack of standardization and modularization, and also because of the strong dependence of control design on system hardware. As discussed in

earlier sections, the concept of PEBB provides a way to hardware standardization of power electronics systems. Based on PEBB and IPEM concept, the new integrated devices are feasible for renewable and distributed energy applications. In addition to that, standardization in power electronics requires standardizing the power flow and signal distribution network, which in turn allows a distributed controller approach. The standardization of communication interface permits division of power electronics system into flexible, easy to use, multifunctional modules or building blocks, which can significantly ease the task of system integration. By using control software that is functionally divided into hierarchical levels and by standardizing interfaces between levels, the application software becomes independent of the hardware specifications of power stage and products from different vendors can communicate and work with each other [51]. Furthermore, if both sides of an interface support device self-identification and system resources assignment, then the so-called plug-and-play implementation is feasible for future power electronic systems [51].

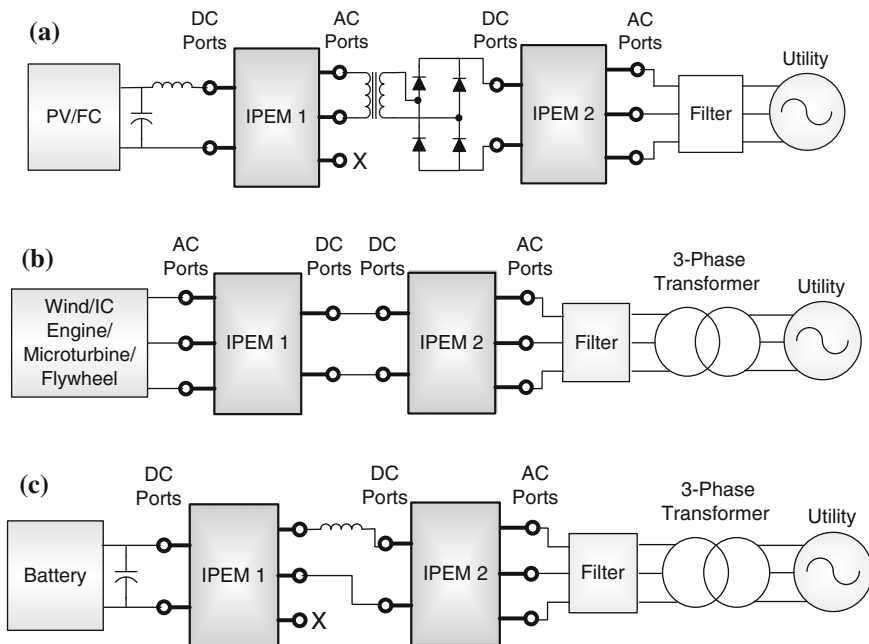
### ***11.4.1 Power Interfaces***

From the generalized IPEM-based power electronics for different distributed energy systems, as shown in Fig. 11.20, following characteristics should be made available for designing the standardized power interfaces:

- Each IPEM should have two ports named DC port and AC port. In case of isolated DC–DC converter, the AC port of IPEM1 should generate high frequency square-wave AC.
- Both ports for the IPEM must be bidirectional and should be able to work either as buck or as boost converting mode. This will be inherently available for a IPEM with three-phase bridge power electronic devices as shown in Fig. 11.19.
- Device ratings for the IPEMs are limited by manufacturer datasheet. Therefore for high power applications, paralleling of the converters may be necessary.
- The wiring will be based on the operational power.
- Filters, transformers, and other external circuits design will be dependent on the operational power. It is always possible to design the circuit for higher power and use it for low power applications, but obvious drawbacks will be inefficient design and higher cost.
- Combining multiple sources and/or storages can be done using the DC bus. In such case, a single IPEM can be used for DC–AC inversion.

### ***11.4.2 Control and Communication Interfaces***

Control of today's medium and high-power converters is primarily based on a centralized digital controller that has several drawbacks, including the large



**Fig. 11.20** Block diagrams of power interfaces for **a** DC sources; **b** variable frequency AC sources and storages; **c** DC storage

number of point-to-point signal links that connect power stage and sensors on one side with the centralized controller to the other [52]. Additionally, the signals in typical power electronic systems are of different formats and are transmitted through a variety of physical media. This makes the standardization and modularization of such systems and subsystems very difficult [52]. The standardization in power electronics requires standardizing control, signal distribution network, and communication interface, which in turn allows for an open-architecture distributed controller partitioned into flexible modules or building blocks, similar to the discussion presented under the PEBB section of this chapter.

For the modular design of the power electronics in renewable and distributed energy applications, the control of the power electronic system can be functionally divided into hierarchical architecture as shown in Fig. 11.21. The controller that is the inherent part of the IPEM is defined as local controller. In the literature it is often called as hardware manager [52, 53]. The higher level controller is defined as application manager. This is the controller typically external to the IPEM that establishes the functions that are the main mission of the power electronics system. In order to achieve the goals required at the system control level, some standard control functions must be performed inside applications manager [16]. If more than one application is combined, for example in a hybrid system with different distributed energy sources/storages, a higher level system manager is required that

coordinates the operation as well as maintains the system data bus for communicating with the individual application managers [16].

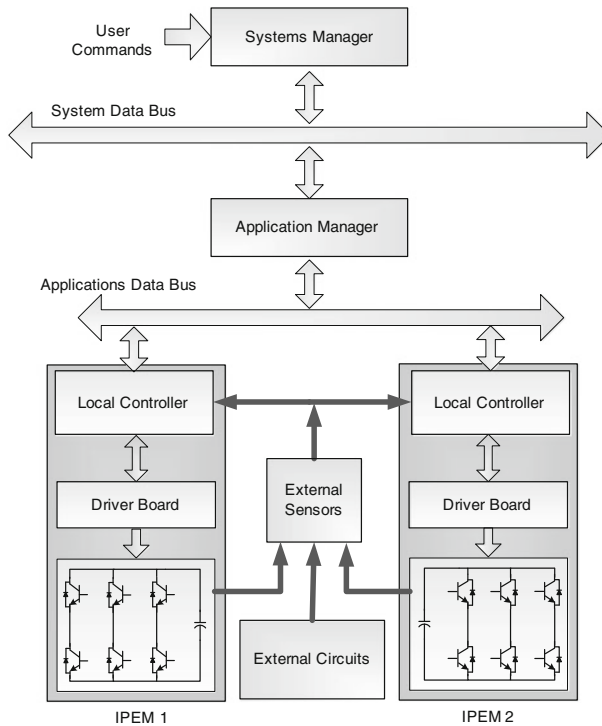
The local controller is designed to provide control and communication functions for the IPEM it is associated with. It is designed to support all module specific control tasks thus making the module specific functions, such as soft switching, invisible to the application manager. From a generalized evaluation of different converters, it can be found that there is a set of common functions shared by all of them and also these common functions are related to the lower levels [53]. For renewable and distributed energy applications, the PWM generation at the lower level always relates to either voltage or current control for the particular converter. The IPEMs provide enough calculation capabilities due to the built-in digital controllers, so it is easier to carry out the voltage and current control inside the local controller along with the PWM generation for the switches to make the system more modularize [16].

In addition, the local controller can be used for over-current protection and indication; current, voltage, and temperature sensing with A/D conversion; and communication of PWM, status, and measurements. Some IPEM manufacturer also offers the IPEM without the built-in digital controller, which in turn provides the user some flexibility of choosing suitable controller hardware depending on the application requirements. In such cases, it is required to define the interfaces for the local controller to maintain the modularity and standardization for the IPEM system [16].

The application manager is the external controller that operates to establish the functions that are the main mission of the power electronic systems [16]. For example, in microturbine applications, the power circuit consists of two IPEMs connected in back-to-back formation having a common DC bus. The application manager operates the individual local controllers in such a way that the source converter works for DC bus voltage control and the grid converter controls the power flow to the grid. In order to achieve these goals required at the system control level, some standard control functions such as converter functionality selection, voltage/current reference generation etc., must be performed in the application manager. The application manager controls the local controller through standard interfaces. It also controls the communications data bus for the local controllers.

The top level system manager performs the controls tasks at the system level, such as responding to users' commands, coordinating performances between different applications, and monitoring system execution [16]. The system manager can also be utilized to determine the mode of operation for each of the renewable and distributed energy systems individually, so that the issues related to islanding and energy cost optimization can be resolved.

The input–output signals and control interfaces for a typical IPEM hierarchical controller are summarized in Table 11.2. For this particular IPEM, it is assumed that the local digital controller is outside the power electronics module. Furthermore, it is assumed that the outputs of the external sensors (ES) are connected directly to the local controller's (LC's) analog input ports. The connection between




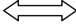
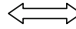
**Fig. 11.21** Hierarchical division of control functionalities for IPEMs

the LC and the applications manager is assumed to follow typical communication protocols such as Controller Area Network (CAN) or asynchronous serial [16]. But different open architecture communications protocols can also be used depending on the application requirements. Both the system manager and application manager is developed in CPU and named as external controllers (EC) in the table. All the measurement signals are routed to the external controllers via local controller.

The communication between the IPEM and local controller is obtained through a D-sub 25 pin connector with ribbon cable. If the controller is inside the IPEM, this communication interface is not available to the user. From [53], it can be observed that the bandwidth of the analog type signals depends on number of signals, switching frequency, and number of bits representing the duty cycle. Analog signals that are not directly related to the switching frequency may require a lower bandwidth. On the other hand, the channel bandwidth requirement for the digital type signal depends on number of signals, ratio of sampling period to transmission time, sampling frequency, and number of bits representing the variables. In most of the renewable and distributed energy applications, the CAN communication is sufficient for data transmission as it can support up to 1 Mb/s bit



**Table 11.2** Input–output signals and control interfaces for hierarchical controller

IPEM	Interface 1	Local Controller (LC)	Interface 2	External Controllers (EC) and External Sensors (ES)
<b>Inputs:</b> <ul style="list-style-type: none"> <li>• PWM signals</li> <li>• Enabling signals</li> </ul> <b>Outputs:</b> <ul style="list-style-type: none"> <li>• dc bus voltage</li> <li>• Phase currents</li> <li>• Heat sink temperature</li> <li>• Fault signals                             <ol style="list-style-type: none"> <li>1. Internal switch short circuit</li> <li>2. Phase over-current</li> <li>3. dc bus over-voltage</li> <li>4. Power supply under-voltage</li> <li>5. Over-temperature at heat sink</li> </ol> </li> </ul>	 D-sub 25 pin connector with ribbon cable	<b>Inputs:</b> <ul style="list-style-type: none"> <li>• Phase currents</li> <li>• Phase voltages</li> <li>• dc bus voltage</li> <li>• Heat sink temperature</li> <li>• Relay sense signals</li> <li>• Encoder inputs</li> <li>• Zero-crossing detection</li> <li>• Fault signals from IPEM</li> <li>• System operation mode signals from EC</li> <li>• Protection signals from EC</li> </ul> <b>Outputs:</b> <ul style="list-style-type: none"> <li>• Gate drive PWM signals</li> <li>• Communication signals for IPEM</li> <li>• Enabling signals to IPEM</li> <li>• PWM status signals to EC</li> <li>• Fault signals to EC</li> </ul>	 Measurement signals from sensors to analog input of digital controller   Control signals from external controller by CAN or asynchronous serial	<b>Inputs:</b> <ul style="list-style-type: none"> <li>• Measurement signals from LC</li> <li>• Measurement signals from ES</li> <li>• Encoder signals</li> <li>• Fault signals</li> <li>• User Inputs</li> <li>• PWM status signals</li> </ul> <b>Outputs:</b> <ul style="list-style-type: none"> <li>• Reference voltage and current signals to LC</li> <li>• Communication signals for external data bus</li> <li>• Relay contactor signals</li> <li>• Protection signals to LC</li> <li>• System operation mode signals to LC</li> </ul>

rate at network lengths below 40 m. But using IPEMs for other type of applications such as active filtering may require new communication protocols as described in [52, 53].

## 11.5 Example of Modular Power Electronics Based Integration

Based on the discussions in this chapter, some simplified case studies will show next how IPEM-based modular power electronics and control can be used to integrate renewable and distributed energy sources to the utility grid.

### 11.5.1 PV Integration Example

An IPEM-based power electronics topology for the PV application includes the DC–DC boost converter with embedded high-frequency transformer, along with the DC–AC inverter. In general, the MPPT and voltage boost are done by the DC–DC converter controller. The power flow control to the utility and the sinusoidal unity power factor current injection to the utility are obtained by the DC–AC inverter controller. A simplified block diagram of the PV system with the power electronics and control is given in Fig. 11.22.

The DC–DC boost converter is based on current-source full-bridge inverter with an embedded high-frequency transformer and rectifier. As this DC–DC stage includes galvanic isolation between the PV string and the grid, the PV strings can

be easily system grounded. The current-source input stage is beneficial since it reduces the requirement for the filter capacitor in parallel with the PV strings. Furthermore, the diodes included in the rectifiers are current commutated, involving low-reverse recovery of the diodes and low-voltage stress [29]. The voltage from the PV string is first converted into a high-frequency AC; galvanic isolation (and in some cases voltage boosting) is accomplished through the use of a high-frequency transformer. The transformer secondary voltage is then rectified using a full-bridge diode rectifier. The rectified DC is then converted into grid compatible AC and connected to the utility by a three-phase voltage-source inverter.

MPPT of a PV array is usually an essential part of a PV system. Over the years, many MPPT methods have been developed and implemented. The names of some of these methods are hill climbing, perturb and observe, incremental conductance, fractional open-circuit voltage, fractional short-circuit current, fuzzy logic, and neural network control, ripple correlation control, current sweep, DC-link capacitor droop control, load-current or load-voltage maximization, and  $dP/dV$  or  $dP/dI$  feedback control. The detailed overview of these MPPT methods can be found in [54]. In Fig. 11.22, a simple method for the MPPT is shown. By measuring the string voltage and current, the PV array output power is calculated and compared to the previous output power. Depending on the result of the comparison, the reference PV current is calculated. The switching is controlled to regulate the input current for the current-source inverter to follow this reference current. This process is repeated until the maximum power point has been reached. Other types of MPPT controllers can also be developed within the same controller framework.

A simplified example of constant power control of the utility-connected inverter is shown in Fig. 11.22. The inner control loop regulates current, and the outer control loop regulates power. To control the active power output of the inverter, the DC bus voltage is regulated. When the DC bus voltage is increasing, it means that the power from PV source is increasing; therefore to maintain the DC bus voltage, active power transfer to the grid needs to be increased. In Fig. 11.22, the reactive power output of the inverter is controlled by the  $q$ -axis current reference ( $i_q^*$ ). In some cases, instead of the  $q$ -axis current reference, a reactive power reference or a power factor reference can be used.

### 11.5.2 Microturbine Integration Example

The IPEM-based power electronics topology for the high speed microturbine includes the back-to-back rectifier–inverter connection which provides the improved power flow control as well as increased efficiency. The voltage-fed converter scheme used in such a system is shown in Fig. 11.23. A PWM-based IGBT bridge rectifies the high-frequency AC from the microturbine generator. The rectifier can also supply the needs for start-up and eliminates the requirement of a gear box. The inverter topology is identical to that of the rectifier, and it supplies the generated power at 60 Hz to the utility grid.

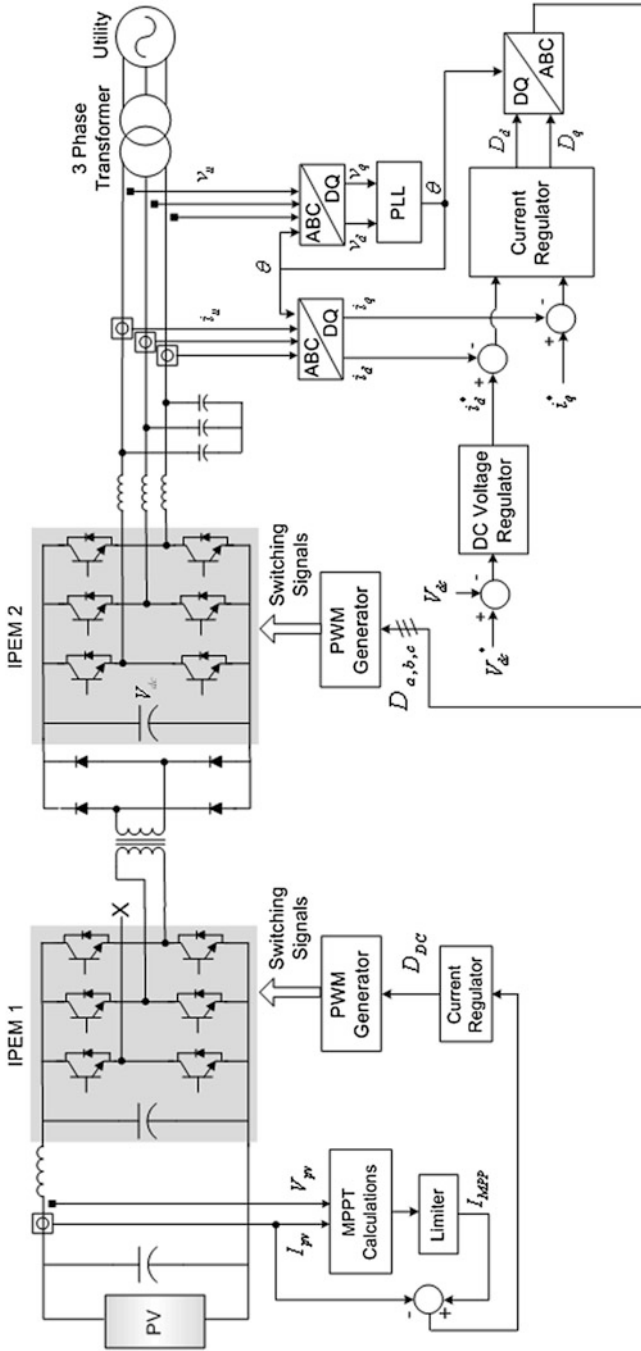


Fig. 11.22 IPEM-based power electronics and control of a PV system

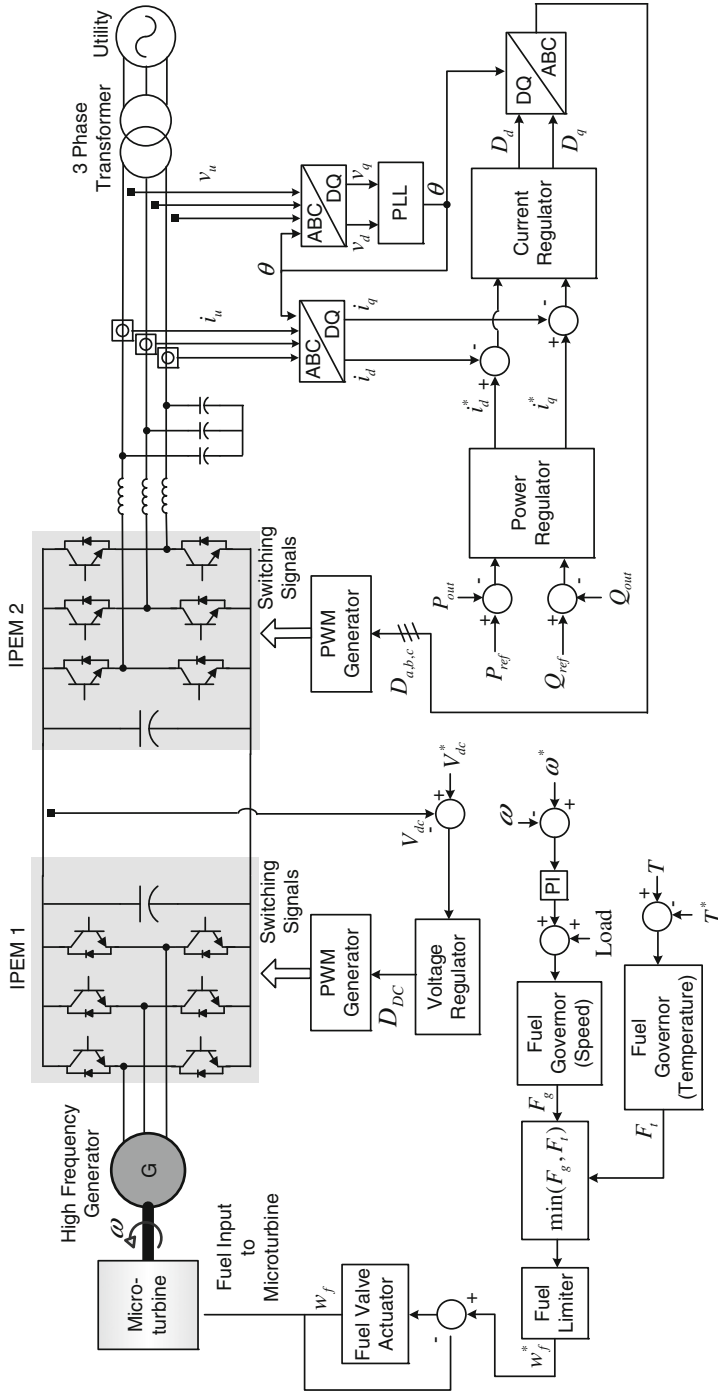


Fig. 11.23 Generalized power electronics and control of a microturbine system

The total efficiency of the microturbine is optimal at a certain temperature and speed, which makes the microturbine more economical if it always runs at the optimum point [36]. The purpose of the control system is to produce the demanded power while maintaining the optimal temperature and speed characteristics. Three basic control loops can be designed for the control of the microturbine and associated power electronics system as shown in Fig. 11.23. The first control loop works to maintain the generator speed, whereas the other two loops maintain the rectifier DC-link voltage and the power flow control by the inverter [45].

The speed control loop's operation depends on several microturbine system components, such as: fuel governor response, temperature rise time, valve position, combustion chamber response, time delay of the combustion chamber, compressor discharge, and turbine expansion [36]. A simplified scheme for the generator speed control is shown in Fig. 11.23. The control system consists of a normal speed regulator that tries to maintain a predefined reference speed. Such speed may not be the optimal for lower power loads, but the regulator tries to maintain the speed by controlling the fuel input to the turbine. It is very difficult to increase the speed without reducing the power load for a short moment and a very complex control must consider all of those variables. The upper performance limit is the limitation of the fuel injectors, and the maximum amount of fuel that can be injected is based on temperature limitations [36]. The fuel demand is the input of a nonlinear transfer function representing the dynamics of the fuel valve actuator system; the output from the valve actuator system is the fuel input required for rotating the turbine shaft at the reference speed [45].

The second control loop works as the DC-link voltage regulator. A reference DC-link voltage is set and the rectifier is controlled to follow the set point. It consists of a PI regulator that provides the PWM signal output required for the three-phase rectifier switches.

The control of the utility connected inverter, as shown in Fig. 11.23, is developed with constant power control [49] and is similar to the one discussed in the previous PV example. As there is no galvanic isolation in the power electronics topologies, a line frequency three-phase transformer is required in case isolation is necessary.

## References

1. Navigant Consulting (2005) DER integration research program power electronics research assessment. California Energy Commission Report CEC-500-2005-206
2. Piff JC (2003) Power electronics building blocks (PEBB) program. Defense Systems Management College Press, USA 32 (2):46-59
3. Ericson T, Hingorani N, Khersonsky Y (2006) PEBB—power electronics building blocks from concept to reality. In: IEEE petroleum and chemical industry conference, pp 1–7
4. Hingorani N (2010) PEBB concept for high power electronics. In: IEEE international symposium on industrial electronics, pp 3684–3688
5. Hingorani NG (2003) Power electronics building block concepts. In: IEEE power engineering society general meeting, pp 1339–1343

6. IEEE (2011) IEEE guide for control architecture for high power electronics (1 MW and greater) used in electric power transmission and distribution systems. IEEE standard 1676–2010, pp 1–47
7. Khersonsky Y, Hingorani N, Peterson KL (2009) IEEE electric ship technologies initiative. In: IEEE petroleum and chemical industry conference, pp 1–10
8. Ericson T (2008) The ship power electronic revolution: issues and answers. In: IEEE petroleum and chemical industry technical conference, pp 1–11
9. Ericson T, Khersonsky Y, Steimer PK (2005) PEBB concept applications in high power electronics converters. In: IEEE power electronics specialists conference, pp 2284–2289
10. Apeldoorn O, Odegard B, Steimer P, Bernet S (2005) A 16 MVA ANPC-PEBB with 6 kA IGBTs. In: IEEE industry applications conference. pp 818–824
11. Wang F, Rosado S, Thacker T, Boroyevich D (2004). Power electronics building blocks for utility power system applications. In: International power electronics and motion control conference, pp 354–359
12. Schwartzberg JW (2003) Application of ac switch power electronic building blocks in medium voltage static transfer switches. In: IEEE power engineering society general meeting, pp 1372–1374
13. ABB Switzerland Ltd. (2003) Dynamic voltage restorer for a critical manufacturing facility. In: Conference presentation in IEEE transmission and distribution conference. [http://grouper.ieee.org/groups/1409/0309\\_linhofer.pdf](http://grouper.ieee.org/groups/1409/0309_linhofer.pdf). Accessed May 2011
14. Silicon power corporation (2008) SSTS<sup>TM</sup> solid state transfer switch: product datasheet. [http://www.siliconpower.com/\\_Documents/SSTS-Datasheet.pdf](http://www.siliconpower.com/_Documents/SSTS-Datasheet.pdf). Accessed May 2011
15. Lee FC, van Wyk JD, Liang ZX, Chen R, Wang S, Lu B (2004) An integrated power electronics modular approach: concept and implementation. In: International power electronics and motion control conference, pp 1–13
16. Kramer W, Chakraborty S, Kroposki B, Thomas H (2008) Advanced power electronic interfaces for distributed energy systems, part 1: systems and topologies. National renewable energy laboratory report TP-581–42672
17. Chakraborty S, Kramer W, Kroposki B (2009) A review of power electronics interfaces for distributed energy systems towards achieving low-cost modular design. Elsevier Renew Sustain Energy Rev 13(9):2323–2335
18. Schugart P (2007) Using AMSC PEBBs to accelerate new technology development of electric power systems. In: Government microcircuit applications and critical technology conference, pp 1–4
19. Stockmeier T (2008) Power modules: demands for renewable energy & electric vehicles. *ElektronikPraxis Electronica Magazine*, pp 92–95
20. Mookken J, Haddad K (2006) Modular approach simplifies power-system design. In: Power electronics technology magazine, pp 46–49
21. Lee FC, van Wyk JD, Boroyevich D, Guo-Quan L, Zhenxian L, Barbosa P (2002) Technology trends toward a system-in-a-module in power electronics. *IEEE Circuits Syst Mag* 2(4):4–22
22. Boroyevich D (2010) Building block integration in power electronics. In: IEEE international symposium on industrial electronics, pp 3673–3678
23. van Wyk JD, Lee FC, Boroyevich D, Zhenxian L, Kaiwei Y (2003) A future approach to integration in power electronics systems. In: IEEE industrial electronics society annual conference, pp 1008–1019
24. Rengang C, Canales F, Bo Y, van Wyk JD (2005) Volumetric optimal design of passive integrated power electronics module (IPEM) for distributed power system (DPS) front-end dc/dc converter. *IEEE Trans Ind Appl* 41(1):9–17
25. Mookken J (2005) Future vehicles drive next generation of power modules. *Power Electronics Europe Magazine*:34–37
26. Newman P (2010) High currents under control: compact vehicle power systems. *Bodo's Power Systems Magazine*, pp 20–22

27. American Superconductor Corporation (2010) PowerModule™ PM1000: product datasheet. [http://www.amsc.com/pdf/PM1000\\_DS\\_PM\\_0510\\_A4\\_forweb.pdf](http://www.amsc.com/pdf/PM1000_DS_PM_0510_A4_forweb.pdf). Accessed May 2011
28. American Superconductor Corporation (2010) PowerModule™ PM1000 system developer kit: product datasheet. [http://www.amsc.com/pdf/PM1000\\_SDK\\_0810.pdf](http://www.amsc.com/pdf/PM1000_SDK_0810.pdf). Accessed May 2011
29. Kjaer SB, Pedersen JK, Blaabjerg F (2005) A review of single-phase grid-connected inverters for photovoltaic modules. *IEEE Trans Ind Appl* 41(5):1292–1306
30. Blaabjerg F, Chen Z, Kjaer SB (2004) Power electronics as efficient interface in dispersed power generation systems. *IEEE Trans Power Electron* 19(5):1184–1194
31. Cheng KWE, Sutanto D, Ho YL, Law KK (2001) Exploring the power conditioning system for fuel cell. In: *IEEE power electronics specialists conference*, pp 2197–2202
32. Chen Z, Blaabjerg F (2006) Wind energy—the world’s fastest growing energy source. *IEEE power electronics society third quarter newsletter*, pp 15–19
33. Carrasco JM, Franquelo LG, Bialasiewicz JT, Galvan E, Guisado RCP, Prats MAM, Leon JI, Moreno-Alfonso N (2006) Power-electronic systems for the grid integration of renewable energy sources: a survey. *IEEE Trans Industr Electron* 53(4):1002–1016
34. Al-Khayat N, Al-Tayie J, Seliga R (2002) Stand alone adjustable speed power generating set. In: *International conference on Harmonics and quality of power*, pp 639–643
35. Kawabata Y, Morine Y, Oka T, Ejiogu EC, Kawabata T (2001) New stand-alone power generating system using wound-rotor induction machine. In: *IEEE conference on power electronics and drive systems*, pp 335–341
36. Farret FA, Simoes MG (2006) *Integration of alternative sources of energy*. Wiley-IEEE Press, New York
37. Staunton RH, Ozpineci B (2003) *Microturbine power conversion technology review*. Oak Ridge National Laboratory Report ORNL/TM-2003/74
38. Nikkhajoei H, Iravani MR (2005) A matrix converter based micro-turbine distributed generation system. *IEEE Trans Power Delivery* 20(3):2182–2192
39. Leung KK, Sutanto D (2000) Using battery energy storage system in a deregulated environment to improve power system performance. In: *International conference on electric utility deregulation and restructuring and power technologies*, pp 614–619
40. Mohan N, Undeland TM, Robbins WP (2002) *Power electronics: converters, applications, and design*. Wiley, New York
41. Inoue S, Akagi H (2007) A bidirectional isolated dc–dc converter as a core circuit of the next-generation medium-voltage power conversion system. *IEEE Trans Power Electron* 22(2):535–542
42. Li H, Peng FZ, Lawler JS (2003) A natural ZVS medium-power bidirectional dc–dc converter with minimum number of devices. *IEEE Trans Ind Appl* 39(2):525–535
43. Lazarewicz ML, Rojas A (2004) Grid frequency regulation by recycling electrical energy in flywheels. In: *Proceedings of IEEE power engineering society general meeting*, pp 2038–2042
44. Simoes MG, Farret FA (2004) *Renewable energy systems: design and analysis with induction generators*. CRC Press, USA
45. Bertani A, Bossi C, Fornari F, Massucco S, Spelta S, Tivegna F (2004) A microturbine generation system for grid connected and islanding operation. In: *IEEE power systems conference and exposition*, pp 360–365
46. Tanrioven M, Alam MS (2004) Modeling, control and power quality evaluation of a PEM fuel cell based power supply system for residential use. In: *IEEE industry applications society annual meeting*, pp 2808–2814
47. Ryan MJ, Lorenz RD (2000) A “power-mapping” variable-speed control technique for a constant-frequency conversion system powered by a IC engine and PM generator. In: *IEEE industry applications conference*, pp 2376–2382
48. Cimuca GO, Saudemont C, Robyns B, Radulescu MM (2006) Control and performance evaluation of a flywheel energy-storage system associated to a variable-speed wind generator. *IEEE Trans Industr Electron* 53(4):1074–1085

49. Ye Z, Walling R, Miller N, Du P, Nelson K, Li L, Zhou R, Garces L, Dame M (2006) Reliable, low-cost distributed generator/utility system interconnect. National Renewable Energy Laboratory Report SR-560-38017
50. Chakraborty S, Kroposki B, Kramer W (2009) Evaluation of VAR control and voltage regulation functionalities in a single-phase utility-connected inverter for distributed energy applications. IEEE energy conversion congress and exposition, pp 1753–s1759
51. Guo J, Celanovic I, Borojevic D (2001) Distributed software architecture of PEBB-based plug and play power electronics systems. In: IEEE applied power electronics conference and exposition, pp 772–777
52. Celanovic I, Celanovic N, Milosavljevic I, Boroyevich D, Cooley R (2000) A new control architecture for future distributed power electronics systems. In: IEEE power electronics specialists conference, pp 113–118
53. Rosado S, Wang F, Boroyevich D, Wachal R (2003) Control interface characterization of power electronics building blocks (PEBB) in utility power system applications. In: IEEE power engineering society general meeting, pp 1350–1355
54. Eram T, Chapman PL (2007) Comparison of photovoltaic array maximum power point tracking techniques. IEEE Trans Energy Convers 22(2):439–449



# Chapter 12

## Resource Aggregation Using Microgrids

Giri Venkataramanan and Sandeep Bala

**Abstract** Microgrids are emerging as a flexible approach to aggregate diverse distributed and renewable energy sources with the electric grid. This chapter presents the salient features of the microgrid, including operating modes, example configurations, control, and dynamic properties. A detailed outline of stability properties of the microgrid in DC and AC configurations is presented. A brief summary of their potential and challenges in the future is discussed in the concluding section.

### 12.1 Introduction

The total capacity of distributed energy generation and storage devices connected to a typical electrical service network today generally makes up a small fraction of the total local electrical load. In order to improve the reliability and greenness of the electrical supply, there is a trend toward installing more distributed energy resources, particularly renewable generation. Increasing the penetration of such energy resources in the local grid requires special care in the design and operation of the local grid. It is desirable to aggregate the distributed energy resources in a way that they can serve the loads either independently in a small grid or in cooperation with a larger utility grid, and this type of operation is enabled by microgrids [1, 2]. While renewable/distributed generation and electrical storage

---

G. Venkataramanan (✉)

Department of Electrical and Computer Engineering, University of Wisconsin-Madison,  
1415 Engineering Drive, WI, Madison, USA  
e-mail: giri@engr.wisc.edu

S. Bala

ABB Corporate Research, Raleigh, NC, USA

devices may be interconnected in an ad-hoc grid, there are three defining properties that distinguish a microgrid from an ad hoc grid:

- Ease of integration of new resources;
- Ease of scaling up or down the size; and
- Equitable role for each resource in determining the operation of the microgrid.

This chapter provides an overview of microgrids within the context of aggregating distributed electrical resources. Section 12.2 presents the conceptual framework that defines a microgrid. Section 12.3 shows various configurations of microgrids along with illustrative examples. Section 12.4 provides a discussion of different control principles for various generation sources that may use power electronic interfaces in forming a microgrid. Section 12.5 discusses various dynamic interactions that may happen within the power electronic systems of different aggregated resources and between the power electronic controllers and the aggregation network. The concluding section provides summarizing remarks.

## 12.2 The Microgrid Concept

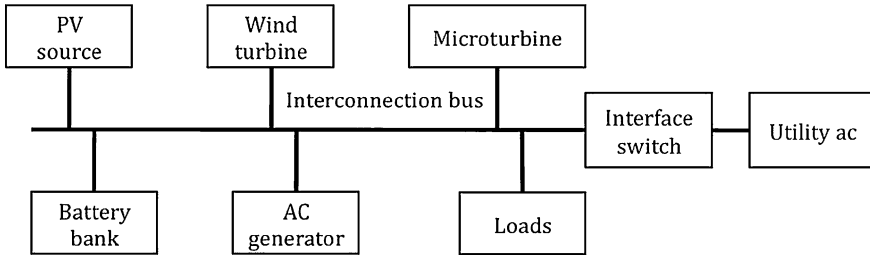
### 12.2.1 Definitions

A microgrid is a local electrical network that (1) comprises power generation units, power consumption units, and a means of delivering power from the generation units to the consumption units, (2) may be connected to a larger utility power system, and (3) operates to balance the power supply and demand within the microgrid [3].

The local electrical network forming the microgrid may include a network within a building or a group of buildings; a section of a distribution network; a group of circuits downstream of a distribution substation; the entirety of an electric customer's facility; the electrical network of a residential subdivision, a district, an industrial park, a remote village, a ship, or an airplane; and so on.

The network would include electric power generation units such as conventional internal combustion driven alternators, microturbines, fuel cell generators, solar thermal power generators, solar photovoltaic installations, induction generators, wind turbine generators, combined heat and power generators, etc. The network would also contain power consumption units including motors, heating and lighting loads, industrial process loads as well as emerging bidirectional loads like electric vehicles with V2G capabilities.

Furthermore, the network would contain appropriate feeder circuits, branch circuits, transformers, grounding, switchgear, and protection elements to provide a safe and reliable means of providing electricity to the power consumption units from the power generation units, while possibly importing and/or exporting power from a large-scale electrical utility that may be connected to the network.



**Fig. 12.1** A simplified schematic illustration of a microgrid

At first glance, the description of the local network of generation and consumption units appears to be no different from that of state-of-the-art grid-connected renewable distributed generation systems. However, the capability to independently balance supply and demand within the local network, particularly in the absence of a large-scale electric utility grid is the defining feature of the microgrid. Such a capability to operate in the absence of the utility grid is salient, since the utility grid is nominally understood to have virtually infinite capability to source as well as sink energy relative to the aggregate supply and demand capabilities of the microgrid. This notional feature of a microgrid is defined by the control features of the generation sources that are located therein.

Figure 12.1 illustrates a schematic of a notional microgrid integrating several generation sources, utilization equipment, and the main electric utility.

## 12.2.2 Operating Modes

The operating modes of a microgrid define the high-level functionality of microgrids, which must then be implemented in appropriate system configurations through system design and control. A microgrid has two distinct steady-state operating modes and two distinct transitional operating modes as described in this section.

### 12.2.2.1 Grid-Interactive Steady State Mode

A microgrid that is electrically connected to the main electric grid is said to be in grid-interactive mode. In grid-interactive mode, the microgrid does not necessarily have to balance its internal supply and its internal demand because any difference between supply and demand can be accommodated by the utility grid.

### **12.2.2.2 Grid-Independent Steady State Mode**

A microgrid that is not connected to any utility grid is said to be in grid-independent mode. In grid-independent mode, the microgrid must balance the internal supply and demand. Any difference between supply and demand will have to be accommodated through appropriate provision of energy storage within the microgrid.

### **12.2.2.3 Seamless Transition Mode**

A microgrid that is capable of transitioning between grid-interactive and grid-independent modes of operation without any discontinuity in service to the loads within the microgrid is said to be capable of seamless mode transitions. This mode of transition would be desired in facilities that require high levels of power quality.

### **12.2.2.4 Transfer Transition Mode**

A microgrid that requires a finite discontinuity in service to the loads within the microgrid in order to transition between grid-interactive and grid-independent modes of operation is said to be capable of performing transfer mode transitions. This mode of transitions would be adequate in facilities that require high levels of reliability, but may be able to ride-through finite loss of supply.

## **12.3 Electrical Configurations**

The choice of electrical configuration of a microgrid depends on the legacy electrical systems (utility network, power generation sources, power consuming loads) present in the ambient installations, protection and safety requirements, and the properties of new resources that are being aggregated in the system.

### ***12.3.1 DC Microgrids***

#### **12.3.1.1 Definition**

A DC microgrid is one that uses direct current (DC) as the means of delivering power from the generation units to the consumption units. They may be configured as systems conductors with positive *and* negative polarity, with a grounded conductor at neutral potential, or as systems with positive *or* negative polarity, with the other conductor grounded [4, 5].

### **12.3.1.2 Exceptions**

Local power distribution systems like those in computing, communications and data management equipment, small mobile applications such as boats, aircrafts, and land vehicles could comprise DC power networks, because these applications typically consist of fixed elements with well-defined operating characteristics. While they do not require the operational features of microgrids, they may be configured in such a manner to increase their robustness and reliability.

### **12.3.1.3 Typical Elements**

A DC microgrid typically includes power converters to interface sources and loads, special protection elements, and an interface to AC grid.

### **12.3.1.4 Benefits**

A DC microgrid decouples the frequency, voltage, and phase of the various AC generation and consumption elements in the microgrid by the use of suitable power converters.

### **12.3.1.5 Challenges**

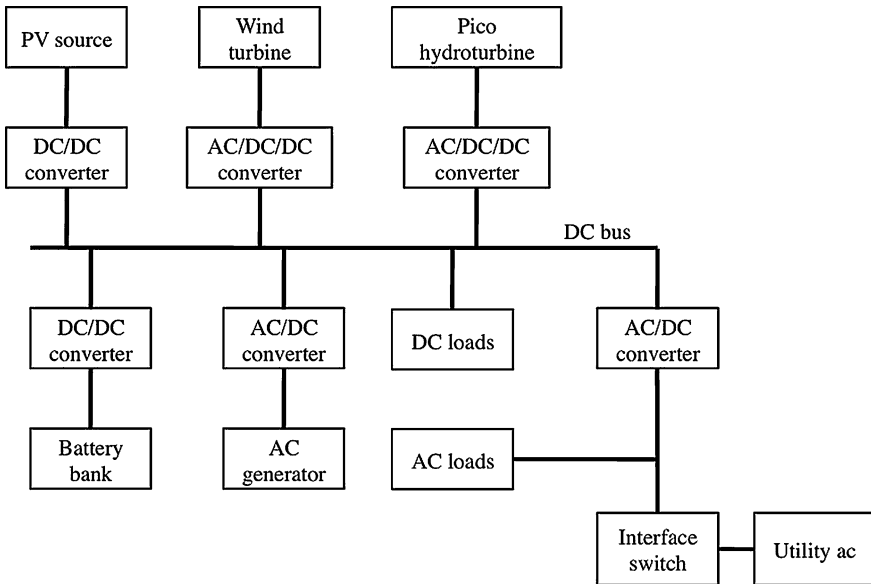
It is challenging to build robust protection systems for DC microgrids, and it often requires integration of protection functions into the converters themselves [6].

Figure 12.2 illustrates a DC bus based microgrid. The interface between each energy source and the DC bus has a power electronic converter (a DC/DC converter, or an AC/DC converter); these converters are described in the chapter on power electronics in this book. Each of the converters may be centrally dispatched in order to regulate the energy flow in or out of the DC bus, or they may be droop controlled in order to share power in a distributed manner.

## ***12.3.2 AC Microgrids***

### **12.3.2.1 Definition**

An AC microgrid is one that uses alternating current (AC) as the means of delivering power from the generation units to the consumption units. Types include single-phase, three-phase, and multi-phase with different grounding options.



**Fig. 12.2** A simplified schematic illustration of a DC microgrid

### 12.3.2.2 Exceptions

Networks with fixed elements and well-defined operating characteristics do not fall under the purview of AC microgrids.

### 12.3.2.3 Typical Elements

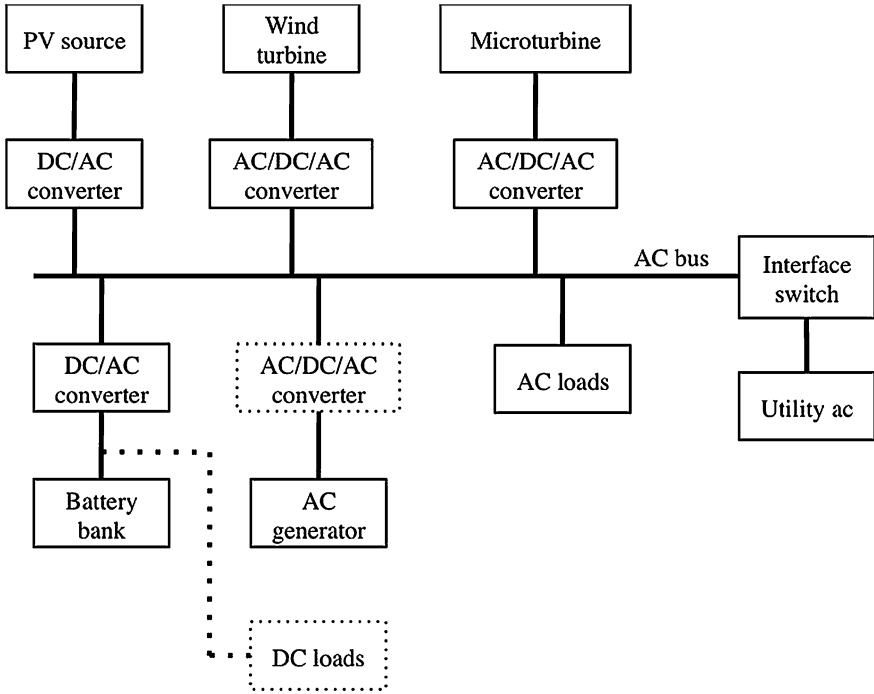
An AC microgrid typically includes transformers and power converters to interface sources and loads as well as protection devices.

### 12.3.2.4 Benefits

The operation of an AC microgrid is analogous to that of a large-scale utility system; it is relatively easy to achieve power flow control, and one can use conventional protection elements.

### 12.3.2.5 Challenges

In an AC microgrid, one may need to modify power conversion interfaces to handle fault scenarios under different operating modes.



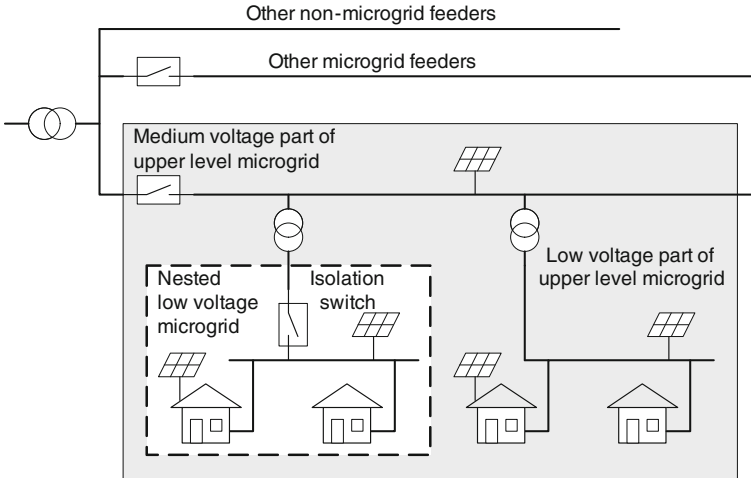
**Fig. 12.3** A simplified schematic illustration of an AC microgrid

Figure 12.3 illustrates AC bus based microgrid. The interconnection between the AC bus and each of the energy sources is realized using power electronic converters (DC/AC or AC/AC) described in the chapter on power electronics in this book. Each of the converters may be centrally dispatched in order to regulate the energy flow in or out of the AC bus, or they may be droop controlled in order to share power among them in an autonomous or distributed manner. Installations of these systems have found application in remote locations where access to a central electricity grid is unreliable and the power quality is poor.

Laboratory-scale and utility-scale field demonstrations have been established in several locations around the world [3].

### 12.3.3 Nested Microgrids

In certain cases, a sub-network of the overall microgrid may need to be operated at a different voltage, at a different frequency, or at a greater degree of reliability than the rest of the microgrid. In such cases, it is possible to nest microgrids. The lower level microgrid does not directly interface with the utility grid; instead it interfaces with the upper level microgrid.



**Fig. 12.4** A simplified schematic illustration of a nested microgrid

An example of nested microgrids is shown in Fig. 12.4. In the example, a group of buildings with local generation is operated as a low-voltage AC microgrid, which is connected via an isolation switch and a transformer to a medium voltage AC microgrid.

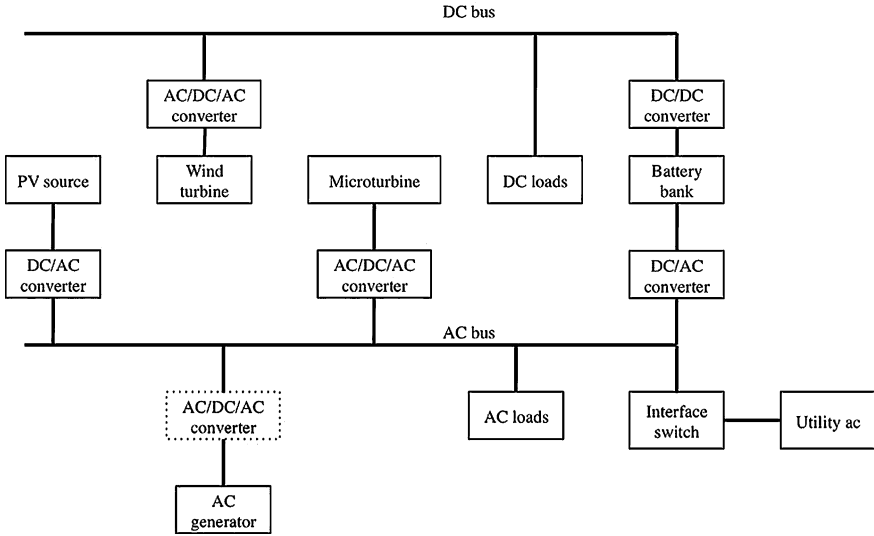
In a military microgrid operating nominally at 50 or 60 Hz, there may be many units that can generate and consume power from a 400 Hz supply. In such a case, the overall system could be designed with a nested low voltage AC microgrid operating at 400 Hz. The system would require a power electronic frequency converter at the interface between the lower and upper level microgrids.

Similarly, one may also choose to design a system with a DC microgrid nested within an AC microgrid or vice versa. The choice of such a nested design would be made only if it enabled lower total cost of system setup and operation. Figure 12.5 illustrates a hybrid microgrid based on a DC bus and an AC bus with the appropriate power electronic converters. Each of the converters may be centrally dispatched in order to regulate the energy flow in or out of the DC and/or AC bus, or they may be droop controlled in order to share power among them in a distributed manner. Similar to the AC microgrid, these systems have found application in remote locations where access to a central electricity grid is unreliable and the power quality is poor [7].

## 12.4 Control Structures

Each source in a microgrid must have an equitable role in determining the operation of the microgrid. If the physical characteristics of the source themselves do not naturally provide such a feature, then an overriding controller must regulate the





**Fig. 12.5** A simplified schematic illustration of a hybrid AC and DC microgrid

operation of the source in a manner that enables such a feature. The type of controller selected would depend on the nature of the source. Each source has a local controller that typically consists of two parts: (1) an inner controller that regulates the terminal quantities like voltage and frequency, and (2) an outer controller that provides the references to the inner controller. In addition to the local controller, the microgrid may have a supervisory controller that updates set points for the individual local controllers depending on the state of the overall microgrid.

This section first describes the two chief types of local control structures: (1) grid-forming control, and (2) grid-following control. Then the section describes the operation of the supervisory controller.

**12.4.1 Grid-Forming Control**

A source with a grid-forming control structure, called a grid-forming source, is a source that actively regulates the voltage and frequency of the grid [8]. In grid-independent mode, there must be at least one source with grid-forming control in the microgrid.

Grid-forming sources must be dispatchable. A fully dispatchable source is one that can deliver any amount of power up to its rated power at any time. A partially dispatchable source is one that has some flexibility in the amount of power it can deliver. Dispatchable sources are always some form of stored energy: chemical (fuels, which interface microgrids through diesel gensets or fuel cells), mechanical

(flywheels, which interface microgrids through electrical machines), electrochemical (batteries, which interface microgrids through power converters), or electromagnetic (superconducting magnetic energy storage, which interface microgrids through power converters).

Equitable roles for the grid-forming sources are ensured by controlling them to share the load power in proportion to their rated powers. The method to ensure power sharing is slightly different for DC and AC power systems.

**12.4.1.1 DC Systems**

Voltage droop is used to share power in DC systems [4, 5]. The controller of the DC source computes the actual output power  $P$  of the source and determines the voltage reference to the voltage regulator according to the equation

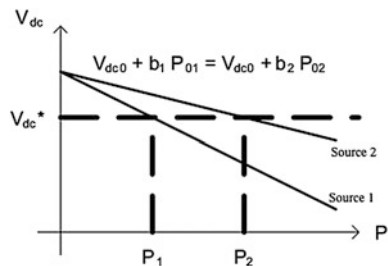
$$V_{DC}^* = V_{DC0} - b(P - P_0). \tag{12.1}$$

For a given DC source, the value of  $P_0$  corresponds to the power output of the source in grid-connected mode when the bus voltage is tightly regulated to be equal to the nominal voltage  $V_{DC0}$ . This value is typically set in proportion to the rated power of the source. The droop  $b$  is typically set to a value in the range 0.5–1 % of the ratio of the nominal voltage and the rated power of the unit [9].

In a DC power system, the power flow depends only on the voltages and the resistances of the sources and the lines between the different nodes in the network. The voltage droop on the source effectively emulates a source resistance, and when each source has the same droop constant (as a percentage of its rated power), then the power outputs are approximately in proportion to the rated powers of the sources.

Figure 12.6 illustrates the power sharing between two DC sources with very low resistance between the sources. In this example, the first source is rated at half the power of the second source. The values of  $V_{DC0}$  in both the sources are set to be equal to the nominal DC voltage of the microgrid, but the value of  $P_{01}$  is half the value of  $P_{02}$ . The voltage of the microgrid settles to a value  $V_{DC}^*$  such that the sum of  $P_1$  and  $P_2$  is equal to the load power, and in this steady state, the value of  $P_1$  is half that of  $P_2$ .

**Fig. 12.6** Illustration of sharing power in a DC microgrid using voltage droop



### 12.4.1.2 AC Systems

In AC systems, power-frequency droop is used to share power [1, 7]. In conventional AC power systems, the synchronous generator driven by a prime mover exhibits a drop in speed when there is an increase in the load; this drop in speed is sensed by the speed governor, which then commands the prime mover to increase its power output. This action has the effect of sharing the load according to the power delivery capability of the sources. The reactive powers are shared by the sources by proportionally drooping the voltage references, which are fed to the field winding control of these synchronous generators. Other sources can emulate synchronous machines by implementing an appropriate control structure. For example, if a voltage source inverter is used to interface a dispatchable source with an AC microgrid, the frequency and voltage references to the inner controller of the inverter are computed by the outer controller. The overall block diagram is shown in Fig. 12.7.

The microgrid control block implements the droop equations:

$$\omega^* = \omega_0 - b_p(P - P_0) \tag{12.2}$$

$$V^* = V_0 - b_q(Q - Q_0). \tag{12.3}$$

Again the droop constants  $b_p$  and  $b_q$  are set to a value of 0.5–1 % of ratio of the nominal frequency and real power or voltage and reactive power respectively.  $P$  and  $Q$  are the active and reactive output powers of the inverter as calculated based on the feedback voltages and currents. In a typical AC network, the reactance is more significant than the resistance, and so the power flow depends on the relative

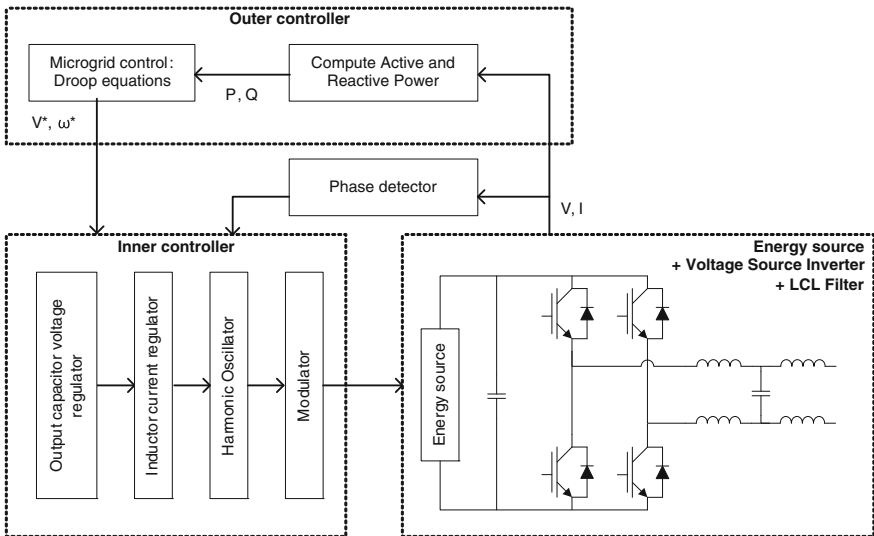
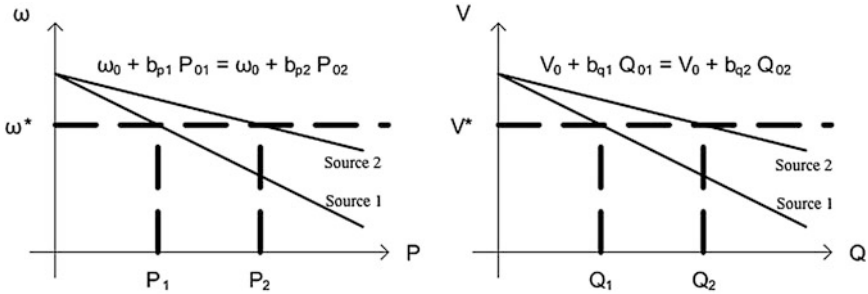


Fig. 12.7 Block diagram of control structure for grid-forming AC source



**Fig. 12.8** Illustration of power-frequency droop and reactive power-voltage droop

phase angles of the sources, the relative voltages of the sources, and the reactances of the lines in the network. The power-frequency droop equation helps set the relative phase angles of the sources, and the reactive power-voltage droop equation helps set the relative voltages of the sources. In steady state, the frequencies of all the sources are equal, and the voltages of the sources are nearly equal. The minor differences in the voltage references occur due to the reactive power drops in the lines in the network, but these drops usually are small compared to the load reactive powers. The power-frequency and reactive power droops and their sharing operation between two grid-forming sources are illustrated in Fig. 12.8.

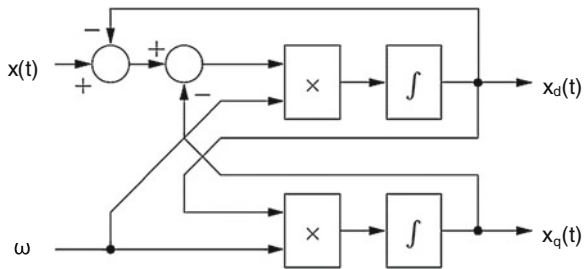
In contrast to the speed governors in prime-mover driven synchronous machines, inverter controllers require explicit computation of the active and reactive powers. In balanced  $n$ -phase systems, the computation of  $P$  and  $Q$  is achieved by the following equations [9]:

$$P = n/2 (v_d i_d + v_q i_q) \tag{12.4}$$

$$Q = n/2 (v_q i_d - v_d i_q). \tag{12.5}$$

For three-phase systems, the direct and quadrature signals ( $v_d, v_q, i_d, i_q$ ) can be computed using the Park transformation [10]. In single-phase systems,  $n = 1$ , and the computation of  $P$  and  $Q$  requires the generation of an artificial quadrature signal. This can be achieved using the filter shown in Fig. 12.9 [11].

**Fig. 12.9** Block diagram of a second-order generalized integrator used to isolate the direct and quadrature components of a single-phase signal [9]



By implementing the appropriate grid-forming control as described above for DC and AC microgrids, dispatchable sources are used to form microgrids.

### 12.4.2 Grid-Following Control

A source with a grid-following control structure, called a grid-following source, is a source that injects power into the microgrid at a voltage and frequency that are regulated by other sources. Most renewable power sources do not regulate their output voltage and frequency, because they are power-constrained sources. A photovoltaic panel connected to a microgrid through a power converter is an example of a grid-following source.

Figure 12.10 shows an example control structure for a grid-following AC source. An outer controller determines the references for the inner controller based on the instantaneous power generation capability. In certain cases, these references may be adjusted according to a supervisory energy management scheme in the microgrid. The control structure is similar for a source in a DC microgrid. The only difference is that a DC source does not require a phase locked loop.

As a final note, any grid-following source can be supplemented with energy storage and then controlled to be grid-forming. For example, a solar source supplemented with a battery can use an inverter programmed to behave as a grid-forming source as long as there is sufficient energy available in the battery.

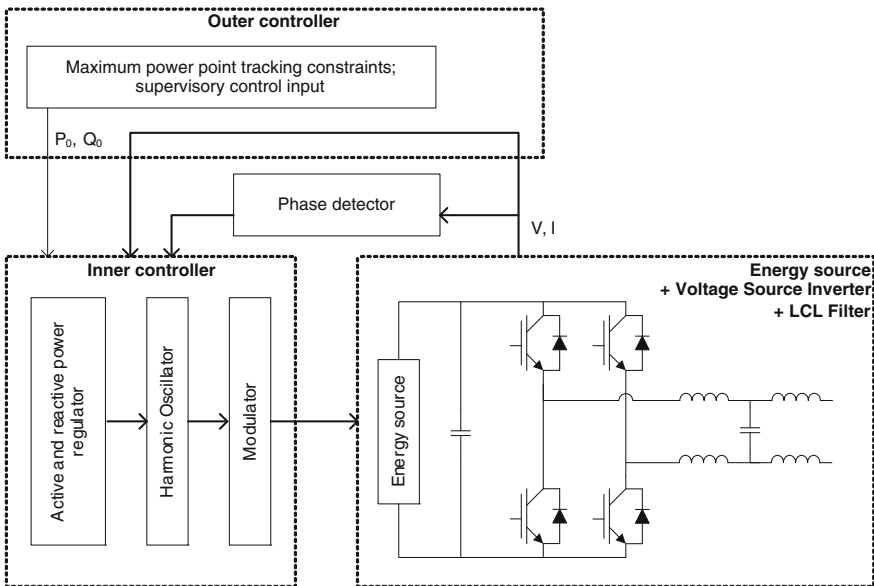


Fig. 12.10 Block diagram of control structure for a grid-following AC source

### 12.4.3 Microgrid Coordination

A microgrid with sufficient grid-forming generation capacity and with the sources using the control structures described in Sects. 12.4.1 and 12.4.2 can operate without any real-time communication between the system components. But in order to ensure the highest level of reliability at the lowest cost, a microgrid operator should incorporate higher level functions such as asset management, economic dispatch, maintenance scheduling, and contingency management. This can be achieved through a supervisory controller that coordinates the operation of the units in the microgrid [12, 13].

The supervisory controller receives information about the electrical states of the units in the microgrid. Since the goal of the supervisory controller is to optimize the system level operation rather than the instantaneous operation, the feedback and actuation can occur at a slower time scale, typically in the order of minutes. The individual units report average voltages, average powers, available generation capacities, operational statuses, and other such information. The supervisory controller uses all the information to determine the set points required for optimal system operation. For both grid-forming and grid-following sources, these are typically the set points  $P_0$  and  $Q_0$ . The controller then transmits these set points to the individual units.

As an example, the supervisory controller may determine the optimal use of energy storage resources to lower the total cost of operation of the system. In most markets, the cost of generation is not fixed; it follows the laws of supply and demand. When there is greater demand from the load relative to the supply, the cost of generation is high; and when there is lower demand, the cost is low. The supervisory controller can observe the cost of generation as it varies and then command the energy storage resources to charge when the cost is low and discharge when the cost is high. This coordination ensures economic dispatch of the various units in the microgrid.

As another example, the supervisory controller may observe that there is not enough generation capacity available to support the total load. In this case, it commands certain switches in the microgrid to open in order to effect load shedding. Thus microgrid coordination can manage contingency events and ensure the highest reliability possible in the system.

## 12.5 Dynamic Properties

This section discusses the stability aspects of microgrids, i.e., the ability to maintain the power supply to the load without unwanted dynamics, such as voltage or power flow oscillations. In extreme cases, such undesirable dynamics could cause the operation of protection devices like breakers or fuses, which in turn would jeopardize the integrity of power supply to at least some of the loads [14].

Microgrids are complex systems with diverse response intervals and time delays among the power generation and consumption units, interconnections, and internal feedback regulators. The design of generation elements in the network and internal feedback regulators are generally constrained by the dynamics of the prime energy source, and desirable terminal properties are dictated by power quality and generation control. The designs of power consumption units and their internal regulators are dictated by their useful function in transforming electricity into end-use. The interconnections among system elements are sized and designed by considerations related to power transfer. Therefore, ensuring stable dynamics of interactions between the disparate devices are of paramount importance in ensuring safe and reliable provision of power within the microgrid.

Stability of microgrids is assessed at two scales—large signal and small signal. Large signal stability refers to the ability of the system to withstand larger perturbations that could be caused by faults or other large step changes in the system, and settle to a different operating point. Analytical tools to study large signal stability are particularly cumbersome because of the nonlinear nature of generic microgrid elements. Only a time-series simulation technique would provide sufficient fidelity for examining the large signal stability of the system.

Small signal stability refers to the stability of an operating point under small perturbations that could be caused by noise and parameter variations. It can be evaluated by a study of the eigenvalues of the system linearized about the operating point. In examining small signal stability, linearized dynamic phasor models that express the system behavior provide significant insight into the small signal behavior of the system over a range of operating conditions, and such models are useful in providing general design guidelines. Furthermore, small signal stable behavior of the system at different operating conditions is a necessary condition for large signal stability and therefore provides a systematic approach to establish reasonable microgrid designs. Small signal models typically use linearized system approximations to transform the complexity of models into a simpler system, typically of fewer dimensions to be analytically tractable in order to provide necessary insight.

In one case of approximate modeling approaches, the internal dynamics of generators are considered to be negligible and the stability of particular inductive interconnections of the microgrid as affected by the generation controllers that regulate the droop in frequency and magnitude of the terminal voltage are considered. It is shown that a stable and diversified microgrid can be formed if each unit in the microgrid is equipped with droop-based active and reactive power controllers that follow particular scaling properties [15, 16].

Several studies for designing internal regulators to decouple the relationships between real and reactive power that occur in resistive interconnections and various approaches of generalized droop controllers and impedance emulating controllers have been proposed [14, 17]. In general, the relationship between the internal voltage control of the power electronic converters and the external control of the generator's real and reactive power output that include the effect of interconnection lines play a critical role in defining system behavior.

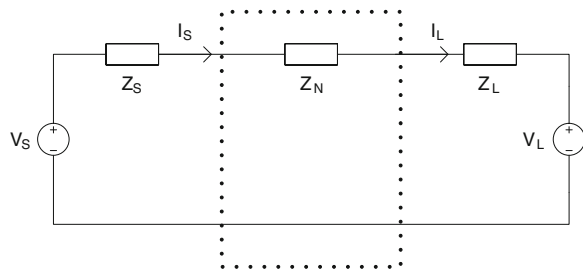
An examination of stability of the microgrid is detailed further in this section within the context of a DC and AC microgrids, where the responsibility of the DC or AC bus regulation is shared among several power converters.

### 12.5.1 Stability in DC Microgrids

The small signal stability of a DC power system is related to the small signal impedances of the sources, loads, and network of the system. The impedance of sources in DC microgrids is usually considered to be resistive (positive small signal impedance) because of the droop characteristic [4, 5]. Loads can be classified as constant power loads, constant current loads, or constant impedance loads, but usually a load behaves as a mix of these three major types of loads. The loads in the DC microgrid that are predominantly constant power loads have negative small signal impedances. The combination of badly scaled positive and negative impedances in the same system causes small signal instability [18]. Furthermore, in the context of microgrids, stability may be examined by computing the loop gain transfer function of the regulation system of the power converters that form the network [19].

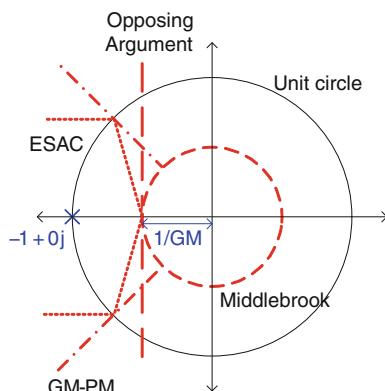
To examine the small signal stability of a simple DC network interconnection shown in Fig. 12.11, one must look at the poles of the closed loop feedback system to verify they are all in the left half plane of the Laplace domain. The poles of the interconnected system may be ensured to be stable by examining the linearized source impedance  $Z_S$  and the linearized load impedance  $Z_L$  at the interconnection (point of common coupling, or PCC). The network impedance  $Z_N$  could be combined with the source impedance or the load impedance. The DC network is stable if and only if the denominator of the small signal closed loop gain transfer function  $(1 + Z_S/Z_L)$  has no zeros in the right half plane, because those zeros may attract poles for a certain high gain. This can be ensured if the Nyquist contour of  $Z_S/Z_L$  (often referred to as the loop gain  $T_e$ ) does not encircle the point  $-1 + 0j$  in the complex plane. A number of approaches have been proposed to ensure this condition is satisfied. Each of the approaches proscribes the loop gain contour from entering a certain vicinity of the point  $-1 + 0j$ . By implementing such a constraint, one gets a sufficient condition for stability, but this condition is not

**Fig. 12.11** A simplified network interconnecting a single DC source and a single DC load





**Fig. 12.12** Nyquist plane of  $Z_S/Z_L$  indicating sufficient conditions for small signal stability of a DC interconnection ( $GM$  gain margin,  $PM$  phase margin)

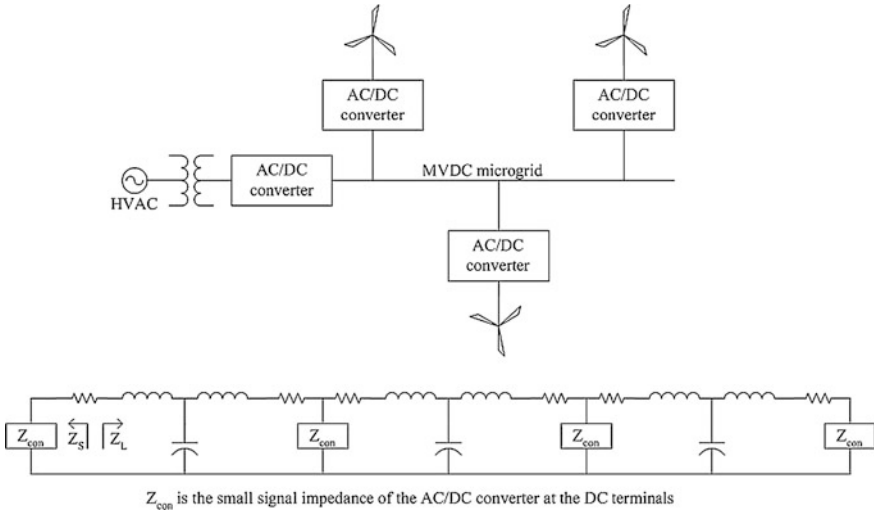


necessary to guarantee the stability. Figure 12.12 illustrates the boundaries of the regions in four different approaches (listed in decreasing order of conservativeness and increasing complexity to establish): the Middlebrook criterion (stay within the circle of radius illustrated by  $1/\text{Gain Margin}$ ), the opposing argument criterion, the gain-margin phase-margin criterion, and the ESAC criterion [20, 21].

An “equivalent source” as well as an “equivalent load” must be considered using electric network theory in order to apply the stability criteria based on physical understanding of the system. If the microgrid system has operating points that exhibit small signal instability, the system must be redesigned by changing the gains of the controllers, changing filter parameters, or changing the choice of the controller altogether. Following this, a full-fledged computer-based simulation would be recommended in order to achieve verification of large signal stability.

### 12.5.1.1 Stability of a DC Microgrid Wind Farm Collection Network

Although state-of-the-art wind farm collection networks are configured as AC networks, a DC microgrid may be an alternative and competitive approach for realizing collection network for future applications [22]. Such a collection network configured as a microgrid is illustrated in Fig. 12.13, along with a small signal equivalent circuit of the system. Parameters of cable components are listed in Table 12.1. The distances between the turbines and AC grid connection are modeled after the park layout at the Cedar Ridge wind park in Fond Du Lac County Wisconsin. The interconnection cable impedance parameters are scaled from cable data provided by HVDC cable manufacturers. In this case, even though the power consuming loads within the DC microgrid itself are insignificant, the power converters to interface between the DC microgrid and the AC utility, and between the DC microgrid and various wind turbines may all be configured to enable the operational features of the microgrid as illustrated in the previous section.



**Fig. 12.13** Simplified diagram of a wind park DC interconnection with distance and impedance values [22]

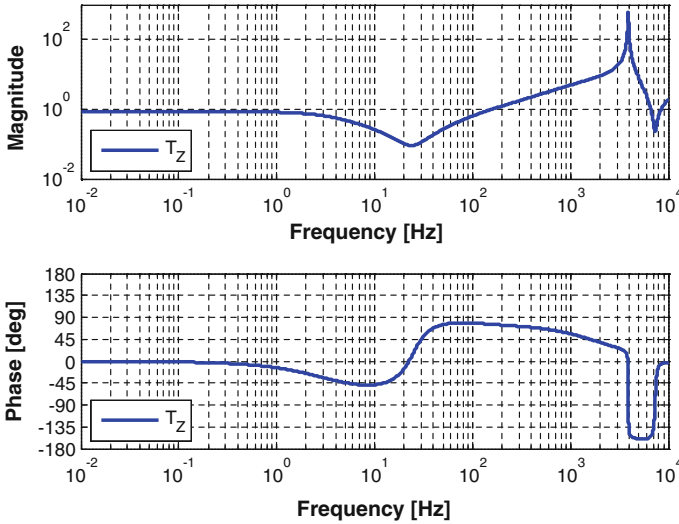
**Table 12.1** 50 kV underground DC cable properties used to illustrate stability analysis of DC microgrid [22]

Parameter	Description	Value	Units
$L_r$	Inductance	76	$\mu\text{H}/\text{km}$
$C_r$	Capacitance	1	$\mu\text{F}/\text{km}$
$R_r$	Resistance	36	$\text{m}\Omega/\text{km}$

A Bode plot of the frequency response of the loop gain transfer function  $T_Z$  (or  $Z_S/Z_L$ ) is illustrated in Fig. 12.14. It may be observed that the system is stable across the entire frequency range (i.e., it does not cross  $180^\circ$ ) and a rather small value of phase margin may be observed in the neighborhood of 5 kHz. Fortunately, the reduced phase margin occurs well above the frequency range in which power conversion takes place and it is likely that unmodeled skin effect losses in the DC interconnection cable will damp these higher frequency resonances introduced by the network cables.

### 12.5.2 Stability in AC Microgrids

An approach similar to the one taken for DC microgrids is not completely applicable to AC microgrids for various reasons: (1) the stability of an AC microgrid depends on the dynamics of the physical network as well as the dynamics of all the devices connected to it and more importantly (2) in grid-forming

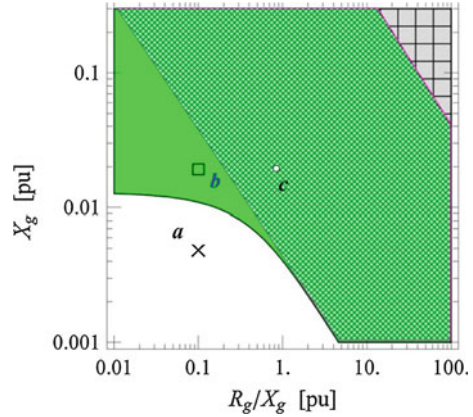


**Fig. 12.14** Magnitude and phase angle frequency response of source ( $Z_{in}$ ) and load ( $Z_o$ ) impedance, and source to load impedance ratio ( $T_Z$ ) to establish small signal stability of the DC microgrid wind farm collection network [22]

inverter-interfaced sources, the interplay between the voltage regulator and the generation controller has a dramatic impact on the overall system stability. Even for a single-phase system, it is no longer sufficient to consider the properties of a single loop gain transfer function that is represented by the impedance ratio at the interface. This is due to the inherent sinusoidal variation of the operating variables at the power frequency. It is common to transform such time varying quantities into complex phasor representation where the time variation is implicit. However, the complex representation also introduces direct and quadrature components for the operating variables. Therefore, the impedance ratio in effect consists of four dimensional transfer functions representing the coupling between *direct-direct*, *direct-quadrature*, *quadrature-quadrature*, and *quadrature-direct* variables. Furthermore, when the power frequency is in itself a dynamic variable in the droop controller, the phasor transformations do not necessarily lead to rather simple system representation. The abstractions and models to study the dynamic behavior using these transfer functions are only emerging at present have not been well established [23]. The stability evaluation is even more complex when considering unbalanced three-phase systems.

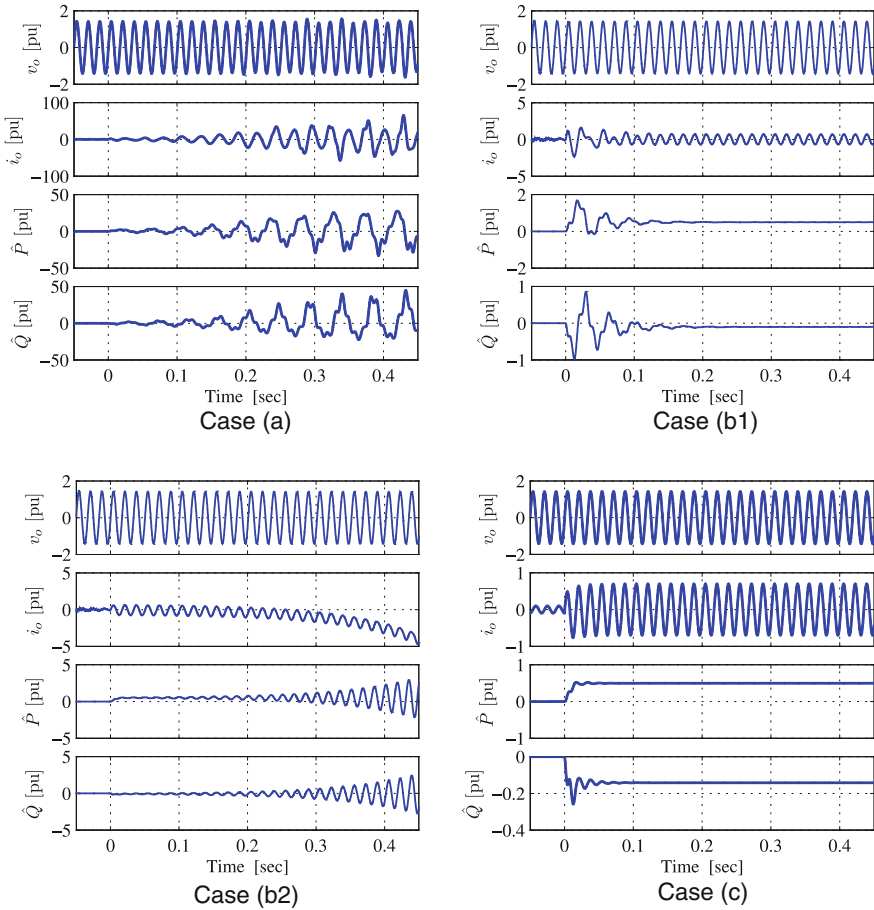
Therefore, by considering the simplest of microgrid systems—a single-inverter infinite bus system—and carrying out an eigenvalue analysis, one can gain useful insight to the relationship between the inverter controller and the interconnection impedance. Typical voltage regulators that may be considered are RMS voltage regulators and voltage waveform regulators. RMS voltage regulators aim to regulate the output voltage of the inverter based on feedback of the terminal voltage

**Fig. 12.15** Range of interconnection impedance parameters of a single inverter-utility interface illustrating stable operating regions for a RMS voltage regulator (*solid shaded region + hatched shaded region*) and a voltage waveform regulator (*hatched shaded region*)



of the inverter including any filters, as illustrated in Fig. 12.7. On the other hand, voltage waveform regulators aim to regulate the output voltage waveform of the inverter by tracking its time variations. A detailed eigenvalue analysis of the system includes a phasor dynamic model for all the state variables and controllers of the inverter. The steady state operating conditions are determined by solving the dynamic model for appropriate power throughput conditions. The model is then linearized at the operating point to determine the Jacobian of the system at the operating point. The locations of the eigenvalues of the Jacobian are examined to establish stability of the system at the operating points. Details of such an eigenvalue analysis of a candidate system may be found in [9], and the selected results are summarized here to illustrate the general properties. In this case, the sensitivity of the interconnection impedance (consisting of reactance  $X_g$ , and resistance  $R_g$ ) between the inverter and the infinite bus are studied. Figure 12.15 shows the range of interconnection impedance parameters of a single inverter-utility interface illustrating stable operating region for a RMS voltage regulator (solid green region) and a voltage waveform regulator (hatched green region). It may be observed that the RMS voltage regulator has the largest range of parameters values that lead to a stable steady state.

The results from the small signal modeling are verified using detailed computer simulation of the overall system including all the time variations and nonlinearities. Selected waveforms that confirm the results from the analytical model are presented in Fig. 12.16. Case (a) presents the waveforms from the unstable operating point (a) as noted in the white region of Fig. 12.15, where the  $X_g$  and  $R_g$  parameters are both quite low. Case (b1) and (b2), respectively, present the waveforms from the operating point (b) as noted in the green region of Fig. 12.15, which is stable while using a RMS voltage regulator, and unstable while using a voltage waveform regulator. Case (c) presents the waveforms from the operating point (c) as noted in the hatched green region of Fig. 12.15, which is stable while using a voltage waveform regulator.



**Fig. 12.16** Simulation results of a single inverter-utility interface illustrating stable and unstable operating points for a RMS voltage regulator and a voltage waveform regulator, respectively

The following key observations may be made from Fig. 12.15, as corroborated by Fig. 12.16:

- Under closed loop voltage control, if the  $X_g$  and  $R_g/X_g$  ratio are too small, the system is unstable (white region).
- If the  $X_g$  and  $R_g/X_g$  ratio are too large, the system does not have a reasonable operating point (gray checkered region).
- For moderate values of  $X_g$  and  $R_g/X_g$ , RMS voltage regulators have larger parameter range for stability when compared to voltage waveform regulators.

In summary, an interconnection reactance of approximately 10 %, with typical R/X values between 1 and 10 % provide a stable interface, particularly with the choice of RMS voltage regulators.

## 12.6 Summary

This chapter has presented an overview of microgrids as they pertain to power electronic interfaces between distributed and renewable energy resources. In particular, the concept of microgrids exploits the capabilities of power electronic interfaces through appropriate control to improve the flexibility in aggregating diverse resources. The focus of the discussion here has been on the power electronic interfaces, but in order to exploit the versatility and flexibility of the microgrid concepts, it can also be employed in aggregating resources that do not have power electronic interfaces, such as synchronous generators, induction generators, etc. with appropriate generation control, as well as storage systems and loads. Such an environment would allow increased penetration of renewable and distributed generation systems to serve the energy needs without compromising levels of reliability and power quality. It is also compatible with various intelligent communication and decision systems that are being considered under the rubric of ‘smart grid’ [24].

The technical features of the conceptual microgrids have been demonstrated in multiple scenarios in laboratory and field installations around the world. However, widespread adoption of the conceptual features would require innovations in commercial, economic, and business frameworks in the provision of electrical service to customers, steering away from the one-size-fits-all type of electric utility model that is common today [25].

## References

1. Lasseter R (2002) MicroGrids. In: Proceedings of the IEEE PES winter meeting 2002, vol 1, pp 305–308
2. Venkataramanan G, Marney C (2008) A larger role for microgrids IEEE power and energy magazine, May/June 2008
3. Barnes M, Kondohi J, Asanoi H, Oyarzabal J, Ventakaramanan G, Lasseter RH, Hatziaargyriou N, Green T (2007) Real-world micro grids—an overview, SoSE '07. IEEE international conference, pp 1–8
4. Johnson BK, Lasseter RH, Alvarado FL, Adapa R (1993) Expandable multiterminal DC systems based on voltage droop. IEEE Trans Power Delivery 8(4):1926–1932
5. Tang W, Lasseter RH (2000) An LVDC industrial power distribution system without central control unit, PESC 2000, vol 2, pp 979–984
6. Cuzner R, Venkataramanan G (2008) The status of DC microgrid protection, conference record of the IEEE IAS annual meeting, Edmonton, Canada
7. Sachau J, Engler A (1999) Static and rotating grid formation for modularly expandable island grids. In: Proceedings of 8th European conference on power electronics and applications. EPE 99, Lausanne, Switzerland
8. Guerrero JM, Berbel N, Matas J, Sosa JL, de Vicuna LG (2007) Control of line-interactive UPS connected in parallel forming a microgrid, IEEE international symposium on industrial electronics, 2007. ISIE 2007, 4–7 June 2007, pp 2667–2672
9. Sandeep Bala (2008) Integration of single-phase microgrids. PhD Dissertation, University of Wisconsin-Madison

10. Illindala MS (2005) Vector control of PWM VSI based distributed resources in a microgrid. PhD Dissertation, University of Wisconsin-Madison
11. Ciobotaru M, Teodorescu R, Blaabjerg F (2006) A new single-phase PLL structure based on second order generalized integrator, in power electronics specialists conference, 2006. PESC'06, 37th IEEE, June 2006, pp 1–6
12. Dimeas AL, Hatziaargyriou ND (2005) Operation of a multiagent system for microgrid control. *IEEE Trans Power Syst* 20(3):1447–1455
13. Barklund E, Pogaku N, Prodanovic M, Hernandez-Aramburo C, Green TC (2007) Energy management system with stability constraints for stand-alone autonomous microgrid. In: *Proceedings of the IEEE international conference on systems of systems engineering*, 16–18 April 2007, pp 1–6
14. Jayawarna N, Wu X, Zhang Y, Jenkins N, Barnes M (2006) Stability of a microgrid. In: *Proceedings of the 3rd IET international conference on power electronics, MACHines and drives*, Mar 2006, pp 316–320
15. Venkataramanan G, Illindala M (2007) Small signal dynamics of inverter interfaced distributed generation in a chain-microgrid. In: *Proceedings of IEEE power engineering society general meeting, 2007*, 24–28 June 2007, pp 1–6
16. Illindala M, Venkataramanan G (2010) Small signal stability of a microgrid with parallel connected distributed generation, special issue on microgrids. *Int J Intell Autom Soft Comput* 16(2)
17. Chung I-Y, Liu W, Cartes DA, Collins EG, Moon S-I (2010) Control methods of inverter-interfaced distributed generators in a microgrid system. *IEEE Trans Ind Appl* 46:1078–1088
18. Middlebrook RD (1976) Input filter consideration in design and application of switching regulators. In: *IEEE proceedings of the IASAM*
19. Carrol J (1992) An input impedance stability criterion allowing more flexibility for multiple loads which are independently designed, naval air warfare center, aircraft division, Indianapolis, B/812, Jan 1992
20. Wildrick M, Lee FC, Cho BH, Choi B (1995) A method of defining the load impedance specification for a stable distributed power system. *IEEE Trans Power Electron* 280–285
21. Sudhoff SD, Glover SF, Lamm PT, Schmucker DH, Delisle DE (2000) Admittance space stability analysis of power electronic systems. *IEEE Trans Aerosp Electron Syst* 36(3): 965–973
22. Ludois D (2012) DC interconnected wind farm using bridge of bridge multilevel converters, PhD Dissertation, University of Wisconsin-Madison, Jan 2012
23. Francis G, Burgos R, Boroyevich D, Wang F, Karimi K (2011) An algorithm and implementation system for measuring impedance in the D-Q domain. In: *Proceedings of 2011 IEEE energy conversion congress and exposition (ECCE)*
24. Lemmon MD, Venkataramanan G, Chapman P (2009) Using microgrids as a path towards smart grids. Position paper presented at NSF workshop in cyber physical energy systems, Baltimore, MD, Jun 2009
25. Marnay C (2007) Microgrids and heterogeneous security, quality, reliability, and availability. In: *Proceedings of the 2007 power conversion conference—Nagoya*

# Chapter 13

## Power Electronics for Smart Distribution Grids

**Danilo I. Brandão, Renata Carnieletto, Phuong H. Nguyen,  
Paulo F. Ribeiro, Marcelo G. Simões and Siddharth Suryanarayanan**

**Abstract** The operation of future electricity grids will have a multi-disciplinary nature via the merging of energy and communication infrastructures, and the interaction of state-of-the-art technologies such as power electronics, computational intelligence, signal processing, or smart metering. This interoperability presents challenges to optimize system performance by improving synergy between actors, i.e., producers, consumers, and network operators. This chapter tackles a part of these challenges by focusing on the role of power electronics in smart grids. First, background information of emerging distribution systems, evolutionary changes, and enabling technologies is presented. Furthermore, a requirement of electronic-based interface systems with smart topologies and controls is explained. Finally, applications of smart interface systems are expounded via three examples: (1) smart inverters, (2) smart power router, and (3) virtual synchronous generator.

### 13.1 Introduction to Emerging Distribution Systems

Worldwide, electric power grids are transforming toward varied levels of modernization at the start of the twenty-first century. Drivers for such transformations include: the need for enhanced reliability and power quality to serve the advanced loads of the new century; accommodation of projected growth in demand levels; and integration of ‘cleaner’/‘greener’ sources of electricity generation and storage. In order to achieve this modernization, governmental mandates such as the Smart

---

D. I. Brandão · R. Carnieletto · P. H. Nguyen (✉) · P. F. Ribeiro · M. G. Simões ·  
S. Suryanarayanan  
Den Dolech 2 CR2.10 (building Corona), P.O. Box 513, 5600 MB Eindhoven,  
The Netherlands  
e-mail: p.nguyen.hong@tue.nl

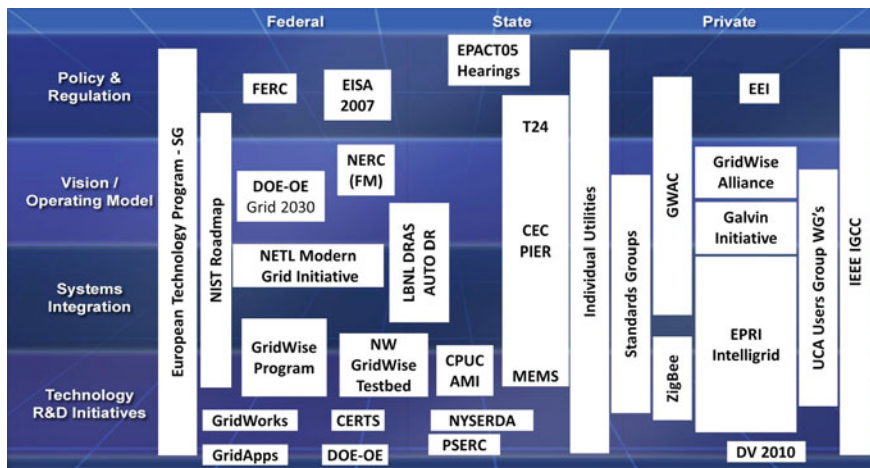


Grid Initiative (SGI) in the USA and European Electricity Grid Initiative in (EEGI) in Europe have been introduced. The popular phrase, *Smart Grid*, which is used as an umbrella term to describe the emerging modernized power grid, promulgates the use of technologies from the control and communications field to greater extent in the power grid so as to achieve greater efficiency in operation and resiliency in the grid. In other words, the *Smart Grid* may be loosely defined as an emerging electricity infrastructure that possesses bidirectional flow of electric power and digital information. Based on current worldwide trends in lowered transmission investments, coupled with retirement of assets at the transmission level, it is expected that the *Smart Grid* will evolve at the distribution levels of the electric grid. An imperative for such an evolution is the integration of flexible and intelligent power electronic devices, across various levels, at the distribution system. In this chapter, an overview of power electronics for emerging distribution systems along with some examples is provided.

### ***13.1.1 Policies and Standards for the Smart Grid***

Globally, efforts are underway to address the needs for sustainable, clean, and secure energy for the future—i.e., the development of a Smart Grid. In order to realize a Smart Grid, it is necessary for legislative policies and regulations to be in place. For example, a Smart Grid project sponsored by the Federal Energy Regulatory Commission (FERC) and the National Association of Regulatory Utility Commissions (NARUC) in the USA is providing the forum for state and federal regulators to discuss issues and make recommendations for state and federal policies to support the Smart Grid development. Grid 2030, the US DOE's long-term vision for the twenty-first century electric infrastructure also calls for introduction of smart controls and appliances to the existing grid [1]. Some other projects in the US include the Electric Power Research Institute (EPRI) IntelliGrid initiative, which has developed a utility-centric technical project framework and engaged in pilot implementations, the Department of Energy (DOE). Modern Grid Initiative efforts to enable and accelerate grid modernization, including providing analytic support, the Grid Wise Alliance which is a coalition of utilities, technology vendors, and others. Figure 13.1 shows the numerous groups involved in Smart Grid initiatives where policy and regulation at federal, state, and private levels are listed as a function of the vision, systems integration, and technology developments.

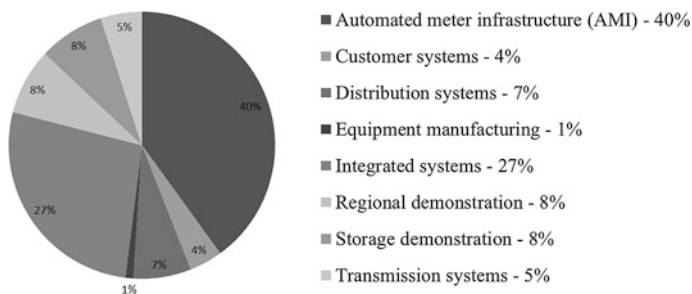
The Energy Independence and Security Act of 2007 (EISA07) passed by the 110th U.S. Congress included the Smart Grid Initiative, which is the official policy of the United States to modernize the electricity grid [3]. A document titled “A Policy Framework for the twenty-first Century Grid: Enabling our Energy Future,” [4], has established a policy framework based on four pillars for a Smart Grid—(1) enabling cost-effective Smart Grid investments; (2) unlocking the potential of innovation in the electric sector; (3) empowering consumers and enabling informed decision making; and (4) securing the grid from cyber-security threats,



**Fig. 13.1** Selected federal, state, and private smart grid initiatives in the USA (Courtesy: E. Lightner, ENERNEX [2])

and which will support key aspects of the transition to a smarter grid and a clean energy future. The American Reinvestment and Recovery Act of 2009 (ARRA09) enacted by the 111th US Congress provides several billions of dollars for investment in the Smart Grid [5]; Fig. 13.2 depicts a histogram of the allocation of Smart Grid projects in the USA as of June [6].

On a global scale, the International Panel on Climate Change (IPCC) Working Group III’s Special Report on Renewable Energy (RE) Sources and Climate Change Mitigation (SRREN) presents an assessment of the literature on the scientific, technological, environmental, economic, and social aspects of the contribution of six renewable energy sources aimed at mitigating the effects of climate change [7]. It is intended to provide policy relevant information to governments, intergovernmental processes, and other interested entities.



**Fig. 13.2** A pie chart of the distribution of various smart grid PROJECTS in the US (as of Jun 2011) according to project type (Figure generated with data from [www.SGICclearinghouse.org](http://www.SGICclearinghouse.org))

As an enabling technology, power electronics has the ability to provide effective and intelligent solutions for the grid of the future; however, the complexity and interaction of the dispersed assets in an emerging distribution system is nontrivial and requires interoperability and compliance with standard procedures. In that regard, in the US, the National Institute of Standards and Technology (NIST), which has been assigned the role of a national coordinator for Smart Grid interoperability standards, released a framework and roadmap for interoperability standards in January 2010 [8]. In September 2011, the Institute of Electrical and Electronics Engineers (IEEE) developed the Standard 2030 guide for “Smart Grid interoperability of energy technology and information technology operation with the electric power system, and end-user applications, and loads” [9]. The International Electrotechnical Commission (IEC) has identified over 100 standards from its repertoire as relevant to the Smart Grid [10]. Interoperability promises the plug-and-play feature of the various devices and assets that may synergistically form the Smart Grid. It is necessary that evolving power electronics adhere to such interoperability standards for controls and communications purposes.

## 13.2 Evolutionary Changes and Enabling Technologies

In this section, the evolutionary changes that are anticipated on legacy distribution systems, and the associated enabling technologies are presented.

### *13.2.1 Evolution of a Smart Distribution System*

Based on the expectations of the Smart Grid Initiative and relevant supporting documents, a survey for identifying the characteristics of a smart distribution system was performed [11].

The major findings from the survey in [12] indicates that an evolving smart distribution system:

1. Will avail of enabling features such as real-time pricing, Automated Metering Infrastructure (AMI), two-way communicating devices, and networked connections between feeders for optimizing distributed assets.
2. Will possess integrated Distributed Energy Resources (DER) at all distribution voltage levels capable of with two-way communications with the service provider via a smart meter, a local energy management system, and with other DERs at the rate of at least once per minute. It is expected that renewable energy sources will make up at least 10–19 % of the total generation, of which less than 50 % of the new DERs will be met by renewable sources. The new DERs will be supported by battery storage and fast-starting dispatchable generation sources. Distributed Storage (DS), primarily batteries will comprise less

than 50 % of rated load for up to four hours, and are expected to support up to 50 % of nondispatchable DER.

3. Will be characterized by massively deployed sensors and smart meters that will engage in two-way meshed communications and be enabled with control algorithms to automatically react to measurements.
4. Will provide avenues for consumer participation in Demand Response (DR) through the widespread use of dynamic pricing, with real-time signals.
5. Will use adaptive and self-healing technologies primarily integrated at the 15 kV class. Smart feeders will be responsible for self-healing actions and will be enabled by digital feeder automation capable of communications.
6. Will utilize advanced tools (including visualization, analysis, and simulation) to streamline routine operations.
7. Will possess smart appliances and consumer devices that are two-way communication enabled and controllable.
8. Will have the ability to operate in either intentionally islanded or grid-connected mode [12].

### ***13.2.2 Operation and Management Philosophies***

As indicated in the previous subsection, the evolving smart distribution grid is projected to have increased levels of RE sources and other assets, hitherto not seen on the legacy distribution system. This infrastructural change is inherently dispersed and calls for provision of timely information on system states and parameters to the various entities engaged in operation and management (O and M) services. The dispersed nature of the emerging distribution grid also introduces scenarios where different O and M service providers may be present in different locations with different expectations and goals. As a result, O and M surfaces as an important aspect of the Smart distribution grid that must take into account the various interactions between entities such as local energy management systems (LEMS), the Distribution Management System (DMS), the utility Supervisory Control And Data Acquisition (SCADA) system and possibly any newly emerging Balancing Authorities (BA), and Power Exchange (PX) markets for distribution systems. It is not inconceivable to envision a distribution system aggregator that sends out price and control signals through the system and charged with the task of balancing the system, much like in contemporary bulk (transmission) power systems. This is more relevant when intentional islanding of distribution systems becomes an accepted practice.

At the end-user level, it is expected that dedicated service providers will provide O and M services; relevant information may be accessed bidirectionally through the Smart meter as a portal. The end-user LEMS may either use software supplied by enterprises or use the portal software provided by the local distribution utility for purposes of communications. The communication network itself could use a variety of the following secure choices: cellular protocols, Home Area

Networks (HAN), WiFi, Wireless mesh networks, Zigbee, Internet, Broadband over Power Lines (BPL), or Fiber-optic [12]. Schedulable home appliances provide the ability to control/cycle them during DR actions [13]. In commercial and industrial loads, the variability in loads is not as dramatic as in the loads of the residential sector, hence the advent of pervasive controls for O and M purposes in the commercial and industrial sectors of the distribution system may not be as profound. Regardless, it is possible that in the coming years, public concern over privacy may introduce litigations against utilities and/or distribution service providers. This may force the utilities and distribution service providers to adopt a rigorous method of authenticating O and M services for the end-user.

As the transportation fleet undergoes transformation into a partially electric fleet, new O and M requirements for electric vehicle management will be required. This could include: vehicle identity registration systems with the utility or DMS; utility or DMS interactions with financial institutions such as credit card companies; utility or DMS interactions parking structure owners who offer electric vehicle recharging and discharging services; and the possible use of registering the vehicles in a DR or energy conservation program.

As end-users being to generate electricity and back feed to the grid, it will be required that they meet the technical requirements of appropriate standards for connecting distributed generation to the grid, such as the IEEE 1547 and UL 1741 [14, 15]. Additionally it will be required to identify and register the devices with the utility, which likely will involve the ability to install a digital certificate on the participating devices—this opens another avenue of new products, services, and markets, as mandated by the SGI.

Increased levels of asset integration will require advanced management of assets and demand through smart metering technologies. M2M (Machine-to-Machine) Interfaces may replace some Human–Machine Interface (HMI) solutions, thus accelerating the deployment of increasingly sophisticated automatic control systems. All of the above O and M aspects must be incorporated into the control algorithms of the front end of the various power electronics devices that will interface the assets to the emerging distribution grid.

### ***13.2.3 Services***

As smart distribution systems emerge on the grid, it is expected that the existing and new assets such as DG, distributed energy storage (DES) units will be adaptable for provision of not only primary service, i.e., supply of electricity, but also a portfolio of ancillary services. It is easy to envision that the provision of such diverse services from the same asset will require power electronics front end, for these assets that are inherently capable of functioning in multiple quadrants. Some of the ancillary services that could be made available from assets with power electronics front ends include:

- Voltage regulation
- Frequency regulation
- Provision of spinning reserves and standby service
- Power quality enhancement
- Power factor correction
- Instantaneous power compensation during load transients
- Intentional islanding for DR.

### ***13.2.4 Communication and Control Infrastructures***

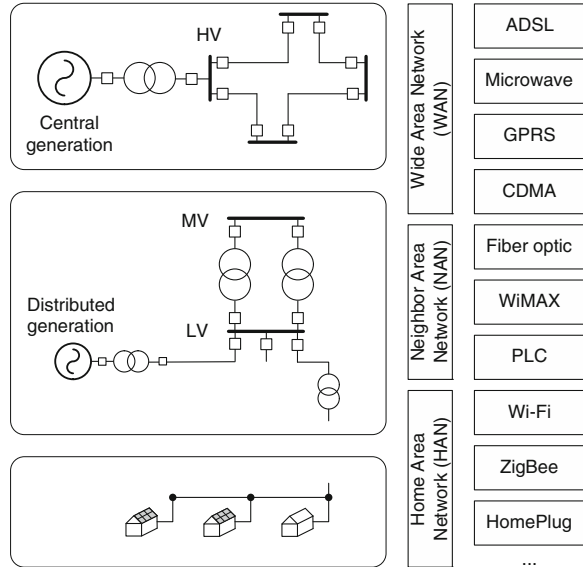
SCADA is an existing application of Information and Communication Technologies (ICT) in the electricity grid. This normally Ethernet-based network is used by operators to fulfill their missions of real-time monitoring and control functions. In emerging distribution networks, the introduction of RE sources is expected to be more efficient, when the development of the ICT-based DMS for meeting grid requirements matures. The ICT infrastructure will have to adapt to the operation of the myriad of small-scale generation units by monitoring a range of variables and ensuring efficiency of generation.

It is desired to have bidirectional power and information flows on the distribution networks with Neighborhood Area Network (NAN) and Home Area Network (HAN). Depending on characteristics of bandwidth, latency, traffic model, and priority level, different wired communication technologies such as Power Line Communications (PLC), Asymmetric Digital Subscribers Line (ADSL), fiber optic, and wireless technologies such as WiMAX, Code Division Multiple Access (CDMA), WiFi, ZigBee, may be used in different communication networks [12]. Figure 13.3 gives an overview about possible integrations of ICT technologies in emerging distribution systems and Smart Grids.

As a part of a Smart Grid, smart metering and sensor systems are under varying levels of development and deployment for distribution networks. This is expected to provide large amounts of information for management and control purposes in smart grids [16]. DR can be implemented and supported by two-way smart meters and smart sensors on equipment communicating through ICT, managing the demand according to the agreements reached with the customers. Advanced ICT infrastructure opens possibilities for real-time and scalable market mechanisms to reduce uncertainty of instantaneously changing prices and to arrange short-time reserves. Near real-time information allows utilities to manage the power network as an integrated system, actively sensing and responding to changes in power demand, supply, costs, and quality across various locations. However, wide-area integration of ICT in the distribution system might also introduce vulnerabilities which might influence the reliability of the power network [17].

Control infrastructures for emerging distribution systems may appear as either centralized or decentralized schema. Regardless of the type of control infrastructure, it is imperative to possess a communication infrastructure for coordinated control

**Fig. 13.3** An overview of possible integration in emerging distribution systems and Smart Grids



actions. Communication is required to effect control actions such as dispatching generation, shedding loads, initiating black start, engaging energy storage elements, and participating in the electricity market [18]. The backbone of a successful communication system in emerging distribution systems is the existence of a minimally redundant sensory network that is capable of communicating among hierarchical agents [18].

### 13.3 Smart Topologies and Controls for Interface Systems

A power electronic interface, e.g., as an inverter, can operate in stand-alone or in grid-connected modes. There are a few interfacing control methodologies that should be used in both cases. In the stand-alone mode, the inverter must maintain the constant output voltage and frequency, and the load will determine the needed operation power factor. The inverter voltage is asynchronous with the grid voltage, and the reactive power is supplied by recirculation current through the free-wheeling diodes of the inverter’s Insulated Gate Bipolar Transistor (IGBT). It is also considered in the international literature as an Uninterruptible Power Supply (UPS) operation mode. In the grid-connected mode, the voltage and frequency are determined by the utility grid. The injected current is defined by the power electronic circuit with a proper feedback control. Therefore, the operation power factor is usually maintained unitary. With the advent of DG based on power electronics, several applications in the last few years have demonstrated the advantages of programming reactive power at the grid, harmonics mitigation, and

even voltage control at the Point of Common Coupling (PCC), as well as the utilization of energy storage systems. However, such features can only be applied in practice if real-time communication is implemented between control system and utility. Smart-grid technological advances has been facilitating these advanced functions [19]. When the inverter is grid connected, an auxiliary security control systems must be implemented in order to isolate the inverter from the grid in case of black-out, and to seamlessly reconnect it back to the grid. IEEE 1547 standards have been developed in USA for distributed generation interconnection to the grid, and power electronic interfaces must comply with IEEE 1547 guidelines.

### ***13.3.1 Interfacing Control Methods***

Grid-connected inverter interfacing methods have historically evolved from front-end PWM rectifiers used in regenerative machine drives [20], where instead of dissipating power on dynamic break (from deceleration or torque reversal transient operation) the efficiency is improved by pumping power back to the grid. Actually, a grid connected inverter has the same control principles as Pulse Width Modulation (PWM) rectifier has; but further flexibilities are required when such systems are primarily injecting power in the grid from renewable energy sources (PV or wind), or from fuel cells, since an overall balance of system must be provided. In order for a Voltage Source Inverter (VSI) be connected to the grid, an impedance must be provided across, typically a decoupling inductor, or interphase reactors can be used to connect power converters with regenerative capabilities [21]. Voltage source converters connected to the grid have been demonstrated to have improved performance by LCL filters, originally proposed by [22] and since then incorporated initially in active rectifiers and latter to DG applications [23–25]. In addition, the control system for injecting power in the grid has been designed by analogy in order to resemble machine control techniques used in designing cascaded loop control—where voltage is commanded in the outer loop (as machine speed in a drive system) and current in the inner loop (as machine torque in a drive system). For the same reasons that a vector controlled drive system has back-EMF cross-coupling motional voltages that must be compensated in the torque control loop, a grid connected inverter presents a cross-coupling voltage drop, i.e., a system reactance multiplied by current term from one axis disturbing the other one. Therefore, a Proportional-Integral (PI) based controller must be properly designed to optimize such cross-coupling effects [21]. Recently, P + Resonant controllers have been used to improve dynamic performance of current control loop [26].

One of the major challenges for a proper decoupled control is the synchronization with the grid frequency. Several research works have applied Phase Locked Loop (PLL) techniques for grid connected inverters, while used LCL filters instead of common interphase reactors. However, there is still a discussion on which



methodology is the most efficient. Three-phase systems are easily controlled with decoupled d-q or p-q theory, whereas single-phase grid connected inverters do not have a proper mathematical formulation. Solutions based on hysteresis band control, approximated solution considering a phase time shifted by  $90^\circ$ , or Hilbert transform have limited capabilities. Some approaches consider the same decoupled d-q or p-q methodologies for single-phase systems [27, 28].

The following sections describe the main approaches for implementing such interfacing control methods for grid connected inverters.

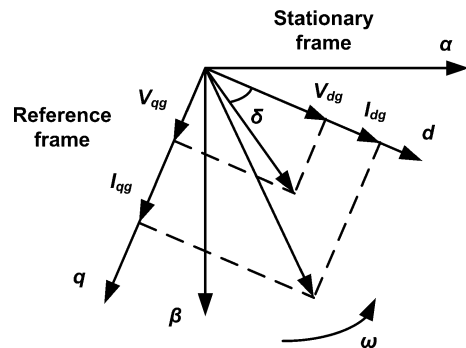
### 13.3.1.1 Constant Current Control

In order to connect to the utility voltage source grid, the inverter is designed to supply constant current output. The constant current control is implemented with reference frame transformation from three-phase to stationary frame (abc/dq). With the unity vector synthesized by a PLL, a reference frame rotates synchronously with the grid, as shown in Fig. 13.4 [29]. Equation (13.1) describes the grid dynamics which is used for the feedback control (typically PI controllers). This feedback loop limits output voltage on the reference frame. Figure 13.5 shows a control diagram that commands the gating pulses of the inverter transistorized bridge. The PLL synthesizes the unit vector that allows synchronization with the utility grid.

$$L \frac{d}{dt} \begin{bmatrix} i_d \\ i_q \end{bmatrix} = \begin{bmatrix} R & -\omega L \\ \omega L & R \end{bmatrix} \begin{bmatrix} i_d \\ i_q \end{bmatrix} + \begin{bmatrix} \Delta e_d \\ \Delta e_q \end{bmatrix} \quad (13.1)$$

where  $i_d$ ,  $i_q$  are the  $d$  and  $q$  axis current components;  $\Delta e_d$  and  $\Delta e_q$  are the instantaneous voltage difference between the PCC and the inverter output voltage of  $d$  and  $q$  axis components;  $R$ ,  $L$ , and  $\omega$  are grid resistance, inductance, and fundamental angular frequency.

**Fig. 13.4** Stationary and reference frame for grid variables



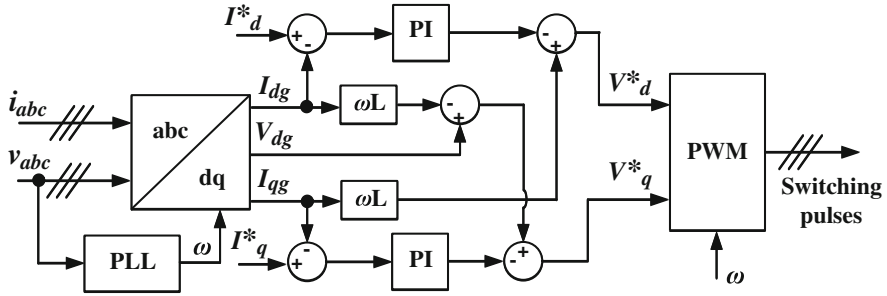


Fig. 13.5 Constant current control technique

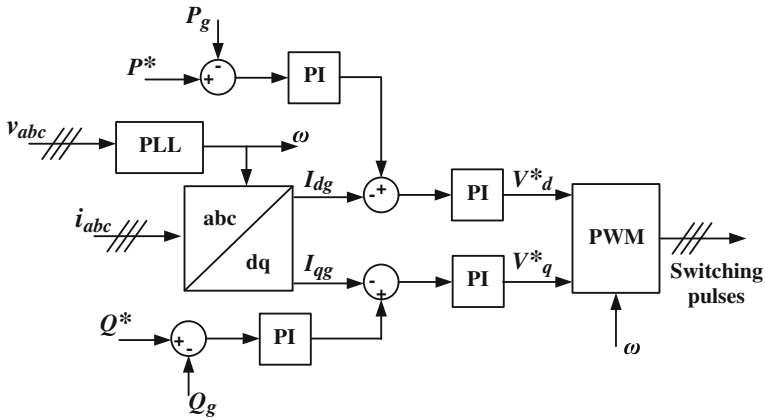


Fig. 13.6 Constant P-Q control technique

### 13.3.1.2 Constant P-Q Control

The generalized theory of the instantaneous reactive power in three-phase circuits has been proposed by Akagi in 1983 [30] and it was used for the first time to control grid-connected inverters in 1991 by Ohnishi [31], as indicated by Eqs. (13.2) and (13.3). There are some advantages of instantaneous power-based controllers: (1) power calculation does not vary by any transformation, (2) it is directly related to energy-constrained sources, such as PV and wind, and (3) it allows instantaneous power balance transactions with the utility grid. Figure 13.6 shows an implementation diagram where active power builds up the q-reference value for current, which is compared to the instantaneous grid q-current, whereas the reactive power loop builds up the reactive power d-reference current value, which is compared to the instantaneous grid d-current. Therefore, a constant P-Q control is an outer loop over a current loop control.

$$p = \frac{3}{2} [v_{ds}i_{ds} + v_{qs}i_{qs}] \tag{13.2}$$

$$q = \frac{3}{2} [v_{qs}i_{ds} - v_{ds}i_{qs}] \tag{13.3}$$

### 13.3.1.3 Constant P-V Control

The grid-connected inverters allow controlling the voltage at the PCC, as shown in Fig. 13.7 [19]. This technique is a slight variation of the previous one, where basically the voltage feedback is used to adjust the amount of reactive power (or d-axis voltage) required for the system. Although it seems simple, there are some challenges in this approach, where the instantaneous peak voltage of the utility grid must be followed at the PCC, the PCC must have an impedance, usually inductive, between the supply system and the inverter and that will affect the stability of the feedback control loop. The P-V control approach is the most suitable for voltage support utility services, but it is very difficult to define stability range of operation by mathematical analysis, and very extensive real-time simulation and experimentation must be conducted in order to implement the hierarchical level of active power and voltage grid control.

### 13.3.1.4 IEEE 1547 and Associated Controls

It is imperative that control algorithms that performs the task of connecting (and intentionally islanding) the Power Electronic (PE) based DG to (and from) the grid confirms with the IEEE 1547 family of standards, as applicable to the installation [14]. Control functionalities must take into account a variety of input parameters such as frequency, phase, and DQ frame voltage of the grid and the PE side. The control algorithm must compare these inputs with the IEEE 1547 recommendations and generate appropriate signals with in the recommended critical time to island or to reconnect the PE-based DG to the grid. It is relevant to note that at the

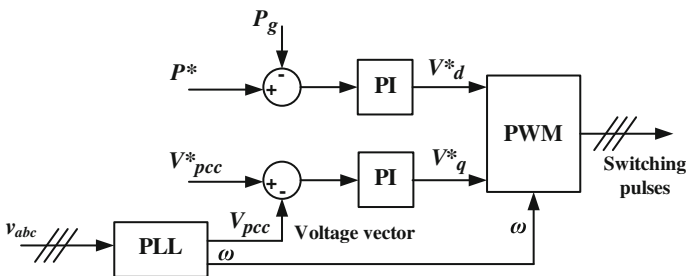


Fig. 13.7 Constant P-V control technique

time of writing this chapter the IEEE 1547 family of standards has begun deliberating the technical considerations for effective provision of both primary and ancillary services. In this chapter, a smart inverter is presented that takes into account the provision of at least one ancillary service in addition to the primary service [19].

## 13.4 Examples of Smart Interfacing Systems

In this section, three examples of power electronics-based smart interfacing systems—a *smart* inverter, a *smart* power router, and a virtual synchronous generator—are presented with the aid of description of the associated models and plots from simulation studies.

### 13.4.1 Smart Inverter

In this subsection, the combined functional ability of the voltage source inverter is defined to: supply power to local loads; supply power to other utility loads up to rated capacity of the inverter; store energy in a local lead acid battery bank; provide voltage support at the PCC of the utility; and provide control options to the consumer based on near real-time electricity information obtained from the utility through advanced metering devices.

General design methodologies for inverters applied in the smart grid systems is presented in [32, 41]; however, the combined smart functionalities described in this section are exclusive of this work. The smart inverter functionalities depicted in this section look beyond the recommendations of the current national technical standard for interconnecting DG sources to the grid—the IEEE Std. 1547 [14], because it may provide voltage support at the PCC, offering an extra service in case of voltage sags scenarios. Usually, in a scenario of voltage sags in distribution systems, the voltage is regulated by utility owned (or) operated capacitor banks; however, with the appearance of the smart inverter functionalities, the ability to regulate voltage at the PCC is brought to the customer. The authors have not probed the safety issues stemming from performing voltage control on the grid side using the proposed inverter setup.

Based on real-time spot pricing of active and reactive power obtained from the utility using an advanced metering device, on the state of charge (SOC) of the battery bank and on settings of the customer, the inverter control algorithm determines the optimal operating mode. This algorithm enables the inverter to: (a) schedule local loads; (b) determine either to locally store energy or sell energy to the grid.

### 13.4.1.1 Models

A voltage source inverter was designed as a 5 kVA single-phase full bridge converter operating at 120 V (60 Hz) to function in two modes: grid-tied and islanded [19]. For it, the voltage source inverter must have two control loops: current control loop and voltage control loop. The entire control is developed in the  $dq$  frame with a virtual  $q$ -axis (as the application is single-phase). According to [33, 34], the  $q$  quantity is obtained either by the derivative of the fundamental signal, or by delaying the real axis quantity by one quarter of the grid-voltage period [19]. In this work, the latter technique is employed. Figure 13.8 depicts the block diagram of the smart inverter topology.

The phase-locked loops (PLL) have been used to provide the phase angle ( $\theta$ ) information to the control loops, as shown in Fig. 13.9. The current and voltage control loops shown use four proportional-integral (PI) controllers: two PIs with the same gains for the current control loop ( $i^*_d$  and  $i^*_q$ ), and two PIs with the same gains for the voltage control loop ( $v^*_d$  and  $v^*_q$ ). The PI compensator generates the modular PWM signal and they have been chosen for its simplicity and ease implementation. According to Fig. 13.9, the main control consists of two control loops: voltage control loop, that is enabled when the inverter operates in islanded mode, and current control loop for the grid-tied mode.

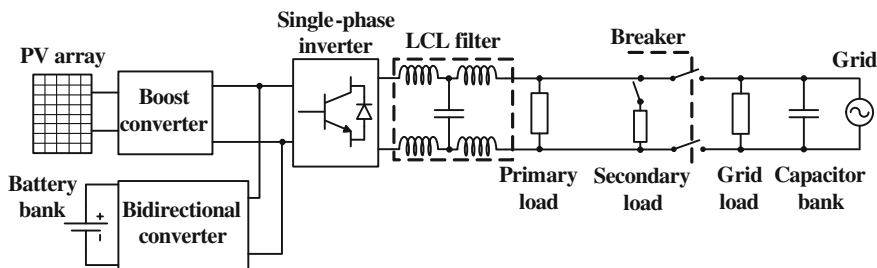


Fig. 13.8 Block diagram of the smart inverter topology

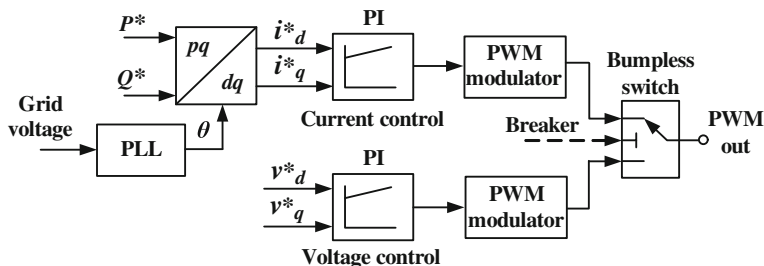


Fig. 13.9 Control loops of the smart inverter

The main goal of the voltage source inverter development with smart functionalities is to enable an efficient interconnection and economical operation for dispersed PV-based DG system to the utility grid. The local load (inverter load) has been modeled as two components: a primary VSI load and a secondary VSI load—which distinguishes the critical loads from others that may be scheduled at the location. Thus, if the inverter is operating at the islanded mode and it does not have enough power to supply all local loads, only the VSI primary load will be supplied. Another convenience of this load set is the ability to operate in the economic mode. This will be explained in the following sections.

The input to the single-phase voltage source inverter is a voltage stabilized at 350 VDC, provided by the set formed by photovoltaic panels and DC–DC boost converter. The nominal output voltage of the PV array is 192 V. Then a DC–DC boost converter has been used in the model to raise the PV voltage level to 350 VDC. The inverter setup also includes a lead-acid battery storage bank with nominal voltage of 192 V and 24 Ah cells, [19], connected to the DC link through a bidirectional DC–DC buck–boost converter modeled as shown in Fig. 13.10. A battery model is from MatLab/Simulink platform simulation [35]. The storage subsystem brings flexibility to the system, e.g., the ability to supply local loads when the inverter is islanded without enough power, to store cheap energy and to sell when the price is higher.

Table 13.1 provides a listing of the various specifications of the DC–DC buck–boost converter of the smart inverter [19].

The smart functionalities of the voltage source inverter are aimed at: provision of active and reactive power support to local loads and to grid loads up to the rated capacity; store energy in a local lead acid battery bank; option to regulate voltage

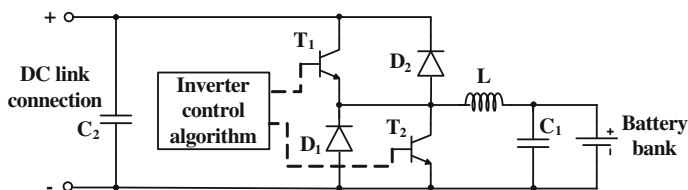


Fig. 13.10 Control diagram of the bidirectional DC–DC buck–boost converter [19]

Table 13.1 Design specifications of the DC–DC buck–boost converter used in the smart inverter [19]

Quantity (symbol)	Value
Buck–boost nominal active power ( $P$ )	5 kW
DC link nominal voltage ( $V_{DC}$ )	350 V
Battery nominal voltage ( $V_B$ )	192 V
Switching frequency ( $f_s$ )	15 kHz
Series resistance of battery bank ( $r_B$ )	0.2 $\Omega$
Inductor resistance ( $r_L$ )	0.02 $\Omega$
Series resistance of the $C_1$ and $C_2$ capacitors ( $r_C$ )	0.05 $\Omega$

at the PCC during voltage sags; and decision-making ability aided by information of real-time pricing obtained through advanced metering devices from the utility grid. Note that the goal of this section is not to discuss how the real-time pricing will be obtained.

Based on the above functionalities, the inverter operation is governed by certain rules, which determine the mode of operation—identified in this section as super-modes and sub-modes. Depending upon the status connection to the grid as determined by compliance with IEEE Std. 1547, there are two super-modes: stand-alone mode (S1) and grid-tied (S2) mode, vide Fig. 13.11.

In super-mode S1, i.e., the stand-alone mode, the inverter is islanded (isolated) from the electric distribution system and it is subject to operation under one of the following three sub-modes viz., s1, s2, s3 depending upon the available inverter active power ( $P_{INV}$ ) and the local active power demand ( $Z_{INV}$ ), where  $P_{INV}$  represents the total active power output of the PV panels and the battery bank output, and  $Z_{INV}$  represents the sum of active power of the primary VSI load plus secondary VSI load.

In sub-mode 1 under super-mode 1, identified as S1s1, when  $P_{INV}$  is lesser than  $Z_{INV}$ , the power output of the PV panels and stored energy are not enough to supply the full demand of the local load. In such case, a prioritization of local demand is effected and selected loads (primary VSI load) are powered by the inverter. If, after the selection of loads there is any remaining power from the PV panel, it will be directed to storage in the battery bank. Typically, such a redirection to the energy storage depends on level of the state of charge (SOC). It is important to note that the SOC control of battery banks will not be discuss in this section.

In sub-mode 2 under super-mode 1, defined as S1s2, when  $P_{INV}$  is greater than  $Z_{INV}$ , the available inverter power is greater than the local demand. In this circumstance the residual power is routed to the battery banks for storage.

In sub-mode 3 under super-mode 1, identified as S1s3,  $P_{INV}$  is equal to  $Z_{INV}$ , wherein the available inverter power is equal to the local load demand. In this case, the inverter feeds the local loads without storage. A prioritization of loads may be effected in this case if there is a need to store some of the energy for later use.

In super-mode S2, i.e., the grid-tied mode, the voltage source inverter is interconnected to the electric distribution system and is subject to operation under one of the following four sub-modes viz., s1, s2, s3, s4 depending upon the

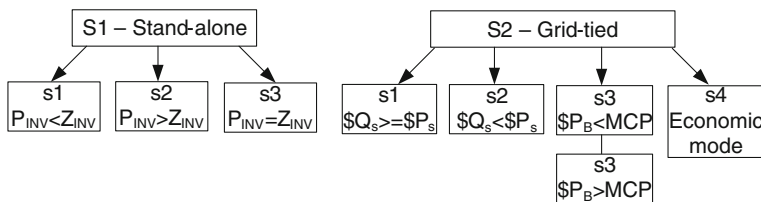


Fig. 13.11 Summarizes operating modes of the smart inverter

available inverter active power ( $P_{INV}$ ), local active power demand ( $Z_{INV}$ ), and economic considerations for trading active and reactive power with the grid on a spot pricing basis. The variables for economic consideration include the spot price to sell active power to grid ( $\$P_S$ ), spot price to sell reactive power to grid ( $\$Q_S$ ), a threshold value of the grid pricing of an electricity unit which will enable the consumer to decide which loads will be powered using the inverter. In this case, it is assumed that the grid has infinite demand, i.e., the grid will acquire whatever the inverter intends to sell.

In sub-mode 1 under super-mode 2, defined as S2s1, when  $\$Q_S$  is greater or equal than  $\$P_S$ , the inverter is controlled to provide voltage support regulation to the grid. If there should exist additional inverter capability to provide active power, then the inverter is controlled so that  $Z_{INV}$  is supplied by the  $P_{INV}$  and any remaining power is sold to the grid and/or stored in the battery bank [13].

In sub-mode 2 under super-mode 2, identified as S2s2, when  $\$Q_S$  is lesser than  $\$P_S$ , the inverter is controlled to fix the reactive power reference to zero and supply only active power to local loads ( $Z_{INV}$ ) and any remaining power is directed to the grid and/or to the battery banks [13].

There exist another sub-mode under this super-mode, i.e., S2s3. This is related to the option of powering local loads using the inverter versus the option of purchasing active power from grid, when there is power available from DG. This can be chosen based on comparison of the real-time electricity pricing obtained from the grid ( $\$P_B$ ) with a threshold value such as the marginal cost of electricity production or a set customer-preference, denoted as MCP. If  $\$P_B$  is lesser than MCP, then the inverter load is fed by the grid and  $P_{INV}$  is stored in a battery storage for consumption or selling to the grid later, possibly during isolation from the grid or when real-time pricing of electricity is conducive to profitability, respectively. Or, if there is no  $P_{INV}$  available, then the electric energy can be bought from grid and stored in battery for later use. If  $\$P_B$  is greater than MCP, then the inverter is so controlled that  $Z_{INV}$  is fed by  $P_{INV}$  and the stored energy in battery bank and any remaining power is sold to the grid. The use of the production marginal cost may not applicable in the case of PV systems; however, if the installation considers customer preferences as input as in [13], then the above rationale can be upheld as shown in case study #1.

The sub-mode 4, under super-mode 2, determined as S2s4, is with regard to the operation at an economic mode—this mode is being proposed as an alternative under the mode, S2s3. This usually occurs when the cost of purchasing electricity from the grid is relatively expensive, i.e., such as described in S2s3; thus, the inverter is setup for powering all its local loads while connected to the grid. However, in such a case, if the inverter power is not enough to supply its loads, the customer has an option to operate at an economic mode, i.e., effecting a prioritization of primary VSI loads and shedding the secondary VSI loads (as in S1s1). This sub-mode is achieved in the simulation by the use of a flag variable; if the flag is set to zero it operates in the economic mode using variable loads; and if the flag is set to one it operates in an “always supplying loads” mode, as the inverter power is not enough, power from grid is purchased to supply the remaining loads.



Figure 13.11 summarizes operating modes of the smart inverter. It is pertinent to note that the study presented here does not consider the time line for powering loads or charging the storage, i.e., in terms of energy demanded and supplied. Consideration of the energy supplied and demanded is inherently tied to hours of available sunlight, and to the PV installation capacity and the battery storage [13].

### 13.4.1.2 Simulation Based Case Study for the Smart Inverter

Based on the foregoing discussion, two case studies describing the smart functionalities of the inverter are presented in this subsection. The power and voltage bases used were 5 kW and 120 V (60 Hz), respectively. The grid side quantities are assumedly measured at the PCC.

#### *Case #1, S2s3: grid-connected mode*

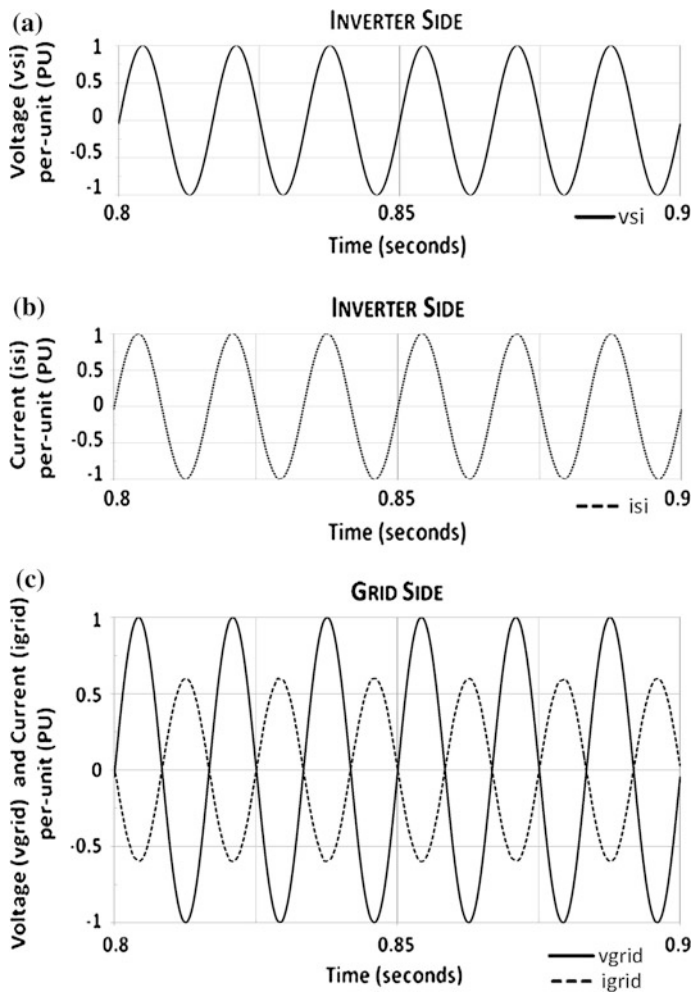
In this simulation, the local demand for an hour is 2 kW, split into the primary VSI load of 1 kW and the secondary VSI load of 1 kW. According to the mode S2s3, the real-time electricity pricing obtained from the grid ( $\$P_B = 2.25 \text{ \$/kW}$ ) is greater than a set customer-preference ( $MCP = 1.5 \text{ \$/kW}$ ). Consequently, the reference points of the inverter are set to provide power to the local loads and to sell the remaining power to the grid. The voltage and current waveforms associated with this operation mode are shown in Fig. 13.12.

From Fig. 13.12 we can see that the voltage and current waveforms on the inverter side are in phase, corresponding to the fact that the inverter provide power to the local loads and to the grid. As the voltage and current are both at 1 pu, then the inverter active power is 5 kW, i.e., at the inverter nominal power. On the grid side, the voltage is 1 pu and the current is 0.6 pu shifted by  $180^\circ$ , indicating that the grid is acquiring 3 kW of active power. (Note: The power and voltage bases used were 5 kW and 120 V, respectively). In this case study, the reactive power demands at the inverter loads were set to zero.

#### *Case #2, S1s2: stand alone mode*

In this simulation, the local demand for an hour is 2 kW, while the available output from the PV modules is 5 kW. According to the mode S1s2, the setup is functioning in the stand alone mode; hence, the real-time electricity pricing ( $\$P_B$ ) or the set customer-preference (MCP) are not relevant for the operation; rather, the option to use any excess generation for charging local energy storage devices is exploited. Consequently, the reference points of the inverter are set such that local loads (2 kW) are powered from the inverter, and the remaining power (3 kW) for that hour is utilized for charging the lead–acid battery. The voltage and current waveforms associated with this operation mode are shown in Fig. 13.13. Once again, in this case study, the reactive power demands at the inverter loads were set to zero.

As can be seen from Fig. 13.13, the voltage and current waveforms on the inverter side are in phase, corresponding to the fact that the inverter is supplying its local loads, without reactive demands.

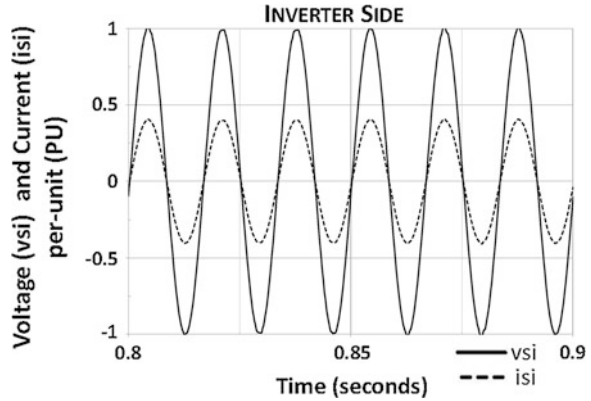


**Fig. 13.12** (a) Voltage and (b) current, on the inverter side; (c) voltage and current on the grid side for Case #1

### 13.4.2 Smart Power Router

The concept of Smart Power Router (SPR) as an intelligent and flexible interface between local control areas is one of the ways in which emerging distribution system will operate [36]. A core of SPR is a back-to-back converter system (hardware), so-called Power Flow Controller (PFC). SPR decides set points for PFC based on distributed control algorithms (software) implementing in the Multi-Agent System (MAS) environment (middleware).

**Fig. 13.13** Voltage and current at the inverter side for Case #2

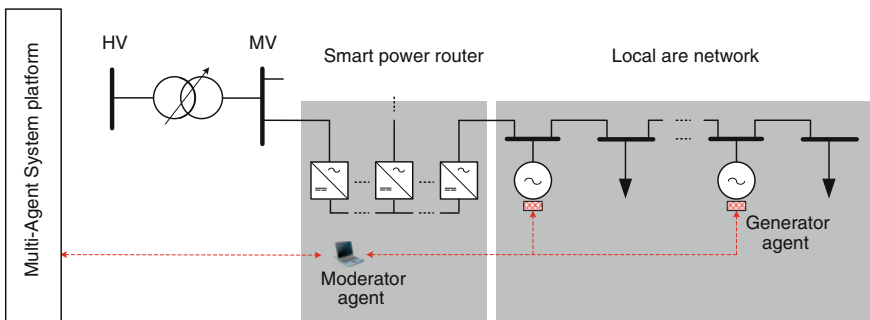


**13.4.2.1 Model**

A configuration of SPR is shown in Fig. 13.14. Each moderator agent representing a local area network can obtain local information such as the power flow on incoming (outgoing) feeders, power generation and reserves, power load demands, cost of production, and load priority. Besides managing autonomous control actions, this moderator agent can send messages to communicate with the same level agents. The PFC is to control the power flow for its feeders based on the set points given by the moderator.

**13.4.2.2 Simulation Based Case Study**

This section describes a 3-phase laboratory setup designed and implemented to demonstrate the performance of SPR. As a popular platform for the application of MAS in power engineering, the Java Agent Development framework (JADE) is used in this setup [37]. The realized setup consists of a physical test network separated into three areas by inverters, as shown in Fig. 13.15. The setup is flexible



**Fig. 13.14** A configuration of smart power router

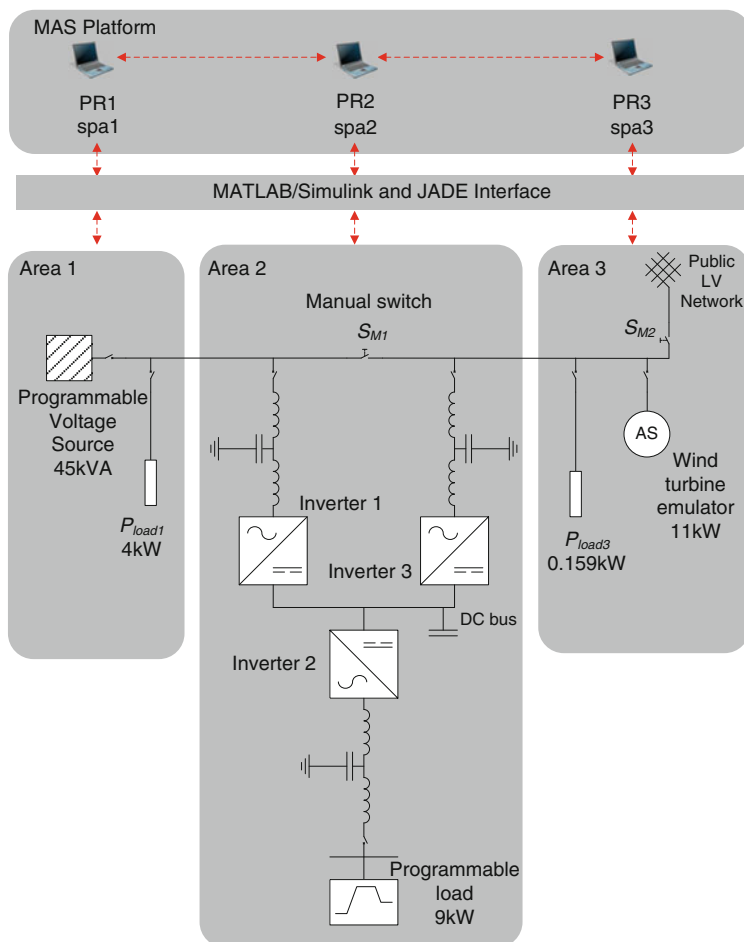


Fig. 13.15 Single-line diagram of the setup

enough to test possibilities for reconfiguring network areas as well as rerouting power flow. In following subsections, the capability of connecting and disconnecting network areas will be shown.

Each inverter with 5 kVA normal power is independently controlled by a scheme shown in Fig. 13.16. The manual switch  $S_{inv-i}$  is to connect the inverter to the grid, feeder, or load; with 10 A maximum current. The input contactor  $K_2^{inv-i}$  is used for charging DC bus via the rectifier whilst the output contactor  $K_1^{inv-i}$  is used for controlling purposes.

*Connecting Inverter and Local Area Network*

In order to illustrate the flexibility of the systems a set of experiments are conducted. The first experiment is to connect area 1 (can be considered as a microgrid)

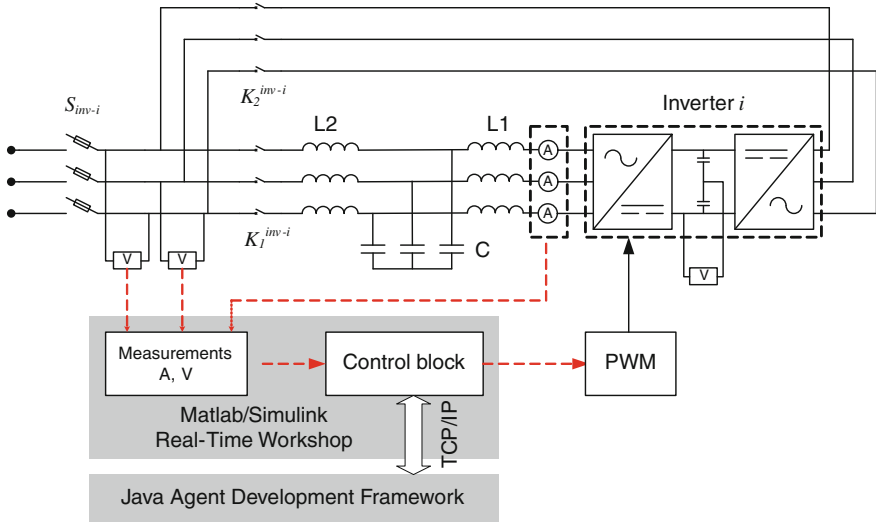


Fig. 13.16 Schematic representation of the SPR

to area 2 and 3 (can be considered as the public grid) via the inverter system. Figure 13.17 shows a simplified diagram for this experiment of connecting area 1 to the rest of grid.

Inverter 3 is connected first to boost the DC bus voltage up to 680 V. Inverter 1 is then used to connect area 1 with the rest of the system. To ensure that the voltages between the two sides of  $K_1^{inv-1}$  be alike, inverter 1 can use reference voltage from inverter 2 for the sake of simplicity. By opening  $S_{inv-2}$  and closing  $K_2^{inv-1}$ , the measured voltage of inverter 2 is equivalent with the voltage at the inverter side of  $K_1^{inv-1}$ . This value will be compared with the grid side voltage of

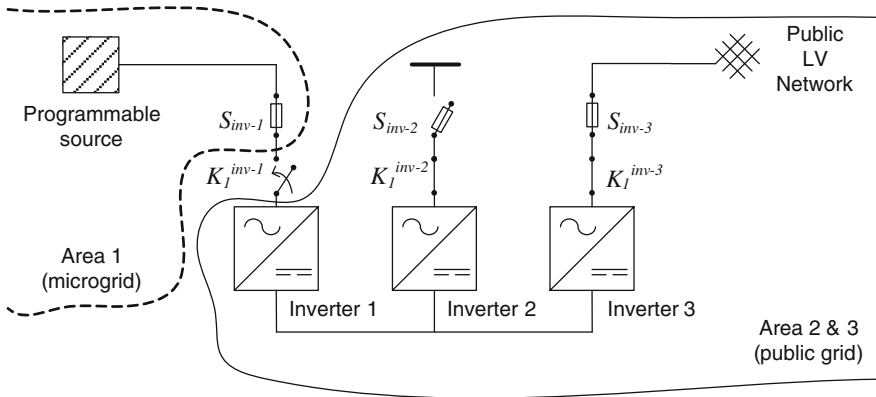


Fig. 13.17 Simplified diagram in case of connecting a microgrid to the public grid

inverter 1 for synchronization. In reality, there will be a separated measurement at inverter 1.

Figure 13.18a shows response of  $V_{DC}$  due to the connection of the inverters. Inverter 1 is first connected to the grid and operated in the DC bus voltage control mode to keep  $V_{DC}$  at 680 V. Connections of inverter 2 and inverter 3 draw also amount of active power from the DC bus. After being connected to the grid, inverter 3 switches to the PQ control mode with set points at zero that causes slight oscillation in  $V_{DC}$ . Power changes in the inverters are shown in Fig. 13.18b, c, and d.

To verify the capability of the PQ control mode, the following steps are deployed. At  $t = 65$  s, the active power reference is stepped to 500 W, as shown in Fig. 13.19a. Then, at  $t = 95$  s, the reactive power reference is stepped to 500 VAR, as shown in Fig. 13.19b. Note that positive value indicates the power flow direction from the grid to the inverter sides. The active power variation at  $t = 95$  s is caused by the change in reactive power.

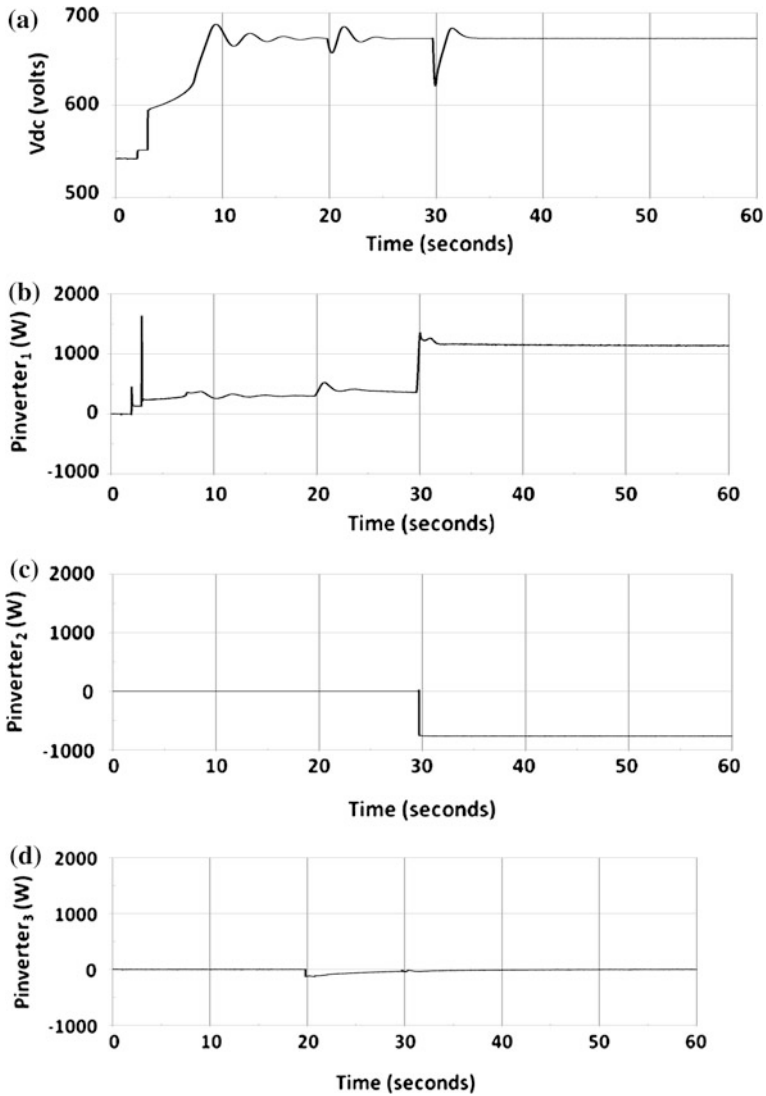
Since area 1 is now connected to the grid, inverter 3 takes the responsibility for the DC bus voltage control while inverter 1 operates in the PQ control mode. Inverter 2 uses a feed forward AC voltage controller and supplies, after switching on, the light resistive load of area 2. When maintenance or a disturbance occurs in an area, the area needs to be isolated from the others. In the setup, the main power stream is from the programmable source of area 1 to supply its local load and the variable load of area 2 via inverters 1 and 2.

#### *Disconnecting a Local Area Network*

The next case study is to adapt to changing conditions when, for instance, intentionally islanding area 1 and 2 (can be considered as a microgrid) from area 3 (the public grid). The DC bus voltage previously controlled by inverter 3 must be maintained to keep the power flow balanced. Inverter 1 can take over this function by changing its operation mode from PQ control to DC bus voltage control. Figure 13.20 shows a simplified diagram for the experiment of islanding local area network. Note that the removal of one of the inverters, limits the robustness and flexibility of the remaining inverters in the system and must be solved as soon as possible.

To keep the supply steady, inverter 1 must take over the DC bus voltage function of inverter 3 at the moment of switching off inverter 3 (at  $t = 40$  s in this case) until the moment that inverter 3 reconnects again (at  $t = 60$  s). Figure 13.21 shows that the test grid is kept stable during the maintenance switching period. There is a small oscillation of  $V_{DC}$  which is damped after nearly ten seconds. The active power through inverter 1 is increased slightly because the load of area 2 was already supplied mainly by the programmable source before disconnection of inverter 3. The reactive power flow of inverter 1 is kept equal to zero. Since the maintenance is finished at  $t = 60$  s, inverter 3 is successfully reconnected to the grid. The inverters are switched back to their previous operation modes.

Bidirectional power electronics converters for topology flexibility, inverters for solar, wind, and other distributed generation applications together with static



**Fig. 13.18** Overall responses and power flows for the inverters. **a** DC bus voltage. **b** Instantaneous active power of inverter 1. **c** Instantaneous active power of inverter 2. **d** Instantaneous active power of inverter 3

switches and other distribution FACTS devices will become crucial for the implementation of smart grids. Together with intelligent controls, protection, and multi-agent technologies the future smart grid will be able to operate with required flexibility and efficiency.

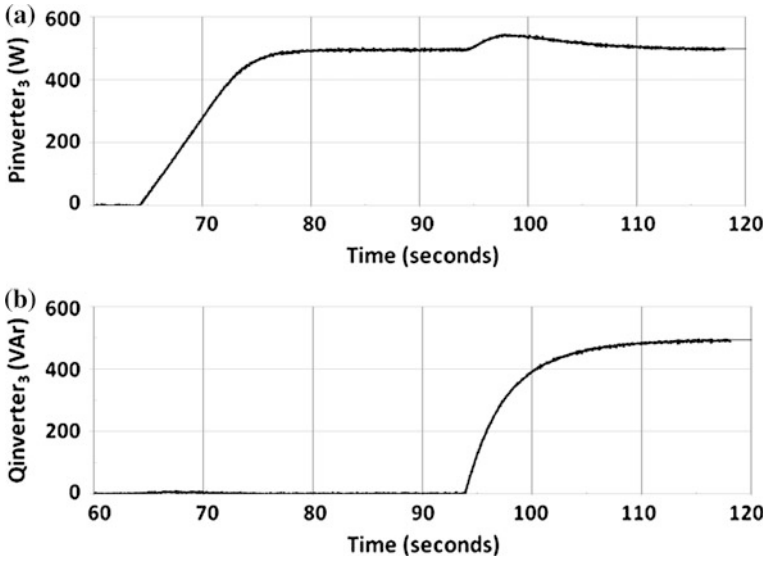


Fig. 13.19 PQ control function for inverter 3. **a** Active power reference changes to 500 W, at  $t = 65$  s. **b** Reactive power reference changes to 500 VAR, at  $t = 95$  s

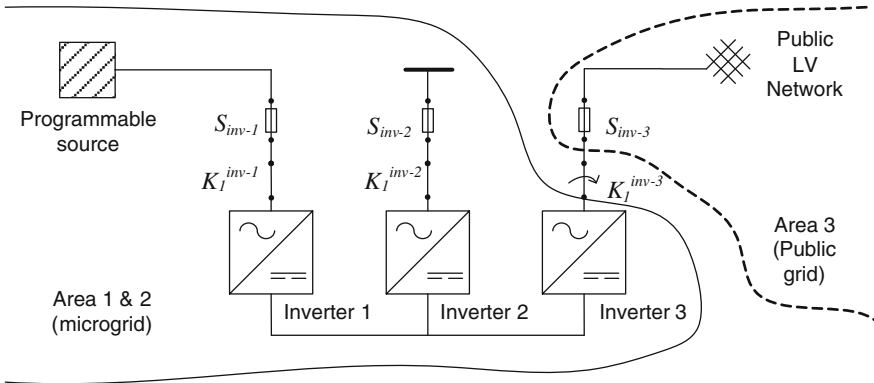
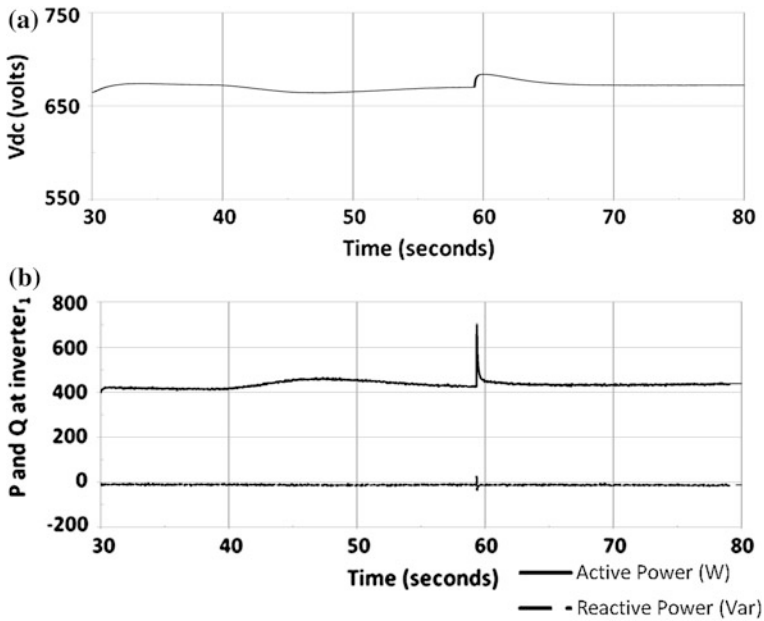


Fig. 13.20 Simplified diagram in case of islanding a local area network

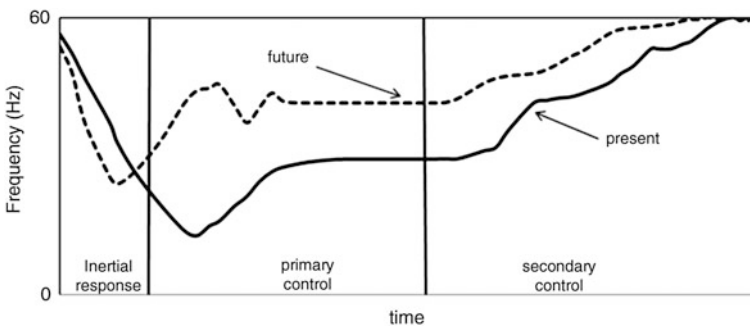
### 13.4.3 Virtual Synchronous Generator

The large-scale implementation of DGs creates both challenges and opportunities on the aspect of frequency control [38]. Increasing the share of small and medium-size generation units leads the whole system inertia to decrease. Unless fast acting primary control, the system frequency will become significantly sensitive with disturbances. Virtual Synchronous Generator (VSG) gives an opportunity for





**Fig. 13.21** Power flow through inverter 1 in case of disconnecting cells. **a** DC bus voltage. **b** Instantaneous active and reactive power



**Fig. 13.22** Frequency control in a power system: nowadays and future with VSGs

inverter-interfaced DG units to participate in preventing fast frequency decay [39]. Figure 13.22 illustrates a probable frequency behavior of the system before and after considering the contribution of VSG. Using the proposed scheme can facilitate and speed up the frequency recovery as illustrated.

**13.4.3.1 Model**

Distributed generation with power electronics interfaced units does not exhibit the inertial properties of typical synchronous generators. However, by emulating virtual rotational inertia to these units, the so-called Virtual Synchronous Generators can reduce the rate of change of frequency (ROCOF) and the frequency deviation. Figure 13.23 illustrates a simplified model of a VSG.

Emulation of rotational inertia by VSG can be implemented by adjustment of active power in the way similar to a synchronous machine in the swing equation as follows:

$$\Delta P_{\text{inertial}} = 2H_{\text{VSG}} \cdot \omega_{\text{grid}} \cdot \frac{d\omega_{\text{grid}}}{dt} \tag{13.4}$$

where  $H_{\text{VSG}}$  is a virtual inertia constant [s], which can be designed to be equal to the inertia constant of synchronous generator with the same power rating;  $\omega_{\text{grid}}$  is grid frequency [pu];  $\Delta P_{\text{inertial}}$  is an adjustment of VSG active power reference for emulation of inertial response.

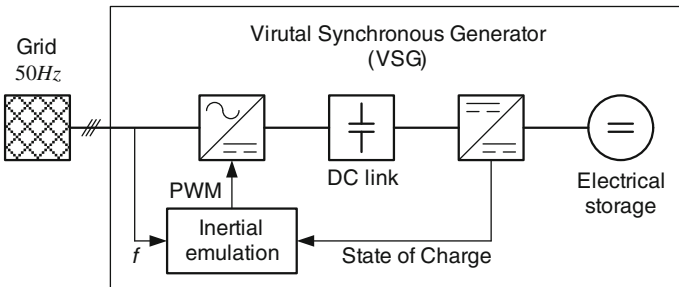
As power adjustment is directly proportional to frequency deviation, the droop control can be added as follows:

$$\Delta P_{\text{droop}} = K_{\text{droop}} \cdot (\omega_{\text{grid}} - \omega_{\text{grid\_ref}}) \tag{13.5}$$

where  $K_{\text{droop}}$  is a designed droop gain, which can be selected in the similar way as droop gains for traditional power plants. The reference of grid frequency,  $\omega_{\text{grid\_ref}}$  is normally set at 1 pu.

Finally, the total active power that has to be adjusted by VSG  $\Delta P_{\text{VSG}}$  can be described as:

$$\Delta P_{\text{VSG}} = \Delta P_{\text{inertia}} + \Delta P_{\text{droop}} \tag{13.6}$$



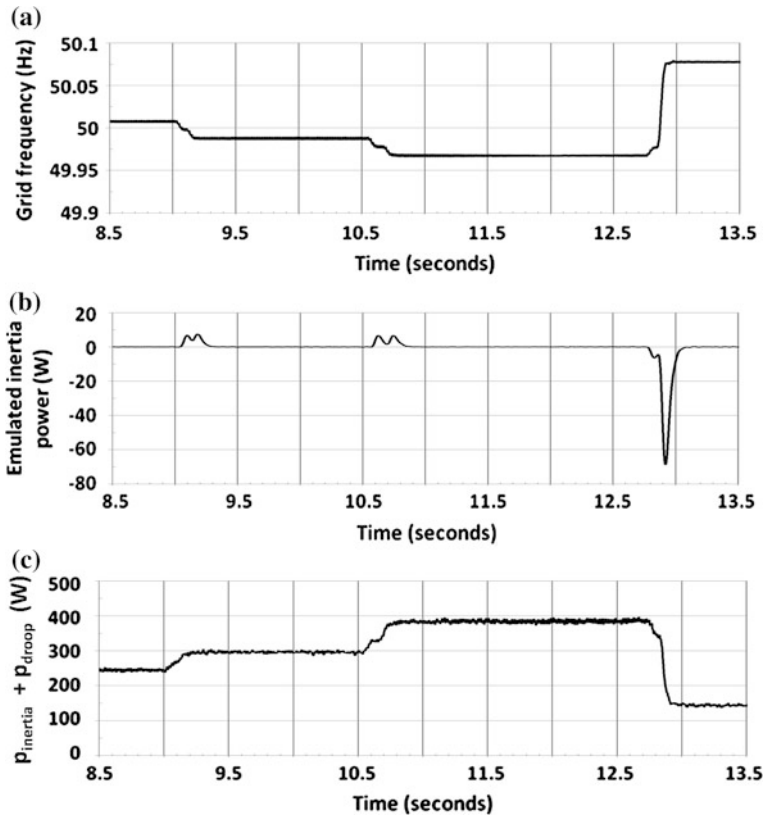
**Fig. 13.23** A simplified model of a virtual synchronous generator

### 13.4.3.2 Simulation Based Case Study

The performance of VSG was tested in a laboratory setup. The setup includes a programmable source, a controllable AC load, and a VSG. By a pre-defined function, the source respectively decreases or increases the voltage and frequency like in the real grid. This emulated change of frequency is given to the model to test VSG control algorithm.

When the AC load was increased at  $t = 9$  s, the programmable source reacts to decrease the frequency, see Fig. 13.24a. VSG start supplying power to the grid as a rotating mass of the synchronous generator when losing speed. Since the frequency increases, VSG absorbs power like slowing down the rotating mass of the synchronous generator. This contributing inertia and droop control power of VSG to support the grid are shown in Fig. 13.24b, c.

This initial experiment shows that the inertia of synchronous generators can be emulated by using inverter-interfaced storage. Virtual rotational inertial and power



**Fig. 13.24** Performance of a virtual synchronous generator (VSG) with variable frequency. **a** Frequency. **b** Emulated inertia. **c** Instantaneous inertia and droop power

droop controls of VSG have been participated to stabilize the frequency change. A further result about field tests of VSG has been implemented with EU VSYNC project [40].

## References

1. United States Department of Energy (2003) "Grid 2030" A national vision for electricity's second 100 years. US Department of Energy. Available [www.ferc.gov/eventcalendar/files/20050608125055-grid-2030.pdf](http://www.ferc.gov/eventcalendar/files/20050608125055-grid-2030.pdf). Cited 24 Apr 2012
2. Lightner E (2008) Evolution and progress of smart grid development at the Department of Energy. FERC-NARUC Smart Grid Collaborative Workshop. Available <http://www.narucmeetings.org/Presentations/Evolution%20and%20Progress%20of%20Smart%20Grid%20Development.pdf>. Cited 24 Apr 2012
3. US Congress (2007) Energy independence and security act of 2007 (EISA07). 110th US Congress
4. National Science and Technology Council (NSTC) (2011) A policy framework for the 21st century grid: Enabling our secure energy future. Executive office of the President: National science and technology council. Available <http://www.whitehouse.gov/sites/default/files/microsites/ostp/nstc-smart-grid-june2011.pdf>. Cited July 2011
5. Strobel CD (2009) American recovery and reinvestment act of 2009 (ARRA09). J Corp Account Financ 20(5):83–85 (111th US Congress)
6. US Department of Energy (2011) Smart grid information clearinghouse. Available [www.sgclearinghouse.org](http://www.sgclearinghouse.org). Cited July 2011
7. (2011) Summary for Policymakers, International Panel on Climate Change, 11th Session of Working Group III of the IPCC, Abu Dhabi, United Arab Emirates
8. Locke G, Gallagher PD (2010) NIST framework and roadmap for Smart Grid interoperability standards, release 1.0. US Department of Commerce. Available [http://www.nist.gov/public\\_affairs/releases/upload/smartgrid\\_interoperability\\_final.pdf](http://www.nist.gov/public_affairs/releases/upload/smartgrid_interoperability_final.pdf). Cited July 2011
9. IEEE Guide for Smart Grid interoperability of energy technology and information technology operation with the electric power system (EPS), and end-use applications and loads. Institute of Electrical and Electronics Engineers (IEEE) Standard 2030. Sept 2011
10. International Electrotechnical Commission (IEC) (2011) Core IEC Standards. Available <http://www.iec.ch/smartgrid/standards/>. Cited July 2011
11. Brown HE, Suryanarayanan S, Heydt GT (2010) Some characteristics of emerging distribution systems under the Smart Grid Initiative. Elsevier Elec J. doi:10.1016/j.tej.2010.05.005
12. Brown HE, Haughton DA, Heydt GT, Suryanarayanan S (2010) Some elements of design and operation of a smart distribution system. Transmission and distribution conference and exposition, 2010 IEEE PES. doi:10.1109/TDC.2010.5484491
13. Armas JM, Suryanarayanan S (2009) A heuristic technique for scheduling a customer-driven residential distributed energy resource installation. Intelligent system applications to power systems, 2009. ISAP'09. 15th international conference, pp 1–7. doi:10.1109/ISAP.2009.5352954
14. Photovoltaics DG, Storage E (2009) IEEE application guide for IEEE Std 1547, IEEE Standard for interconnecting distributed resources with electric power systems. Institute of Electrical and Electronics Engineers (IEEE). doi:10.1109/IEEESTD.2008.4816078
15. Inverters C (2005) Controllers and interconnection system equipment for use with distributed energy resources. UL 1741. Underwriters Laboratory (UL)

16. Deconinck G, Vanthournout K, Beitollahi et al (2008) A robust semantic overlay network for microgrid control applications. In: Lemos R et al (eds) *A robust semantic overlay network for microgrid control applications*. Springer, Berlin
17. La Poutre H, Kling WL, Cobben S (2009) *Intelligent systems for green developments*. ERCIM News 79:38–39
18. Suryanarayanan S, Mitra J, Biswas S (2010) A conceptual framework of hierarchically networked agent-based microgrid architecture. IEEE PES Trans Distrib Conf Exposition. doi:[10.1109/TDC.2010.5484332](https://doi.org/10.1109/TDC.2010.5484332)
19. Carnieletto R, Brandão D, Suryanarayanan S et al (2011) A multifunctional single-phase voltage source inverter in perspective of the Smart Grid Initiative. IEEE Ind Apps Mag. doi:[10.1109/MIAS.2010.939651](https://doi.org/10.1109/MIAS.2010.939651)
20. Malinowski M, Kazmierkowski MP, Trzynadlowski AM (2003) A comparative study of control techniques for PWM rectifiers in AC adjustable speed drives. IEEE Trans Power Electron. doi:[10.1109/TPEL.2003.818871](https://doi.org/10.1109/TPEL.2003.818871)
21. Sukegawa T, Kamiyama K, Takahashi J et al (1992) A multiple PW GTO line-side converter for unity power factor and reduced harmonics. IEEE Trans Ind Apps 28(6):1302–1308. doi:[10.1109/28.175281](https://doi.org/10.1109/28.175281)
22. Lindgren MB (1995) Feedforward-time efficient control of a voltage source converter connected to the grid by lowpass filters. Power Electron Spec Conf. doi:[10.1109/PESC.1995.474942](https://doi.org/10.1109/PESC.1995.474942)
23. Liserre M, Blaabjerg F, Hansen S (2005) Design and control of an LCL-filter-based three-phase active rectifier. IEEE Trans Ind Apps. doi:[10.1109/TIA.2005.853373](https://doi.org/10.1109/TIA.2005.853373)
24. Mao J, Wu G, Wu A et al (2011) Modeling and decoupling control of grid-connected voltage source inverter for wind energy applications. Adv Mat Res. doi:[10.4028/www.scientific.net/AMR.213.369](https://doi.org/10.4028/www.scientific.net/AMR.213.369)
25. Ko SH, Lee SR, Dehbonei H et al (2006) Application of voltage- and current-controlled voltage source inverters for distributed generation systems. IEEE Trans Energy Conv 21(3):782–792. doi:[10.1109/TEC.2006.877371](https://doi.org/10.1109/TEC.2006.877371)
26. Carnieletto R, Ramos DB, Simões MG, et al (2009) Simulation and analysis of DQ frame and P + Resonant controls for voltage source inverter to distributed generation. Power Electron Conf 104–109. doi: [10.1109/COBEP.2009.5347677](https://doi.org/10.1109/COBEP.2009.5347677)
27. Hassaine L, Olias E, Quintero J et al (2009) Digital power factor control and reactive power regulation for grid-connected photovoltaic inverter. Renewable Energy 34(1):315–321. doi:[10.1016/j.renene.2008.03.016](https://doi.org/10.1016/j.renene.2008.03.016)
28. Kjaer SB, Pedersen JK, Blaabjerg F (2005) A review of single-phase grid-connected inverters for photovoltaic modules. IEEE Trans Ind Apps. doi:[10.1109/TIA.2005.853371](https://doi.org/10.1109/TIA.2005.853371)
29. Duarte JL, van Zwam A, Wijnands C, et al (1999) Reference frames fit for controlling PWM rectifiers. IEEE Trans Ind Elec 46(3):628–630. doi: [10.1109/41.767071](https://doi.org/10.1109/41.767071)
30. Akagi H, Kanazawa Y, Fujita K, et al (2007) *Generalized theory of instantaneous reactive power and its application*. Wiley, London, vol 103, pp 58–66, doi:[10.1002/eej.4391030409](https://doi.org/10.1002/eej.4391030409)
31. Ohnishi T (1991) Three phase PWM converter/inverter by means of instantaneous active and reactive power control. Indus Electron Control Instrum. doi:[10.1109/IECON.1991.239183](https://doi.org/10.1109/IECON.1991.239183)
32. Ortjohann E, Lingemann M, Mohd A et al (2008) A general architecture for modular smart inverter. Indus Electron. doi:[10.1109/ISIE.2008.4676908](https://doi.org/10.1109/ISIE.2008.4676908)
33. Roshan A, Burgos B, Baisden BC, et al (2007) A D-Q frame controller for a full-bridge single phase inverter used in small distributed power generation systems. Applied Power Electronics Conference, APEC 2007–Twenty Second Annual IEEE. doi:[10.1109/APEX.2007.357582](https://doi.org/10.1109/APEX.2007.357582)
34. Miranda UA, Aredes M, Rolim LGB (2005) A DQ synchronous reference frame current control for single-phase converters. IEEE Power Electron Spec Conf. doi:[10.1109/PESC.2005.1581809](https://doi.org/10.1109/PESC.2005.1581809)
35. Math works Inc (2011) SimPowerSystems: model and simulate electrical power systems. Available: <http://www.mathworks.com/products/simpower/>. Cited July 2011

36. Nguyen PH, Kling WL, Ribeiro PF (2011) Smart power router: a flexible agent-based converter interface in active distribution networks. *IEEE Trans Smrt Gr.* doi:[10.1109/TSG.2011.2159405](https://doi.org/10.1109/TSG.2011.2159405)
37. Telecom Italia SpA (2010) Java agent development framework. Available: <http://jade.tilab.com/>. Cited 24 Apr 2012
38. Ishchenko A, Kling WL, Myrzik J (2009) Control aspects and the design of a small-scale test virtual power plant. *Power and Energy Society General Meeting-Conversion and Delivery of Electrical Energy in the 21st Century.* doi: [10.1109/PES.2009.5260225](https://doi.org/10.1109/PES.2009.5260225)
39. Driesen J, Visscher K (2008) Virtual synchronous generators. *Power and Energy Society General Meeting-Conversion and Delivery of Electrical Energy in the 21st Century.* doi: [10.1109/PES.2008.4596800](https://doi.org/10.1109/PES.2008.4596800)
40. (2010) Virtual synchronous project. European Union. Available <http://www.vsync.eu/>. Cited July 2011
41. Xue XY, Chang L, Kjaer SB et al (2004) Topologies of single-phase inverters for small distributed power generators: an overview. *IEEE Trans Power Electron.* doi:[10.1109/TPEL.2004.833460](https://doi.org/10.1109/TPEL.2004.833460)

# Chapter 14

## Advanced Electric Vehicles

Giampaolo Carli, Arash Shafiei and Sheldon S. Williamson

**Abstract** This chapter primarily aims at addressing the practical issues for commercialization of current and future plug-in hybrid electric vehicles (PHEVs), and focuses primarily on power electronics based solutions for both current as well as future electric vehicle (EV) technologies. New PHEV power system architectures are discussed in detail. Key EV battery technologies are explained as well as corresponding battery management issues are summarized. Advanced power electronics intensive charging infrastructures for EVs and PHEVs are also discussed in detail.

### 14.1 Introduction

Conventional vehicles (CVs), which use petroleum as the only source of energy, represent majority of the existing vehicles today. As shortage of petroleum is considered as one of the most critical world-wide issues, costly fuel becomes a major challenge for CV users. Moreover, CVs emit greenhouse gases (GHG), thus, making it harder to satisfy stringent environmental regulations.

One of the most attractive alternatives includes electric vehicles (EVs) or zero emission vehicles (ZEVs), which only consume electric energy. However, due to the limited energy densities of the current commercially available battery packs, the performance of EVs is restrained as neighborhood vehicles, with limitations of low speed, short autonomy, and heavy battery packs. As a successful example,

---

G. Carli · A. Shafiei · S. S. Williamson (✉)  
Power Electronics and Energy Research (PEER) Group,  
Department of Electrical and Computer Engineering, Concordia University,  
1455 de Maisonneuve Blvd. W, Montreal, QC H3G 1M8, Canada  
e-mail: sheldon@ece.concordia.ca

Canada-based ZENN's commercialized EV has an average speed of 25 mph and 30–40 miles driving range per charge.

Currently, the most promising and practical solution is the hybrid electric vehicles (HEVs). Its propulsion energy is usually from more than two types of energy storage devices or sources, and one of them has to be electric. HEV drive trains are basically divided into series and parallel hybrids. Series hybrids are electric-intensive vehicles, as the electric motor is the only traction source, and the internal combustion engine (ICE) merely works at its maximum efficiency, as an on-board generator, to charge the battery.

Keeping in mind the goals of creating an energy wise, cost-effective, and overall sustainable society, plug-in hybrid electric vehicles (PHEVs) are recently being widely touted as a viable alternative to both conventional as well as regular HEVs. PHEVs are equipped with sufficient on-board electric power, to support daily driving (an average of 40 miles/day) in an all-electric mode, only using the energy stored in batteries, without consuming a drop of fuel. This, in turn, causes the embedded ICE to use only a minimal amount of fossil fuel to support further driving beyond 40 miles, which further results in reduced GHG emissions.

PHEVs can reduce fuel consumption by charging its battery from the grid. It is, thus, a valid assumption that moving into the future, a large number of PHEV users will most definitely exist, and the overall influence of charging the on-board energy storage system (ESS) cannot be neglected. Related literature firmly states that by the year 2020, the market share of PHEVs will increase to about 25 %. Based on this data, the additional electric energy demanded from the distribution grid for 5 million PHEVs would be roughly about 50 GWh per day. Also, the typical charging time would be 7–8 h, which might make it hard to accommodate these additional loads in the load curve without increasing the peak load. Also, the required additional charging energy would have a possible impact on the utility system.

Expanding the electric system the conventional way, with large generating plants located far from the load centers, would require upgrading the transmission and distribution systems too. Besides the high costs, this can take many years before obtaining the right of way. Alternatively, smaller power plants based on renewable energy, such as wind energy, which is a cost-effective renewable energy addition to many utilities. Also, solar energy can be installed in a fraction of that time on the distribution system, which is commonly referred to as “distributed generation (DG).” Photovoltaic (PV) presents a modular characteristic and can be easily deployed in the roof top and facades of residences and buildings. Many corporations are adopting the green approach for distributed energy generation. For instance, *Google* has installed 9 MWh per day of PV on its headquarters, Googleplex, in Mountain View, California. At the moment, it is connected to Mountain View's section of electricity grid. Alternatively, it could be used for charging PHEVs during work hours, being a great perk for environmentally concerned employees. The energy stored in the batteries could also be used for back-up during faults. In Canada, the latest projections (2000) indicate that by 2010, renewable DG sources will represent at least 5 % of the total energy produced and 20 % of cogeneration, from



the actual figures of 1 and 4 %, respectively. Therefore, from the environment point of view, charging PHEVs with solar power will be the most attractive solution.

This chapter primarily aims at addressing the practical issues for commercialization of current and future PHEVs, and focuses primarily on power electronics based solutions for both current as well as future EV technologies. New PHEV power system architectures are discussed in detail. Key EV battery technologies are explained as well as corresponding battery management issues are summarized. Advanced power electronics intensive charging infrastructures for EVs and PHEVs are also discussed in detail.

## **14.2 Electric, Hybrid Electric, and Plug-In Hybrid Electric Vehicle Topologies**

### ***14.2.1 Electric Vehicles***

The EVs are powered only by electricity. Therefore, they include electric motors for propulsion, batteries and/or fuel cells for long-term storage, and sometimes ultra capacitors for transient stabilization, making a combination called hybrid energy storage system (HESS). The technology of EVs is retrofit to other EVs such as electric bikes, electric boats, and electric airplanes. and so on. EVs supplied from batteries (the most common) are called battery electric vehicles (BEVs). Historically, the very first cars by the middle of the nineteenth century were BEVs because of the simplicity of electric motors compared to ICEs. However, ICE cars replaced BEVs due to the low range of BEVs and low specific energy batteries when compared to gasoline.

Batteries must be properly sized for achieving a given driving range. Therefore, many cells should be put in series and parallel in a battery pack to provide suitable voltage and rating for driving the EV motors. Various issues must be considered in designing battery packs, such as charging methods for improved battery lifetime as presented in [Sect. 14.3.1.4](#).

### ***14.2.2 Hybrid Electric Vehicles***

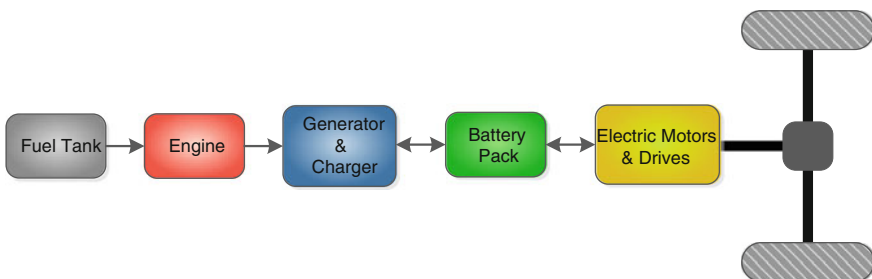
A hybrid vehicle utilizes two or more sources of energy for propulsion e.g., gasoline, natural gas, hydrogen, liquid nitrogen, compressed air, wind, solar, electricity, or any other. If one of these sources is electricity, this vehicle is called HEV. This electricity is usually provided by a battery pack or a fuel cell. HEVs generally combine ICEs with electric motors to run the vehicle. They may include vehicles other than cars but hybrid electric cars are the most common ones. The main purpose of using HEVs, the same as EVs is to reduce the amount of

emissions and fuel consumption. This can be achieved in different ways, the simplest could be turning off the ICE during idle times such as during the waiting time at stop lights (called by stop–start control strategy). Another possibility is by converting the car kinetic energy to electric energy during breaking, instead of wasting such energy as heat in the brakes. This can improve the gas efficiency (mile per gallon range) to approximately 15 %. This efficiency increases as the efficiency of the wheel to battery path components are improved by better design. Different configurations of ICE and electric motor are possible in a HEV. They will be described in the following section as follows.

#### 14.2.2.1 Hybrid Electric Vehicles Topologies [1, 2]

##### *Series Hybrid*

In a series hybrid, the ICE acts as a prime mover to run a generator. This generator charges a battery pack and this battery pack will supply power to the electric motors. In fact, the ICE is the main primary source of power; however, the HEV runs by the direct mechanical coupling of the electric motor and not from the ICE. The benefit rises from the fact that the ICE engine can be smaller compared to a standard car. In addition, the ICE in a series hybrid operates at the most efficient operating point most of the time, resulting in improved overall efficiency of the system. In terms of power flow analysis, the power from generator may supply the electric motors directly, however, to smooth the power transients or variable power demand from electric motors, the battery pack is necessary to act as an energy buffer. Depending on the design, in order to minimize the stress on the battery pack leading to improved life cycle of the battery pack, banks of ultra capacitors may also be used to supply highly transient currents. As mentioned before, during the vehicle braking the kinetic energy can be transformed to electrical energy using a generator; therefore, the electric machine and the motor drive in a series hybrid is designed to act as a motor generator. Generally, series hybrids are more



**Fig. 14.1** Typical series-hybrid topology

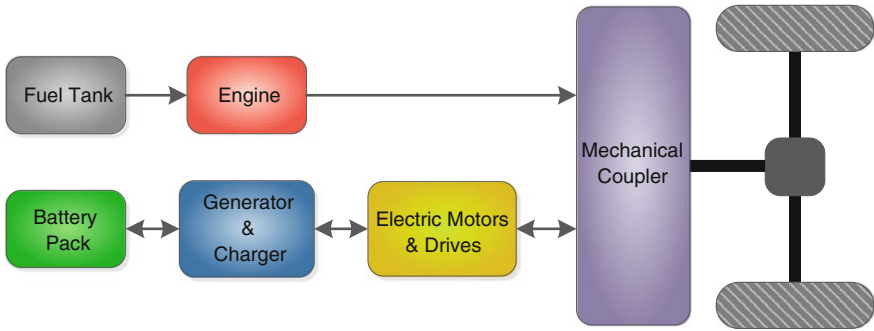


Fig. 14.2 Typical parallel-hybrid topology

efficient for low-speed range and urban areas. A typical series hybrid power train is illustrated in Fig 14.1.

*Parallel Hybrid*

In a parallel hybrid, the ICE can directly run the HEV in parallel to the electric motor. In other words, the transmission is governed by ICE, electric motors, or both of them at the same time depending on the driving condition and control strategy. The typical configuration of parallel hybrid is shown in Fig. 14.2. In general, parallel hybrid is more efficient for high-speed ranges, i.e., highways. In today’s parallel HEV market, the electric motors are low power and usually rated less than 30 kW with a relatively small size battery pack since in parallel hybrid the electric motor is accompanied by ICE and does not supply all the power. Regenerative braking can be supported in parallel hybrids also.

*Series-Parallel Hybrid*

This configuration is shown in Fig. 14.3, it is also known as power split topology and combines the features of series and parallel hybrid. As shown in the figure, a power split is utilized to share the output mechanical power from ICE to the drive shaft or to the electric generator. This ensures the battery pack is always

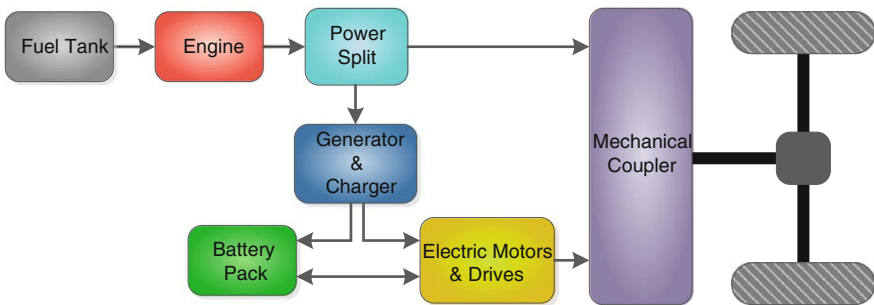


Fig. 14.3 Typical series-parallel hybrid architecture

maintained charged to be able to run the electric motors when needed. A series-parallel hybrid can operate in series hybrid mode or in parallel hybrid mode, depending on the driving conditions and supervisory control strategy. A series-parallel hybrid benefits from advantages of both series and parallel hybrid, so it is efficient in both urban areas and highways.

### ***14.2.3 Plug-In Hybrid Electric Vehicles***

A PHEV is the combination of a HEV and an EV which can be recharged using an electric plug. In fact, a PHEV benefits from both the hybrid nature of a HEV and the noticeable all-electric range (AER) of an EV. AER simply shows the distance that the PHEV or EV can go only using the batteries. For instance, PHEV-30 means that the PHEV can go 30 miles only on electricity. In a simple HEV, the AER is relatively small because of the small capacity of the battery pack. However, in a PHEV the vehicle can run long ranges only on batteries. The battery pack of a PHEV is much bigger than a HEV to be able to store the required amount of energy. The overall efficiency of PHEVs is much higher than ICE cars. The final usage cost highly depends on the price of electricity, since PHEVs require a relatively significant amount of input electric energy to get charge. To get a rough idea, it can be mentioned that charging a PHEV once per day doubles the electrical energy consumption of a mid-size home. Besides, the reduction amount of pollutants depends on the source of electricity, i.e., fossil fuel, natural gas, hydro, wind, and solar.

PHEVs have same three main topologies as HEVs, i.e., series, parallel, and series parallel. PHEVs can operate in three different modes of operation: charge depleting, charge sustaining, and blended mode. If the battery has enough charge, PHEV can operate using only electricity until it reaches the minimum state of charge (SOC), this is called charge-depleting mode. The battery pack cannot provide enough energy and power for acceleration if its SOC is low. In contrast, the battery pack cannot absorb available energy from regenerative braking if it is fully charged. Thus, it is desired that the SOC of the battery pack is kept in a range from 60 to 80 %. If the control strategy operates the ICE and other subsystems to achieve this, it is called charge-sustaining mode. In some PHEVs, the control strategy operates in such a way that for low speeds, e.g., less than 60 km/h the vehicle works in charge-depleting mode and for high speeds it works in charge-sustaining mode. This is called blended mode. In other cases, the PHEV may operate in different modes of operation for different speed ranges depending on the driving condition and control strategy, this mode is called mixed mode of operation.

## 14.3 EV and PHEV Charging Infrastructures

### *14.3.1 EV and PHEV Batteries and Charging Regimes*

Replacing the conventional ICE vehicles with EVs and PHEVs in a large scale can result to tremendous prosperities in saving our world from the dangerous ever-increasing rate of pollutants. The majority of benefits such as pollution reduction and decrease of oil consumption resulting from moving toward using EVs and PHEVs are mainly based on using batteries as a green source of energy. The electrochemical nature of batteries has a highly nonlinear behavior and dependant on many factors such as materials, temperature, aging, load profile, and charging algorithm. A very important concern is related to storage, because in order to have a given amount of energy for a reasonable AER, tens or hundreds of cells should be connected in series and parallel for the desirable voltage and current ratings of the battery pack. This causes the nonlinear behavior of cells to be more prominent. Furthermore, there are some phenomena that are observed only in battery packs and not in single cells, such as thermal unbalance among the cells in pack.

EV and PHEV battery packs are relatively expensive compared to the price of the whole car, because of high number of cells, chemistry types such as Lithium-based, and protection circuits. Accordingly, the life cycle of these battery packs are very important for a cost-effective user's point of view. Therefore, lower cost for final customer can be achieved with increasing the battery pack life cycle, resulting in less frequent replacements of the whole pack. As a real example related to Honda Civic: recently, there has been news [3] about Honda Company regarding the battery packs of Honda Civics produced during 2006–2008. Apparently, some of the battery packs in the second-generation Honda Civic hybrids are failing prematurely after five years. According to regulations in California, there is a 10 year, 150,000 mile warranty requirement on the components of the hybrid system. Although Honda Company took recall actions, some customers were not satisfied and preferred to change themselves the battery packs. It has been reported that those battery packs cost about \$2,000 excluding shipping and installation.

This case shows the importance of the battery packs price in the commercialization of EVs and PHEVs in a large scale. A factor that highly impacts the life cycle of battery packs is the charging algorithm. There are other factors also involved such as the charging time that plays an important role in high attraction to EVs and PHEVs. These topics and all other ones related to this area should be mainly handled with a multi-level control and power system called battery management system (BMS) which takes care of all or some of the aspects affecting batteries in any way. The more accurate and comprehensive the BMS is the more reliable, safer and faster the charging procedure can be done. Designing a high efficient BMS needs very good understanding of the behavior of single cells according to the variations of different parameters and also parameter variation and behavior change in a packed large number of cells.

The following section describes basic definitions of battery technology and appropriate charging algorithms that optimize the life cycle of batteries. Such definitions help understanding the applications in HEVs.

#### 14.3.1.1 Battery Parameters

- (1) *Battery Capacity*: This parameter indicates the amount of charge that can be drawn from a fully charged battery until it gets fully discharged. An important effect in batteries is that the higher amount of current drawn from a battery, the lower capacity the battery will have. Hence, theoretically, battery capacity is defined as the amount of current drawn from a battery that completely discharges it in exactly 1 h; for example, a battery capacity of 10 Ah means that a constant current of 10 A is drawn from the battery will discharge completely the battery after 1 h. However, in practice, battery manufacturers specify a table showing the amount of time the battery runs with several constant current loads and several constant power loads. In practice, this table provides much more practical information rather standard definitions, because after production different loads with different characteristics may be connected to the battery. Nevertheless, the amount of time that a battery runs is not exactly predictable, because in general the loads are not necessarily constant current or constant power loads. In addition, these manufacturer tables are valid for new batteries and they change with aging. Therefore, in many design methodologies just estimates of battery runtime calculated. The battery capacity is shown with variables defined as “C” or “Q” or similar notations. The main unit for battery capacity is Ampere-hour (Ah), but based on the battery size other units such as mAh or even mAs (for very small batteries) can be used.
- (2) *C Rate*: This parameter is used to show the amount of current used for charging the battery. For example, for a 10 Ah battery, when it is mentioned to terminate the charging process while the charging current falls below C/10 rate (10 h rate), it means the charging should be stopped when current becomes less than the amount of current with which the battery is discharged after 10 h, or specifically  $10 \text{ Ah}/10 \text{ h} = 1 \text{ A}$ .
- (3) *State of Charge*: State of charge (SoC) is the percentage of charge available from a battery to the whole capacity of the battery. SoC is very difficult to measure because a complex electrochemical model is required, and there are other effects such as relaxation (described in the following section). Besides, according to aging the rated capacity of the battery reduces over time, hence, for determining SoC, the rated capacity should be measured or calculated regularly.
- (4) *Depth of Discharge*: Depth of discharge (DoD) is defined as  $(100 - \text{SoC})$  in percentage, i.e., how much from the total energy of the battery has been utilized. This parameter is usually used in discharge patterns

recommendations. For example, the battery manufacturer may recommend the user not to go over 70 % DoD according to lifetime.

- (5) *Energy Density*: Energy density can be defined based on volume or weight, i.e., Wh/L or Wh/Kg. The “Volumetric Energy Density”, which is defined as the amount of available energy from a fully charged battery per unit volume (Wh/Litre). The unit Litre is mainly used for measuring the volume of liquids. Mostly, the batteries have liquid electrolyte, so in such cases it easily makes sense, however, even for solid-state electrolytes such as Lithium Polymer batteries, the same unit is usually used. The other way of defining the energy density is “Gravimetric Energy Density” which is also referred as “Specific Energy” and defined as the available energy from a fully charged battery per unit weight (Wh/Kg). Based on application and based on the importance of the volume or weight, either definition can be used. In the case of EVs and PHEVs usually weight is a more important factor than volume, so, mostly specific energy is seen in the literature for EVs and PHEVs.
- (6) *Charging Efficiency*: The chemical reactions inside the battery during charge and discharge are not ideal and there are always losses involved. Therefore, not all the energy used to charge the battery, is available during discharge. Some of this energy is wasted as heat dissipation. The charging efficiency can be defined as the ratio of available energy from the battery in a complete discharge to the amount of energy needed to completely charge the battery. This parameter may be mentioned by other names such coulombic efficiency or charge acceptance. The types of losses that reduce coulombic efficiency are mainly losses in charging process due to chemical reactions, such as electrolysis of water or other redoxation reactions in the battery. In general, the coulombic efficiency for a new battery is high, however, reducing as the battery ages.

Next section discusses some aspects of batteries of EVs and PHEVs regarding charging battery packs. This will help in designing more efficient and flexible chargers based on battery behaviors which will finally lead to improvement of battery packs lifetime.

#### 14.3.1.2 Main Characteristics of Commonly Used Batteries

There are hundreds types of batteries described in reference books [4] and technical literature.

Most of them are demonstration prototypes, working under laboratory conditions and still under investigation, not commercialized maybe because of costs, nonmature technology, low energy density, safety, toxic components, and so on. The most widely available batteries are Pb–Acid, Ni–Cd, Ni–MH, Li–ion, and Li–polymer.

Batteries can be mainly divided into primary batteries and secondary batteries. Primary batteries are those which can be used only once and after a full discharge they are no longer used, because the internal chemical reactions are irreversible.

Secondary batteries can be used many times by recharging such as the ones used for automotive and traction applications and as energy storage for renewable energy systems.

Here, we will only consider secondary type batteries and when we are talking about batteries we mean secondary batteries, otherwise stated.

- (1) *Lead–Acid (Pb–Acid) Batteries*: For over one century, lead–acid batteries have been utilized for various applications including traction. Their well-improved structure has led to valve regulated lead–acid (VRLA) batteries which can be considered as maintenance free batteries, which is a desirable characteristic for PHEVs. In terms of efficiency they have a high efficiency in the range of 95–99 %. The main disadvantage of lead–acid batteries is their weight, in other words, they have a low specific energy (30–40 Wh/Kg) compared to their counterparts.
- (2) *Nickel–Cadmium (Ni–Cd) Batteries*: Considering low power applications Nickel–Cadmium (Ni–Cd) batteries also benefit from a mature technology but considering traction applications their specific energy is low as well. The typical specific energy for this type is 45–60 Wh/Kg. The main applications are in portable devices, but they are also recommended when high instantaneous currents must be provided. They are typically used when long life and reasonable costs are desired. However, they have environmental concerns for recycling because they contain toxic metals [5].
- (3) *Nickel–Metal Hydride (Ni–MH) batteries*: Comparing to previous types they have higher specific energy at the expense of lower cycle life. In general, for the same size batteries, Ni–MH batteries can have up to two or three times more energy than a Ni–Cd type. The typical value for the specific energy of the present technology Ni–MH batteries is in the range of 75–100 Wh/Kg. This type is widely used in EV and PHEV applications.
- (4) *Lithium–Ion (Li–Ion) batteries*: This type has noticeably high specific energy, specific power, and great potential for technological improvements providing EVs and PHEVs with perfect performance characteristics such as acceleration performance. Their specific energy is in the range of 100–250 Wh/Kg. Because of their nature, Li–ion batteries can be charged and discharged faster than Pb–Acid and Ni–MH batteries, making them a good candidate for EV and PHEV applications. Besides all, Li–ion batteries have an outstanding potential for long life if managed in proper conditions, otherwise, their life can be a disadvantage. One of the main reasons is almost the absence of memory effect in Li-based batteries. A weak point of Li-based batteries is safety since they are highly potential for explosion due to overheating caused by overcharging. They can almost easily absorb extra charge and get exploded. The use of advanced BMS can ensure reliable range of operation of Li–ion batteries even in cases of accidents. Another advantage is that Li–ion batteries have environmentally friendly materials when compared with Ni-based batteries.
- (5) *Lithium–Polymer (Li–Po) batteries*: Li–Po batteries have the same energy density as the Li–ion batteries but with lower cost. This specific chemistry is



one of the most potential choices for applications in EVs and PHEVs. There have been significant improvements in this technology. Formerly, the maximum discharge current of Li-Po batteries was limited to about 1 C rate; however, recent enhancements have led to maximum discharge rates of almost 30 times the 1 C rate, which greatly improves and simplifies the storage part of the EVs and PHEVs in terms of power density, since this can even eliminate the need of ultra-capacitors. Besides, there have been outstanding improvements in charging times. Recent advances in this technology have led to some types which can reach over 90 % SoC in a couple of minutes which can significantly increase the attraction toward EVs and PHEVs because of noticeable reduction of charging time. Because this type is a solid-state battery, having solid electrolyte, the materials would not leak out even in the case of accidents. One of the other advantages of this type is that it can be produced in any size or shape which offers flexibility to vehicle manufacturers.

### 14.3.1.3 Basic Requirements of EV and PHEV Batteries

The basic preferred characteristics of PHEV batteries can be summarized as follows [6]:

- (1) High specific energy which results in higher AER and less recharge cycles required.
- (2) High specific power which results in high acceleration characteristics of the PHEV due to high rates of currents available from the battery without causing any permanent damage to the battery pack.
- (3) High number of charge/discharge cycles available and high safety mechanisms built into the battery because of high power ratings of battery packs.
- (4) Environmental friendly aspect of the battery, i.e., being recyclable and including low amounts of toxic materials.
- (5) Cost is also an important concern for commercializing EVs and PHEVs in a large scale.

### 14.3.1.4 Charging Methods

Charging in general is the action of putting energy back to the battery i.e., restoring energy. Different chemistries require different charging methods. Other factors affecting choosing the charging method are capacity, required time, or other factors. The most common techniques are mentioned here:

- (1) *Constant Voltage Charge*: As it is clear from the name “Constant Voltage” or CV is when a constant voltage is applied to the battery pack. This voltage is a pre-set value given by the manufacturer. This method is accompanied with a current limiting circuit most of the time, especially for the beginning periods

of charging where the battery easily takes high rates of current comparing to its capacity. The current limitation value mainly depends on the capacity of the battery. Depending on the battery type to be charged, this preset voltage value is chosen. For example, for Li-ion cells the value of  $4.200 \pm 50$  mV is desirable. An accurate set point is necessary, since overvoltage can damage the cell and under voltage causes partial charge which will reduce life cycle over time. Therefore, the circuit used for charging, which can be a simple buck, boost or buck-boost topology depending on the voltage ratio of input and output, should be accompanied with a controller to compensate for source and load changes over time. When the cell reaches the preset voltage value, this causes the battery to be in a standby mode, ready for later use. The amount of this idle time should not be very long and should be limited based on the manufacturer recommendations. This method is usually used for lead-acid batteries, also for Li-ion batteries while using current limiter to avoid overheating the battery especially in the first stages of the charging process [7].

- (2) *Constant Current Charge*: Constant current charging simply means applying a constant current to the battery with a low percentage of current ripple independent of the battery SoC or temperature. The abbreviation for this method is CC in the literature. This is achieved by varying the voltage applied to the battery using control techniques such as current mode control to keep the current constant. CC technique can be implemented using a “Single Rate Current” or “Split Rate Current”. In single rate only one preset current value is applied to the battery which is useful in balancing the cells. However, backup circuits must be used to avoid overcharging. In the split rate, CC different rates of current are applied based on time of charge, voltage, or both in different stages of charging. This gives more accurate and balanced charging and circuits should be used to avoid overvoltage of the cells. In some cases, for prolonging dead batteries, CC method with high rates and low duration can be utilized to extend the lifetime of the battery. But, this is a very cautious procedure and must be done carefully. Ni-Cd and Ni-MH batteries are charged using this method. Ni-MH batteries can be easily damaged due to overcharging, so they should be accurately monitored during charging [8].
- (3) *Taper Current Charge*: This method can be used when the source is a non-regulated DC source. It is usually implemented with a transformer with a high output voltage comparing to the battery voltage. A resistance should be used to limit the current flowing to the battery. A diode can also be used to ensure unidirectional power flow to the battery. In this method, the current starts at full rating and gradually decreases as the cell gets charged. As an example, for 24 V 12 A battery, the charging begins with 12 A when the battery voltage is 24 V, then 6 A when the voltage reaches 25 and then 3 A for 26 V and finally 0.5 A for 26.5 V. (This is just a hypothetical example and the values are not necessarily valid). This technique is only applicable to sealed lead-acid (SLA) batteries. Taper charging has other disadvantages. As mentioned before, this technique uses transformers which adds to the weight of charger and generates heat.

- (4) *Pulse Charge*: This technique involves using short-time current or voltage pulses for charging. By changing the width of pulses the average of the current or voltage can be controlled. Pulse charging provides two significant advantages, (1) it reduces charging time, and (2) the conditioning effect of this technique highly improves the life cycle. The intervals between pulses called rest times play an important role, they provide some time for chemical reactions inside the battery to take place and stabilize. Since in this method high rates of current or voltage can be used, it reduces undesirable chemical reactions that happen at the electrodes, such as gas formation and crystal growth, which are the most important reasons of life cycle reduction in batteries. This technique may remind us pulse width modulation (PWM) technique which is a control technique with very low voltage rates and higher frequency ranges which is different from pulse charging.
- (5) *Reflex Charge*: During charging procedure some gas bubbles appear on the electrodes, especially amplified during fast charging. This phenomenon is called “burping”. Applying very short discharge pulses or negative pulses which can be achieved for example by short circuiting the battery for very small time intervals compared to charging time intervals in a current limited fashion, typically 2–3 times bigger than the charging pulses during the charging rest period resulting in depolarizing the cell will speed up the stabilization process and hence the overall charging process. This technique is called with other names such as “Burp Charging” or “Negative Pulse Charging”. Different control modes of charging along with waveforms and diagrams are described in [9]. There are other charging methods such as current interrupt (CI) which will be thoroughly explained in the charging algorithm section.
- (6) *Float charge*: For some applications when the charging process is complete and the battery is fully charged, the batteries should be maintained at 100 % SoC for a long time to be ready for time of use uninterruptable power supplies (UPS) are one of such applications where the batteries should always remain fully charged. However, because of self discharge of batteries, they get discharged over time; for example, they may lose 20 or 30 % of their charge per month. To compensate for self-discharge, a constant voltage which is determined based on the battery chemistry and ambient temperature is applied permanently. This voltage is called “Float Voltage”. In general, float voltage should be decreased with the increase of temperature. This causes a very low rate of current, for example C/300–C/100 rate to the battery which continuously compensates for the self discharge rate and also prevents sulfate formation on the plates. This technique is not recommended for Li-ion and Li-Po batteries and it is not necessary for EV/PHEVs which are frequently used every day. In addition, float charging involves a protection circuit which avoids overcharging. This circuit adjusts the float voltage automatically and interrupts charging at some intervals based on battery voltage and temperature.

- (7) *Trickle charge*: Mainly, trickle charging is the same as float charging just with small differences. One is the usual absence of protection circuit which avoids overcharging. Hence, it is very important to make sure in the design procedure that the charging current is less than self discharge rate. If so, they can be left connected to the battery pack for long times.

#### 14.3.1.5 Termination Methods

When the charging is in procedure, it is very important to decide when to terminate the charging. This is because of two main reasons. One is to avoid undercharge, i.e., making sure the battery is fully charged, not partially, in order to use the full capacity of the batteries. The other one is to avoid overcharging which is very dangerous, especially in the case of high energy density Lithium-based EV/PHEV battery packs. If not terminated on time, the overcharging of batteries can lead to over gassing of the cells, especially in liquid electrolyte cells which results in increase in the volume of individual cells, a situation that cannot be tolerated in a rigidly packed battery pack. Another issue is overheating of the cells, especially in Lithium-based batteries which can easily lead to the explosion and firing of the whole pack, since; Lithium is a very active material and easily combines with oxygen in the air. The only thing needed to begin the combination is enough heat.

Choosing different termination criteria leads to different termination methods. Selecting the type of termination of charging process depends on different factors such as the application and the environment where the battery is used. The conventional termination methods that can be used are mentioned here:

- (1) *Time*: Using time is one of the simplest methods which is mainly used as a backup for fast charging or normally used for regular charging for specific types of batteries. This method is very simple and inexpensive, but because of diminishing battery capacity over time due to aging, the time should be reset for a reduced capacity aged battery to avoid overcharging of old batteries. Therefore, the charger will not work well for new batteries and will lead to life time reduction.
- (2) *Voltage*: As mentioned before, voltage can be used as a termination factor, i.e., terminating the charging process when the battery voltage reaches a specific value. This method has some inaccuracies, because real open circuit voltage is obtained when the battery is left disconnected for some time after the charging. This is because chemical actions happening inside the battery need some time to stabilize. Nevertheless, this method is widely used. In addition, this technique is usually used with constant current technique to avoid overheating damage to the battery.
- (3) *Voltage Drop ( $dV/dT$ )*: In some chemistries like Ni–Cd when charged using constant current method, the voltage increases up to the fully charged state point and then the voltage begins to decrease. This is due to oxygen build-up inside the battery. This decrease is significant, so the negative derivative of the voltage versus time can be measured to indicate overcharge. When this

parameter becomes negative, it shows that we have passed the fully charged state and the temperature begins to rise. After this point the charging method can be switched to trickle, or float charge, or terminated completely.

- (4) *Current*: In the last stages of charging, if constant voltage method is used, the current begins to decrease as the battery reaches fully charge state. A preset current value such as  $C/10$  rate can be defined and when the current goes below this value the charging would be terminated.
- (5) *Temperature*: In general, increase in temperature is a sign of overcharge. However, using temperature sensors highly adds to the cost of system. Nevertheless, for some chemistries such as Ni–MH, methods such as voltage drop is not recommended, because the voltage drop after full charge state is not significant to be relied on. In this case, temperature increase is a good indication of overcharge and can be used.

#### 14.3.1.6 Cell Balancing

For high power/energy demanding applications such as EV/PHEVs a large number of cells should be connected in series to provide a high voltage stack and connected in parallel in order to provide a high output current. There are some concerns related to a battery stack. Single cells produced by different manufactures can be recharged hundreds of times, but when connected in series the life cycle dramatically decreases. This is because of cell imbalances. Just to get an idea about the significance of this effect, the results of a real experiment from [10] is mentioned here. In an experiment, 12 cells were connected in series. Despite claiming life cycle of 400 cycles by the manufacturer, it reduced to only 25–30 cycles in a string. This shows how devastating cell imbalance can be. To deal with this, the reasons of cell imbalance should be known and managed. Batteries are electro-chemical devices. Even in the case of a simple resistor while manufactured there is a percentage of inaccuracy. In the case of batteries this is magnified. Two different cells produced in the same factory at the same time will have slightly difference in their parameters. One of these parameters is capacity difference. In the case of a battery pack there are different reasons leading to cell imbalance. As mentioned in [11] there are four fundamental factors leading to cell imbalance. They are manufacturing variations, differences in self-discharge rate, differences in cell age, and also charge acceptance variance. Similarly, in [12] cell imbalance is classified as internal sources which include “Variations in Charge Storage Volume” and “Variations in Internal Battery Impedance” and external sources resulting from “Protection Circuits” and “Thermal Differential Across the Battery Pack”.

A simple analogy can be made with water tanks in order to understand how different battery cells, with different capacities, operate when connected in series. By assuming that water tanks have different volumes connected to each other using pipes at the bottom of tanks, if the first tank is supplied with water the level of water in all the tanks evenly rises. After sometime, the tanks with lower capacity

get full of water while others with higher capacity are partially filled with water. To completely fill up higher capacity tanks, there is no way other than over filling the lower capacity tanks.

Coming back to the real situation, now it is easy to guess what happens in the case of battery strings. Fully charging the high capacity cells involves overcharging low capacity cells. This will lead to excessive gassing and premature dry out of lower capacity cells and at the same time sulfate formation in partially charged cells leading to lifetime reduction. The only way to manage such situation is with cell equalization circuits and custom control algorithms. An important distinction between batteries for EVs versus PHEVs is that for the first case the batteries are usually charged up to 100 % SoC (cell balancing becomes an important issue), while for PHEVs the batteries are usually kept in the range of 40–80 % enabling them to provide enough energy, while being able to absorb regenerative power at the same time.

It is important to note that in cell balancing SoC is the main factor and not voltage. Measuring actual SoC involves discharging the battery completely and calculating the percentage of charge which is not practical. Hence, usually SoC is estimated. Voltage is correlated with SoC and can be used as an indicator of SoC. Accuracy of estimated SoC using voltage depends on battery chemistry and other factors. If other techniques can be used that can determine SoC more accurately, they may be used depending on the allowable cost of the system. Different SoC estimation techniques will be presented in (Sect. 14.3.1.7). Cell balancing in a series string really means equalizing the SoC of the cells which is approximately equivalent to voltage balancing [13].

There are three main cell equalization techniques: (1) charging (2) passive, and (3) active:

- (1) *Charging*: Charging method is simply continuing charging the cells until they are all balanced to some degree. This implies overcharging the cells in a controlled manner which leads to the full charge of high capacity cells. This method is applicable to lead–acid and Nickel-based batteries since they can tolerate some overcharge without significant damage. However, this technique should be carefully implemented since extra overcharge leads to overheating of the cells and finally premature drying of the electrolyte. Despite simplicity and low cost of this method, there are disadvantages such as low efficiency and long times required to obtain cell balance. Experimental results [14] show that for complete cell equalization of 48 V batteries of a specific chemistry, a time on the range of weeks is required. Furthermore, results from [10] show that the extra time required for cell balancing of more cells using this method increases with the square ratio of the number of cells added to the string.
- (2) *Passive*: In this method, extra energy in lower capacity cells is dissipated in resistive elements connecting two terminals of the cells. This will provide enough time for higher capacity cells to get fully charged. This method has low efficiency because of energy dissipation but has a higher speed than the charging method. Passive technique is inexpensive, easy to implement and the control algorithm can be easily designed.

- (3) *Active*: Active cell balancing uses active devices such as transistors, op-amps, and diodes to control the power flow between different cells. This flow can be between groups of cells or single cells. Extra charge is removed from lower capacity cells and transferred to higher capacity cells. This technique highly speeds up the charging procedure and no energy is dissipated. Of course, a small amount of power is dissipated in the circuitry which can be minimized using zero-voltage or zero-current switching techniques.

Lithium-ion batteries are one of the most attractive candidates for EV/PHEVs. Their voltage should be carefully monitored and rigorously controlled in the range of 4.1–4.3 V/cell since the threshold voltage leading to break down of the cell is very close to the fully charged cell voltage rating. Because Lithium batteries do not tolerate overcharging, the charging technique is not applicable to them. According to safety considerations, for Lithium-based batteries the only reliable cell equalization technique is active balancing.

Various types of cell balancing techniques can be found in the literature. Hence, there is a need to categorize them based on a criterion. Based on energy flow they can be classified into four different groups: (1) dissipative, (2) single cell to pack, (3) pack to single cell, and (4) single cell to single cell. It is possible to imagine the operation of each category based on the name with some pros and cons for each group. For instance, dissipative shunting resistor technique is an inexpensive technique and easy to control because of simple structure leading to simple implementation [15].

In addition to energy flow criterion for categorizing, cell balancing techniques can be split into three main groups based on the circuit topology: (1) shunting, (2) shuttling, and (3) energy converter.

Nondissipative techniques like PWM controlled shunting technique have high efficiency but it needs accurate voltage sensing and is somewhat complex to control [16]. Besides, the high number of elements leads to an expensive system. Using resonant converters highly increases the efficiency because of very low switching losses but on the other hand increases further the complexity of the control system [17].

Shuttling techniques work based on transferring extra charge of high capacity cell or cells to an energy storage element such as a capacitor or a group of capacitors, and then transferring it to the low capacity cell or cells [18]. The system would be cheaper using only one high capacity capacitor, but the equalization is faster when a group of capacitors are used. Utilizing a group of low capacity cells instead of one high capacity cell is a good idea, although it increases the complexity of the control system.

Most of the energy converter cell equalization techniques utilize transformers where isolation becomes an advantage at the expense of weight and costs. A model and transfer function of the energy converter cell equalization system is derived in [19] which can be used for control designing purposes.

The above-mentioned cell balancing techniques are all summarized and explained along with circuit topologies in [20]. The question that arises here is that

how much the cells should be balanced. The balance should be in the range of volt, mill volt, or some other range? As experiments from [13] show for lead–acid batteries, cell-to-cell voltage matching should be in the range of 10 mV which corresponds to a SoC range that provides reasonable improvement in life cycle. This is an important factor, since, for example if the voltage matching should be in the range of 1 mV, it means that the sensors should be 10 times more accurate and also the algorithm may be needs to be improved for this case. This means more cost and complexity. Therefore, there is a trade-off between cost and life cycle. This parameter should be experimentally verified for different chemistries, environments, and applications.

Since EV/PEHV battery packs do not possess a mature technology and also not many experimental data are available, sometimes contradictory claims may be seen in the literature, one of which is mentioned here. As mentioned before, battery packs used in HEVs are usually controlled to remain in the mid-range of SoC. The principle is that the battery should be in a state with the ability of absorbing regenerative energy while being able to support enough power during acceleration. If the battery is in 100 % SoC, absorbing regenerative current will lead to the overcharge of the battery. Cell overcharge is usually sensed through measuring the cell voltage. Some literature supports that switched capacitor cell equalization technique (shuttling method) is a suitable candidate for applications with no end of charge state like HEVs, because there is no need for intelligent control and it can work in both charge and discharge mode [20]. On the other hand, some researchers support that according to the nearly flat shape of open circuit terminal voltage of Lithium–Ion cells in the range of 40–80 %, the suitability of charge shuttling methods for HEV applications is denied because of the negligible voltage deviation of cells [15], and more complex estimation of SoC should be implemented, as discussed in the next section.

#### 14.3.1.7 SoC Estimation

One of the most important information needed for safe charging is SoC. Charging algorithms is mainly based on SoC directly or indirectly. Hence, the knowledge of SoC value is a key parameter in accurate charging. Unfortunately, directly measuring SoC is somehow impossible or at least very hard and expensive to implement and in some applications does not make sense, so mostly SoC is estimated based on other variables or states of the battery. This involves battery models based on which different estimation methods can be utilized or observers can be designed. Precise estimation of SoC is not an easy task, although in typical applications battery voltage which is a sign of SoC can be used. In the case of high power/high energy EV/PHEV battery packs more accurate methods are advisable, although being more expensive and complex in implementation. The more accurate the SoC estimation is, the better the charging algorithms can be implemented resulting in life cycle improvement.



As mentioned before, SoC is mainly the ratio of available charge to the rated capacity of the cell. One of the important points in SoC estimation to take care of is rated capacity change over time due to aging resulting from degradation of electrolyte, corrosion of plated and other factors. Research in this field is defined as “State of Health Estimation” where the readers are encouraged to study in the specialized literature.

Here we mention and describe some SoC estimation techniques. One of the simplest methods is to completely *discharge* the battery and measure the SoC. Although simple, it is very time consuming and it is not practical to completely discharge a battery just to measure SoC. Knowledge of the SoC is useful for the current situation of the battery, so if the battery is discharged the state of the battery has changed and there is no more use of previous state SoC knowledge. Especially, in the case EV/PHEV this method is not applicable. Although this method is not used online, it may be used periodically after long intervals just to calibrate other SoC methods.

Another method is *Ah Counting* which measures and calculates the amount of charge entering the battery or leaving it by integrating the current over time. This is one of the most common methods used; however, there are some deficiencies and drawbacks. Initially, because there is always inaccuracy in the sensors. Even very small, because it is being integrated over time it can sum up to a considerable value leading to significant errors. Besides, even supposing a very accurate current sensor, because this integration is being implemented usually by the use of digital circuits and numerical methods, there are always calculations errors involved and again can show up in high errors over time. Even if assuming both deficiencies to be solved in some way there is another reason leading to inaccuracy. Even if the amount of charge entering the battery is exactly calculated, because of coulomb efficiency where a certain amount of current entering to charge will not be the same when leaving the battery, this method has some inaccuracy. One way to reduce these inaccuracies is to recalibrate the integration process every time a specific known set point (such as fully discharged state or fully charged state) is reached.

Another method for SoC estimation is called *Measurement of Physical Characteristics of Electrolyte*. Obviously, this method is applicable only to liquid electrolyte batteries, not solid ones like Li-Po. In this method, a chemical fact is used and that is the relation of change of some parameters in electrolyte with change of SoC. One of these parameters is the density of the acid. There is an almost linear relation between changes in acid density versus SoC. This method is very well-known specially in lead-acid batteries. Acid density can be measured directly or indirectly using parameters such as viscosity, conductivity, ion concentration, refractive index, ultrasonic response, and so on.

As discussed before, the *Open Circuit Voltage* of the batteries can also be used as an indicator of SoC. The uncertainty in this method is due to the fact that batteries under operation need some rest time for their open circuit voltage to stabilize. This time for some cases can be up to hours; however, this method is also widely used. The key point in this method is the linear relationship of open circuit

voltage versus SoC in a specific range of SoC. This range and its slope are variant for different chemistries which should be taken into account.

There are other techniques categorized under soft computation techniques such as fuzzy neural network [21] or adaptive neuro-fuzzy modeling [22] which can also be utilized for SoC estimation. Other approaches categorized as heuristic interpretation of measurement curves mentioned in [23] such as Coup de Fouet, Linear Model, Artificial Neural Network, Impedance Spectroscopy, Internal resistance, and Kalman filters can also be utilized which are more precise methods but more complicated to implement.

#### 14.3.1.8 Charging Algorithm

Charging algorithm can be defined as the combination of what was mentioned up to here and controlling all or part of the parameters affecting battery performance and life cycle in such a way to achieve charging the battery pack with safety, efficiently, and terminated on time. Managing the charging procedure of a high power battery pack with hundreds of cells involves many issues as already discussed in this chapter. To control all of these parameters, efficient and accurate algorithms with reliable safety and backup circuits are required. The trend toward fast charging with huge amounts of current flowing to the battery pack producing lots of heat requires accurate and reliable supervisory control algorithms to ensure safe charge. Managing such complex task can be handled with advanced control techniques like fuzzy logic, supervisory control, and decentralized control, and so on. In general, each battery chemistry requires a unique charging algorithm. Depending on the algorithm it may be applied to other types as well; however, this should be carefully done according to life cycle and safety issues.

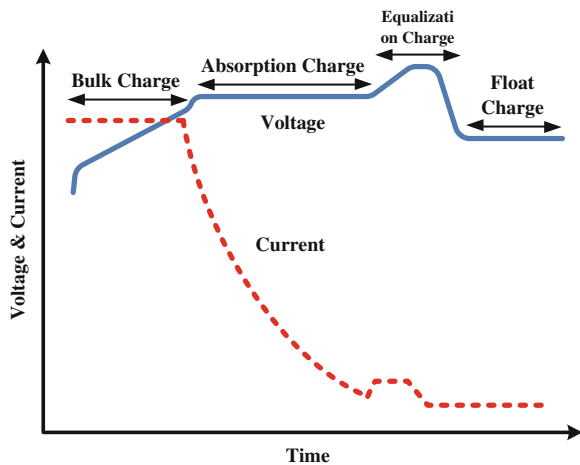
For precise battery charging, the charge/discharge profile of the battery provided by the manufacturer must be used. However, the profile is valid for brand new batteries; hence, some techniques like data acquisition methods must be used to acquire the charge/discharge profile of the battery with deterioration due to aging. Novel techniques regarding this issue is being introduced in the literature every often [24].

As mentioned before, lead–acid batteries have mature technology and infrastructure already exists, but they still have poor life cycles in the order of 300–400 cycles. A lot of efforts have been put into research for increasing the life cycle of lead–acid batteries because of their advantages such as low cost and availability. This chemistry has a common charging algorithm which includes four different stages or three based on the application, as indicated in Fig. 14.4. In the first stage, a predefined constant current is applied to the battery pack which charges the cells rapidly. In this stage, the cell voltages increase gradually because of SoC increase. This stage is called *Bulk Charge* stage. The process is continued until a predefined maximum voltage is reached. These values are all recommended by the manufacturer in the datasheet. In the next stage called *Absorption Charge* stage, a constant voltage is applied to the battery pack. At this stage, the current decreases

gradually until it reaches a predefined C rate value and the cells are approximately charged but not equalized because of cell imbalance. At this stage, a relatively higher voltage than constant voltage in absorption stage can be applied to the pack for some time to balance all the cells inside the pack. This stage is called *Equalization Charge* stage. The equalization can also be achieved with other techniques as mentioned before. After some prescribed time, the charger applies a lower constant voltage in order to keep the battery in a ready to use state. This is called *Float Charge* stage and depending on the application it can be utilized or omitted.

As the battery ages, its internal characteristics also change; hence, an adaptive charging algorithm could be used to take into account these parameter variations. Experimental results show that the value of voltage of the third stage should be increased over time to get the same amount of energy as the battery ages [25–27]. The equalization stage is the key part of this algorithm and has great influence on the life cycle of the battery. As mentioned before, the voltage of this stage should be increased but this increases the current and also the heat generated which has a negative impact on the life cycle. One way to get the same amount of current with lower heat dissipation is by using pulses of current. Although this technique seems the same as pulse charging, it is actually different, because the time intervals are significantly bigger than pulse charge time periods which are in the range of kilo hertz. This method is called CI. This technique has shown significant life cycle improvements [28]. Using this algorithm, the battery can reach 50 % of the initial capacity after 500 cycles which is a significant improvement in life cycle. Although this algorithm is useful, it puts the battery under stress while it reaches the end of life because of permanently increasing the overvoltage value. This algorithm can be implemented in an alternative way. Instead of using this method for each cycle, which puts high stress on the battery, it can be utilized every 10 cycles. This algorithm is called partial-state-of-recharge cycling (PSOR) [28] and has approximately the same effect with the advantage of less stress on the battery. This algorithm has been claimed to

**Fig. 14.4** Charging algorithm of a typical lead–acid battery



enable the battery deliver up to 80 % of initial capacity even after 780 cycles [28] which is a really noticeable improvement in life cycle.

As can be seen, these complicated algorithms cannot be done using simple PI, PID controllers. They require DSP-based controllers to be programmable with numerical data dependent on the battery chemistry, state of health, and other factors.

Continuously, different algorithms are being proposed and tested for improving life cycle of the batteries. This is a vast research area and is currently still under development, getting a lot of attention as EV/PHEVs become popular and available in the market.

## 14.4 Power Electronics for EV and PHEV Charging Infrastructure

In its simplest incarnation, a charging facility for EVs would merely consist of a unidirectional AC/DC converter charger connected to the power grid. Power would simply flow on demand from the power grid through a power conditioner into the vehicle battery pack; once the battery is fully charged, the connection to the grid no longer performs any useful work. This simple set up may have been appropriate for small private commercial vehicle fleets, or where electric cars represented a very small fraction of the active road vehicles. However, as society's efforts to electrify our means of transportation intensify, it is clear that a smarter exploitation of the vehicle-to-grid (V2G) interaction is in order. To the power utility, the bulk of EVs connected to its grid appears as an energy storage agent that is too significant to be left untapped. This view is reinforced by the outcome of several statistical studies [29] that show that more than 90 % of all vehicles are parked at all times, thus potentially connected to the grid. Assuming a 50 % EV market penetration, simple calculations show that, the total storage capacity available would be in the order of thousands of GW-hour! Therefore, the V2G connection should be bi-directional, giving the owner of each vehicle the ability to "sell" back a portion of this stored energy to the utility, presumably at an advantageous rate. The same requirement of

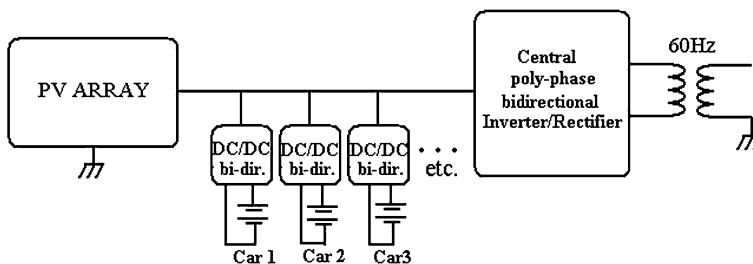


Fig. 14.5 Typical PV-powered grid-tied carport architecture

bi-directionality also applies when the vehicle is connected to a microgrid powered by a distributed resource. In a grid-connected solar carport for instance, many vehicles can be charged by PV panels or by the grid or by both, depending on load and insolation (time of day, meteorological conditions, time of year, etc.). In the case of overproduction, energy from the panels can be fed back to the grid for a profit, while the EV batteries function to buffer the characteristic solar intermittence. Similarly, the DC–DC converters that condition the power from the solar panels to each charging vehicle should also be bi-directional in order to allow the owner of a plugin electric vehicle (PEV) to exchange a portion of his energy with the operator of the micro grid (Fig. 14.5).

These considerations demonstrate that bi-directionality is a highly desirable feature in any power conditioner utilized in vehicle charging–discharging applications, including interactions to and from the grid, microgrid, or residential loads and renewable energy generators. On this basis, the reader should note that the discussion that follows makes no distinction between V2G and grid-to-vehicle communication, both being classified by the acronym V2G. Similarly, V2H will designate either the vehicle-to-home or the home-to-vehicle interface.

Other requirements for the optimal charging infrastructure are harder to identify. This is due to pervasive lack of standardization involving battery technology and nominal voltage, safety strategy, connector configuration, communication protocols, location of charger (on-board or off-board), and more. In the following paragraphs, these issues are treated especially in reference to their impact on local power generation and utilization.

### ***14.4.1 Charging Hardware Strategy***

Like any other means of transportation, EV/PHEV's benefit markedly from minimizing their weight. These vehicles are even more sensitive to that issue, considering the unavoidable presence of heavy battery/ultra capacitor energy packs. The electronic power converters intended for the charging function can be bulky and heavy in their own right, and their deployment on-board seems to make little engineering sense. Yet, at the time of this writing, the great majority of PEVs in North America contain their own power rectifier and connect directly to 120 or 240 V household plugs. This can be explained by two considerations. First, while the household AC voltages are fully standardized, at least within a country, the DC nominal battery voltage for PEVs is definitely not. Different manufacturers have adopted ad hoc energy storage technologies and safety strategies, resulting in strikingly different bus voltages and current requirements. An unsophisticated external converter could then be optimized for only one vehicle brand or model.

Second, some techniques have been developed that do not add significant weight to the vehicle. The critical idea is to utilize the power electronic circuitry that is already on-board in order to perform the rectifying function. This charging circuit is commonly referred to as an “integrated charger”; it makes use of the

bi-directional inverter that drives the electric motor as well as the windings of the motor itself. Figure 14.6 shows a well-known example of this concept:

With regard to Fig. 14.6, it is important to realize that inductors LS1, LS2, and LS3 are not added magnetic devices, but the actual winding leakage inductances of the electric motor. Thus, the only added components are the two relays K1 and K2, which are activated in order to reconfigure the schematic from a three-phase motor driver, during normal vehicle propulsion operation, to a single-phase boost rectifier, during charging.

The above two considerations are consistent with relatively slow charging strategies. In the first instance, because the amount of electric power available in a residential setting does not usually exceed 10 kW at a household plug. In the second instance, because the electronics that drive a PEV electric machine are sized for its propulsion needs. Thus, the average charging power must be limited to a level comparable to the motor’s rated power, which is of the order of 10–50 kW in smaller cars.

Slow charging strategies are commonly referred to as level 1 and level 2. The former is associated with a connection to a regular AC household plug (120 V, 15 A), while the latter involves powers that can be as high as 14.4 kW or 240 V at 60 A, which is also normally available in residential settings. Moreover, these power levels are compatible with the average generating capacity of microgrids and corresponding distributed resources. Then, it would appear that whether a car

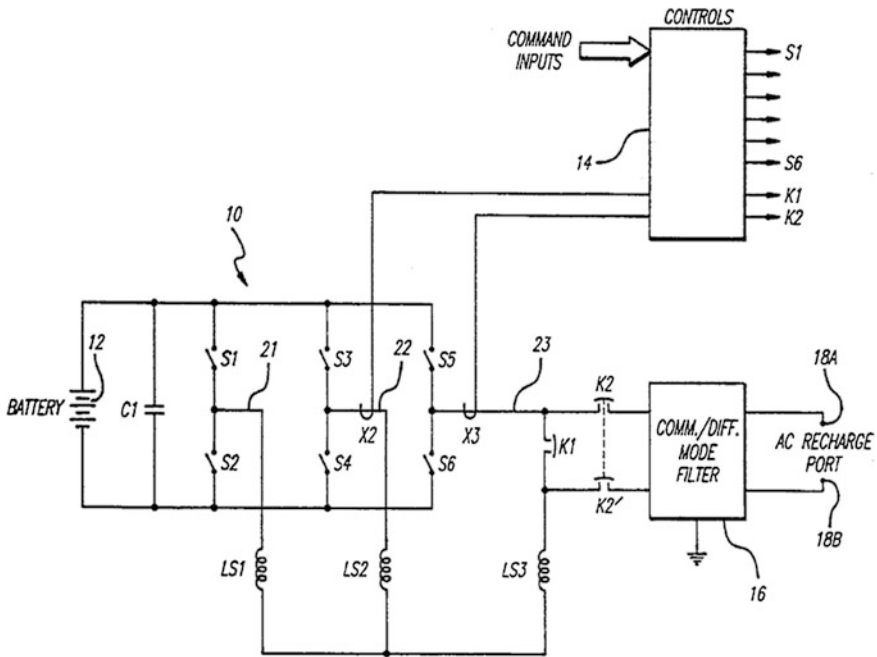


Fig. 14.6 Integrated charger based on boost converter [47]

is charged through a regular residential wall socket, or a microgrid outlet, the available power levels justify the location of the rectifier on-board the vehicle.

On the other hand, EV manufacturers are quickly recognizing that long charging periods may be acceptable to consumers only if quick charging is available as well, albeit at higher cost. Two solutions are presently under consideration. The first solution is the so-called battery swapping, whereby a car owner simply drives to a service station and allows an automated system to safely replace a spent battery with a fully charged one. Along the same lines, the battery could be of the redox flow type. In this case, the battery casing is not replaced; rather, it is drained and then filled with fresh liquid electrolyte. In either forms, the obvious drawback is the need for the exact standardization of battery size, chemistry, and capacity.

The second solution consists of allowing direct access to the battery DC terminals, so that a large off-board rectifier can be connected and re-energize the battery pack using powers of the order of up to several hundred kilowatts. This is known as level 3 charging, allowing an electric “fill-up” service stop to last only a few minutes. In this instance, although the battery itself may not need a high level of standardization, it would be subject to extremely high currents at high voltages. This renders the practical implementation of this second solution strongly dependent on needed improvements to battery and ultra capacitor technologies. Furthermore, a public charging station capable of servicing many cars simultaneously would represent a local load of several megawatts as seen by the grid.

Despite these difficulties, it is highly likely that either the battery swapping or the fast-charging strategy will eventually be universally available to complement, or even replace, the onboard charger.

### ***14.4.2 Grid-Tied Infrastructure***

Assuming fast-charging through direct DC connection becomes the method of choice, car owners will have two options. They may still prefer to slow charge their vehicles overnight by plugging to a AC–DC charger [or electric vehicle supply equipment (EVSE)], most probably in their homes. This converter will deliver relatively low powers of the order of 5–10 kW because limited by the residential connection, as mentioned earlier. However, as further explained in [Sect. 14.5](#), this method may involve some financial returns. The alternative method will be to use a fast-charging public facility, corresponding to a familiar service gas station that is capable of multi-megawatt power transfers. Although the cost per kW-hour will be high, the owner benefits from charge times in the order of minutes rather than hours.

In both cases, V2G capability, enabled by smart grid technology will become a standard feature with all EVSE’s, whether they are public, commercial, semi-public, or private. This will allow the subsistence of a very significant distributed storage resource at the disposal of electric utilities. More specifically, the PEV fleet will be optimally positioned to become a significant provider of some

ancillary services and play a role in offering dispatchable peak power. These services to the electricity supplier will be analyzed separately:

#### *PEVs as “Peakers”*

A peaker is a small but nimble generating units that can supply the grid with relatively fast response. Historically, natural gas turbines or small hydroelectric plants were the devices of choice for this task. They are active for only a few hours every day and therefore provide only limited energy. Thus, a substantial fleet of PEVs can carry out this task as a highly distributed resource without significantly depleting their batteries. Unfortunately, as long as peak power is not considered a “service”, the utility operator will compensate the car owner solely for the energy sold, albeit at a higher peak demand rate [30]. This may not constitute a strong enough incentive to the car owner who has to consider other factors, such as the additional battery and power electronic wear and tear for his vehicle. Nevertheless, future adjustments in energy market models are under study to address this among other issues.

#### *PEVs as Spinning and Nonspinning Reserve*

One of the most lucrative ancillary service is the spinning and nonspinning reserve. The former consists of generators that are online, but normally run at very low capacity. In the case of a disruption, such as a failure in base load generation or transmission, these generators are commanded to provide the missing power. They must be able to ramp up in less than 10 min and provide power for as long as 1 h or more. Nonspinning reserves are not online and are required to ramp up to full power within 30 min. Because this is a service, the utility company will pay for the availability of the power as well as its amount. In fact, this service is paid even when no power is ever delivered. A PEV owner can provide this service naturally and be reimbursed starting at the time he plugs his vehicle to the grid even if the battery is never discharged. Also, it must be noted that PHEVs have smaller battery capacity than all-EVs, but contain an ICE that can be started on a V2G command to generate electricity and function as a spinning reserve as well.

#### *PEVs as Voltage Frequency Regulation Agents*

An ancillary service that is even better tailored for PEVs is regulation. It consists of delivering or absorbing limited amounts of energy on demand and in real time. Normally, the request is automated in order to match exactly the instantaneous power generation with the instantaneous load. Failure to do so results in dangerous shifts in line frequency and voltage. The dispatched amount of energy has short duration—in the order of few minutes—but it is requested relatively frequently. Therefore this is a continuous service. It is important to underline that the amount of energy involved is relatively small and changes direction quite rapidly and regularly, implying minimal PEV battery discharge for any reasonably short-time interval. The near instantaneous response time and the distributed nature of the PEV fleet explains why regulation is probably the most competitive application for V2G from the point of view of the utility operators.



### *PEVs as Reactive Power Providers* [31]

Most electronic topologies used for the inverter/rectifier function in the interface of the PEV to the grid are fully capable of shaping the line current to have low distortion and varying amounts of phase shift with respect to the AC line voltage. This implies that reactive power can be injected into the grid on demand and in real time. Furthermore, since reactive power translates in no net DC currents, this service can be provided without any added stress to the PEV battery.

## 14.5 The V2G and V2H Concepts

The advantages described in the preceding sections are not presently exploitable due to a general lack of the required hardware infrastructure, as well as the thorny transition to new business models that include the V2G concept. The roadmap toward achieving this goal will probably consist of the following several milestones.

- (1) The first milestone is rather rudimentary as it does not yet require bidirectional converters. It will consist of a simple owner-selectable option afforded by the vehicle BMS user interface that allows the grid to schedule when to activate and deactivate charging. In return, the owner pays lower per-kW-hour rates. Communication between the grid operator and the BMS can be done through the existing cell phone technology, requiring no additional infrastructure or hardware.
- (2) The straightforward “grid-friendly” charging time-window strategy described above will evolve to include more sophisticated algorithms. For instance, the grid might broadcast any updates to the current per-kW-hour cost and let the vehicles BMS choose whether to activate charging. Some ancillary services, such as regulation “down” could become feasible, while regulation “up” will be limited by the lack of reverse power flow capability of the EVSE at this stage. The use of aggregators will also become widespread. Aggregators are intermediate communication and power distribution nodes between a group of vehicles, located in proximity to each other, and the grid. This allows the grid to macromanage a single installment of several vehicles, corresponding to significant power level blocks with somewhat predictable behavior, akin the other distributed energy resources. Furthermore, because the aggregator’s consumption will be in the MW range, it will allow purchases of power on the wholesale market, reducing the cost for each participant vehicle.
- (3) Eventually, bidirectionality will become a standard feature for all EVSEs. However, this capability will not be immediately harnessed to achieve controlled reverse power flow to the grid. Rather, the PEV battery will, most likely, initially service the surrounding premises, probably the owner’s home. This scenario, called V2H, will probably precede the full implementation of V2G [32], because it effectively bypasses several large infrastructure and

technical issues needed for V2G, while achieving many of the same results. Through pricing incentives, a PEV parked in the residential premises and connected on the customer's side of the meter, can be exploited to absorb energy from the grid during times of low demand, and transfer it to the household appliances, during times of high demand. This will indirectly shrink the power peaking for the grid while reducing the electrical bill to the user. It will also reduce overall transmission losses over the V2G strategy, because line current will flow only in one direction, from grid to vehicle, and will then be consumed locally. Moreover, if the household is geared with renewable source generators, the vehicle can immediately serve as storage and, during blackouts, as backup power. Although one can find some similarities between the concepts of V2H and V2G, there are important distinctions. In practical terms, these differences stem from the fact that V2H cannot take advantage of the high predictability deriving from statistical averages afforded by very high numbers of vehicles available for V2G operations. Simply stated, the real benefits of V2H are not easily estimated, because they are dependent on many exceedingly uncertain variables. Some of these are: the number of available vehicles, commute schedule, time duration and distance, PEV energy storage capacity, presence and quantity of quasi-predictable local generation (example: solar panels), presence and quantity of unpredictable local generation (example: wind power), residence-specific energy consumption profile, and presence of additional storage. Despite the fact that these issues will require complicated management algorithms in order to optimize the use of V2H, some benefits, such as emergency back-up, are available immediately with a relatively minor upgrades to the residential infrastructure. These upgrades consist mainly in the installation of a transfer switch to disconnect the residence from the grid during backup operation, and expand the design of the power converter to detect islanding conditions. Furthermore, the EVSE must be capable of controlling output current into the line when connected to the grid, but reverting to controlling output voltage when acting as a backup generator.

- (4) Full V2G implemented with automated options for V2H. The connection will be metered and could also include any locally generated renewable energy management.

### ***14.5.1 Grid Upgrade Strategy***

The electric transmission and distribution networks in most industrialized nations must consider changes and upgrades in order to fully benefit from the introduction of PEVs as distributed resources. First we must consider the extent by which the current production capacity will have to be expanded. Various studies [33] have suggested that once the typical charging profile for a PEV is scrutinized and hopefully optimized—charging mostly at night—the installation of new generation

will be unnecessary or minimal at most. In fact, it will have the effect of diminishing reliance on more expensive load-following plants, since the overall 24 h demand curve will average closer to the base load. Therefore, the main effort should be in effectively introducing intelligence into the grid. The hardware and communication standards for implementing such intelligence are still under study. Wideband digital interface can take the form of PLC (Power Line Communication) or utilize separate communication channels that have some market penetration already. In either case, the EV will most likely be treated as any other managed load by this smart grid, with the exception of a sophisticated on-board metering device that will have to be reconciled with the utility's pricing model. Presently, the two major obstacles to the utilization of PEVs as distributed resources are the lack of bi-directionality in the power converters and the lack of recognized standards, both software protocols and hardware, for the smart grid function. Of the two, the former is by far the easiest to implement, given the well-established characterization of suitable power electronic topologies.

#### *Renewable and Other Intermittent Resource Market Penetration*

Due to recent well-known trends, renewable resources are increasingly prominent in the complex energy market mosaic. As long as their penetration level is low, they can be easily handled by the current infrastructure, but at present incremental rates this will not be the case in the future. The intermittent nature of solar and wind generation will require a far more flexible compensation mechanism than what is available now. Because of this, today's renewable energy installations are invariably accompanied by large battery banks that act as buffers between the generator and the grid. Wind power, in particular, is not only intermittent but has no day-average predictability, as winds can differ hour to hour as easily as night as during the day, adding an extra amount of irregularity to an already varying load. This suggests that PEVs will be called to perform not only the more manageable regulation task, but also aid in providing peak power. As noted earlier, this may not find the approval of the PEV owner unless the pricing model is modified. Nevertheless, it is reasonable to ask whether a large PEV contracted fleet could perform this task on a national (US) level. Studies have shown [34] that the answer is yes. With an overconfident, 50 % estimation for the market penetration of wind energy and 70 million PEVs available, peak power can be provided at the expense of approximately 7 kW-h of battery energy per day or about 10–20 % of an average PEV reserve.

#### *Dedicated Charging Infrastructure from Renewable Resources*

The traditional microgrid often relies on diesel generators as a single source of energy. Even in this case, any load fluctuations are quite difficult to negotiate, relying solely on the intrinsically slow ramp up speeds of the generator itself. The new trend toward integrating renewable resources into microgrids greatly amplifies this problem due to their notorious intermittent nature. On the other hand, the dedicated generation from renewables for the explicit purpose of PEV charging is gaining more credibility as a means to eliminate transmission losses and greatly

reduce the overall carbon foot-print associated with EVs. Such installation would fall in two categories: (1) small installations with or without a grid tie, (2) large installation with grid-tie. Small installations can be somewhat arbitrarily defined at less than a total of 250 kW of peak production. This would be sufficient to slow-charge about 20 vehicles and would certainly require local external storage in order to buffer the peaks and valleys in local energy production. This is more evident in the case of islanded installations; if any energy is produced in excess, it cannot be sent back to the grid, so it will need long-term storage capability. Large installation with a grid-tie can inject or draw power to and from the grid as a means to equalize the grid during overproduction and draw from the line. However, depending on the number of vehicles connected, which can be accurately predicted with statistical methods, some of the PEV resource can be utilized to minimize the size of the external storage. Nonetheless, it appears that PEVs can alleviate the inherent issues associated with local renewable production for the dedicated purpose of PEV charging, but not totally eliminate them.

## 14.6 Power Electronics for PEV Charging

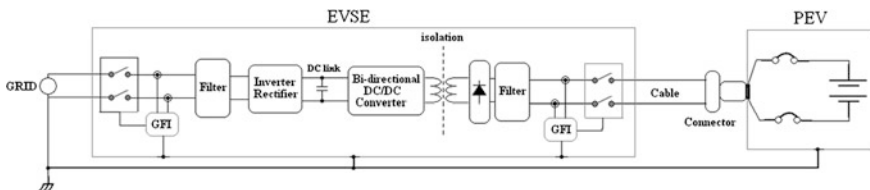
The PEV charging process will be enabled by the sophisticated power electronic circuits found in the EVSE. Such equipment will be optimally designed depending on the different possible sites and types of power connection. We will begin by looking at EVSE connected to the main power grid and then analyze dual-sourced systems such as grid-tied renewable energy installations dedicated to PEV charging. A short discussion on basic safety compliance strategy follows.

### *Safety Considerations*

For off-board chargers there are only a few important safety needs that affect significantly the power converter design. These are (1) isolation of the battery pack with respect to chassis and the grid terminals, (2) ground fault interrupters (GFI) to detect any dangerous leakage current from either the grid or the battery circuit, (3) connector interface, and (4) software.

A typical EVSE and related connections is shown in Fig. 14.7.

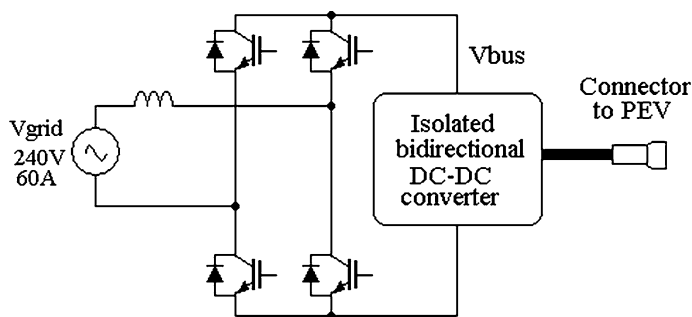
Two GFIs detect any breakdown or current leakage on either side of the isolation barrier in order to insure complete protection to the user and disconnect the



**Fig. 14.7** Typical EVSE safety configuration

high-power circuit immediately in case of fault. The battery pack is fully isolated from the chassis since it cannot be grounded properly during charging without heavily over sizing the connector cable. In fact, some existing safety recommendations require that an active breakdown test be performed on the battery pack prior to every charging cycle. At the time of writing, the de facto standard for level 3 DC charging is the CHAdeMO standard developed by the Tokyo Electric Power Company. Although competing standards may eventually overtake it in popularity, the description the CHAdeMO connector demonstrates the safety concerns involved. The connector itself will have mechanical means to lock itself onto the car receptacle in order to prevent accidental removal when energized. It will carry the power leads, but also communication wires that include a CAN bus digital interface as well as several optically isolated analog lines for critical commands such as on/off, start/stop, etc. Every analog signal sent by the PEV to the charger (or vice versa) is received and acknowledged through the analog lines. This analog interface is sturdier than a digital one and less susceptible to electromagnetic interference. The CAN bus is activated only when more complex information is exchanged. Prior to the start-charge command, the EVSE communicates its parameters to the PEV (maximum output voltage and currents, error flag convention, etc.), and the PEV communicates its parameters to the EVSE (target voltage, battery capacity, thermal limits, etc.), and a compatibility check is performed. During charging, the PEV continuously updates the EVSE with its instantaneous current request (every 100 ms or so) and all accompanying status flags. Once charging is finished, the operator can safely unlock the connector and drive away.

As can be seen, the presence of safety devices, such as the GFIs as well as a sturdy method of analog and digital communications renders the charging process extremely safe, leaving the power electronic designer of the EVSE with the relatively simple task of ensuring only the isolation barrier between the grid voltage and the PEV floating battery. In fact, the utilization of an isolation transformer can actually simplify some designs due to the added voltage amplification capability afforded by the transformer's turns ratio. This could prove very beneficial if much higher battery voltages become necessary in order to increase storage capacity.



**Fig. 14.8** Canonical single-phase EVSE configuration

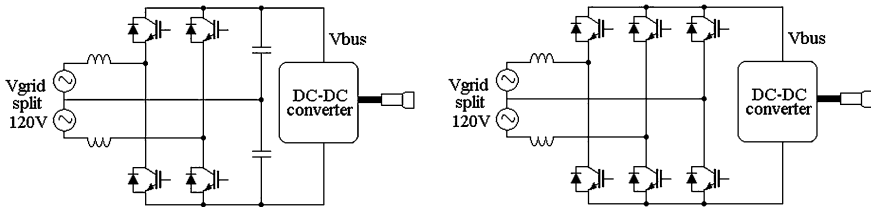


Fig. 14.9 Split phase sourced EVSE configurations

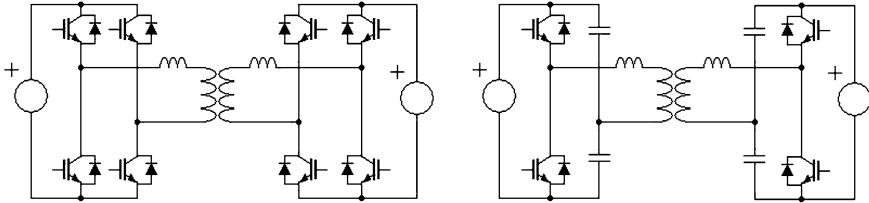


Fig. 14.10 Typical isolated bidirectional buck-boost DC-DC converter topologies

### Grid-tied Residential Systems

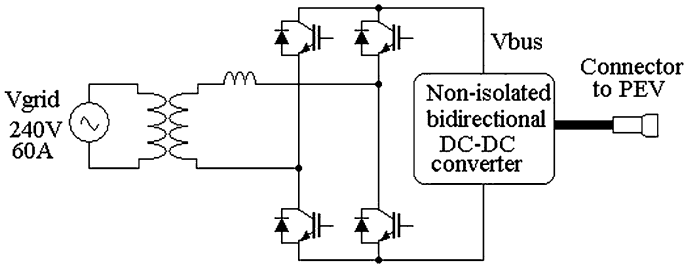
As noted earlier, only level 1 and level 2 are feasible within the confines of a residential setting. This can be accomplished through integrated chargers when available or an external EVSE. In the latter case, the most obvious circuit configuration is a single-phase bi-directional rectifier/inverter powered by a 60A/240 VAC circuit that is readily available from the distribution transformer. The DC-link voltage is then processed by a bi-directional DC-DC converter that performs the isolation function. This simple topology shown in Fig. 14.8 can be called the canonical topology as will be repeated, with minor changes, for most grid-tied system irrespective of power rating.

In North America, the 240 V from the residential distribution transformer is in the form of a split 120 V supply, suggesting small modifications to the canonical topology. Figure 14.9 shows two possibilities:

The two topologies in the figure are similar, but the one on the right has better voltage utilization and is better equipped to counter unbalanced loads on the split supply [35].

For the DC-DC converter, many bi-directional isolated circuit topologies have been proposed [36]. Typical circuits are shown in Fig. 14.10.

When the two controlled bridges are independently driven in phase-shift modulation (PSM), these are generally referred to as dual active bridge (DAB) topologies. In their simplest operation mode, when power needs to be transferred from the left-side circuit to the right-side circuit, for instance, the right-side IGBT switches are left undriven, leaving their antiparallel diodes in the form of a regular diode bridge. Under these circumstances, the topology becomes identical to a regular PSM converter, which is simple to operate, but not very flexible in terms of voltage gain. On the other hand, when both bridges are modulated, power transfer



**Fig. 14.11** Configuration with isolation at the grid

can be accomplished in both directions and with great variability ranges on the input and output voltages. In addition, zero voltage switching (ZVS) can be assured for all switches for reduced switching loss and generated electrical noise (EMI).

Other topologies [37, 38] based on the DAB have been proposed with purported additional benefits, such as better switch utilization, extended ZVS operating range, and more flexible voltage amplification.

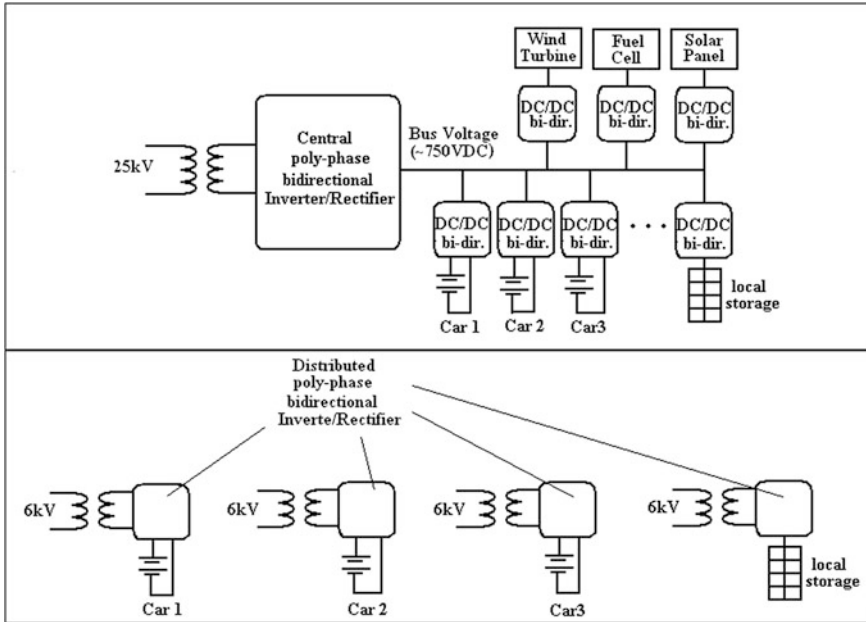
#### *Grid-tied Public Systems*

A public parking/charging installation would deliver only level 2 power, given the relatively long plugin times. Because there are several parking locations in close proximity, the power configuration used for residential use may not be optimal. Rather, a single transformer can be installed at the grid, delivering isolated power to all vehicles in the facility. This way, cheaper and more efficient nonisolated DC–DC converters can be used without violating safety rules.

Figure 14.11 illustrates this configuration for each charging station. For the whole installation, the architectures shown in Fig. 14.12 are possible:

In the centralized architecture [39] a single, large poly-phase, 50/60 Hz step-down transformer connects to the grid, providing isolation for the whole facility. This is followed by a large bidirectional rectifier that produces a single high-voltage DC bus. Each parking station uses inexpensive high-efficiency nonisolated DC–DC converters to process this bus voltage into the appropriate charging current for the individual PEVs. Because isolation is either desirable or required, especially on PV panels depending on local electrical codes, additional storage or generating resources, such as wind turbines and fuel cells, can also benefit from a simpler interface to the DC bus. Moreover, the single transformer connection guarantees that no DC current is injected into the grid, doing away with complicated active techniques to achieve the same purpose.

The advantages just noted for centralized configuration are somewhat offset by the following drawbacks: (1) the need for a bulky and usually inefficient line-frequency transformer, (2) an expensive high-power polyphase inverter/rectifier, (3) single-fault vulnerability in the transformer and central inverter/rectifier, and



**Fig. 14.12** Central architecture (*top*). distributed architecture (*bottom*)

(4) lack of voltage amplification in each non-isolated DC–DC converter (otherwise afforded by the turns ratio of the high frequency transformer in isolated topologies).

In a level 3 (fast charging) public facility, other technical challenges must be considered. For instance, with battery pack rated voltages in the range of 200–600 V, the overall currents required for fast charging will be of the order of thousands of amps. These currents must necessarily flow through cables and especially connectors, causing local thermal issues and loss of efficiency due to ohmic loss. In addition, the charging stations will appear as a concentrated loads to the grid, so that any power transients produced by the stations are very likely to cause local sags or surges.

The first issue can be partially countered by brute force methods such as the development of advanced sub-milliohm connectors and minimizing cable lengths by placing the grid step-down transformer in physical proximity of the vehicle. It is obvious that any intervening power conditioning electronic circuit should be added only when absolutely necessary. This immediately suggests that the architecture of the charging station should be distributed rather than central. As can be seen from Fig. 14.12 (bottom), a distributed architecture could potentially reduce the number of processors from grid to battery from two to one. To be fair, this single stage may not be feasible when managing large input–output voltage ranges, especially if buck–boost operation is required (see discussion on the Z-converter later in this section). Nevertheless, if an additional DC–DC stage should prove necessary, it will be easily integrated locally with the inverter for improved



efficiency. Furthermore, a central processor, besides constituting a single point of failure as already noted, would have to be rated for the full service station power, which could be of the order of a megawatt. On the contrary, a distributed architecture benefits from repeated circuitry (economies of scale), redundancy for higher reliability, and the possibility of power conditioning in physical proximity to the vehicles, reducing ohmic loss.

The issue of power line quality deterioration caused by the service station operating transients has only been studied for specific geographic locations [40], but possible voltage fluctuation of up to 10 % have been reported depending on the length of the feeding high-voltage transmission line. The obvious and perhaps sole approach to mitigate this problem is the integration of flywheel, battery, or ultracapacitor banks into the charging station. This storage will smooth out the load transients by delivering local power when needed and storing power during periods of lower demand. Moreover, it will average out the draw from the grid, so that the distribution equipment can be rated at much lower peak powers (as much as 40 % [41]).

The task of discriminating between the various available electronic topologies is made easier when considering the sheer power handled by fast chargers; to wit, up to 250 kW. Obviously, a good candidate must be very efficient, inherently low noise, with low component count and capable of high-frequency operation in order to control physical size. For the inverter/rectifier section, we must also add the requirement that no significant harmonic content should be present in the line current. In order to obtain input currents that are sinusoidal and free of ripple noise, several methods of increasing complexity exist.

One method uses a three-phase thyristor bridge. The devices are very rugged and efficient in terms of conduction loss and have enough controllability to roughly regulate the DC bus [15]. In order to remove unwanted current harmonics, an active filter is added. This filter is based on IGBT devices, but only processes a small portion of the total power. A second method uses a fully controlled IGBT bridge in order to achieve excellent input current shaping for extremely low input current distortion and well regulated, ripple-free DC bus voltage.

Moreover, fewer components and much higher switching frequencies can be achieved resulting in smaller magnetic components. On the other hand, IGBTs

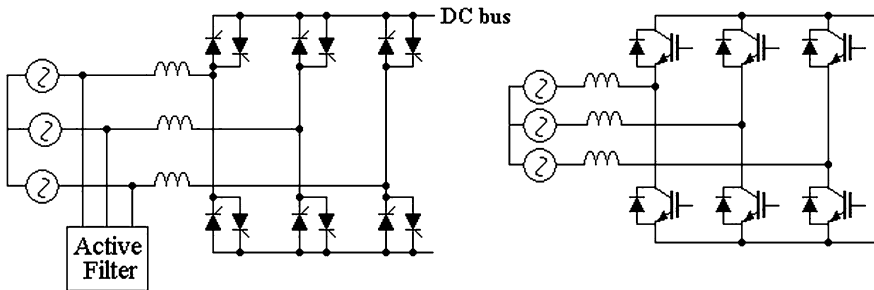


Fig. 14.13 Thyristor bridge and active line filter (left), IGBT bridge (right)

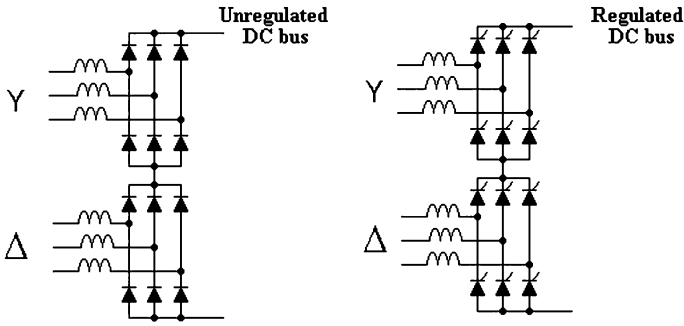


Fig. 14.14 12-pulse rectifier circuits

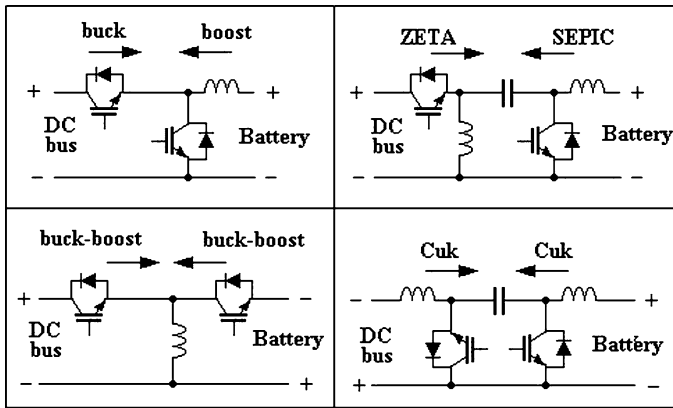


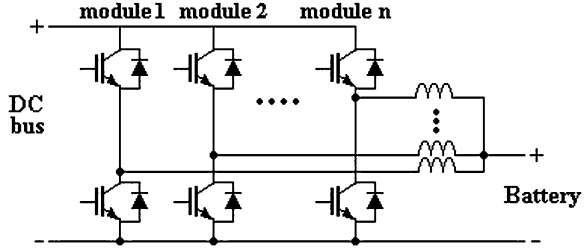
Fig. 14.15 Basic bidirectional nonisolated topologies

have switching losses and more significant conduction losses than thyristors. Yet other techniques, although less sophisticated, have the potential of realizing the required low current distortion limit without the addition of an active filter. The uncontrolled 12-pulse rectifier shown in Fig. 14.13 (left) can certainly do this, albeit with the addition of significant inductive filtering. Because the output DC bus will not be regulated, the subsequent DC–DC converter design cannot be optimized. Using thyristors can achieve regulation of the bus and possibly still achieve the required input current shaping.

It is important to note that of the four topologies mentioned here, only those in Fig. 14.14 are bidirectional, and therefore,, the only choice if V2G is to be implemented.

For the final DC–DC converter, all common basic topologies, that is, boost, buck boost, buck, Cuk, SEPIC, and ZETA can be used so long as they are rendered bi-directional by replacing the diode with a transistor device. In this case, these

**Fig. 14.16** Interleaved modular approach for the DC-DC converter



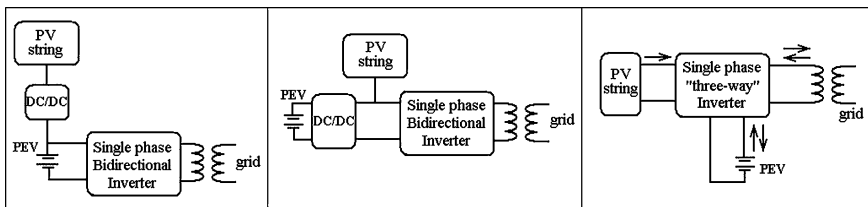
topologies function differently depending on the direction of power flow (see Fig. 14.15).

Different design requirements might suggest different topologies [39], but some of these are objectively more difficult to justify. For instance, using the buck boost/buck boost (bottom left in Fig. 14.15), produces a voltage inversion from positive to negative that may be undesirable. It also places higher electrical stress on the switches; it requires a more sophisticated design for the inductor and draws pulsed current from the battery. Similarly, the ZETA/SEPIC topology has a higher part count, including a capacitive, rather than inductive energy-transferring element. On the other hand, as long as the DC bus is guaranteed to exceed the battery voltage—a requirement that is assured by the use of the controlled bridge discussed earlier—the buck-boost topology (top left in the figure) is quite attractive. Furthermore, this topology is readily modified in order to divide the task of handling a very large power flow among paralleled modules [40].

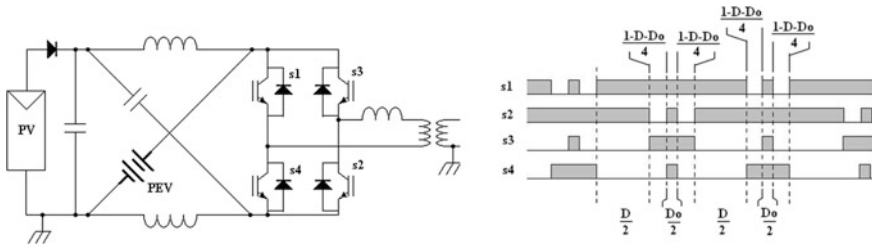
This is shown in Fig. 14.16; the amount of converted power can be split among n identical sections and the battery ripple current greatly reduced by the well-known technique of phase-shift interleaving. Using this circuit with n = 3 and a switching frequency of 2 kHz, for a typical 125 kW application, efficiencies as high as 98.5 % have been reported.

*Grid-tied Systems with Local Renewable Energy Production*

As noted earlier, when relatively large energy production from intermittent sources is to be tied to the grid, a statistically predictable PEV presence could serve the purpose of minimizing on-site dedicated storage. This would be the case for municipal carports powered by wind and/or solar generation and where the vehicles must be able to interact intelligently with both locally generated and grid



**Fig. 14.17** Possible configurations for solar carport



**Fig. 14.18** Z-loaded rectifier (*left*), gating pattern (*right*)

distributed power at the same time. The possible scenario described in Fig. 14.12 (top) may not be ideal when the renewable resource is meant to generate the dominant share of PEV charging energy. Rather, by realizing the advantages of the distributed configuration, as in Fig. 14.12 (bottom), one stage of conversion can be eliminated so long as a conversion topology with wide input–output voltage range capability can be found.

Figure 14.17 shows some possible configurations for one of the several charging stations in a solar carport. The architecture depicted on the left has the disadvantage of inserting a DC–DC converter into the main intended power flow, from PV to battery. Moreover, the power drawn from a single phase connection is pulsed at twice the line frequency. This pulsating power takes the form of an undesirably high ripple current into the battery. The configuration shown in the middle of Fig. 14.17 removes the ripple issue, but adds an additional conversion stage between the grid and the battery. The configuration on the right requires a converter that is capable of bidirectional flow between the PEV and the grid, as well as steering of PV power to either the PEV or the grid in a controlled fashion. Furthermore, this should ideally be achieved by a single conversion stage for all power flow paths and with wide voltage range capability. A good candidate for this task is the Z-loaded inverter/rectifier topology shown in Fig. 14.18.

The operating characteristics of the Z-loaded converter have been described extensively in the literature [42–44]. The most salient feature of this conversion topology is its controllability through two distinct modulation modes within the same switching cycle, designated by duty cycle  $D$  and “shoot-through” duty cycle  $D_o$ . The gating patterns shown in Fig. 14.18 describe the meaning of  $D$  and  $D_o$ . As can be seen, during period  $D_o$ , all four switches are closed simultaneously, causing the inductors to charge and ultimately boost the voltage across the capacitor, the battery, and the grid terminals. Thus,  $D_o$  can be understood as the duty cycle associated with operation akin to that of a current sourced inverter. During period  $D$ , on the other hand, the bridge operates in a manner similar to that of a voltage sourced inverter, which is essentially a buck. Therefore, with the appropriate utilization of  $D$  and  $D_o$ , both buck–boost operation can be achieved, so that the battery voltage can be either higher or lower than the peak of the line voltage. This allows a wide line and battery voltage range. Most significantly, due to the double modulation, both the grid and the battery current can be controlled precisely in

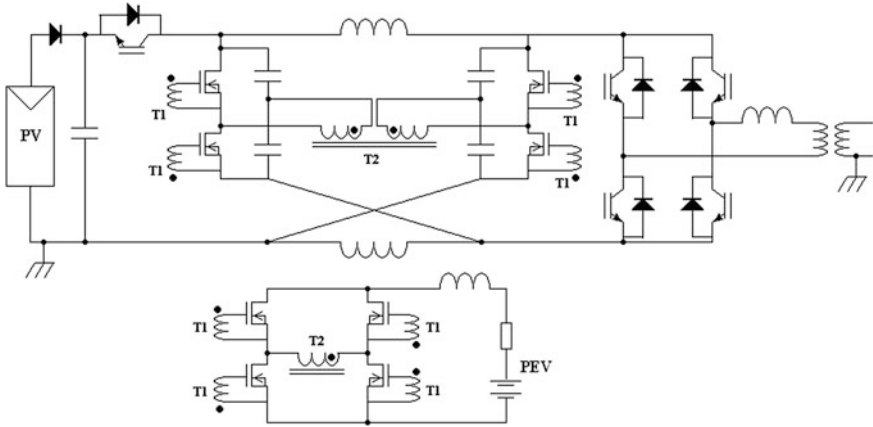


Fig. 14.19 Z-converter application to single phase, grid tied PV charging station

amplitude and shape (sinusoidal for the line current and ripple-less DC for the battery). The maximum power point tracking (MPPT) function for the PV string can then be achieved by managing the simple addition of these two power flows.

The topology shown in Fig. 14.18 must be modified in order to achieve isolation of the battery pack. Therefore, the DAB converter shown in Fig. 14.10 (right) can be integrated resulting in the detailed schematic of Fig. 14.19. The apparent complexity of the isolation stage is deceptive; in fact, this is a simple bidirectional converter that uses a small and inexpensive high-frequency transformer and that runs in open loop at full duty cycle and where all eight switches are driven by the same signal. In addition, since the duty cycle is always 100 %, ZVS is assured, resulting in efficient operation executed by relatively small devices.

With the inclusion of the isolated DC–DC converter, the need for the 50/60 Hz isolation transformer may be called into question. In North America, the grounding of one side of the PV panel has traditionally been the required norm. Although recent conditional exceptions to this safety regulation have been allowed by the National Electric Code, utility companies have resisted this change, mainly because a direct connection to the AC–DC bridge converter can inject dangerous

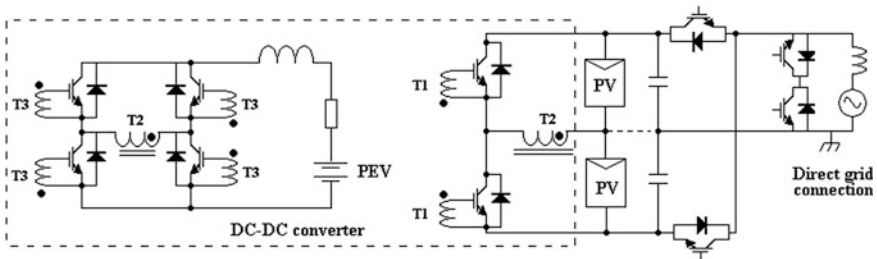


Fig. 14.20 Transformerless topology

levels of DC current into the distribution transformer. On the other hand, should this constraint become less binding in North America, as it is currently in Europe, other circuits could be proposed that could prove more reliable and efficient. Many so-called transformer less topologies have been proposed [45, 46] and Fig. 14.20 depicts a simplified schematic for one such possibility.

In this case, the DC–DC conversion and the rectifier/inverter section are controlled separately, rendering the control strategy much simpler. On the other hand, the DC–DC converter is now governed by a feedback loop, meaning that it no longer takes advantage of the low switching loss normally associated with 100 % duty cycle operation. With allowances from the regulatory safety agencies, the PV panels can be floating as long as the circuit has additional protection afforded by GFIs and that it produce no leakage currents to ground during normal operation. The last requirement is attained only if the topology guarantees very little common mode voltage on the PV panels during normal operation (note that this cannot be achieved with the Z-converter). Nevertheless, the mid-point can still be grounded, as indicated by the dashed line in the figure, but at the expense of performance.

Whichever architecture is chosen it is clear that the energy transfer cannot be controlled to fully satisfy any arbitrary current demands of the PV, the grid and the PEV battery simultaneously. In fact, many renewable resources are themselves subject to MPPT control, so that the simple power balance in Eq. (14.1) must be satisfied:

$$P_{\text{MPPT}} = P_{\text{PEV}} + P_G \quad (14.1)$$

where  $P_{\text{MPPT}}$  is the power draw requested by the distributed resource. It has to equal the sum of the power absorbed by the grid and the PEV battery ( $P_{\text{PEV}}$  and  $P_G$  respectively). Since  $P_{\text{MPPT}}$  is determined by external factors, such as clouding in the case of PV, either  $P_{\text{PEV}}$  or  $P_G$  can be controlled independently, but not both. Which of these is controlled will depend heavily on how the PEV owner decides to utilize his vehicle storage resource. Thus, in installations where charging power comes primarily from intermittent sources, the need for a significant presence of additional storage on the premises will be diminished, but not eliminated.

## References

1. Ehsani M, Gao Y, Emadi A (2010) Modern electric, hybrid electric and fuel cell vehicles, fundamentals, theory and design, 2nd edn. CRC Press, New York
2. Husain I (2005) Electric and hybrid vehicles, design fundamentals. CRC Press, New York
3. IEEE spectrum, software fix extends failing batteries in 2006–2008 Honda Civic Hybrids: is cost acceptable? <http://spectrum.ieee.org/riskfactor/green-tech/advanced-cars/software-fix-extends-failing-batteries-in-20062008-honda-civic-hybrids-is-cost-acceptable>. Accessed 23 August 2011
4. Crompton TR (2000) Battery reference book, 3rd edn. Newnes, London
5. Buchmann I (2001) Batteries in a portable world: a handbook on rechargeable batteries for non-engineers, 2nd edn. Cadex Electronics Inc, Canada
6. Dhameja S (2002) Electric vehicle battery systems. Newnes, London

7. Chen LR (2008) Design of duty-varied voltage pulse charger for improving li-ion battery-charging response. *IEEE Trans Ind Electron* 56(2):480–487
8. Park SY, Miwa H, Clark BT, Ditzler D, Malone G, D'souza NS, Lai JS (2008) A universal battery charging algorithm for Ni-Cd, Ni-MH, SLA, and Li-Ion for wide range voltage in portable applications. In: *Proceedings of the IEEE power electronics specialists conference, Rhodes*, pp 4689–4694
9. Hua CC, Lin MY (2000) A study of charging control of lead acid battery for electric vehicles. In: *Proceedings of IEEE international Symposium on industrial electronics, vol 1*, pp 135–140
10. West S, Krein PT (2000) Equalization of valve-regulated lead acid batteries: issues and life tests. In: *Proceedings of IEEE international telecommunications energy conference*, pp 439–446
11. Brost RD (1998) Performance of valve-regulated lead acid batteries in EV1 extended series strings. In: *Proceedings of IEEE battery conference on applications and advances, Long Beach*, pp 25–29
12. Bentley WF (1997) Cell balancing considerations for lithium-ion battery systems. In: *Proceedings of IEEE battery conference on applications and advances, Long Beach*, pp 223–226
13. Krein PT, Balog RS (2002) Life extension through charge equalization of lead-acid batteries. In: *Proceedings of IEEE international telecommunications energy conference*, pp 516–523
14. Lohner A, Karden E, DeDoncker RW (1997) Charge equalizing and lifetime increasing with a new charging method for VRLA batteries. In: *Proceedings of IEEE international telecommunications energy conference*, pp 407–411
15. Moore SW, Schneider PJ (2001) A review of cell equalization methods for lithium ion and lithium polymer battery systems. In: *Proceedings of SAE 2001 world congress, Detroit*
16. Nishijima K, Sakamoto H, Harada K (2000) A PWM controlled simple and high performance battery balancing system. In: *Proceedings of IEEE 31st annual power electronics specialists conference, vol 1, Galway*, pp 517–520
17. Isaacson MJ, Hoolandsworth RP, Giampaoli PJ (2000) Advanced lithium ion battery charger. In: *Proceedings of IEEE battery conference on applications and advances*, pp 193–198
18. Pascual C, Krein PT (1997) Switched capacitor system for automatic series battery equalization. In: *Proceedings of 12th annual applied power electronics conference and exposition, Atlanta, vol 2*, pp 848–854
19. Hung ST, Hopkins DC, Mosling CR (1993) Extension of battery life via charge equalization control. *IEEE Trans Ind Electron* 40(1):96–104
20. Cao J, Schofield N, Emadi A (2008) Battery balancing methods: a comprehensive review. In: *Proceedings of IEEE vehicle power and propulsion conference, Harbin*, pp 1–6
21. Lee YS, Wang WY, Kuo TY (2008) Soft computing for battery state-of-charge (BSOC) estimation in battery string systems. *IEEE Trans Ind Electron* 55(1):229–239
22. Shen WX, Chan CC, Lo EWC, Chau KT (2002) Adaptive neuro-fuzzy modeling of battery residual capacity for electric vehicles. *IEEE Trans Ind Electron* 49(3):677–684
23. Piller S, Perrin M, Jossen A (2001) Methods for state-of-charge determination and their applications. *J Power Sources* 96(1):113–120
24. Ullah Z, Burford B, Dillip S (1996) Fast intelligent battery charging: neural-fuzzy approach. *IEEE Aerosp Electron Syst Mag* 11(6):26–34
25. Atlung S, Zachau-Christiansen B (1994) Failure mode of the negative plate in recombinant lead/acid batteries. *J Power Sources* 52(2):201–209
26. Feder DO, Jones WEM (1996) Gas evolution, dry out, and lifetime of VRLA cells an attempt to clarify fifteen years of confusion and misunderstanding. In: *Proceedings of IEEE international telecommunications energy conference*, pp 184–192
27. Jones WEM, Feder DO (1996) Behavior of VRLA cells on long term float. II. The effects of temperature, voltage and catalysis on gas evolution and consequent water loss. In: *Proceedings of IEEE international telecommunications energy conference*, pp 358–366

28. Nelson RF, Sexton ED, Olson JB, Keyser M, Pesaran A (2000) Search for an optimized cyclic charging algorithm for valve-regulated lead–acid batteries. *J Power Sources* 88(1):44–52
29. Kempton W, Tomic J, Brooks A, Lipman T, Davis (2001) Vehicle-to-grid power: battery, hybrid, and fuel cell vehicles as resources for distributed electric power in California, UCD-ITS-RR-01-03
30. Kempton W, Kubo T (2000) Electric-drive vehicles for peak power in Japan, *Energy Policy*
31. Kisacikoglu MC, Ozpineci B, Tolbert LM (2010) Examination of a PHEV bidirectional charger system for V2G reactive power compensation, IEEE applied power electronics conference, Palm Springs
32. Tuttle DP, Baldick R (2012) The Evolution of plug-in electric vehicle-grid interactions, The University of Texas at Austin department of electrical and computer engineering
33. Jenkins SD, Rossmair JR, Ferdowsi M (2008) Utilization and effect of plug-in hybrid electric vehicles in the United States power grid, vehicle power and propulsion conference
34. Kempton W, Tomic J (2005) Vehicle-to-grid power implementation: from stabilizing the grid to supporting large-scale renewable energy. *J Power Sources* 144(1):280–294
35. Wang J, Peng FZ, Anderson J, Joseph A, Buffenbarger R (2004) Low cost fuel cell converter system for residential power generation, *IEEE Trans Power Electron* 19(5), pp 1315–1322
36. Han S, Divan D (2008) Bi-directional DC/DC converters for plug-in hybrid electric vehicle (PHEV) applications, applied power electronics conference and exposition, APEC
37. Peng FZ, Li H, Su G-J, Lawler JS, (2004) A new ZVS bidirectional DC–DC converter for fuel cell and battery application. *IEEE Trans Power Electron* 19(1):54–65
38. Xiao H, Guo L, Xie L (2007) A new ZVS bidirectional DC–DC converter with phase-shift plus PWM control scheme, applied power electronics conference, APEC
39. Du Y, Zhou X, Bai S, Lukic S, Huang A (2010) Review of non-isolated bi-directional DC–DC converters for plug-in hybrid electric vehicle charge station application at municipal parking decks, applied power electronics conference and exposition (APEC)
40. Aggeler D, Canales F, Zelaya H, Parra DL, Coccia A, Butcher N, Apeldoorn O (2010) Ultra-fast DC-charge infrastructures for EV-mobility and future smart grids, innovative smart grid technologies conference Europe (ISGT Europe), IEEE PES
41. Bai S, Du Y, Lukic S (2010) Optimum design of an EV/PHEV charging station with DC bus and storage system, energy conversion congress and exposition (ECCE)
42. Peng Z (2003) Z-source inverter. *IEEE Trans Ind Appl* 39(2):504–510
43. Peng FZ, Shen M, Holland K (2007) Application of Z-source inverter for traction drive of fuel cell—battery hybrid electric vehicles. *IEEE Trans Power Electron* 22(3):1054–1061
44. Carli G, Williamson S (2009) On the elimination of pulsed output current in Z-loaded chargers/rectifiers. In: Proceedings of IEEE applied power electronics conference and exposition, Washington
45. González R, López J, Sanchis P, Marroyo L (2007) Transformer-less inverter for single-phase photovoltaic systems, *IEEE Trans Power Electron* 22(2)
46. Kerekes T, Teodorescu R, Borup U (2007) Transformer-less photovoltaic inverters connected to the grid. In: Proceedings of IEEE applied power electronics conference and Exposition
47. Cocconi AG (1994) Combined motor drive and battery recharge system, US Patent no 5,341,075



# Chapter 15

## Multi-Agent Technology for Power System Control

**Robin Roche, Fabrice Lauri, Benjamin Blunier, Abdellatif Miraoui and Abderrafiâa Koukam**

**Abstract** The electric grid is evolving toward what has been defined as the “smart grid paradigm”. The development of communication infrastructures provides power electronics interfaces with the ability to control complex power systems in efficient and scalable ways and in real time. Multi-agent systems (MAS) are based on distributing information and computing algorithms for complex networks, and are an excellent technological solution for this application. This chapter focuses on applications of MAS in power systems and describes how they can be used with other artificial intelligence techniques in order to make the grid smarter and more flexible. In addition to presenting the basics of multi-agent theory, this chapter covers some design procedures and provides several examples, as well as perspectives for future developments of MAS in power systems control.

### 15.1 Introduction

With the recent developments in smart grid technology, communication plays an increasingly central role in power systems, particularly at the distribution level. Although supervisory control and data acquisition (SCADA) systems have long been used for monitoring and remote control at the transmission and sub-transmission levels, they are expected to be utilized for further control in a more encompassing way than before, especially due to the new possibilities offered by power electronic interfaces. As shown in [Chap. 2](#), power converters, for example, can accommodate various levels of current and voltage, manage power flows, and directly interact with renewable or alternative energy sources, storage units, and sophisticated loads.

---

R. Roche (✉) · F. Lauri · B. Blunier · A. Miraoui · A. Koukam  
Université de Technologie de Belfort-Montbéliard, IRTES-SET, 90010 Belfort, France  
e-mail: robin.roche@utbm.fr

As energy prices and demand keep rising with depletion of fossil fuel resources and growing environmental concerns, the necessity to integrate distributed energy resources (renewable or alternative) has become of paramount importance. The increasing penetration of sources such as solar panels and wind turbines contributes to the intermittent nature of generation, requiring storage compensation that needs to be controlled adequately. The concept of smart grid control originated from such dispersed generation model, with the requirement of demand-side management (for example by shedding or shifting the use of some loads when required), while taking into account additional parameters such as customer behavioral expectations.

Three clear trends can be observed in contemporary power systems: they are becoming at the same time more complex, more distributed, and less predictable. Therefore, control systems have to evolve from their monolithic and centralized structures and adapt to more decentralized ones, where the intelligence of the system can be achieved through cooperation of multiple entities and components. Multi-agents systems (MAS), which have been applied in computer science studies for years, have characteristics that make them suitable for acting as a basis for building modern distributed control systems. In addition, artificial intelligence techniques can be embedded in some agents with smart features, particularly in automating tasks traditionally performed by human operators.

The next sections discuss the following important questions that are related to how MAS can be developed for controlling power systems:

- What do modern control systems require?
- What are MAS and why are they relevant in this field?
- How to design a MAS and what choices do designer have to face?
- What choices need to be made in the design process, among which alternatives?
- For which applications are MAS used or could MAS be used?
- How may MAS uses evolve in the future?

## 15.2 Distributed Control Systems

Control systems are at the core of all power systems, in that they allow them to operate efficiently and safely. Control is a term related to a wide variety of processes with different objectives and constraints. The following discussion provides some useful analysis in how such systems may evolve toward distributed, intelligent and autonomous paradigms, especially relevant to smart grid control needs.

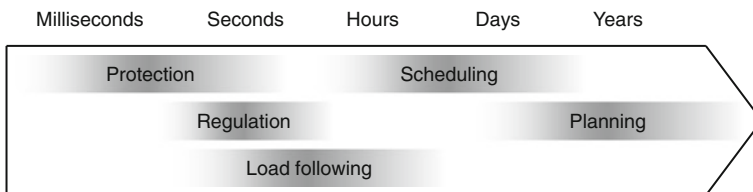
### 15.2.1 Control Systems Objectives

The main objectives of control systems can be sorted according to these priorities:

1. **Safety:** The first one is the overall safety of the system, for example in avoiding a catastrophe such as the ones of Chernobyl and Fukushima or even a simple black out that requires distributed generation to be disconnected from distribution lines.
2. **Protection:** A control system must protect equipment from self-inflicted or external damages.
3. **Stability and reliability:** The system must operate correctly (e.g., regulate voltage and reactive power, manage storage in conditions that do not degrade the performance, etc.) as long as possible while providing its customers with power of satisfactory quality. Therefore, stability and reliability must be taken in consideration in the overall control system design.
4. **Economics:** All other system priorities must be fulfilled while minimizing costs. Traditional energy management control primarily focuses on economics, but a broader paradigm should be considered in taking all technical specifications and economics as well.

From the above requirements, several complementary (sometimes overlapping) control system functionalities must be understood over several timescales (Fig. 15.1), related to the following physical constraints:

- *Protection* (milliseconds–seconds): In order to meet the first two priorities, control systems for utility-connected equipments must react very quickly to disturbances, such as short circuits and overvoltages.
- *Regulation* (seconds): Systems need to regulate voltage levels and reactive power in order to maintain stability and reliability.
- *Load following* (minutes–hours): Generation needs to meet demand, resulting in frequency control. Such characteristic overlaps with further economic constraints.
- *Scheduling* (hours–days): Unit commitment or maintenance scheduling are required functionalities for operating power systems, typically affecting all the above priorities.



**Fig. 15.1** Control systems can be divided into several complementary applications, each with its prevailing timescale, from milliseconds to years

- *Investment/expansion planning* (months to years): When and how the power system needs to evolve (by building new power plants, expanding transmission lines, etc.) is typically the slowest deciding priority.

From these requirements and functionalities, a four level hierarchy in which several complementary layers can be defined for control systems:

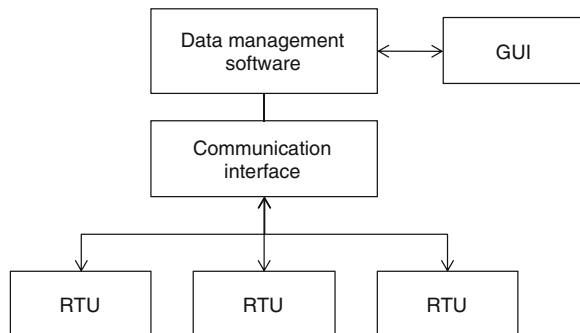
- A physical layer uses actuators and sensors to monitor multiple information.
- A grid operation level with control strategies related to sources, load shedding, and so on.
- A decision-making layer considers energy management supporting scheduling and forecasting.
- And a user level, in which operators interact with the system.

### 15.2.2 Modern Architectures for Power Systems Control

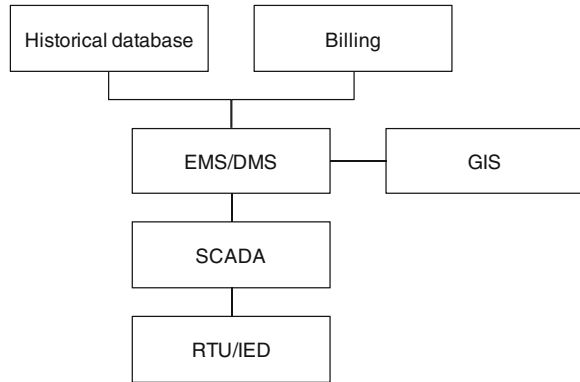
Modern control systems used by utilities are based on SCADA systems. SCADAs are information systems used for monitoring and supervising power systems or industrial processes, but without control functionalities. However, with recent popularization of the term, SCADAs are now associated with extensive systems, sometimes performing control actions. Figure 15.2 shows the structure of a basic SCADA, which is a fully centralized architecture, where remote terminal units (RTUs) provide communication interfaces with physical components such as sources, loads, and so on.

With the development of communication interfaces, distributed control systems (DCS) have emerged. They have many similarities with SCADAs, but the intelligence is not centralized but rather distributed in several subsystems called intelligent electronic devices (IED). IEDs are usually implemented with micro-controllers and are similar to RTUs. However, they have extended capabilities such as the ability to autonomously issue control commands; an IED can command a circuit breaker by detecting an abnormal voltage, current or frequency, for example.

**Fig. 15.2** A typical SCADA system consists in several remote terminal units (RTUs) connected to a central controller the operator can interact with through a GUI



**Fig. 15.3** An integrated control system includes several interconnected systems such as SCADA, EMS/DMS, etc



SCADAs only provide communication interfaces between a control system and physical end-points. Further control capabilities can be integrated, including (Fig. 15.3):

- Distribution management systems (DMS) achieve or facilitate numerous functionalities, such as substation automation, condition monitoring, fault location, voltage control, and load flow calculations.
- Energy management systems (EMS) include computer-aided tools that enable controlling and scheduling the operation of a power system under given constraints (e.g., at a minimal cost), without affecting the capability to meet their technical requirements and quality standards.
- Outage management systems (OMS) are used to assist operators for system restoration after a failure.
- Geographical information systems (GIS) contain geographically referenced data, for visualizing events in a distribution grid.
- Additional systems for network analysis, demand response management, business management, billing, customer information, etc.

### 15.2.3 Distributed Control Systems

The SCADA and associated control systems described in the previous section have been utilized for monitoring and controlling power systems relying on a traditional centralized structure, with a limited number of large power plants used for generation. However, distribution and transmission systems are under transformation toward further incorporation of distributed energy resources, and monitoring and control systems must therefore undertake changes such as:

- Distributing decision making, by moving from centralized analysis and decision systems to distributed approaches, where several components (instead of one) are able to reach a goal through cooperative tasks. This process begun with the

deployment of IEDs, but further features are required due to the evolution of the grid and associated communication infrastructures.

- Automating complex decision processes, such as scheduling and planning, today often conducted by human operators. There is a need for advanced computational resources, with complex decision-making and decision-support algorithms.

MAS have been showing a great promise to fulfill those needs. The following section explains their importance and how MAS can contribute in making control systems deeply distributed, further autonomous and more intelligent.

## 15.3 MAS for Power Systems

Although MAS have been used for over two decades, their application in power systems have appeared in the last decade. This section explains what are MAS and why they are so important as a distributed paradigm for strategies used in modern power systems control.

### 15.3.1 Principles of MAS

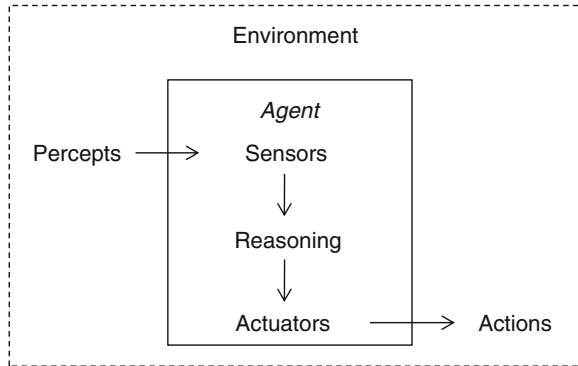
MAS support a framework of modeling and control of multiple structures that can be decomposed into several interacting entities. Formal definitions for MAS have been proposed by Wooldridge and Weiss [1] and Ferber [2]. The following definition provides a simple overview of the MAS concept:

A multi-agent system is a system composed of a collection of autonomous and interacting entities called agents, evolving in an environment where they can autonomously perceive and act to satisfy their needs and objectives (Fig. 15.4).

Based on such definition, many existing systems from various domains can be classified as MAS, such as:

- A society or a group, in which agents are people, and can communicate with each other, cooperate, compete, and so on.
- A network of computers, where agents are software algorithms, interacting with each other by exchanging messages and data, for example to solve a problem faster than a single computer.
- Robots of a production line, where they need to cooperate and coordinate themselves to perform a given task.
- A power system, where the components of the grid are agents and must interact with each other to serve consumers reliably and at least cost.

**Fig. 15.4** An agent perceives its environment through sensors and acts on it using its actuators



There are multiple definitions for what can be defined as “the environment” of an agent. It can be defined as to all external entities and resources the MAS can interact with. From a power system point of view, the environment of an agent can be considered as everything but itself. The agent can be (geographically) situated in this environment, and other agents may be part of it. There are various means of interacting with their environment, through communication, by controlling actuators, or by evaluating a particular index of performance, for instance. Agents receive data from their environment, called percepts, and take decisions on the basis of current and possibly past percepts.

Agents can exhibit different behaviors and properties which give them a certain degree of autonomy with various degrees of intelligence. The most common ones are:

- *Reactive agents*: They only show some simple reactions to excitations (stimuli). They are useful when fast response times are needed. Their representation of the world, i.e. the environment, is minimal. But by interacting with each other, such agents can together lead to important results, difficult to achieve if the system had been modeled as a single agent. Protection systems for utility distribution can be considered as reactive agents.
- *Cognitive or intelligent agents*: They have extended intellectual capabilities and can use their resources and skills to reach their goals. Those agents can have beliefs, desires and intentions, as in the beliefs, desires, intentions model (BDI) [3]. Fully automated building EMS, and gas turbine control systems are examples of such agents.
- *Learning agents*: They can gain knowledge, for example by analyzing the results of their actions and usually have a much better knowledge of the environment, which is required to take complex decisions. A building energy management system with the ability to learn the habits of its occupants and take decisions accordingly would be an example.

Additional explanations are given in [Sect. 15.4.5](#).

Therefore, MAS have the following properties:

- They are inherently *distributed*, due to the separation between agents and their environment. An agent may not be handicapped by a change of environment or else they will react differently depending on their surroundings. Agents do not need to have a global knowledge of the whole environment, since their perception is local.
- They are *pro-active* and follow their own objectives, or the ones prescribed for the whole system. These objectives can be reached by using their own resources and skills, autonomously, or by interacting with other agents, e.g., for cooperating.
- They have a *social* ability, i.e., by interacting with each other and their environment, agents can form groups and cooperate or compete, depending on their goals. Together, agents are thus a form of distributed or collective intelligence.

Therefore, the methodology of formulating a MAS-based modeling and control system design requires formalizing how the agents coordinate themselves, cooperate, take decisions, plan their actions, and build their representations of the environment.

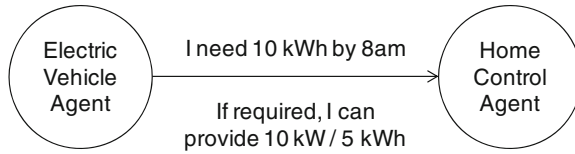
### ***15.3.2 Relevance of MAS for Power Systems***

In order to discuss the advantages of MAS-based control versus classical methodologies for applications in power systems, it is important to understand how the power grid evolved over the last decades. Classical control methods implemented in SCADAs are fully functional in today's grid. But the contemporary developments toward the future smart grid will require to integrate millions of devices such as distributed storage, intelligent loads, and distributed energy resources. Control systems will then have to operate efficiently on a large scale system, despite very disperse faults that may occur. In order to analyze practical advantages of MAS for tackling these conditions, the following properties (distributed, pro-active, and social) will be discussed in more details.

#### **15.3.2.1 Distributed Architecture**

MAS are distributed by design with three main attributes: (1) local knowledge, (2) flexible interactions, and (3) bottom-up control approach. Local knowledge means that agents' view of the environment are local, and as a consequence their knowledge is limited to only what they can or need to know. The perception of agents can be limited to their neighbors, which enables reducing data transfer. For example, for a microgrid, an agent for a distributed generator does not need to receive information about a small load, which can be several miles away. Therefore, a distributed MAS architecture contributes to a scalable distribution grid.





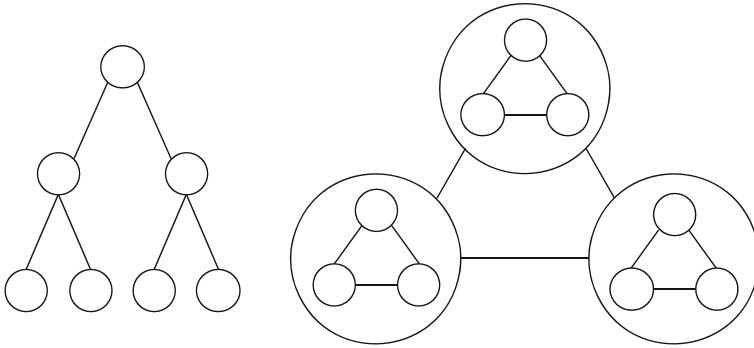
**Fig. 15.5** When an agent joins an existing MAS, it can announce its name and services to the other agents so that they can interact with him. This figure illustrates an example with an electric vehicle

A flexible designed MAS incorporates plug-and-play, robust and fault-tolerant procedures when required by changes in the environment. For example, if a generator or load agent is disconnected, i.e., turned on or off (independently of whether it has been scheduled or not) or loses communication, the MAS will acknowledge this modification and adapt to it. It will take it into account when taking decisions toward reaching its objectives (e.g., maintaining the system stable) after the event has been detected. This property is an evolution when compared to most analytical control methods, where all possible events, changes, and faulty conditions have to be predicted when designing the control system in order to command the system for corrective reaction. In addition, a flexible MAS can add or remove new functionalities without requiring to completely redesigning the system, which could help lower development and maintenance costs. This characteristic is similar to how computer systems use their plug-and-play internal operations. The operation of electric vehicles with the distribution grid for charging could, for example, benefit from this property (Fig. 15.5).

The previous two features enable the third one, i.e., a bottom-up control approach. This feature is well suited for complex and distributed problems. Agents can operate autonomously, and cooperate or compete with each other if required. The complexity of the control system can be reduced by distributing tasks among communicating agents. This property could play an important role in a MAS designed for a smart grid with a high penetration of distributed energy sources. The grid would be divided into many microgrids containing local generators, loads, and storage devices (Fig. 15.6). Intermediate layers, consisting of groups of microgrids for example, could also be added. When compared to control methodologies applied in current power systems, this would correspond to a bottom-up approach where decisions would be taken locally, in a decentralized way.

### 15.3.2.2 Proactivity

Proactive agents have goals which can be local and/or global. A single agent usually has local goals while a group of agents may have global goals. For example, maintaining a voltage steady is mainly a local goal for a power source, while maintaining balance between generation and supply is a global objective and cannot be reached by a single agent, hence requiring cooperation. Such proactivity

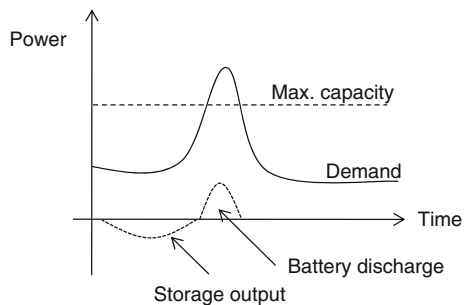


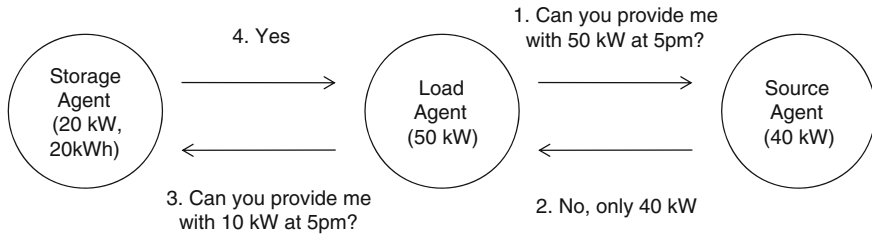
**Fig. 15.6** One of the expected evolutions of future power grids is a change from a centralized and radial architecture (*left*) to a decentralized network of microgrids (*right*). Circles represent energy sources and loads, but also the corresponding agents

might be enabled by autonomous intelligence with information based on knowledge about the environment (e.g., the grid), and when appropriate with further information by asking other agents, and knowledge of required actions requested by other agents through communication that may help achieving global goals. Agents can then take decisions based on such on-line knowledge and their goals, plan actions to perform, and finally execute them for achieving the required actions.

Figures 15.7 and 15.8 illustrate an example where a storage manager schedules a distribution procedure: if the system knows (based on forecasting) that demand is going to peak and conventional generation sources will not be sufficient to match it, the battery agent may take preemptive actions by charging the battery to its maximum state-of-charge. This would enable the system to meet future demand during such peak. Other examples could be procedures to start, synchronize and reconnect a turbine to the grid, and planning of required reactive power for such connection.

**Fig. 15.7** In this fictitious example, the total generation capacity is not sufficient to meet demand during a *peak*. Storage enables to meet this demand, even during the *peak*, but requires charging before discharging





**Fig. 15.8** A simplified example of how three agents could interact to find a solution to an insufficient capacity problem

### 15.3.2.3 Social Behavior

Agents need to have a social behavior compatible with other fellow agents, expressed under various forms. Their social organization can vary from one system to another and with time, as well as the way they interact with each other and take decisions. In other words, agents can coordinate themselves and cooperate for reaching goals that may not be reachable by a single agent. Agents can influence the actions of others or act as interfaces for negotiations, requests, and contracts, as described in [Sect. 15.4.8](#).

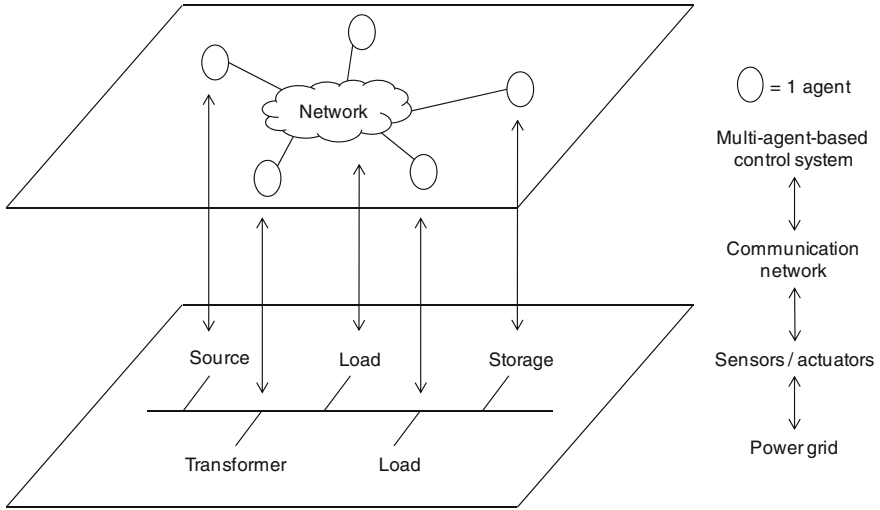
Continuing the previous example on peak demand with storage, before the MAS decides that the battery should absorb the peak, a “discussion” with other agents (such as power system brokers) may happen about whether the load can be taken by another source and maybe a better solution would arise from economics and technical points of view. Another scenario is when a small dc microgrid has a bus voltage maintained by a battery. If such battery tends to run toward a low state-of-charge, the battery agent can ask other agents to replace it in order to control the bus voltage.

### 15.3.2.4 Practical Implications

MAS also enable to specify communication aspects, that are not commonly considered in power systems studies, and are an important feature of smart grids. This property enables MAS-based prototype systems to be closer to implementation, as the system is already distributed and is easier to deploy. Defining what each system entity (i.e., agent) does also facilitates specifying the required hardware.

## 15.3.3 Applications of MAS for Power System Control

Smart-grid control requires flexibility and extensibility, and those are inherent features of MAS. Figure 15.9 shows how MAS enable communication and decision-making for power systems, where agents are associated to sensors, actuators, operators and other physical or virtual entities. MAS have been showing promises



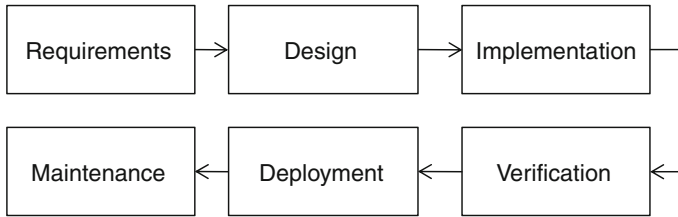
**Fig. 15.9** MAS are well suited for monitoring and controlling power grids, and especially for smart grids where communication and distributed assets are intensively present

as an efficient control framework for developing the technology of smart grids, including voltage/VAR control, restoration, energy management, monitoring, and fault analysis (several examples are described in Sect. 15.5). A comprehensive state-of-the-art review can be found in McArthur et al. [4, 5].

## 15.4 MAS Design

This section gives the fundamentals on how MAS can be applied to power systems. It is described how existing standards, methodologies, languages, tools, architectures, and choices to make can support design specifications such as when and how should which agents interact (cooperate and/or compete) to successfully meet their design objectives. The following items are discussed:

- MAS design methodologies and their characteristics and protocols.
- Standards that MAS should adhere for power systems control.
- Communication protocols between agents.
- Types of services in agent platforms.
- Reactive and intelligent agents structures.
- Use of learning techniques for MAS.
- MAS for planning actions.
- MAS development platforms to facilitate MAS design and prototyping.



**Fig. 15.10** The waterfall model of software development

### 15.4.1 Development Methodologies

With a growing number of applications of MAS in various disciplinary fields, several methodologies have been created to enable developers to follow a formal process when designing MAS. These methodologies describe the tasks and activities that take place during the development process.

Similarly to most standard software development methodologies, or life cycles, most MAS development methodologies follow the same steps, sometimes referred to as the waterfall model: requirements specification, architecture definition and design, implementation, testing/verification, deployment, and maintenance (Fig. 15.10). However, due to the distributed nature of MAS, such methods require some adaptations, which are directly related to how agents are structured and how they interact with each other. Most MAS methodologies rely on similar basic steps and abstractions.

Two abstraction levels are distinguished for specifying the system and its objectives in order to enable designing MAS:

- The individual agent level, for defining the autonomy, proactivity, and cognitive, deliberation, and control abilities of each agent.
- The multi-agent level is split into the four following processes:
  - The environment, to identify what the MAS can influence.
  - The roles and interactions of agents.
  - The organizational rules, to identify how roles and protocols depend on and interact with each other.
  - The organizational structures, to identify the topology of the MAS.

Several development methodologies can be used for MAS design, such a GAIA [6]. Table 15.1 contains a summary of the analysis and design steps of this methodology. Other possibilities include SODA [7], MaSE [8], MESSAGE [9], TROPOS [10], or ADELFE [11]. MAS-CommonKADS [12] and DESIRE [13] are alternatives based on knowledge engineering. Comparisons of these methodologies can be found in [14–16].

These methodologies use top-down approaches, but when designing a MAS with an expected emergent behavior, a bottom-up approach (where specific agent-level capabilities can result in coherent multi-agent-level behaviors), should be

**Table 15.1** A summary of the main steps of the GAIA methodology

1. Analysis	2. Architectural design	3. Detailed design
1.1 Division into sub-organizations	2.1 Organizational structure	3.1 Agent models
1.2 Environmental model	2.2 Final role models	3.2 Service models
1.3 Initial role models	2.3 Final interaction models	
1.4 Initial interaction models		
1.5 Organization rules		

preferred [17]. It has been observed that, at the time of writing, such methodologies are rarely used in designing MAS for power systems, and that standards are rarely considered.

### 15.4.2 Standards

The is an on-going development of the “Internet of things” is expected to enable all kinds of products (including energy sources and loads) to be interconnected. These products will need to use a common language to interact coherently. Interoperability between products from different designers and vendors is an important concern if the designed system needs to communicate with other devices to be used or maintained on a regular basis, which is usually the case for power systems applications. The benefits of using standards are important: they enable lower development costs, faster development and better flexibility, interoperability and integration with the existing systems. As a consequence, several standards and specifications have been developed by various groups such as FIPA [18] and IEC [19].

Three main categories of standards are important for considering MAS applied to power system control: (1) FIPA standards for agents, (2) standards for communication between systems, and (3) data structuring for power system applications.

The first set of standards were designed by the foundation for intelligent physical agents (FIPA), an IEEE Computer Society organization. It was specifically developed for interoperability of agents and MAS and contains five main sections. The first one deals with particular application domains, such as entertainment or travel assistance, while the second section refers to the abstract architecture of MAS, i.e., the entities required to build agent services and environment. The third part describes agent communication with interaction protocols, communicative acts, and content languages. The fourth section deals with agent management specifications and the fifth part presents the agent message transport protocol (MTP), used for transport and representation of messages. Two of these specifications are widely adopted and will be described in detail in the subsequent subsections: Agent management (SC00023), and agent communication language (ACL) (SC00061).

The second category of standards deals with how systems such as substations and other power systems should communicate. As communication is one of the most important tools of MAS, they need to be integrated in the design process of any industrial MAS. The authors selected three main standards to be discussed in this chapter: IEC 61850, IEC 60870, and DNP3.

- The International Electrotechnical Committee (IEC) has several technical committees, such as the TC57 [20], that is responsible for the development of standards for information exchange in power systems, including SCADA, EMS, and distribution. One of the main standards published by this committee is IEC 61850 [21], originally a standard for the design of electrical substation automation, with a focus on communication. As adaptations and extensions of the standard were also published for particular applications such as hydroelectric power plants, distributed energy resources or wind turbines, the standard now applies to a variety of power systems, including energy storage and demand response. IEC 61850 includes several communication protocols based on Ethernet.
- IEC 60870 is another IEC standard for SCADAs, which has six parts. Its fifth and sixth parts define the communication profiles and protocols for interaction between systems.
- The distributed network protocol DNP3 [22] is a set of communication protocols for process automation, commonly used by utilities in SCADA systems. Its main focus is on reliable communications between master stations and IEDs/RTUs. DNP3 was adopted as an IEEE standard (1815–2010).

The third and last set of standards defines how data should be structured, mainly for SCADA applications. These specifications impact how agents may structure their representation of the environment, and how they interact with each other.

- In addition to its specifications for communication, IEC 61850 also defines naming and object modeling schemes. It specifies a substation configuration description language (SCL) for the configuration of substations, based on XML, as well as a representation of modeled data and communication services.
- The common information model (CIM) [23, 24] was developed by the electric power industry for generation, transmission, and distribution. Its aim is to define how application software can exchange information about the configuration and status of an electrical network. This is achieved through a common vocabulary and ontology. The CIM is based on other standards, such as IEC 61970 for interfaces with energy management systems, and IEC 61968 for interfacing the main applications for electrical distribution in a utility. Although CIM and SCL share some similarities, they are distinct standards and should not be mixed. A distinction is the focus of SCL on substations, whereas CIM is applied to various other systems.
- MultiSpeak [25] is another standard designed for interfacing software applications of utilities. It defines common data semantics (in XML form), the message structure for data exchange, and the messages required to support specific

business process steps. Here too, although CIM and MultiSpeak have similarities, the latter is rather oriented toward distribution and US-based electric cooperatives.

Due to the multiplicity of these standards, there is a lot of harmonization work underway between MultiSpeak, IEC 61968 and IEC 61970, and CIM and SCL.

Using a MAS for operating a power system requires combining these three types of standards. Achieving a coherent system respecting these specifications is difficult and has been the subject of some works, as in [26, 27]. Moreover, there are additional standards for other topics, such as security (IEC 62351) and automatic meter reading (DLMS/IEC 62056).

### 15.4.3 Communication, Languages, and Ontologies

A common language and vocabulary is required for agents to communicate. Therefore, languages such as ACL and knowledge query and manipulation language (KQML) were created and can be used for MAS development. ACL is a FIPA specification [28] and is usually preferred. Similarly to protocols such as TCP, each message is given several attributes, including the content of the message, and information about the participants and the ownership of the conversation. The structure of an ACL message should contain the following parameters:

- A parameter defining the type of communication, called “performative”; this field indicates whether the message is a request, a reply, an information, etc.
- Participants in the conversation, with information on the sender, receiver(s), and reply-to fields, including the names of the corresponding agents.
- The content of the message.
- A description of the content, with the used language, encoding and vocabulary, called “ontology”.
- Conversation control parameters, such as a conversation identifier and protocol.

Table 15.2 shows the structure of an ACL message. The performative is the only mandatory parameter in the specification, but others should also be included when necessary.

For complex conversations between heterogeneous agents, ontologies may be needed to define the vocabulary agents use in their conversations. As for humans, using a common language may indeed not be sufficient. An ontology is a formal representation of knowledge, under the form of a set of concepts and of relationships between these concepts. FIPA–SL is an ontology standard adopted by FIPA that is implemented in several MAS development tools (see Sect. 15.4.10). Its includes three types of elements:

- Concepts can include all lot of different elements from physical components to datasets. Concept examples can include components, data types, etc.



**Table 15.2** Sample ACL message fields

Field	Value	Description
(inform		Performative
:sender	agent1	Sender name
:receiver	agent2	Receiver name
:content	How are you?	Content of the message
:in-reply-to	hello-round-0	Other parameters
:reply-with	hello-round-1	
:language	sl	
:ontology	hello-ontology	
)		

- Agent actions are a particular type of concept corresponding to communication acts. For example, the action *connect()* would require the subject of the action to connect to the rest of the system after having been isolated.
- Predicates specify relationships between concepts which result in binary values (true or false). An example could be the predicate *isStorageUnitCharged()*, to determine whether a storage unit is fully charged or not.

In large systems, where several subsystems have to interact, may arise the need for multiple ontologies. An ontology agent can then be used to handle these multiple ontologies, or an upper ontology may be developed to serve as a general models for designing more specific ontologies. As described in McArthur et al. [5], standards specifying data models, such as CIM, can be used as a basis to build ontologies. A CIM-based ontology was, for example, made available by the IEEE PES MAS Working Group [29].

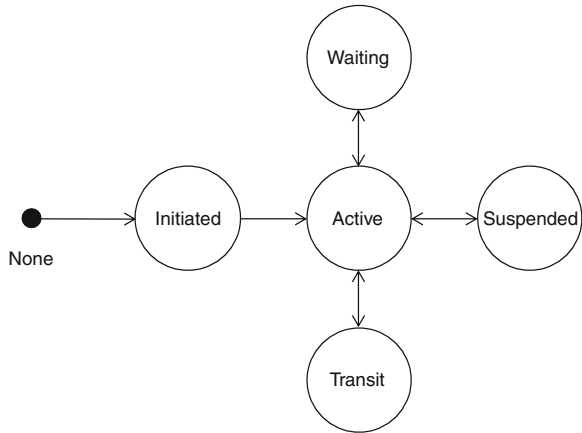
#### 15.4.4 Agent Management

FIPA specification SC00023 [30] defines two levels in how agents should be managed, exist, and operate. The first level, called “agent level”, corresponds to each agent itself, while the second relates to groups of agents and how they interact with each other, called the “MAS level”. At the agent level, the specification defines the life cycle of the agent, and at the MAS level, it proposes agent management services and a message transport system (MTS). These services are essential in enabling the MAS to operate in a distributed and flexible manner.

The first level defines how agents have their life cycles, from their creation to their end. During their lifetime, agents can be in five possible states:

- Initiated, just after their creation. In this state, the agent executes a series of instructions, defined by the user and run once as an initialization procedure.
- Active, that is the “normal” state, in which the agent operates.
- Waiting, when it is pooling for an external event and has not been woken up.

**Fig. 15.11** The life cycle of an agent starts with its creation and its transition to the initiated state. It can then switch to four other states, the most common one being the active mode. Destroying the agent means it does not exist anymore [30]



- Suspended, when it has been halted from the active state.
- In transit, when the agent is physically moving from one agent platform (AP) to another (e.g., from a computer to another).

Figure 15.11 shows a finite-state automaton representing all the possible states in an agent.

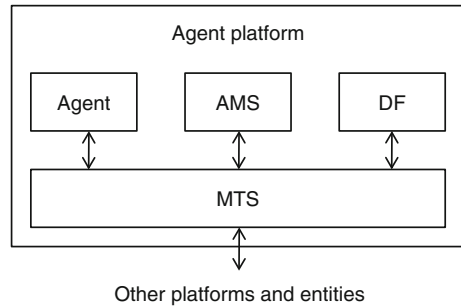
At the MAS level, each AP contains several entities and at least one agent. A single platform can consist of agents located in different physical locations, such as on remote computers. It should implement the agent management reference model (Fig. 15.12), which defines service entities including:

- The agent itself, which communicates with other agents using the ACL language and may have access to external software.
- A directory facilitator (DF) that provides a yellow-pages service to agents, i.e., a list of agents with their respective capabilities. Each agent can register its services in the DF and then query it for knowing if other agents have a certain service registered. Implementing a DF is optional, and multiple DFs can exist in a single AP.
- A unique agent management system (AMS), which supervises the AP and maintains a list of all agents and their addresses in the AP. This functionality is similar to a white-pages service, i.e., a list of agents and their name and address, to which each agent must register.
- A MTS, which enables messages to be transported from one agent to the other. A MTP is used for physically transferring messages between agents on possibly different platforms; all messages exchanged between platforms go through the MTP.

For enabling the previous services to operate properly, each agent is assigned a unique agent identifier (AID). Each AID is composed of three parameters:

- A unique name, usually consisting of a local name and the address of the AP.

**Fig. 15.12** FIPA's agent management reference model [30]



- An address list, to which the messages should be delivered.
- A resolver, used by the AMS for resolving the transport address of the agent.

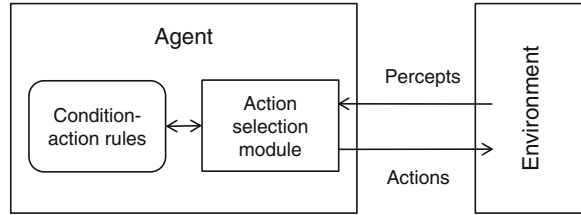
### 15.4.5 Agent Anatomies

As described by Russell and Norvig [31], the internal architecture (or anatomy) of an agent defines its behavior, i.e., there is a function mapping every sequence of percepts (what the agent perceives) into actions. This function can be simple, as in reactive agents, or quite complex as in cognitive agents. An architecture such as subsumption may be used for reactive agents [32]. Cognitive agents may be based on the Soar architecture [33], while the work of Albus on the reference model architecture [34] is applicable for hybrid types. There are four main classes of agents classified in accordance to their level of autonomy, the way percepts are used, and how they can be modeled:

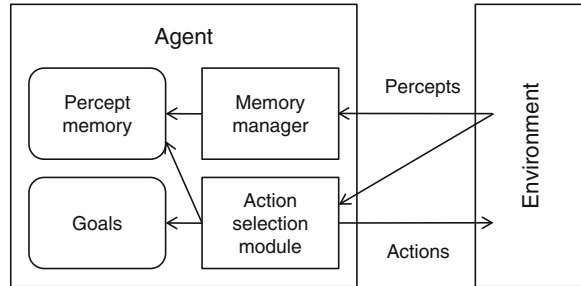
- *Reflex agents* perform simple actions based on current percepts (Fig. 15.13) and their behavior is based on an action selection module that receives percepts from the environment and consults a database of condition–action rules, similar to if-then rules, to take a decision. Such agents can be useful when fast response times are needed, e.g., for protection. Their representation of the world (the environment) is minimal, but they may support emergent behaviors. Emergence occurs when new characteristics appear at a certain level of complexity.
- *Goal-based agents* are directed by goals set a priori by the user. They have an internal representation of their environment and can memorize previous percepts so as to take more elaborate decisions. More precisely, once a percept is received by the agent, the memory manager stores the information in the percept memory. A sequence of percepts is then built in order to be used subsequently by the action selection module to select suitable actions in order to reach given goals (Fig. 15.14).

The BDI agent model [3] is a type of goal-based agent that enables a designer to build agents having beliefs about the world, with desires, i.e., objectives and goals, plus intentions, i.e., plans. The BDI architecture enables a separation between plan

**Fig. 15.13** Structure of a simple reflex agent



**Fig. 15.14** Structure of a goal-based agent



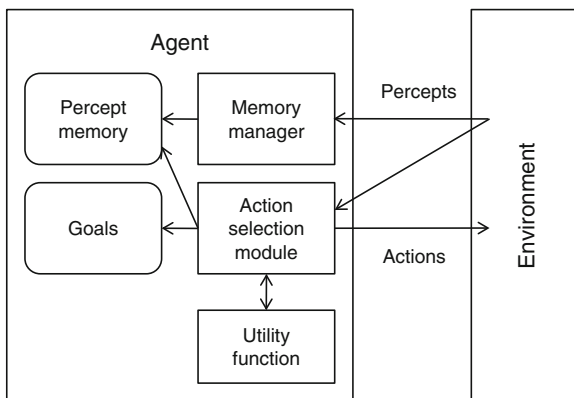
(actions) selection and execution. Such agents can therefore be used for planning, which consists in finding a sequence of actions in order to reach a given goal. The concept of planning will be further explained in [Sect. 15.4.9](#).

- *Utility-based agents* use a performance measurement index, commonly called utility function, in order to evaluate their behavior. Suppose a goal-based agent has to search for a sequence of towns that have to be visited. Some paths may be shorter, safer, or cheaper than others. A goal-based agent will select any path among the possible ones. On the other hand, an utility-based agent can select a specific path that optimizes a given utility function, taking into account some compromise. Figure 15.15 summarizes the processes used by a utility-based agent. A utility-based agent that always optimizes its utility is called a *rational agent*, as it behaves in an efficient manner, given its prior knowledge of the environment. An agent running an economic dispatch algorithm is an example.
- *Learning agents* belong to one of the previous classes and in addition can learn to perform a given task more effectively. They are able to modify the function that codes their behavior while interacting with their environment, so as to be more confident at performing a given task. An agent running a load forecasting algorithm would be a typical example. These types of agents are described with more details in the next section.

### 15.4.6 Learning Agents

Since the beginning of artificial intelligence in the 1950s, scientists have been developing computer programs with the purpose of *learning* how to perform a

**Fig. 15.15** Structure of a utility-based agent



specific task. Machine learning became a very exciting branch of artificial intelligence, for it aims at designing machines that can improve their performance without having to actually program them explicitly.

Instead of defining algorithms as functions that map inputs into correct outputs, with the risk of forgetting some inputs when defining the function, machine learning advocates the design of algorithms that enable a machine to learn a function using empirical data. Such data can be either gathered prior to the learning phase of the task at hand, or collected by the machine as it interacts with its environment, i.e., within a network or a physical or virtual world.

Machine learning is traditionally divided into three main branches:

- *Supervised learning* deals with problems of prediction or classification. It consists in determining the underlying function that has generated a set of data. This function is assumed to map inputs to desired outputs. Artificial neural networks, support vector machines, and decision trees are some of the techniques widely used in supervised learning. An application of supervised learning in power systems is for load forecasting, where historical and weather data are used to predict the load.
- *Unsupervised learning* consists in identifying some regularities in the given data, in order to constitute classes. K-means, mixture models, principal component analysis (PCA), independent component analysis, or some artificial neural networks like the self-organizing map are some of the most widely used approaches for solving unsupervised learning problems. Such techniques can be used for blind source separation (that is the separation of a set of signals from a set of mixed signals), text clustering (grouping documents that share similar contents), and dimensionality reduction (which consists in reducing the quantity of data under consideration when taking a decision). In power systems, an algorithm analyzing large fault datasets to detect the origin of an issue could use such techniques.
- *Reinforcement learning* tackles sequential decision-making problems, that is problems where a rational agent has to determine the best sequence of actions

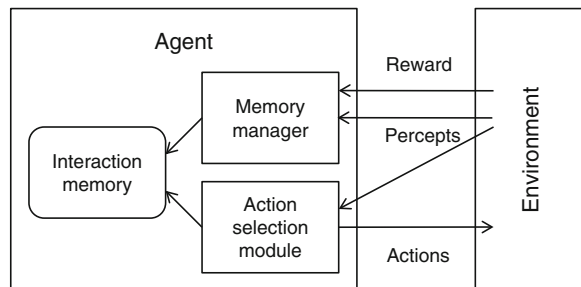
that enables it to efficiently perform a given task. For example, a chess program willing to win should perform the best sequence of moves at every encountered game configuration. A reinforcement learning agent usually interacts with its environment using three kinds of signals: percept, action, and reward signals. Rewards are typically generated by a reward function defined by the system designer. This reward function must formalize what the agent has to do, i.e., its task, and not how it should do it. An agent bidding on power markets could integrate such capability to improve its strategy over time.

Each time the agent receives a percept, its action selection module consults a memory constituted by information about its interactions with its environment and then selects an action that is performed by the agent in the environment. A new percept and reward are sent to the memory manager of the agent to update its interaction memory (Fig. 15.16). These steps of interaction and learning of the agent are continuously repeated. The figure below assumes the agent has a global perception of its environment.

Machine learning techniques have been applied successfully to solve complex problems in various applications. Their success can be explained by the fact that they can intrinsically handle partial observability and uncertainties coming from different sources, for example due to measurements by imperfect sensors. Several free software suites are available for experimentation on a variety of machine learning algorithms such as RapidMiner [35], KNIME [36], Weka [37], or Shogun toolbox [38].

In the fields of control and energy management, machine learning techniques can be used advantageously for carrying out different important tasks. Supervised learning can be applied to handle renewable generation forecasting [39, 40] as well as demand forecasting [41, 42]. Renewable generation from photovoltaic panels and wind generators can be predicted from data mapping time-stamped meteorological conditions (like wind speed, solar irradiation, or humidity) to the optimized corresponding generation of different types of renewable devices. Supervised learning techniques take advantage of these data to determine underlying functions (one for each possible renewable energy source) that can precisely predict generation from information about meteorological conditions. Similarly, demand forecasting can be handled by using supervised learning techniques that

**Fig. 15.16** Structure of a simple learning agent



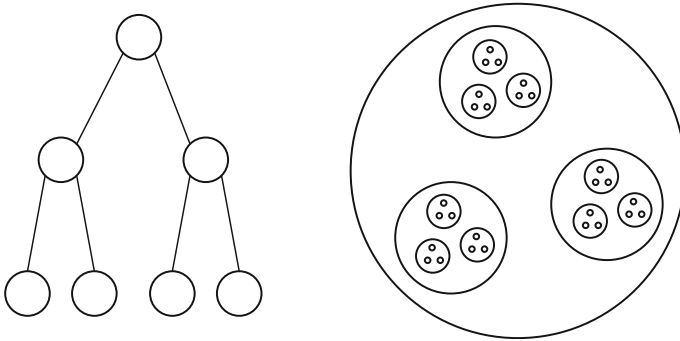
uses time-stamped data extracted from historical and meteorological measurement databases.

Reinforcement learning techniques can for example be used to reliably damp electromechanical oscillations in flexible ac transmission systems (FACTS) [43]. Reinforcement learning could also be valuable for supporting the behavior control of energy trading agents. Such techniques can be based on nonlinear, stochastic, and nonstationary assumptions, so that agents can continuously learn to act rationally in environments whose dynamics or the operating conditions can possibly change. Moreover, they could be used in combination with some classical approaches and enable them to operate faster by suggesting solutions based on historical data. For example, PCA might be used from an initial set of information to extract the important features on which some agents could rely in order to learn to act intelligently.

### 15.4.7 Organizational Topologies

The collection of roles, authority relationships, data flow, resource allocation, and coordination patterns that guide the behaviors of all agents are defined as an organizational topology. The major topologies used in MAS include hierarchies, holarchies, coalitions, teams, congregations, societies, federations, markets, and matrix organizations [44]. Each has its own strengths and weaknesses, and some topologies are more appropriate than others depending on the application:

- A *hierarchy* (Fig. 15.17) is the earliest and the most widely used topology, in which agents are arranged in a tree-like structure. Agents higher in the tree have a more global view than agents below them. Lower level agents transmit the information perceived locally to higher level agents, which provide directions to those below them, on the basis of a more complete amount of information. This topology is typically used in most current control systems.
- *Holarchies* consist of agents (called holons) that are constituted by several entities and are at same time part of a larger entity. Biological species, individuals, cells, and atoms can each be viewed as holons sharing this dual characteristic. Hierarchies and holarchies are more easily applied to problems where goals can be decomposed into tasks that can be assigned to those agents.
- *Coalitions* are dynamic and short lived, and emerge as soon as a goal has to be fulfilled by a subset of an agent population. The coalition is destroyed when the constituent agents have managed to perform the task. The structure of a coalition is typically flat, although there can exist a leading agent that represents the coalition as a whole. In a coalition, agents are “selfish,” i.e., they try to maximize their own profit. Such topology may for example be used for power restoration after a blackout.
- *Teams* are an “altruist” type of organization, as opposed to coalitions; they attempt to maximize the utility of the whole team, and coordinate their actions



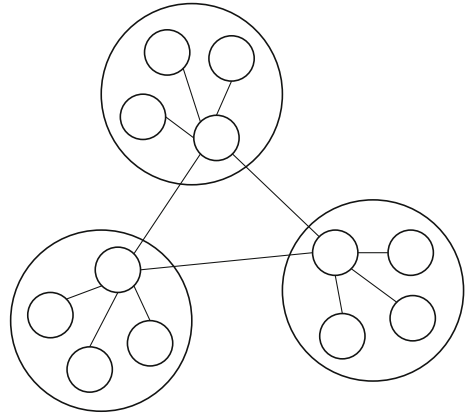
**Fig. 15.17** A hierarchy (*left*) and an holarchy (*right*)

in order to efficiently fulfill a common task. Team agents have an explicit representation of the shared tasks and know the means by which cooperation should progress.

- *Congregations* are generally long lived and are formed from heterogeneous agents that have great interest to get together. Some simple examples of congregations are clubs or academic departments. Congregating agents are expected to be rational, by maximizing their own long-term utility. Congregations are formed if agents want to increase information gain or to decrease commitment failure.
- *Societies* are inherently long lived and open. Agents living in a society may have different goals, levels of rationality and heterogeneous capabilities. They meet and interact according to social laws (or norms), which dictate how they should coexist. Vehicular traffic laws are an example of social laws that minimize conflicts and encourage efficient solutions.
- *Federations* are arranged such that some agents delegate a part of their autonomy to a single agent that represents the group (Fig. 15.18). Group members interact only with this delegate (also called facilitator, mediator, or broker), which acts as an interface between the group and the outside world. The delegate typically receives undirected messages from its group members and sends information to the delegates of other federations. Messages from group members include skill descriptions, task requirements, or status information, whereas messages from or to other delegates include task requests or capability notifications. This structure could for example be used to interface several microgrids, where the central controller of each microgrid would be the delegate.
- *Marketplaces*, or market-based organizations, enable buyers and sellers to send and receive bids for a common set of items, such as shared resources or tasks. Like for federations, an individual or a group of individuals in a marketplace is responsible for coordinating the actions of other agents. Unlike a federation though, agents within a marketplace are competitive. This topology is already used in power markets, where independent power providers and utilities (among other players) bid to sell and buy power.



**Fig. 15.18** A federation example



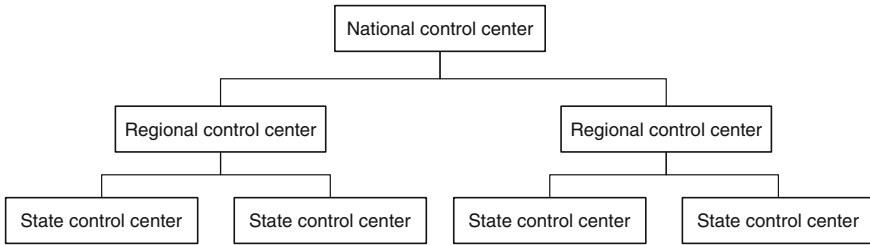
- *Matrix* organizations mimic how humans influence one another, i.e., the behavior of an agent or of an agent group may be influenced by multiple centers of authority. How the agent perceives these influences can influence other agents as well. Simple examples of such influences include someone receiving guidance or pressures from its boss, spouse, children, or colleagues.

For power systems, no preferred topology is considered better than others. Several parameters may influence the choice of a topology:

- The structure of the real world organization of the system or the power grid.
- Needs for reliability, especially regarding communication.
- Whether decisions require negotiations, for example based on market mechanisms.
- The scale of the system and possible evolutions.
- The necessity to change of topology to reach goals.

Such choice is a tradeoff several parameters including computation, coordination simplicity, and organizational rules, plus the simplicity of the architecture itself. An analysis according to these criteria defines the topology of the system and its control regime (the way agents interact, as described in the next section). It should also be noted that the architecture of a MAS may change over time, depending on what it is trying to achieve and how the environment evolves.

Contemporary control systems are frequently based on hierarchical topologies, because they have been the most intuitive to the human mind when designing control systems, especially in single layer applications. For layered architectures, there are other possibilities that enable dividing the global system into several interacting subsystems, such as the reference model architecture [34]. An example is the hierarchy of grid control centers in a country (Fig. 15.19). However, there are several drawbacks; the main one being that they are prone to single-point failures, for example if the central controller or communication fails. Their reliability and resilience are thus limited.



**Fig. 15.19** Most of today’s control systems are organized in a hierarchical topology based on geographical subdivisions

More decentralized topologies are theoretically well suited for the needs of modernized, distributed, and liberalized power systems. But they are also more complex to design as they impose a change of paradigm. A fully distributed architecture, where all agents would be “equal,” would be ideal and would constitute the ultimate level of resilience to communication failures, as there would not be any centralization of data (the need for communication would certainly increase though). Until such topologies become feasible, hybrid ones, such as the ones listed earlier, are thus to privilege. The Internet is an example of an hybrid architecture, where there is no global controller, and decisions are taken at least partially locally, although some nodes are most important than others.

### ***15.4.8 Inter-Agent Interaction***

The described topologies define the interaction of an agent with another one, or entity, but it is still needed to define how they interact. Interactions are paramount notions for defining MAS [2]. An interaction between agents can only take place if they can act or communicate and if there are situations where they can get together, such as the need to fulfill a common objective. Interactions may be conducted under the form of discussions between at least two agents and can occur in numerous situations: the rescue of an agent by others, a conversation between two agents, the implicit agreement when two agents have to decide which one goes first, the cooperation of several agents to fulfill a common task, and so on.

Interactions are usually required when agents have to satisfy a common objective while taking into account their limited resources and individual skills. Getting together to fulfill a common objective involves that some agents are part of a possibly emerging organization, as described in the previous section. Therefore, every agent organization is the result of these interactions and of the place where they take place. The dynamical characteristics of interactions then implies that new agent organizations are likely to be formed as new objectives have to be satisfied. Agents can for example form coalitions [45] if it helps them reach their goals.

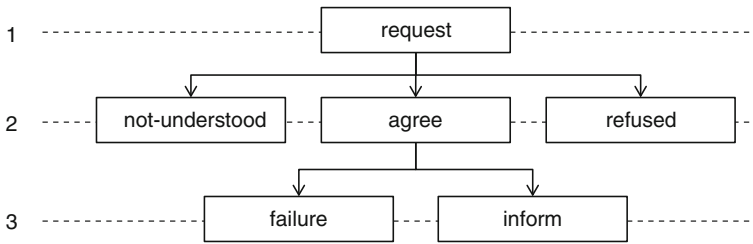
Defining interactions between agents depends on answers to the following questions: What is the nature of their goals? What are their resources? Which skills do they possess to fulfill these goals? Several criteria can be used to classify interactions. These criteria include the nature of the goals pursued by the agents, their relationship to external resources, and their individual skills with respect to the task at hand:

- Typically, agents are engaged in competitive tasks when their goals are contradictory, whereas they cooperate or co-evolve when their individual goals are compatible (that is when the satisfaction of a goal by an agent does not interfere with the possibility of satisfying another goal by another agent). Maintaining the balance between electricity supply and generation is an example of problem where cooperation is essential.
- External resources include all environment elements that agents need to satisfy a goal, such as raw materials, energy, available amounts of space and time, etc. For example, every energy source or power line has a limited capacity. Limited resources can lead agents to conflicts as they will likely need the same resources at the same moment and at the same place than other agents. Such conflictual situations can generally be resolved by the coordination of agent actions.
- The last criterion relates to whether the task can be pursued by a single agent rather than by a group of agents, and if each one of them has the appropriate skills to perform its subtask. An energy source can for example not store energy, and neither does a load.

To enable interoperability, interactions are structured and follow common rules called protocols. Basic and common types of interactions are requests, queries, subscriptions, and propositions. An example is the FIPA-Request protocol [46]: an agent can formulate a request, that other agents can accept or refuse (Fig. 15.20).

Those interactions are limited, and combinations of them are often used instead. There are several types of such complex interaction protocols: contracting, auctions, bargaining, voting, and brokering.

- The *contract-net protocol* is an example of contracting, defined in FIPA specification SC00029 [47]. This task-sharing protocol consists in a collection of agents forming a contract network. Two categories of agents are distinguished: the manager, and contractor agents. A typical round (see Table 15.3) starts with a call for proposals sent by the initiator. A deadline can be set to limit the duration spent waiting for answers. Contractors (participants) can then emit proposals (prices, time to execute an action, etc.) or refuse. The initiator evaluates the proposals and selects zero, one or several agents to perform the task to be fulfilled. The selected participants are free to accept or refuse this offer.
- Agents can interact and distribute tasks through *auctions*. Four main types of auctions are commonly used: English, Dutch, sealed first price or Vickrey, and Walrasian auctions.



**Fig. 15.20** The FIPA-Request protocol enables an agent to formulate a request that other agents may accept or refuse. The corresponding conversation is divided into three consecutive steps

- English auctions are the most common ones. Participants bid openly against each other, with each subsequent bid higher than the previous one. A reservation price (the minimum price) may be set by the auctioneer. The auction ends when no participant is willing to bid further. FIPA defines a specification for English auctions in XC00031 [48].
- In Dutch auctions, the auctioneer starts with a high price which is lowered until some participant accepts the announced price. This type of auctions is also defined by FIPA in its XC00032 specification [49].
- With sealed first-price auctions, all bidders simultaneously submit their bids, and the winner is the one with the highest bid. Bidders can only submit a single bid. Vickrey auctions are identical except that the winner pays the second highest submitted price [50].
- Walrasian auctions are more complex and enable matching supply and demand in a market of perfect competition. A market clearing price is set so that the total demand equals the amount of sold goods, and leads to a general equilibrium [51]. This type of auctions was proposed for use on electricity markets using locational margin pricing [52].
- *Bargaining* is an alternative to auctions for pricing goods, i.e., when prices are not fixed and can be negotiated. The goods can for example be split into several parts and be themselves subject to bargaining. As humans, agents can employ various strategies to reach their goals.
- Interactions can also happen under the form of votes. *Voting protocols*, such as Robert’s rules of order (RONR) [53], define procedures for conducting votes

**Table 15.3** A summary of the conversation between the initiator and the participants (contractors) in a contract-net protocol according to the FIPA specification

Initiator	Direction	Participants
Call for proposals	→	
	←	Propose or refuse
Accept or reject proposals	→	
	←	Inform of the end/result of the round or of a failure

between agents. Voting can be used to take decisions when votes are very simple (e.g., yes or no). Similarly to votes during elections, various rules can be adopted for selecting the winner(s).

- Another interaction type specified by FIPA is *brokering* [54]. An agent can for example request a broker to find other agents who can answer a query; the broker would then relay the answer back to the initiator.

Numerous other interaction protocols, sometimes derived from domains such as game theory, can be employed. Custom interactions can for example be based on Petri nets; consensus theory can be used for reaching a group agreement even in the presence of faults [55, 56]; the Shapley value can help finding solutions to cooperative games [57, 58]; etc.

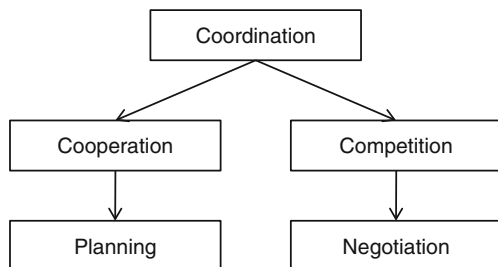
### 15.4.9 Multi-Agent Planning

In order to attain their goals, agents are sometimes required to coordinate themselves to cooperate or compete with each other, and dispatch tasks using interaction protocols. In some cases, agents may be required to plan their actions before executing them. Actions can include rounds of interactions that must happen in a given order, for example if their outcomes are interdependent. As shown in Fig. 15.21, planning enables advanced agent cooperation, whereas negotiations are used for managing competing agents.

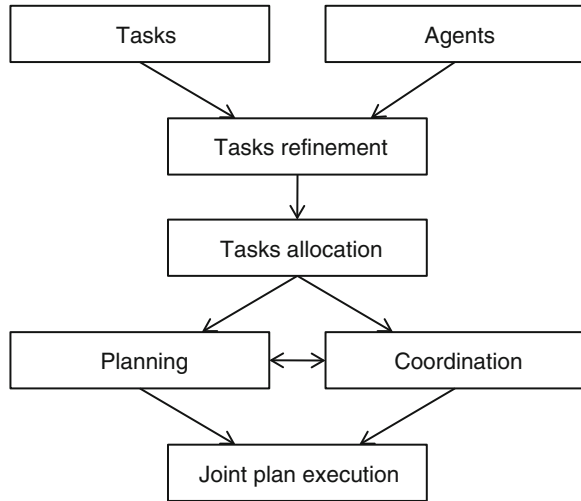
Similarly to interactions, planning involves action selection, sequencing, and resources handling. The established plans can be action sequences or action trees resulting from policies and strategies defined by the designer or by other agents. Figure 15.7 provides a simple example: to be able to provide the required power during the demand peak, the storage unit needs to charge before the peak occurs.

Three main elements differentiate multi-agent planning techniques: where the plans are created, when coordination occurs, and how plans are coordinated. As for MAS architectures, planning can be centralized, or partially or fully distributed. In centralized planning, one agent plans for the others. It is potentially optimal and requires communication only before and after planning. On the other hand, in distributed planning, computation time is reduced, privacy is easier to ensure, the

**Fig. 15.21** Agents can coordinate themselves in two different manners: by cooperating, and planning is then required, or by competing, requiring negotiation



**Fig. 15.22** Planning and coordination are complementary in establishing joint plans in MAS. Coordination can happen *before*, during (as pictured here) or after planning [59, 60]



system is scalable and distributed control and execution are enabled. For partially distributed planning, only parts of agents' plans are shared. Regarding when coordination occurs, three main approaches exist: before, during and after planning (Fig. 15.22). Coordination can also happen during plan execution, especially when communication is unreliable.

Existing planning techniques include STRIPS, ACT, partial plans, plan space refinement, HTN, or Petri nets [54]. Choosing a planning and coordination technique depends on the behavior of the agents and of the technical environment. Similarly to what was detailed in the previous sections, agents for planning can:

- Be strongly related or independent.
- Be cooperative or self-interested.
- Try to resolve conflicts or to exploit efficiency.
- Have no communication or reliable communication available.
- Have to bear with a low or high incident rate.

The interested reader may refer to [31, 59–61] for more information on this topic.

#### 15.4.10 Development Platforms

Although it is possible to develop a MAS from scratch, using a dedicated development platform (middleware) is, in most cases, a much simpler solution. Many different toolkits were created over the years, as shown in [62]. These platforms include tools and functionalities that facilitate the development of MAS. Some of them comply with FIPA standards, especially for messaging and agent management. A list of such platforms is available in [63].

In the field of MAS for power system applications, the Java agent development framework (JADE [64]) is the most popular. It has extensive documentation, third-party plug-ins (e.g., for mobile devices, for BDI agents [65], etc.) and full FIPA compatibility. Among the other existing platforms, some general-purpose examples include AgentBuilder, MadKit, and ZEUS. Some others may be of interest for specific users: NetLogo enables beginners to get started with MAS programming, JANUS simplifies holonic agents building, Cougaar enables very large-scale simulations, JADEX proposes a framework for developing intelligent agents according to the BDI model, JACK for autonomous agents, etc. Most of these platforms are developed in Java, which enables cross-platform (i.e., operating systems) compatibility, but other languages can be used.

Because of the multiple definitions and applications of MAS, most of these platforms are quite different, and a careful selection needs to be operated. This selection can be done according to the following criteria: documentation availability, compliance with standards, performance [66], scalability, built-in development tools, GUI friendliness, etc.

## 15.5 Applications of MAS to Power Systems

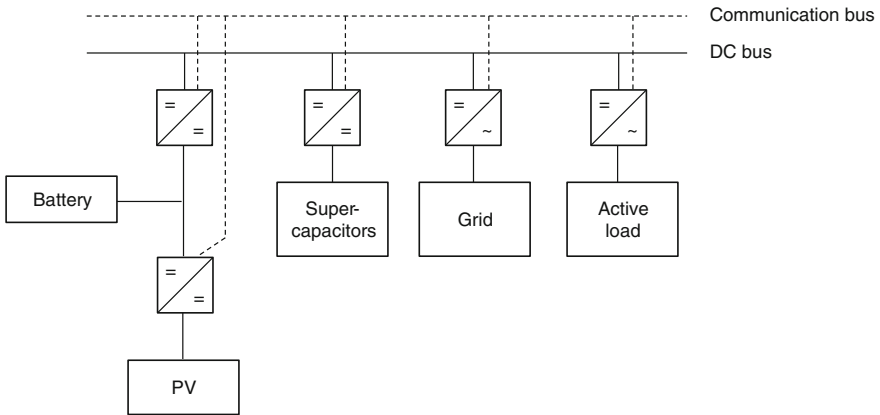
For all the reasons listed in the previous sections, MAS have been applied to solve several problems in power systems. The following four examples were published in the last decade. Based on the explanations from the previous sections, the reader is encouraged to analyze what choices the designers of the presented MAS have conducted. Other existing applications [4] also constitute interesting concepts.

### 15.5.1 Coordinated DC Bus Voltage Control

Lagorse et al. proposed a MAS-based coordinated DC bus voltage control scheme, described in [67]. The objective of this algorithm is to automatically maintain the bus voltage at a constant value, which can be considered as the DC equivalent of frequency control in AC networks: as soon as there is a difference between supply and demand, the voltage level (resp. the frequency) moves away from its reference value and compromises system stability.

The DC bus can be the central part of an islanded network where various loads, sources, and storage units are connected. In the described test case, the microgrid includes a PV source, a battery, supercapacitors, a grid access point (to import/export energy from/to the distribution system), and an active load, all connected to a common DC bus (see Fig. 15.23).

Each source and storage unit is connected to a power electronic converter controlled by an agent (Fig. 15.24). The agents cooperate to ensure that the bus voltage remains constant, using a token system to select which inverter controls

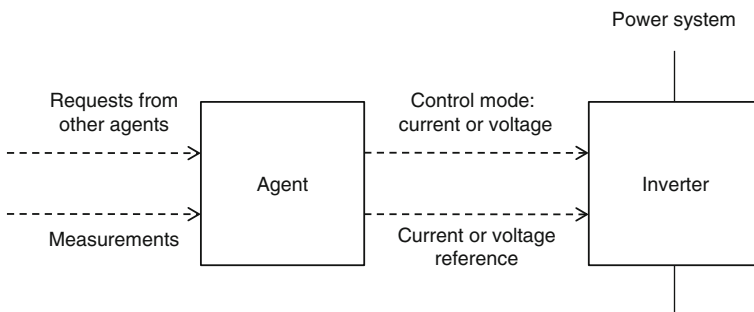


**Fig. 15.23** A single-wire schema of the hardware architecture studied in this DC bus voltage control application. Agents directly control inverters by cooperating with each other [67]

the bus voltage. A secondary objective is to minimize energy imported from the grid.

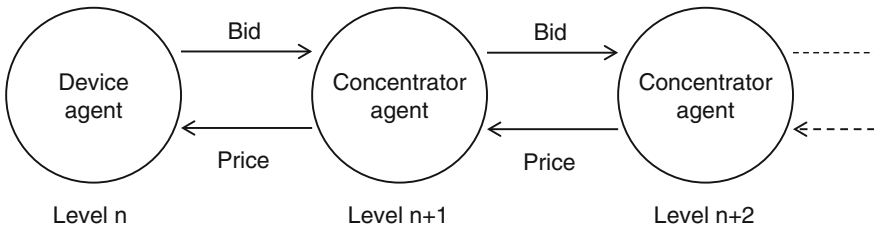
The inverter that has the token regulates the bus voltage while the other inverters are current controlled through PI controllers. The agents coordinate themselves to define two outputs: how each inverter should be controlled (voltage or current), and the corresponding voltage and current references.

For example, if a storage unit holds the token and its state-of-charge reaches its lower limit, the unit is not able to keep controlling the bus voltage anymore and needs to give the token to another agent. It then requests another agent to replace it. This request may or may not be accepted. If it is, then the other agent switches its inverter to voltage-controlled mode, while the agent that had the token switches it to current-controlled mode (Table 15.4). If the request is rejected, then the agent can ask another agent connected to the bus to replace it.



**Fig. 15.24** Each agent receives requests from other agents and decides whether its inverter should be current- or voltage controlled and with which reference [67]





**Fig. 15.25** Each device and concentrator agent emits a bid for the power it wants to sell or buy, and receives a price computed by the auctioneer in return. This price is back propagated through all layers of the system by the concentrator agents

**Table 15.4** An idealized discussion between two agents when transferring the token to control the voltage of the DC bus [67]

Agent 1	Token	Direction	Token	Agent 2
I cannot keep controlling the bus voltage. Can you take the token?	x	→		
	x	←		Yes
Here, take the token		→	x	
		←	x	Thank you

Each agent has a similar internal architecture, based on a finite-state machine which gives the agent a different behavior depending on whether it has the token or not. Each agent has its own characteristics derived from the type of hardware it is connected to: source, load, or storage unit. For example, as grid imports have to be minimized, the grid agent never asks to control the voltage, and can only receive requests. On the contrary, supercapacitors agents have the highest priority to regulate the bus voltage, because of their high voltage and very short response time compared to other sources.

The main interest of this voltage control algorithm resides in its decentralized nature, its flexibility and its fault tolerance. Other components can be added and/or deleted without requiring manual adaptation of the system, as long as the system is capable of knowing that these components are available and what are their main characteristics are. On the other hand, this scheme does not optimize how the resources used, which would require a different approach.

### 15.5.2 Market-Based Coordination of Distributed Generation

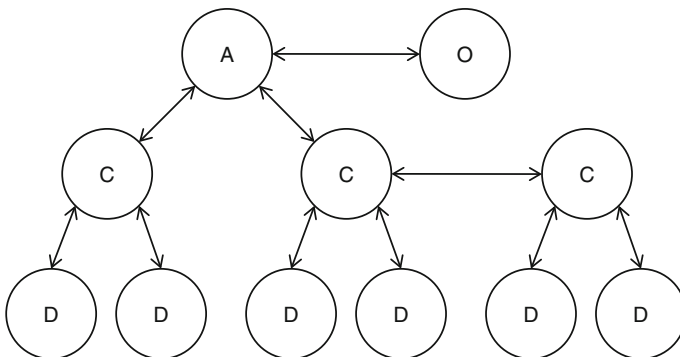
Coordinating distributed energy sources in modernized power markets is another field where MAS-based cooperation can be employed. PowerMatcher, a concept developed by ECN in the Netherlands [51, 68, 69], is an example. The objective is

to coordinate agents so as to balance supply and demand in an economically efficient way. To solve this problem, agents have the capability to competitively trade energy on a common market. These market-based negotiations provide a decision-making framework based on microeconomics.

The negotiation process relies on dynamic pricing schemes, in which prices can vary throughout the day depending on the balance between supply and demand: the higher the demand, the higher the prices, and vice versa. Each agent buys or sells energy depending on its type (load, source, etc.), and commits to this bought or sold amount. In this competitive general equilibrium market, all agents have access to the same information on price, obtained by searching for the equilibrium between supply and demand.

The PowerMatcher architecture is based on a logical tree structure, as shown in Fig. 15.26. Each group of agents is coordinated by a concentrator agent, which is in turn coordinated by another concentrator at a higher level. Four types of agents are used:

- *Device agents* control the distributed sources, loads, and storage units of the system, and are able to converse with concentrators. They have their own goals and properties, and issue bids based on what they are willing to pay (resp. be paid) for a given amount of energy to consume (resp. produce).
- *Concentrator agents* (Fig. 15.25) locally concentrate and aggregate the bids they receive, and back propagate the price chosen by the auctioneer to lower level agents (device agents and other concentrators).
- The *auctioneer agent*, at the top of the tree, centralizes the bids of the agents connected to it and finds the equilibrium price based on bids it has received to clear the market. The obtained price is then sent back to the agents if it has significantly changed from its earlier value.
- The *objective agent* is connected to the auctioneer agent and defines the objective of the system.



**Fig. 15.26** The MAS proposed in PowerMatcher uses a hierarchical architecture, based on four types of agents: an auctioneer (*A*), an objective agent (*O*), concentrator agents (*C*) and device agents (*D*). The above diagram shows an example with a limited number of agents

Each agent, whether it is a device or a concentrator, only knows its direct neighbors.

A negotiation round is initiated with a given frequency (of a few minutes) by the auctioneer agent. The agent starts by asking other agents to submit their bids, and computes the equilibrium price based on information it has gathered. Other events can trigger a round, such as a sudden change in demand. DF and AMS agents are used, so that each agent can find other agents to negotiate with.

The main interests of this concept are its ability to operate in environments with a large share of renewable energy sources, where the energy sector has been fully liberalized, and consumers can also be producers. The selected bottom-up approach, combined with the decentralized decision-making process, enable a very flexible architecture, where a change in the structure, by adding or removing functionalities or agents, does not affect the overall operation of the system. This structure is plug-and-play and scalable: contrary to other architectures, this solution is not based on a central optimization algorithm that would hinder the ability to scale the system. By aggregating local bids, the need for intensive data communication is avoided. Similar concepts can also be applied to trade other commodities, such as heat in a microgrid where cogeneration is available. The system is being tested in a demonstration project called PowerMatching city,<sup>1</sup> located in the Netherlands.

Comparable and interesting MAS- and market-based approaches were proposed by other researchers, such as DEZENT [70], MASCEM [71], work by Dimeas and Hatziargyriou [72, 73], Pipattanasomporn et al. [74], and Funabashi et al. [75].

### ***15.5.3 Restoration***

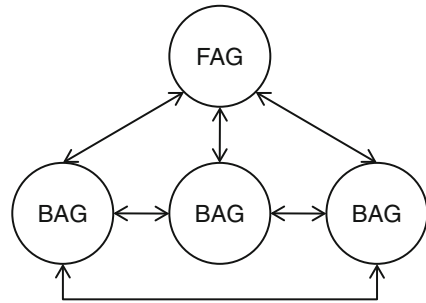
One of the earliest applications of MAS in power systems is for restoration, as described in Nagata and Sasaki [76]. Restoration is needed after a partial or global blackout has occurred. Operators usually employ an OMS to automatically restore power, by sequentially re-energizing all the buses in the grid so as to serve the loads. At the end of the process, the grid is back to its normal operation mode, as before the event. The objective is to serve the maximum of loads connected to the buses. Several constraints have to be respected: the balance between supply and demand, the capacity of each source, and the voltage limits on each bus and branch.

In the proposed approach, two types of agents are used (Fig. 15.27): bus agents (BAG, one for each bus), and a facilitator agent (FAG). Each BAG tries to restore power to the load connected to its bus and can only communicate with its geographical neighbors and with the FAG. Its behavior follows simple rules:

---

<sup>1</sup> <http://www.powermatchingcity.nl>. Last visited June 27, 2011.

**Fig. 15.27** The proposed MAS is made of two types of agents, each with their own roles: bus agents (*BAG*) and a facilitator agent (*FAG*) [76]



- If the bus can be powered by several branches, then the agent chooses the branch with the highest power in order to restore power as quickly as possible.
- If the available power is not sufficient, the agent negotiates with its neighbors to find another solution and get a higher power to energize its load.
- If no satisfying solution can be found, the agent sheds its loads to its minimum power.

The FAG facilitates the negotiation by classifying buses according to their voltage level, and choosing one BAG at each voltage level to initiate the restoration process. Several restoration processes can be run in parallel at different voltage levels, which accelerates the overall restoration.

In a later paper [77], the authors proposed another version of this concept, where FAGs are feeder agents and act as managers for the decision-making process. The architecture shown in Fig. 15.27 is replicated at each feeder, and feeder agents can communicate with each other. This enables the system to operate on a much larger scale, with restoration “groups” cooperating with each other. This approach is an improvement compared to traditional OMS, where everything is coordinated by a central controller. The proposed system is much less complex, as the same algorithms can be replicated and cooperate to achieve their objectives, but could be expected to provide results similar to the ones obtained by centralized algorithms.

Other MAS-based restoration concepts are presented in the literature, such as in [78, 79]. Pan and Tsai [80] also propose a BDI-based solution to this problem.

### 15.5.4 Protection Fault Analysis and Management

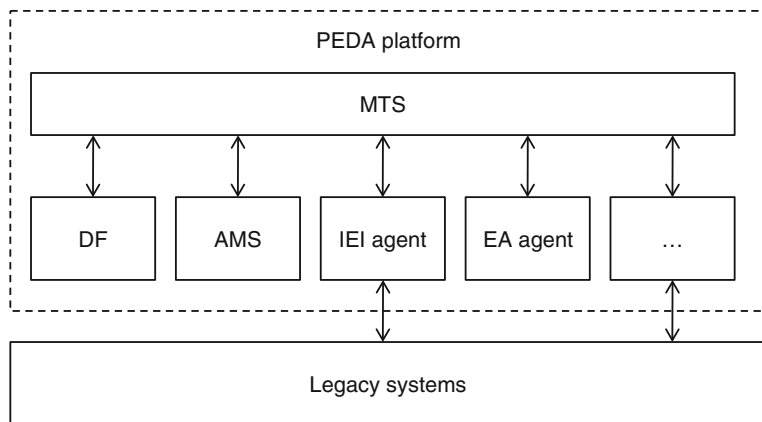
Davidson et al. [81] propose a fault diagnosis and management called PEDA, for protection engineering diagnosis agents (PEDA). PEDA has been used since 2004 by a British utility. Its objective is to automate the analysis and management of faults recorded by SCADAs and digital fault recorders (DFR). As thousands of faults can be recorded during an event such as a storm, engineers need to be supported by a system capable of extracting the most important information from the mass of collected data.

In this case, MAS technology was used as a medium for system integration. The hardware and software used to achieve fault analysis and management can indeed change rather frequently over time, and the system has to be able to accommodate such evolutions. The proposed MAS integrates several tools, including a rule-based expert system to classify and interpret data from SCADAs, and a model-based reasoning system to validate protection operations using DFR data.

The architecture of PEDA is based on FIPA’s agent management reference model presented earlier, and therefore implements both DF and AMS services. As shown in Fig. 15.28, additional agents are used for retrieving, interpreting, analyzing, etc. data, each with its own role in the system. Some of these agents encapsulate systems that were already being used in the legacy system.

ACL and FIPA subscription protocols are used for inter-agent interaction and communication, together with an ontology for disturbance diagnosis. For example, all agents subscribe to IEI agents (telemetry processors), which in turn inform them when they have identified an incident. The AMS and DF enable the MAS to acknowledge when an agent joins the system: each agent autonomously searches for other agents that can provide them the information they need.

This MAS is one of the first applications tested in the power industry. The problems the authors had to face when transferring their laboratory prototype to the real system provide useful lessons (e.g., on platform choice (here JADE), standards, user interfaces, etc.) for other projects that may try to achieve similar tests. It also builds on an approach different from the ones used in traditional MAS work, as it does not primarily focus on distributed intelligence, but rather on the flexibility of the approach, transforming a legacy fault analysis and management system into a flexible and extensible tool, in which software and hardware parts can be easily changed.



**Fig. 15.28** In this MAS, both DF and AMS agents are used, in addition to agents encapsulating legacy systems, and to other agents such as the EA agent that interacts with operators. Only a part of all agents is represented in this diagram [81]

## 15.6 Future Developments

Although they are very promising, MAS are still an emerging technology in the field of power systems. Topics to explore in the future include:

- *Making agents smarter.* Most agents used in MAS for power systems tend to be closer to reactive agents than to cognitive agents. Making them smarter would enable a greater autonomy and more complex decision-making processes with additional parameters taken into account. The learning capability of agents could for example have many applications, from forecasting to scheduling, and could partially pre-solve some problems. Similarly, the planning capacity of agent is rarely used.
- *Fully distributing and automating the decision-making process.* Decision-making processes are usually partially centralized, i.e., not fully distributed. If one or more central controller fails, or if a communication channel is cut [82], then the whole system operation may be compromised. Redundancy can partially help avoid such situations, but increases costs. Achieving a fully distributed decision-making process would solve this problem: if each agent takes his own decisions, sometimes after discussing with others, it would not be greatly impacted by the failure of another agent. However, distributing decision-making often comes at the cost of having more intensive communication.
- *Creating a modeling and simulation tool to facilitate the development and testing of MAS for power systems.* Current solutions require co-simulation between a MAS and a simulation tool such as Matlab/Simulink or PowerWorld Simulator [83]. A tool mixing both would highly simplify simulation, development and testing MAS for these applications.
- *Testing MAS on very large-scale grids.* In most research papers, MAS are tested on small-scale systems and show good results. However, very few work has focused on the scalability of MAS for such applications: how would the system perform when the grid size increases? Will communication and computation requirements explode? How will the system behave in case of perturbations or attacks? Such studies will be essential to determine the optimal decentralization degree to use, as well as the corresponding infrastructure costs for developing smart grid communication infrastructures.
- *Testing MAS for control on real-scale industrial systems.* So far, MAS have been mostly a subject of research in the field of power systems, but their industrial and commercial applications are rare, with exceptions such as the application presented in Sect. 15.5.4. Feedback and lessons learned from early experiments will be essential to foster the adoption of MAS technology in the industry. Three main difficulties have to be faced: utilities are sometime reluctant to investigate the use of MAS, which are still widely unknown due to a lack of practical experience; communication costs are high because MAS often require new equipment, especially at the distribution level; and power system standards are not written with MAS in mind. These difficulties also apply to most new smart grid technologies.

- *Integrating user behavior models.* As consumers are and will remain central players in smart grids, arises the need to model consumer behavior. In the future, so-called “prosumers” may take decisions using their home energy management interface and will directly impact how and when electricity is consumed, for example through demand response mechanisms that may affect consumers’ comfort level and billing, but also utilities. Qualitative studies provide important and useful information, but quantitative results are required to make regulatory and investment decisions, and to develop potentially successful new products. In parallel to modeling such consumer agents, real experiments will also have to take place to make these models more accurate and validate them.
- *Securing MAS communication.* A prerequisite to any commercial application is that systems must be secure and resist to attacks of all sorts. Although this problem is much wider than only for MAS, its importance was stressed by the recent concerns raised by worms such as Stuxnet, which aimed at disrupting industrial processes controlled by PLCs (programmable logic controllers). MAS thus have to include the most efficient and secure technologies before being deployed in the industry.

## References

1. Wooldridge M, Weiss G (1999) Multi-agent systems. The MIT Press, Cambridge
2. Ferber J (1999) Multi-agent systems: an introduction to artificial intelligence. Addison-Wesley, Cambridge
3. Rao AS, Georgeff MP (1991) Modeling rational agents within a BDI-Architecture. In: Allen J, Fikes R, Sandewall E (eds) Proceedings of the 2nd international conference on principles of knowledge representation and reasoning. Morgan Kaufmann publishers Inc., San Mateo, pp 473–484
4. McArthur S, Davidson E, Catterson V, Dimeas A, Hatziaargyriou N, Ponci F, Funabashi T (2007) Multi-agent systems for power engineering applications—part I: concepts, approaches, and technical challenges. IEEE Trans Power Syst 22:1743–1752
5. McArthur S, Davidson E, Catterson V, Dimeas A, Hatziaargyriou N, Ponci F, Funabashi T (2007) Multi-agent systems for power engineering applications—part II: technologies, standards, and tools for building multi-agent systems. IEEE Trans Power Syst 22:1753–1759
6. Zambonelli F, Jennings N and Wooldridge M (2003) Developing multiagent systems: the Gaia methodology. ACM Trans Softw Eng Methodol (TOSEM) 12:370
7. Omicini A (2001) SODA: societies and infrastructures in the analysis and design of agent-based systems. In: Ciancarini P, Wooldridge M (eds) Agent-oriented software engineering. Lecture notes in computer science, vol 1957. Springer, Berlin, pp 311–326
8. Wood M, DeLoach S (2001) An overview of the multiagent systems engineering methodology. Agent-Oriented Software Engineering, Springer, Berlin, pp 1–53
9. Caire G, Coulier W, Garijo F, Gomez-Sanz J, Pavon J, Kearney P, Massonet P (2004) The MESSAGE methodology. Methodologies and software engineering for agent systems. Springer, Berlin, pp 177–194
10. Bresciani P, Perini A, Giorgini P, Giunchiglia F, Mylopoulos J (2004) Tropos: an agent-oriented software development methodology. Auton Agents Multi-Agent Syst 8(3):203–236 Springer

11. Bernon C, Gleizes MP, Peyruqueou S, Picard G (2003) ADELFE: a methodology for adaptive multi-agent systems engineering. *Engineering societies in the agents World III*. Springer Berlin, pp 70–78
12. Iglesias C, Garijo M, González J, Velasco J (1996) A methodological proposal for multiagent systems development extending CommonKADS. In: *Proceedings of the 10th Banff knowledge acquisition for knowledge-based systems workshop*
13. Brazier F, Dunin-Keplicz B, Jennings N, Treur J (1997) Desire: modeling multi-agent systems in a compositional formal framework. *Int J Coop Inf Syst* 6:67
14. Henderson-Sellers B, Giorgini P (2005) *Agent-oriented methodologies*. IGI Global, Hershey
15. Dam KH, Winikoff M (2004) *Comparing agent-oriented methodologies*. Agent-oriented information systems. Springer, Berlin, pp 78–93
16. Gomez C, Isern D, Moreno A (2007) *Software engineering methodologies to develop multi-agent systems: state-of-the-art*, Research report DEIM-RR-07-003. Universitat Rovira i Virgili
17. Crespi V, Galstyan A, Lerman K (2008) Top-down vs bottom-up methodologies in multi-agent system design. *Auton Robots* 24:303–313 Springer
18. Foundation for Intelligent Physical Agents (FIPA) (2011) Available from: <http://www.fipa.org>. Accessed 1 July 2011
19. International Electrotechnical Commission (IEC) (2011) Available from: <http://www.iec.ch>. Accessed 1 July 2011
20. International Electrotechnical Commission (2011) IEC TC 57 Power systems management and associated information exchange. Available from: <http://tc57.iec.ch>. Accessed 1 July 2011
21. Liang Y, Campbell RH (2008) Understanding and simulating the IEC 61850 standard. Available from: <https://www.ideals.illinois.edu/handle/2142/11457>. Accessed 1 July 2011
22. DNP users group (2005) A DNP3 Protocol Primer. Available from: <http://www.dnp.org/About/DNP3%20Primer%20Rev%20A.pdf>. Accessed 1 July 2011
23. CIM users group (2009) Available from: <http://cimug.ucauiug.org>. Accessed 1 July 2011
24. Britton JP, Devos AN (2005) CIM-based standards and CIM evolution. *IEEE Trans Power Syst* 20(2):758–764
25. McNaughton G, McNaughton W (2006) *MultiSpeak Version 3.0 User's Guide*. Available from: [http://www.multispeak.org/utilities/UserGuides/Documents/MultiSpeak\\_V3\\_UserGuideFinal\\_013006.pdf](http://www.multispeak.org/utilities/UserGuides/Documents/MultiSpeak_V3_UserGuideFinal_013006.pdf). Accessed 1 July 2011
26. Saleem A, Honeth N, Nordström L (2010) A case study of multi-agent interoperability in IEC 61850 environments. *Innovative smart grid technologies conference Europe (ISGT Europe)*, 2010 IEEE PES, pp 1–8
27. Apostolov A (2006) Multi-agent systems and IEC 61850. *IEEE power engineering society general meeting*
28. FIPA (2002) FIPA ACL Message structure specification. SC00061G
29. Catterson VM, Baker PC, Davidson EM, McArthur SDJ (2010) An upper ontology for power engineering applications. Available from <http://ewh.ieee.org/mu/pes-mas/>. Accessed 1 July 2011
30. FIPA (2004) FIPA agent management specification. SC00023 K
31. Russell S, Norvig P (2010) *Artificial intelligence, a modern approach*. 3rd edn. Prentice Hall, New Jersey
32. Brooks R (1986) A robust layered control system for a mobile robot. *Rob Autom IEEE J [legacy, pre-1988]* 2(1):14–23. doi:10.1109/JRA.1986.1087032
33. Laird J, Newell A, Rosenbloom P (1987) SOAR: An architecture for general intelligence. *Artificial Intelligence* 33(1):1–64. <http://www.sciencedirect.com/science/article/pii/0004370287900506>
34. Albus JS (1993) A reference model architecture for intelligent systems design. In: Antsaklis PJ, Passino KM (eds) *An introduction to intelligent and autonomous control*. Kluwer Academic Publishers, Dordrecht
35. Rapid-I. Available from <http://rapid-i.com>. Accessed 4 Apr 2012



36. KNIME. Available from <http://www.knime.org>. Accessed 4 Apr 2012
37. WEKA. Available from <http://www.cs.waikato.ac.nz/~ml/weka>. Accessed 4 Apr 2012
38. Sonnenburg S, Rätsch G, Henschel S, Widmer C, Behr J, Zien A, De Bona F, Binder A, Gehler C, Franc V (2010) The SHOGUN machine learning toolbox. *J Mach Learn Res* 11:1799–1802
39. Mellit A (2008) Artificial Intelligence technique for modeling and forecasting of solar radiation data: a review. *Int J Artif Intell Soft Comput Indersci* 1(1):52–76
40. Bhaskar M, Jain A, Srinath V (2010) Wind speed forecasting: present status. International Conference on Power system technology (POWERCON) pp 1–6
41. Metaxiotis K, Kagiannas A, Askounis D, Psarras J (2003) Artificial intelligence in short term electric load forecasting: a state-of-the-art survey for the researcher. *Energ Convers Manage* 44(9):1525–1534 Elsevier
42. Kodogiannis VS, Anagnostakis EM (2002) Soft computing based techniques for short-term load forecasting. *Fuzzy Sets Syst* 128(3):413–426 Elsevier
43. Ernst D, Glavic M, Wehenkel L (2004) Power systems stability control: reinforcement learning framework. *IEEE Trans Power Syst* 19(1):427–435
44. Horling B, Lesser V (2005) A survey of multi-agent organizational paradigms. *Knowl Eng Rev* 19(4):281–316
45. Yen J, Yan YH, Wang BJ, Sin PKH, Wu FF (1998) Multi-agent coalition formation in power transmission planning. In: System SCIENCES, Proceedings of the Thirty-First Hawaii IEEE international conference on, vol 4, pp 433–443
46. FIPA (2001) FIPA request interaction protocol specification. XC00026F
47. FIPA (2002) FIPA contract net interaction protocol specification. SC00029H
48. FIPA (2001) FIPA English auction interaction protocol specification. XC00031F
49. FIPA (2001) FIPA Dutch auction interaction protocol specification. XC00032F
50. Ausubel LM, Milgrom P (2006) The lovely but lonely Vickrey auction. In: Cramton P, Shoham Y, Steinberg R (eds) *Combinatorial Auctions*, pp 17–40
51. Kok JK, Scheepers MJJ, Kamphuis IG (2010) Intelligence in electricity networks for embedding renewables and distributed generation. *Intelligent Infrastructures*. Springer, Berlin, pp 179–209
52. Motto AL, Galiana FD, Conejo AJ, Huneault M (2002) On Walrasian equilibrium for pool-based electricity markets. *IEEE Trans Power Syst* 17(3):774–781
53. Pitt J, Kamara L, Sergot M, Artikis A (2006) Voting in multi-agent systems. *Comput J* 49(2):156
54. FIPA (2001) FIPA brokering interaction protocol specification. SC00033H
55. Pease M, Shostak R, Lamport L (1980) Reaching agreement in the presence of faults. *J ACM* 27(2):228–234
56. Olfati-Saber R, Fax JA, Murray RM (2007) Consensus and cooperation in networked multi-agent systems. *Proc IEEE* 95(1):215–233
57. Kamboj S, Pearre N, Kempton W, Decker K, Trnka K, Kern C (2010) Exploring the formation of electric vehicle coalitions for vehicle-to-grid power regulation. AAMAS workshop on agent technologies for energy systems (ATES 2010)
58. Contreras J, Klusch M, Yen J (1998) Multi-agent coalition formation in power transmission planning: a bilateral Shapley value approach. In: Proceedings of 4th international conference artificial intelligence planning systems, pp 19–26
59. De Weerd M, Ter Mors A, Witteveen C (2005) Multi-agent planning: An introduction to planning and coordination. Available from: <http://www.st.ewi.tudelft.nl/~mathijs/publications/eass05.pdf>. Accessed 1 July 2011
60. Ziparo VA (2005) Multi-agent planning. Available from: [http://www.dis.uniroma1.it/~dottoratoii/db/relazioni/relaz\\_ziparo\\_1.pdf](http://www.dis.uniroma1.it/~dottoratoii/db/relazioni/relaz_ziparo_1.pdf). Accessed 1 July 2011
61. Marinova ZL (2002) Planning in multiagent systems. Msc thesis submitted to the Faculty of Mathematics and informatics of Sofia University “St. Kliment Ohridski”. Available from: <http://www.ontotext.com/sites/default/files/publications/theis-zm.pdf>. Accessed 1 July 2011

62. Comparison of agent-based modeling software (2011) In: Wikipedia, The free encyclopedia. Available from: [http://en.wikipedia.org/w/index.php?title=Comparison\\_of\\_agent-based\\_modeling\\_software&oldid=434070966](http://en.wikipedia.org/w/index.php?title=Comparison_of_agent-based_modeling_software&oldid=434070966). Accessed 1 July 2011
63. FIPA (2003) Publicly available agent platform implementations. Available from: <http://www.fipa.org/resources/livesystems.html>. Accessed 1 July 2011
64. Bellifemine F, Caire G, Greenwood D (2007) Developing multi-agent systems with JADE. Wiley, Hoboken
65. BDI4JADE: a BDI layer on top of JADE (2011) Available from: <http://www.inf.puc-rio.br/~ionunes/bdi4jade/>. Accessed 1 July 2011
66. Camacho D, Aler R, Castro C, Molina JM (2002) Performance evaluation of ZEUS, JADE and Skeletonagent frameworks. Systems, man and cybernetics, 2002 IEEE international conference on, vol 4, p 6
67. Lagorse J, Paire D, Miraoui A (2010) A multi-agent system for energy management of distributed power sources. *Renew Energ* 35:174–182
68. Hommelberg MPF, Van der Velde BJ, Warmer CJ, Kamphuis IG, Kok JK (2008) A novel architecture for real-time operation of multi-agent based coordination of demand and supply. IEEE power and energy society general meeting-conversion and delivery of electrical energy in the 21st Century
69. Kamphuis R, Kok K, Warmer C, HommelbergM (2008) Architectures for novel energy infrastructures: multi-agent based coordination patterns. Infrastructure systems and services: building networks for a brighter future (INFRA), 2008, First international conference on
70. Wedde HF, Lehnhoff S, Handschin E, Krause O (2006) Real-time multi-agent support for decentralized management of electric power. Real-Time Systems, 2006. 18th Euromicro conference on
71. Praca I, Ramos C, Vale Z, Cordeiro M (2003) MASCEM: A multiagent system that simulates competitive electricity markets. *IEEE Intell Syst* 18(6):54–60
72. Dimeas AL, Hatziaargyriou ND (2005) Operation of a multiagent system for microgrid control. *IEEE Trans Power Syst* 20(3):1447–1455
73. Dimeas AL, Hatziaargyriou ND (2007) Agent based control of virtual power plants. International conference on intelligent systems applications to power systems (ISAP 2007) pp 536–541
74. Pipattanasomporn M, Feroze H, Rahman S (2009) Multi-agent systems in a distributed smart grid: design and implementation. IEEE/PES power systems conference and exposition, 2009 (PSC'09)
75. Funabashi T, Tanabe T, Nagata T, Yokoyama R (2008) An autonomous agent for reliable operation of power market and systems including microgrids. Third international conference on electric utility deregulation and restructuring and power technologies (DRPT 2008) pp 173–177
76. Nagata T, Sasaki H (2002) A multi-agent approach to power system restoration. *IEEE Trans Power Syst* 17:457–462
77. Nagata T, Tao Y, Kimura K, Sasaki H, Fujita H (2004) A multi-agent approach to distribution system restoration. The 2004 47th Midwest symposium on circuits and systems (MWSCAS'04), vol 2, pp 333–336
78. Solanki JM, Khushalani S, Schulz NN (2007) A multi-agent solution to distribution systems restoration. *IEEE Trans Power Syst* 22(3):1026–1034
79. Xu Y, Liu W (2011) Novel multiagent based load restoration algorithm for microgrids. *IEEE Trans Smart Grid* 2(1):152–161
80. Pan YT, Tsai MS (2009) Development a BDI-based intelligent agent architecture for distribution systems restoration planning. Intelligent system applications to power systems (ISAP'09) 15th International conference on
81. Davidson EM, McArthur SDJ, McDonald JR, Cumming T, Watt I (2006) Applying multi-agent system technology in practice: automated management and analysis of SCADA and digital fault recorder data. *IEEE Trans Power Syst* 21(2):559–567

82. Buldyrev S, Parshani R, Paul G, Stanley H, Havlin S (2009) Catastrophic cascade of failures in interdependent networks. *Nature* 464:1025–1028
83. Roche R, Natarajan S, Bhattacharyya A, Suryanarayanan S (2012) A Framework for Co-simulation of AI Tools with a power systems analysis software. 23rd International Workshop on Database and Expert Systems Applications (DEXA) pp 350–354